University of Salford MANCHESTER

IMPACT OF ACQUISITION PROTOCOL VARIATIONS ON EFFECTIVE DOSE AND RISK FOR CT HEAD EXAMINATIONS

MOHAMED RAJAB BENHALIM

Ph.D. Thesis **2018**

University of Salford MANCHESTER

Impact of acquisition protocol variations on effective dose and risk for CT head examinations

Mohamed Rajab Benhalim

School of Health Sciences

College of Health and Social Care

University of Salford, Manchester, UK

Submitted in partial fulfilment of the requirements of the

Degree of Doctor of Philosophy (PhD),

February 2018.

Supervision and research area information

Impact of acquisition protocol variations on effective dose and risk for CT head examinations

Research area: Radiography/Medical physics/ Medical imaging/Dosimetry/ Dose optimization

Name of student: Mohamed Rajab Benhalim **Student ID number:** @00372767

The following academics supervised this PhD thesis:

1. **Dr. Andrew England – First Supervisor**

   Senior Lecturer

   Directorate of Radiography

   L613, Allerton Building, University of Salford, Salford, M5 4WT

   Telephone: +44 (0) 161 295 0703

   Email: a.england@salford.ac.uk / www.salford.ac.uk

2. **Professor Peter Hogg – Co-Supervisor**

   Professor of Radiography,

   Director, Centre for Health Sciences Research,

   Research Dean,

   School of Health Sciences

   University of Salford

   Room L608, Allerton Building, University of Salford, Salford, M5 4WT

   Telephone: +44 (0) 161 295 2492

   Email: P.Hogg@Salford.ac.uk / www.salford.ac.uk

3. Dr. Lucy A Walton – Co-Supervisor

Research Fellow, Deputy Director Postgraduate Research / Health Sciences

Address: Room L601, Allerton Building, University of Salford, Salford M5 4WT

Telephone: +44 (0) 161 295 5145 / m +44 (0) 7564 088851

Email: l.a.walton@salford.ac.uk / www.salford.ac.uk

Advisors

1. Dr. Katy Szczepura – Lecturer

Directorate of Radiography

L617, Allerton Building

University of Salford, Salford, M5 4WT

Telephone: +44(0)161 295 2192

Email: k.szczepura@salford.ac.uk / www.salford.ac.uk

Table of contents

Contents

List of figures

List of tables

List of publications, Conference Presentations and Seminars

Differences in effective dose between different paediatric CT brain scan protocols. Mohamed R. Benhalim, Peter Hogg, Katy Szczepura, Andrew England, presented in the United Kingdom Radiological Congress; Liverpool 2016. [**Poster**].

Methods for direct measurement of radiation dose: TLD and MOSFET. In P Hogg, R H Thompson, C Buissink (Eds.), ***OPTIMAX 2016,*** R M.K. M.Ali, M Alrowily, Mohamed R. Benhalim, A Tootell; 2017. [**Book chapter**].

Impact of acquisition protocol variations on effective dose for CT head examinations. Mohamed R. Benhalim, Katy Szczepura, Peter Hogg & Andrew England; presented in the European Congress of Radiology; Vienna 2017. [**Conference paper**].

"How to make MOSFET x-radiation dose measurements in phantoms"; Mohamed R. Benhalim; School of Health Science Research Seminar Series – Direct X-ray radiation dose measurement's in human phantoms on 01.04.2016. [**Research seminar**].

Paediatric lifetime cancer risk for head CT protocols of a 1-year old child. Mohamed R. Benhalim, Peter Hogg, Walton Lucy, Katy Szczepura, Andrew England. [**Conference paper**].

Impact of changing CT gantry angulation on eye dose during paediatric head examinations. Mohamed R. Benhalim, Peter Hogg, Walton Lucy, Katy Szczepura, Andrew England. [**Conference paper and Electronic Poster**].

An investigation of the impact of image viewing parameter settings on the performance of 2.4 MP colour monitor in visualising low contrast detail using the CDRAD phantom. Sadeq Al-Murshedi, Peter Hogg, Mohamed R. Benhalim, Maily Alrowily & Andrew England. [**Conference paper**].

Acknowledgement

Thanks be to almighty God who created me from nothing for allowing me to complete this piece of work.

I would like to take this opportunity to express my sincere gratitude to all those who have supported me to complete this thesis; First of all, I am deeply indebted and thankful to my Primary Supervisor **Dr. Andrew England,** for his help, guidance and encouragement during my time at the University of Salford. It has been my great fortune to have him as academic supervisor. I am grateful his advice, feedback, useful discussions, and constructive criticism. Words would not be enough to express my feelings for his tremendous help and support.
Also, I would like to extend my heart-felt gratitude to my Co-supervisor **Professor Peter Hogg;** the person who has inspired and assisted me and also helped in resolving many challenges during my research journey. His rich expertise and in-depth knowledge of conducting research has been of great help to me in the course of my PhD.

I would also like to express my sincere thanks to my Co-supervisor **Dr. Lucy Walton** for her valuable statistical and mathematical support and for all her feedback throughout of my thesis. I do not think I would have been able to finish this PhD without the help of her.

Also, I am very grateful to **Dr. Katy Szczepura**, who has been great advisor to me for her sharing expertise about providing valuable support about medical physics and giving sincere and valuable guidance.

Some of my work would not be completed without the help of my **colleagues and fellow PhD students** who have always given me help, research advice and tips regarding how the data should be presented. Also, I am grateful to all of the Directorate of Radiography staff, especially **Mr Christopher Beaumont**, for their significant support in facilitating access to the imaging facilities.
I am extremely grateful to my **Libyan Ministry of Higher Education** for supporting me in finishing this PhD.

Finally, I would like to take the opportunity to thank the number one person in my life, to my **Mother**; for her endless support, encouragement and attention and also expressing my deepest appreciation to my **Father**, my **brothers and sisters** for their deep moral support throughout all my overseas studies. I am also grateful to my beloved and lovely children: **Aya, Ansam, Ahmed and the youngest one Areej** for their support, kindness and patience as they accompanied me along this PhD journey. It is to them I dedicate this work.

List of abbreviations

2D – Two-dimensional

3D – Three-dimensional

ABM – Active Bone Marrow

ABS – Atomic Bomb Survivors

ACR - American College of Radiology

ALARA – As Low As Reasonably Achievable

ALARP – As Low As Reasonably Practicable

ANOVA – Analysis of variance

ANS - American Nuclear Society

AP – Anterior-Posterior

AR – Attributable Risk

ART – Algebraic Reconstruction Technique

ATCM – Automatic Tube Current Modulation

BEIR - Committee on the Biological Effects of Ionising Radiation

CBV – Cerebral Blood Volume

CI – Confidence Interval

CIRS – Computerized Imaging Reference Systems

cm – Centimetre

CNR - Contrast to Noise Ratio

CNS – Central Nervous System

CSF – Cerebrospinal Fluid

CT – Computed Tomography

CTDI – CT Dose Index

$CTDI_{vol}$ – CT Dose Index Volume

$CTDI_{w}$ – Weighted CT Dose Index

CTP – CT Perfusion

DAS – Data Acquisition System

DDREF - Dose and Dose Rate Effectiveness Factor

DLP – Dose Length Product

DRLs - Diagnostic Reference Levels

DSCT – Dual Source CT

ED – Effective Dose

EAR - Excess Absolute Risk

EBCT – Electron Beam CT

EF – Effective Risk

EPA – Environmental Protection Agency

ERR - Excess Relative Risk

ET – Extrathoracic Region

FBP – Filtered Back Projection

FDA – The US Food and Drug Administration

g – Gram

GCS – Glasgow Coma Scale

Gray (Gy) - unit used for the absorbed dose. A tissue is said to have received a dose of 1 gray (Gy) when the energy transferred by the radiation to the tissue is 1joule/kg.

HP – Helical Pitch

i.e. – That is

IAEA - International Atomic Energy Agency

ICC – Intraclass Correlation Coefficient

ICRP - International Commission on Radiological Protection

ImPACT – Immediate Post-Concussion Assessment and Cognitive Testing

IPEM - Institute of Physics and Engineering in Medicine

IR(ME)R – Ionising Radiation (Medical Exposure) Regulations

kg – Kilogram

kVp – Peak Kilovoltage

LAR - Lifetime Attributable Risk

LET – Linear Energy Transfer

LNT – Linear No Threshold Model

LSS - Life Span Study

mAs – milliampere-second

MC – Monte Carlo

MDCT - Multiple Row Detector CT

MDS – Myelodysplastic Syndromes

mGy – Milligray

MIRD – Models for Ionizing Radiation Dosimetry

mm – Millimetres

MOSFETs - Metal Oxide Semiconductor Field Effect Transistors

MRI – Magnetic Resonance Imaging

MSAD – Multiple-Scan Average Dose

MSCT – Multi-Slice CT

mSv – Millisievert

NAS - The US National Academy of Sciences

nC – Nanocoulomb

NICE – National Institute for Health and Care Excellence

NRC - National Research Council

NRPB – The UK National Radiation Protection Board

OSL – Optically-Stimulated Luminescence

PA – Posterior-Anterior

PF – Pitch Factor

PMMA – Polymethyl Methacrylate

PNS – Peripheral Nervous System

QA – Quality Assurance

R – Roentgens

RBM – Red Bone Marrow

SD – Standard Deviation

SDCT – Single Row Detector CT

SIRT – Simultaneous Iterative Reconstruction Technique

SPR – The Society for Paediatric Radiology

SSCT – Single-Slice CT

Sv – Sievert

TLDs - Thermoluminescence Dosemeters

T_w – Tissue Weighting Factor

UK – United Kingdom

UNSCEAR - United Nations Scientific Commission on Effects of Atomic Radiation

US – Ultrasound

µGy – Micro Gray

Abstract

PURPOSE: To propose a method for estimating the effective lifetime risk of radiation-induced cancer from different brain CT scan protocols in both paediatrics and adults and to develop a prospective method for estimating the number of cancer cases for patients undergoing CT brain scans when using different scanning parameters.

MATERIALS AND METHODS: A series of CT dosimetry experiments were conducted at the University of Salford. Both adult and paediatric ATOM phantoms were imaged using standard CT head protocols across a wide range of protocol variations. Dose measurements were made using metal oxide semiconductor field effect transducers (MOSFETs). Effective doses and lifetime attributable cancer risks were calculated from MOSFETs organ and tissue absorbed dose measurements in both phantoms. The method for lifetime cancer risk prospective estimation allowed the production of prospective risk data (Excel spreadsheet). This can predict attributable lifetime cancer risk, before undertaking a CT scan, and is of critical importance in order to predict more accurately the radiation risks from CT. Whilst such a tool has benefits for all patient ages, it would have particularly value for children - due to their increased radio-sensitivity. Using such a tool, dose optimisation can then occur on a more informed basis, by adjusting protocol parameters with a view to minimising organ and eye dose. Together with advanced image quality preserving techniques, like ACTM, the tool would allow for more informed clinical decisions to be taken to balance image quality and radiation dose on a patient by patient basis.

RESULTS: The brain, thyroid, thymus, lung, salivary glands, oral mucosa, extrathoracic region and bone marrow all receive more than 0.03 mSv during CT brain scanning. The range in effective dose across a range of CT brain protocols were 0.27 to 1.13 mSv and 0.34 to 1.55 mSv for adult sequential and helical protocols, respectively. For paediatric helical protocols, the effective dose ranged from 0.30 to 2.06 mSv. In addition to scan parameters, differences in risk are also attributed to patient age at the time of scanning and gender. As an example, the lifetime attributable cancer risk for a 30-year-old patient when undertaking either an adult sequential or helical CT brain scan were 8 females and 6 males per 10^6 and 16 females and 9 males per 10^6, respectively. By contrast, for the two paediatric helical CT brains protocols the effective risk (using 3 months to 3 years CT protocol) were 71 females and 36 males per 10^6 at birth and for the 3 years to 5 years protocol this decreases to 69 females and 35 males per 10^6 when aged 5. Using the risk data, a novel interactive spreadsheet has been developed and is

reported within this thesis, which allows the proactive / prospective estimation of radiation risk for CT head examinations.

CONCLUSION: Data collected within this thesis has identified that the most dominant factors effecting absorbed dose are tube current, tube rotation time, detector configuration and helical pitch. When these factors increase the absorbed dose to body organs and tissues increases as well. The only effect of gantry angle is in decreasing the dose to the lens of the eye, this quantity does not factor into effective dose estimates due to the nature of the lens tissue.

This thesis proposes a novel method to estimate effective lifetime risk of radiation-induced cancer from CT brain examinations in order to compare different brain CT protocols (acquisition parameters). Absorbed dose measurements when considered in relation to the age and gender of the patient can help provide estimations of effective risk, a potentially more useful indicator of the possible effects of radiation exposure from CT head examinations. This risk estimation method can be used to compare different CT brain protocol parameters immediately prior to imaging. Risk should be prospectively taken into account when planning a CT brain examination, especially for young ages and those undergoing serial imaging. Using the prospective risk data (spreadsheet) provided in this thesis can help to estimate the probability of cancer induction from specific CT brain protocols and can be considered by practitioners and manufacturers when developing CT examinations in the future.

Overview and Structure of the Thesis

The structure of this thesis is presented in **(Figure 7-1)** on page **XXVII**. The PhD thesis is divided into seven chapters:

Chapter one, is to introduce and provide an overview of the key issues and also provide an outline of the structure of the thesis in order to orientate the reader. In this chapter, an overview of the problem of CT radiation dose and its impact on patients and the awareness of radiation risk has been explained. This also includes a selection of relevant information including reviewing the literature which describes the role of CT in head injury, the rationale for the thesis and aims for the work, thesis scope, objectives and the research question.

Chapter two, provides an overview of the nervous system including a detailed description of the relevant anatomy and embryology. This chapter will highlight the main areas of the brain and provide detailed information on the anatomy of the key areas relevant to radiation dosimetry.

Chapter three, includes a brief history of CT, a literature review of the evolution of CT technology. Details on the CT acquisition factors and mA modulation technology is also provided within this section. Also, this chapter explains the radiation dosimetry options including metal oxide semiconductor field effect transistors (MOSFETs) which are used extensively throughout this PhD thesis. The associated risks from ionizing radiation are discussed together with the methods for estimating the radiation dose from CT examinations. Computational and direct measurement methods for obtaining organ absorbed dose, effective dose and effective risk for adult and paediatric CT are explored within this section.

Chapter four, provides an overview of medical radiation exposure. The current knowledge of risk associated with exposure to low radiation doses is explored and worldwide trends in CT imaging are considered. These issues are further discussed in relation to adult and children and CT dose reduction techniques for adult and paediatrics patients are reviewed.

Chapter five, provides a description of the main experiment work (MOSFET experiments) using the ATOM phantom representing an adult and a one-year old child. Organ and tissue absorbed doses are quantified for CT brain examinations across a range of acquisition parameters. Chapter five also provides estimates of effective dose for the different types of CT

examinations / protocols included within the work. In this chapter, using the BEIR VII data, the method for lifetime attributable risk estimation will be explained.

Chapter six, the results of both experiments using the adult and paediatric ATOM phantoms, for a range of different CT protocols, will be presented using descriptive and inferential statistics. There will also be a comparison of a subset of the different protocols parameters with dose measurements made using MOSFETs. In addition, the absorbed dose to the eye and the results from the cancer risk calculations are presented.

Finally, **Chapter seven**, provides the overall discussion and conclusion of the thesis. In addition, there are limitations and suggestions for future work. The novelty of the work in thesis will be highlighted in this section.

Structure of the Thesis

Chapter 1: (Introduction)	• Overview of the problem and the potential impact on patients. • Thesis aims, objectives and scope.
Chapter 2: (Anatomy of the brain)	• Brain anatomy. • Brain radiological anatomy.
Chapter 3: (Background and radiation dosimetry options for CT scanning)	• Brief summary of the history of CT technology. • CT acquisition factors influencing radiation dose. • Radiation dosimetry. • CT Dose measurement parameters. • Dosimeters for measuring absorbed dose.
Chapter 4: (Literature review of medical exposure and radiation)	• Radiation from medical exposures. • CT and concerns regarding radiation dose. • CT usage and radiation exposure. • Paediatric and adult CT scanning.
Chapter 5: (Methodology)	• Developing a method for absorbed dose measurements using MOSFET. • Using the method to calculate effective dose. • Method for estimating Lifetime attributable risk (LAR).
Chapter 6: (Results)	• Data (effective dose) is presented for the different CT protocols, using MOSFET measurements for both ATOM phantoms representing an adult and 1-year-old child. • Eye absorbed doses for both phantoms. • Effective risk results.
Chapter 7: (Discussion & conclusion)	• Key discussion points • Novelty of the thesis. • Limitations and recommendations for future research. • Summary of the thesis.

Figure 7-1: Flowchart explaining the structure of the thesis.

Chapter 1 : Introduction and Background

1.1 Introduction and rationale

An incredible opportunity was given to medical scientists following the discovery of X-rays by the German scientist Dr. Wilhelm Roentgen in 1895. X-rays being electromagnetic radiation can penetrate through the body and help produce images of organs and body parts under investigation (Graham & Cloke, 2003). Diagnostic imaging, using X-rays, is one of the most useful and valuable medical tools available today. It provides opportunities to study anatomy and physiology, and to diagnose and investigate disease. Advances in technology have led to improved image quality and the ability to gain added diagnostic information that can affect patient management. However, there are notable risks from the use of ionising radiation and one of the main concerns is the induction of cancer. This risk arises not only from higher radiation dose techniques, but also from the increased use of medical imaging using X-rays. As with all fields of medicine, diagnostic imaging involves an element of risk that must be fully understood and balanced against the benefits that it provides.

Computed Tomography (CT) plays an important role in diagnostic radiology. Since its introduction in 1972, CT scanners have greatly increased in technological complexity (Bushberg & Boone, 2011; Fuchs, Kachelrieß, & Kalender, 2000; A. J. van der Molen, Schilham, Stoop, Prokop, & Geleijns, 2013). The introduction of spiral CT in 1989 opened the door to many applications of CT that were not previously possible, such as CT angiography (Fuchs et al., 2000). With the continued advancement, particularly the introduction of multi-detector CT in 1998, the number of CT scans performed annually has continued to rise (D. J. Brenner & Hall, 2007 & 2008). CT is a non-invasive method of acquiring cross-sectional images inside the human body without superimposition of overlapping anatomical structures.

Many authors have investigated the association between radiation exposure and the risk of cancer. Epidemiological studies, such as the Life Span Study of atomic bomb survivors; medical studies and experimental animal research have established a relationship between radiation exposure, cancer induction and cellular damage. However, as reported by ICRP (2007) there is a lack of consensus on the effects of radiation at low doses and low dose rates, with the linear no threshold hypothesis being widely accepted and the basis of the international system of radiation protection (ICRP, 2007b). Medical radiation exposure for diagnostic

purposes usually falls into this low dose category, where the radiation risks are yet to be observed and modelled by epidemiological studies.

CT has been shown to account for the highest contribution to population radiation dose amongst diagnostic imaging modalities (Lehnert & Bree, 2010; NCRP., 2009b). Despite the uncertainties inherent in risk assessments for low dose exposures, some researchers (D. J. Brenner, Elliston, Hall, & Berdon, 2001a; D. J. Brenner & Hall, 2007) have stated that when considering population health, the lifetime cancer risk attributable to CT examinations is not negligible. Furthermore, this risk is higher in children who are more radiosensitive than adults and have a longer remaining lifetime for cancer to become evident. Since 2001 and the publication of a series of articles (D. J. Brenner et al., 2001a; Donnelly et al., 2001) about the risks of radiation induced cancer in children from diagnostic CT scans, there has been a strong international focus on reducing paediatric CT dose (Vassileva et al., 2013).

CT scans of the brain are one of the most common CT examinations performed in Europe (30-40% of all CT scans), and they also contribute significantly to total collective effective dose of the population (Lehnert & Bree, 2010; T. Mulkens, Salgado, & Bellinck, 2007). This contribution is inevitable, as it results from a combination of high radiation dose per examination and frequent use of CT examinations in diagnoses of head trauma and suspected intracranial pathology. The increased use of this high dose procedure has been of great concern globally because of the high possibility of inducing undesired health effects in patients, such as cancer. Furthermore, the significant radiation dose delivered to superficial radiosensitive organs such as the lens of the eye, which is often irradiated during CT examinations of the head, is of great concern (Korir, Wambani, & Korir, 2012; Ngaile & Msaki, 2006; Zarb, McEntee, & Rainford, 2012).

The Head Injury guidelines produced by the National Institute for Health and Care Excellence (NICE) in 2014 (NICE Clinical Guideline 176) defines a head injury as any trauma to the head other than superficial injuries to the face. This guideline indicates that in the UK head injury is the dominant cause for death and disability among the people aged from 1 to 40 years. In England and Wales, 1.4 million people attend the Emergency Departments each year as a result of a head injury. Children under 15 years account for 33% to 50% of these cases. In total, the annual number of people admitted to hospital with a head injury is around 200,000. Based on these figures one-fifth of those who are admitted have evidence of skull fracture or brain injury (Davis & Ings, 2014; Wood & Boucher, 2012).

Farrell et al., (2013) indicates that brain injury is an important cause of morbidity and mortality in childhood. Injury severity is related to the mechanism of trauma, which itself varies with age. For paediatric patients, reporting the incidence of head injury varies amongst authors because of differences in definitions and methodologies. Canadian studies by Gordon et al., (2006) and Mehta (2007) reported that the annual rate ranges from 130 to 200 cases per 100,000 population. These authors further reported that head injuries lead to at least 20,000 Emergency Department (ED) visits. Data from physician groups across the United States have reported that head injuries account for nearly 650,000 ED visits per year, 80% of these admissions presented as minor head injuries often involving loss of consciousness, amnesia and/or a Glasgow coma scale (GCS) score between 13 and 15. With increasing access to CT scanners, nearly 27,000 CT scans are now performed per year (Mehta, 2007). A study by Miglioretti et al., (2013), investigating the use of CT for children aged 15 years or younger, reported that head CT scans were the most commonly scanned body part, increasing by approximately 50% from 1996 to 2010.

CT scans require high radiation doses to produce diagnostic images and it is known that childhood exposure to ionizing radiation can influence adult cognition. Paediatric literature has also reported that exposure to ionizing radiation at an early age can increase the risk of developing tumours during adulthood (D. J. Brenner et al., 2001a; Donnelly & Frush, 2001; Mehta, 2007; Preston, 2008; Thomas et al., 2006). As a result, it is common practice for all CT examinations to adopt the "as low as reasonably achievable" approach to radiation exposure with strong enforcement that scans should not be overused (D. J. Brenner & Hall, 2007; Thomas et al., 2006).

There has been an increase not only in the absolute number of CT examinations, but also in the size of anatomical coverage and the number of acquisition phases obtained while scanning (Bushberg & Boone, 2011; Fuchs et al., 2000). In some places, this is the product of an expedient exchange of the ease and speed of acquisition against appropriateness; however, there is misuse of the technique. There are some suggestions that for some examinations, due to the rapid introduction of new CT technologies and its wider application that suboptimal protocols have been adopted (Bushberg & Boone, 2011). The problem is confounded by scanners that seem simple to operate, but are in fact becoming increasingly complex, favouring the adoption of new practices without giving full regard to the optimal use of dose reduction strategies or algorithms. It is thus possible that a given CT system, in a single department, as used by various

operators for examination of a single body area may yield radiation doses that no longer depend predominantly on the limits of the machine but are operator dependent, with the important implications that some choices of the practitioners and radiologists may not be justifiable from diagnostic or dose limitation perspectives (Bushberg & Boone, 2011).

There is no doubt that CT investigations are increasing from every point of view: numbers of requests, extension, and scan phases (Bushberg & Boone, 2011; Fuchs et al., 2000). In light of the growing awareness of the issue of radiation dose and the possible risk for the individual and population there is a need for all concerned to take on an active role in dose management.

While there have been technological advancements in CT to reduce dose, such as automatic kV selection and iterative reconstruction, patient dose is an important issue, especially for paediatric patients. The estimated lifetime attributable risk of death from cancer is much higher in paediatric patients than in adult patients. For a head scan, the risk of death from cancer for a 5-year-old patient is more than 6 times greater than that for a 30-year-old patient (D. J. Brenner & Hall, 2007). With this knowledge, the importance of accurately measuring or estimating paediatric CT dose is vital. CT plays important role in diagnostic radiology. Even though, MRI is widely used in brain imaging, CT continues to be on the rise due to its varied advantages such as fast image acquisition with wide clinical applications (Livingstone, Eapen, Dip, & Hubert, 2006).

Radiographers face a universal problem in decision-making in clinical practice because of a lack of radiation risk data. Little is known about the difference in radiation risks between different CT acquisition protocols which makes optimisation (from a dose minimisation perspective) challenging. Various uncertainties are associated with these risk estimates, both in terms of the radiation dose for a given CT examination and in terms of the cancer risk per unit dose. Worldwide, there is a large volume of published material on CT and radiation attributable risk, although there is a lack of specific information for people that combines these aspects, particularly for children. As stated by Mathews et al., (2013), practitioners will increasingly need to weigh the undoubted benefits of CT scanning in clinical practice against the potential risks in order to justify each CT scan decision. Fortunately, many radiologists are now aware of the risks, and technological advances have already allowed CT scan doses to be reduced below those used in earlier decades. However, decision tools to objectively assess the need for CT are still not used routinely—for example, minor head trauma or suspected appendicitis are often managed using CT, rather than by observation, ultrasound, or magnetic

resonance imaging. Imaging for head trauma still accounts for the most CT scans in children. It is timely to alert the wider community, as well as the non-radiology healthcare professionals who refer patients for CT examinations, to the potential risks. All parties, including patients and families, need to work together to ensure that CT scans are limited to situations where there is a definite clinical indication, and where every scan is optimised to provide a diagnostic CT image at the lowest possible radiation dose. Within in practice, it has been observed that there is limited understanding of the magnitude of radiation doses and associated risks. Therefore, there is a strong research interest in this area and there is a gap in the current knowledge and understanding, which would inform decision-making, and potentially policy in the medical, public and government sectors.

1.2 Thesis Aims

Although CT scans are very useful clinically, potential cancer risks exist from the associated use of ionising radiation, in particular for children who are more radiosensitive than adults. The primary research aim is to estimate the lifetime attributable cancer risk for brain CT examinations in adults and children. Secondly, to investigate by using direct dosimetry measurements, the effect of varying CT brain protocols parameters on effective radiation dose and risk for adult and paediatric patients. This PhD thesis estimates the radiation dose from brain CT scans across a range of scanning parameters using ATOM phantoms representing a 1-year old and adult. In doing so, this thesis seeks to investigate dose variations due to changes in rotation times, gantry angulations and detector configurations using both sequential and helical protocols. The thesis provides an estimate of effective dose and evaluates the stochastic risk. A key ambition of this thesis is to provide a prospective risk modelling tool that could be used by practitioners in proactively evaluating the potential radiation risk prior to undertaking the CT examination. This risk tool may also have potential as an educational aid to assist in learning about CT parameters and their effects of radiation dose and risk.

1.3 Thesis Objectives

This thesis seeks to evaluate experimentally the radiation dose and risk for adult and paediatric CT brain examinations. The objectives of the thesis are:

1. Comparing between TLDs and MOSFET data to validate the method of using MOSFETs for direct CT brain dosimetry.

2. To use direct dose measurements and two ATOM phantoms to measure absorbed dose to organs/tissues, estimate the effective dose and eye dose for a range of brain CT scanning protocols for adult (helical and sequential) and paediatric (helical) patients.
3. Determine the lifetime attributable radiation risk (cancer induced per million people having the brain CT examination) for ages from 0 to 80 years from CT brain scanning for adult (helical and sequential) and paediatric (helical) protocols.
4. To develop a prospective risk calculation tool to estimate the lifetime attributable radiation risk and eye dose for adults and paediatrics for a variety of brain CT protocols.

This thesis addresses these objectives by:

1. Developing and implementing a method of organ dosimetry for adult and paediatric CT exposures using ATOM phantoms and MOSFET dosimeters.
2. Quantifying organ absorbed doses for typical adult and paediatric CT examinations of the brain for clinically employed protocols.
3. Projecting cancer risks for the population due to adult and paediatric CT examinations based on measured organ absorbed doses and radiation risk coefficients.

1.4 RESEARCH QUESTION

How can changes in CT protocols affect the effective risk from CT head scans in adults and children?

Chapter 2 : Overview of Brain Anatomy and Pathology

2.1 Chapter Overview

This chapter serves to provide an overview of two main areas, 1) an introduction to the neurological anatomy of the brain and 2) an illustration of the common pathology and radiological anatomy of the CT brain. The brain in the primary anatomical region which is the focus of this thesis and as such it is useful for the reader to have a basic anatomical and pathological overview.

The anatomy and pathology discussed in this chapter are relevant when considering the acquisition parameters investigated in this thesis and the potential radiation dose absorbed by the brain. There are many factors, such as the number of CT scans, total scanning time, irradiated volume and imaging protocol parameters, which will lead to an increase in the total absorbed and cumulative dose to organs and tissues irradiated directly or from scattered radiation.

The first section provides information on the basic anatomy of the central nervous system (CNS) and its development, and then the basic organisation of the brain. Secondly, this chapter addresses, in brief, the CT radiological anatomy of common CNS structures as well as an overview of the common pathologies that CT of the brain can be used to diagnose in both paediatric and adult patients.

2.2 Basic Development and Organisation of the Brain

The brain is the largest part of the CNS and consists of three main general areas which are: the brainstem, the cerebellum, and the cerebrum and the cerebral cortex which the outer surface of the cerebral hemispheres (Nowinski, 2011). The basic structural unit of the nervous system is the nerve cell (neurone), which is responsible for conducting the information away from the neuronal cell body and receiving the information from the other neurons. The main function of nervous tissue is to receive stimuli and transmits signals from one part of the organism to another (Van De Graaff, Morton, & Crawley, 2012). The brain itself lies within the cranial cavity resting on the bony skull and protected by cerebrospinal fluid (CSF) **(**Error! Reference source not found.**)** (Kandel & Tollet, 2016; Nowinski, 2011; Van De Graaff et al., 2012).

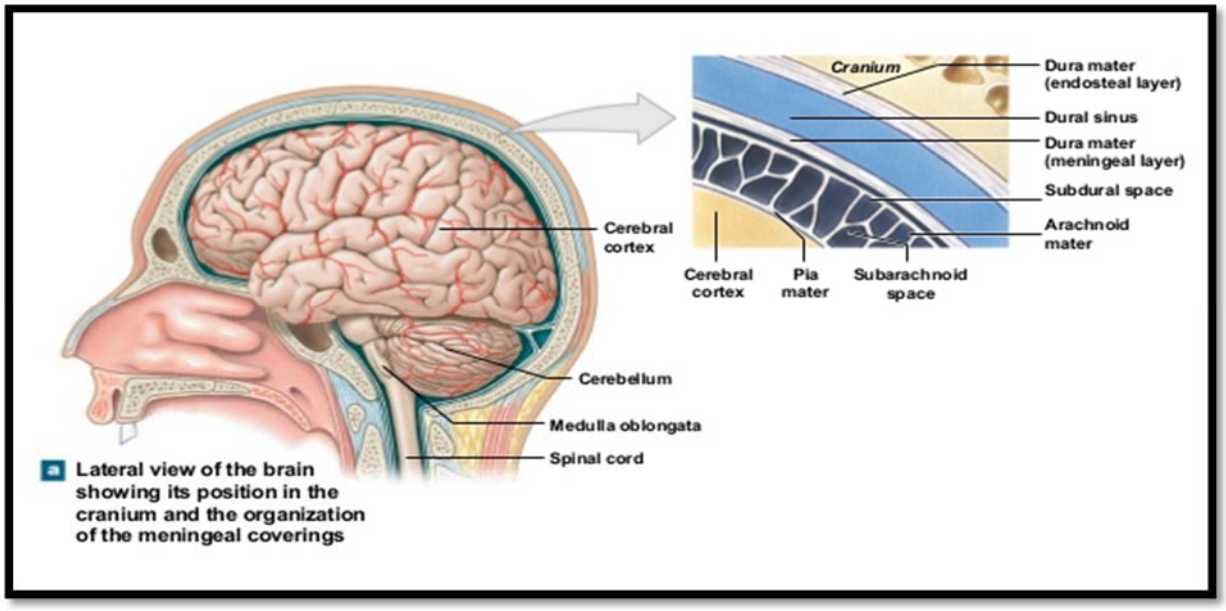

Figure 2-1: Position of the brain within the cranial cavity (Pearson Education, Inc., 2012).

Brain size is one of its most impressive features and our distinctively human mental capacity is commonly attributed to this. At birth the brain weighs around 400g, and this weight during the first three years of life triples as illustrated in **(Table 2-1**, **Figure 2-2** and **Figure 2-3)**.

The relative size of the brain in children is of paramount importance when calculating the radiation dose and risk for imaging examinations in children due to the paediatric head and brain being much larger when compared to the overall size of the body (Dekaban & Sadowsky, 1978; Giedd, 2008). The disproportionately large head size, together with a relatively small body, leads to an increased absorbed radiation dose to other organs and tissues compared with adults. Consequently these differences should be taken into account when selecting acquisition parameters for adult and particularly paediatric brain CT examinations. The general trend it that organ dose is inversely related to patient size; as patient size decreases, organ absorbed dose increases. The location of the organ with respect to the scan's start and stop locations and the angular position of the tube relative to the organs, are all factors that contribute to the average organ dose. This will obviously vary from individual to individual, even when using the same relative start and stop locations among the scanning volume.

After three years the rate of brain growth becomes slower and at the age of eighteen the maximum brain weight is approximately 1400g (Gray, 2014). The weight of the brain holds steady until about the age of fifty when a slow decline sets in. In adults, the average weight of 1400g can vary and studies have demonstrated that normal individuals will have brain weights from 1100g to around 1700g (Nolte, 2002).

Table 2-1: Relation of brain weights to body heights and body weights (Dekaban & Sadowsky, 1978).							
Age group	**Age (yrs)**	**Male**			**Female**		
		Brain Weight (g)	**Body weight (Kg)**	**Body Height (cm)**	**Brain Weight (g)**	**Body weight (Kg)**	**Body Height (cm)**
1	Newborn	380	2.95	50	360	2.88	49
2	1 year	970	9.47	76	940	8.89	72
3	2 years	1,120	13.20	85	1,040	11.58	84
4	3 years	1,270	15.55	94	1,090	14.10	94
5	6 – 7 years	1,330	22.94	116	1,210	21.28	116
6	10 - 12 years	1,440	39.45	143	1,260	39.37	137
7	19 - 21 years	1,450	68.58	174	1,310	51.11	161
8	56 - 60 years	1,370	70.52	174	1,250	60.32	162
9	81 - 85 years	1,310	67.01	1.73	1,170	53.42	159

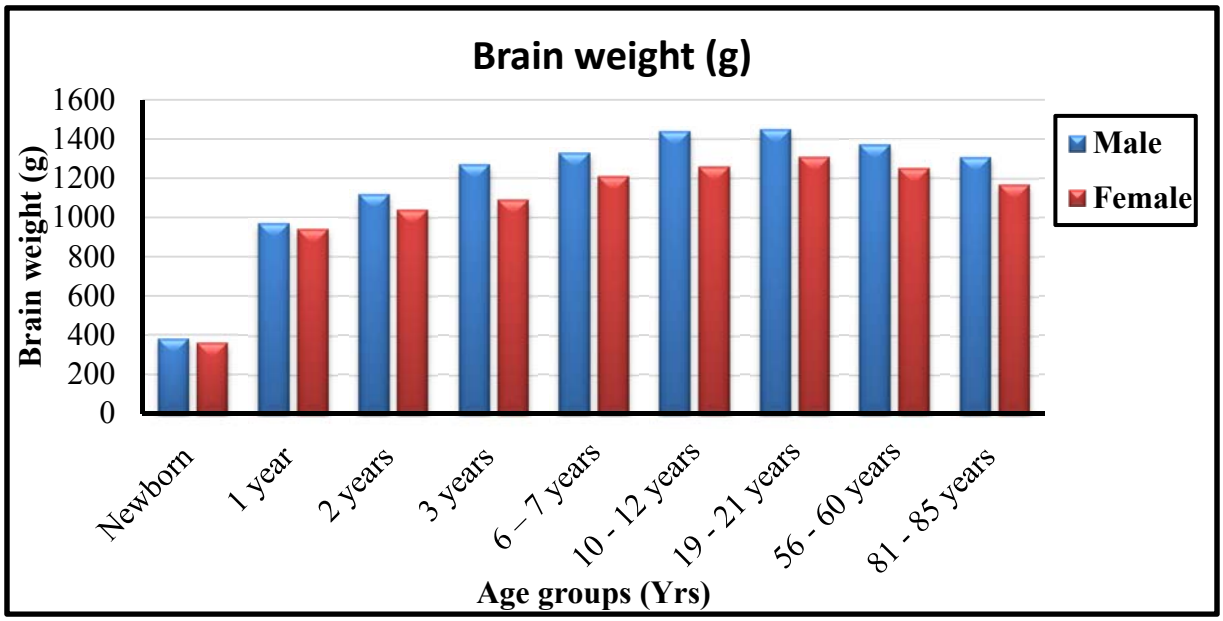

Figure 2-2: Average brain weight for both male and females at different ages (Dekaban & Sadowsky, 1978).

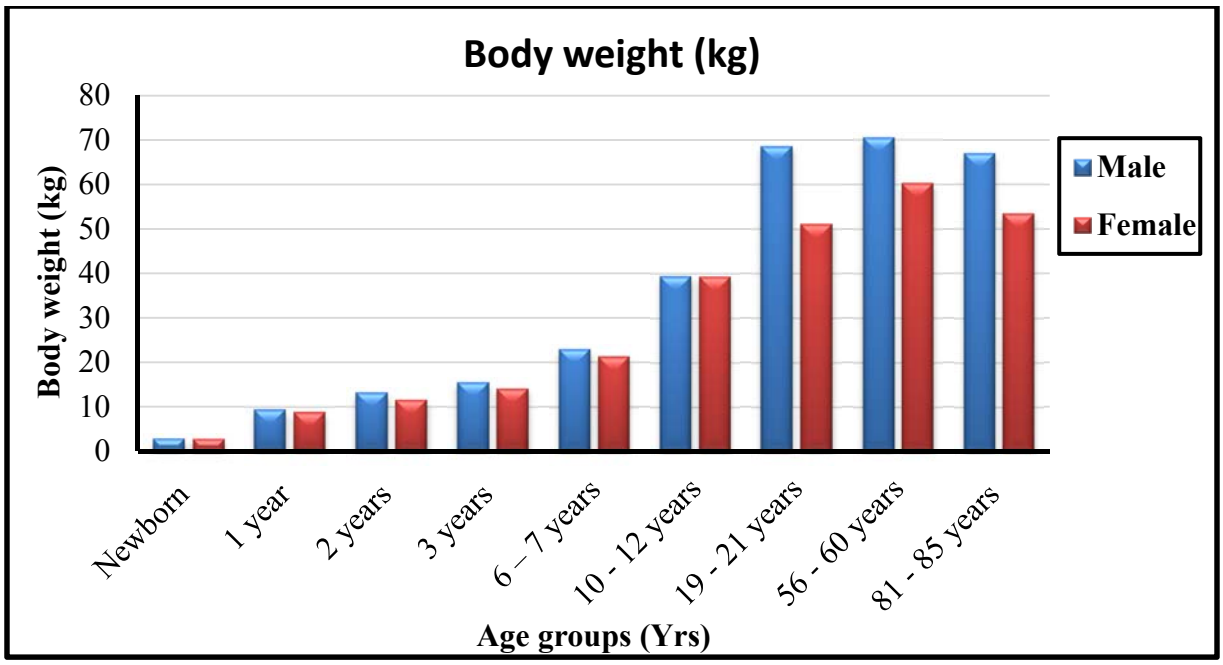

Figure 2-3: Average body weight for both male and females at different ages (Dekaban & Sadowsky, 1978).

2.3 The Central Nervous System (CNS) Anatomy

On the anatomic basis the CNS consisting of the brain and the spinal cord. Also, can be subdivide into parts that are concerned primarily with the regulation of visceral organs and the internal milieu and parts that are concentrated mainly with the more or less conscious adaptation to the external world (Brodal, 2004).

2.3.1 Cerebral Hemispheres

This part of brain is the largest and most highly developed part of the human brain. The cerebral hemispheres consist of the cerebrum and the structures hidden beneath of it. The cerebrum includes the two cerebral hemispheres (left and right) that are connected to each other through white matter tracts called the corpus callosum **(Figure 2-4)** (Rohen, Yokochi, & Lütjen-Drecoll, 2006). These cerebral hemispheres are the largest major division of the brain that are separated from each other by the longitudinal fissure which contains a crescent-shaped fold of the dura matter, the falx cerebri. The other hidden structure of the telencephalon is the diencephalon which is hidden from view by the cerebral hemispheres as shown in **(Figure 2-4)**, **(Figure 2-5)** and **(Figure 2-6)**. Each hemisphere consists of an external highly convoluted cortex, beneath which lies an extensive internal mass of white matter that partly encloses the basal ganglia. Each hemisphere also contains a lateral ventricle that is continuous with the third ventricle

through the interventricular foramen. The commissural fibres of the corpus callosum are linked the two cerebral hemispheres (Standring, 2008).

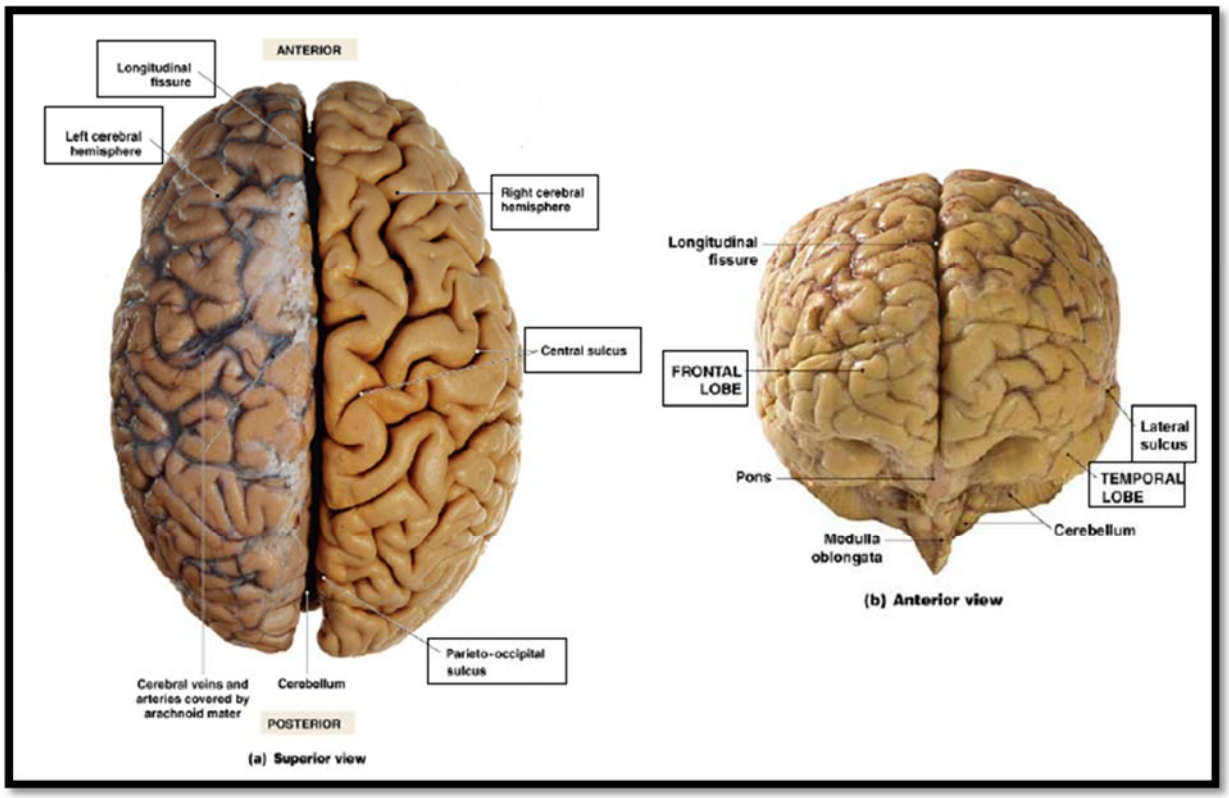

Figure 2-4: Brain cerebral hemispheres, superior and anterior views (Martini, Timmons, & Tallitsch, 2005).

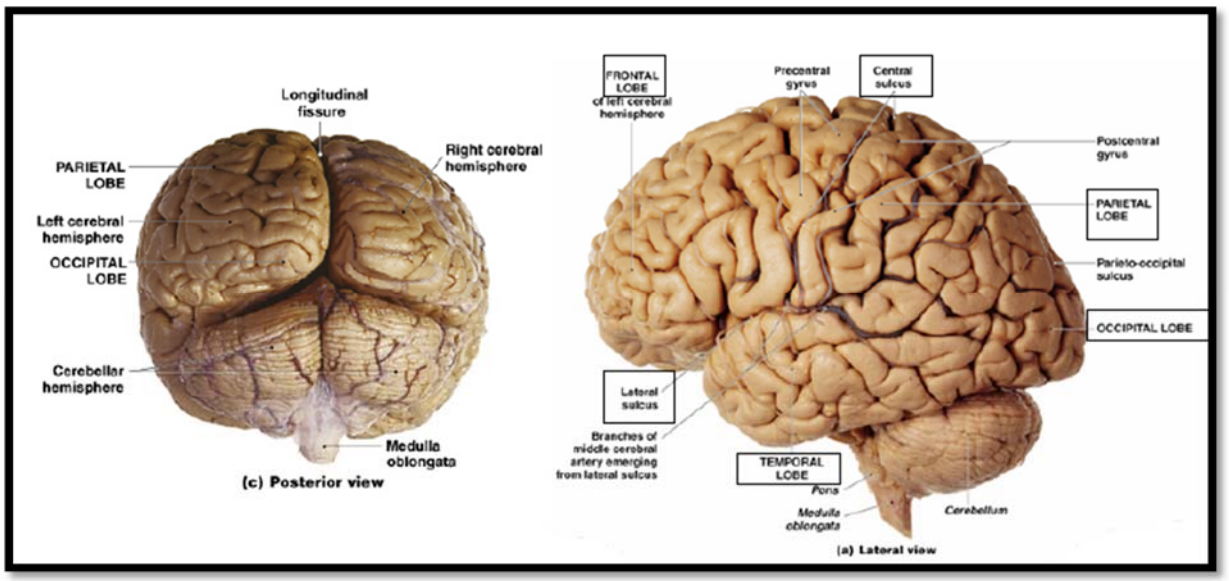

Figure 2-5: The cerebral hemispheres posterior and lateral views (Martini et al., 2005).

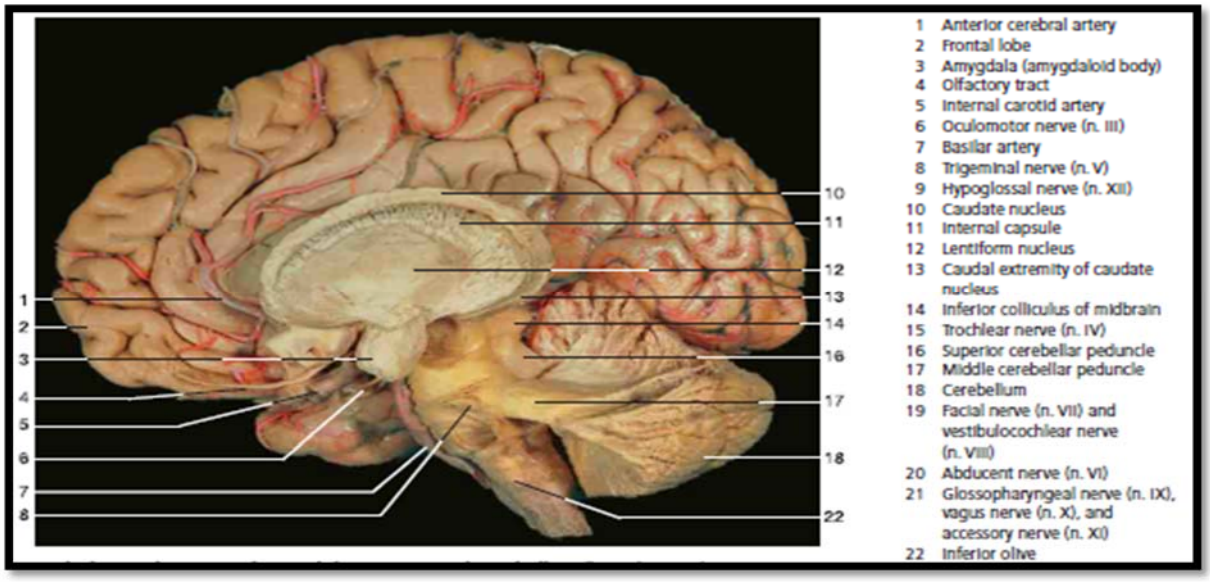

Figure 2-6: Right hemisphere together with brain stem and cerebellum (lateral aspect), the connection of the brain stem with the cerebellum is dissected. The amygdala of the left hemisphere is shown. The corpus callosum has been partly removed (Rohen et al., 2006).

2.3.2 Cerebral Cortex

Key features of the cerebral hemispheres are the shape and the degree to which their surface is folded and convoluted. Each ridge is called a gyrus; and each groove between ridges is called a sulcus **(Figure 2-4**, **Figure 2-5** and **Figure 2-6)**. Particularly deep sulci are often called fissures. Cortext foldings into the gyri and sulci is a mechanism for increasing the total cortical area; each human has about 2.5 sq ft of cortex, two thirds of which is hidden from view in the walls of sulci (Nolte, 2002). The gyri and sulci provide part of the basis for the division of the hemisphere into lobes. The frontal, parietal, temporal, and occipital lobes approximately correspond in terms of surface location to the overlying cranial bones from which they take their names. The anterior and posterior extremities of the hemispheres from the frontal and occipital poles respectively and the temporal pole are the anterior extremity of the temporal lobe. The cortical regions hidden within the depths of the lateral fissure by overlying parts of the frontal, parietal and temporal lobes is known as the insula. The key features on the superolateral cerebral surface of the brain are two prominent furrows, the lateral (sylvian) fissure and the central sulcus **(Figure 2-5)**. The lateral fissure is a deep cleft on the lateral and inferior surface. It separates the frontal and parietal lobes above from the temporal lobe below and accommodates the middle cerebral vessels. The central sulcus is the boundary between the

frontal and parietal lobes and demarcates the primary motor and somatosensory areas of the cortex, located in the precentral and postcentral gyri, respectively (Standring, 2008).

2.3.3 Cerebral Lobes

The surface of each cerebral hemisphere has folded aspects which makes it possible to identify the lobes. Each cerebral hemisphere is divided into several lobes, namely frontal lobe, parietal lobe, temporal lobe, and occipital lobe and the insular cortex see **(Figure 2-7 & Figure 2-8)**. These lobes are separated by sulci: the central sulcus also known as the Fissure of Rolando, the lateral sulcus or Sylvain Fissure, the parietooccipital sulcus and the temporal-occipital sulcus. For a functional prospective each hemisphere has its own specific functions especially for the most complex functions for instance language in the frontal and temporal areas of the dominate hemisphere, spatial orientation in the right parietal lobe, the organisation of complex gestures in frontal lobe, etc. (Kandel & Tollet, 2016).

Frontal lobe: this extends from the anterior tip of the brain to the central sulcus, inferiorly, it ends at the lateral sulcus. On the medial surface of the brain it extends posteriorly to an imaginary line from the top of the central sulcus to the corpus callosum, the area of frontal lobe anterior to the precentral sulcus is divided into the superior, middle and inferior frontal gyri **(Figure 2-7)**, the frontal pole lies in front of these gyri. The ventral surface of the frontal lobe, the orbitofrontal cortex, overlies the bony orbit. The medial surface extends from the frontal pole to the paracentral lobule and consists of the medial frontal cortex and the anterior cingulate cortex (Nolte, 2002; Standring, 2008).

Parietal lobe: this extends from the central sulcus to an imaginary line connecting the top of the parietooccipital sulcus and the preoccipital notch **(Figure 2-7)**. Inferiorly, it is bounded by the lateral sulcus and the imaginary continuation of this sulcus to the posterior boundary of the parietal lobe. On the medial surface of the brain it is bounded inferiorly by the corpus callosum and calcarine sulcus, where anteriorly by the front lobe and posteriorly by the parietooccipital sulcus (Nolte, 2002; Standring, 2008).

Temporal lobe: this extends superiorly to the lateral sulcus and the line forming the inferior boundary of the parietal lobe; posteriorly it extends to the line connecting the top of the parietooccipital sulcus and the preoccipital notch. On the medial surface its posterior boundary is an imaginary line from the preoccipital notch to the splenium of the corpus callosum. Its lateral surface is divided into three parallel gyri by the superior and inferior temporal sulci. The superior temporal sulcus beings near the temporal pole and slops slightly up and backwards

parallel to the posterior ramus of the lateral sulcus. Its end curves up into the parietal lobe. The inferior temporal sulcus is subjacent and parallel to the superior and is often divided into two or three short sulci. Its posterior end also ascends into the parietal lobe posterior and parallel to the upturned end of the superior sulcus **(Figure 2-7)** (Nolte, 2002; Standring, 2008).

Occipital lobe: this is bound anteriorly by the parietal and temporal lobes on both the lateral and medial surfaces of the hemispheres (Nolte, 2002). The occipital lobe is more or less exclusively concerned with visual functions. Primary visual cortex is contained in the walls of the calcarine sulcus and a bit of the surrounding cortex. The remainder of the lobe is referred to as visual association cortex and is involved in higher order processing of visual information (Standring, 2008).

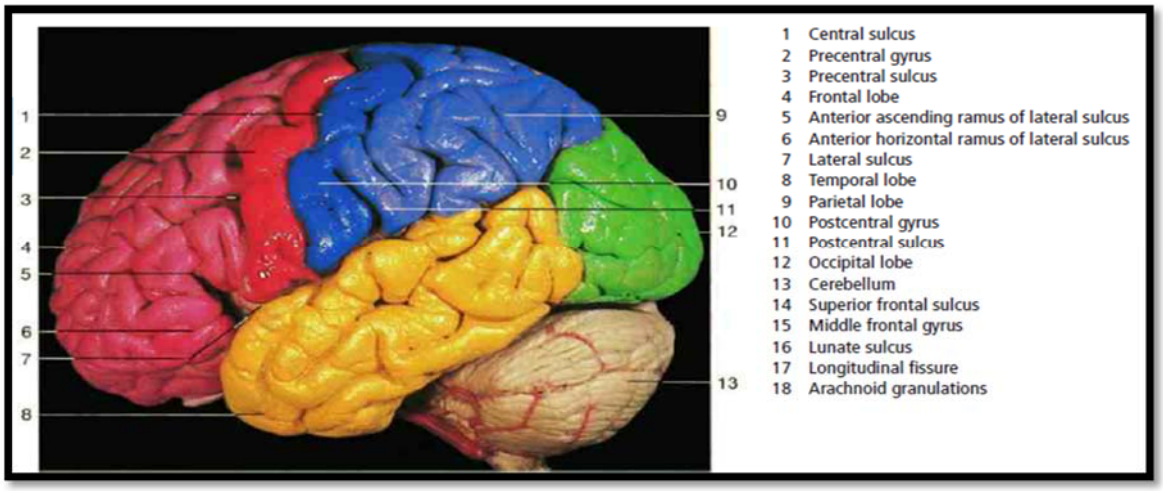

Figure 2-7: Lateral aspect of left cerebral hemisphere (Rohen et al., 2006).

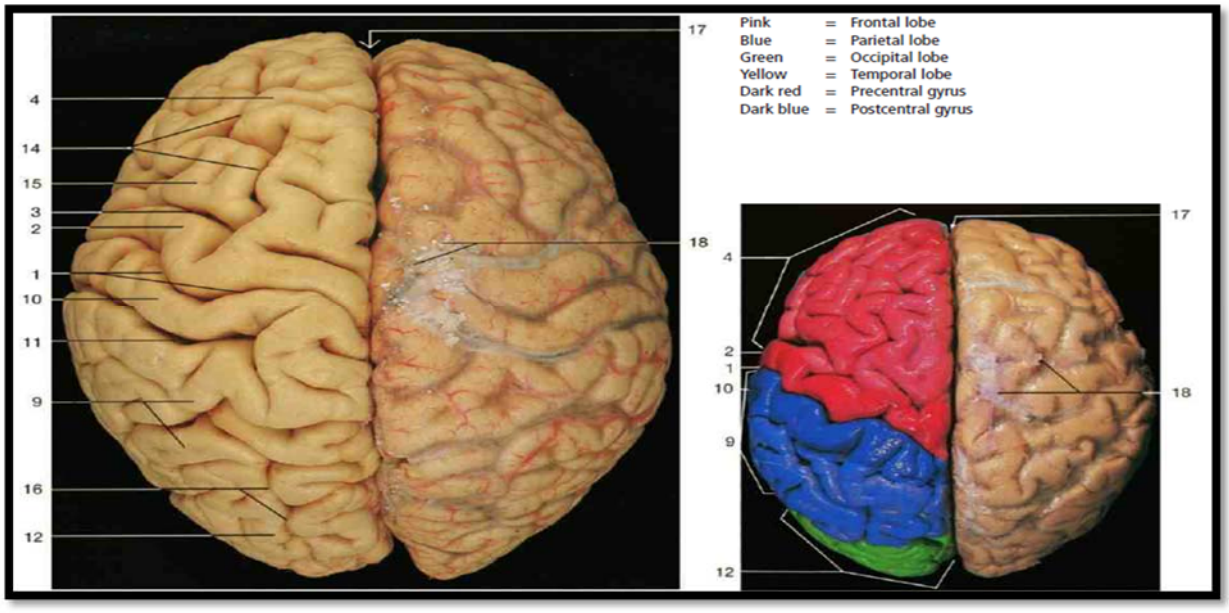

Figure 2-8: Brain superior aspects, right hemisphere with arachnoid and pia matter and lobes of the left hemisphere indicated by colour (Rohen et al., 2006).

The limbic lobe is an additional area of the cerebral cortex not usually included in any of the four lobes discussed above and lies buried in the depths of the lateral sulcus, concealed from view by portions of the frontal, parietal, and temporal lobes. This cortex, called the insula, overlies the site where the telencephalon and diencephalon fused during embryological development. It can be revealed by prying open the lateral sulcus or by removing the overlying portions of other lobes. The portion of a given lobe overlying the insula is called an operculum; there are frontal, parietal, and temporal opercula. The circular sulcus outlines the insula and marks its borders with the opercular areas of cortex. The cingulate gyrus, immediately superior to the corpus callosum, can be followed posteriorly to the splenium of the corpus callous, where it turns inferiorly as the narrow isthmus of the cingulate gyrus and continues as the parahippocampal gyrus of the temporal lobe. These two gyri give the appearance of the encircling the diencephalon and they are together with the olfactory bulb, olfactory tract, and certain other small cortical areas are often referred to separately as the limbic lobe. As indicated by the red colour in **(Figure 2-9)** the limbic lobe therefore contains portions of what would otherwise be considered frontal, parietal, and temporal cortex. The limbic lobe and many of the structures with which it is interconnected make up the limbic system, which is important in emotional responses and drive-related behavior (Nolte, 2002; Standring, 2008).

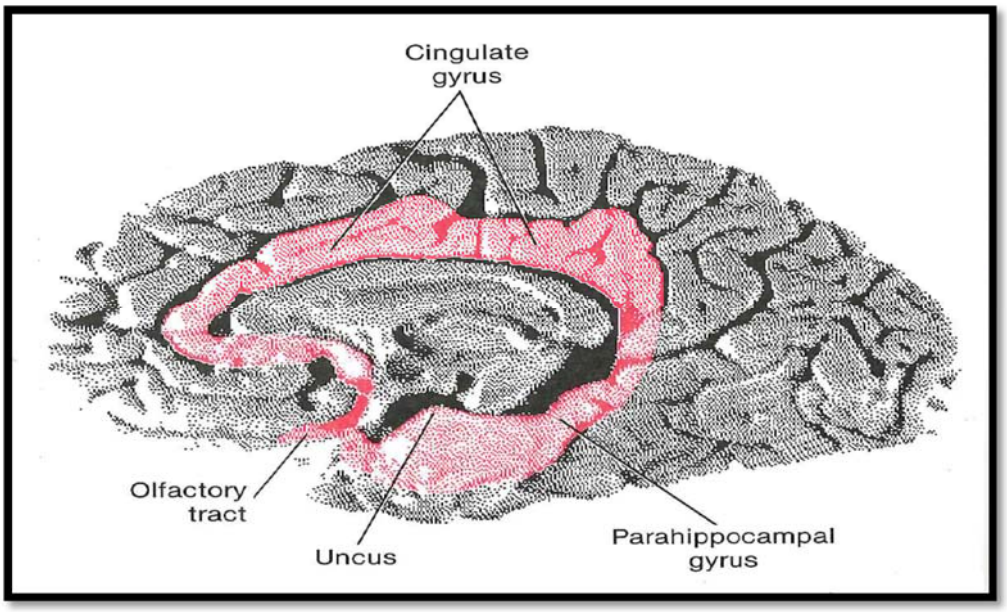

Figure 2-9: Limbic lobe as seen on the medial surface of a hemisected brain from which the brainstem and cerebellum were removed (Nolte, 2002).

2.4 White and Gray Matter

The brain and spinal cord are composed of two kinds of nervous substances known for their colour as the white and grey matter, respectively. This difference in their arrangement that in the brain the grey matter is situated chiefly in the outside forming the brain cortex whilst in the spinal cord the white matter substance is located externally and the grey matter forms the central core. The cortex which is located on the surface of brain hemispheres is composed of gray matter that contains neuron cells bodies and is organized into six layers. The basal ganglia are located at the base of hemispheres. These are also composed of gray matter. White matter contains myelinate axons from CNS neurons and it makes it possible to establish connections between different parts of the CNS through associative fibers that connect parts of the cortex to each other or to the basal ganglia and through fibres that stretch out toward the spinal cord (Kandel & Tollet, 2016). **(Figure 2-10)** provides an illustration of the arrangement of gray and white matter in the brain.

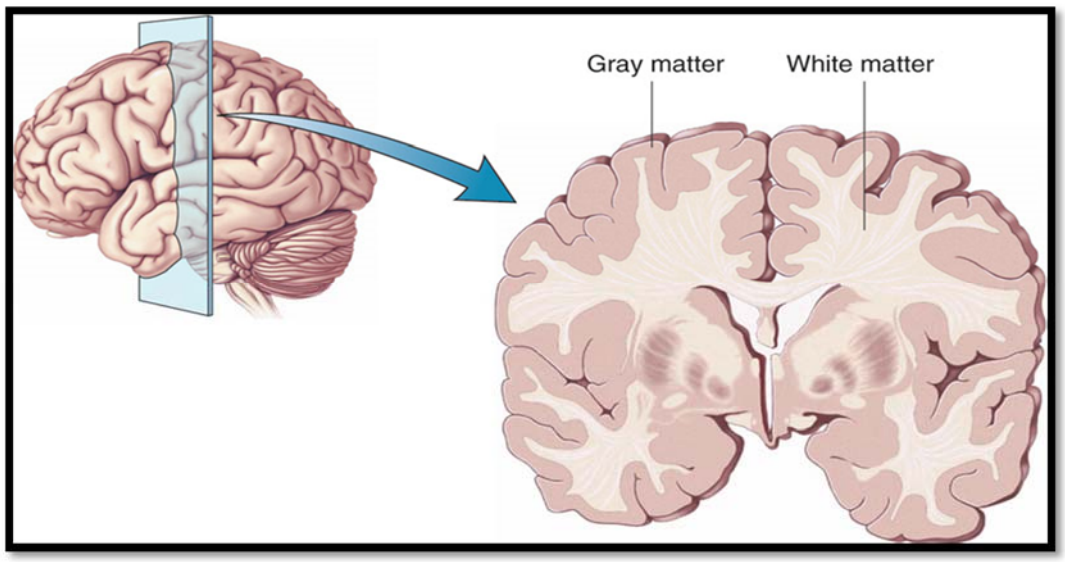

Figure 2-10: Coronal brain section showing the gray and white matter (Martini et al., 2005).

2.5 CT Radiological Anatomy

Gray and white matter structures are differentiated on CT images by differences in density (Butler & Mitchell, 2012; Johns, 2014). White matter consists of high content of myelinated axons while gray matter contains a relatively few axons and a high number of cell bodies. Due to myelin being a fatty structured substance it has low density compared to the cellular gray matter **(Figure 2-11)** (Hofer, 2010; Mary, 2016).

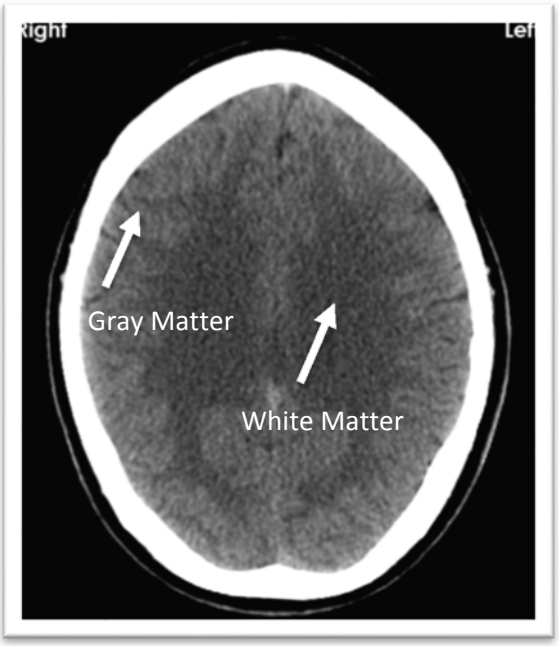

Figure 2-11: Gray and white matter (Mary, 2016).

In general, the various shades of grey demonstrated on CT images are summarized in the following **(Table 2-2)** which illustrates the white to black densities seen in selected tissues in CT (Haines, 2004; Johns, 2014).

Table 2-2: The brain and related structures in CT (Haines, 2004 & CrashMaster, 2011).	
Structure / Fluid / Space	**Gray Scale**
Bone, acute blood	Very white
Enhanced tumour	Very white
Subacute blood	Light gray
Muscles	Light gray
Gray matter	Light gray
White matter	Medium gray
Cerebrospinal fluid	Medium gray to black
Air, fat	On CT, structures are assigned a Hounsfield unit representing their relative density. Air is assigned a value of -1000 UH, water 0 HU, and bone +1000 HU. Fat, being less dense than water but more dense than air has a value of approximately -50 HU.

2.6 CT Brain Pathologies and Clinical Aspects in Adults and Paediatrics

The use of CT is of growing importance in children and adults; however, it is also a major source of radiation dose too. In general brain CT scanning is typically used in adult and paediatric to detect and provide information on haemorrhage, brain injury and skull fractures in

patients with head injuries. Over the last few decades the introduction of increasingly sophisticated imaging techniques has been transferred to neurological diagnosis. CT based imaging techniques play an essential part in assessment and management of neurological disease in both paediatric and adult patients (Renowden, 2012).

Non-contrast CT (NCCT) is the standard brain imaging technique for the initial evaluation of patients with acute stroke symptoms; CT is currently the modality of first choice for imaging patients with acute stroke. Worldwide stroke is the main cause of neurologic morbidity and mortality and it constitutes the second or third most cause of death with cardiovascular disease and cancer in industrialised countries and also in older age group it composes the second most common cause of dementia after Alzheimer disease (de Mendivil et al., 2013). There are effective treatments for patients with embolic occlusion of cerebral arteries by using systemic or local fibrinolysis with the aim of turning strokes from fatal to treatable. For patients with suspected stroke there is also a need to exclude cerebral haemorrhage, CT is used routinely in most situations as the primary imaging modality due to its ability to detect early signs of stroke. Cerebral ischemia is the cause of about 70% of acute strokes due to regional reduction of perfusion (Klotz & König, 1999, Hua et al., 2009). Furthermore, it is also used to assess bleeding caused by a ruptured or leaking aneurysm in patients with a sudden severe headache. Further assessment of brain tumours, enlarged brain cavities (e.g. ventricles) in patients with hydrocephalus and disease or malformations of the skull vault (Broder & Preston, 2011; de Mendivil et al., 2013) are indications for CT.

CT has been reported to have a sensitivity of 90% and a specificity of 100% to accurately detect the type and the extent of the under lying ischemic process (de Mendivil et al., 2013). The advantage of CT scan is that it is rapid which is extremely important in trauma situations. CT clearly shows acute and subacute haemorrhages into the meningeal spaces and the deep brain tissues (Haines, 2004).

Although NCCT is initially used to exclude intracranial hemorrhage and other non-stroke pathologies, advanced CT techniques are increasingly recognized as a modality to characterize early signs of ischemia (Rossaint et al., 2016; Nagel et al., 2017).

CT perfusion (CTP) is an imaging technique for detecting functional abnormalities by measuring tissue-level blood flow, which can be assessed by utilising variety of parameters: cerebral blood flow, cerebral blood volume (CBV) and mean transit time (de Mendivil et al.,

2013). With the use of multislice CT scanners, the potential information available from a CT scan has increased. CT angiography and CT perfusion techniques can refine the current clinical criteria for patient selection for thrombolysis. CT angiography–source images (CTA-SI) can be rapidly obtained with minimal delays after a NCCT in the emergency room. Although CTA has been shown to have value in identifying vessel occlusion, CTA-SI may also aid in the assessment of tissue status (Coutts et al., 2004).

CTA-SI can also be useful in predicting final infarct volume. Brain tissue with a low cerebral blood volume appears as a region without enhancement on CTA-SI, effectively delineating the regions of ischemia. The Alberta Stroke Program Early CT Score (ASPECTS) was developed as a grading instrument to assess early ischemic changes on pre-treatment CT scans in patients with acute ischemic stroke of the middle cerebral artery (MCA). The ASPECTS divides the MCA territory into 10 regions of interest. With training and experience, the early changes of acute ischemia can be reliably detected. One advantage of ASPECTS is that it combines a semiquantitative estimate of volume along with localization. It weights smaller volumes in the basal ganglia and internal capsule equally with larger volumes of brain designated M1 through M6. This approach is useful because lesion volume alone on NCCT is only weakly correlated with neurological outcome (Coutts et al., 2004; Rossaint et al., 2016).

CT is also helps diagnosis and management of many head and neck disorders (Kidwell et al., 2004; Metter et al., 2011; Tijssen et al., 2014). The detection of acute intracranial haemorrhage in paediatric and adult populations is highly sensitive and specific using CT scanning for pathologies such as subdural hematoma, subarachnoid, and intraventricular haemorrhage and haemorrhagic contusions. Also, CT is useful in the diagnosis of secondary parenchymal low density cerebral oedema, ischemia and fractions (Dubbins et al., 2008). CT is a useful and necessary tool which helps to establish the diagnosis and to determine the treatment for urgent surgical intervention (Younis et al., 2002).

CT can be performed quickly, thus it is useful in emergency/trauma situations illustrating many abnormalities in brain structure including: swelling, bleeding arising from ruptured aneurysms, haemorrhagic stroke and head injury (Asbury, 2011). CT is also used prior to brain surgery in order to improve the positioning accuracy and guidance of delicate surgical instruments (Kwoh et al., 1988).

In addition to the above indications, CT scanning can also be performed to determine the following:

- Evaluate the extent of bone and soft tissue damage in patients with facial trauma and planning surgical reconstruction by providing more details to the region of interest through acquiring thinner slices or changing the patient position in the scanner during image acquisition.
- Diagnose diseases of the temporal bone on the side of the skull which may be causing hearing problems.
- Determine whether inflammation or other changes are present in the paranasal sinuses.
- Plan radiation therapy for cancer of the brain or other tissues.
- Guide the passage of a needle used to obtain a tissue sample (biopsy) from the brain.
- Assess aneurysms or arteriovenous malformations through a technique called CT angiography (Broder & Preston, 2011).

CT scanning has provided the most valuable information to date regarding the evolution of brain edema after head injury. Modern CT scanners are able to clearly define areas of low density in relation to focal brain injury such as contusions and hematomas, and some authors have sought to relate increases in CT density values to brain engorgement by correlating those values with cerebral blood volume and cerebral blood flow measurement (Orrison et al., 2011).

General radiological information can be obtained from non-contrast head CT, while contrast enhanced head CT is performed usually following non-contrast CT and then the two procedures are compared. As illustrated in **(Table 2-3)** the pathological signs on non-contrast head CT images can be used to indicate different abnormalities within the brain region (Broder & Preston, 2011).

Table 2-3: Interpretation of pathology from non-contrast CT head images (Broder & Preston, 2011).	
Brain pathology	**Signs of this pathology**
Air-filled space Mastoid air-cells Sinuses	Fractures Infections
Bones	Fractures
Blood	Epidural haemorrhage Intraparenchymal haemorrhage Subarachnoid haemorrhage Subdural haemorrhage
Brain	Midline shift or mass effect Edema Infarction Masses
CSF spaces Cisterns Sulci Ventricles	Atrophy Edema Hydrocephalus Subarachnoid haemorrhage in these structures

2.7 Chapter Summary

While the benefits of CT exceed the harmful effects of radiation exposure in patients, increasing radiation doses to the population have raised a compelling case for reduction of radiation exposure from CT. This chapter has explored important anatomical and radiological factors which make brain / head CT imaging demanding in relation to radiation dose optimisation and risk. This is related to the relative differential size of paediatric and adult head/brain in relation to overall body size. Also outlined in this chapter are potential conditions that can be demonstrated in CT.

Chapter 3 : CT Scanning: Development, Physical Principles and Radiation Dose Parameters

3.1 Chapter Overview

The key focus of this thesis is radiation dosimetry from CT scans. Consequently, the purpose of this section is to provide an introduction to the theoretical concepts and processes of CT scanning. Within this discussion there will be commentary on the key technology developments as well the CT acquisition factors that influence radiation dose. The CT image reconstruction process will be described briefly as there are a number of methods, each having an effect on image quality and radiation dose. This section is related directly to the thesis aims; to investigate organ and tissue absorbed doses (directly) and use the acquired values to estimate the effective dose and radiation risk. The radiation exposure for patients undergoing CT examinations are determined by two main factors: 1) equipment related factors such as the design of the scanner and 2) acquisition parameters chosen by the radiographers and radiologists. This chapter also, provide an overview of how to use Metal Oxide Semiconductor Field Effect Transistors (MOSFETs) for direct radiation dose measurements in human phantoms. The option for using CT derived estimations of radiation dose, dose length product (DLP) and volume CT Dose Index $CTDI_{vol}$ will also be explored. Monte Carlo simulation for mathematical dose estimation will be discussed. The final element of this chapter will be to discuss the utilisation of lifetime attributable risks relevant to CT radiation doses.

Currently there is no definitive method for undertaking CT dosimetry and multiple experimental and computational approaches exist. The choice between dosimetry methods is often more difficult when considering children, since the dose estimates need to be age-specific or reflect the range of ages necessary to accurately represent the paediatric population. Furthermore, with a wide variety of methods available, there is potential for radiation doses to differ. Since organ and tissue absorbed doses are used for risk assessment and effective dose for radiation protection purposes, it is important to explain the extent of the variability between different methods and identify the most suitable.

3.2 CT History and Technology Development

The first CT scanner was developed in 1972 by Sir Godfrey Hounsfield, an engineer at THORN EMI Central Research Laboratories in the United Kingdom (UK). Since then CT scanner technology has rapidly evolved in terms of both technical performance and clinical use, and has resulted in five developmental generations of equipment. The novelty of CT is to reconstruct images mathematically from measured attenuation data and to display and archive them in digital form. The renaissance period of CT followed the introduction of spiral (helical) imaging. This meant a transition from slice-by-slice imaging to true volume imaging and by the 1990s CT had the ability to image whole organs or even the whole body within 5 to 20 seconds with sub-millimeter isotropic resolution. As a result, most of the commercially available CT scanners today are based on a third-generation design. The evolution of CT technology is illustrated in **(Table 3-1)**.

Table 3-1: The evolution of CT technology (Kalender, 2011; Romans, 201; Halliburton et al., 2008; Ulzheimer & Flohr, 2009; Goldman, 2008; Seeram, 2015; Nagel, 2005; Romans, 2011; Hsieh, 2009; Mohan et al., 2011).

CT generation & developments	Year	Number of Detectors	Scan Time	Movement Type	Tube Rotation Degree	Beam Dimensions
First	1970	Single detector	3 - 5 min/slice	Translate - Rotate	1^{o} at a time (together translate through 180^{o})	Pencil Beam
Second	1972	Curved array of more than 30 detectors	30 sec / slice	Translate – Rotate	Rotate through 180^{o}	Fan Beam
Third	1976	Large curvilinear row of hundred detectors	1 sec / slice	Rotate - Rotate	Rotate through 360^{o}	Wider Fan Beam
fourth	1976	Ring of thousand detectors	1 sec / slice	Rotate - Fixed	Rotate through 360^{o}	Wider Fan Beam
Fifth	1984	Hundred of curved detectors	Millisecond / slice	No moving parts	No rotation	Wider Fan Beam
Helical or spiral CT scanners	1990	Hundred of curved detectors	Sub-second	Rotate - Rotate	Rotate through 360^{o}	Wider Fan Beam
Multislice CT scanners (MSCT)	1998	Multi rows of detectors up to 320	Sub-second	Rotate - Rotate	Angle of rotation of 360^{o}	Wider Fan Beam
Cone shaped x-ray beam	1996 & 2001	Flat panel detector	Sub-second	Rotate - Rotate	Angle of rotation of 360^{o}	Cone Beam
Dual source CT scanners	2006	Hundred of curved detectors	Sub-second	Rotate - Rotate	Rotate through 90^{o}	Wider Fan Beam

3.3 Factors Influencing Radiation Dose in CT

CT scanners are a major contributor to the radiation dose received in radiology departments. CT protocols are not set by regulation authorities but are followed locally in hospitals, but they are audited through Dose Reference Level (DRL) analysis (Colagrande et al., 2014). The setting of CT acquisition parameters such as tube current, tube rotation time, peak tube voltage, pitch, and collimation is a major contributor to the radiation dose received during a CT examination. Typically, if one of these parameters is decreased, another needs to be increased to maintain the radiation dose to an acceptable level in order to generate an image with sufficient diagnostic information. The majority of CT scanners used in developed countries are multi-slice CT (MSCT) and therefore this chapter focuses primarily on acquisition parameters and their effect on dose in relation to MSCT only. There are many variables within each examination procedure that influence radiation dose, in particular:

Tube Voltage (kVp): Higher peak voltages will result in more X-rays passing through the body; hence increases the dose and the ratio of dose at depth to surface dose, however, there is lower image contrast. Because of image noise and beam-hardening artifacts (which appear as nonuniformities in the CT numbers), sometimes the trend to decrease tube voltage (and correspondingly, the radiation dose) was not successful (Cody et al., 2004; Nakayama et al., 2005). So, tube voltage reduction is allowed only on the condition that it does not affect the ability to detect low-visibility structures (Akhlaghi et al., 2014).

Tube Current (mA): mA is directly proportional to radiation dose, as tube current increases, more X-rays are incident onto the patient leading to higher patient dose.

Pitch: For MSCT, the most commonly used definition is the table feed/distance (mm/s) of the CT table per 360^{o} rotation of the X-ray tube, divided by the X-ray beam collimation width. This parameter has a direct influence on patient radiation dose. The radiation dose is inversely proportional to pitch when all other factors are held constant. This is essentially because as pitch increases, the time that any one point in space spends in the X-ray beam is decreased.

Effective mAs: The effective mAs takes into account pitch. As stated patient doses are directly proportional to mAs since the photon fluence, as influenced by the tube current–time product (milliampere-seconds), has a direct influence on patient radiation dose. On some CT scanners, the user inputs a parameter labelled mAs, but that parameter is really the effective mAs, which

is milliamperage multiplied by time/pitch. On these scanners, when pitch is varied, mAs varies in a corresponding fashion to keep effective mAs constant. The effects of pitch are discussed in **(Section 3.3.2.3)** on page **30** (McNitt-Gray, 2002; Huda et al., 2007).

Slice Collimation (mm): Defines the thickness of the slice to be imaged. The wider collimation has more mass being irradiated than a thinner one, thus indicating that the radiation dose for wider and thin collimations may be close to equivalent (the difference is attributed to the higher scatter expected in the thicker section).

Beam Collimation (MSCT only): This is the product of the number of active detector channels used and the effective detector row thickness. The number of active detectors determines MSCT slice thickness. In single slice CT (SSCT) the slice thickness is determined alone by the collimation width. In fact, early reports from early versions of MSCT showed significant dependence on X-ray beam collimation. These effects result from differences in X-ray beam collimation, even when the same reconstructed section thickness is used (McNitt-Gray et al., 2002).

Feed: The table travel (or movement) per rotation. An increased table movement can decrease the radiation dose to the patient if all other parameters remain constant.

Tube Rotation: The speed of gantry rotation. This parameter has an inverse effect on radiation dose.

Gantry Angulation: The craniocaudal angle of the X-ray tube and detector array relative to the table. In clinical situations, a patient's head is adjusted to avoid irradiating eye lenses whereas in laboratory studies using phantoms this is not possible and instead the CT gantry is tiled. Also, in some clinical situations where patient's cannot effectively move their head and hence the additional need for angulation.

The parameters described above can be divided into three categories: 1) factors related to CT scanner design, 2) helical CT protocol related factors and 3) CT scan acquisition parameters.

3.3.1 CT scanner design factors (equipment-related factors)

These factors include X-ray tube filtration, X-ray beam shaping filters, collimator design and focus to axis distance, which are explained in detail elsewhere in the literature (McNitt-Gray, 2002; Ulzheimer & Flohr, 2009; Nagel, 2007).

3.3.2 CT helical protocol related factors (spiral interpolation)

As reported by Lewis, 2005, two major technological developments have led to an increase in patient radiation dose and image quality: helical scanning and the changes to the detector array in the Z-axis of the patient (Lewis, 2005).

Data acquisition in spiral/helical scanning mode requires an additional interpolation step to obtain axial slices and is called "over-ranging". These extra rotations are needed for helical interpolation; as a result, there is additional irradiated tissue outside of the selected imaging volume. In helical scanning, extra image data is required at each end of the image plane in order to interpolate the required axial image slices (Nagel, 2007). There are also other sources of excess radiation from helical scans, termed over-beaming, which are described in detail by Cody and Mahesh (2007); it refers to the radiation delivered by the "penumbra" which is not used for image date reconstruction. This over-beaming radiation passes through the patient and contributes to the patient dose but not to the generation of images (Cody & Mahesh, 2007; Sorantin et al., 2013).

3.3.2.1 Over-ranging

Over-ranging is the increase in dose-length product due to the additional rotations at the beginning and at the end of a spiral/helical scan required for data interpolation to reconstruct the first and the last slice of the imaged body region, because the reconstruction algorithm requires additional raw data on both sides of the planned scan **(Figure 3-1)**. Over-ranging effects can be expressed both in terms of the additional number of rotations and the increase in scan length (Nagel, 2007; Schilham, van der Molen et al., 2010; van der Molen & Geleijns, 2007). These extra rotations will lead to exposure of tissue above and below the planned scan length. This adds to the radiation dose to the patient and is therefore important for accurate dose calculations. In single-section spiral CT, the number of over-range rotations is well known—for example, 1.0 and 2.0 for the 180° and 360° linear interpolation algorithms, respectively (Kalender, 2011). In MSCT, image reconstruction algorithms are more variable and scanner specific and little data on over-ranging currently exists (Nicholson & Fetherston, 2002; Tzedakis, Damilakis, Perisinakis, Stratakis, & Gourtsoyiannis, 2005; Aart J van der Molen & Geleijns, 2007).

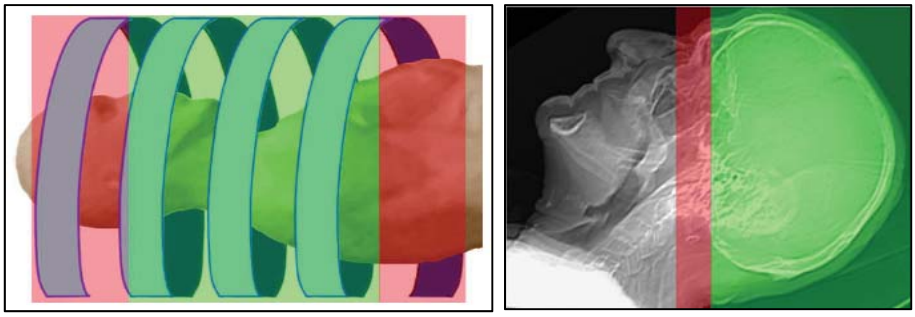

Figure 3-1: This figure illustrates how at least an extra half rotation (red) is needed before the start and beyond the end of the imaged volume (green); and the second image shows how a user would plan a brain CT scan so that the imaged area (green) excludes the eyes. If the scan is helical, however, over-ranging will cause exposure to an additional area (red).

In clinical practice, over-ranging can mean that any organs that were carefully positioned just outside the imaging volume could, in fact, be exposed to primary beam radiation. The exact extent of over-ranging depends on several scanning parameters as well as on the manufacturer and the type of CT scanner. As reported by Schilham et al., (2010) the extent of additional irradiation increases as scan length (table feed) per rotation increases. Over-ranging becomes a serious problem since the current trend in CT scanner development is to decrease scanning time by increasing the scan length covered in one rotation, this makes a substantial contribution to patient radiation dose, even though this dose portion is not used for imaging (Schilham et al., 2010). As described by Schilham et al., (2010) the only two scanning parameters that influence over-ranging are pitch and detector collimation, assuming that the rotation time and the effective milliamperage are kept constant. The over-range length and dose have to increase (linearly) with increasing pitch **(Figure 3-2)**; pitch and detector collimation vary, from a pitch of 2 and a small detector collimation (left), to a pitch slightly larger than 1 and a small detector collimation (middle), to a pitch slightly larger than 1 and a large detector collimation (right). In **(Figure 3-2)**, the top row illustrates the helical motion of the detector array around the patient, the middle row shows X-ray–like images that indicate the region where enough data are present for image reconstruction while the bottom row shows the relative dose profiles as functions of scan position along the direction of table motion (Schilham et al., 2010). A large detector collimation has the same effect on over-ranging as a higher pitch. At least one extra over-ranging rotation is still needed, meaning that over-range length and radiation dose have to increase (linearly) with increasing detector collimation **(Figure 3-2)** (Schilham et al., 2010). The contribution of over-ranging to the total CT dose is, therefore, considerably higher for CT

examinations with shorter scan ranges such as paediatric and cardiac CT. Fortunately, adaptive section collimation technology was developed, as reported by Goo (2012), to eliminate over-ranging during spiral CT scanning. This useful collimation technology is currently available only in some of the CT models.

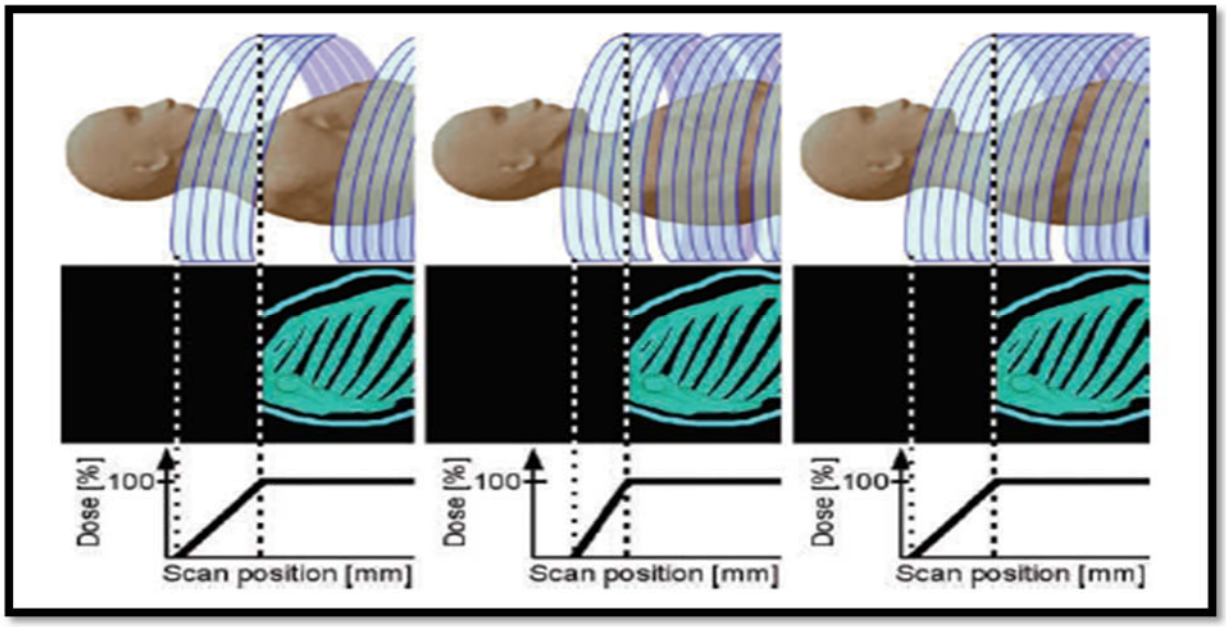

Figure 3-2: Diagram illustrating how over-ranging is influenced as pitch and detector collimation vary (Schilham et al., 2010).

3.3.2.2 Over-beaming

Over-beaming is the excess dose beyond the edge of the detector rows of a MSCT slice per rotation that results if focal spot penumbra falls outside the area of active detector and is not used for imaging purposes **(Figure 3-3)**. The magnitude of over-beaming is inversely proportional to the number of detector rows, therefore, it contributes unnecessary radiation exposure to patients (Goo, 2012; Sorantin et al., 2013). There is no need to exclude the penumbra from imaging with SSCT because most single slice scanners make full use of the entire dose profile. Only at collimator settings below 2 mm, some scanners employ restrictive post-patient collimation. However, different situations arise with MSCT, as more than one active detector channel is used; there is a need to serve all channels equally well. Consequently, penumbra must either totally or partially be excluded from detection. As a result the detectors are 'over-beamed', and a certain portion of the radiation that exposes the patient remains unused

(Figure 3-3), where N is the number of slices acquired simultaneously and h_{col} is the slice collimation (Nagel, 2005; Sorantin et al., 2013).

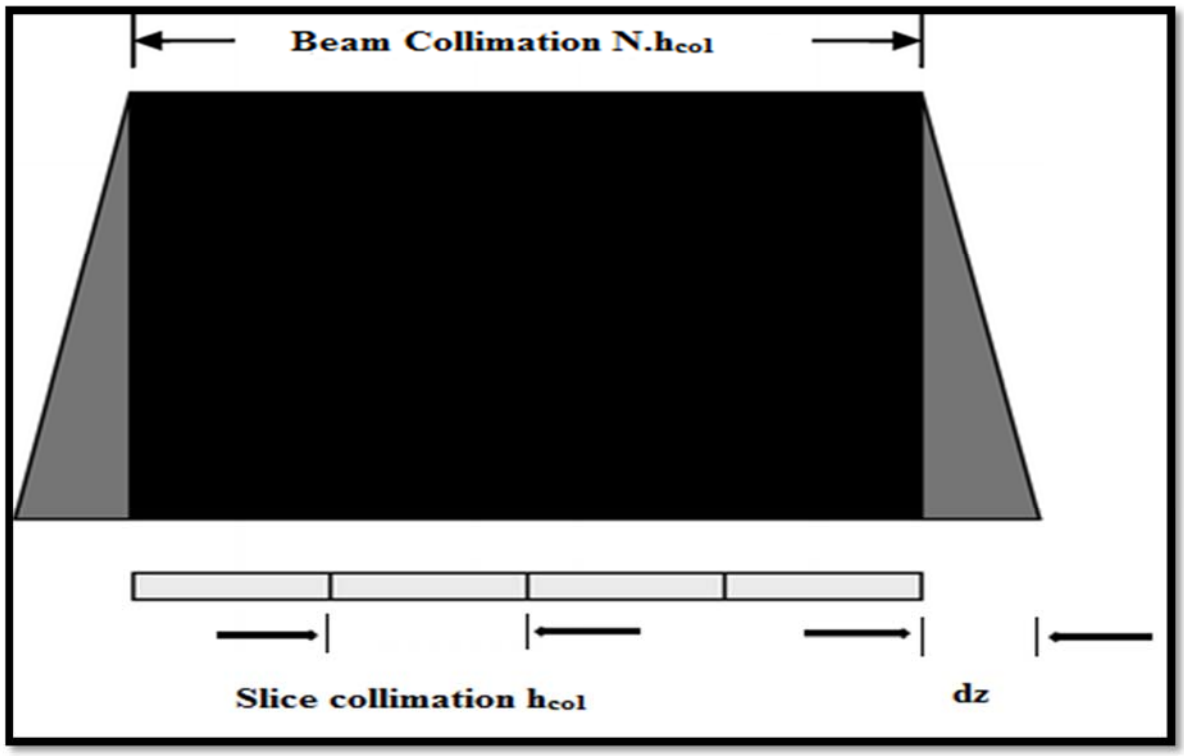

Figure 3-3: Dose profile in free-in-air for a quad-slice scanner (dark grey: umbra, light grey: penumbra); over-beaming is characterized by the parameter dz (Nagel, 2005).

Over-beaming can be determined for a particular type of scanner by a set of CTDI measurements made free-in air at the axis of rotation for all of the collimator settings available. Over-beaming characteristics can be fairly well described by a single parameter (the over-beaming parameter dz) that usually represents the combined width of both penumbra triangles, **(Figure 3-3)**. Typically, for the majority of single-slice scanners (dz) amounts to 0 mm, to 1 mm for single-slice scanners with restrictive post-patient collimation and most dual-slice scanners, and to 3 mm for MSCT scanners with four and more slices acquired simultaneously (Nagel, 2005; Sorantin et al., 2013).

3.3.2.3 Pitch (P)

Most manufacturers report a pitch value with respect to the nominal slice thickness instead of the total active collimation length in the z-axis. In helical CT protocols, the pitch parameter has a direct influence on patient radiation dose. This is essentially because as pitch increases, the time that any one point in space spends in the X-ray beam is decreased. Selecting a higher

pitch will reduce the DLP of the patient but not the CTDI, by reducing the number of rotations over the same plane (GE Medical Systems, 2001; Seeram, 2015).

The determinants of pitch are beam collimation and table speed, both parameters are intrinsically linked to image quality and radiation dose (Rehani, 2010; Paterson & Frush, 2007; Valentin, 2007). A beam-pitch of 1.0 facilitates an acquisition with no overlap or gap, a beam-pitch of less than 1.0 facilitates an overlapping acquisition, and a beam-pitch of greater than 1.0 facilitates an interspersed acquisition. Pitch has a smaller effect on image quality with the use of MSCT scanners than it does with use of SSCT scanners (Flohr et al., 2005). There are three modes of helical pitch (HP) or pitch factor (PF) used in the Toshiba Aquillion 16 CT scanner: HP 11.0/(detail PF 0.688), HP 15.0/(standard PF 0.938) and HP 23.0/(fast PF 1.438) (Toshiba Medical Systems). Generally, radiation dose is inversely proportional to pitch when all other factors are held constant. Therefore, increasing pitch is one consistent way to reduce radiation dose. A study by Michael, (2002), showed that as the pitch decreased the $CTDI_{vol}$ (which is the only CTDI descriptor that takes pitch into account) increased and the radiation dose acquired in head phantom was doubled compared to that acquired in body phantom.

3.3.3 Dose effects relating to CT acquisition parameters (application-related factors)

This section will discuss the main CT scan parameters of interest that have a direct influence on radiation dose, such as the X-ray beam energy (kilovolt peak), tube current (in milliamperes), rotation or exposure time, dose reduction techniques such as tube current variation or modulation and CT gantry angulation. Patient doses in CT examinations depend on the choice of radiographic parameters used to perform the scanning. Key parameters that affect patient dose, and which need to be defined in CT protocols, are the following (Raman et al., 2013; Szczykutowicz et al., 2015 and AAPM Practice Guideline 1.a., 2015):

3.3.3.1 X-ray Tube Potential (kVp)

X-ray tube voltage is the electrical potential applied across the X-ray tube to accelerate electrons toward the target material. The radiation dose increases approximately proportionally to the percentage change in tube voltage. The tube voltage values for routine CT brain scans for adult patients typically range from 110 kVp to 140 kVp (Dowsett et al., 2006; Livingstone et al., 2006; Smith, et al., 2007; Tsapaki et al., 2006).

The tube potential determines the energy of the incident X-ray beam. This parameter has not routinely been adjusted in the past for body CT exams in infants and children, with the majority traditionally being performed at 120-140 kVp (Paterson & Frush, 2007). Increasing tube potential improves both the tube output and penetrating ability of the beam, while image contrast is decreased. Increased tube voltages have been reported to improve tube loading and image quality due to both the tube output and the penetrating ability of the beam being improved, while image contrast is adversely affected. Contrary to the case for mAs, the consequences of variations in kV cannot easily be assessed (Galanski et al., 2007).

As illustrated by Galanski et al., (2007) the relationship between radiation dose and tube potential is not linear. Studies have shown an exponential relationship which varies according to specific circumstances, such as factors related to CT machine design and patient size. Reducing the peak kilovoltage can result in a substantial drop in the radiation dose, though the exact dose saving is in part related to the geometry of individual CT machines, and thus, varies between different manufacturers (Paterson & Frush, 2007). Tack and Gevenois, (2004) highlighted the additional CT acquisition factors which include the inherent tube filtration and the physical distance between X-ray tube and patient. As tube filtration increases the beam becomes harder; this results in lower energy photons being removed and therefore a larger proportion of higher kVp values are emitted. X-ray beam intensity reduces as filtration increases. A report by Huda et al., (2002) demonstrates a four-fold decrease in the radiation dose when the tube kilovoltage was reduced from 140 kVp to 80 kVp for body and head CT protocols.

Generally, higher kV photons are used in diagnostic imaging to increase photon penetration of the patient. This will result in increasing the high contrast resolution of the images (Matsumoto et al., 2011). In CT brain imaging, a high kV (e.g. 120 kV) is used because it yields lower noise in the acquired image and lower noise is required to maximize the resolution of the brain image. It has been determined that an increase in tube potential will decrease the noise of the image, however the patient dose will increase (Duzenli et al., 2005).

3.3.3.2 Tube Current Time-Product (mAs)

The photon flux during image acquisition is controlled by tube current (mA) and time (s); the CT operator can adjust the tube current-time (mAs) in order to reduce the dose (i.e. reduce the number of incident photons) or reduce the noise (i.e. increase the number of incident photons).

The number of photons that are produced in X-ray filament will increase linearly with increasing mAs and the load on the tube also increases. On the other hand, increasing the photons that are incident on the object will allow more photons to reach the image detector (assuming that the beam has adequate penetrating power through appropriate kVp selection). The reduction in noise follows statistical photon counting, and is approximately $1/\sqrt{N}$, where N is the number of incident photons (Seeram, 2015).

There is a linear relationship between tube current and radiation dose (Paterson & Frush, 2007). The typical mAs values for a routine brain CT scan for adult patients, as reported by Livingstone et al. (2006), Smith et al., (2007) and Tsapaki et al. (2006), are 100, 200 – 350 and 250 – 270, respectively (Livingstone et al., 2006; Smith et al., 2007). Whereas typical mAs values for routine peadiatric brain CT scans range from 180 – 230 and 90 – 320, as reported by Huda et al., (2007) and Mazonakis et al., (2007), respectively. As reported by Huda et al., (2004; 2007); for head CT examinations, the mAs can be reduced substantially when scanning infants, and that use of the lowest X-ray tube voltage will generally reduce patient doses. For reasonable dose management in paediatric applications, however, smaller volumes are scanned and tube load parameters can be reduced. Lower mAs can be applied routinely and it is appropriate to reduce the mAs value of adult CT head scan by approximately a factor of 2 to 2.5 when scanning newborns. Manual adjustment of tube current based on patient weight or dimensions can aid in establishing an appropriate balance between image noise and radiation exposure. However, these adjustments do not guarantee constant image quality throughout the entire volume scanned and are not necessarily widely implemented into clinical practice.

For single sequential CT scans the mA time-product (Q) is obtained by multiplying the tube current (I) and exposure time (t). In spiral scanning mode, Q can be calculated as the product of tube current (I) and tube rotation time ($t_{rot)}$ for a single slice, which is different from total scan mAs product that accounts for the product of tube current (I) and total scan time (T) (Nagel H D., 2007).

Tube current-time product is often used as surrogate of measuring patient radiation dose when compared to computed tomography dose index (CTDI), which is defined as the average dose imparted by a single axial acquisition to a standard 100 mm pencil chamber dosimeter inside a PMMA phantom over the width of 14 CT slices (McCollough et al., 2008). As presented by Galanski et al. (2007), this is highly misleading as the normalized values of CTDI and thus the radiation dose resulting from the same mAs settings can vary by up to a factor of 6 between

different scanners. It is not realistic to communicate dose information or related recommendations on the basis of mAs values. Instead, only $CTDI_{vol}$ (and DLP) should be used for this purpose. $CTDI_{vol}$ is the volume computed tomography dose index and specifies the radiation intensity used to perform a specific CT examination. $CTDI_{vol}$ simply indicates the intensity of the radiation being directed at that patient, whereas DLP is the dose length product and defined as the number of slices acquired multiplied by the total scan length (Huda et al., 2011). Further details of CT dose descriptors are discussed in (section **3.5**) page **41**.

With advancement of technology additional ambiguity has been introduced from MSCT scanners with the introduction of pitch-corrected mAs (effective mAs or mAs per slice). Most MSCT scanners benefit from a multipoint spiral interpolation scheme and effective mAs is the most appropriate notation. Nonetheless, some scanners still prefer the traditional mAs notation, for example General Electric and Toshiba, and this introduces an additional complexity when comparing mAs settings between vendors (Galanski et al., 2007).

In paediatric CT, as reported by Paterson and Frush (2007), tube current should be reduced since there is no need for the same number of X-ray photons when imaging a child. A decrease in tube current will lead to higher image noise and the operator must balance savings in radiation dose against increased noise. Studies by Shah et al., (2005); Mathias Cohnen et al., (2000); and Rustemeyer et al., (2004) support a reduction in tube current for head CT scans. A further two studies suggest that a simple way to decrease the radiation dose is by reducing the values of the tube current and peak voltage used to generate the scout images, below those recommended by the manufacturer (O'Daniel et al., 2005; Perisinakis et al., 2001; Matsumoto et al., 2011).

3.3.3.3 Automatic Tube Current Modulation (ATCM)

This is an automated technique used in CT to adjust the X-ray tube current in real-time in response to variations in X-ray intensity received at the detector array caused by different body thicknesses / densities. As reported by Galanski et al., (2007) the mA modulation is used for both body and head CT examinations. The tube current is modulated instead of remaining fixed in order to meet a particular image quality/noise level along the full scan length. Large variations in attenuation can occur both with projection angle and along the anatomical volume (z-axis). Consequentially there is a strong rationale for moving away from using a fixed tube current (FTC). mA modulation can be achieved in near real-time by using a feedback mechanism or incorporate pre-programming and a feedback loop, it can also occur angularly

about the patient or along the long axis (z) of the patient (McCollough, 2005 & 2009). The basic idea behind tube current modulation is to adapt the tube current to attenuation of the body region by increasing the tube current for more attenuating areas and decreasing it for less attenuating areas. Extremely large variations in patient radiation absorption occur with variations in projection angle and anatomic region. Since the projection with the most noise primarily determines the amount of noise on the final image, it is possible to reduce the radiation dose (photons) for other projections without increasing the noise on the final image (Graser et al., 2006; McCollough, 2005, 2006 & 2009; Mulkens et al., 2005). Most currently used scanning protocols, which involve manual selection of tube current for radiation dose optimization and image quality, need to be modified (Tian et al., 2015; Strauss et al., 2010). Within the literature there are three reported methods for automatically modulating the tube current:

- **Angular (x, y) mA modulation:** in this type of modulation the tube current varies as the X-ray tube rotates around the patient (e.g in the A.P. versus lateral direction) as shown in **(Figure 3-4)**. The initial mA value should be chosen by the operator then the mA is modulated upward or downward from the initial value within a period of one gantry rotation. The mA can be varied as the X-ray tube rotates between the AP and lateral positions according to the attenuation information determined from the CT scout image or in near real-time according to the measured attenuation from the 180^{o} previous projection (Graser et al., 2006; Kalra et al., 2004 & 2005; Marco, 2013; McCollough et al., 2009; Raman et al., 2013).

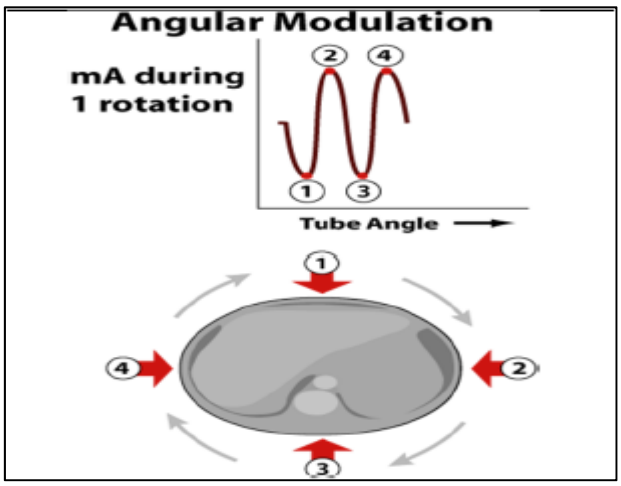

Figure 3-4: mA angular modulation (Marco, 2013).

- **Longitudinal (z) mA modulation:** The longitudinal (z-axis) mA modulation involves the variation of the radiation dose along the anatomical regions according to its attenuation by varying the tube current along the z-axis of the patient (e.g. shoulders versus abdomen) as illustrated in **(Figure 3-5)**. This is different from angular tube modulation in which the tube current is varied cyclically in relation to the starting tube current value. The main function of the z-axis modulation is to produce uniform noise levels across the various regions of the anatomy. To achieve this, the operator must select the desired level of image quality by using scanner presets which are relatively manufacturer-specific (the reference noise index, reference image acquisition, reference tube current–time product value, or reference standard deviation or image quality level as recommended by Toshiba Medical Systems, Tokyo, Japan) (Graser et al., 2006; Kalra et al., 2004 & 2005; Marco, 2013; McCollough et al., 2006 & 2009).

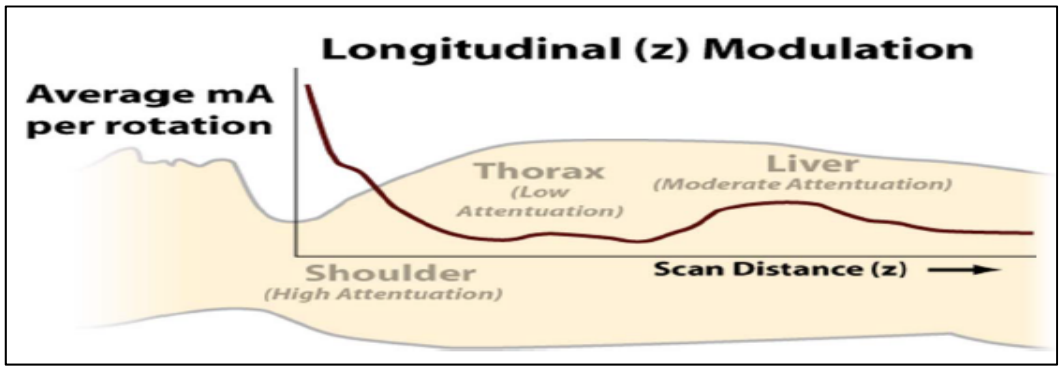

Figure 3-5: Longitudinal (z) modulation (Marco, 2013).

- **Angular and longitudinal (x, y, z) modulation:** This modulation technique combines the two methods mentioned above to vary the mA both during gantry rotation and along the z-axis of the patient (i.e from the anteroposterior direction to the lateral direction and from shoulder to abdomen **(Figure 3-6)**). The desired level of image quality must be selected by the operator using one of the following methods: the reference noise index (GE Healthcare Technologies, Waukesha, Wis), reference image acquisition (Philips Medical Systems, Best, the Netherlands), reference tube current–time product value (Siemens Medical Solutions, Forchheim, Germany), or reference standard deviation or image quality level (Toshiba Medical Systems, Tokyo, Japan) (Kalra et al., 2005; Marco, 2013; McCollough et al., 2009; Raman et al., 2013). This type of mA modulation is used by the Toshiba CT machine employed in this thesis.

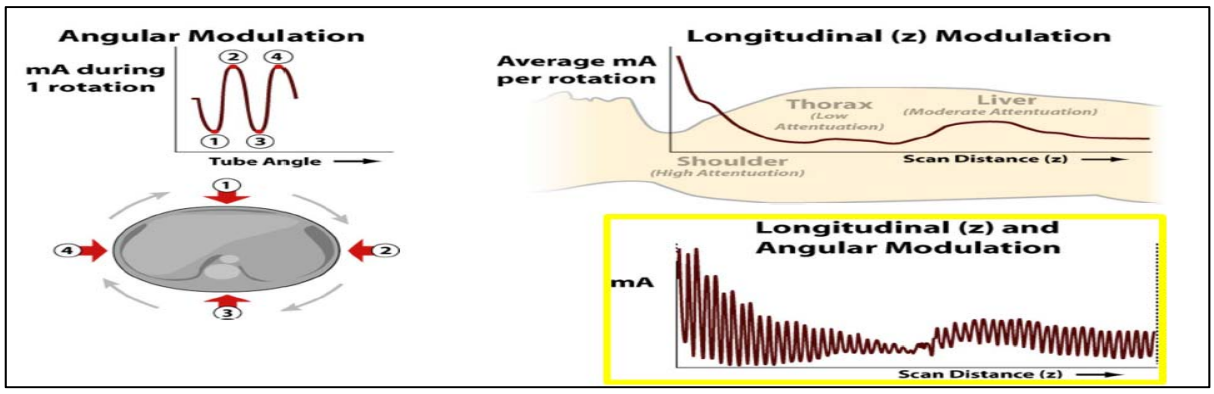

Figure 3-6: Longitudinal (z) and angular modulations (Marco, 2013).

All modern CT systems are now delivered with ATCM systems that modulate tube current in three dimensions. Each of these systems has different specifications and operates somewhat differently. However, the main principle is to manage the required image quality and radiation dose in a reproducible manner by adapting the tube current to the patient's size, shape, and attenuation. Since the radiographers are asked to avoid inferior images, they usually select scan parameters that are 'on the safe side'. This often leads to exposures higher than necessary to achieve the required diagnostic image quality. ATCM systems have a number of benefits: better control of the absorbed dose to the patient, improved consistency of image quality among patients, reduction of certain image artefacts, and reduced load on the X-ray tube, which increases its lifetime (Keat, 2005). With these benefits in mind, users should learn how to use and apply the systems properly (Lee et al., 2008).

Radiographer rely on ATCM systems to reduce dose to patients. The AEC relies on constant noise levels, however, the desired noise levels cannot be easily predicted and the necessary noise levels are not constant for all anatomical regions. If a constant noise level were required for all organs, the dose for regions with high attenuation would increase, while in these regions higher noise levels can be usually tolerated. The tube current is modified relative to normal data for the attenuation of the different organs. But if the required level of noise cannot be predicted the ATCM will set mAs values to the maximum which will lead to a dose increase to the patient (Suess & Chen, (2002).

Optimization of CT scanning protocols involves many parameters, including tube voltage, tube current, section thickness, collimation, and pitch. The image reconstruction kernel is also important. Changing even one of these parameters can affect ATCM systems in different ways, depending on the CT scanner being used. For example, changing the reconstruction kernel will

alter the tube current used by the Toshiba Sure-Exposure system, which tries to maintain the image noise in response to variations in scanning and reconstruction parameters, but will not alter the tube current used by other systems. Therefore, users should know about each of their system's characteristics and the effect that changing scanning and reconstruction parameters will have on the image quality and radiation dose. Nevertheless, in the use of ATCM systems, selecting an appropriate noise index, standard deviation, reference milliamperage, or reference image is vital. This process is not straightforward, however, as stated by Lee et al., (2008), there are two ways to determine appropriate values for the use of ATCM systems. The European Guidelines on Quality Criteria for CT are a good standard for optimizing scanning protocol with reasonable radiation dose. These guideline values are provided in relation to technique for a standard-sized patient for each type of CT examination considered. Another way to optimize protocol is to use simulation software before scanning, although this technique is not currently available to most CT practitioners. This software can simulate the effect of increasing image noise, and the resultant simulated data can be reconstructed. Thereafter, users will be able to evaluate image quality with radiation dose modulation (Lee et al., (2008).

In general, the introduction of ATCM techniques in modern CT scanners represents an important step toward standardization of tube current protocols, with elimination of arbitrary selection by radiologists and radiographers. As reported by McCollough et al., (2009), the use of ATCM greatly enhances and simplifies efforts to decrease patient dose. It has demonstrated reductions in dose of about 20–40% when image quality is appropriately specified.

3.3.3.4 Rotation Time

The tube rotation time determines the speed at which the tube rotates around the patient. In conjunction with table speed it defines the length of table movement for each rotation of the X-ray tube. The X-ray tube in CT irradiates only a narrow section of the anatomy when it makes a full rotation around the patient and does so for multiple rotations along the length of the patient. In general, tube rotation times should be kept as low as possible in order to yield minimal movement artefacts, short scan time (and hence short breath-hold), and the opportunity for scanning a range that is as large as possible. Longer rotation times might be necessary if the required radiographic exposure cannot be achieved for the shortest scan time. In principle, the radiation dose is proportional to rotation time when all other CT scan parameters remain constant. Standard paediatric CT head clinical protocols are usually obtained with 0.5 or 0.75-second rotation times and for adults this is increased to 1-second tube rotation times. However,

for some clinical indications where specific information is needed and to reduce the motion artefacts such as centrum semiovale, corona radiata at the lateral ventricles, middle cranial fossa/skull base, and posterior fossa/palate, the rotation time is reduced and this leads to an increase in radiation absorbed dose (Mullins et al., 2004).

Current MSCT machines have sub-second gantry rotation times. Since there is a linear relationship between tube current (mAs) and radiation dose, if the rotation time is reduced from 1 to 0.5 seconds then the radiation dose will be halved. Both rotation time and tube current are important in paediatric CT. The reduction in examination time has been an important factor for reducing the need to use sedation or general anaesthesia for children undergoing this type of imaging. On the other hand, faster imaging times mean images are less likely to show motion artefact, which in the past may have required an examination to be repeated, with an obvious increase in the radiation dose to the patient. Reducing the tube current will increase image noise, and this must be factored in, when selecting these parameters (Paterson & Frush, 2007).

3.3.3.5 Gantry Angle

Commonly, for CT brain scans, the examination is undertaken in an axial (sequential) mode in order to allow angulation of the gantry in order to reduce the radiation dose to the lens of the eye (Stewart et al., 2012). The lens of the eye does not need to be considered for stochastic effects. However, it is useful to consider the deterministic effects, such as cataracts, which have a threshold of about 0.5 Gy (ICRP Publication 118, 2012) (Stewart et al., 2012). Evidence from within the literature commonly advocates the need to angle the CT gantry in order to avoid direct irradiation of the eye lens (Schilham et al., 2010).

In CT, the radiation dose at the surface of the patient depends upon the distance from the x-ray target to the beam entrance, together with the contribution from the primary and secondary X-ray photons entering the patient from other points. The major contribution to the absorbed dose at any point superficially located arises from the entrance dose. For the eye lens, the frontal X-ray projections contribute to the major part of the absorbed dose. In head scanning, if the frontal 90^{o} is omitted and the scan is performed with an angular rotation rather than this angle (in head, partial rotation degree of 270^{o}), then the eyes receive a reduced dose (ICRP Publication 87, 2000; Rehani et al., 2000).

3.4 Radiation Dosimetry

Radiation dose can be defined as the amount of energy absorbed in the body from radiation interactions. Early measures of radiation dose were non-quantitative; based on skin erythema, and were subsequently replaced by measures of absorbed dose (e.g. energy absorption, measured initially in radiation absorbed dose or (rad) and more recently in gray (Gy) or milligray (mGy) [1 Gy = 100 rad; 1 rad = 10 mGy or 0.01 Gy] (Linet et al., 2012).

Dosimetry is the act of measuring or estimating the radiation doses and calculating those doses to individuals or populations undergoing radiation procedures. There are two types of radiation exposure; namely external exposure, which occurs when the radiation source or nuclear substance is outside of the body and internal exposure, which occurs when the radiation is emitted by nuclear substances inside the body. External exposures are typically monitored by the use of small radiation detectors such as thermoluminescence phosphors, which are worn on the person or patient. Monitoring a patient for external exposure is called patient dosimetry (Attix & Tochilin, 2016; Hine & Brownell, 2013). When discussing the results from dosimetry experiments and calculations the following terminology may arise: -

Absorbed dose: this is the mean energy imparted to the material (tissue) by ionizing radiation per unit mass of that material, expressed as absorbed dose measured with unit of Gray (Gy) (Sabarudin & Sun, 2013).

Equivalent Dose: is referred to as the amount of absorbed radiation dose multiplied by a radiation weighting factor. It is measured in Sieverts (Sv) and can be used to compare all types of ionizing radiation equally against the biological effect (Sabarudin & Sun, 2013).

Effective Dose (ED): accounts for the biological effect of ionizing radiation received during a specific examination. It is also reflects the absorption of non-uniform radiation from partial body exposure relative to whole body radiation dose that is received. ED calculations allow risk to be compared amongst different radiological imaging examinations. The unit of measurement for effective dose is the Sievert (Sv) or Millisieverts (mSv) (Morin et al., 2003; Sabarudin & Sun, 2013).

3.5 CT Dose Descriptors (Quantities for Assessing Radiation Dose in CT)

Radiation doses for patients undergoing CT scan examinations can be measured directly using MOSFETs or TLDs and dosimetry phantoms. Dose estimations, on the other hand, can be carried out indirectly by obtaining indices from the CT scanner which may include CT Dose Index (CTDI), Volume CT Dose Index ($CTDI_{vol}$), Dose Length Product (DLP) or Multiple-Scan Average Dose (MSAD), which is the primary metric used in CT to describe the radiation output from a scanner (McCollough et al., 2008 & 2011). The most commonly used metrics for radiation dose estimates for CT examinations are the CT volume dose index ($CTDI_{vol}$), dose-length product (DLP) and ED.

3.5.1 Computed Tomography Dose Index (CTDI)

As defined by the Food and Drug Administration (FDA or USFDA) in 1984, the original incarnation of the CTDI was based on an axial CT scanner. This original definition represented the dose from the primary beam plus scatter from surrounding slices measured in Milligray (mGy). Variations in CTDI have been defined due to developments in technology and these have been introduced into MSCT equipment. These CTDI variations include $CTDI_{100}$, $CTDI_{w}$ and $CTDI_{vol}$. A summary of CTDI radiation dose parameters described in this section are provided in **(Table 3-2)**, whereas **(Table 3-3)** gives short summary of the CT dose parameters definitions and their effects on radiation dose, the first three parameters are discussed in chapter three section **(3.3)** on page **25** (Goo, 2012).

Table 3-2: Parameters of radiation dose (Gerber et al., 2005).

Variable	Parameter	Physical equivalent	SI unit
Radiation exposure	$CTDI_{100}$	Number of ions produced in air by photons	coulomb/kg (C/kg)
Absorbed radiation dose	CTDI, $CTDI_{w}$, $CTDI_{vol}$	Radiation energy absorbed by patient's body	Gray (Gy)
Cumulative radiation dose	DLP	Total radiation energy absorbed by patient's body	mGy x cm
Effective dose	ED	Biological effect of radiation dose received	Sievert (Sv)

Table 3-3: Definitions of CT parameters and their effects on radiation dose (Goo, 2012).			
Dose Parameter	**Definition**	**Effects on Radiation Dose**	**Unit**
Tube potential or voltage	X-ray beam energy	Proportional to square of tube voltage change	kV
Product of tube current and time	Photon fluence; number of photons in defined exposure time	Directly proportional to radiation dose	mAs
Pitch	Ratio of table feed per gantry rotation to nominal width of beam collimation	Inversely proportional to radiation dose	-
$CTDI_w$	Average radiation dose in scan volume measured in standard CT phantoms; 1/3 CTDI center + 2/3 CTDI periphery	Directly proportional to radiation dose in unit volume, influenced by pitch factor	mGy
$CTDI_{vol}$	$CTDI_w$/pitch	Directly proportional to radiation dose in unit volume, irrespective of pitch factor	mGy
Dose-length product	$CTDI_{vol}$ x scan length (cm)	Directly proportional to total scanned radiation dose	mGy·cm
Effective dose	Overall risk-related radiation exposure; Σ W_T (tissue weighting factor) x H_T (tissue equivalent dose)	Directly proportional to total scanned radiation dose and overall risk of irradiated tissue	mSv

3.5.2 CTDI:

CTDI is the fundamental parameter of absorbed radiation dose in CT. During its calculation, most manufacturers use a 16 cm phantom for head and 32 cm phantom for body examinations. As reported by Shrimpton and Wall, (2000), the smaller phantom is also used for dose assessment in paediatric examinations. The CTDI dose is measured at the centre and near the periphery of the phantom **(Figure 3-7)**. Thus, the dose values obtained are denoted as $CTDI_{H,c}$ and $CTDI_{H,p}$ and also $CTDI_{B,c}$ and $CTDI_{B,p}$ with H = head, B = body, c = centre, p = periphery (Gerber et al., 2005; Nagel, 2007; Shrimpton & Wall, 2000).

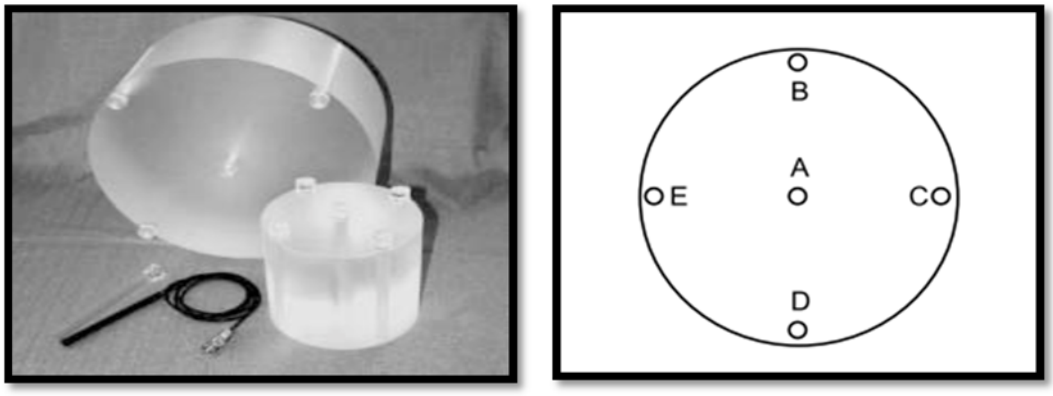

Figure 3-7: Cylindrical standard CT dosimetry phantoms (16 and 32 cm in diameter) and arrangement of the locations A to E for the determination of CTDI in a standard CT dosimetry phantom (Nagel, 2007).

The CTDI is derived from the dose distributed along a line parallel to the axis of rotation for the scanner (= z axis) that is recorded for single rotation of the radiation source as represented by **(Figure 3-8)**. This means CTDI is the equivalent dose value inside the irradiated slice (beam) that would result if the absorbed radiation dose profile were entirely concentrated to a rectangular profile of width equal to the nominal beam width $N \cdot h_{col}$, with *N* being the number of independent (i.e. non-overlapping) slices that are acquired simultaneously. Accordingly, all dose contributions from outside the nominal beam width, i.e. the areas under the tails of the dose profile, are added to the area inside the slice (Nagel, 2007).

The mathematical definition corresponding to CTDI describes the summation of all dose distributions along the z-axis:

$$\boldsymbol{CTDI} = \frac{1}{N.h_{col}} . \int_{-\infty}^{+\infty} D(z).dz$$

Where D(z) is the value of the dose at a given location, z, and $N \cdot h_{col}$ is the nominal value of the total collimation (beam width) that is used for data acquisition. CTDI is therefore equal to the area of the dose profile (the dose profile integral) divided by the nominal beam width. In practice, the dose profile is accumulated in a range of –50 mm to + 50 mm relative to the centre of the beam, i.e. over a distance of 100 mm (Nagel, 2007).

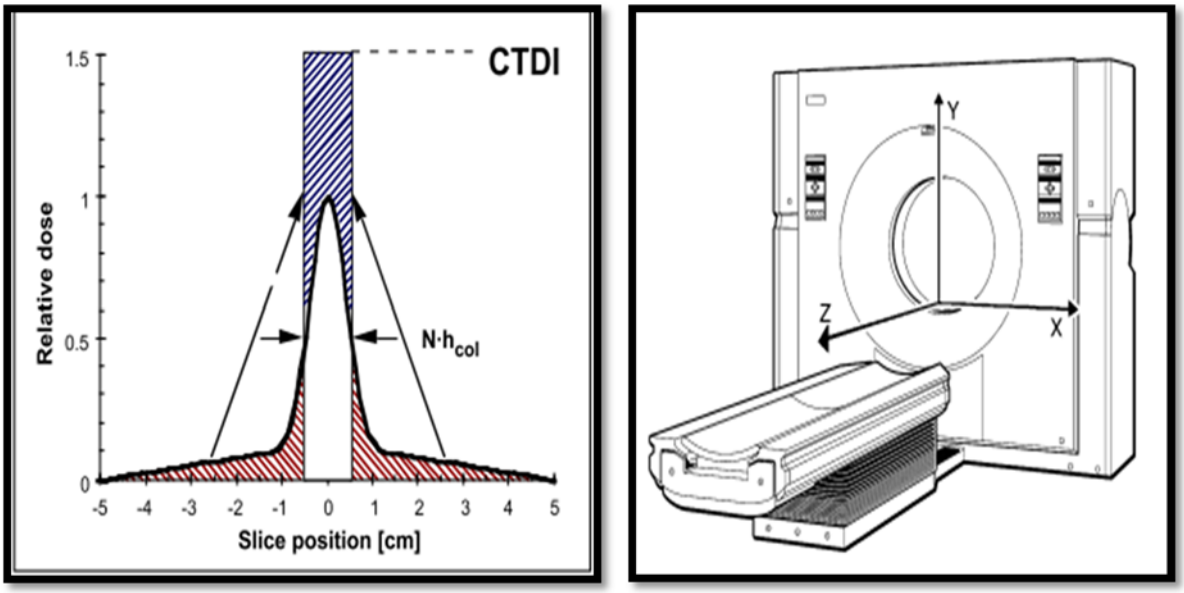

Figure 3-8: Radiation dose profile (left image) of a single computed tomographic slice (Nagel, 2007). The second image denotes the axis system used in CT (Gerber et al., 2005).

For **(Figure 3-8)**, the first image illustrates CTDI, which is the equivalent of the dose value inside the irradiated slice (beam) that would result if the absorbed radiation dose profile were entirely concentrated to a rectangular profile of width equal to the nominal beam width $N \cdot h_{col}$ (Nagel, 2007). There are tails at the edges of the slice of the radiation dose profile which are caused by the divergence of the X-ray beam and scattering photons by the body tissue. For the estimation of radiation dose these tails have important implications because, depending on the width of the individual slice in the z-axis and distance between adjacent slices, the tails can overlap and lead to an accumulation of radiation dose. For **(Figure 3-8)**, the second image is the CT axis system used to acquire the slice profile. The x- and y-axes (transaxial) represent the two dimensions of each individual slice. The z-axis (axial, ‘‘third’’ dimension) is the axis along which successive slices are arranged (Gerber et al., 2005).

3.5.3 $CTDI_{100}$:

The $CTDI_{100}$ reflects the dose contribution from a 100 mm range centred on the index slice over the z-axis in the phantom and is expressed in the SI units of coulomb/kg (C/kg). It can be measured by using a 100 mm long pencil-shaped ionization chamber in two different cylindrical acrylic phantoms (16 and 32 cm diameter) which is placed at the isocenter of the CT scanner. The $CTDI_{100}$ varies within the slice plane and for body imaging is higher at the periphery than at the centre of the field of view (Gerber et al., 2005).

3.5.4 $CTDI_w$:

The weighted CTDI ($CTDI_w$) is expressed in the SI units of gray (Gy), and was introduced to account for the non-uniform dose delivery when using $CTDI_{100}$. When applying an X-ray beam to a patient the beam often passes directly on to entire surface of the patient's body. The primary bean contains the most photons and is mostly attenuated by a patient's tissues. As a result, the energy received by patient's skin is higher than in the centre of the body. Even though the X-ray beam irradiates 360^o around the patient's body and passes through the ioscentre. Accordingly, the surface is exposed to more photons than the centre portion (Cody & Mahesh, 2007; McCollough et al., 2011).

The $CTDI_w$ reflects the weighted sum of two thirds peripheral dose and one third central dose in a 100 mm range in acrylic phantoms locations. This quantity reflects the average absorbed dose over the two-dimensions (x and y) of the average radiation dose to a cross-section of a patient’s body (Cody & Mahesh, 2007; Coursey & Frush, 2008; Cretti & Perugini, 2016;

Einstein et al., 2007; Sabarudin & Sun, 2013; Tootell et al., 2014). The $CTDI_w$ parameter combines the values of CTDI at central and peripheral of the phantoms into one single name represented mathematically by the following equation:

$$\boldsymbol{CTDI_w} = {}^{2}/_{3} \, . CTDI_{100 \text{ at periphery}} + {}^{1}/_{3} \, . CTDI_{100 \text{ at center}}$$

3.5.5 $CTDI_{vol}$:

CT scans commonly consist of more than one slice, this means that the radiation dose received from a complete CT examination consisting of multiple parallel slices is higher than the sum of the $CTDI_{100}$'s of the individual slices due to the overlap of the tails of the individual radiation dose profiles (Commission, Medicines, & Healthcare, 2010; Gerber et al., 2005). The volume CTDI ($CTDI_{vol}$) was introduced to adjust for pitch (the gap or overlap of the helical pattern of radiation) by calculating what is known as volume CTDI ($CTDI_{vol}$). It is the most commonly cited index for modern MDCT equipment and defined as $CTDI_w$ divided by the beam pitch factor ($CTDI_{vol} = CTDI_w/pitch$). It's distinctly different from $CTDI_w$ in that it represents the average radiation dose over the volume scan (*x*, *y*, and *z* directions). It is a useful tool for radiologists and radiographers because it specifies the radiation intensity used to perform a specific CT examination and not to quantify how much radiation that each patient receives from the CT examination. $CTDI_{vol}$ provides a method for comparing the absorbed radiation dose received from different scanning protocols because incorporates all information specific to a scanning protocol and, expressed in SI units of gray (Gy) (Cody & Mahesh, 2007; Coursey & Frush, 2008; Rehani et al., 2000; Sabarudin & Sun, 2013; Tootell et al., 2014; Valentin, 2007).

$$\boldsymbol{CTDI_{vol}} = CTDI_w/Pitch$$

$$= CTDI_w \, x \, \frac{\text{total nominal scan width}}{\text{distance between scans}}$$

The equation demonstrates that the numeric value of the $CTDI_{vol}$ is directly related to the degree of overlap between adjacent slices. This degree of overlap is determined by the width of the individual slices and by the distance between the slices in the z-axis (Commission, Medicines, & Healthcare, 2010; Gerber et al., 2005).

The distance between adjacent slices in the helical scanning mode is dependent on how far the patient table moves during one gantry rotation; this is known as pitch. Pitch is defined as the

patient table increment (expressed in millimetres) during one CT gantry rotation divided by the combined width of all simultaneously acquired slices and can hence be expressed as:

$$\boldsymbol{Pitch} = \frac{I}{N \times T}$$

Where I is the distance between slices defined by the table advance during one gantry rotation (mm) in helical scanning mode, N is the number of slices, and T is the nominal width of one slice (Commission, Medicines, & Healthcare, 2010; Gerber et al., 2005).

Thus, $CTDI_{vol}$ for the axial scanning mode can be expressed mathematically as following:

$$\boldsymbol{CTDI_{vol}} = \frac{N \times T}{I} \times CTDI_w$$

According to pitch definition above, the $CTDI_{vol}$ for the helical scanning mode can be expressed as:

$$\boldsymbol{CTDI_{vol}} = \frac{1}{Pitch} \times CTDI_w$$

$CTDI_{vol}$ can be used in turn to determine the dose-length product (DLP). Measured in SI units of mGy·cm, DLP reflects the integrated radiation dose for a complete CT examination.

CTDIvol represents the radiation produced by the CT scanner, not the radiation dose to an individual patient. The limitations of CTDIvol include using index-based values to describe dose in CT, modified by a series of adjustments to reflect the dose of radiation that the scanner delivers to a plastic phantom. Although customized dose calculations for individual patients theoretically can be generated by using data present in the CT images themselves, no automated method has been developed that can recognize and segment the various tissues and organs for individual patients (Strauss & Goske, 2011). However, the $CTDI_{vol}$, by definition, assumes the patient is either the 16-cm or 32-cm diameter cylindrical plastic phantom However, the CTDI phantom is rarely a reasonable model for an individual patient with respect to attenuation. In addition, clinical structures, e.g., bone and lung, will change the dose distribution relative to that found in a cylindrical, homogeneous, plastic phantom.

3.5.6 Dose Length Product (DLP)

In most CT scanners, the values of $CTDI_{vol}$ and Dose Length Product (DLP) are displayed on the scanner console during the CT examinations, which is the most commonly quoted value of the radiation dose received by a patient. The DLP is calculated to account for the differences in the scan extent for a CT examination (Cody & Mahesh, 2007).

The Dose Length Product (DLP) is defined as the $CTDI_{vol}$ multiplied by the scan length (slice thickness × number of slices) in centimetres and can be calculated using the following formula, where $CTDI_{vol,}$ is the volume CT dose index and L, is the length of the scanned volume of the anatomical region being scanned.

$$\boldsymbol{DLP} = CTDI_{vol} \times \text{Irradiated Scan Length (L)}$$

These parameters are precisely defined to allow comparisons of the radiation doses among different CT imaging protocols (Cretti & Perugini, 2016; Einstein et al., 2007; Gerber et al., 2005).

3.6 Radiation Dose Measurement Instrumentations

In many situations, i.e. legislative requirements, measurements of CTDI and DLP or absorbed dose are required. It is also required to optimise image quality and patient radiation dose (Simantirakis et al., 2014). Since the radiation doses from diagnostic radiology are small, accurate and long-term stability dosimeters are required (IAEA, 2007). In diagnostic radiology, there are several types of radiation dosimeters that can be used. The most frequently used dosimeters are either ionisation chambers or solid state detectors which include thermo-luminescence detectors (TLD), optically stimulated luminescence dosimeters (OSL), semiconductors detectors, and more recently, scintillation phosphors coupled with optical fibre (Bushong, 2013). The choice of the most suitable dosimeter depends on the clinical situation in which the measurements are required (Lemoigne & Caner, 2011). For instance, the measuring instrument should have the same properties (absorbed the same amount of energy) as the medium in which the dose is measured (Hobbie & Roth, 2007; Hendee & Ritenour, 2002).

3.6.1 Ionisation Chambers

An ionisation chamber detector consists of two electrodes within an air-filled chamber. An electric field across the two electrodes is used to collect the charges produced in the air by the ionisation due to incidence radiation. Since the ionisation chambers used in diagnostic radiology are vented air, correction factors should be applied to the readings. The correction factor is calculated using the following equation:

$$K_{TP} = (P_0.T) / (P.T_0)$$

Where P, T are the pressure and temperature of the ambient and P_0, T_0 are the pressure and temperature of the reference condition – 101.3 kPa and 293.2 k. The ionisation detectors are available in different types such as: free-air ionisation chambers, chambers for dose or air kerma measurement, and kerma area product (KAP) chambers (Hourdakis & Nowotny, 2014).

3.6.2 Semiconductor Detectors

These types of detectors are widely used in diagnostic radiology because of the small size and instantaneous response of the detectors (IAEA, 2007). There are two types of semiconductor detectors, namely, silicon diodes and metal oxide semiconductor field effect transistor (MOSFETs) (Hourdakis & Nowotny, 2014).

3.6.2.1 Silicon Diode Detectors

Electron-holes are formed in the diode body when a silicon p-n junction diode dosimeter is exposed to X-rays, resulting in an electrical current in the reverse direction. The magnitude of generated electrical current is proportional to the radiation dose. The main advantages of diode dosimeters over ionising chambers are their higher sensitivity and reproducibility. However, the sensitivity of the diode dosimeter is dependent on dose rate and diode temperature (Lemoigne & Caner, 2011).

3.6.2.2 MOSFET Detectors

MOSFET dosimeters have several advantages, including small size, immediate readout, high sensitivity and ease of use (Siebel et al., 2015). The first applications of MOSFET dosimeters to radiotherapy were in the late 1990s and since then they have been widely used in various medical applications such as dose verification in radiotherapy and diagnostic procedures (Wang et al., 2005). As reported by various researchers the metal oxide semiconductor field effect

transistor (MOSFET) is a measurement device which is finding increasing applications in diagnostic radiation field dosimetry (Frush & Yoshizumi, 2006; Hollingsworth et al., 2007; Hurwitz et al., 2007 & 2009; Jones et al., 2005; Miksys et al., 2010; Mukundan Jr et al., 2007; Sessions et al., 2002; Wang et al., 2005; Yoshizumi et al., 2003).

This type of detector consists of silicon transistor capacitors. One of the capacitor electrodes is replaced by semiconductor material. The basic structure of a MOSFET dosimeter is presented in **(Figure 3-9)**. The MOSFET comprises of a four-tier based structure with a source, drain, gate and body. The source and drain are about 1μm apart and metalized contacts are made to the both source and drain, generally aluminum. The rest of the substrate surface is covered with a thin oxide film, typically about 0.05 μm thick. On top of the insulating oxide layer, the gate electrode is laid. The body electrode is mounted against the gate as shown in **(Figure 3-9)** below. The detectors physical dimensions are approximately 3 mm diameter and 3 mm thick and are encapsulated in solid water material to produce a tissue equivalent protective layer around the detector. The types of MOSFET gate can be divided into two categories according to the polysilicon material (N–type or P– type), which consider the resistance of polysilicon gate power trench MOSFET. The N–type trench power MOSFET is usually lower gate resistance than P–type, due to lower sheet resistance of N-type in situ doped polysilicon (Baliga, 2008; Galup-Montoro & Schneider, 2007; Koivisto et al., 2015; Liou & Schwierz, 2003; Oktyabrsky & Peide, 2010).

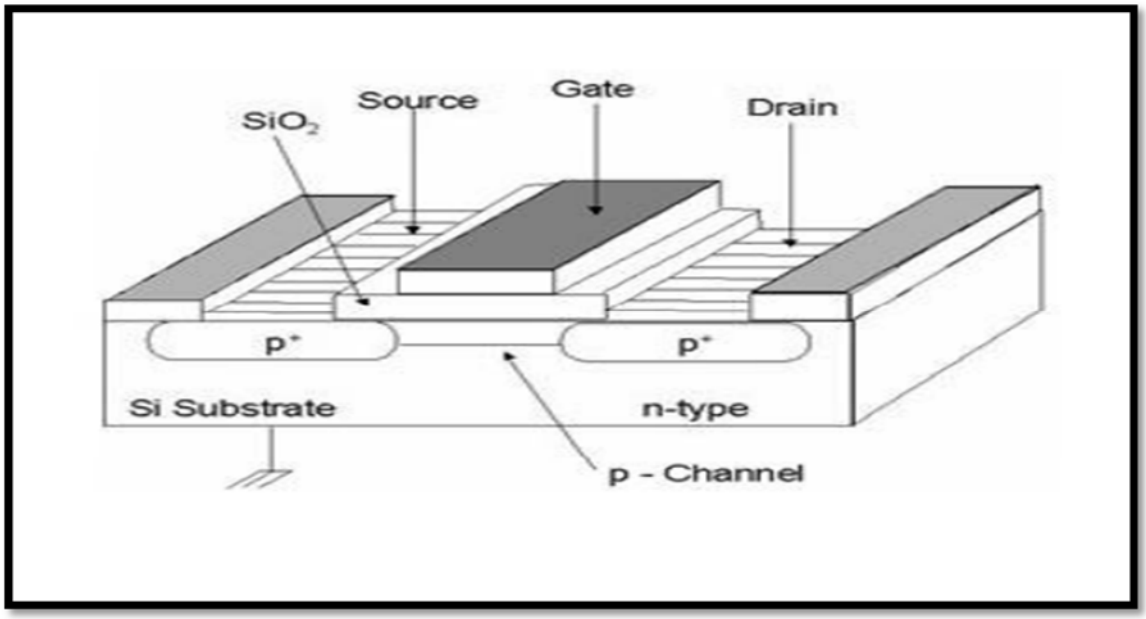

Figure 3-9: Basic schematic of a MOSFET dosimeter (Galup-Montoro & Schneider, 2007).

The main idea behind the operation of a MOSFET detector is the charging of the gate of the MOSFET detector by a build-up of charge produced by ionizing radiation (Oktyabrsky & Peide, 2010; VanDam & Marinello, 2006). The incidence of the X-ray in the gate region of the MOSFET will produce electron-holes pairs. The holes will move towards the silicon-gate interface producing a charge in the current of the n-type channel. Consequentially, a shift in the threshold voltage of the gate bias will occur. The value of this shift is directly proportional to the amount of the absorbed dose. Therefore, during irradiation MOSFET requires a connection to a bias voltage. This type of detector is mostly used for patient dosimetry (Hourdakis & Nowotny, 2014).

3.6.3 Thermo-Luminescence Dosimeters (TLDs)

3.6.3.1 TLD Principle

Thermo-Luminescence is a phenomena of light emission from an insulator or a semiconductor, resulting from previous energy absorption from a source of ionising radiation. It was initially discovered in 1663. Since then, many theories have been proposed to explain the thermo-luminescence of semiconductors or insulators. The explanation which depends on the electric energy band theory is the most acceptable one (Rivera, 2012).

There are many crystal materials which have the phenomenon of thermoluminescence when exposed to radiation. The crystal absorbs a fraction of the incidence radiation and it stores this in its lattice. If the crystal is heated then this absorbed energy can be released in the form of visible light. The TLD measures ionizing radiation exposure by measuring the visible light intensity emitted from the detector's crystal when is heated (Rivera, 2012). In a perfect semiconductor or insulator crystals, most electrons occupy the valance band which is detached from the conduction band, the highest energy level, by a forbidden gap (Bos, 2007). According to one trap-one centre model, there are two levels in the forbidden band gap: T level, which is located down to the conduction band above the Fermi level of equilibrium, and R level which is located above the valence band and below the equilibrium Fermi level. At equilibrium, both these levels are empty (Bos, 2007).

In brief, and as indicated by Bos, (2001), the thermoluminescence process occurs in several steps: a) the production electron-hole pairs in thermo-luminesce material by the absorption of ionising radiation energy, b) the trapping of the charge carriers in R and T levels, c) the de-

trapping of charge carriers by temperature rising, d) light production by recombination of charge carriers in luminescence centres at R level (Bos, 2001; Khan & Gibbons, 2014).

3.6.3.2 Thermoluminescence Dosimetry

In the middle of the twentieth century, tissue equivalency of some thermoluminescence materials led to the first utilisation of thermoluminescence as a radiation dosimeter. The perfect dosimetric materials should have an atomic number similar to that of human tissue which is 7.42 (Bos, 2001; Kitis et al., 2000). In addition to tissue equivalency, several characteristics are required for thermoluminescence which make it of interest as a dosimeter in clinical radiation dosimetry are the following: a) linearity, a linear response over wide range absorbed radiation dose; b) sensitivity, the amount of light produced per unit absorbed dose; c) independency of radiation energy; d) simple glow carve, resulting in a simple heating protocol; e) good mechanical strength and static chemical activity; f) low fading (Kortov, 2007; Rivera, 2012). The fading comprises of two components: pre-fad, which the decrease in thermoluminescence dosimeter response to radiation; and post-fad, which is the reduction in the storage signal in thermoluminescence dosimeter with time (Luo, 2008).

Currently, there are several commercial types of TLD. These TLD groups or types are divided according to the materials from which dosimeters are manufactured. Owing to this they are classified into three groups: LiF, CaF_2, and Al_2O_3. The first group (LiF) include TLD-100, TLD-100H, TLD-600, and TLD-600H. TLD-100; LiF was the first used TL dosimeter. It has good tissue equivalency ($Z_{eff\,TLD} = 8.04$ compared to $Z_{eff\,tissue} = 7.42$) which makes them have similar response to radiation as human tissue, also it is sensitive to low doses of radiation, it has a wide range of linear response (10μGy-10Gy) and also its low fading rate of around 5-10% per year (Bartolotta, & Marrale, 2006). Whereas TLD-100H dosimeters can be used in diagnostic radiology and are around 20 times more sensitive than TLD-100 detectors. They have a wide dose range (1 μGy – 20 Gy), and lower fading rate of around 3% per year. The TLD-600H dosimeter is used for neutron dosimetry. The dosimeter that is made of Al_2O_3 is the TLD-500 which has a useful dose range of 0.05 μGy – 10 Gy, with a 3% per year fading rate (Kortov, 2007). The chosen of the dosimeter depends on the dose range and which field to be used in. As reported by Rivera (2012), in diagnostic radiology the required dose range is of the order of 0.001 to 10 mSv, while that for radiotherapy is 0.1 to 100 mSv (Rivera, 2012).

3.6.4 Optically Stimulated Luminescence Dosimeters (OSLD)

These type of detectors were developed in the late 1990s. The operating principle of these dosimeters is similar to that of TLDs but the luminescence process is stimulated by laser light rather than heat (Canadian Nuclear Safety Commission [CNSC], 2012). These detectors are made of aluminium oxide (Al_2O_3) which emits visible light. The amount of emitted light is proportional to the absorbed radiation dose. For occupational radiation monitoring purposes OSLDs are preferred over TLDs (Bushong, 2013).

3.7 CIRS ATOM Dosimetry Phantoms

Phantoms made of tissue substitutes have been used extensively to physically represent human anatomy and mimic its radiation characteristics in dosimetric studies (Winslow et al., 2009). The purpose of using phantoms in dosimetric studies is to simulate patient's radiation exposure during specific radiological producers in order to measure dose or to mimic conditions for reference calibration of a dosimeter system or beam (e.g. radiotherapy beam calibrations by the use of water phantoms). In diagnostic imaging procedures, materials that have similar X-ray scattering and absorption to tissue are useful phantom materials, where such measurements have been used by several authors to calculate average organ doses as well as effective dose in both adult and paediatric diagnostic radiology examinations. Additional requirements for phantom materials are that they should remain stable/consistent over time, especially those with complex designs which need to be used for a long time. Phantoms are also necessary for the evaluation of radiographic equipment by the interpretation of phantoms images (Byng et al., 1998).

Quantifying organ doses in physical phantoms offers a distinct advantage over computational methods (Monte Carlo and DLP) because knowledge of the exact photon energy spectrum or irradiation geometry is not required. This is especially useful considering the increasing use of proprietary scanning techniques that are difficult to model, such as automatic tube current modulation in CT and automatic exposure control (AEC) in fluoroscopy. The majority of organ dose studies in diagnostic imaging utilise commercially available phantoms such as RANDO (The Phantom Laboratory, Salem, NY) or CIRS ATOM phantoms (Computerized Imaging Reference Systems, Inc, Norfolk, VA). In order to provide a representation of the human anatomy, these commercially available phantoms typically use three tissue equivalent materials imitating bone, lung, and soft tissue. To allow access to organ locations for the placement of

dosimeters, the RANDO and ATOM phantoms are assembled in axial slices 2.5 cm thick (Hurwitz, Yoshizumi, et al., 2007). Unfortunately, the widespread clinical use of these phantoms has been limited by their prohibitive costs (Winslow et al., 2009).

For organ dose or whole body dose measurements, Computerized Imaging Reference Systems (CIRS) currently produce different ATOM dosimetry phantom models covering a wide range in sizes (newborn to adult). Six models are available: newborn, 1-year, 5-year and 10-year old paediatric phantoms as well as adult male and female phantoms. The phantoms are made of tissue-equivalent epoxy resins, offer superior tissue simulation by covering a wider range of energy levels from diagnostic to therapeutic. Each phantom is sectional in design with traditional 25 mm thick sections. The sectional surfaces are extremely flat and smooth and do not require any special coatings or treatment. This results in minimal interfaces between the slabs when viewed in a scout or projection X-ray. The ATOM line also differs from other dosimetry phantoms by providing optimized TLD locations specific to 22 inner organs (CIRS, 2013).

3.8 Absorbed Dose Measuring Methods

According to the guidelines of national and international authorities, e.g. EU directives, the absorbed doses from diagnostic radiology to patients exposed to ionising radiation need to be determined. Therefore, *in vivo* dose estimations from patients undergoing radiological examinations or nuclear medicine procedures are performed. In addition, in diagnostic imaging anatomical phantoms are often used for direct absorbed dose measurements or indirectly via using software simulations (Hine & Brownell, 2013).

There are two main methods of measuring/estimating absorbed and effective doses. The first method uses dosimeters such as TLDs or MOSFETs and is known as direct measurement methods, the second method uses computer based simulations and is known as mathematical or Monte Carlo methods.

3.8.1 Direct Methods

As previously stated, in clinical dosimetry the main detectors used for absorbed dose measurements are ionisation chambers, TLDs and semiconductors. This direct approach of CT dosimetry uses a physical phantom. Radiation doses are measured in the location of organs or tissues of interest either by using TLDs or MOSFETs, the effective dose and effective risk can

then be calculated. This is can be an intensive laborious procedure but the time can be reduced by switching from TLDs to a near real-time MOSFET based dosimetry system (Hashemi-Malayeri & Williams, 2003).

3.8.2 Mathematical Modelling Methods to Estimate Dose

During a radiographic procedure there are many aids which may be to help estimate the radiation dose from an examination. For CT based acquisitions the two incides that are the most commonly used in day to day clinical practice are $CTDI_{vol}$ and DLP (Tootell et al., 2014). Other methods exist and estimate the absorbed dose to a patient using Monte Carlo software in order to simulate the CT scan geometry, protocol parameters and geometric patient models.

As reported by Hashemi-Malayeri and Williams, (2003), the first approach is the standard method based on the Food and Drug Administration (FDA) definition of Computed Tomography Dose Index (CTDI). This method is normally used for QA measurement and does not provide a direct assessment of the risk to the patient resulting from CT examinations (Hashemi-Malayeri & Williams, 2003). However, it is used to derive DLP which can be converted to patient dose using a set of conversion factors previously calculated for different regions of the body to give a value for effective dose (Paul et al., 2010), see **(Section 3.8.2.1)** on page **54**.

A second approach is the ImPACT method which uses the Monte Carlo (MC) computer technique that is combined with free in air values of CTDI. The MC computer techniques are used to simulate the absorption and scattering of x-ray photons within a mathematical phantom. This gives organ doses normalised to the free in air dose on the axis of rotation of the scanner, from which effective dose could be derived (Hashemi-Malayeri & Williams, 2003).

3.8.2.1 Estimating Effective Dose (ED) from DLP Using Conversion Factors

The CT-specific dose descriptors (CTDI and DLP) do not allow for comparisons with other sources of radiation exposures e.g. general radiography, nuclear medicine or natural background radiation. The only common factor which can achieve such comparisons is the effective dose which can be estimated mathematically using the value of DLP displayed on the scan console and the conversion factors which depend on the region of the body being scanned (Elbakri & Kirkpatrick, 2013; Nagel, 2007).

Effective dose can be calculated by multiplying the DLP by a conversation factor (k). The k coefficients are related only to the tissue involved in the volume being scanned and have been derived from Monte Carol (MC) simulation techniques and experimental measurements (Christner et al., 2010; Galanski et al., 2005; McCollough). Such k values are averaged over a number of CT systems and calculations are limited in that this provides only large determination of effective dose for a thin patient size and as noted by McCollough et al (2011), this standard patient is a little thin by today's standards (nominal body mass of 70 kg). Conversion coefficients are available in several publications including the American Association of Physicists in Medicine (AAPM) Report 96 and the National Council on Radiation Protection and Measurements (NCRP) Report 160 (McCollough et al., 2008; Prins et al., 2011; Schauer & Linton, 2009). Effective dose calculations in this way are limited in that they are independent of age, gender and scanner model (Kalender, 2014). During the 1990s, the k coefficient values were derived using ICRP report 60; however, in 2007, the ICRP published updated tissue factors. Owing to this, new k factor values were updated according to the new tissue weighting factors released by ICRP in 2007. The use of ICRP 103 weighting factors increased EDs in the head by ~11%, increased EDs in the chest by ~20%, and decreased EDs for pelvic scans by ~25% (Huda et al., 2011; Huda & Mettler, 2011; Kobayashi et al., 2015). Further limitations of this method include the possible underestimation of calculations in CT dose from differences in beam geometry between physical phantoms and the computer simulation software (Tootell et al., 2014). When estimating effective dose for helical scanning, using DLP and $CTDI_{vol,}$ there will be a possible underestimate of effective dose values due to the actual scan length which often exceeds the prescribed scan length. Most modern CT scanners calculate and display the values of DLP, with respect to integral scan length instead of prescribed length indicated with by the laser lights (Christner et al., 2010). The DLP cannot be used to estimate effective dose or detrimental cancer risk to individual patients, because as mentioned the k coefficients are for standard sized patients (Bauhs et al., 2008; McCollough et al., 2011) and calculations do not take into account the actual anatomy included within the scan volume.

3.8.2.2 Monte Carlo Simulations

With the continued growth and development of CT as a diagnostic imaging tool, as well the increasing utilization of MSCT and the complexity of MSCT scanning protocols, there is a greater need for accurate dose calculation tools. Owing to this, there is continued motivation to develop methods to accurately estimate absorbed radiation dose and, ultimately, the

radiological risk from CT examinations. While methods of radiological risk estimation using the effective dose approach have been developed (ICRP, 1991a; McCollough & Schueler, 2000), these methods require knowledge of the radiation dose delivered to each radiosensitive organ during CT scan examinations. However, direct measurements of CT organ doses *in vivo* are not possible, and estimates may be problematic because of the highly localized patterns of exposure in CT. These exposure patterns are characteristic of the scanning protocol and location, and yield variable doses to different organs (DeMarco et al., 2007).

Commercially available software for dose modelling is relatively quick and easy to use. The software employs Monte Carlo modelling techniques which are mathematical in origin and they simulate as closely as possible the real interactions suffered by photons. Such a technique allows for both organ and effective dose values for conventional radiographic techniques and CT imaging examinations to be estimated (Tootell et al., 2014).

The earliest methods of calculating the dose to the organs from CT scan examinations applied Monte Carlo simulation methods that used the mathematical geometric hermaphrodite model of a standard man MIRD phantom or they use the results of these methods to derive it (ImPACT, 2006; Kalender et al., 2011 & 2014).

One of the earliest attempts was by Zankl et al.; (1995) who investigated organ doses to paediatric patients using voxelized models (the GSF tomographic paediatric models). Both baby and child models were available and were generated from whole body CT data of real patients. Within this work they created a catalogue of organ dose exposures normalized to air kerma free-in-air on the axis of rotation by simulated CT scans; they tabulated these for two beam energies and two scan geometries (tube voltage: 80 and 125 kv, total filtration: 2.2 mm Al + 0.2 Cu, mean photon energy: 50.5 kev and 64.4 kev, half-value layer: 5.38 mm Al and 7.98 mm Al) (Zankl et al., 1995). The effective dose has been estimated by Caon et al.; (1999), using a voxelized model of a 14-year-old female and different CT scan protocols. In this work fifty-four consecutive CT scans were used to construct a tomographic computational model of a 14-year-old female torso suitable for the determination of organ doses from CT (Caon et al., 1999). In 2002, Schmidt and Kalender developed a fast voxel-based Monto Carlo simulation program known as (ImpactMC) to calculate dose distributions specifically for both the respective CT scanner and the individual patient anatomy. The calculations were performed on a 3-D voxel volume that can be filled with either the CT data of patients or mathematical phantoms converted to voxel volume data (Schmidt & Kalender, 2002). The effects of scan

protocol, specifically over-scanning; on voxelized cylindrical and anthropomorphic phantoms from a MSCT were been simulated by Tzedakis et al.; (2005). They estimated the effective doses for four standard CT examinations, (head and neck, chest, abdomen and pelvis, and trunk studies). The boundaries of these regions at the z axis were 0–70, 0–43, 43–70, and 70–95 cm for trunk, abdomen and pelvis, chest, and head and neck, respectively. Data were obtained for both axial and helical modes of operation taking into account the helical z-axis over-scanning. The validity of the MC simulation was verified by a comparison of calculated and measured standard computed tomography dose index (CTDI) dosimetric data, and a comparison of calculated and measured dose profiles along the z axis (Tzedakis et al., 2005).

Advances in computer technologies have led to the introduction of MC methods to simulate complex problems (Guimaraes, Moralles, & Okuno, 2008). The MC simulation methods applied to calculate the organ dose from CT examinations uses a CT dose spreadsheet developed by the UK's ImPACT group (ImPACT, UK). The ImPACT work is based on the simulations performed by the National Radiological Protection Board (NRPB) (ImPACT, 2006) using a standard mathematical anthropomorphic model (MIRD V) model and voxelized patient data. Although some of these methods allow the user to input either axial or spiral CT scanning protocols, radiation dose estimates from the helical scan protocols are approximated from the contiguous axial scan data and are not derived directly from simulations of a spiral acquisition (DeMarco et al., 2007; Jansen & Shrimpton, 2011; Jarry et al., 2003).

3.8.2.3 Modelling Absorbed Dose

The dose modelling process involves the computer simulation of a phantom being exposed to a large number of photons of varying energies emitted from a point source (Tootell et al., 2014). Calculation of photon transport is based on stochastic mathematical simulation of interactions between photons and matter. By following the path of the photons that are emitted from a point source into the solid angle specified by the focal distance and the X-ray field dimensions, while they interact with the phantom according to the physical processes that they may undergo photo-electric absorption, coherent (Rayleigh) scattering or incoherent (Compton) scattering. This chain of interactions forms a so-called individual photon history. The deposition of energy to the organ at each interaction point is calculated and stored for dose calculation. A large number of independent photon histories is generated, and estimates of the mean values of energy depositions in the various organs of the phantom are used for calculating the doses in these organs (Tapiovaara et al, 1997; Tootell et al., 2014).

3.8.2.4 ImPACT CT Dosimetry Software

ImPACT software is a quick and easy method for calculating of both organ and effective dose. **(Figure 3-10)** shows a sample of the dose report generated using the ImPACT CT Dosimetry software, as calculations take into account specific features of each CT unit (e.g. radiation quality and field geometry), the results are dependent on selecting the correct imaging parameters and CT model (Tootell et al., 2014). The NRPB have published organ doses for several models of CT scanners normalised to CTDI measured in air. Effective dose can be easly calculated using these data, however, as the new CT scaning technology and systems are constantly being introduced which makes it not always possible to select the correct scanner. Currently, the dose simulation software does not include many new systems and in this situation means dose simulations often have to rely on a "best fitting" approach to the attributes of these scanners to those of a similar design (Huda et al., 2011; Tootell et al., 2014). As reported by Groves et al., (2014) this can lead to the potential of introducing a significant error in the estimated dose (Groves et al., 2014). Also, automatic manipulation of mA by the scanner (ATCM) can introduce an error as the software only allows a single value to be used (Tootell et al., 2014). The main objectives of this simulation software are to determine the effective dose. In order to achieve a calculation of effective dose the average equivalent dose to 12 organs and tissues for which weighting factor have been assigned and other of eight reminder organs must be assigned (ICRP, 1991a). The total average of the equivalent dose multiplied by the relevant weighting factor is summed to give the effective dose.

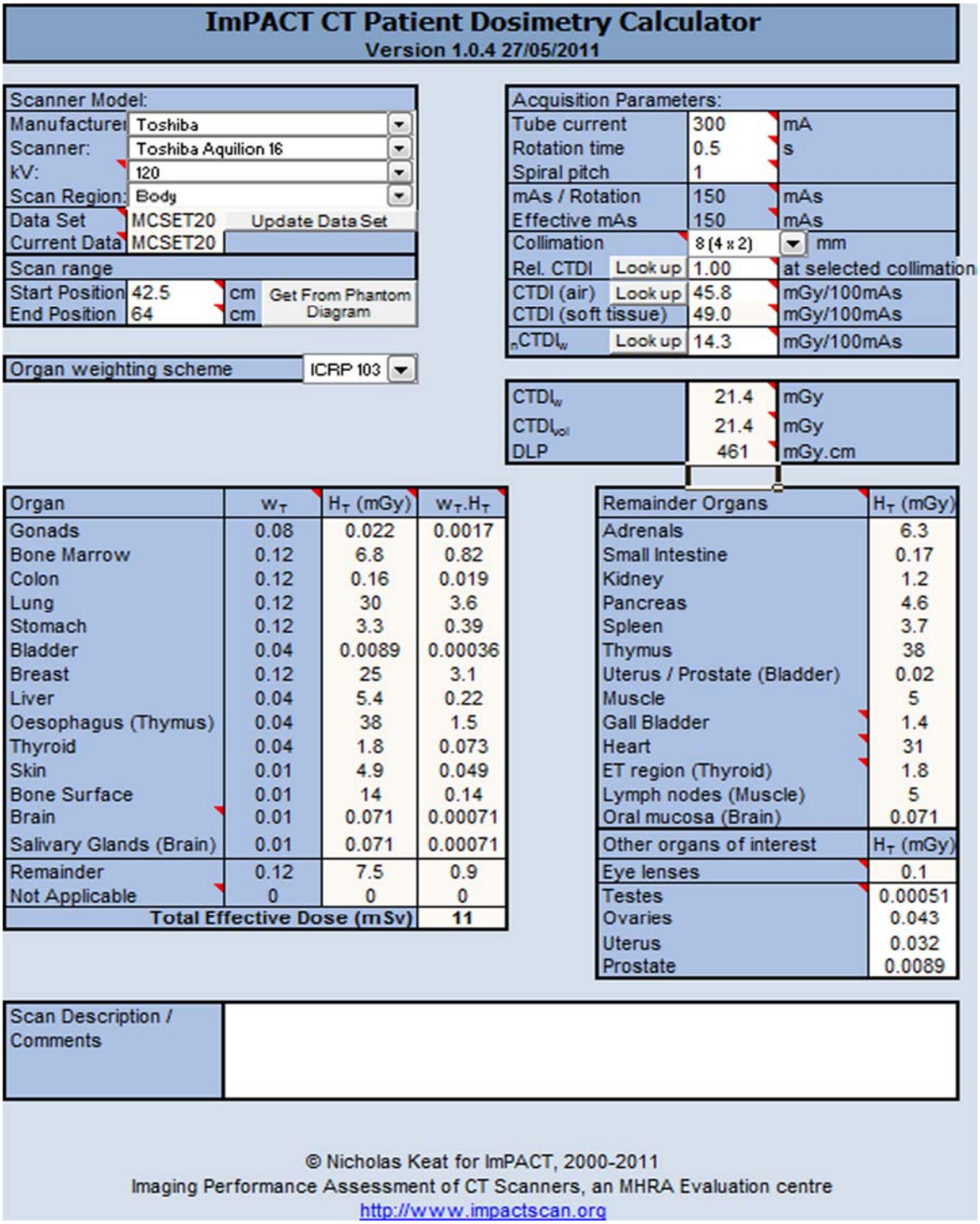

ImPACT CT Patient Dosimetry Calculator
Version 1.0.4 27/05/2011

Scanner Model:			
Manufacturer	Toshiba		
Scanner:	Toshiba Aquilion 16		
kV:	120		
Scan Region:	Body		
Data Set	MCSET20	Update Data Set	
Current Data	MCSET20		
Scan range			
Start Position	42.5	cm	Get From Phantom Diagram
End Position	64	cm	

Acquisition Parameters:			
Tube current	300	mA	
Rotation time	0.5	s	
Spiral pitch	1		
mAs / Rotation	150	mAs	
Effective mAs	150	mAs	
Collimation	8 (4 x 2)	mm	
Rel. CTDI	Look up 1.00	at selected collimation	
CTDI (air)	Look up 45.8	mGy/100mAs	
CTDI (soft tissue)	49.0	mGy/100mAs	
$_nCTDI_w$	Look up 14.3	mGy/100mAs	

Organ weighting scheme: ICRP 103

$CTDI_w$	21.4	mGy
$CTDI_{vol}$	21.4	mGy
DLP	461	mGy.cm

Organ	w_T	H_T (mGy)	$w_T.H_T$
Gonads	0.08	0.022	0.0017
Bone Marrow	0.12	6.8	0.82
Colon	0.12	0.16	0.019
Lung	0.12	30	3.6
Stomach	0.12	3.3	0.39
Bladder	0.04	0.0089	0.00036
Breast	0.12	25	3.1
Liver	0.04	5.4	0.22
Oesophagus (Thymus)	0.04	38	1.5
Thyroid	0.04	1.8	0.073
Skin	0.01	4.9	0.049
Bone Surface	0.01	14	0.14
Brain	0.01	0.071	0.00071
Salivary Glands (Brain)	0.01	0.071	0.00071
Remainder	0.12	7.5	0.9
Not Applicable	0	0	0
Total Effective Dose (mSv)			11

Remainder Organs	H_T (mGy)
Adrenals	6.3
Small Intestine	0.17
Kidney	1.2
Pancreas	4.6
Spleen	3.7
Thymus	38
Uterus / Prostate (Bladder)	0.02
Muscle	5
Gall Bladder	1.4
Heart	31
ET region (Thyroid)	1.8
Lymph nodes (Muscle)	5
Oral mucosa (Brain)	0.071

Other organs of interest	H_T (mGy)
Eye lenses	0.1
Testes	0.00051
Ovaries	0.043
Uterus	0.032
Prostate	0.0089

Scan Description / Comments

Figure 3-10: Example of an ImPact CT Dosimetry software dose report (Tootell et al., 2014).

As reported by Tootell et al., (2014) computer simulation is frequently reported as underestimating CT doses in the range of between 18 and 40% (ICRP, 1977, 1991a; Tootell et al., 2014). Explanations for these underestimations are due to the differences in the physical dosimetry phantoms and the virtual phantoms used by the dose modelling software and the simplified geometric shapes of the organs.

Salvado et al. (2005) used MC based methods to estimate doses to both phantoms and some patient-based voxel models and compared these to $CTDI_w$. They demonstrated that $CTDI_w$ values significantly underestimate organ doses to both phantoms and patients. They reported the percentage differences in the normalized effective dose between contiguous axial and helical scans with a pitch =1, many reach 13.1%, 35.8%, 29.0%, and 21.5%, for head and neck, chest, abdomen and pelvis, and trunk studies, respectively (Tzedakis et al., 2005).

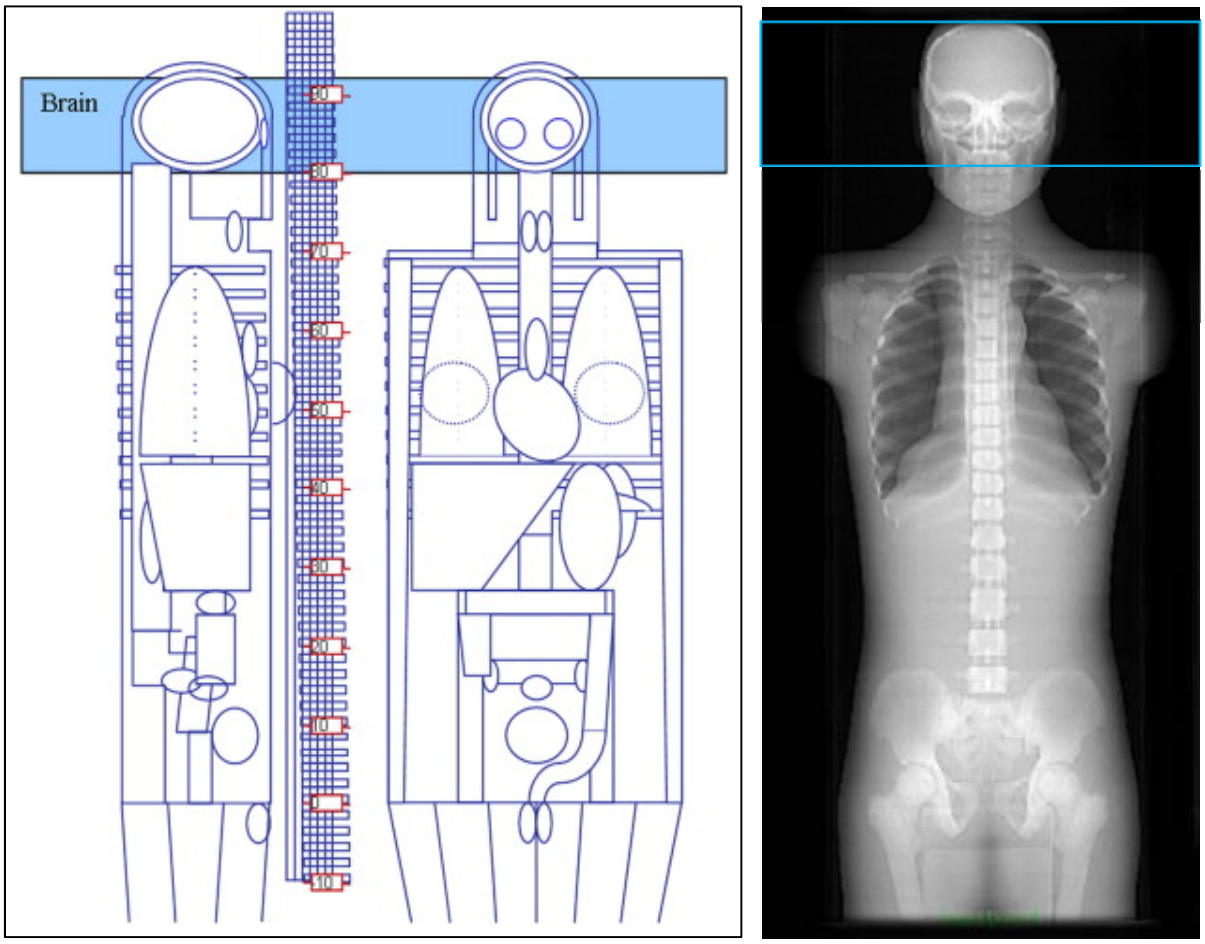

Figure 3-11: ImPACT image showing a typical brain scan acquisition volume, staring at 80 cm and ending at 93 cm (Elbakri & Kirkpatrick, 2013) and an anterior-posterior scout view of the adult ATOM phantom (CIRS, 2013).

3.9 Risk from Exposure to Low Radiation Doses

The term risk according to the epidemiologists is utilised to describe the association of data of cancer incidence and radiation exposure in two different patterns: relative risk that relates to the ratio of cancer incidence rate in an exposed population to that in an unexposed population;

and absolute risk which is the simple rate of cancer incidence in a specific population (NAS, 2006). To express the lifetime risk several methods can be used:

1. Excess Lifetime Risk (ELR), this type of risk compares cancer incidence or mortality in two groups of the same population - one of them is theoretically exposed to radiation and the other is not;
2. Risk of Exposure Induced-death (REID), that compares the death rate of specific causes in theoretically unexposed and exposed groups of a certain age and gender;
3. Loss of Life Expectancy (LLE), which gives an impression of the period of life lost due to radiation;
4. Lifetime Attributable Risk (LAR), which gives an account of excess mortality or incidence of cancer over a study period, with the backgrounds defined by a theoretically unexposed population (ICRP, 2007).

As stated by Statkiewicz-Sherer, et al., (2010), the damage produced by ionising radiation due to energy deposition in tissue is referred to as the radiation risk. This energy may result in ionisation within the tissue if the photons pass near an orbital electron and provide sufficient energy for the electron to be liberated from the atom. The amount of damage to tissue is related to radiation dose, type of radiation, whether it is internal or external, time of exposure, radiation distribution (type of exposed tissue) and the individual's sensitivity which influenced by gender and age (HPA, 2011). Females are at higher risk of radiation induced cancer than males (Balonov & Shrimpton, 2012). Young patients are at higher risk because they have a longer remaining life span. For example, as illustrated by Lin, (2010) the risk of radiation damage for a 20 years old patient is twice to that of a 40 years old patient. The latter has double the risk when compared to a 60-year-old patient. The radiosensitivity of young children is 3-4 times more than that of adults.

Generally, the interactions of radiation with tissue are either direct, when the radiation energy is directly transferred to the DNA causing structural change in its molecules; or indirect interaction, wherein the radiation energy is absorbed by water molecules forming free radicals which in turn cause damage to the DNA molecules. As reported by Suzuki & Yamashita (2012), it has been found that for X-ray exposures of 100 mGy, 30-40% of the DNA damage is due to direct interaction and the remaining 60-70% of the damage results from indirect interactions. The adverse health effects of radiation can be classified into two groups: deterministic effects, that follow high radiation doses and result in relatively immediate and

predictable tissue reactions and damage (this damage can occur within minutes, hour, days and even weeks); and stochastic effects, which follow low radiation doses and may result in cancer development (ICRP, 2007). Development is based on probability, the lag period between irradiation and cancer development for stochastic effects is at least 5 years and may reach to 10 or 20 years (Lin, 2010).

Stochastic effects usually occur due to mutations in DNA which occur randomly. In general, the probability of stochastic effects occurrence increases as the radiation dose increases. The dose-response curve determines the probability of stochastic effects occurrence with radiation dose being the root cause. Both linear and linear-quadratic dose-response carves are used to describe the relationship. However, the severity of the resultant disease is not related to radiation dose because the cancer produced by 2 Sv radiation dose is not more severe than cancer produced by 0.2 Sv radiation dose. Stochastic effects are classified into radiation-induced cancer and reproductive cell damage which affects sperm and ova and causes defects in offspring (Statkiewicz-Sherer, et al., 2010). As stated by Brenner, (2014), for radiological doses ranged from 5 to 100 mSv, data from life-span studies (LSS) of atomic bombs survivors revealed that the risk of radiation-induced cancer was strongly related to the radiation dose received. However, for low doses and since more than 60% of the LSS cohort received radiation doses between 5 and 100 mSv, no strong evidence available to describe the relationship between the risk of radiation-induced cancer and these low doses.

Persistent controversy exists in the literature regarding the risk of radiation-induced cancer from low dose ionising radiation. This creates big challenge for epidemiological studies. In this context controversy arises in questions about the dose threshold of cancer production, linearity and gradient of dose-response curves (Griffery & Sodickson, 2009). Overall there are two opposing risk models to estimate the risk of low radiation doses. The first one adopt the linear no-threshold principle (Griffery & Sodickson, 2009). Based in this model any dose however small can result in cancer incidence. Whereas the second model propose that there is a specific threshold for radiation induced cancer and below this threshold the radiation dose can be considered as safe (Prasad et al., 2004). Although, the ICRP (2007), and the National Academy of Sciences (NAS) (2006), have adopted the linear no-threshold (LNT) model, United Nations Scientific Committee on the Effects of Atomic Radiation UNSCEAR (2008), considered the LNT to be uncertain at radiation doses less than 100 mSv and it is no longer recommended for

radiation-induced cancer assessment from such doses. This has motivated many researchers to investigate the reliability of this model using different data sources.

A study conducted by Dobrzynski et al., (2015), evaluated the risk of radiation-induced cancer and early childhood death for populations living in regions with different natural background radiation. They concluded that the risk of radiation-induced cancer due to such small doses and dose rates tends not to exist or is lower than expected by the LNT model. This can be explained by the adaptive physiological mechanism of tissue. In conclusion, they reported that for low doses and low dose rates the LNT model is exaggerating the risk of radiation-induced cancer. The analysis of LSS cohort data for participants who received radiation doses ranging between 0-150 mSv illustrated that the risk of radiation-induced solid cancers is linear but at less than 100 mSv the cancer incidence increment is statistically insignificant (Suzuki & Yamashita, 2012).

The feasibility of LNT model has been investigated by Kleinerman, (2006); Linet et al., (2009) using risk data in children after diagnostic and/or therapeutic radiation exposure. Several major studies that investigated childhood cancers following benign disease radiation treatment and diagnostic procedures were reviewed by Kleinerman, (2006). The study reported that the rates of brain, thyroid, breast, skin (non-melanoma) cancers, and leukemia, were seen to be increased due to childhood irradiation. This study also found that cancer risk increases with dose increment (Kleinerman, 2006). More recently Linet at al., (2009) highlighted studies that investigated the association of maternal prenatal and postnatal newborn radiation with childhood cancers. They stated that the data about this relationship is limited and more research is required (Linet et al., 2009).

The low dose risk of radiation-induced cancer in patients subjected to recurrent CT examinations has been evaluated by several investigators. Pearce et al., (2012) carried out a retrospective cohort study for patients who had CT examinations and the subsequent risk of radiation-induced leukemia and brain tumours. In their cohort they analysed data for patients younger than 22 years who had attended CT scan examinations within the UK NHS between 1985 and 2002, with the follow-up process continuing until the end of 2008. They found that when the patient radiation cumulative dose increased from 5 mSv to approximately 50 mSv the relative risk of radiation-induced leukemia became 3.18, and 2.82 for brain tumours when the cumulative dose increased from 5 mSv to approximately 60 mSv. Similarly, Mathews et al., (2013), evaluated the cancer incidence in 680.211 patients (0-9 years old) who had undergone

CT scan examinations between 1985 and 2005 with follow-up until 2007. A 24% increase in different tissue cancers was noted when compared to the general Australian population within the same age range (Mathews et al., 2013).

In conclusion, as stated by Brenner (2014); and de Gonzalez & Darby (2004), the accurate determination of radiation-induced cancer from low radiation dose is not easy. The limited data available about the risk from low radiation dose has resulted in controversy and uncertainty. According to the available data, the risk of radiation-induced cancer from low dose radiation is very small but unlikely to be zero (Wall et al., 2006). Therefore, the linear no-threshold (LNT) model may be the best reasonable risk model for describing the relationship between the exposure to low energy radiation and solid cancer incidence (ICRP, 2007; Little et al., 2009; NAS, 2006). To overcome uncertainty about the LNT model (Dobrzynski et al., 2015), Wall et al., (2006) recommended the classification of low dose radiation cancer into four categories, as illustrated below in **(Table 3-4)**.

Table 3-4: X-ray examinations divided into four broad risk bands (Wall et al., 2006).

Risk Band	Risk Range	Typical type of X-ray examination
Negligible	< 1 in a million	Radiography of chest, limbs and teeth
Minimal	1 in a million to 1 in 100 000	Radiography of head, neck and joints
Very low	1 in 100 000 to 1 in 10 000	Radiography of spine, abdomen and pelvis
Low	1 in 10 000 to 1 in 1000	CT, angiography, contrast studies of the alimentary, biliary and urinary tracts, and interventional radiology

3.10 Chapter Summary

This chapter gave an overview of CT scanner history and technology developments. This chapter also discusses the most important parameters within each CT examination that influences the radiation dose, as well the different CT physical dose measurement parameters. The examination protocol used in imaging procedures is the decisive factor that determines the radiation dose. It is important to note that it is extremely difficult for radiographers or radiologists to predict the amount of dose the patient will receive based on the chosen protocol and therefore they may not always be using the lowest dose practically possible. It is therefore possible that a new proactive way of estimating dose to patient is rapidly needed.

All modern CT scanners display CTDIw which takes all scan parameters into account, including the pitch in helical scans and a series of axial scans. It is a reasonable representation of the

average dose in the scanned volume. However, the displayed dose is for a specific phantom setup, e.g., the 32-cm or 16-cm PMMA phantoms in body and paediatric or head scans, respectively. As reported by Suess & Chen, (2002), in many cases these phantoms used to determine the displayed $CTDI_w$ may not represent the actual patient. This is also true in paediatric CT: because of the significantly smaller cross-sectional diameter, the patient receives a higher dose than indicated by the displayed reading. Also, they indicated that depending on object size the dose in phantoms/patients of, for example, 16-cm diameter can be two times higher than the displayed $CTDI_w$ of that obtained using 32-cm phantom. Knowledge of the dose in the scanned volume is essential to optimize scan protocols, but for reasonable dose management one has to consider the biological effect of this dose, i.e. the radiation risk caused by the CT examination. The deterministic radiation risk is best represented by the ‘‘effective dose’’. However, for low radiation doses such as doses from CT scans examinations, the best way to consider that is to estimate the life time cancer risk inductions. This takes into account the dose to all sensitive organs and their radiation risk factors for both genders at different age. This is the focus of this thesis, which aims to provide prospective way to estimate the lifetime cancer induced per 10^6, effective dose and eye dose for adult (helical and sequential) and paediatric (helical) CT protocols. This prospective risk method, is essential for analysis of radiation dose and risk versus benefit and should be used to give risk estimates to patients and help justify the examination. Presently, no CT manufacturer provides such information on the scanner console to either the radiographer or radiologist.

Radiation risk has been regularly reviewed by a variety of organisations nationally and internationally. At the international level, there are the ICRP and the United Nations Scientific Committee on the Effects of Atomic Radiation (UNSCEAR). At national levels, there are the UK Radiation Protection Division of the Health Protection Agency and the US National Council on Radiological Protection and Measurements (NCRP), as well as the US National Academy of Sciences Biological Effects of Ionizing Radiation (BEIR) committees (Hall & Brenner, 2014). All of these bodies agreed that, for doses < 100 mSv, the most appropriate risk model for radiation protection purposes is one in which the risk of radiation induced stochastic effects, is particular cancer induction, is assumed to decrease linearly with decreasing dose with no threshold which so-called linear no-threshold (LNT) model (Hall & Brenner, 2014; ICRP, 2007c; NCRP., 2001). The risks to individuals from diagnostic radiation exposures are generally small; it is often difficult to study them directly. However, because of the large

number of people exposed annually, even small risks could translate into a considerable number of future cancers.

Chapter 4 : Literature Review

4.1 Chapter Overview

The largest contributor to population radiation dose from diagnostic imaging is CT, this will now be considered in further detail including an examination of the global frequency of CT examinations and the resultant radiation doses. CT scans are an extremely useful part of modern medical practice although it is well acknowledged that potential cancer risks exist from the use of ionising radiation. The discussion reported in this chapter reviews the current status of opinion regarding the perceived risks (lifetime attributable risks) from radiation exposure at the low dose levels relevant to diagnostic CT examinations. Also within this chapter there is a focused discussion of the radiation risks associated with paediatric CT imaging and a summary of the current attitudes within this area.

4.2 Research Strategy

A comprehensive literature search was conducted of scientific online databases, in order to identify literature relevant to this thesis using the following search engines: EBSCO Information Services, CINAHL, Ovid-Medline, Cochrane, SCOPUS, Pub-med, and Google Scholar. In addition, books were also used for background information relevant for the purposes of this thesis. To acquire scientific literature on the radiation dose from adult and paediatric CT scan head/brain examinations, lifetime attributable cancer risk, the following key words were used: CT brain examinations, CT brain radiation dose or high radiation dose among imaging modalities, CT acquisition protocols, CT head/brain protocol parameters and techniques for CT dose reduction and CT organs and tissues absorbed dose or CT effective dose or X-ray radiation risk calculation and estimation.

To ensure that important seminal studies conducted many years ago were also captured in the search results, there was no time limit on the search. The entire search was limited to English-language journals, and related to human and animal subjects. The search operators (AND, OR, NOT) were used where necessary to refine the search. For the purposes of this thesis, the literature review was presented in a narrative format, under a series of key themes.

4.3 Radiation from Medical Exposures

The use of ionising radiation in modern medicine is necessary for both diagnosis and treatment. As reported by the United Nations Scientific Committee on the Effects of Atomic Radiation, UNSCEAR, (2010), there is now more than one diagnostic examination performed per person across the population every year in countries with advanced health care systems (UNSCEAR, 2010). The UNSCEAR reported that globally, there are approximately 3.6 billion diagnostic examinations and six million therapeutic treatments performed annually. These medical practises involving the use of ionising radiation include diagnostic examinations, interventional procedures and radiotherapy treatments and are typically undertaken in radiology, nuclear medicine and radiation oncology departments or clinics (UNSCEAR, 2010). For medical purposes, the people exposed to ionising radiation are the patients themselves. Recent figures demonstrate that diagnostic medical exposures, including radiology and nuclear medicine, account for about one-fifth of the average annual per caput dose to the global population from all sources (UNSCEAR, 2010). The National Council on Radiation Protection & Measurements (NCRP) (2009) reported that from all of the diagnostic imaging modalities, CT is the highest contributor to population dose, even though it accounts for a much smaller proportion of the total number of examinations (Schauer & Linton, 2009).

Evidence from epidemiological studies prove that it is impossible to deny the association between an increase in cancer incidence and morbidity and ionising radiation exposure (ICRP, 2005). By contrast, quantifying the risk associated with low dose radiation exposures, such as a typical CT scan, is more complex and contentious. As reported by Brenner and Hricak, (2010) and Brenner et al., (2003) despite the uncertainty surrounding risk associated with low dose exposures, the societal risk may not necessarily be negligible and must still be considered, this concern arises when an increasingly large population is exposed to small individual risks (Brenner et al., 2003; Brenner & Hricak, 2010; Wall et al., 2014). Children are more radiosensitive than adults thus; the risk of radiation exposure is even higher than for adults. The difficulties involved in quantifying the risks of low dose radiation are well known, two important questions have been addressed by many researchers, firstly, what is the lowest radiation dose which provides good evidence regarding increasing existing cancer risks in humans? According to the most recent literature and epidemiological evidence this is approximately 10 – 50 mSv for an acute exposure and approximately 50 – 100 mSv for a protracted exposure (Hendee & O'Connor, 2012). The second question is what is the most

appropriate way to extrapolate such cancer risk estimates to even lower doses? As supported by experimentally grounded, quantifiable, biophysical arguments, a linear extrapolation of cancer risks from intermediate to very low doses currently appears to be the most appropriate methodology (Brenner et al., 2003; Brenner & Hall, 2012; Hricak et al., 2011; Wall et al., 2006).

4.4 CT Usage and Radiation Exposure

Introducing CT into routine care has improved healthcare outcomes, however, CT delivers higher radiation dose than conventional diagnostic X-ray examinations. The radiation dose to a patient from CT, for some examinations, can reach more than 100 times the dose received from routine radiographic examinations (de González et al., 2009). In the last decade, a number of research studies have focused on the cancer risk associated with radiation exposure due to medical diagnostic imaging modalities. These discussions focused on CT being a relatively high dose modality, which is potentially over-utilised and due to lack of understanding of the risk associated with certain acquisition parameters (Brenner, 2002; Brenner et al., 2001a; Brenner & Hall, 2007; de González et al., 2009; Einstein, Henzlova, & Rajagopalan, 2007; Fazel et al., 2009; Hall & Brenner, 2008; Hammer et al., 2011; Smith-Bindman, 2010; Smith-Bindman et al., 2009; Brenner, 2010). Even deterministic effects, as reported by the US Food and Drug Administration (FDA), such as hair loss, have been reported in incidents in the US from apparent erroneous over-doses due to CT brain perfusion scans (FDA, 2009, 2010).

CT imaging procedure delivers approximately 70% of the overall radiation dose to the paediatric population. Crude estimations showed that the ED ranges from between 6 and 100 mSv for paediatric patients. CT is a major source of medical radiation and its availability and frequency of scanning is responsible for increasing the population dose. Due to the high ED of CT, an effort to minimize it is critically important. This is especially important in children, because the younger the patient is at the time of exposure to radiation, the greater the risk (BEIR VII Phase 2, 2006). Due to the higher radiosensitivity of children's cells, the lifetime cancer risk associated with an individual CT examination is higher in children than in adults (ICRP, 2007a) and there is an increased risk for thyroid, skin, brain and breast cancer in children (UNSCEAR report, Annex I, 2000). In addition, due to a child's longer lifetime to manifest radiation-induced cancer, and the fact that cancer risk is cumulative over a lifetime, radiation risk from CT in children is one of the major current concerns in CT dosimetry (Akhlaghi, Hakimabad, & Motavalli, 2014).

Over the years, CT technology has evolved, with various impact on the radiation dose. After the introduction of conventional CT, helical CT became commercially available in 1991. Because of its new advantages, the use of CT imaging increased in the paediatric population. Although helical technology provides additional opportunities for CT in children, the radiation dose associated with helical CT is much greater than the radiation dose associated with sequential CT.

In all developed countries the use of CT scans has increased rapidly since its inception in the 1970s, although its usage rates vary greatly from one country to another. A worldwide survey conducted by UNSCEAR from the mid-1990s, has shown increases in the number of CT machines per million population in nine countries as shown in **(Figure 4-1)**, the number of CT scanners per million populations was 64 in Japan, 26 in the US and 6 in the UK (Hall & Brenner, 2008; UNSCEAR, 2000c, 2010).

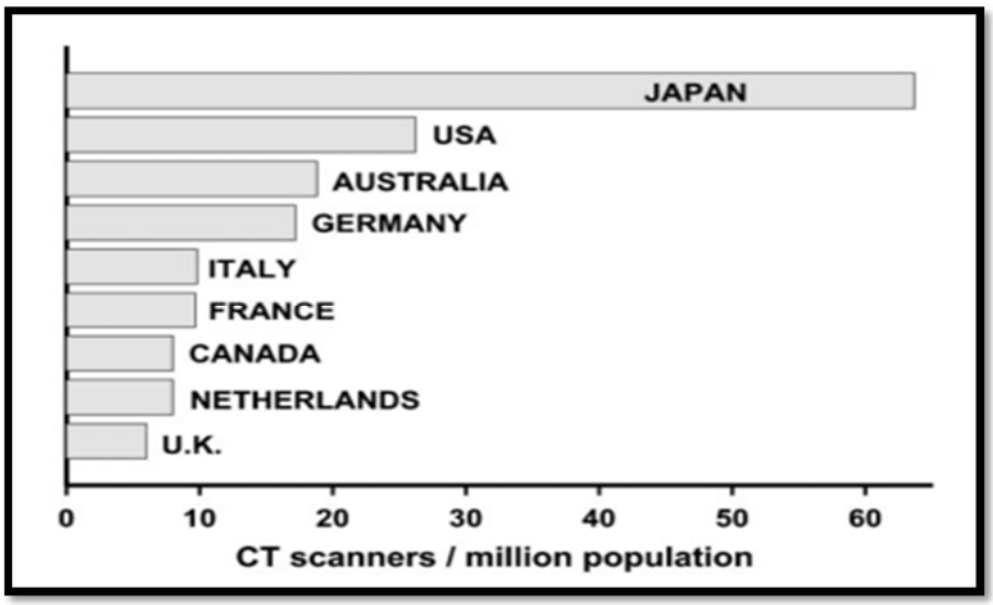

Figure 4-1: Number of CT scanners per million population in selected countries in the 1990s (Hall & Brenner, 2008).

A retrospective study was conducted by Miglioretti et al., (2013), the use of CT for children up to 15 years old from 1996 to 2010, including 4,857,736 child-years of observation. Radiation doses were calculated for 744 CT scans performed between 2001 and 2011. As stated in **(Figure 4-2)**, their results showed that the use of CT increased between 1996 and 2005, remained stable between 2005 and 2007, and then began to decline. The solid lines show rates for children younger than 5 years of age; the dashed lines show rates for children 5 to 14 years

of age. The gray lines show rates at each health system, and the red lines show the average rates across health systems.

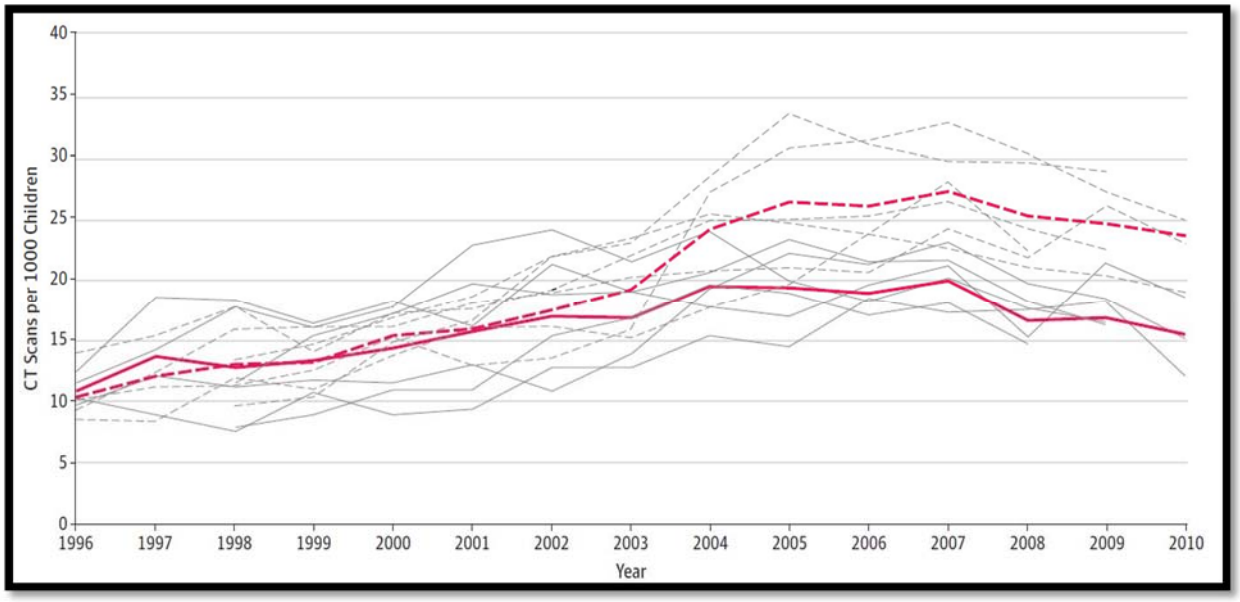

Figure 4-2: Trends in the use of CT over time, by age group and year (Miglioretti et al., 2013).

De Gonzalez et al., (2009) pointed out that the total number of CT scan examinations performed annually in the US has increased approximately sevenfold between 1981 to 1995 (from 2.8 million to 20 million). By 2007, the number of CT examinations had increased to approximately 70 million scans per year, including at least 4 million for children. In Britain, it has been estimated that about 11% of diagnostic radiology procedures are CT examinations, however, their contribution to the collective dose is approximately 70% (Brenner & Hall, 2007; de González et al., 2009; Elliott, 2009; Dougeni et al, 2012).

There is a substantial variation in the radiation dose for the same type of CT examination between sites, this information was identified by a number of studies and surveys and potentially means that using the average radiation dose as an indicator of CT dose levels may be misleading. Their results show there is a large variability in scanning technique and a resultant large range of ED obtained, reflecting the increasing complexity of CT scanning. High radiation doses were observed in some centres that carry out limited paediatric studies (Moss and McLean, 2006). Effective dose was closely associated with mAs, with most centres using lower mAs for younger patients, but few centres reducing the kVp for paediatric patients. It is often difficult to achieve a balance between radiation dose and the attainment of diagnostic

information. The indication for the CT often affects the protocol and scanning parameters chosen. Feedback and education for these centres is needed to avoid inappropriate high radiation doses in the potentially susceptible paediatric patient population. It is important that CT technique is tailored to the child and that CT is only used when there are good clinical indications. Surveys of practice in the UK suggested a 40-fold variation of ED for a given examination between departments, and an Australian survey found up to 36-fold variation in ED for comparable studies between centres (Moss and McLean, 2006). A survey was conducted to investigate the frequency of CT examinations for paediatric patients below 15 years of age in 128 CT facilities in 28 developing countries of Africa, Asia and Eastern Europe and to assess the magnitude of CT doses (Muhogora et al., 2010). Eleven CT facilities in six countries were found to use adult CT exposure parameters for paediatric patients, thus indicating limited awareness and the need for optimisation. The results of the studies and surveys emphasize the need for continuing education and protocol review, particularly in paediatric CT examinations, in a complex and fast changing environment (Moss & McLean, 2006; Muhogora et al., 2010; Shrimpton et al., 2006; Smith-Bindman et al., 2009; Wallace et al., 2010).

Brenner, (2002) suggests that more attention should be given to the radiation dose from multiple CT examinations. This increase in radiation dose from CT is partially due to the increased speed of image acquisition allowing multiphase examinations, all associated with higher doses (Smith-Bindman et al., 2009). There has been evidence linking the exposure from low level of ionising radiation, at doses used in medical imaging, to development of cancer (Smith-Bindman et al., 2009). The risks to individuals are likely to be small, but because of the large number of persons exposed annually, even small risks could translate into a considerable number of future cancers. There has been a comprehensive reviewed by The National Academy of Sciences' National Research Council into the biological and epidemiological data related to health risks from exposure to ionising radiation, published as the Biological Effects of Ionizing Radiation (BEIR) VII Phase 2 report (Smith-Bindman et al., 2009). The radiation doses associated with a given CT scan may vary considerably between different machines and institutions as reported by the US Food and Drug Administration (FDA) in their survey during 2000 – 2001. This included data on CT head scans from 203 facilities and found that the institution-to-institution multiple-scan average dose varied by as much as a factor of 10 (Hall & Brenner, 2008).

Since children and adolescents are more sensitive to radiation than adults, it is meaningful to analyse paediatric CT doses and imaging trends (Radiation, 2013; UNSCEAR, 2010). There are already some surveys that have been conducted on paediatric CT utilisation rates (Blackwell et al., 2007; Dorfman et al., 2011; Larson et al., 2011; Mettler Jr et al., 2000; Townsend et al., 2010), and the IAEA is assessing paediatric CT utilisation in developing countries (Muhogora et al., 2010). The main purpose of these surveys were to collect information regarding the dose levels during the most common CT examinations in adults and paediatrics. Whereas the key messages of the studies were that the exposure parameters are not always adjusted appropriately to the clinical question or to patient size, especially for children. Dose reduction techniques, such as tube-current modulation, low-tube voltage protocols, and iterative reconstruction algorithms can substantially decrease radiation doses. A summary of the the key points discussed above are:

- Number of CT scans are increasing and they contribute most to the radiation dose received by patients, as they are in general higher dose procedures.
- There is variability in practice and, therefore, the dose received by patients at different sites/within different countries will vary.
- Children are more radiosensitive and, therefore, it is particularly important to consider the radiation dose to children and understand ways in which the dose can be reduced.

4.5 CT Dosimetry and Concerns Regarding Radiation Dose

Medical imaging represents the major source of man-made ionising radiation to people (Olarinoye & Sharifat, 2010; Zenone et al., 2012). Therefore for all radiographic procedures image quality should be produced with the least possible radiation dose; as low as reasonably achievable (ALARA) principle (Uffmann & Schaefer-Prokop, 2009).

As indicated in the literature due to advances in technology and improvements in training the radiation dose from diagnostic X-ray procedures has generally decreased with just two exceptions: CT and Interventional Radiology (Dawson, 2004; Lumbreras et al., 2016; Paterson & Frush, 2007). Also as reported by the UK National Radiation Protection Board (NRPB) survey in 2003, CT scans accounted for 9% of all medical radiological examinations, this type of imaging modality was responsible for approximately 47% of the total radiation patient effective dose (Shrimpton et al., 2006; Pearce et al., 2012; Dougeni et al, 2012). The more recent report in the UK is the third national CT survey by the NRPB (2011). The review

included data from nearly a third of all CT scanners (all MSCT) and provides a substantial snapshot of the UK CT practice in relation to 13 common types of examination on adults and also head examinations for children (collated into three age bands). This survey focused on establishing dose indicators $CTDI_{vol}$ and DLP, for 47,000 individual patients, representing some 900 examination protocol/scanner combinations and 24,000 separate scan sequences (Shrimpton et al., 2014). Whereas the previous two national reviews focused on standard CT protocols (Shrimpton et al., 2006; Shrimpton, Hillier, Lewis, & Dunn, 2005). This more recent survey found there are still variations apparent in typical practice between CT centres for similar procedures. For adults typical examination doses are reported higher than the previous results from the 2003 review in connection to overall national practice that is includes both SSCT and MSCT. The increases for levels of $CTDI_{vol}$ are within 20% and those for DLP within 40%, also more significant changes are in relation to high resolution scans of the chest, where two quite different techniques are currently used; typical doses for axial-only scanning are significantly lower by factors of more than three compared with those for helical-only scanning. In children, the survey found slight differences in typical values of $CTDI_{vol}$ for examinations of head were between -10% and + 20%, where those for DLP are between +40% and +50%, with the smallest changes for the youngest age band (0–1 year) and the largest for the oldest age band (>5 years) (Shrimpton et al., 2014).

Lockwood et al., in 2007, reported the ED for common diagnostic imaging tests **(Table 4-1)**, on page **76**. The use of CT is categorized by Brenner and Hall, 2007 according to the population of patients either adult or paediatric and the purpose of imaging: diagnosis in symptomatic patients or screening of asymptomatic patients. The largest of these categories are CT-based diagnostic tests in adults; about half of diagnostic CT examinations in adults are scans of the body, and about one third are scans of the head. Approximately 75% of scans are obtained in a general hospital setting and 25% in a single-specialty practice setting. In CT, exposure to ionising radiation is a problem that is becoming progressively more important as CT has acquired the role of a rapid, total-body exploratory examination; it is very popular with both patients and clinicians and is considered a ‘‘defensive’’ tool in the diagnostic setting. An increase not only in the absolute number of CT examinations, but also in terms of both length of coverage and number of phases obtained while scanning (arterial, venous) has been observed (Colagrande et al., 2014). The largest increase in CT use has been observed in the categories of paediatric diagnosis and private whole body adult screening, for example ‘Life Scan’ and these trends can be expected to continue. This is primarily due to the decrease in time needed

for the scan and the superior detection capabilities e.g. solitary lung nodules. A large part of the projected increase in CT scanning for adults will probably come from new CT-based screening programs for asymptomatic patients. The four areas attracting the most interest are CT colonography (virtual colonoscopy), CT lung screening for current and former smokers, CT cardiac screening, and CT whole body screening. An average adult CT scan of the head or abdomen delivers a radiation dose to the organ being scanned typically in the range of 15 mSv, and for neonate 30 mSv for a single CT scan, with an average of 2 to 3 CT scans per study (Brenner & Hall, 2007). In the US, a study conducted by Mettler and colleagues (2008) reported that among all patients undergoing CT, at least three scans were obtained in 30% of patients, more than five in 7%, and more than eight in 4% of patients. Within this work it was identified that repeat scans were conducted because some of the patients had a prior CT examination on an earlier date, others had pre- and post-contrast scans. In addition, a single CT examination often consists of multiple scan sequences (phases) across the same anatomical range. This is further illustrated within the literature where a single CT scan gives radiation doses in the range of 10–30 mSv. In relation to multiple CT scans on the same patient, benefits should be considered relative to potential carcinogenesis since tissue doses are in the range of 50–200 mSv, which have been shown to cause an increase in cancer rate among the Japanese atomic bomb survivors (Mettler et al., 2008; Brenner, 2010). These references directly relate the average CT dose with the magnitude of doses found in the atomic bomb survivors (ABS) and large-scale radiation worker (LSR) studies. Risks at these dose levels are real, with dose and risk increasing simultaneously. With improvements in CT dosimetry more accurate and reliable information can be provided regarding the ED to patients.

Table 4-1: Estimated effective radiation dose for common diagnostic imaging tests (Lockwood D. et al., 2007; Table 1, p 122).	
Imaging Study	**Effective Dose (mSv)**
Chest radiography (PA and lateral)	0.06
Screening mammography	0.6
Gastric emptying study	1.4
Kidney-ureters-bladder radiography	1.7
CT of the head	1.8
Lumbar spine radiography	2.1
Background radiation, annual dose	3.6
Radionuclide bone scan	4.4
Ventilation-perfusion (V/Q) scan	6.8
CT of the pelvis	7.1
CT of the abdomen	7.6
CT of the chest	7.8
Barium enema radiography	8.7
CT angiography of coronary arteries	10
Positron emission tomography (whole body)	14
Small bowel series (barium swallow x-ray study)	15
Intravenous urography	10.0 - 20.0
Whole-body screening CT	22.5
Three-phase hepatic CT scan	29.9
Dual-isotope myocardial rest and stress perfusion CT study	32.5
CT urographic study	44.1

As reported by Lockwood et al., (2007), quantifying the radiation dose is not a simple matter. The energy and quantity of the photons, the size of the patient, and the vulnerability of irradiated tissues must be factored into any estimate. The concept of ED allows many of these factors to be compared and controlled. On the other hand everyone is constantly exposed to naturally occurring ionizing radiation, commonly called background radiation. Background radiation comes from radioactive elements present in the earth since its formation is primordial radionuclides, such as uranium and the natural products of its decay, radium and the gas radon. Other background radiation is in the form of cosmic rays, high-energy particles that constantly bombard the atmosphere and create radioisotopes of carbon and nitrogen. The average annual ED from background radiation is estimated at 3.6 mSv (Lockwood et al., 2007). As showed in **(Table 4-1)** some diagnostic procedures involve an ED that is a tiny fraction of background radiation, whereas many impart several times that amount.

Lockwood et al., (2007) further pointed out that CT examinations account for two thirds of the cumulative patient dose from diagnostic radiologic procedures, and the cumulative dose from CT scanning is rising as advances in technology increases the number of indications for and the capabilities of CT. For instance, new CT scanners are faster than old machines due to multiple

detector rows that have increased the speed of scanning and enabled high-resolution reconstruction of images in all anatomical planes, permitting consideration of volume CT acquisition. Also, development of iterative reconstruction algorithm software packages also have been developed to utilise these benefits, with modern scanners being able to reconstruct a study of 1000 images in less than 30s rotation time which allow imaging in multiple phases after contrast administration (Elliott, 2009). CT urography typically consists of three consecutive CT examinations of the abdomen and pelvis, and it exposes the patient to the highest radiation dose of any commonly used diagnostic imaging studies **(Table 4-1)**, on page **76**.

To quantify radiation risk the International Commission on Radiation Projection (ICRP) uses the concept of ED. Generally, as reported by ICRP (2007) in the annual publication report (103) the risk of fatal cancer for adults is estimated at 5% Sv but is higher for children. There is some debate about the use of ED, but it remains the useful tool to estimate risk (Borrás et al, 2010; Ma et al., 2013; Martin, 2014). *In vivo*, the ED cannot be directly measured but it can be estimated by measuring organ dose in representative phantoms or MC simulations as discussed in **(Section 3.8)** on page **53** of this chapter.

Brenner, (2008), has argued that there are three major problems with the concept of ED:

1. Tissue weighting factors represent a committee determined subjective balance between the different stochastic endpoints of cancer incidence, mortality, life shortening and hereditary risks. These weighting factors, for some organs, are changing over a period of time and make historical ED estimates unreliable (D. Brenner, 2008).

2. The other major problem with ED is that it is independent of age at the time of exposure, whereas data suggest that attributable radiation risks, supported by experimental data, are often highly age-dependent (D. Brenner, 2008).

3. The third major problem with the ED is that it is often confused and misused. The equivalent dose that refers to a given tissue and ED that is a weighted average over the entire body are both measured in Sieverts. So, the equivalent dose and even the absorbed dose have been confused with one another (Brenner, 2008).

The risk associated with radiation exposure is related to the biological effects induced due to that amount of radiation deposit in the body. These types of effects are measured by using the

direct data from human epidemiological studies of atomic bomb survivors in Hiroshima and Nagasaki in Japan in 1945. For a long time, a large group of survivors were studied and as time passes the statistical confidence of estimating the cancer risk improves. As reported by Brenner and Hall, (2007), Cardis et al., (2007) and Preston et al (2008), the number of survivors who received doses of radiation less than 50 mSv is around 25,000 people, this amount of radiation is similar to the doses received by those undergoing some CT examinations (Brenner & Hall, 2007; Cardis et al., 2007; Preston, 2008).

The main key points that should be understood are that CT examinations are among the highest sources of radiation to population. $CTDI_{vol}$ and DLP are the most common parameters for computing the radiation dose delivered to the scan volume from particular CT examinations. Also, dose to particular organs are depend on the scan parameters used. Effective dose is not a suitable quantity for considering stochastic risk from low radiation dose procedures. The new quantity should take into account patient age and gender at the time of scanning.

4.6 Paediatric and Adult CT Scanning

The clinical value of CT is unquestioned, and the uses of newer helical and multislice units are growing. The dose received by some patients, particularly children, is higher than desired and must and can be reduced without any significant loss of diagnostic information (Linton & Mettler Jr, 2003).

A US conference talk in 2002, on the subject of CT dose reduction, described adult CT scanning as being incredibly effective and has become a routine part of radiology because it provides much more detail than conventional X-ray imaging. It also increases the confidence of our referring physicians in our contributions in almost every clinical area. In paediatric CT, there has been a 200% increase in utilisation over the past few years (Donnelly et al., 2001; Linton & Mettler Jr, 2003).

For medical imaging modalities, especially CT diagnostic reference levels (DRLs) are becoming more common. DRLs represent the lower bound of potentially unacceptable practice, rather than being an upper limit not to be exceeded. These can be set at a practice, regional and/or national level and are calculated by surveying doses for standard patients across practices and generally established on the basis of the rounded third quartile value of the dose distributions (Shrimpton & Wall, 2000). Dose surveys can then be conducted at a practice level and compared with national DRLs to determine when local practice should be reviewed,

particularly when the DRL is consistently exceeded. DRLs have been used for some time in European countries (Bongartz et al., 2004) but fail to take into account the quality of the resultant images.

Diagnostic reference levels (DRLs) have been defined in European guidelines for CT examinations since 2000 (McCollough, 2010). DRLs, appropriate to CT in examinations in adult patients have already been specified, utilising the dosimetric concepts of weighted computed tomography dose index per slice in serial scanning or per rotation in helical scanning, and dose-length product per complete examination. This methodology can also be applied to CT examinations on children, with reference dosimetry for all types of examination on children of all ages being based solely on measurements involving the smaller (16 cm diameter) of the two standard CT dosimetry phantoms. Some initial DRLs for paediatric CT have been set on the basis of the rounded third quartiles of the dose distributions provided by a survey of typical practice at over 40 scanners from seven European countries. Values are presented in relation to three patient ages (<1 year, 5 and 10 years) and five types of procedure (Shrimpton and Wall, 2000).

Even though DRLs should not be applied to individual exposures but are reference doses for common examinations, they can help to optimise radiation protection to avoid unnecessarily high doses to the patient. The DRLs are provided for four major anatomical regions, they are: head, chest, abdomen, and pelvis whereas for CT, the $CTDI_W$ and the DLP were suitable quantities to be used as DRLs. These DRLs are derived from a European document based on a British study performed in the early 1990s (McCollough, 2010). Since that time the CT machines have undergone major evaluation and $CTDI_w$ has been replaced by the $CTDI_{vol}$ which is commonly displayed by the CT scanner console (Colagrande et al., 2014). A national survey was published in 2006 by Shrimpton et al., which reviewed the radiation dose from CT examinations in the UK in 2003. Data reported is based on data received from over a quarter of all UK scanners, of which 37% had MSCT capabilities. The study included data collected from the protocols established on each scanner for 12 common types of CT examination on adults and children. The study concluded that, the mean UK doses for adult patients were in general lower by up to 50% than previous ones for 1991, although doses were slightly higher for MSCT relative to SSCT scanners. The relative increase in reference dose was larger for scans of the head and the chest (high resolution) (Shrimpton et al., 2006). A similar study was conducted in Italy in 2004 and published in 2006; the study aimed to establish the first Italian

survey of radiation dose in CT prior to the widespread adoption of MSCT. The study was carried out in 29 Italian hospitals, covered 48 CT scanners and 232 examinations for seven adult clinical CT protocols, and showed that $CTDI_w$ and DLP were always below the DRLs set by the European guidelines (Origgi et al., 2006).

Analysis of the risks associated with paediatric CT mainly refers to the study by Brenner et al., (2010), which highlighted the increase in the probability of occurrence of tumours when the patient's age is decreased. It should be noted that some CT examinations in a child could increase the probability of tumour occurrence to more than 20% (Brenner et al., 2010a; Colagrande et al., 2014). However, the main dosimetric aspects connected with the use of CT in paediatrics are still poorly standardised due to following: Firstly, the weighting factors for effective dose are not age specific, and therefore, some authors suggest estimating them on an organ-by-organ basis (Huda & Vance, 2007) and secondly, the classic CT dose descriptors are based on phantoms with diameters simulating the geometry of an adult and introducing significant uncertainties in the evaluation of organ doses in children (Colagrande et al., 2014).

Different research groups have used various tools to perform size-dependent dose evaluations. Two studies, one by Axelsons et al., (1996) and the other by Giacco et al., (2001) used a physical anthropomorphic phantom (Axelsson et al., 1996; Giacco et al., 2001), while other investigators used MC voxelized phantoms (Lee et al., 2007). In both methodologies, unlike for adults, the phantoms are size and age specific (the new-born baby (0-year-old) and the 1-, 5- and 10-year-old child, the 15-year-old adolescent and adult to represent the age groups) (Varchena, 2002). Another study by Khursheed et al., (2002) used the MC N-particle (MCNP) radiation transport code to calculate normalised ED values for three different scanners and mathematical anthropomorphic phantoms with ages ranging from new-born to adult. They demonstrated the high dependence on patient age and size: the ED in a new-born was 1.5 times greater than that of an adult for all types of examinations, as well in all cases an inverse trend is observed between normalised effective dose and phantom age, with the dose to the new-born from head and neck scans being 2.2–2.5 times higher than that to the adult, depending on scanner model. Other dosimetric aspects associated with paediatric CT have been focused on optimisation procedures (Kalra et al., 2004; Khursheed et al., 2002). Brady et al., (2011) noted paediatric CT imaging trends in Australia from 1994 – 2009; they illustrated that 2.1 million CT examinations were performed in Medicare in Australia for children and adults. The average annual growth in the number of CT scans provided since 1994 was 8.5% which was more than the population growth

of 1.4%. Combining the data sets showed that over the last 20 years, there has been an average annual increase of 5.1% in the CT imaging rate for 0 to 18-year-olds, which accounts for more than the increase seen in adult CT protocols (Brady et al., 2011).

As reported by Brenner & Hall, (2012), a number of pioneering researchers publishing in the Journal of the American College of Roentgenology have raised concerns regarding the possibility of cancer induction from paediatric CT scans. This in turn attracted attention from the media in the US regarding the radiation dose to children from CT scanning (Brenner & Hall, 2012). This resulted in a strong public reaction and also encouraged the medical community to become more aware of paediatric CT dose. This focused the efforts of the CT manufacturers to reduce dose and previous endeavours in this area were limited (Donnelly, 2005).

As mentioned by Paterson et al., (2001) and Ghotbi et al., (2006) one of the important conclusions was that CT protocols for adults were in some cases being used on children. In early CT scanners operators were not allowed to adjust the scanner parameters, however, advancing technology provided operators with the ability to lower the dose for younger or smaller patients although it appeared that this was not being utilised in some cases. There is a large variability in body size in the paediatric population, so adjustments of acquisition parameters are necessary because they are the main determinants of radiation dose received by the child. Paterson et al., in 2001 indicated in their paediatric CT survey that no appreciable adjustment of parameters were being made based on the examination type or patient age (Paterson et al., 2001). According to Blackwell et al., (2007); Brenner et al., (2001a) and Wiest et al., (2002) the number of CT scans being performed on children appeared to be increasing, this can be attributed to advances in technology that allow faster scanning times and hence greater feasibility for conducting scans on uncooperative children and (or) sick patients as well the availability of CT scanners makes them readily accessible (Blackwell et al., 2007; Brenner et al., 2001a; Wiest et al., 2002). According to Brenner et al., (2001a), compared with adults the combination of using adult parameters and the higher radiation risk for children leads to a significantly higher attributable lifetime cancer mortality rate in children, for example in the US 600,000 abdominal and head CT scans are performed annually on children under the age of 15 years, approximately 500 of these children might ultimately die of radiation induced cancer. It must be noted that Brenner's work reflected the status of paediatric CT over a decade ago. Scanner technology and clinical protocols have adapted, however, paediatric CT is still a high dose examination and highly prevalent. It is also important to make comparisons with other

causes of cancer than simply radiation induced cancer rates. Approximately 140,000 of the 600,000 children will eventually die from cancer from non-radiation related causes and the radiation induced cancer risk increases this rate by only 0.35% (Brenner et al., 2001a).

Moreover, the wider benefits of using CT scans in healthcare must be considered. Brenner et al., (2010) has calculated the radiation attributable cancer rate equates to about 1 in every 1,200 abdominal and head CT scans leading to a fatal cancer in the age group under 15 years. The significant proportion of these examinations as expected would have a diagnostic benefit changing patient management and even being lifesaving. Thus, the ratio of benefit to risk must be considered in this context and is ultimately a decision that the child's clinician must make. Furthermore, Brenner et al., (2001a & 2010) stated that risks calculated are likely to be high since it was based on the use of adult scanning parameters. In fact, these risks are lower for a properly optimized and clinically justified examination (Brenner et al., 2001a & 2010).

Following the press coverage of the articles published in 2001, the Society for Paediatric Radiology (SPR) responded stating that the views were unbalanced and potentially dangerous, they further stated that the benefits of CT imaging had not been highlighted sufficiently (Paediatric Radiology, 2001). This agreed with that reported by Brenner et al., (2001c), the risks are almost always outweighed by the benefits, but when the risks are applied to such a large population they become a public health issue. For an individual patient the benefits are justified, but from a population perspective the risks must be considered (Brenner et al, 2001c).

As mentioned by Picano, (2004) in terms of radiation risk it will always be a challenging question of defining what is acceptable. Better knowledge of such risks will help us to avoid small individual risks translating into substantial population risks. Radiological awareness is essential to help doctors in the difficult task of balancing what is good for the individual patient against what is acceptable for society. Human nature tends to lead us to overreact when presented with a small risk, while larger risks, such as dying from lung cancer due to smoking are often disregarded (de Gonzalez & Darby, 2004; Picano, 2004a, 2004b).

Donnelly (2002) discusses issues related to radiation exposure from an historic perspective and draws the parallel with the introduction of X-ray imaging in medicine and the delay in realising its harmful effects. It also raises caution that over-utilization can result from the successful introduction of new technology, without realizing its unforeseen dangers which leads to belated

optimization of techniques and implementation of appropriate safety and protection measures (Donnelly, 2002).

In 2003, Linton and Mettler published an article on dose reduction in CT and concluded that the clinical value of CT is unquestioned, and the uses of newer helical and multidetector units are growing but that further optimisation of the radiation dose to children and adults is necessary (Linton & Mettler, 2003). Particularly from 2001 onwards it was becoming apparent in the literature that dose reduction was needed for paediatric CT, despite the known controversy regarding quantifying the risk associated with low radiation doses.

Dose reduction is one of the main problems in CT, and many techniques have been developed to face this problem. However, radiation dose is linked to image quality and the factors contributing to each should be balanced to ensure images have sufficient diagnostic information and the radiation dose is minimised (Colagrande et al., 2014). CT dose reduction will require a combination of approaches. These include user education for physicians and radiologic technologists, development of technique charts by medical physicists, development of automatic exposure control devices by manufacturers, and possible retrofits of these devices for older machines. It also will require creation of a climate of opinion in which radiologists will demand attention to dose reduction in their purchase of new CT scanners, one industry participant commented. There is the added possibility that radiation dose from paediatric CT can be reduced further using alternative image reconstruction methods (Singh et al., 2012; Tricarico et al., 2013; Vorona et al., 2011). Within adult CT scanning iterative reconstruction techniques have emerged as significant dose reducing methods, in patients, low-dose CT with adaptive statistical iterative reconstruction was associated with CT dose index reductions of 32–65% compared with routine imaging and had the least noise both quantitatively and qualitatively (Hara et al., 2009; Korn et al., 2012; Silva et al., 2010; Singh et al., 2011). It should now be standard practice of adjusting the examination parameters for children based on age, weight, size or a combination of these and there is much in the literature about addressing these techniques (Boone et al, 2003; Donnelly et al., 2001; Haaga, 2001; Huda et al., 2000; Lucaya et al., 2000; Paterson & Frush, 2007; Suess & Chen, 2002; Verdun et al., 2004). An excellent review has been provided by Paterson et al., (2007) for some of the suggested protocols for children and manufacturers which provide age- or weight-based technique charts. These technique charts / tables provide guidelines for MSCT parameters in paediatric CT chest, abdomen/pelvis, extremity skeletal examination, and CT angiography (Paterson & Frush,

2007). However, there is no direct method that can help practitioners to assess the radiation risk prospectively prior to undertaking a CT scan. Thus, there is a need for a method that can aid the radiographers and CT users to obtain risk data on possible cancer induction for specific CT protocols and when changing acquisition parameters.

4.7 CT Brain Acquisition Protocols and Radiation Dose

The choice of scanning protocol in CT will affect the radiation dose delivered to the patient. There are two types of CT protocols commonly used to scan the brain, sequential and helical or spiral. For the Toshiba Aquilion 16 CT scanner used in this study, the standard sequential protocol parameters are: axial scanning with a 120kVp tube potential, 320 mAs, and a rotation time of 1 second and the detector width x rows = beam collimation is 0.5 mm x 16 = 8 mm. Whereas the standard helical protocol uses 120kVp and 1 second rotation time, mA is controlled automatically (100 – 450) and the detector width x rows = is 0.5 mm x 16 = 8 mm.

As reported by McCollough (2006 & 2011), most radiation dose reduction efforts have been focused on alterations in tube current by using ATCM. Wide variations in patient radiation absorption occur with changes in the CT projection angle and anatomic region, and the projection with the most noise initially determines the amount of noise on the final image (McCollough et al., 2006 & 2011). Mettler Jr. et al, 2000 and McCollough et al., 2006 argued that differences in patient doses from CT can be linked to multiple causes. A systematic review study by Dougeni et al., (2012), reported on evaluating patient dose from CT scan examinations using a variety of published literature. The report investigated the ED during common CT scan examinations in adult and paediatric patients. The CT dose is still the highest among the radiation diagnostic modalities and there is variation in dose reported for similar producers for different scan types that is because different scanner types by different manufacturers and different scan protocols (kVp, mAs), the variations are also related to the selected length of the region to be scanned, tube rotation speed, helical pitch, collimation, filtration, and patient weight (Dougeni et al., 2012; Kubo et al., 2008; McNitt-Gray, 2002). The ED values for adult and paediatric CT examinations obtained from the report are illustrated in **(Table 4-2)** and **(Table 4-3)**, on page **85** and **87**, respectively.

Table 4-2: Adult head CT ED (mean values in brackets) (A. Cohen et al., 2016; Dougeni, Faulkner, & Panayiotakis, 2012; Rapalino et al., 2012).	
Reference	**Effective doses from CT scanning in Adult (mSv)**
Clarke et al., 2000	0.98 – 2.1 (1.9 3rd quartile)
Tsapaki et al., 2001	1.4
Huda et al., 2001	1.2 – 1.5 (1.3)
Papadimitriou et al., 2003	0.7 – 3.7 (2.1) Greece 1.6 Italy
Hatziioannou et al., 2003	0.4 – 2.5 (1.6) (2.00 3 [rd] quartile)
Cohnen et al., 2003	2.8 (neck)
Shrimpton et al., 2003	1.5 mean, 1.7 3 [rd] quartile
Brix et al., 2003	2.2
Yates and Pike., 2004	0.9–2.4 (1.7)
Heggie, 2005	1.5
Ngaile et al., 2006	2.2
Tsapaki et al., 2006	1.2
Moss and McLean, 2006	1.6 – 2.8
Aldrich et al., 2006	1.7 – 4.9 (2.8)
Origgi et al., 2006	0.5 – 3.1 (1.7) Experimental 0.6 – 4.1 (1.8) Monte Carlo
Muhogora et al., 2006	6.1 – 7.9
Cohnen et al., 2006	1.7 head CT 1.9 intracranial angiography 2.8 cervical angiography 1.1 – 5.0 cerebral perfusion
Huda and Vance, 2007	0.9
Van der Molen et al., 2007	1.9
Teeuwisse et al., 2007	0.6 – 2.4 (1.4) acute stroke 0.2 – 1.9 hearing loss
Tsai et al., 2007	1.6
Kharuzhyk et al., 2010	0.9 – 2.0 (1.4)
E. Dougeni et al., 2012	0.4 – 7.9
O. Rapalino et al., 2012	1.95 – 2.66 ± 0.04
Andrew et al., 2016	2.0 – 2.3 ± 0.7
World Health Organization 2016	2
Overall	**Mean: 2.0** **SD: 1.2**

Advances in CT technology have increased and extended the use of CT clinically, this has resulted in two advantages, more frequent CT examinations (short scan time, improve in speed of image acquisition, also the technique of retrospective image acquisition scanning with overlapping of slices) and the introduction of new CT protocols such as spectral CT (Budoff, 2009; Dawson, 2014). In comparison to projection radiography, where technological developments have steadily driven dose down, patient doses in spite of CT technological evolutions have still remained among the highest in diagnostic radiology. The widespread introduction of MSCT resulted in a considerable increase in both the frequency of CT procedures and patient exposure levels. The associated increase in radiation dose with MSCT, see **(Sections 3.3.2.1 and 3.3.2.2)** on pages **27** and **29**, is partly due to the need to scan a slightly larger volume than is planned. Over-beaming occurs in order to get sufficient data interpolated

to reconstruct the first and last slice. Usually there is an additional half rotation at the beginning and the end of the intended scan length, which may account for an increase in dose 10–20% for head–neck and trunk studies and may reach up to 30–35% for chest and abdomen pelvis studies (Dawson, 2014; Kalender, 2006, 2011, 2014; Tzedakis et al., 2005; Brix et al., 2003; Budoff, 2009; Dawson, 2014; Huda & Vance, 2007; ICRP Publication 102, 2007; Mayo et al., 2003; UNSCEAR, 2000a, 2000b; U. N. S. C. o. t. E. o. A. R. UNSCEAR, 2008).

A review was completed by Dougeni in (2012), about the ED from CT scanning in paediatric patients for head CT examinations and the results as illustrated in **(Table 4-3)**. It was observed that there were large dose variations and some individual clinical sites exceeded the recommended DRLs. On this basis alone, it is clear that there is potential for CT dose reduction, this is especially true for exposure factors which are not always adjusted appropriately for the clinical question or to patient size, especially for children. Dose reduction techniques, such as ATCM, low-tube voltage protocols, prospective echocardiography-triggered coronary angiography and iterative reconstruction algorithms can substantially decrease dose.

Verdun F R. et al., (2008) and Shrimpton et al., (2005 & 2014) have reported large variations in doses in adult and paediatric CT for a similar type of procedure, especially in paediatric examinations where the range of patient size is wider within the same age band (Shrimpton et al., 2005 & 2014; Verdun et al., 2008; Wall et al., 2011). The variation in patient dose from CT is more dependent on scan protocols than on scanner type. For example, for the same head CT scan (140 kVp, 340 mAs, 5 mm contiguous section) with a single and multi-detector row CT scanner, the dose is 205% higher for the spiral scan (increase from 60 mGy to 123 mGy). This arises not only from geometrical differences but also from differences in beam filtration, X-ray spectrum and beam profile but could be eliminated by applying an optimised protocol (Hamberg et al., 2003).

Table 4-3: Effective dose from CT scanning in paediatric patients for head examination (mean values in brackets) (Dougeni et al., 2012; Miglioretti et al., 2013; Vilar-Palop, Vilar, Hernández-Aguado, González-Álvarez, & Lumbreras, 2016; WHO, 2016)					
Effective doses from CT scanning in children (mSv)					**Reference**
Neonate	**1 year**	**5 years**	**10 years**	**15 years**	
1.6 – 2.4 [2 months]	1.7 – 2.7 [2 years]	1.60 – 2.5 [7 years]		1.3–2.2	Papadimitriou et al., 2000
3.5–14.5 (7.6)					Huda et al., 2001
8.4	2.3	1.5	1.7		Chapple et al., 2002
6	4.9	4	2.8	1.7	Huda et al., 2003
	0.3–1.5	0.5–1.6	0.6 – 2.3		Pages et al., 2003
	2.5	1.5	1.6		Shrimpton et al. 2006
1.3–2.3 [2 months]		1.5 – 2.0 [5–7 years]			Moss and McLean, 2006
0.8–2.4					Staton et al., 2006
3.6					Huda and Vance, 2007
2.0–5.0 (4.2)	2.7–5.6 (3.6)	2.0–3.6 (2.4)	1.6 – 2.7 (2.0)	1.0 – 2.1 (1.4)	Thomas KE, and Wang B., 2008
		0.7			Feng et al., 2010
4.3 ± 2.6	3.9 ± 0.6	4.1 ± 1.2	3.6 ± 0.5	3.9 ± 0.7	Papadakis et al. 2011
(3.5) [< 5 years]		(1.5) [5-9 years]	(1.1) [10-14 years]		Miglioretti et al., 2013
1.7 [< 1 year]	1.6 [1-5 years]		1.8 [6-10 years]	1.6 [11-15 years]	Vilar-Palop et al. 2016
6	3.7	2	2.2	2 [< 15 years]	World Health Organization 2016
3.3		**2.4**	**2.4**		EU DRL, 2000
2.6 [battered child-trauma]		**1.8 [hydrocephalus]**			EU DRL, 2004
3.0		**1.9**	**2.0**		UK DRL, 2003, 2006

A report by Hara et al., (2010), reported on the radiation dose delivered from CT brain examinations using $CTDI_{vol}$ indices measured using a PMMA head phantom. These values were then compared with actual measured values using TLDs and an Alderson RANDO anthropomorphic phantom. The X-ray tube voltage and current were varied and included 90, 120, and 140 kVp and 25 to 300 mAs. Conclusions from this study indicated that there were no real differences between $CTDI_{vol}$ and TLDs based dose estimations at 90 kVp. Study findings did indicate that as the tube voltage increased (120 and 140 kVp) the actual TLDs values were less than the $CTDI_{vol}$ based values. **(Table 4-4)** and **(Table 4-5)** report the measured doses from Hara et al., (2010) using TLD and $CTDI_{vol}$ with tube currents of between

25 and 300 mAs for the three different values of tube voltage (90, 120, and 140 kVp) (Hara et al., 2010).

Table 4-4: Absorbed doses to the brain during CT head scans (Hara et al., 2010).				
kVp	**mAs**	**Measured dose using TLD (mGy)**	**$CTDI_{vol}$ (mGy)**	**% Different**
90	25	1.39	1.8	12.9
90	300	17.00	21.2	11
120	25	3.21	3.8	8.42
120	300	37.79	47.7	11.6
140	25	5.08	5.5	4
140	25	65.07	65.6	0.41

Table 4-5: Eye exposure dose from CT head scans (Hara et al., 2010).				
kVp	**mAs**	**Measured dose using TLD (mGy)**	**$CTDI_{vol}$ (mGy)**	**% Different**
90	25	1.94	1.8	3.74
90	300	20.31	21.2	2.14
120	25	3.71	3.8	1.20
120	300	49.72	47.7	2.07
140	25	5.44	5.5	0.55
140	25	69.76	65.6	3.07

With a dosimetry phantom, the measured values of the brain gradually deviated from the corresponding index values as the current increased, whereas no deviations from the index values were observed for the measured values of the eyes as the current increased. Scans of the brain and eyes in the head region were acquired under the same conditions. In the head region the calculated TLD value–to–$CTDI_{vol}$ ratios, show the TLD values of were lower than the CTDIvol (TLD value–to–CTDIvol ratio, 0.93 ± 0.12) as illustrated in **(Table 4-4)** (Hara et al., 2010).

4.8 Chapter Summary

The use of ionising radiation in modern medicine is necessary for both diagnosis and treatment. As reported by the UNSCEAR, (2010), there is now more than one diagnostic examination performed per person across the population every year in countries with advanced health care systems (UNSCEAR, 2010). The UNSCEAR reported that globally, there are approximately 3.6 billion diagnostic examinations and six million therapeutic treatments performed annually. These medical practises involving the use of ionising radiation include diagnostic examinations, interventional procedures and radiotherapy treatments and are typically undertaken in radiology, nuclear medicine and radiation oncology departments or clinics (UNSCEAR, 2010). For medical purposes, the people exposed to ionising radiation are the patients themselves.

Recent figures demonstrate that diagnostic medical exposures, including radiology and nuclear medicine, account for about one-fifth of the average annual per caput dose to the global population from all sources (UNSCEAR, 2010). The National Council on Radiation Protection & Measurements (NCRP) (2009) reported that from all of the diagnostic imaging modalities, CT is the highest contributor to population dose, even though it accounts for a much smaller proportion of the total number of examinations (Schauer & Linton, 2009).

Evidence from epidemiological studies prove that it is impossible to deny the association between an increase in cancer incidence and morbidity due to ionising radiation exposure at high doses (ICRP, 2005). By contrast, quantifying the risk associated with low dose radiation exposures, such as a typical CT scan, is more complex and contentious. As reported by Brenner and Hricak, (2010) and Brenner et al., (2003) despite the uncertainty surrounding low dose exposure, the societal risk may not necessarily be negligible and must still be considered, this concern arises when an increasingly large population is exposed to small individual risks (Brenner et al., 2003; Brenner & Hricak, 2010; Wall et al., 2014). Children are more radiosensitive than adults thus; the risk of radiation exposure is even higher than for adults. The risks from low doses of radiation are likely to be lower, progressively larger epidemiological studies are required in order to quantify the risk to a useful degree of precision and establish a low dose response. On the other hand, the necessary sample size increases approximately as the inverse square of the radiation dose in order to maintain statistical precision and power (Brenner et al., 2003; ICRP, 2005). The difficulties involved in quantifying the risks of low dose radiation are well known, two important questions have been addressed by many researchers, firstly, what is the lowest radiation dose which provides good evidence regarding increasing existing cancer risks in humans? According to the most recent literature and epidemiological evidence this is approximately 10 – 50 mSv for an acute exposure and approximately 50 – 100 mSv for a protracted exposure (Hendee & O'Connor, 2012). The second question is what is the most appropriate way to extrapolate such cancer risk estimates to even lower doses? As supported by experimentally grounded, quantifiable, biophysical arguments, a linear extrapolation of cancer risks from intermediate to very low doses currently appears to be the most appropriate methodology (Brenner et al., 2003; Brenner & Hall, 2012; Hricak et al., 2011; Wall et al., 2006).

Chapter 5 : Materials and Methods

5.1 Chapter Overview

This thesis assessed effective dose directly, using MOSFETs, to provide an understanding of the radiation dose variations across a range of helical and sequential CT brain imaging protocols (432) for both paediatric and adult patients, respectively. Absorbed dose was used to calculate both effective dose (ED) and the lifetime cancer risk induction for both males and females of different ages, ranging from 0 to 80 years. It was initially the intention to carry out the experiments using TLDs, however, due to the huge number of protocols utilised and the long time required to collect the data and analyse the results (which was beyond the PhD time frame) a decision was made to use only MOSFET dosimeters. Comparing the doses measured between MOSFET and TLDs was undertaken for number of CT brain protocols to valid the MOSFET method.

Organ and tissue absorbed doses were directly measured using MOSFETs for CT examination of the adult brain (sequential and helical) and paediatric (helical) using a Toshiba Aquilion 16 CT scanner and ATOM phantoms representing both adult and paediatric patients. Within the method a series of acquisition parameters were varied which included tube potential, rotation time, gantry angulation, mA modulation (ATCM), detector configuration and helical pitch.

5.2 Thesis Aim/Rationale

The aim of this study was to measure the organ and tissue absorbed dose and to estimate the ED during a CT scan of the brain using two dosimetry (ATOM) phantoms, then provide further estimations of the attributable lifetime cancer risk. The main reason behind carrying out this study was to develop a great understanding of a CT radiation dose and its effect in inducing cancer risk due to stochastic effects and developing excel spreadsheet/tool to estimate cancer risk from CT brain examinations cases/10^6 for male and females aged from 0 to 80 years, see thesis aims and objectives **(Sections 1.2** and **1.3)** on page **5**.

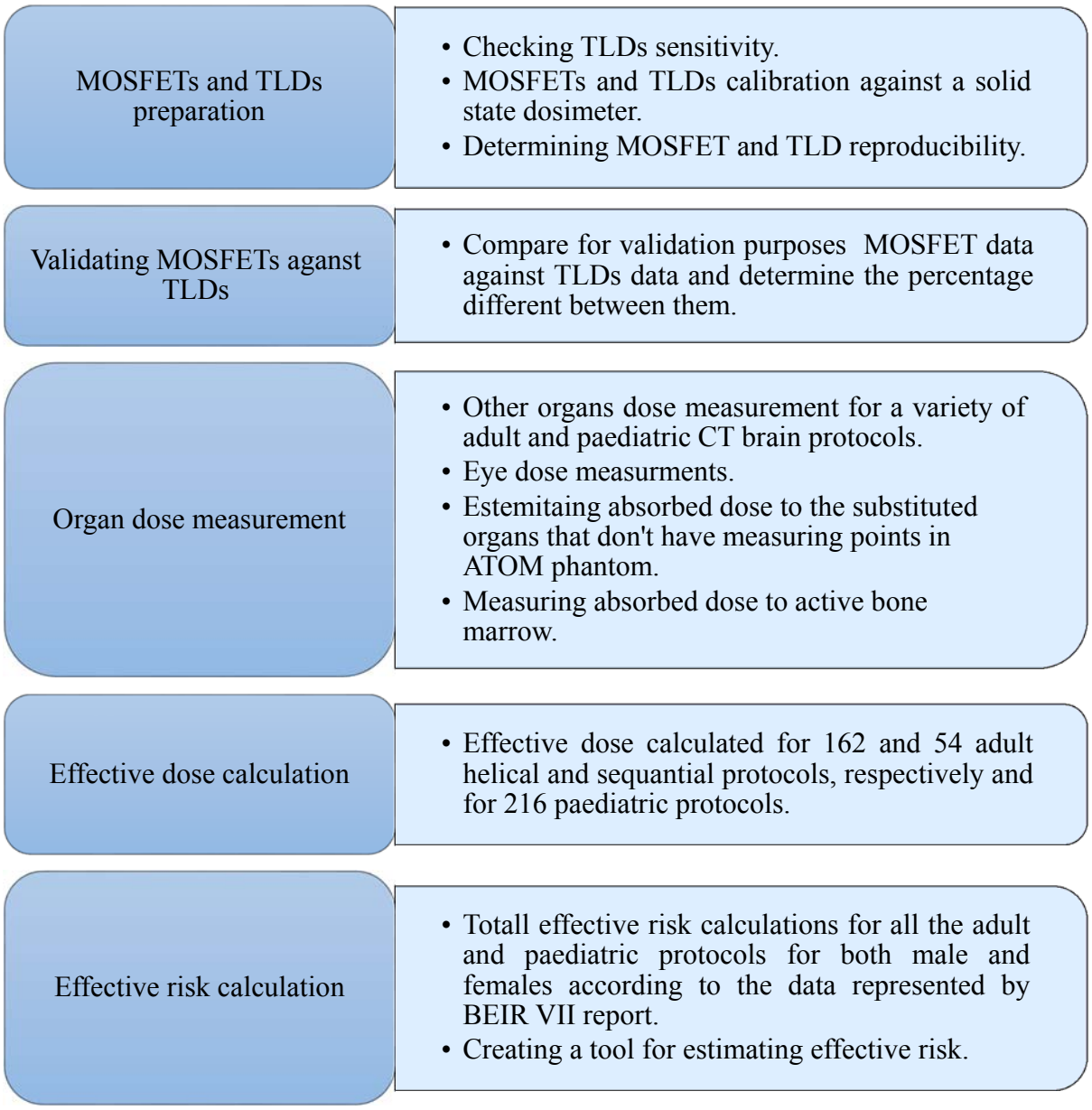

Figure 5-1: A flowchart illustrating the methods used in this PhD thesis.

5.3 MOSFET validation using TLD data

TLDs are traditionally the gold standard dosimeter generally employed for diagnostic radiology. As indicated in the literature, TLDs are used extensively in many medical dosimetry and personal monitoring applications, owing to their suitable dosimetric characteristics, reliability, small size and tissue equivalence as well as their accuracy and precision (Moscovitch & Horowitz, 2007; Rivera, 2012; Mukundan et al., 2007; Yoshizumi et al., 2007). The use of TLDs are particularly labour intensive and time consuming. It typically takes around 7 hours for routine dosimetry due to the additional steps of annealing and read out which are needed in

order to generate accurate results. As a result, within this thesis due to the large number of protocol evaluations (n=432), it was necessary to explore a new method for organ dose measurement. Within the literature MOSFETs have been introduced as an alternative to TLD but with the advantage of a much faster dose acquisition time.

Some of the known limitations of MOSFETs are the energy and angular dependence, particularly for lower energies typically encountered in diagnostic radiology (Dong et al., 2002; Ehringfeld et al., 2005; Jones et al., 2005; Wang et al., 2005). However, these may be addressed to some extent with consistent positioning and appropriate correction factors. Dong et al. (2002) have demonstrated an increased sensitivity of MOSFET sensors at low doses (below about 5 mGy) compared with TLD-100H chips which varied less than 3% over the same dose range, suggesting that TLDs may be more suitable at the very low doses typically used in conventional radiography. The MOSFET dosimeter is small and has several advantages, such as multiple point dose measurements, real time readout, and ability to immediately reuse.

This section serves two main purposes: (1) to validate the MOSFET dose measurement method by comparing with TLDs as the standard of reference and (2) to compare the calculated ED of both method against values published in the literature to compare the accuracy of the measured results from MOSFETs.

In this study both the TLDs and MOSFETs detectors were calibrated against a solid-state dosimeter using a conventional X-ray machine (Varian) with an X-ray beam equivalent in quality to that of a Toshiba Aquilion 16 CT scanner (half-value layer, ≈ 5 mm Al at 120 kVp). The MOSFETs were experimentally evaluated against TLDs by placing them in an ATOM dosimetry phantom model representing an average adult male and measuring the absorbed and calculating ED for 54 CT brain protocols at three different CT gantry angulations, 0^{o}, 15^{o} and 27^{o}.

The absorbed doses measured with the MOSFETs in the scanned volume demonstrated reasonable agreement (on average within 6% to 13%) against the TLD measurements. The percentage difference between absorbed dose measured with MOSFET over TLD for organs in the scan volume were as follows: brain, 13% (23.82 mGy for TLD compared to 27.48 mGy for MOSFET); active bone marrow of the cranium 6% (2.25 mGy for TLD compared to 2.11 mGy for MOSFET). A study by Yoshizumi et al. (2007) compared the same high sensitivity MOSFETs against TLD-100H chips for CT examinations in an adult phantom. They found the

difference between the dosimetry methods ranged from 1% to 27% in the scanned volume (Yoshizumi et al., 2007). The disparity was much greater for organs outside of the field of view, due to the lower limit of detection for MOSFETs compared with TLDs (Yoshizumi et al., 2007). For the individual TLDs which measured absorbed doses to body organs from the brain CT, only 48% of the measured doses were greater than 1.4 mGy. This was for all TLDs, including those placed at a distance from the scanned volume (e.g. testes for a CT brain examination). However, for the TLDs placed in the directly irradiated volume, the measured absorbed doses were predominantly above 5 mGy. For this thesis the measurements for selected organ doses and the percentage difference for TLDs and MOSFETs, respectively, were as follows (thyroid, 0.36 mGy & 0.42 mGy, difference=16.6%; active bone marrow of the thoracic spine, 0.02 mGy & 0.023 mGy, difference=13%; breast, 0.12 mGy & 0.10 mGy, difference=16%; testes, 0.004 mGy & 0.011 mGy, difference=63%). Overall, ED estimates for adult CT brain examinations are on average 10% higher for MOSFET (mean ED 0.82 ± 0.07) than the TLD (mean ED 0.74 ± 0.04) measurements. As such, MOSFETs appear to be a reasonable alternative to TLDs for measuring CT organ absorbed doses in the scanned volume.

In these validation measurements the lower limit of MOSFET detection was 0.0018 mGy and the majority of the measurements taken were above this threshold. It was decided that the dose in the primary beam was most important for the experiments and it was for this reason that MOSFETs were considered to be a reasonable alternative to TLDs. But the potential impact would be on risk is that the ratio of MOSFET to TLD effective dose (ED) estimates for adult CT brain examinations are on average 10% higher than the TLD measurements, which mean the estimated risk of lifetime cancer induced will be overestimated by 10%. Intraclass correlation coefficients were used to quantify the reliability, an ICC value of 0.949 (95% CI 0.805 to 0.991) was obtained. The TLD ED_{mean} was 0.74 ± 0.04 with 95% confidence interval (CI) (0.49 – 0.98 mGy) and MOSFET ED_{mean} was 0.82 ± 0.07 with 95% confidence interval (CI) (0.54 – 1.1 mGy). Overall, there was good agreement between MOSFET measurement and the TLD method.

5.4 CT Equipment

A Toshiba Aquilion 16 CT scanner (Toshiba Medical Systems, Tokyo, Japan), as shown in **(Figure 5-2)** below, was used throughout this study. The Toshiba Aquilion 16 is a third-generation multi-slice helical CT scanner, featuring a 60-kW generator, 7.5 MHU tube and a minimum standard gantry rotation time of 0.5 seconds. In helical mode, it is capable of

acquiring 16 parallel rows of data per rotation, with collimations of 16 x 0.5 mm, 16 x 1.0 mm and 16 x 2.0 mm. A full specification of the Toshiba Aquilion 16-slice CT scanner is illustrated in **(Table 5-1)** (TOSHIBA, 2004).

Figure 5-2: Toshiba Aquilion 16 CT Scanner (TOSHIBA, 2004).

Table 5-1: Specification: Toshiba Aquilion 16-slice Computed Tomography (CT) scanner		
Operating parameters	**Acceptable**	**Preferred**
Fastest 360º rotation time (s)	≤ 0.6 + other	
Min nominal imaged slice width in axial mode (mm)	≤ 0.6 + 4 other	
Min kV range (kVp)	≥ 80 – 130	
Min mA range	≥ 30 – 345 (10 mA steps)	
Pitch range available for routine scanning	0.6 – 1.5	
Scanner gantry	**Acceptable**	**Preferred**
Min aperture diameter (cm)	≥ 70	
Min ranging gantry tilt (degrees)	≥ ± 30 (with gantry control)	
Laser positioning lights	Scan plane (internal & external)	Sagittal, coronal
Coincidence of laser light with scan plane (mm)	≤ ± 2	≤ ± 1
Gantry and couch controls	On both left & right of gantry	
X-ray tube	**Acceptable**	**Preferred**
Minimum filtration (mm Al)	≥ 2.5	
Continuous scan time (s)	≥ 100	
Detection system	**Acceptable**	**Preferred**
Detector type	Ceramic, solid state	
Scan field of view: extent of x-ray fan beam at isocentre in x-ray plane (cm)	≥ 50	
No. simultaneous z-axis data channels acquired per rotation	≥ 16	
Length of z-axis coverage per rotation (mm)	≥ 19	
Dose	**Acceptable**	**Preferred**
Display of $CTDI_{vol}$ on main console	Prospective	
Display of Geometric efficiency if < 70% on main console	Prospective	
Automatic control of tube current	To account for patient attenuation variation in x-ray plane	To account for patient attenuation variation in z-axis
Display monitor	**Complies with RCR SIG** (TOSHIBA, 2004)	
Screen size	19"	
Image display matrix	1024x1024	

The CT scanner was warmed up prior to each scanning session and was checked at regular intervals by a team of engineers from the manufacturer and local medical physicists (once

yearly by the engineers and twice yearly by a medical physicist as part of planned physics and manufacturer contracts). Within this process quality assurance tests were undertaken and the results were within acceptable levels recommended by the manufacturer and also complied with the radiation protection legislation of the international committee on radiation protection (ICRP) (ICRP, 2007a). **(Table 5-2)** and **(Table 5-3)** illustrates the list of the specific tests which were carried out by Medical Physics and Toshiba Medical Systems.

Table 5-2: List of Measurements Performed (Christie Medical physics & Engineering, 2015)

Measurement	Tolerance	Outcome		
		Pass	Fail	Ref
General Radiation Safety				
Operation of controls and warning devices	Functioning as expected	Pass		
CT System				
Dosimetry CTDI	Baseline ±15%	Pass		2.1.1*
Variation of output with helical pitch	Mean ±20%	Pass		
Image noise analysis	Inter slice mean ±10% Baseline ±10%	Pass		
CT number values	Baseline ±5HU(water) or ±10HU	Pass		
CT number uniformity	Difference between centre/periphery Body: Small ±10HU, Large ±20HU	Pass		
Artefacts	No visible artefacts	Pass		
Automatic Exposure Control/Dose Modulation	Functioning as expected	Pass		

* Computed Tomography Dose Index (CTDI)

Table 5-3: 2.1.1 Computed Tomography Dose Index (CTDI), the measured $CTDI_{100}$ at the isocentre in air (Christie Medical physics & Engineering, 2015)			
kV	Beam/detector collimation (mm)	Mode/SFOV	$CTDI_{100}$ (mGy/100 mAs)
120	12 (4x3)	Head/Small	28.7
"	2 (4x0.5)		71.5
"	4(1x4)		46.7
"	8 (4x2)		33.8
"	16 (4x4)		29.1
"	24 (4x6)		27.9
"	32 (4x8)		28.3
80	12 (4x3)		12.1
100	12 (4x3)		19.5
135	12 (4x3)		36.3
120	12 (4x3)	Body/Large	96.0
"	2 (4x0.5)		63.9
"	4(1x4)		46.2
"	8 (4x2)		43.3
"	16 (4x4)		39.8
"	24 (4x6)		40.7
"	32 (4x8)		38.5
80	12 (4x3)		21.7
100	12 (4x3)		32.2
135	12 (4x3)		53.4

5.5 Experimental Equipment

MOSFET (TN-RD-70-W Best Medical Canada, Ottawa, Ontario, Canada) and two Computerised Imaging Reference Systems (CIRS) ATOM dosimetry phantoms were used to carry out the dosimetry measurements. The two ATOM phantoms were representative of an adult patient and a one-year old child (CIRS, Inc, Norfolk, Virginia, US). There are several commercially available phantoms, including a number of paediatric options. The adult phantom represented the dimensions of an average adult person (ATOM Model 701-D; height: 173 cm, weight: 73 kg, and thorax dimensions: 12 x 14 cm, **Figure (5-3)**). The one-year old child was an ATOM Model 705-D with a height of 75 cm, weight: 10 kg, and thorax dimensions: 23 x 32 cm), **(Figure 5-3)** (Xu & Eckerman, 2010). ATOM phantoms are made from epoxy resin, with photon attenuation values within 1% for bone and soft tissue and 3% for lung tissue at photon energies from 30 keV to 20 MeV, as claimed by the manufacturer (CIRS, 2006; CIRS, 2010; Varchena, 2002); **(Figure 5-4)**. The adult phantom provides 281 dosimetry locations and the

phantom model representing the paediatric has 167 locations for dosimeters; for both the adult and paediatric phantom the locations are within 22 organs (CIRS, 2006; CIRS, 2013).

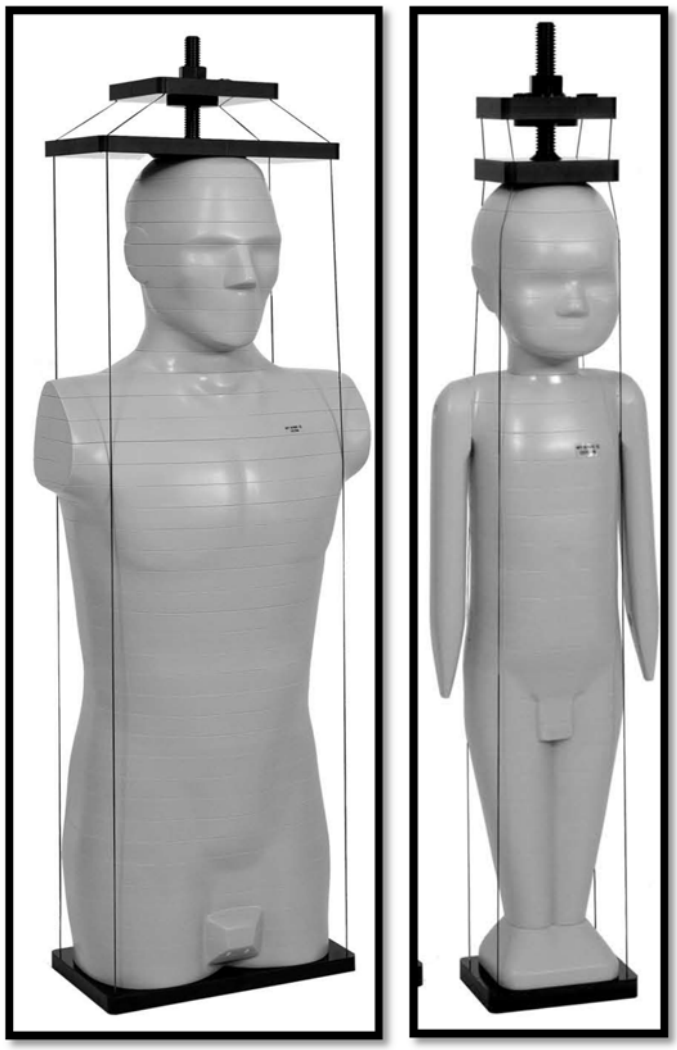

Figure 5-3: Illustrations of the adult and child ATOM dosimetry phantoms (Models: 701-D and 705-D CIRS, Inc., Norfolk, Virginia, US, 2013) (CIRS, 2013).

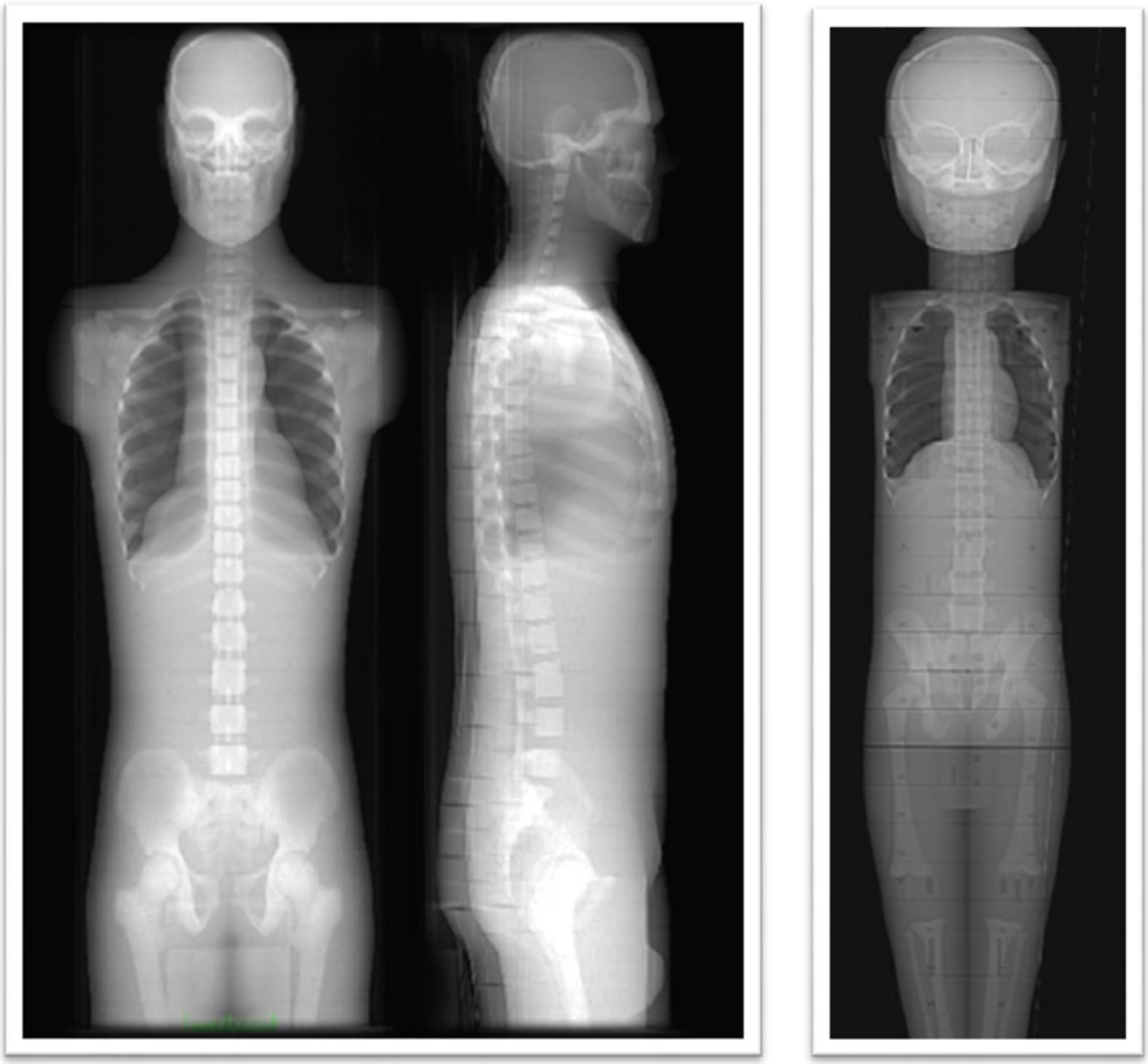

Figure 5-4: Anterior-posterior and lateral views of the dosimetry phantom of an adult and anterior-posterior view of the paediatric phantom (CIRS, 2013; Huda, Ogden, Lavallee, Roskopf, & Scalzetti, 2012).

CIRS currently produce five different paediatric phantoms each representative of an age bracket as shown in **(Table 5-4)**. Organ dimensions for children within each bracket do not vary by more than 15% and the phantoms are representative of age variations and both sexes (Varchena, 2002). For children, height is more indicative of body size than age, particularly when considering children suffering from an illness who may be undergoing CT examinations in a hospital. Hence, for dosimetry purposes, children falling within the height ranges specified in **(Table 5-4)** are best represented by the corresponding phantom. The phantom used in this experiment represents children 66-95 cm tall, which broadly corresponds to 0.5 to 3 years old (Varchena, 2002).

Table 5-4: CIRS paediatric anthropomorphic phantom range (Varchena, 2002).		
Phantom Name	**Age Range (years)**	**Height Range (cm)**
Newborn	0 - 0.5	Up to 66
1-year-old	0.5 - 3	66 - 95
5-year-old	3 - 7	95 - 124
10-year-old	7 - 13	124 - 156
15-year-old	13 - 17	156 – 168

(Table 5-5) displays the parameters of each tissue type used in the phantoms (CIRS, Norfolk, VA) (CIRS, 2013).

Table 5-5: Parameters of Anthropomorphic Phantom (CIRS, Norfolk, VA) (CIRS, 2013).		
Tissue Type	**Physical Density (g/cc)**	**Electron Density (g/cc)**
Bone	1.60	5.030 x 1023
Soft Tissue	1.05	3.434 x1023
Spinal Cord	1.07	3.448 x 10 23
Spinal Disks	1.15	3.694 x1023
Lung	0.21	0.681 x 1023
Brain	1.07	3.470 x 1023

The phantom representing an adult used in this thesis consisted of 39 sections each 25-mm thick (legs and arms are not included); and the phantom representing a 1-year old child consisted of 29 sections each 25-mm thick (arms and legs included). Dosimetry measurement locations are provided in holes drilled within these sections; these holes are plugged when not in use with soft tissue, bone or lung equivalent material depending on their location. The pre-drilled holes are 5mm; each hole is spaced in a 30 x 30 mm matrix. Within each hole plugs which are 5 mm diameter x 25 mm long can sit and accommodate TLD chips, TLD rods, TLD bars, TLD cubes, MOSFET detectors, and Landauer OSL Micro Dot and Nano Dot holders **(Figure 5-5)**. The selection of hole position is supported by detailed anatomical information about the average position of the 22 organs. A set of maps outlining the most frequently observed organ locations and also the optimised detector hole distributions within each organ accompanies each phantom with "-D" configuration. The hypothetical outline of the internal organs appropriate for each section is shown on an organ map. The map also shows the drilled holes into each section along with the corresponding unique hole ID as shown in **(Figure 5-6)**. These holes are in optimised locations in order to allow precise calculations using the minimum number of detectors necessary.

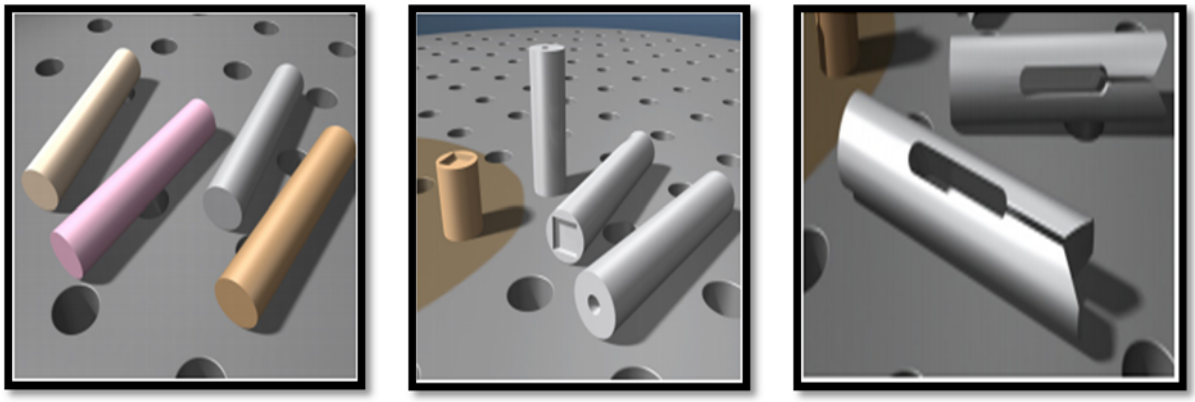

Figure 5-5: Standard solid tissue equivalent (TE) plugs, TLDs and chip rod holders and MOSEFT cartridges (CIRS, 2013).

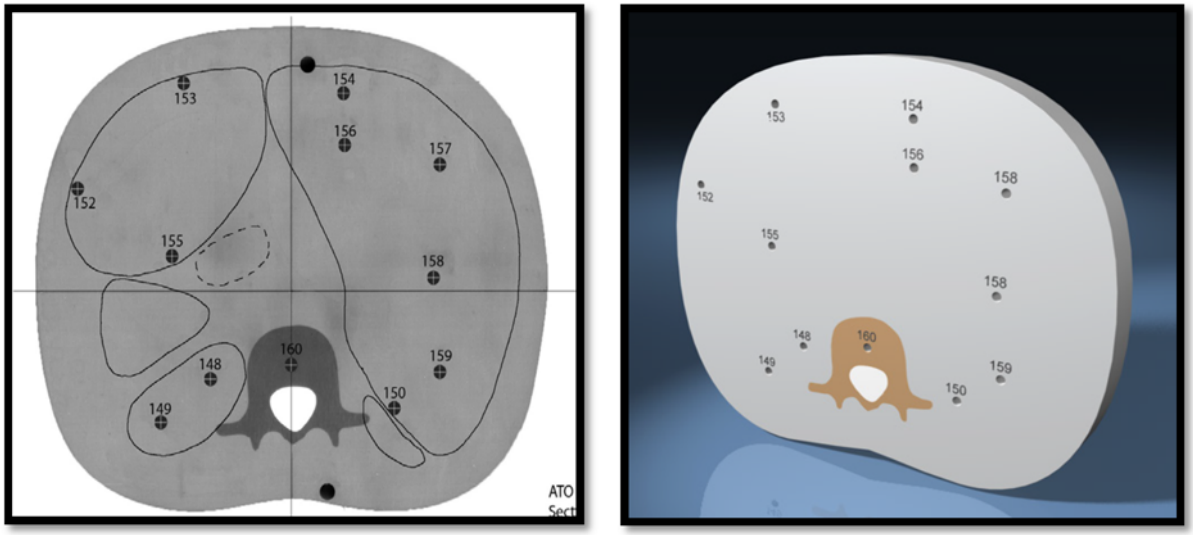

Figure 5-6: Model 702-D Section 23 organ map, the first image showing theoretical organ outlines and the second image showing organ dosimetry option (CIRS, 2013).

The organ map is used in conjunction with a lookup table that indicates for each organ, the number of detectors to insert, the hole number for each inserted detector and the corresponding detector depth for each hole. This can help the user for minimising the quantity of detectors to be used.

As indicated by CIRS, the ATOM phantoms manufacture company, the Model 701 adult ATOM male can also represent a larger female patient than the Model 702. For this reason, breast attachments are available for use with the Model 701 to calculate the absorbed dose to the female breast. One standard shaped size, 350cc, is available and is provided drilled with 5mm diameter thru holes in a 2cm X 2cm grid pattern **(Figure 5-7)** (CIRS, 2013). These breasts were used to measure absorbed dose to female breasts and facilitate ED and risk calculations.

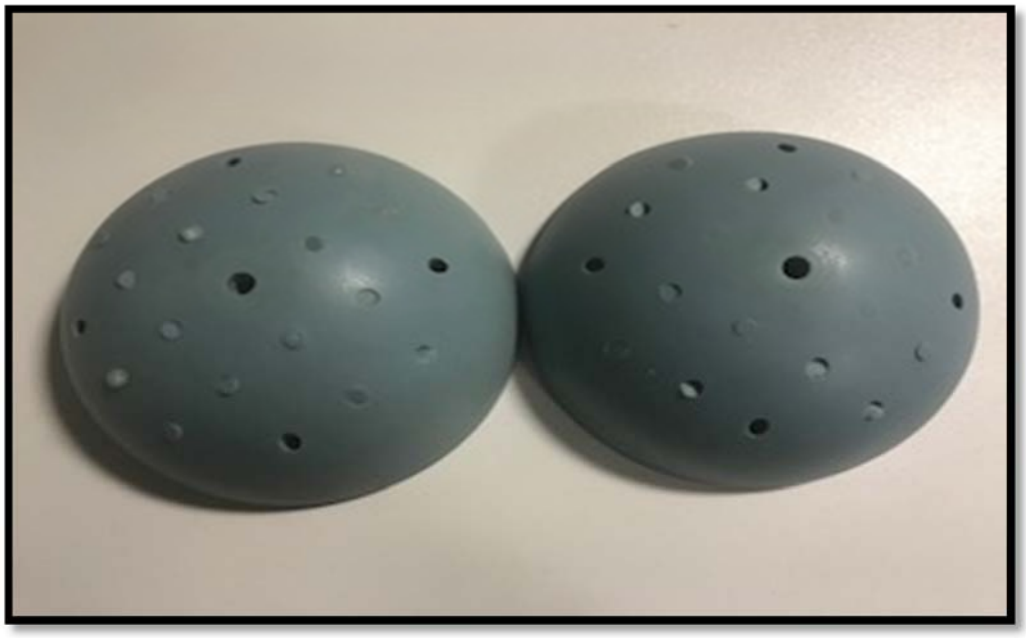

Figure 5-7: Female single breasts attachment (350cc) 701-BR-350 (CIRS, 2013). The unplugged holes were used for MOSFET accommodation.

(Table 5-6) and **(Table 5 -7)** show the number of dosimeters located in each organs and tissues for adult and paediatric ATOM phantoms, respectively. More details of the location and number of dosimeters within the slices of the Adult and paediatric ATOM phantoms are illustrated in **Appendix (A)** within **(Table A - 1)** and **(Table A - 2)** on pages **197** and **199**, respectively.

Table 5-6: Location and number of dosimeters within the organs and tissues of the ATOM phantom model representing an Adult person.					
No	**Organs**	**Number of Dosimeters**	**No**	**Remainder Organs and tissues**	**Number of Dosimeters**
1	Brain	11	13	Adrenals	2
2	Eyes*	2	14	Thymus	4
3	Breast male/female	2/8	15	Heart	2
4	Thyroid	6	16	Spleen	12
5	Oesophagus♠	3	17	Pancreas	5
6	Lung	36	18	Gall bladder	5
7	Stomach	14	19	Small intestine	5
8	Liver	29	20	Kidney	16
9	Colon	11	21	Prostate	3
10	Bladder•	16	22	Ovary	2
11	Tests	2			
12	Bone marrow	85			
	Cranium	4			
	Cervical Spine♠	2			
	Clavicle	10			
	Scapular	10			
	Sternum	4			
	Femora	4			
	Mandible ♣ ◊	6			
	Pelvis	18			
	Ribs	18			
	Thoraco-lumber Spine	9			
Total number of dosimeters		**281**			

* Not included in effective dose calculations.

♠ Dosimeters located in the anterior of C2 and upper oesophagus were used to calculate extra thoracic organ dose.

• Dosimeters located in the bladder were used to estimate the dose to the uterus.

♣ Dosimeters located in the left and right lingula of the mandible and to the left and right of the sublingual fossa were used to calculate salivary gland organ dose.

◊ Dosimeters located in the left and right lingula of the mandible were used to calculate oral mucosa organ dose (Tootell et al., 2014).

Table 5 -7: Dosimeter location in organs and tissues within ATOM phantom model representing one year child.			
Organs and Tissues	**Number of detectors**	**Organs and Tissues**	**Number of detectors**
Brain	9	Thymus	2
Bone Marrow (ABM)♣ ◊	64	Spleen	4
Eyes*	2	Kidneys	8
Thyroid	2	Adrenals	2
Oesophagus♠	3	Heart	2
Lungs	25	Pancreas	3
Breasts	2	Gall Bladder	2
Stomach	6	Prostate	4
Bladder	6	Oral Mucosa	3
Colon	8	Small Intestine	4
Salivary Glands	3	Extrathoracic	2
Testes	2		
Total number of dosimeters	**167**		

* Not included in effective dose calculations.

♠ Dosimeters located in the anterior of C2 and upper oesophagus were used to calculate extra thoracic organ dose.

♣ Dosimeters located in the left and right lingula of the mandible and to the left and right of the sublingual fossa were used to calculate salivary gland organ dose.

◊ Dosimeters located in the left and right lingula of the mandible were used to calculate oral mucosa organ dose (Tootell et al., 2014).

5.5.1 Mobile MOSFET Dosimetry System

For brain scans using the phantoms dose measurements were made using a mobile MOSFET wireless dosimetry system (Model TN-RD-70-W, Best Medical Canada Ltd., Ottawa, Canada) (MobileMOSFET, 2007). The mobile MOSFET device TN-RD-70-W comprises a TN-RD-38 wireless Bluetooth transceiver, four TN-RD-16 reader modules, twenty high-sensitivity TN-1002RD-H dosimeters, and TN-RD-75M software. In this study, TN-RD-16 reader modules that can be independently set to control five dosimeters were operated using the high bias voltage, 13.6 V, to obtain the best possible accuracy **(Figure 5-8)**. A TN-RD-38 wireless transceiver was used for data communication between the TN-RD-16 reader modules and a PC (Ottawa, Best Medical Canada Ltd.) (Koivisto et al., 2015). The MOSFET system measures the difference in threshold voltage before and after an X-ray exposure. This difference in voltage is proportional to the absorbed dose (Carvajal et al., 2010). Threshold voltages were

read immediately after each exposure. Four readers can be simultaneously used during a single procedure if required, allowing for a total of 20 dosimeters to be in operation. More information about the structure of the MOSFETs response to ionising radiation are illustrated in (background) chapter section **(3.6.2.2)** on page **48**.

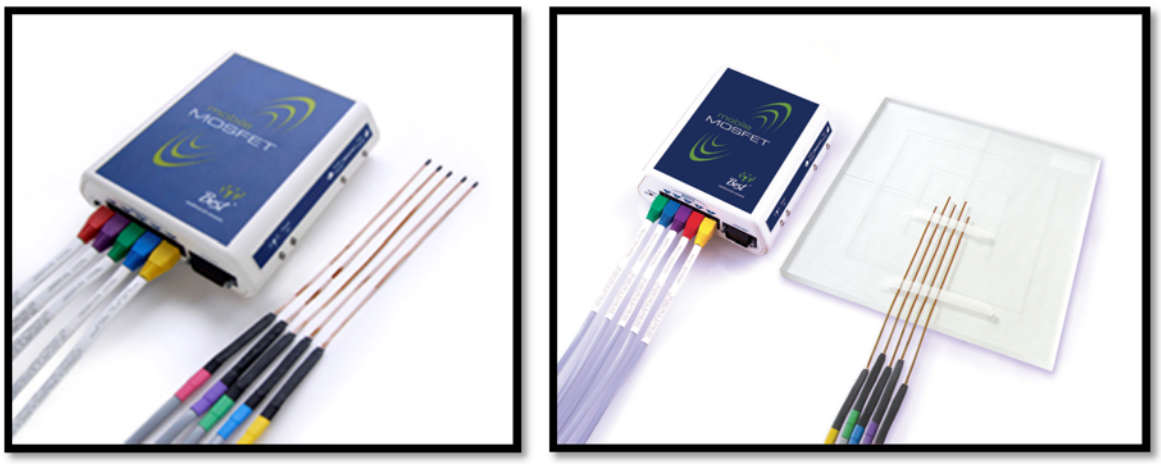

Figure 5-8: MOSFET reader with five dosimeters and the calibration jug (Best medical Canada Ltd.) (MobileMOSFET, 2007).

5.5.2 MOSFET Calibration

Five individual MOSFETs were connected to each reader module, which transferred data wirelessly to a laptop. Four reader modules with 20 high sensitivity MOSFETs were calibrated and used. The MOSFETs were calibrated using a general radiography X-ray tube (Wolverson Arcoma, Willenhall, UK X-ray tube and CMP 200 DR generator) matched to the CT scanner beam quality to be used during the measurements. This was achieved on the general X-ray tube by using 120 kVp and adding 1 mm Al filter. When measured with a calibrated solid state detector, the Unfors Mult-O-Meter (Unfors RaySafe, Billdal, Sweden) digital dosimeter; Model 503L (Unfors Instruments, AB). For calibration, each set of five MOSFETs connected to a reader module was placed adjacent to the solid-state detector **(Figure 5-9)**. The MOSFETs were placed at a source-to-dosimeter distance of 60 cm, as recommended by the manufacturer with the black bulb side of the dosimeters facing the beam and with no build-up material on the dosimeter (Best Medical Canada, 2007).

Each MOSFET wire was colour coded and connected to the same terminal in the same bias reader for calibration and subsequent measurements. Three exposures were made at different tube currents of 100, 160, 250, 360 and 450 mAs and millivolt to milligray (mV/mGy)

conversion factors were computed using the MOSFET software (DXPOSURE Software, Version 2.2, Best Medical Canada, Ottawa, Ontario, Canada) (MobileMOSFET, 2007). All MOSFET measurements were read out immediately after exposure to avoid any additional charge build up. All the steps mentioned above have been repeated for all four readers and the calibration factors obtained for all 20 dosimeters are summarised in **(Table 5-8)** on page **107**.

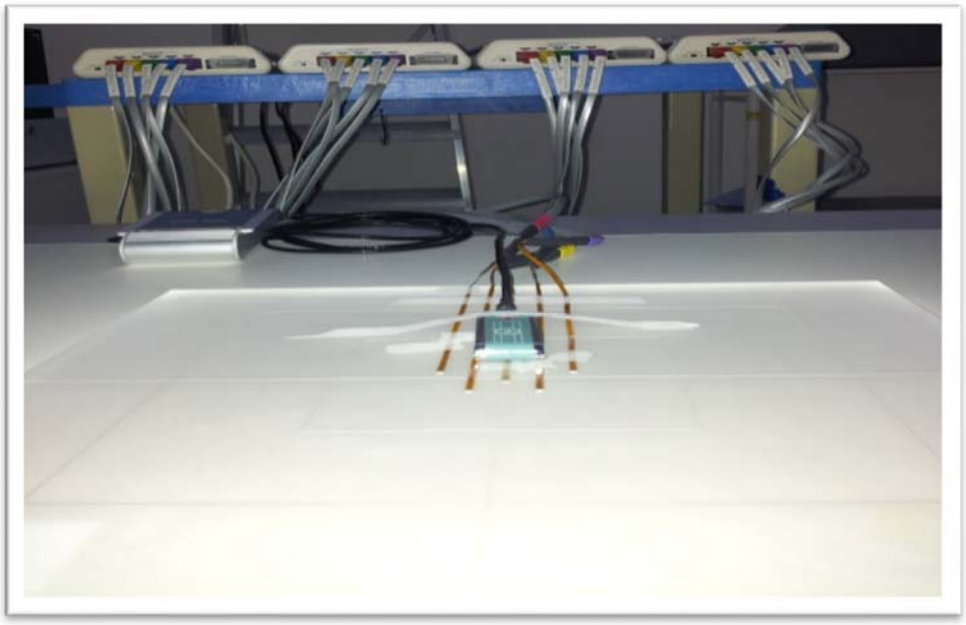

Figure 5-9: First image shows MOSFET reader and 5 dosimetries and the second image illustrates calibration set up.

Table 5-8: Calibration factors summarised across all four readers (1, 2, 3 & 4) and for all 20 dosimeters.					
mAs	100	160	250	360	450
Solid State Entrance Surface Dose (ESD) mGy	9.875	15.430	24.110	34.780	43.660
Reader 1 (0737) Calibration Factors mV/mGy	MOSFET #1	MOSFET #2	MOSFET #3	MOSFET #4	MOSFET #5
	1.66	**1.76**	**1.67**	**1.59**	**1.65**
mAs	100	160	250	360	450
Solid State Entrance Surface Dose (ESD) mGy	9.875	15.45	24.14	34.84	43.73
Reader 2 (0738) Calibration Factors mV/mGy	MOSFET #1	MOSFET #2	MOSFET #3	MOSFET #4	MOSFET #5
	1.54	**1.62**	**1.62**	**1.69**	**1.67**
mAs	100	160	250	360	450
Solid State Entrance Surface Dose (ESD) mGy	10	15.65	24.44	35.26	44.26
Reader 3 (0735) Calibration Factors mV/mGy	MOSFET #1	MOSFET #2	MOSFET #3	MOSFET #4	MOSFET #5
	1.70	**1.76**	**1.73**	**1.72**	**1.65**
mAs	100	160	250	360	450
Solid State Entrance Surface Dose (ESD) mGy	9.947	15.53	24.27	35.04	43.96
Reader 4 (0736) Calibration Factors mV/mGy	MOSFET #1	MOSFET #2	MOSFET #3	MOSFET #4	MOSFET #5
	1.61	**1.70**	**1.67**	**1.65**	**1.61**

5.5.3 Determining MOSFET Reproducibility

The reliability of an instrument is the ability of that instrument to produce consistent results under the same measurement conditions over time (Field, 2013, Pallant, 2010). To ensure that the findings of the study are valid, and to increase confidence in the results, it is important to perform a reliability study on the MOSFET dosimetry system. To achieve this, similar to TLDs and before collecting all experimental data, MOSFET dosimeters were checked for dose measurement reproducibility. After obtaining the calibration factors for all the 20 dosimeters, before exposure in the CT scanner, the 20 MOSFET dosimeters were deployed throughout the

paediatric ATOM phantom organs and tissues for 167 locations. The dosimetry phantom was scanned using a commercially available 16-MDCT scanner (Toshiba Aquilion 16). The helical axial brain (5.0-mm-thick slices, ATC mAs, 100 kVp) paediatric protocols were selected. CT scanning was repeated three times (same protocol) and each time the absorbed dose was recorded and then the ED calculated for each of the three examinations and the results are illustrated in **(Table 5-9)**. Intraclass correlation coefficients were used to quantify the reliability, an ICC value of 0.998 (95% CI 0.987 to 0.997) was obtained.

Table 5-9: MOSFET method reproducibility testing results (model phantom representing adult data).

Scan No	Angle	Rotation Time (Secs)	Detector Configuration (mm)	kV	mAs (fixed)	Scan Length (mm)	Effective Dose (mSv)
1	0	0.5	0.5x16	100	ATCM	136	1.3
2	0	0.5	0.5x16	100	ATCM	136	1.4
3	0	0.5	0.5x16	100	ATCM	136	1.4

Obtaining and calculating the average absorbed dose for large organs or tissues can be a challenge. MOSFETs need to be placed at all available locations within the phantom. Multiple MOSFETs at each location improves the accuracy of measurement (Scalzetti et al., 2008). In an adult male phantom, Scalzetti et al., (2008) recommend a system involving 187 measurement points in order to properly obtain the average organ absorbed dose. Whereas other studies used a varying number of measurement locations ranging from 20 to 66 in order to make an assessment of ED in CT examinations (Groves et al., 2014; Hollingsworth et al., 2007; Hunold et al., 2003; Hurwitz et al., 2007; Kawaura et al., 2006; Scalzetti et al., 2008).

5.6 CT Protocols

The experiment conducted within this thesis utilised two different brain protocols (helical and sequential for adult) and helical for paediatric with various scan parameters. Within clinical practice a CT brain examination is commonly undertaken in sequential mode in order to allow angulation of the gantry to reduce the dose to the lens of the eye. Depending on the clinical indication in adult patients both helical and sequential modes can be used but more commonly only a helical mode is used for paediatric CT examinations. Justification for helical modes in paediatric examinations is based on the need to eliminate or reduce any movement (motion)

artefacts. With helical CT, eye dose can be reduced by using a faster helical scanning protocol or by utilising shorter rotation time.

5.6.1 Adult CT Protocols

As mentioned previously two standard brain protocols (adult sequential and adult helical) were assessed together with changes in the different scan parameters as shown in **(Table 5-10)** and **(Table 5-11)** for helical and sequential protocols, respectively. The standard helical protocol scan parameters used by Toshiba Aquilion 16 protocol (Brain 5mm Helical) are: 120 kV, mA range: 300, rotation time: 1.0 seconds, range: 140 mm, D-FOV: 240.0 (S), effective mAs: 437, total scan time: 28.365, CE: off, thickness: 16 rows – 0.5x16, detail: PF. 0.688 / HP 11.0. Head brain axial, image thickness: 5.0 mm, reconstruction interval: 5.0 mm, Sure Exp. 3D: high quality: SD: 1.80, max range: 310.0, max scan time: 59.274 focus: small. Whereas the main scans parameters of sequential protocol (Head Brain Axial 4mm) are: kV: 120, mA Range: 280, rotation time: 1.0, range: 8.0, D-FOV: 240.0 (S), effective mAs: 280, couch movement: out 8.0, direction: out, image thickness: 4.0 mm, sure Exp. 3D: off, slice thickness: standard 2.0x4, CE: off, focus: small. Full details of CT scan protocols parameters are shown within **(Table B - 1)** and within **(Table B - 2)** in **Appendix (B)** on pages **204** and **211**, respectively.

Table 5-10: Adult brain helical CT protocol scans parameters examined using MOSFETs.

Rotation Time (S)	Gantry Angle (Degrees)	Detector Configuration (mm)	Pitch Factor / Helical Pitch	Sure Exp. 3D (ATC)
0.5 and 1.0	0, 15 and 27	0.5x16, 1.0x16 and 2.0x16	Detail PF 0.688/HP11.0, Standard PF 0.938/HP15.0 and Fast PF 1.438/HP 23.0	High Quality SD 1.80, Standard SD 2.00 and Low Dose SD 2.20

Table 5-11: Adult brain sequential CT protocol scans parameters examined using MOSFETs.

Rotation Time (S)	Gantry Angle (Degrees)	Detector Configuration (mm)	Sure Exp. 3D
0.5 and 1.0	0, 15 and 27	0.5x4, 1.0x4 and 2.0x4	High Quality SD 1.80, Standard SD 2.00 and Low Dose SD 2.20

5.6.2 Paediatric Protocols

Using the paediatric ATOM phantom, the brain was scanned using a helical protocol only with changes in scanning parameters as illustrated in **(Table 5-12)** and **(Table 5-13)**. The main scan parameters of Toshiba Aquilion 16 paediatric protocol (Brain Infant 0-3 Yrs HCT 5mm) were as follows: KV: 120, mA: 150, rotation time: 0.5 Secs, range: 125.0 mm, D-FOV: 240.0 (S), effective mAs: 110, total scan time: 12.819, direction: out, CE: off, thickness: 16 row – 0.5x16: detail: Pitch Factor 0.688/Helical Pitch 11.0, paediatric brain baby, image thickness: 5.0 mm, reconstruction interval: 5.0 mm, max range: 1080.0, max scan time: 99.638, focus: small. Full details of CT scan protocols parameters are shown within **(Table C - 1)** and **(Table C - 2)** in **Appendix (C)** on pages **213** and **220**.

Table 5-12: Paediatric brain infant CT helical protocol scans parameters.

Rotation Time (S)	Gantry Angle (Degrees)	Detector Configuration (mm)	Pitch Factor / Helical Pitch	Sure Exp. 3D
0.5 and 0.75	0, 15 and 27	0.5x16, 1.0x16 and 2.0x16	Detail PF* 0.688/HP♠ 11.0, Standard PF 0.938/HP15.0 and Fast PF 1.438/HP 23.0	High Quality SD 4.00, Standard SD 6.00 and Low Dose SD 8.00

PF*= Pitch Factor, HP♠= Helical Pitch, ATC= Automatic Tube Current, SD= standard deviation.

Table 5-13: A detailed of paediatric protocol changes examined using MOSFET.

No	Gantry Angle (Degrees)	Rotation Time (S)	Detector Configuration (mm)	kV	mAs
1	0, 15 and 27	0.5, 0.75 and 1.0	0.5x16	100 & 120	120, 160, 180 & 200
2					
3					

5.7 Quantification of Absorbed Radiation Dose Method

5.7.1 Adult CT Head Acquisitions

The adult phantom scanning procedure is outlined in the following flow chart diagram for MOSFET dosimeters, **(Figure 5-10)**.

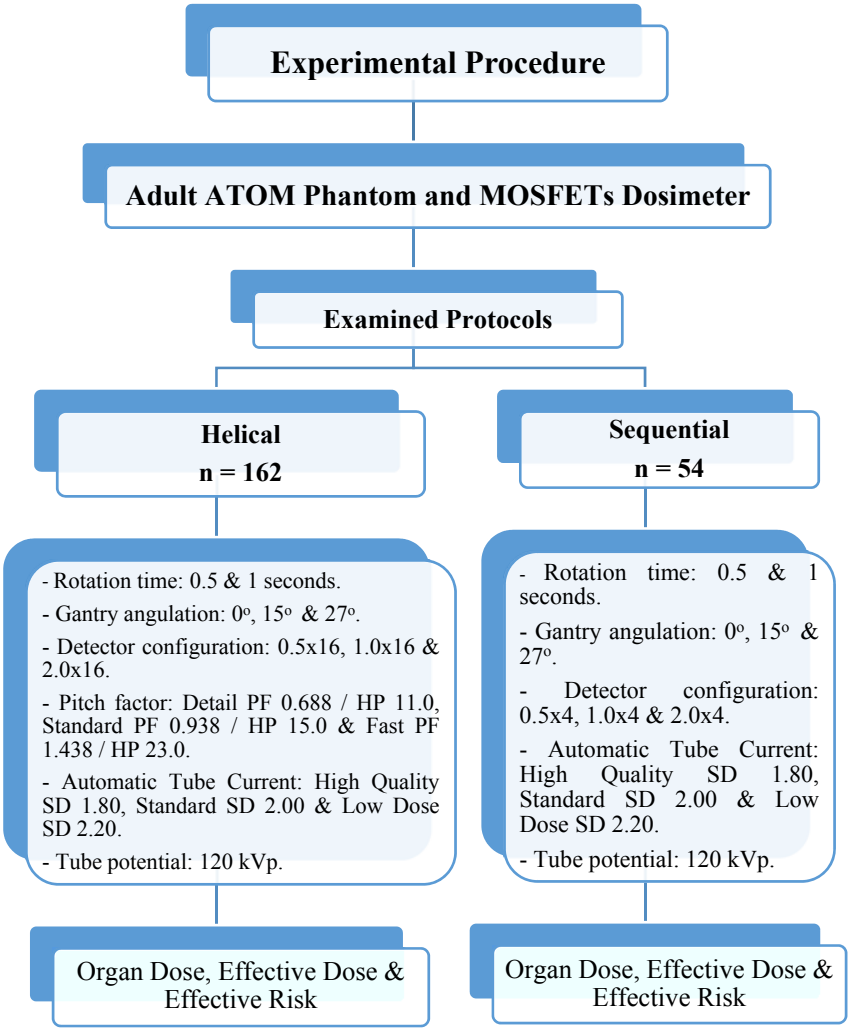

Figure 5-10: Illustrates adult ATOM phantom experiment procedure flow chart.

For the adult phantom, following each of the CT acquisitions **(Figure 5-11)**, the radiation dose was measured using the twenty MOSFET dosimeters pre-loaded in different locations **(Figure 5-12)**. With only 20 dosimeters available the phantom was loaded and irradiated in the order of locations 1-20, then 21-40 and so on. The obtained values (mV/mGy) were sent to the computer via wireless network and saved as an Excel file. This was then repeated until all of the 281 dosimetry locations had mV readings. Once the data had been gathered they were automatically divided via mobile MOSFET software by the respective calibration factors **(Table 5-8)** on page **107**, section **(5.5.2)** for each MOSFET dosimeter in order to determine organ and tissues absorbed dose. These were then multiplied by tissue weighting factors as recommended by ICRP 103 report (2007) in order to allow the estimation of ED (ICRP, 2007c). This procedure was repeated for all parameters of the CT adult protocols (helical and sequential)

at three different gantry angles (0º, 15º & 27º) 162 and 54 acquisitions for helical and sequential protocols respectively **(Figure 5-13)**.

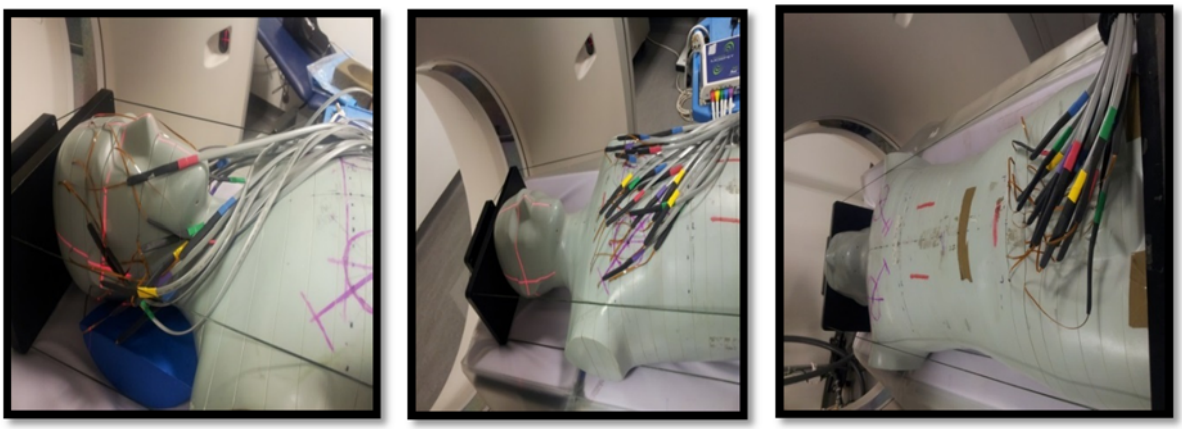

Figure 5-11: Brain CT scanning acquisitions.

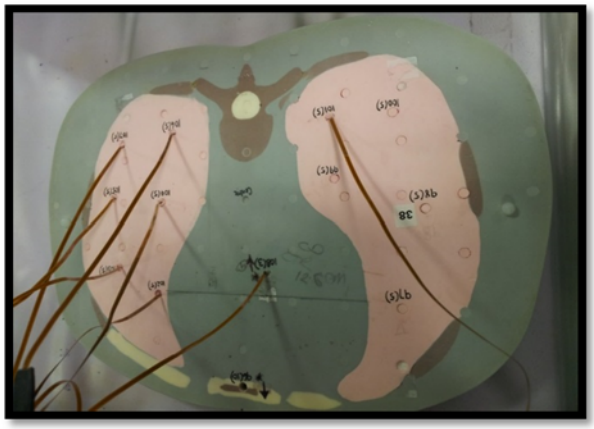

Figure 5-12: MOSFET dosimeters pre-loaded at different locations within adult ATOM phantom.

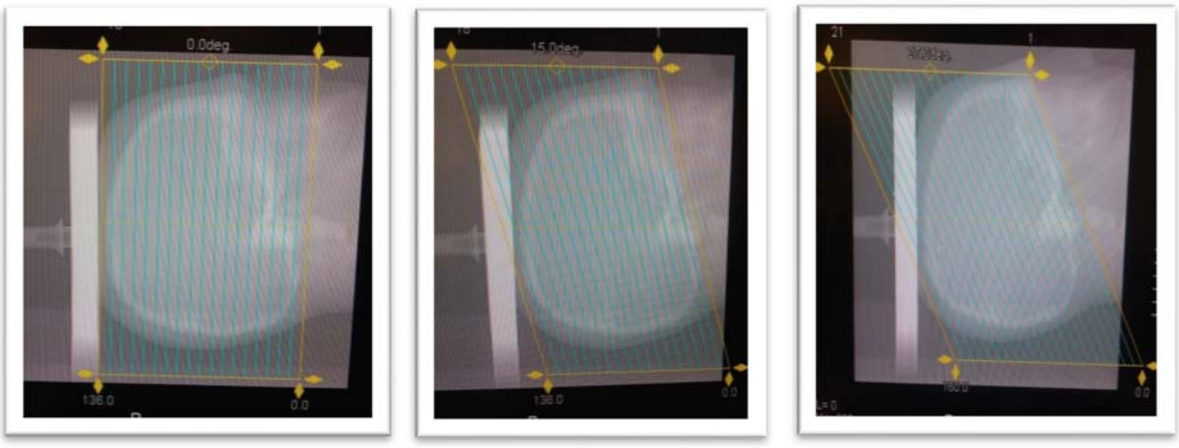

Figure 5-13: CT image of scout view showing the three angles of scan acquisitions at 0°, 15° and 27°, respectively.

5.7.2 Paediatric CT Head Acquisitions

Paediatric organs and tissues absorbed doses were obtained using MOSFETs and helical CT scanning protocol as illustrated by the follow flow chart diagram, **(Figure 5-14)**.

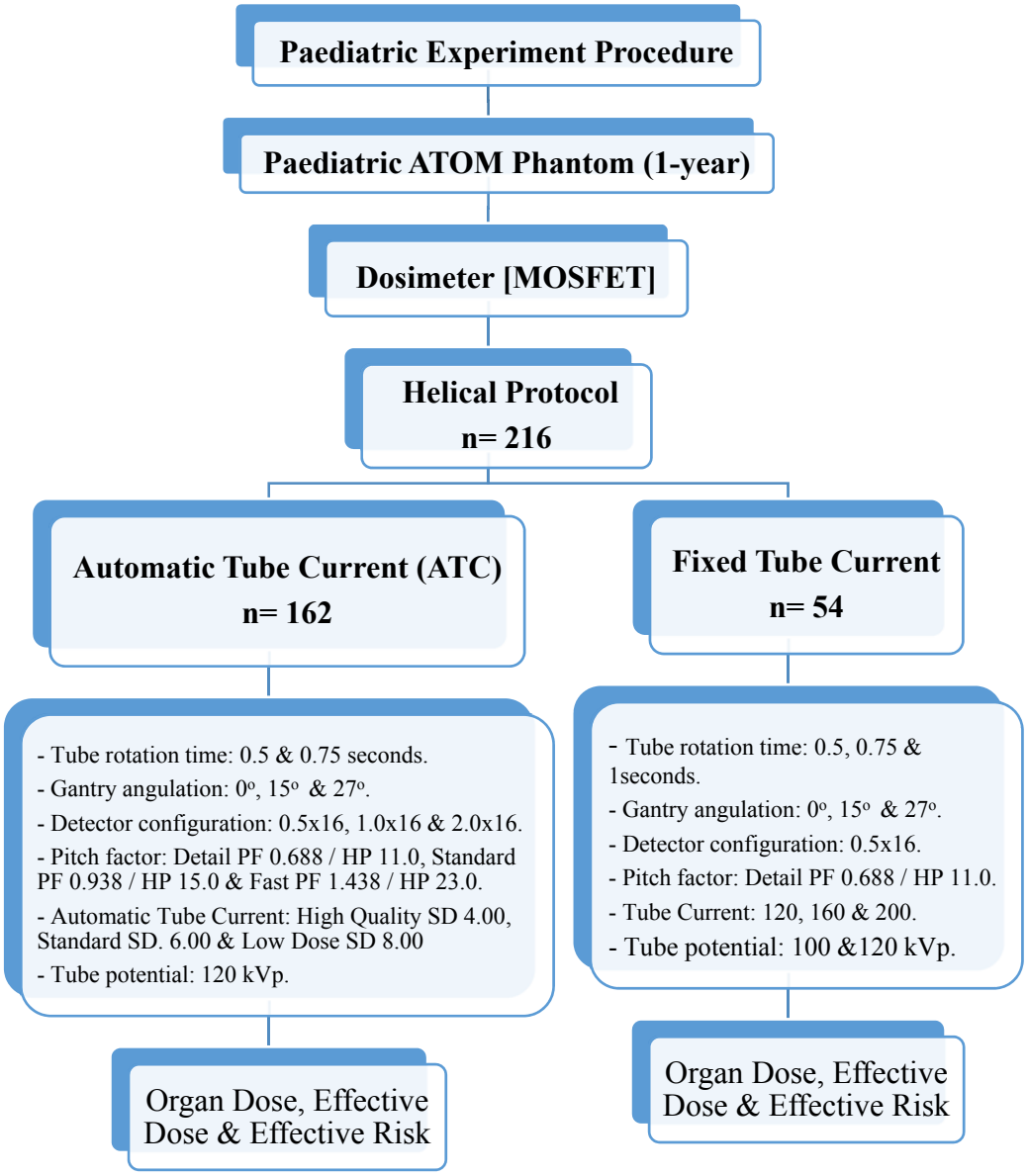

Figure 5-14: Paediatric brain CT scanning experiment procedure flow chart.

For the paediatric dosimetry 20 MOSFETs were loaded in the phantom at define of different locations. Locations of the MOSFETs are displayed in **(Table 5 -7)** section **(5.5)** on page **104**. The combination of the MOSFET wire and tape resulted in a small gap between adjacent phantom slabs. Care was taken when moving the phantom for the experimental set up as the MOSFET wires protruded when the phantom was fully assembled. For measurements of absorbed dose for CT examinations, the MOSFETs were placed inside the provided locations

of tissues and organs within the dosimetry phantom which is a total of 167 locations **(Figure 5-15)**, whereas **(Figure 5-16)** illustrated the scout view of the three gantry angles used for all the measurements. The calibration factor calculated for each MOSFET relative to the solid-state dosimeter measurement already takes into account the conversion from mV to cGy then converted to mGy.

Full paediatric head CT dosimetry measurements were taken with tube potential of 100 and 120 (kVp), mAs of 100, 120, 160 and 200. Whereas the angulation and rotations time varies from 0, 15 & 27 and 0.5, 0.75 and 1 seconds respectively at slice thickness of 0.5 mm x 16 to account in total for (54) acquisitions are illustrated in **Appendix (C)** within **(Table C - 2)** on page **220**. Additionally, the 0 to 3 years clinical paediatric protocol was also tested and a detailed list of (162) acquisitions of this protocol changes are illustrated in **Appendix (C)** within **(Table C - 1)** on page **213**. The protocol parameters were manipulated to assess all of the available options for each parameter, except the tube voltage which was kept consistent (kVp: 120). The following parameters were used; Sure Exposure automatic tube current (High Quality SD 4.00, Standard SD 6.00, and Low Dose SD 8.00), helical pitch factors (Detail pitch factor 0.688 / helical pitch 11.0, Standard pitch factor 0.938 / helical pitch factor 15.0 and Fast pitch factor 1.438 / helical pitch 23.0), also three different detector configurations (0.5x16 mm, 1.0x16 mm and 2.0x16 mm) as well as two rotation times and three gantry angulation (0.5 & 0.75 seconds) and (0^{o}, 15^{o} and 27^{o}), respectively.

Figure 5-15: Paediatric phantom MOSFET loading and scan set up.

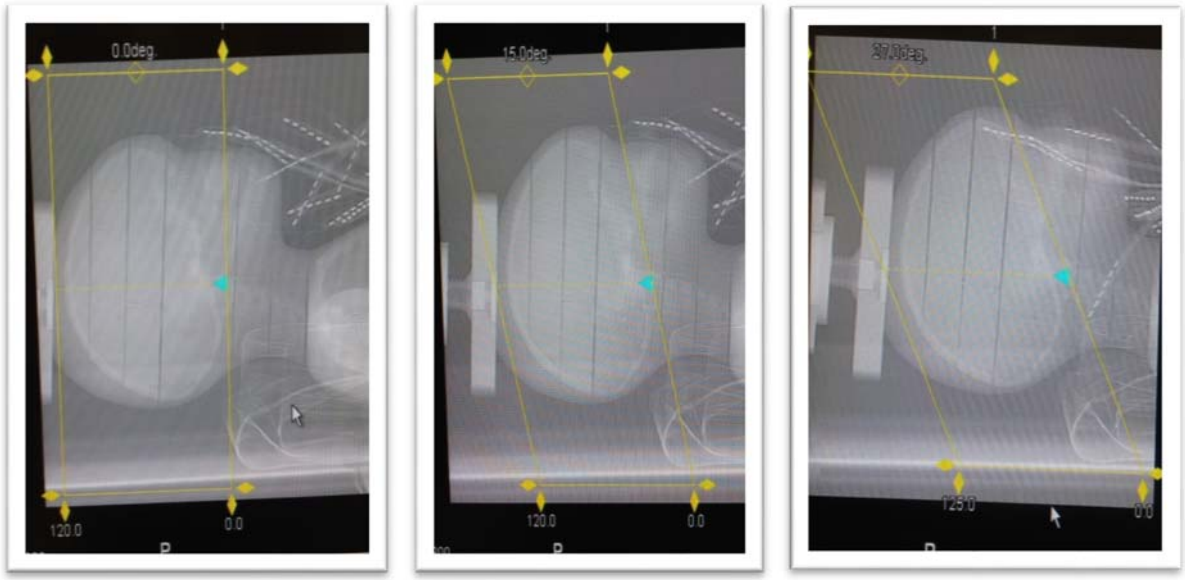

Figure 5-16: Scout view of the paediatric brain showing the three angles of scan acquisitions at 0°, 15° and 27° respectively.

5.8 Measuring Absorbed Dose and Calculating Effective Dose

The absorbed dose to selected organs (red bone-marrow), colon, lung, stomach, breast, gonads, bladder, oesophagus, liver, thyroid, brain, salivary glands and remaining tissues: adrenals, extrathoracic region, gall bladder, heart, kidneys, oral mucosa, pancreas, prostate, small intestine, spleen, thymus, uterus/cervix) and eye. ED were calculated from average measured absorbed doses to the organs using both the adult and paediatric phantoms. The absorbed dose to the eyes were measured for the purpose of quantifying the detrimental effects to see if exceed the threshold level proposed by ICRP.

In order to calculate the ED using the absorbed dose measurements the following procedure was followed. The absorbed doses for each organ and tissue were summed and then an averaged, this figure was then multiplied by a radiation weighting factors (a radiation weight factor of 1 was used since all experiments involved X-ray photons) as reported by ICRP in their 103 report, (2007) (ICRP, 2007c) using the following equation.

$$H_T = W_R \,.\, D_{T,R}$$

Where H_T is the equivalent dose.

W_R is the radiation weighting factor

$D_{T,R}$ is the absorbed dose in the tissue (T) by radiation type (R).

Organ and tissue doses were measured for the CT head imaging protocols (helical and sequential) using MOSFET dosimeters (adult and paediatric). Only helical protocols were tested for paediatric CT head imaging as this was thought to best reflect current clinical trends. The methodology used to measure and evaluate ED are discussed in sections **(5.7.1)** and **(5.7.2)** on pages **110** and **113** for MOSFET methods, respectively.

Radiation and tissue weighting factors are provided by the International Commission on Radiological Protection (ICRP) and the factors are updated over time based on advances in the scientific understanding of the effects of radiation on the human body **(Table 5-14)**.

Table 5-14: Tissue weighing factors from ICRP 103 (ICRP, 2007d).

Organ	Tissue Weighting Factor
Gonads	0.08
Bone marrow	0.12
Colon	0.12
Lung	0.12
Stomach	0.12
Breast	0.12
Bladder	0.04
Liver	0.04
Oesophagus	0.04
Thyroid	0.04
Skin	0.01
Bone (surface)	0.01
Salivary Glands	0.01
Brain	0.01
Remainder: Adrenals, Extrathoracic (ET) region, Gall bladder, Heart, Kidneys, Lymphatic nodes, Muscle, Oral mucosa, Pancreas, Prostate (♂), Small intestine, Spleen, Thymus, Uterus/cervix (♀).	0.12
TOTAL	1.00

The most recent recommendations of tissue weighting factors which published in 2007 are contained in ICRP Publication 103 (ICRP 103) (ICRP, 2007b; Jack Valentin, 2007), which updated ICRP Publication 60 (ICRP 60) (ICRP, 1991b) that having been in use for about 20 years. Contributions to ED were assessed from all tissues except for bone surface, skin, lymphatic nodes, and muscle, which did not have locations for dosimeters within the ATOM

phantoms. The absorbed dose for each tissue was multiplied by the tissue weighting factor to determine the contribution of each tissue toward effective dose using equation below. **(Table 5-15)** representing an example of calculating ED from organs and tissues absorbed dose for both adult and paediatric protocols. For bones which contained bone marrow, the organ dose data were multiplied by its relevant percentage of active bone marrow as recommended by Cristy, 1981 (Cristy, 1981) see (Section **5.8.3)** below on page **118**.

$$E = \Sigma W_T \, . \, H_T$$

Where E is the effective dose to the whole body

W_T =tissue weighting factor of tissue (T) defined by ICRP 103

H_T equivalent dose absorbed by tissue (T)

Table 5-15: An example of an ED calculation, mGy.

Organ	Absorbed Dose (mGy)	Tissue Weighting Factor	Effective Dose (mSv)
Brain	27.482	0.01	0.275
ABM	2.261	0.12	0.271
Eyes	32.050	0	0.000
Thyroid	0.362	0.04	0.014
Oesophagus	0.000	0.04	0.000
Lungs	0.255	0.12	0.031
Breasts	0.012	0.12	0.001
Liver	0.072	0.04	0.003
Stomach	0.063	0.12	0.008
Bladder	0.096	0.04	0.004
Colon	0.112	0.12	0.013
Salivary Glands	3.008	0.01	0.030
Testes	0.039	0.08	0.003
Total			**0.654**
Remaining Organs			
Thymus	0.105	0.12	
Spleen	0.117		
Kidneys	0.039		
Adrenals	0.144		
Heart	0.000		
Pancreas	0.011		
Gall Bladder	0.046		
Prostate	0.295		
Oral Mucosa	3.008		
Small Intestine	0.028		
Extrathoracic	1.035		
Total	**4.829**		
Grand Total	**4.829/11= 0.439**	**0.439*0.12 = 0.053**	**0.053+0.654 = 0.706**

5.8.1 Calculating Substituted Organ Absorbed Dose

The ATOM dosimetry phantom does not model all organs and tissues listed in ICRP 60 and ICRP 103 and often other organ absorbed doses are used as a substitute to approximate these doses (Z Brady, Cain, & Johnston, 2012). For tissues where there is no specific location to site a dosimeter within the phantom e.g. oral mucosa and salivary glands, the absorbed dose to the mandible was used. Similarly, the extrathoracic region (ET) is not specified in the dosimetry phantom and instead a point identified as the cervical spine (C2) and the superior margin of the oesophagus were used as surrogates. The measurement for this MOSFET was used for the extrathoracic region absorbed dose and was also combined with the other cervical spine and oesophageal MOSFET measurements to calculate the average cervical spine and oesophagus absorbed dose. These approximations are also used by the ImPACT group, (2011); The ICRP Publication No. 66, (1994); Roberts et al., (2014); Theodorakou et al., (2014) and Tootell et al., (2014). MOSFET dosimeters which are placed at the location of the lens of the eye, this is not specified in the organs and tissues at risk of stochastic effects by the ICRP. The dose to the eye was measured in order to assess deterministic effects but was not used in any ED calculations (ImPACT, 2011).

5.8.2 Measuring Absorbed Dose to Colon

The absorbed dose to the colon as specified by the ICRP 103 Recommendations (ICRP, 2007b) is calculated as the mass-weighted mean of the absorbed dose to the upper large intestine (D_{ULI}) and lower large intestine (D_{LLI}). The upper large intestine was listed as a remainder organ in ICRP 60 (ICRP, 1991a) and the lower large intestine absorbed dose was used for the colon absorbed dose, although this definition was revised in ICRP Publication 69 (ICRP, 1995). The absorbed dose to the ULI is the mass-weighted average of the absorbed dose to the ascending (D_{asc}) and transverse colon (D_{trans}) and the absorbed dose to the LLI is the mass-weighted average of the absorbed dose to the descending (D_{desc}) and recto-sigmoid colon (D_{recto}) (ICRP 103).

5.8.3 Measuring Absorbed Dose to Active Bone Marrow

The active bone marrow is distributed into nine different bone tissues within the human body as follows: (cranium, mandible, vertebrae spine, clavicle, sternum, scapular, ribs, pelvis and femora). As reported by M. Cristy; 1981, the quantity of marrow in each bone has been expressed as a percentage of the whole marrow in each cadaver, and then these values are

averaged (Cristy, 1981). Absorbed dose to active bone marrow was calculated using the data for age 1 and 40 years in active bone marrow distribution from Christy **(Table 5-16)**, by averaging the absorbed radiation dose to each bone marrow tissue and multiplying by their relevant percentage of active bone marrow using equation below. Then the overall active bone marrow dose is added and multiplied by its tissue weighting factor.

$$D_{abm} \sum_{k} Ak \,.\, Dk$$

Where D_{abm} = Dose to active bone marrow

A_k = proportion of active bone marrow described by Cristy, ($\Sigma Ak = 1$)

Table 5-16: Active bone marrow (ABM) in a given bone expressed as a percentage of active bone marrow in the body (Cristy, 1981).

	Percentage of active marrow at various ages						
Bone	0	1	5	10	15	25	40
Cranium	25.3 (27.0)[a]	24.2 (25.1)	15.9	11.6	9.2	7.7	7.6
Mandible	2.5 (2.5)	2.4 (2.4)	1.6	1.1	0.9	0.8	0.8
Scapulae	2.3 (2.7)	2.5 (2.7)	2.7	2.9	3.3	2.9	2.8
Clavicles	0.7 (0.8)	0.8 (0.8)	0.9	0.9	1.0	0.8	0.8
Sternum	1.4 (0)	1.5 (0.8)	1.7	2.1	2.7	3.0	3.1
Ribs	7.0 (9.2)	7.6(8.9)	8.8	10.9	13.6	15.2	16.1
Cervical vertebrae	1.7 (3.4)	1.9 (2.8)	2.2	2.7	3.3	3.7	3.9
Thoracic vertebrae	7.1 (8.3)	7.7(8.4)	8.9	10.9	13.7	15.3	16.1
Lumbar vertebrae	5.4 (2.4)	5.9(4.3)	6.8	8.4	10.5	11.7	12.3
Sacrum	4.3 (0.1)	4.7 (2.4)	5.5	6.7	8.4	9.4	9.9
Os coxae	11.2 (9.2)	12.1 (11.1)	13.1	15.6	18.5	19.5	17.5
Femora, upper half	3.3 (3.7)	3.9(4.1)	6.8	9.4	9.2	7.4	6.7
Femora, lower half	3.3 (3.7)	3.6(3.9)	6.3	6.1	2.0	0	0
Tibiae, fibulae, patellae	7.0 (8.0)	8.1 (8.7)	9.0	5.5	0	0	0
Ankle and foot bones	7.2 (8.3)	4.4 (4.7)	2.5	0	0	0	0
Humeri, upper half	2.2 (2.3)	2.3 (2.4)	2.4	2.5	3.1	2.5	2.3
Humeri, lower half	2.2 (2.3)	2.2 (2.3)	2.2	1.6	0.7	0	0
Ulnae and radii	2.4 (2.5)	2.4 (2.5)	2.0	1.1	0	0	0
Wrist and hand bones	3.4 (3.6)	1.9 (1.9)	0.9	0	0	0	0

[a] Numbers in parentheses following the age nought and age one values are adjustments the model values.
Basis for these adjustments is discussed in conjunction with table 6.

5.9 Lifetime Risk Estimation

The life-time risks of fatal cancer induction associated with the standardized clinical helical and sequential adult protocols and standard helical paediatric protocol were calculated using the

equation below. The calculation involves collecting absorbed dose data of different organs and tissues then using factors of organ-specific radiation-induced cancer risk published by The Nuclear and Radiation Studies board, BEIR VII phase 2 report for ages 0 to 15 with an interval gap of 5 years and from 20 to 80 years with an interval gap of 10 years for both males and females **(Table 5-17)** (BEIR VII, 2006).

Table 5-17: Organ-specific radiation-induced cancer risk factors published by American National Academy of Sciences (BEIR VII, 2006).

TABLE 12D-1 Lifetime Attributable Risk of Cancer Incidence[a]											
	Age at Exposure (years)										
Cancer Site	0	5	10	15	20	30	40	50	60	70	80
Males											
Stomach	76	65	55	46	40	28	27	25	20	14	7
Colon	336	285	241	204	173	125	122	113	94	65	30
Liver	61	50	43	36	30	22	21	19	14	8	3
Lung	314	261	216	180	149	105	104	101	89	65	34
Prostate	93	80	67	57	48	35	35	33	26	14	5
Bladder	209	177	150	127	108	79	79	76	66	47	23
Other	1123	672	503	394	312	198	172	140	98	57	23
Thyroid	115	76	50	33	21	9	3	1	0.3	0.1	0.0
All solid	2326	1667	1325	1076	881	602	564	507	407	270	126
Leukemia	237	149	120	105	96	84	84	84	82	73	48
All cancers	2563	1816	1445	1182	977	686	648	591	489	343	174
Females											
Stomach	101	85	72	61	52	36	35	32	27	19	11
Colon	220	187	158	134	114	82	79	73	62	45	23
Liver	28	23	20	16	14	10	10	9	7	5	2
Lung	733	608	504	417	346	242	240	230	201	147	77
Breast	1171	914	712	553	429	253	141	70	31	12	4
Uterus	50	42	36	30	26	18	16	13	9	5	2
Ovary	104	87	73	60	50	34	31	25	18	11	5
Bladder	212	180	152	129	109	79	78	74	64	47	24
Other	1339	719	523	409	323	207	181	148	109	68	30
Thyroid	634	419	275	178	113	41	14	4	1	0.3	0.0
All solid	4592	3265	2525	1988	1575	1002	824	678	529	358	177
Leukemia	185	112	86	76	71	63	62	62	57	51	37
All cancers	4777	3377	2611	2064	1646	1065	886	740	586	409	214

NOTE: Number of cases per 100,000 persons exposed to a single dose of 0.1 Gy.
[a]These estimates are obtained as combined estimates based on relative and absolute risk transport and have been adjusted by a DDREF of 1.5, except for leukemia, which is based on a linear-quadratic model.

The absorbed dose determined for the adult and paediatric examinations was scaled by these gender specific factors to calculate the estimated future risk of cancer induction. **(Table 5-18)** and **(Table 5-19)** are two examples of calculating lifetime cancer risk induced cancer for both adult and paediatric CT brain examinations, respectively.

$$R = \sum_{T} r_T \, H_T$$

Where *R*= effective risk

rT = life time radiation attributable tissue –specific cancer risks (per unit equivalent dose to tissue T)

H_T = is the equivalent dose absorbed by tissue (*T*)

In this thesis, the number of cases of cancer induction is per 1 000 000 persons exposed to a single dose of 100 mGy.

Table 5-18: An example of calculating adult cancer risk case/10^6 for 10 years old female.

Organ	Absorbed Dose (mGy)	Organ-specific radiation-induced cancer risk factors	Organ Effective risk case/10^6
Stomach	0.100	0.72	0.072
Colon	0.035	1.58	0.055
Lungs	0.277	5.04	1.397
Breasts	0.341	7.12	2.424
Uterus	0.067	0.36	0.024
Ovary	0.034	0.73	0.025
Thyroid	1.744	2.75	4.795
bladder	0.067	1.52	0.102
Liver	0.085	0.2	0.017
Total			**8.912**
Remaining Organs			
Thymus	0.317	5.23	
Spleen	0.108		
Kidneys	0.033		
Adrenals	0.000		
Heart	0.214		
Pancreas	0.035		
Gall Bladder	0.028		
ABM	3.773		
Brain	45.082		
Small Intestine	0.1034		
Extrathoracic	3.668		
Total	**53.360**		
Grand Total	**53.360/11= 4.851**	**4.851*5.23 = 25.370**	**25.370 + 8.912 = 34**

Table 5-19: An example of calculating paediatric cancer risk case/[106] for 0 years old female.			
Organ	**Absorbed Dose (mGy)**	**Organ-specific radiation-induced cancer risk factors**	**Organ Effective risk case/10^6**
Stomach	0.271	1.01	0.273
Colon	0.086	2.2	0.190
Lungs	0.740	7.33	5.422
Breasts	0.881	11.71	10.311
Uterus	0.064	0.5	0.032
Ovary	0.044	1.04	0.046
Thyroid	5.460	6.34	34.616
bladder	0.074	2.12	0.157
Liver	0.183	0.28	0.051
Total			**51.099**
Remaining Organs			
Thymus	1.205	13.39	
Spleen	0.183		
Kidneys	0.144		
Adrenals	0.454		
Heart	0.468		
Pancreas	0.222		
Gall Bladder	0.056		
ABM	7.987		
Brain	27.544		
Small Intestine	0.0122		
Extrathoracic	3.805		
Total	**42.078**		
Grand Total	**42.078/11= 3.825**	**3.825*13.39 = 51.220**	**51.220+51.099 = 102**

5.9.1 Lifetime Cancer Risk Estimation Tool

Using the effective risk data an Excel spreadsheet was created for both paediatric and adult clinical head CT protocols and the resultant data represents the number of cancer induction cases per 1,000,000 in relation to each protocol. The spreadsheet can be used to look up the estimated risk associated with a brain CT scan according to patient age and gender and the relevant protocol. The tool can also be used to compare the risks associated with a variety of different protocols. The tool is presented in **chapter 6** (results), page **157**. The **(Figure 6-24)** illustrates the different parameters within the risk estimation tool (detector configuration [mm] , pitch factors / helical pitch, sure Exp. 3D [ATC], tube rotation time [S], tube angulation [degrees], protocol number, estimated number of exposures [1-5], and eye dose [mGy]) and

(Figure 6-25) on page **158**, represents the tool outcome (lifetime risk of cancer [case/10^6] for both males and females aged from 0-5 and 10-80 for paediatric and adult respectively.

The tool provides a theoretical approach to consider eye dose and lifetime cancer risk from brain CT. The purpose of the tool is to demonstrate an approach to displaying the absorbed eye dose and lifetime risk of cancer from brain CT scans, for use by practitioners. The tool enables the practitioner to specify the settings they are considering using and view the resultant estimated absorbed eye dose and lifetime risk for a range of patients of different ages and genders, of which they can select the most relevant to their patient. The tool can also be used to estimate the accumulative dose and risk that are likely to occur in patients as a result of repeated brain CT scans. This may be useful where the patient is expected to require multiple brain CT scans in the future. The novelty of this tool is it enables practitioners to consider the risk prospectively and may therefore inform practitioner decision making. It is emphasised that currently this spreadsheet is only applicable for a Toshiba Aquilion 16 CT scanner (Toshiba Medical Systems, Tokyo, Japan).

The tool can be used by downloading and opening the workbook in Microsoft Excel. There are two workbooks. Workbook 1 displays the paediatric eye dose and lifetime risk of cancer for paediatrics (male and female) 0 (newborn) and 5 years. Workbook 2 displays the estimated eye dose and lifetime risk of cancer for 10, 15, 20, 30, 40, 50, 60, 70 and 80-year-old males and females. The spreadsheet is interactive and enables the eye dose and risk data to be displayed for a specified protocol/s by using the downward arrows in row 3 to modify the acquisition parameter/s, protocol number and/or estimated number of exposures. The risk estimation tool together with an instruction manual are both included on a CD-ROM in the back of this thesis.

5.10 Statistical Analysis

All data were analysed using SPSS version 24 (IBM Corp, Armonk, NY). The figures and tables represent the mean values plus or minus the standard deviation unless otherwise stated. For inferential statistics, a p-value of less than 0.05 was deemed significant. Data presented on the lifetime risk of cancer, was rounded to the nearest integer. When lifetime risk of cancer was estimated to be below 1, risk was rounded up to 1 in 1 million.

5.10.1 Normality Test

An assessment of the normality of data is a prerequisite for many statistical tests because normal data is an underlying assumption in parametric testing. There are two well-known tests of normality, namely the Kolmogorov-Smirnov Test and the Shapiro-Wilk Test. Shapiro-Wilk Test is more appropriate for small sample sizes (< 50 samples). For this reason, the Shapiro-Wilk test is used as a numerical means of assessing normality. Tests for normality were performed for the ED estimated for the following acquisition parameters: (1) gantry rotation time (S), (2) gantry angulation (degrees), (3) detector configuration (mm), (4) helical pitch (mm) and (5) sure Exp. 3D settings (ATCM). The initial tests showed that the data were not normally distributed, hence the decision to split the data into two groups based on the tube rotation times. After splitting all data presented within this thesis were normally distributed, thus parametric tests were subsequently used to compare means between groups.

5.10.2 Inferential Statistics

A paired-samples t-test was used to make comparisons between two variables. Where more than two variables were compared, analysis of variance (ANOVA) was performed. An ANOVA was performed to determine the effect of different acquisition parameters on ED. To calculate the variation in ED, for each CT protocol, both correlation and regression analyses were undertaken to see which parameters had the most impact on the ED.

5.10.3 Association Statistics

A common task in data analysis is to investigate an association between two variables. This can be a correlation to see if two variables vary together, or a regression to see how one variable affects another.

5.10.3.1 Correlation

A correlation test was used to test the variation among the different CT protocol parameters and the ED. This include the following variables: (1) gantry rotation time (S), (2) gantry angulation (degrees), (3) detector configuration (mm), (4) helical pitch (mm) and (5) sure Exp. 3D settings (ATCM) and Pearson correlation was used for this purpose.

5.10.3.2 Intraclass Correlation Coefficient (ICC)

The Intraclass Correlation Coefficient (ICC) was used to determine the reliability of the MOSFET dosimetry measurements. The reliability of a dosimeter is the ability of that dosimeter to produce consistent results under the same measurement conditions over time. This was calculated for the data obtained on both the adult and paediatric (1-year) ATOM phantom models for three sets of measurements using MOSFET, under the same conditions. The main aim of repeating the experiment is not to test statistical significance, but rather to test the feasibility and the validity of the methods and data collection dosimetry and in turn minimise error that might arise in the main study.

5.10.3.3 Multiple Linear Regression

Regression is used when there is a reason to believe that changes in one variable cause the changes in the other. In this thesis, a regression analysis was performed to establish a reliable regression equation to predict the ED. The regression model included multiple factors (independent variables): (1) gantry rotation time (S), (2) gantry angulation (degrees), (3) detector configuration (mm), (4) helical pitch (mm) and (5) sure Exp. 3D settings (ATCM) and therefore multiple linear regression was performed. A stepwise approach was used during which the variables within the model and the order in which they were inserted was dependent on the strength of their association with the measured effective dose and their statistical significance.

5.11 Chapter Summary

This chapter explained the method used to estimate ED for adult and paediatric brain CT scan examinations of helical and sequential adult protocols and helical paediatric protocols. This approach was the direct measurement method using the two ATOM phantoms representing of adult and 1-years old child examined with solid-state dosimeters MOSFET. Finally, the attributable lifetime risk was calculated for both males and females according to the data published by American National Academy of Sciences in their report (BEIR VII – Phase 2), 2006. Full results from the experiments and the subsequent attributable lifetime cancer risk calculations, including the spreadsheet are described in the results chapter **(6)** within sections **(6.1 – 6.7)**.

Chapter 6 : Results

6.1 Results Overview

This chapter presents the results of a series of dosimetry experiments carried out at the University of Salford using a Toshiba 16 Aquilion CT scanner with ATOM phantoms representing an adult and one year old child. The data was assessed for normality and then, a number of inferential stats (ANOVA, correlation and regression) were undertaken to compare the data and to see if there was correlation as well as to see the effect of each variable on effective dose. The results will be presented in descriptive format using means and standard deviations (SD), tables and graphs. The main purpose of conducting this study was to provide data necessary for the novel calculations of the lifetime risk from CT brain scan protocols for different ages and both genders, when considering individual acquisition parameters. To improve the usability of this data, towards to end of this result section a mode for the presentation of the data has been suggested (interactive Excel spreadsheet). The purpose of this is to (1) estimate the lifetime attributable cancer risk for brain CT examinations in adult and paediatric to improve the ability of practitioners to ascertain estimated risk for a patient prospectively, (2) investigate using direct dose measurement method the effect of varying CT brain protocols parameters on effective radiation dose and risk for adult and paediatric patients to enable practitioners to consider the accumulative risk for patients who may be subject to multiple CT brain scans within a time frame, see aims and objectives **(Sections 1.2 and 1.3)** on page **5**.

6.2 Summary of Dosimetry Calculations

Data collection in the study was conducted using two ATOM phantoms, an adult and a one year old paediatric phantom. For each phantom, a variety of CT brain protocols were undertaken and repeated three times. For both phantoms, organ dose measurements were obtained using MOSFET dosimeters.

Effective doses, were calculated from mean absorbed organ and tissue dose using the MOSFET dosimeters for each protocol. The values of effective dose were calculated for each of the original locations of 281 dosimetry data sets in the adult phantom and 167 in the paediatric phantom. These were obtained using the helical settings for paediatric CT brain examinations and both sequential and helical protocols for adult CT brain examinations. An example of the

absorbed and effective dose calculations for a single protocol are presented in **(Table 6-1)**. These exemplary data were obtained using the following protocol parameters: 0.5 second tube rotation time, 0° gantry angle, 2 mm image thickness, 0.5 x 16 mm detector configuration, detail (0.688 / HP 11.0) pitch factor, a High Quality Sure Exp. 3D setting (SD 1.8) and scan length 140 mm.

Table 6-1: An example of the absorbed and effective radiation doses to body organs and tissues from an adult CT brain scan.

Organ	Measuring Points	Average Absorbed Dose (mGy)	Tissue Weighting Factors (ICRP 103)	Weighted Dose (mSv)
Brain	11	27.48	0.01	0.28
ABM	85	2.26	0.12	0.27
Eyes	2	32.05	0	0.00
Thyroid	6	0.36	0.04	0.01
Oesophagus	3	0.00	0.04	0.00
Lungs	36	0.26	0.12	0.03
Breasts	2	0.01	0.12	0.001
Liver	29	0.07	0.04	0.003
Stomach	14	0.06	0.12	0.01
Bladder	16	9.581E-02	0.04	0.004
Colon	11	0.112	0.12	0.01
Salivary Glands	6	13.0	0.01	0.03
Testes	2	40.0	0.08	0.003
Total	**223**			**0.65**
Remaining Organs			0.12	
Thymus	4	10.1		
Spleen	12	0.12		
Kidneys	16	0.04		
Adrenals	2	0.14		
Heart	2	0.00		
Pancreas	5	0.01		
Gall Bladder	5	0.05		
Prostate	3	0.30		
Oral Mucosa	6	3.01		
Small Intestine	5	0.03		
Extrathoracic	2	1.04		
Total	**62**	**4.83**		
Grand Total	**285**	**4.83/11= 0.44**	**0.44*0.12 = 0.05**	**0.65+0.05 = 0.71**

The relationships between different CT scan parameters and effective doses are provided in subsequent tables and graphs presented in **(Sections 6.3 and 6.4)** on pages **128** and **140**. The presentation of the results is organised into three distinct themes: one focuses on data obtained

from the adult phantom / protocols and the second on paediatric brain CT examinations. The third theme focuses on estimating attributable cancer risk from brain CT scan protocols for different ages and genders and is a distinctly novel aspect of this thesis. The third theme includes the development of a risk estimation tool as a way of displaying the potential utility of such information for clinical practice.

6.3 Adult Phantom Effective Dose Calculations (using MOSFET)

6.3.1 Descriptive Data - Statistical Tests

6.3.1.1 Tests of Normality

Before carrying out any inferential statistical tests, the data was assessed for normality using histograms and the Shapiro-Wilk test. The results of both analyses revealed that the dosimetry data were normally distributed across all the CT parameters investigated (P> 0.05), except for helical pitch experiments where the corresponding *p* value for the Shapiro-Wilk test was less than 0.05. Further analysis of the data suggested the reason the helical pitch data was not normally distributed was a result of the automatic tube current modulation (ATCM) system not correctly modulating the mA for some acquisitions **(as illustrated in Figure 6-1)**. The ATCM is used to adjust the mA according to the patient size which will reduce the radiation dose (tube current) to the patient as discussed in **chapter three (section 3.3.3.3)** on page **34**. The ATCM option on the Toshiba Aquilion 16 CT scanner is called Sure Exp. 3D which has a variety of options available for controlling the noise levels (High quality [SD 1.80], Standard [SD 2.00] and Low dose [SD 2.20]). Selecting one of these settings during a CT scan will preset the required noise level according to the chosen standard deviation (SD) value. In some instances, the CT scanner struggled to reduce the noise to an acceptable level due to the limited anatomical information available within the dosimetry phantom. As the scanner struggled to accurately assess the noise level it increased the tube current to a maximum level. This created problems when assessing the Sure Exp. 3D data and this will be subject to further discussion within this thesis. To verify that the ATCM was not modulating the tube current as would have been expected, a t-test was conducted to determine whether there were significant differences in mean effective dose between 0.5 and 1.0 tube rotation times. The t-test indicated a statistically significant difference in the effective dose (0.5 seconds, mean = 0.60, SD = 0.13 mSv; 1.0 seconds, mean = 0.91, SD = 0.20 mSv, $p \leq 0.001$). The difference in the mean effective dose between the two rotation times was 0.30 mSv.

Figure 6-1: Angular and longitudinal mA modulation.

To overcome this issue the data collected were split into two groups according to the CT gantry rotation time (0.5 and 1.0 Secs). A normality test was run again and the results showed a normal distribution ($P > 0.05$); hence from this point forward parametric statistical tests were used.

The results of descriptive statistics and test of normality for the adult phantom, data obtained at 0.5 and 1.0 second rotation times are illustrated in **(Table 6-2)** and **(Table 6-3)**. The paediatric data are included in **(Appendix M)** within **(Table M - 1)** on page **251**, for normality tests.

Table 6-2: Adult effective dose (mSv) summary statistics including an indication of the normality of the data (0.5 second rotation time)

Protocol Parameters		**Mean, SD**	**Minimum**	**Maximum**	**P -Value Shapiro-Wilk**
Gantry angulation (degree)	0º	0.61 ± 0.11	0.43	0.76	0.20
	15º	0.56 ± 0.13	0.34	0.81	0.20
	27º	0.62 ± 0.14	0.42	0.88	0.20
Detector configuration (mm)	0.5x16	0.60 ± 0.14	0.39	0.88	0.18
	1.0x16	0.57 ± 0.14	0.34	0.81	0.20
	2.0x16	0.62 ± 0.09	0.43	0.82	0.20
Helical Pitch (mm/rotation)	11	0.73 ± 0.07	0.60	0.88	0.20
	15	0.60 ± 0.06	0.47	0.71	0.20
	23	0.47 ± 0.07	0.34	0.62	0.20
Sure Exp. 3D (SD)	1.80	0.63 ± 0.13	0.39	0.88	0.20
	2.00	0.60 ± 0.12	0.38	0.83	0.20
	2.20	0.55 ± 0.11	0.34	0.78	0.20

Table 6-3: Adult effective dose (mSv) summary statistics including an indication of the normality of the data (1.0 second rotation time)

Parameter/Factor		**Mean, SD**	**Minimum**	**Maximum**	**P -Value Shapiro -Wilk**
Gantry angulation (degree)	0	0.95 ± 0.16	0.64	1.24	0.20
	15	0.85 ± 0.20	0.58	1.35	0.18
	27	0.93 ± 0.21	0.56	1.55	0.17
Detector configuration (mm)	0.5x16	0.89 ± 0.15	0.64	1.25	0.13
	1.0x16	0.99 ± 0.24	0.64	1.55	0.20
	2.0x16	0.84 ± 0.17	0.56	1.12	0.20
Helical Pitch (mm/rotation)	11	1.03 ± 0.22	0.62	1.55	0.20
	15	0.87 ± 0.18	0.56	1.24	0.20
	23	0.82 ± 0.12	0.64	1.12	0.20
Sure Exp. 3D (SD)	1.80	1.02 ± 0.20	0.70	1.55	0.20
	2.00	0.91 ± 0.18	0.64	1.28	0.20
	2.20	0.79 ± 0.14	0.56	1.10	0.18

6.3.1.2 Association Statistics

The association statistics were used in this thesis to measure the statistical strength of the relationship on the variables of interest (tube rotation time, CT gantry angulation, detector

configuration, sure exposure (ATCM) and helical pitch); these measures of strength, or association, can be described in several ways, depending on the analysis. The correlation coefficient is a measure of the degree of linear association between two continuous variables (describes the strength of an association between two variables), i.e. when plotted together, how close to a straight line is the scatter of points. Correlation simply measures the degree to which the two vary together. A positive correlation indicates that as the values of one variable increase the values of the other variable increase, whereas a negative correlation indicates that as the values of one variable increase the values of the other variable decrease. Regression is used to examine the magnitude of the relationship between one dependent and one independent variable. After performing an analysis, the regression statistics can be used to predict the dependent variable when the independent variable is known.

6.3.1.2.1 Correlation

The Pearson product-moment correlation coefficient (*r*) was conducted for normally-distributed (parametric) data, and the Spearman rank-order correlation coefficient (*r*s) was used for data that are not normally distributed (non-parametric data). Both vary from +1 (perfect correlation) through 0 (no correlation) to –1 (perfect negative correlation) (Field, 2015; Millar, 2001).

The result of correlation tests are represent in **(Table 6-4)**. This table shows the correlation of different CT parameters with effective dose (for the 162 adult protocols). The analysis reveals that there is a weak negative correlation between effective dose (mSv) and helical pitch, moderate positive correlation between effective dose and tube rotation time and finally negative weak correlation between effective dose and ATCM, respectively. The other CT parameters (gantry angulation and detector configuration) were, not significantly correlated with effective dose.

Table 6-4: Adult CT brain protocol correlation test results.

		Tube Rotation Time (seconds)	Gantry Angulation (Degrees)	Detector Configuration (mm)	Helical Pitch	Sure Exp. 3D (ATC)
Effective Dose (mSv)	Pearson Correlation	0.687**	-0.019	-0.015	-0.402	-0.285**
	Sig. (1-tailed)	0.000	0.406	0.426	0.000	0.000
	N	162	162	162	162	162
**. Correlation is significant at the 0.01 level (2-tailed).						

6.3.1.2.2 Linear Regression

Regression is used when we have reason to believe that changes in one variable cause changes in the other. The end result of such tests is a probability (*P*) that the 'null hypothesis' (which always states that there is no difference between the sets of data) is true. The regression was conducted to predicate the relationship between the independent variables and effective dose and if the change in effective dose is influenced by the intendant factors.

Given that the data were analysed using linear regression, the value of R^2 is 0.751, which tells us that the CT gantry angulation, detector configuration, helical pitch and Sure Exp. 3D (ATC) can account for 75.1% of the variation in effective dose. The F-ratio of the model mean squares (MS_M) divided by the residual mean squares (MS_R) and as reported by Field (2015) indicates a reliable model should have a large F-ratio (greater than 1). The F-ratio value of regression model is 68.8, which is significant at $P< 0.001$, this tells us that there is less than a 0.1% chance that an F-ratio this large would happen if the null hypothesis were true. In short, the regression model overall predicts effective dose significantly well. The contribution of each of the parameters to the R^2, i.e. the R^2 value for CT gantry angulation 1%, detector configuration 14%, helical pitch 0.02% and sure expos 39%. The most influential was the R^2 value for tube rotation time which was 62.1%. The regression model can, however, predict up to 75.1% of effective dose variability.

Regression equation: ED = 0.729 + 0.621 x tube rotation time -0.01 x CT gantry angulation – 0.01 x detector configuration + 0.14 x Helical pitch – 0.393 x sure Exp. 3D

R square = 75.1%.

6.3.2 Helical Acquisitions

The values of effective dose estimated from the CT experiments (helical protocol, gantry angulations 0^o, 15^o & 27^o) are given below. The results for all 162 protocols are illustrated in **(Appendix D**) within **(Table D - 1)** to **(Table D - 6)** on pages **222** to **227** and are summarised by the acquisition angulation.

The main effect of varying the acquisition parameters of tube rotation time, detector configuration, helical pitch and Sure Exp. 3D (ATCM) for the three different gantry angulations (0^o, 15^o and 27^o) on effective dose are described below: -

6.3.2.1 Tube Rotation Time (S)

This data shows the effect of tube rotation time and CT gantry angle on the effective dose. As shown in table **(Table 6-5)** and **(Figure 6-2)**, the effective dose for the two tube rotation times, at three different CT gantry angulations, indicate there is an increase in the effective dose by around 39%, as a result of the increase in rotation time from 0.5 to 1.0 second.

Table 6-5: Adult helical effective doses estimates for the three gantry angulations at the two different tube rotation times (mean/SD).

Gantry Angulation (Degrees)	Tube Rotation Time (Seconds)		
	0.5	1.0	P values
0°	0.71 ± 0.01 (mSv)	1.17 ± 0.01 (mSv)	0.01
15°	0.81 ± 0.01 (mSv)	1.25 ± 0.02 (mSv)	0.05
27°	0.88 ± 0.01 (mSv)	1.13 ± 0.01 (mSv)	0.03
P values	>0.05	>0.05	

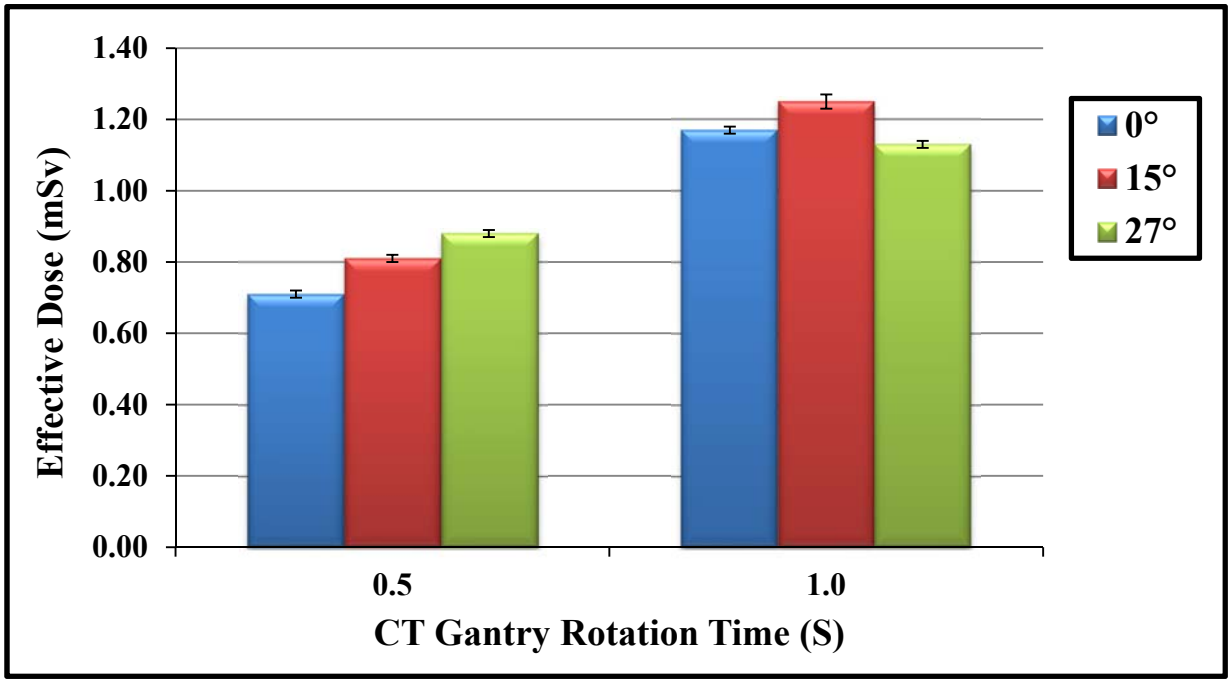

Figure 6-2: A bar chart comparing the effective dose and the tube rotation time for the three different gantry angulations. Error bars denote the standard deviation of the data.

6.3.2.2 Detector Configuration (mm)

This data shows the effect of detector configuration and CT gantry angle on the effective dose. As shown in **(Table 6-6)** and **(Figure 6-3)** the gantry angulation and detector configuration has no effect on effective dose.

Table 6-6: Adult helical effective dose estimates for three different detector configurations across three different gantry angulations (mean/SD).				
Detector Configuration (mm)	**Gantry Angulation (Degrees)**			
	0°	**15°**	**27°**	**P values**
0.5x16	0.71 ± 0.01 (mSv)	0.81 ± 0.05 (mSv)	0.88 ± 0.03 (mSv)	>0.05
1.0x16	0.76 ± 0.01 (mSv)	0.70 ± 0.03 (mSv)	0.81± 0.05 (mSv)	>0.05
2.0x16	0.73 ± 0.04 (mSv)	0.79 ± 0.07 (mSv)	0.82 ± 0.08 (mSv)	>0.05
P values	>0.05	>0.05	>0.05	

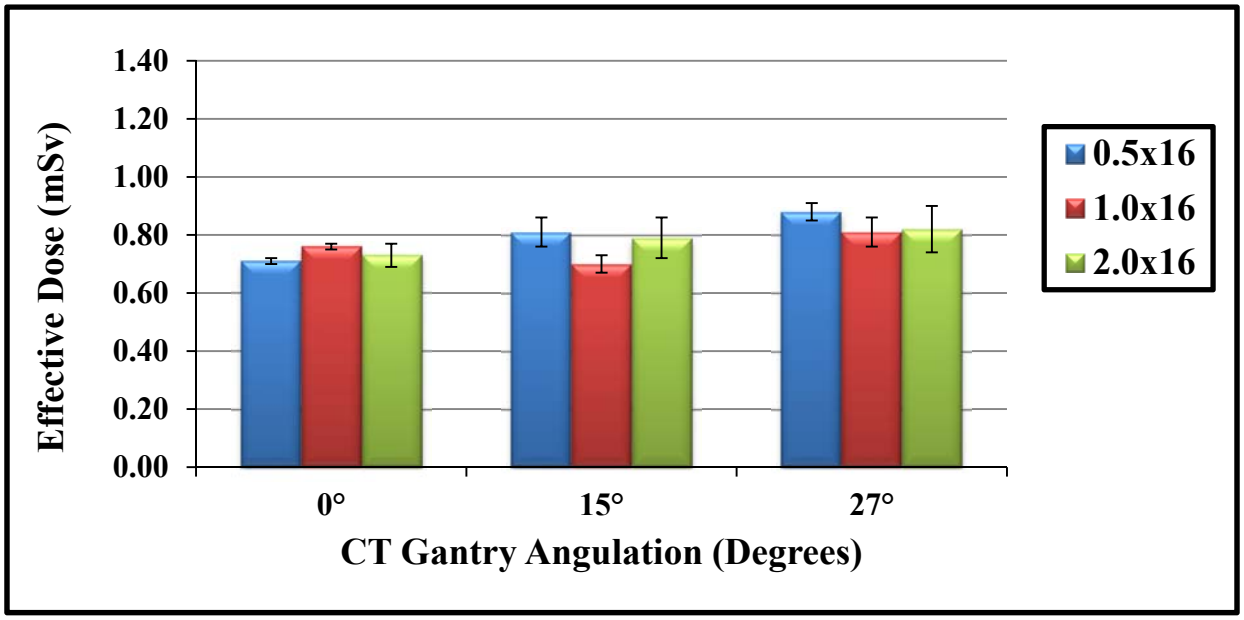

Figure 6-3: A bar chart comparing the effective dose for three different detector configurations at three different gantry angulations. Error bars denote the standard deviation of the data.

6.3.2.3 Helical Pitch

This data shows the effect of helical pitch and CT gantry angle on the effective dose. As shown in **(Table 6-7)** and **(Figure 6-4)** the effective dose estimates for the three helical pitch factors, at the three CT gantry angulations, are described below. The results indicate that as the helical pitch increases the effective dose decreased. There was only a slight decrease in effective dose when moving from detail to standard but a more noticeable decrease between detail and fast, see **(Table 6-7)** and **(Figure 6-4)**. Accordingly, the change in helical pitch from detail to fast resulted in the effective dose being decreased by 35% for the 0° gantry angulation and by 47% for the 15° and 27° gantry angulations.

Table 6-7: Adult effective dose estimates for three different helical pitch factors at three different gantry angulations (mean/SD).				
Helical Pitch	**Gantry Angulation (Degrees)**			
	0°	**15°**	**27°**	**P values**
Detail	0.71 ± 0.01 (mSv)	0.81± 0.05 (mSv)	0.88 ± 0.04 (mSv)	0.04
Standard	0.63 ± 0.03 (mSv)	0.58 ± 0.02 (mSv)	0.70 ± 0.05 (mSv)	0.16
Fast	0.46 ± 0.01 (mSv)	0.43 ± 0.01 (mSv)	0.47 ± 0.01 (mSv)	0.03
P values	<0.05	<0.05	<0.05	

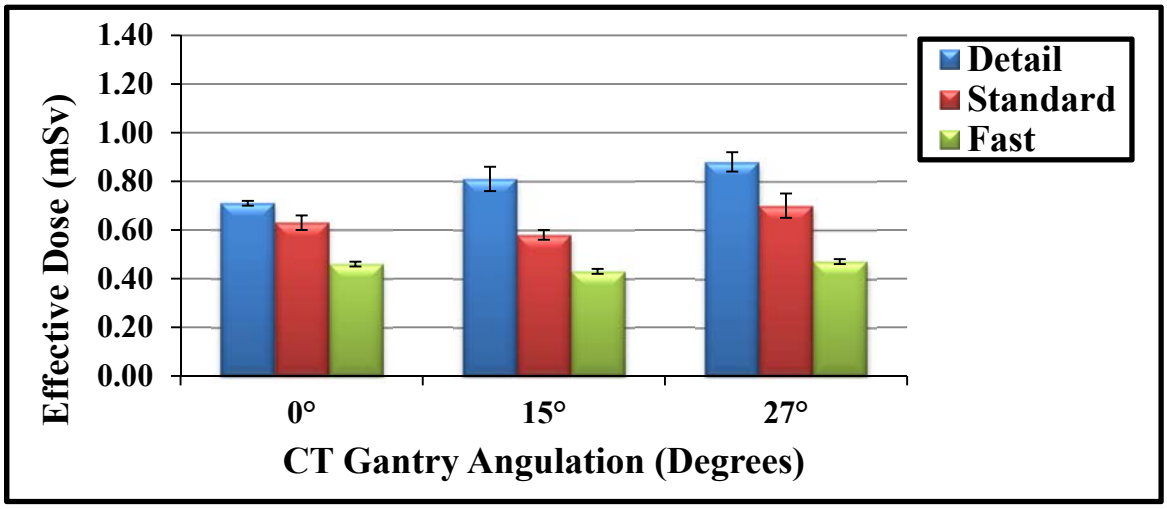

Figure 6-4: A bar chart showing the effective dose against the three gantry angulations for the three different helical pitch factors. Error bars denote the standard deviation of the data.

6.3.2.4 Automatic Tube Current Modulation (Sure Exp. 3D)

This data shows the effect of ATCM and CT gantry angle on the effective dose. The values of effective dose obtained at three different ATCM settings are shown in **(Table 6-8)** and are plotted in **(Figure 6-5)**. As is illustrated from the graph all the three ATCM settings have the same effect on effective dose at 0° CT gantry angulation, however, there is a slight increase in effective dose for the two other gantry angulations (15° and 27°) from low dose through to the high quality setting.

Table 6-8: Adult effective dose estimates for three different ATCM settings at three different gantry angulations (mean/SD).				
ATCM setting	**CT Gantry Angulation (Degrees)**			
	0°	**15°**	**27°**	**P values**
High Quality	0.71 ± 0.09 (mSv)	0.81 ± 0.04 (mSv)	0.88 ± 0.05 (mSv)	>0.05
Standard	0.70 ± 0.09 (mSv)	0.72 ± 0.09 (mSv)	0.83 ± 0.03 (mSv)	>0.05
Low Dose	0.70 ± 0.09 (mSv)	0.68 ± 0.09 (mSv)	0.78 ± 0.02 (mSv)	>0.05
P values	>0.05	>0.05	>0.05	

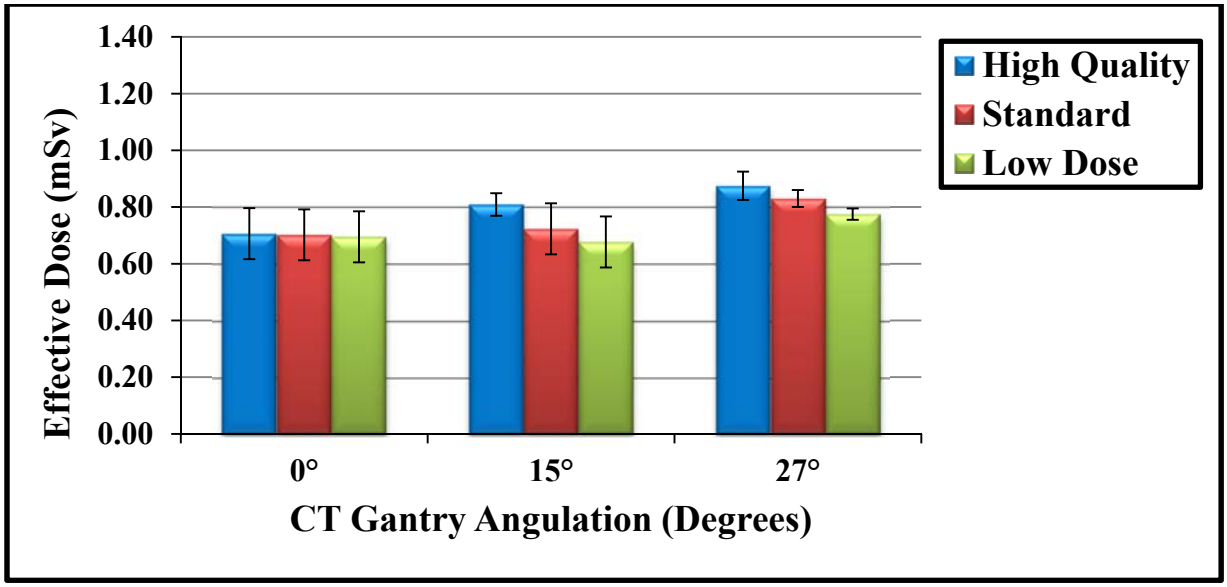

Figure 6-5: A bar chart illustrating the effective dose values for different gantry angulations for the three different ATCM settings. Error bars denote the standard deviation of the data.

6.3.3 Sequential Acquisitions

This section provides the results of 54 brain sequential protocols obtained using the following parameters: two different gantry rotation times (0.5 and 1.0 seconds), three different detector configurations (0.5 x 4, 1.0 x 4 and 2.0 x 4 mm) and three different ATCM settings (high quality, standard and low dose). All the measurements were conducted at three different gantry angulations, 0°, 15° and 27°.

Comparison of the estimated effective dose for different scan parameters is provided in the figures below for an adult sequential brain CT examination.

6.3.3.1 Tube Rotation Time

The effective dose calculations for two rotation times and three different gantry angulations are outlined in **(Table 6-9)**. The effective dose values for the two rotation times are illustrated in **(Figure 6-6)**. This data shows there is significant different in effective dose values, as the rotation time changed from 0.5 seconds to 1 second the effective dose increased by 48.7% for 0° CT gantry angulation.

Table 6-9: Effective dose estimates for an adult sequential protocol for two rotation times and three different gantry angulations (mean/SD).				
CT Gantry Rotation Time (S)	**CT Gantry Angulation (Degrees)**			
	0º	**15º**	**27º**	**P values**
0.5	0.37 ± 0.01 (mSv)	0.30 ± 0.01 (mSv)	0.38 ± 0.01 (mSv)	>0.05
1.0	0.55 ± 0.02 (mSv)	0.64 ± 0.01 (mSv)	0.75 ± 0.02 (mSv)	>0.05
P values	0.02	0.01	<0.001	

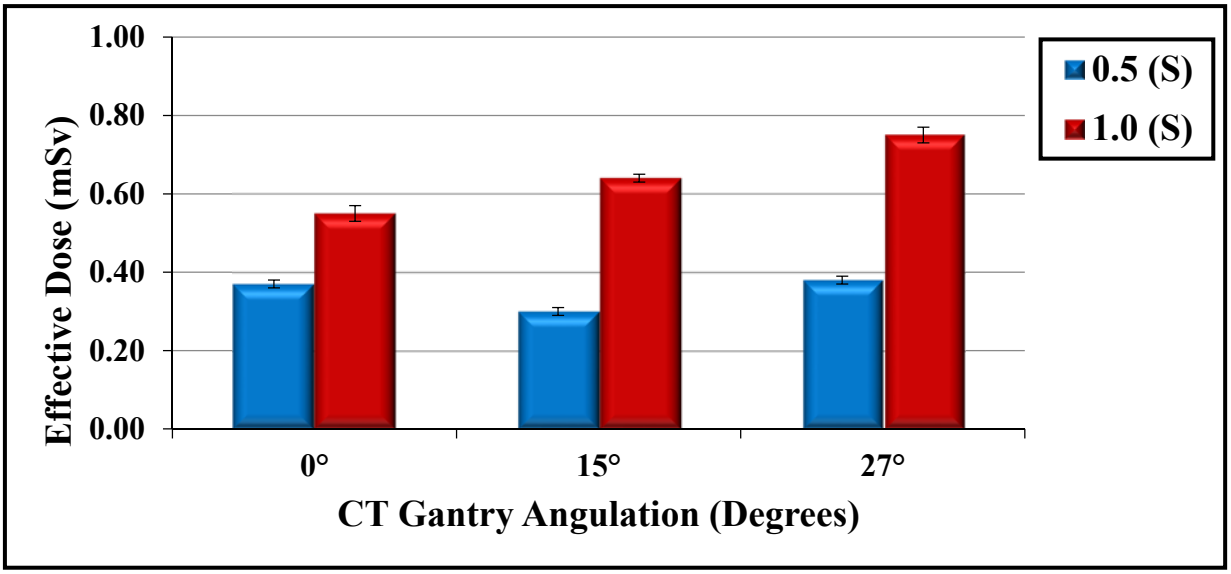

Figure 6-6: A bar chart representing the effective dose for adult sequential protocols, at three different gantry angulations and for two different tube rotation times (S, seconds). Error bars denote the standard deviation of the data.

6.3.3.2 Gantry Angulation

Table 6-10 shows the effective dose estimates for the three different gantry angulations across the two rotation times (0.5 and 1.0 second). The difference in effective dose as the gantry angulation and the tube rotation time's change are shown in **(Figure 6-7)**, as the rotation time increases the effective dose also increases ($P<0.05$). By contrast, changing the gantry angulation has no statistically significant effect on effective dose ($P>0.05$). However, as can be seen from the data in **(Table 6-10)**, for 1 second tube rotation times, the effective dose increases from 0.55 to 0.75 mSv when angling the gantry, this equates to a 27% increase in dose.

Table 6-10: Adult brain sequential protocol effective dose estimates for three different CT gantry angulations and two different rotation times (mean/SD).			
CT Gantry Angulations (Degrees)	**Tube Rotation Time (seconds)**		
	0.5	**1.0**	**P values**
0º	0.37 ± 0.02 (mSv)	0.55 ± 0.02 (mSv)	0.005
15º	0.30 ± 0.03 (mSv)	0.64 ± 0.06 (mSv)	0.005
27º	0.38 ± 0.03 (mSv)	0.75 ± 0.06 (mSv)	0.004
P values	0.06	0.06	

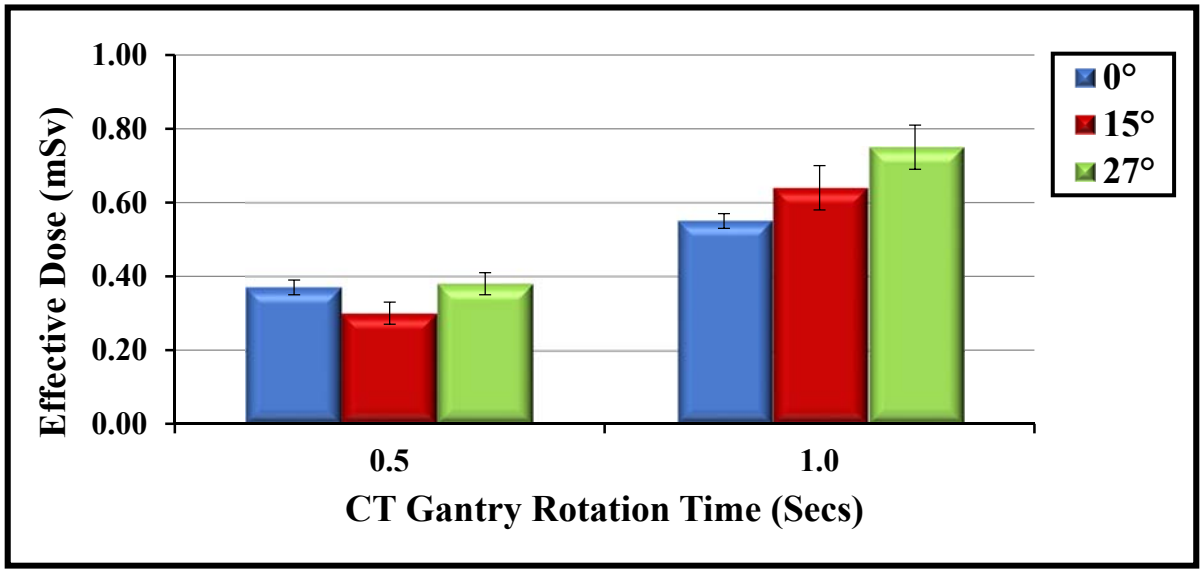

Figure 6-7: A bar chart illustrating the effective dose for adult brain sequential protocols at three different CT gantry angulation degrees and two rotation times. Error bars denote the standard deviation of the data.

6.3.3.3 Detector Configuration

A comparison of the effective dose estimates obtained at three gantry angulations with three different detector configurations are presented in **(Table 6-11)**. These data are plotted graphically showing there are statistically significant differences ED across the three detector configurations (P<0.05), **(Figure 6-8)**.

Table 6-11: Effective dose estimates for different CT detector configurations and angulations (mean/SD).				
Detector Configuration (mm)	**CT Gantry Angulation (Degrees)**			
	0º	**15º**	**27º**	**P values**
0.5 x 4	0.37 ± 0.02 (mSv)	0.30 ± 0.02 (mSv)	0.38 ± 0.02 (mSv)	0.06
1.0 x 4	0.43 ± 0.03 (mSv)	0.39 ± 0.02 (mSv)	0.44 ± 0.02 (mSv)	0.19
2.0 x 4	0.61 ± 0.05 (mSv)	0.51 ± 0.02 (mSv)	0.63 ± 0.03 (mSv)	0.09
P values	0.007	<0.001	<0.001	

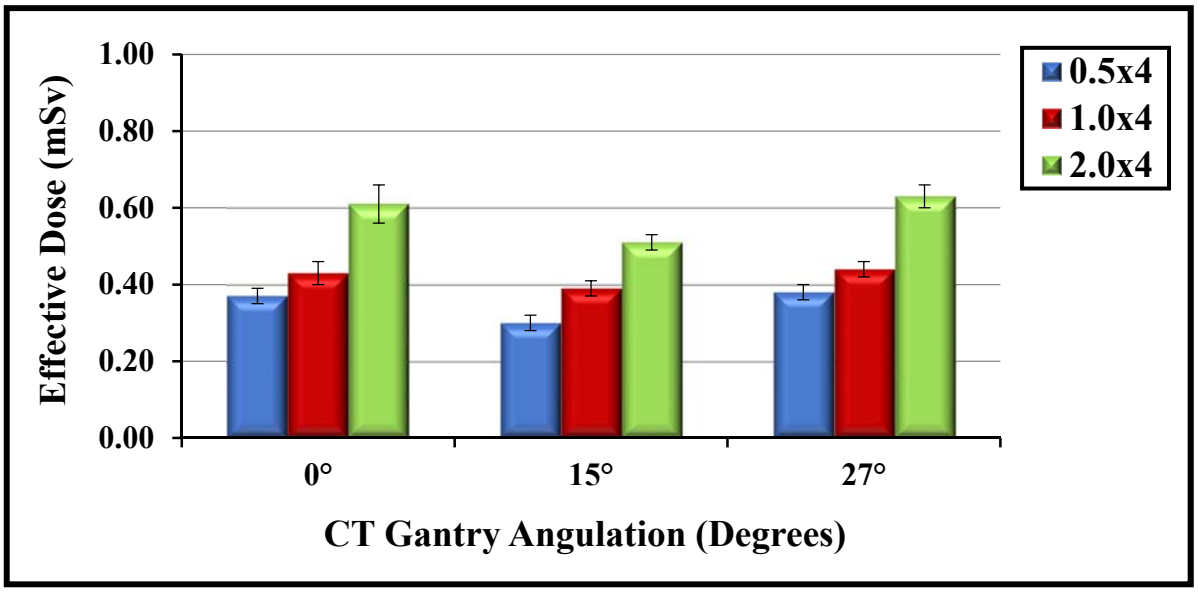

Figure 6-8: A bar chart showing the effect of different detector configurations on effective dose for the three different gantry angulations. Error bars denote the standard deviation of the data.

6.3.3.4 Automatic Tube Current Modulation (Sure Exp. 3D)

The data presented here shows the different effective dose values obtained for three different ATCM settings at three different CT gantry angulations. Comparison of effective dose values for a range of different automatic tube current modulation settings and gantry angulations are illustrated in **(Table 6-12)**. The range of effective dose calculated for ATCM settings are shown in **(Figure 6-9)**. At 0^{o} gantry angulation there were no differences in effective dose values between high quality and low dose mA modulation techniques, however, as the CT gantry changed to 27^{o} the effective dose is decreased by 10.5%.

Table 6-12: Effective dose estimates for the three different gantry angulations and the three-automatic tube current modulation settings (mean/SD).

ATCM setting	CT Gantry Angulation (Degrees)			
	0^{o}	15^{o}	27^{o}	P values
High Quality	0.37 ± 0.01 (mSv)	0.30 ± 0.09 (mSv)	0.38 ± 0.09 (mSv)	>0.05
Standard	0.33 ± 0.08 (mSv)	0.32 ± 0.07 (mSv)	0.39 ± 0.08 (mSv)	>0.05
Low Dose	0.37 ± 0.05 (mSv)	0.27 ± 0.08 (mSv)	0.34 ± 0.09 (mSv)	>0.05
P values	>0.05	>0.05	>0.05	

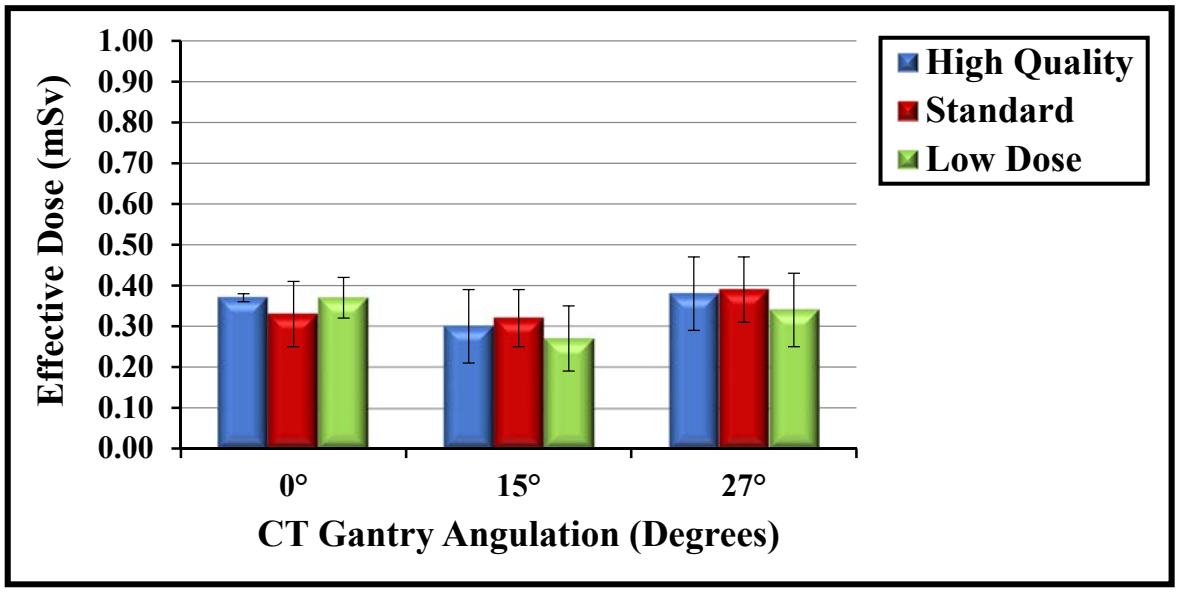

Figure 6-9: A bar chart of effective dose estimates for adult CT brain examinations using three different ATCM settings, for three different gantry angulations. Error bars denote the standard deviation of the data.

6.4 Paediatric Phantom Effective Dose Estimates (using MOSFET)

This section presents the results of effective dose calculations from absorbed dose measurements to organs and tissue using MOSFET dosimeters in 167 locations using a one year old representative paediatric ATOM phantom. Dose estimates were obtained using two different approaches, one using all possible scanning options available and the second used a protocol for a CT brain examination for children aged from 3 months to 3 years creating 162 protocols and the other different fixed values of tube current and voltage as well as different CT angulations and rotation times creating 54 protocols, see **(Appendix F)** which displays the full list of protocols within tables NO. **(Table F - 1)** to **(Table F - 6)** on pages **234** to **236**.

6.4.1 Descriptive Data - Statistical Tests

6.4.1.1 Tests of Normality

Testing normality of the data from the 162 protocols was necessary to examine the appropriateness of the overall data for further analysis. Data were again analysed using histograms and the Shapiro-Wilk test. For the data presented in this section the Shapiro-Wilk test demonstrated that the data conformed to a normal distribution ($P > 0.05$), see **(Appendix M)**, **(Table M - 1)** on page **251**.

6.4.1.2 Association Statistics

6.4.1.2.1 Correlations

The data also, checked using correlation to assess the characterization of relationships among multiple protocol factors, the correlation statistical test results are show in **(Table 6-13)**. This table shows the correlation of different CT parameters with effective dose (for the 162 paediatric protocols). The analysis reveals that there is a moderate negative correlation between effective dose (mSv) and both detector configuration and ATCM, respectively. The other CT parameters (tube rotation time, gantry angulation and helical pitch) were, not significantly correlated with effective dose (mSv).

Table 6-13: Paediatric CT brain protocol correlation test results.

		Tube Rotation Time (seconds)	Gantry Angulation (Degrees)	Detector Configuration (mm)	Helical Pitch	Sure Exp. 3D (ATC)
Effective Dose (mSv)	Pearson Correlation	0.021	-0.091	-.604**	0.075	-.674**
	Sig. (2-tailed)	0.000	0.252	0.000	0.341	0.000
	N	162	162	162	162	162
**. Correlation is significant at the 0.01 level (2-tailed).						

6.4.1.2.2 Linear Regression

The linear regression models have been established for further assessment of the relationship between effective radiation doses for each parameter used to acquire the absorbed dose in order to investigate the possibility of predicting individual effective dose. The linear regression the value of R^2 is 0.858, which tells us that the rotation time, the CT gantry angulation, detector configuration, helical pitch and Sure Exp. 3D (ATC) can account for 85.8% of the variation in effective dose. The contribution of each of the parameter was to the R^2, i.e. the R^2 value for tube rotation time was 7.2%, CT gantry angulation 1.3%, helical pitch 0.6% and sure expos 17%. The most influential was the R^2 value for detector configuration 67.5%.

6.4.2 Paediatric Helical Brain CT Protocols using ATCM

The difference in the estimated effective dose between four scan parameters was investigated for three gantry angulations. Protocol variations include CT gantry angulation, tube rotation time, detector configuration, helical pitch and ATCM settings.

6.4.2.1 Tube Rotation Time

Effective dose was calculated from absorbed dose measured at two different tube rotation times (0.5 and 0.75 seconds) and three different gantry angulations (0º, 15º and 27º). 81 protocols were tested for each CT scan tube rotation time giving a total of 162 protocols. The effective dose values and the relationship between the two rotation times are shown in **(Table 6-14)** and illustrated in **(Figure 6-10)**. There was no significant effect of tube rotation time or gantry angulation on the effective dose ($p>0.05$).

Table 6-14: Paediatric effective dose estimates for the two tube rotation times across the three different gantry angulations (mean/SD).

CT Gantry Angulation (Degrees)	Tube Rotation Time (seconds)		
	0.5	0.75	P values
0º	2.01 ± 0.02 (mSv)	1.95 ± 0.02 (mSv)	0.23
15º	1.82 ± 0.02 (mSv)	1.76 ± 0.01 (mSv)	0.27
27º	1.73 ± 0.01 (mSv)	1.73 ± 0.01 (mSv)	0.20
P values	0.44	0.14	

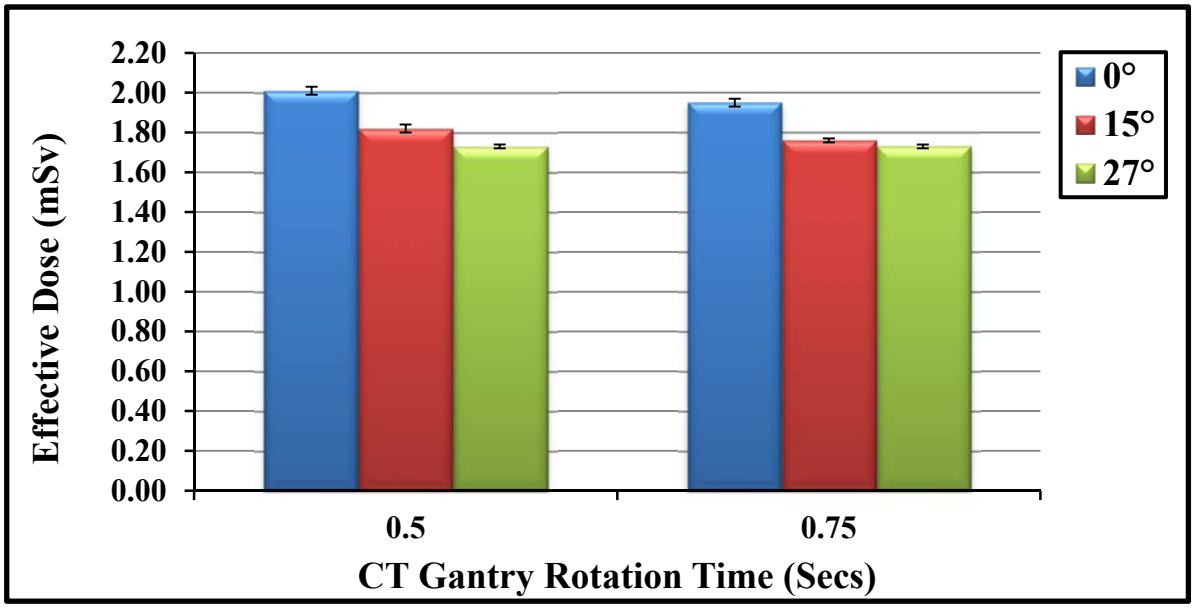

Figure 6-10: A bar chart comparing the effective dose and tube rotation times for three different gantry angulations. Error bars denote the standard deviation of the data.

6.4.2.2 Detector Configuration

The effective dose was calculated for three setting of detector configuration (0.5x16 mm, 1.0x16 mm and 2.0x16 mm) at three different gantry angulations (0º, 15º and 27º). As shown

in **(Table 6-15)** and **(Figure 6-11)** the effective dose decreased significantly according to the change in detector configuration from 0.5x16 mm through to 2.0x16 mm.

Table 6-15: Effective dose estimates for different detector configurations and gantry angulations (mean/SD).

Detector Configuration (mm)	Gantry Angulation (Degrees)			
	0º	**15º**	**27º**	**P values**
0.5 x 16	2.01 ± 0.07 (mSv)	1.82 ± 0.04 (mSv)	1.73 ± 0.09 (mSv)	0.36
1.0 x 16	1.02 ± 0.08 (mSv)	0.98 ± 0.06 (mSv)	0.93 ± 0.07 (mSv)	0.46
2.0 x 16	0.71 ± 0.04 (mSv)	0.63 ± 0.02 (mSv)	0.66 ± 0.09 (mSv)	0.98
P values	<0.001	<0.001	<0.001	

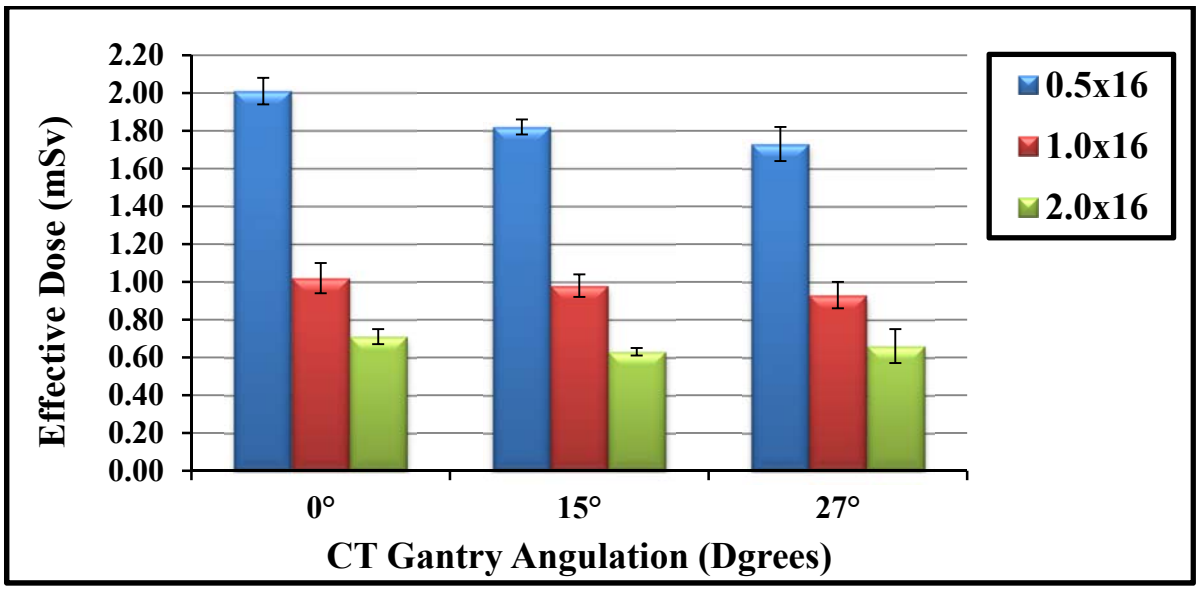

Figure 6-11: A bar chart comparing effective dose across the three different detector configurations, for the three gantry angulations. Error bars denote the standard deviation of the data.

6.4.2.3 Helical Pitch Factors

The helical protocol for the Toshiba Aquilion 16 scanner has three different helical pitch values. These are Detail PF 0.688 / HP 11.0, Standard PF 0.938 / HP 15.0 and Fast PF 1.438 / HP 23.0. The estimated effective dose for the three different helical pitch factors at three gantry angulations are presented in **(Table 6-16).** The comparison of the effective dose between helical pitch factors and gantry angulations are illustrated graphically in **(Figure 6-12).** This highlights there was a reduction in effective dose from 0º through to 27º using a detailed, standard and fast helical pitch factors (when changing from detail to standard helical pitch factor

the reduction was 14.9% and changing helical pitch setting from detail to fast the reduction was 21.4%.

Table 6-16: A comparison of the effective dose for different helical pitch factors and CT gantry angulations (mean/SD).				
Helical Pitch	**Gantry Angulations (Degrees)**			
	0º	**15º**	**27º**	**P values**
Detail	2.01 ± 0.07 (mSv)	1.82 ± 0.06 (mSv)	1.73 ± 0.06 (mSv)	0.94
Standard	1.71 ± 0.06 (mSv)	1.58 ± 0.05 (mSv)	1.50 ± 0.05 (mSv)	0.94
Fast	1.58 ± 0.04 (mSv)	1.52 ± 0.04 (mSv)	1.49 ± 0.04 (mSv)	0.91
P values	0.05	0.05	0.05	

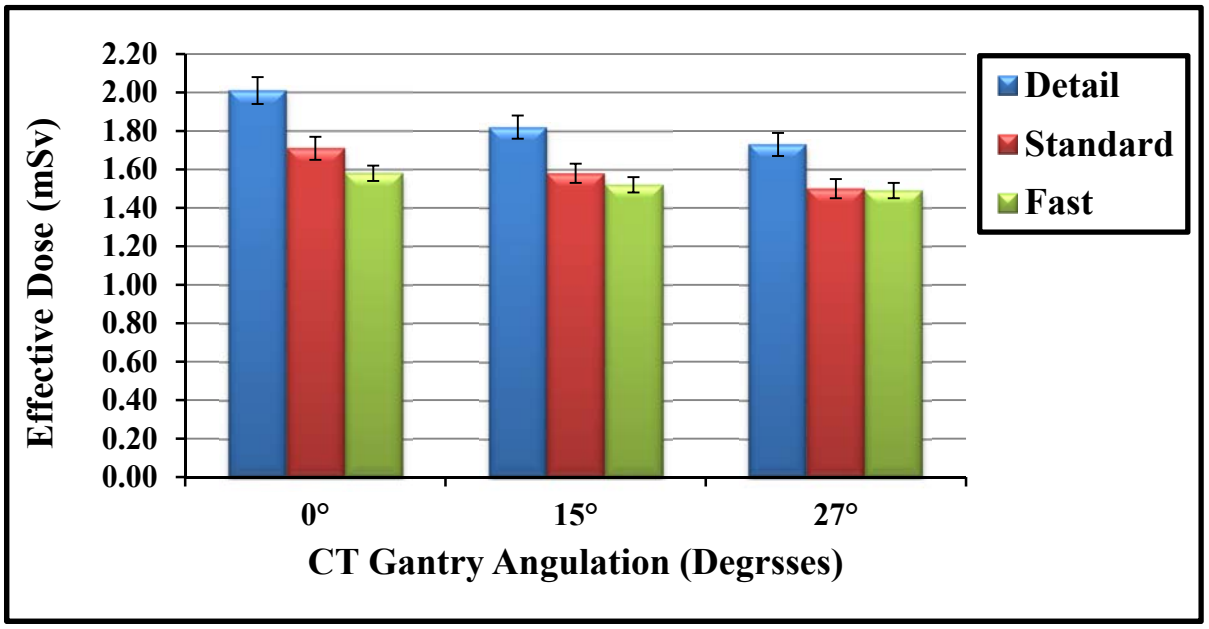

Figure 6-12: A bar chart comparing effective dose for the three helical pitch factors across the three CT gantry angulations. Error bars denote the standard deviation of the data.

6.4.2.4 Automatic Tube Current Modulation (Sure Exp. 3D)

Table 6-17 below reports the effective dose estimates for three different ATCM settings including High Quality (SD 4.00), Standard (SD 6.00) and Low Dose (SD 8.00) for the different gantry angulations. The relationship between these parameters and effective dose are represented graphically in **(Figure 6-13)**. The effective dose was reduced by 66% when changing the ATCM settings from high quality to low dose. The effective dose was reduced by 12% when changing the CT gantry angle from 0º to 27º.

Table 6-17: Effective dose estimates for ATCM settings across three gantry angulations (mean/SD).				
ATCM setting	**Gantry Angulations**			
	0º	**15º**	**27º**	**P values**
High Quality	2.01 ± 0.05 (mSv)	1.82 ± 0.06 (mSv)	1.73 ± 0.07 (mSv)	0.4
Standard	1.08 ± 0.05 (mSv)	0.99 ± 0.03 (mSv)	0.90 ± 0.07 (mSv)	0.4
Low Dose	0.68 ± 0.06 (mSv)	0.61 ± 0.05 (mSv)	0.60 ± 0.02 (mSv)	0.2
P values	<0.001	<0.001	<0.001	

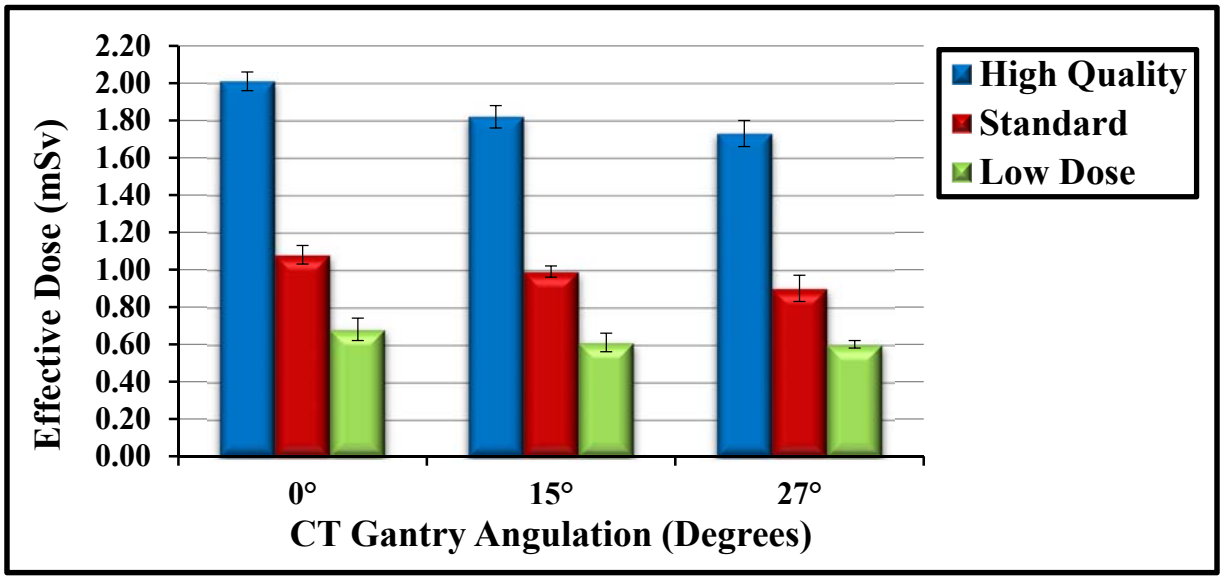

Figure 6-13: A bar chart comparing the effective dose for three ATCM settings obtained at three different gantry angulations. Error bars denote the standard deviation of the data.

6.4.3 Paediatric Helical Brain CT Protocol Using Different Values of Fixed Tube Current and Tube Potential

The protocol for helical paediatric brain CT scan was further varied and created a further 54 protocols to investigate additional effect. The detector configuration was kept fixed at 0.5 x 16 mm. The tube potential was varied between 100 and 120 kVp together with three different values of tube current 120, 160 and 200mA. The rotation time was also varied at 0.5, 0.75 and 1.0 seconds. All parameters were examined at three different CT gantry angulations including 0º, 15º and 27º. The results of this section were divided into four groups to investigate the relationship between effective dose and the following parameters: tube rotation time, tube current and tube potential. See **(Appendix G)** which displays the full list of protocols within **(Table G - 1)** to **(Table G - 3)** on page **240**.

6.4.3.1 Tube Rotation Time

Data shown in **(Table 6-18)** illustrates the effect of changing tube rotation time on effective dose estimates for a range of gantry angulations. As represented in **(Figure 6-14)** there was only a small reduction in effective dose when changing gantry angle from 0º to 15º or 27º, approximately 6%. On the contrary, increasing the rotation time from 0.5 seconds to 1 second increased the effective dose by 86.0%.

Table 6-18: A comparison of effective dose for different tube rotation times and gantry angulations (mean/SD).

Tube Rotation Time (seconds)	Gantry Angulation (Degrees)			
	0º	**15º**	**27º**	**P values**
0.5	1.07 ± 0.03 (mSv)	1.01 ± 0.03 (mSv)	1.01 ± 0.03 (mSv)	0.95
0.75	1.49 ± 0.04 (mSv)	1.50 ± 0.04 (mSv)	1.53 ± 0.03 (mSv)	0.98
1.0	1.99 ± 0.05 (mSv)	1.88 ± 0.04 (mSv)	2.02 ± 0.05 (mSv)	0.88
P values	0.05	0.05	0.04	

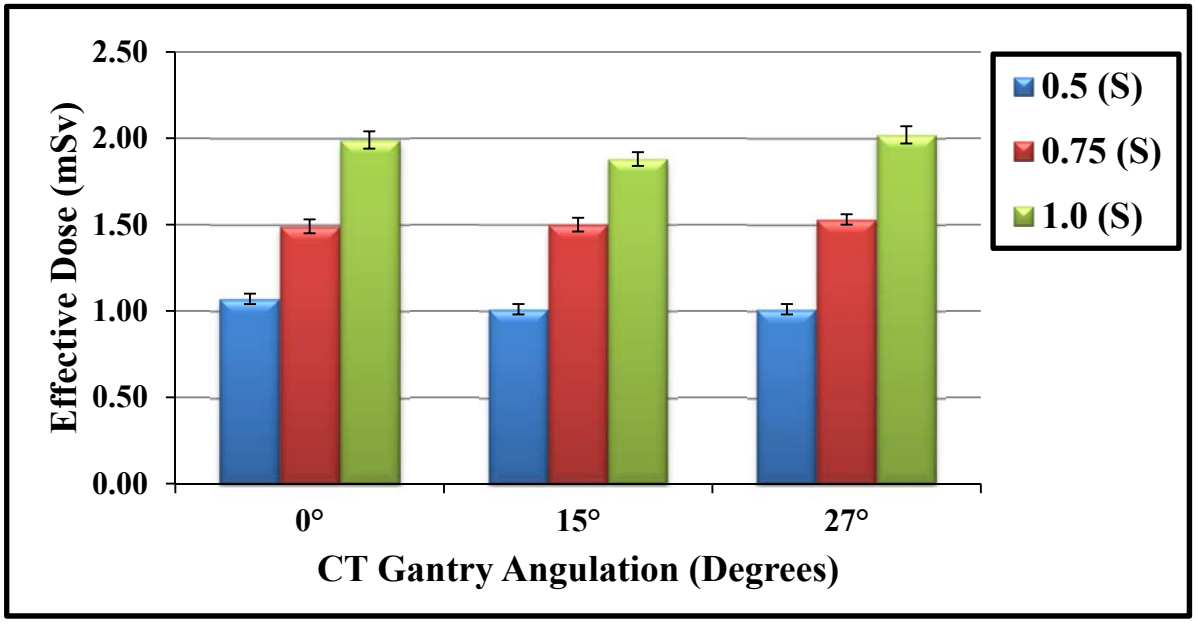

Figure 6-14: A bar chart illustrating effective dose estimates for different gantry angulations for three tube rotation times. Error bars denote the standard deviation of the data.

6.4.3.2 Tube Potential (kVp)

Two values of tube potential (kVp) were used in these paediatric protocols and the results on effective dose are illustrated in **(Table 6-19)** and **(Figure 6-15)**. In this experiment, the effective dose increased by 39.3%, 39.6% and 58.4% when changing the tube kilovoltage from 100 to 120 kVp for the three CT gantry angulation 0º, 15º and 27º, respectively.

Table 6-19: Effective dose estimates obtained at two tube potentials (100 and 120 kVp) for three different gantry angulations (mean/SD).				
Tube potential (kVp)	**Gantry Angulation (Degrees)**			
	0º	**15º**	**27º**	**P values**
100	1.07 ± 0.04 (mSv)	1.01 ± 0.04 (mSv)	1.01 ± 0.04 (mSv)	0.99
120	1.49 ± 0.07 (mSv)	1.41 ± 0.06 (mSv)	1.60 ± 0.06 (mSv)	0.95
P values	0.03	0.04	0.01	

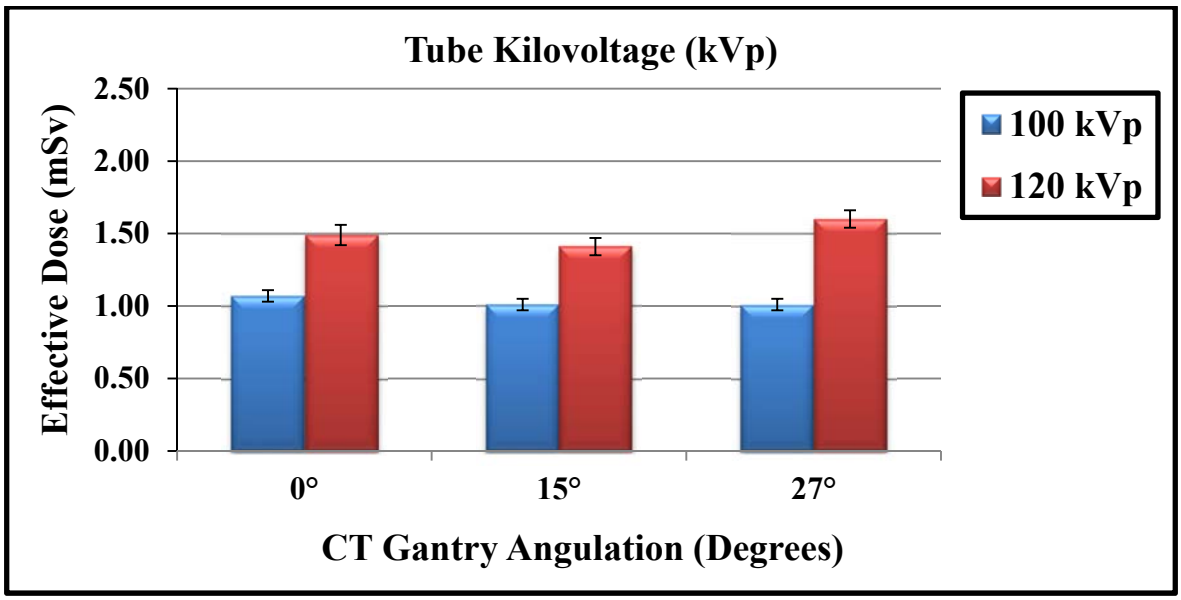

Figure 6-15: A bar chart illustrating the effect of changing tube potential on effective dose for three different gantry angulations. Error bars denote the standard deviation of the data.

6.4.3.3 Tube Current

The main effect of tube current on effective dose was investigated by varying the values of mA within the paediatric protocol and the results were illustrated in **(Table 6-20)** and **(Figure 6-16)**. By calculating the percentage difference between the different values of effective dose obtained, the dose was increased on average by approximately 43% when raising the tube current from 120 to 200 mA.

Table 6-20: Effective dose for different tube currents at different gantry angulations (mean/SD).				
Tube Current (mA)	**Gantry Angulations (Degrees)**			
	0º	**15º**	**27º**	**P values**
120	1.07 ± 0.04 (mSv)	1.01 ± 0.04 (mSv)	1.01 ± 0.4 (mSv)	0.99
160	1.49 ± 0.05 (mSv)	1.23 ± 0.05 (mSv)	1.61 ± 0.04 (mSv)	0.90
200	1.72 ± 0.06 (mSv)	1.76 ± 0.05 (mSv)	1.58 ± 0.07 (mSv)	0.96
P values	0.02	0.02	0.03	

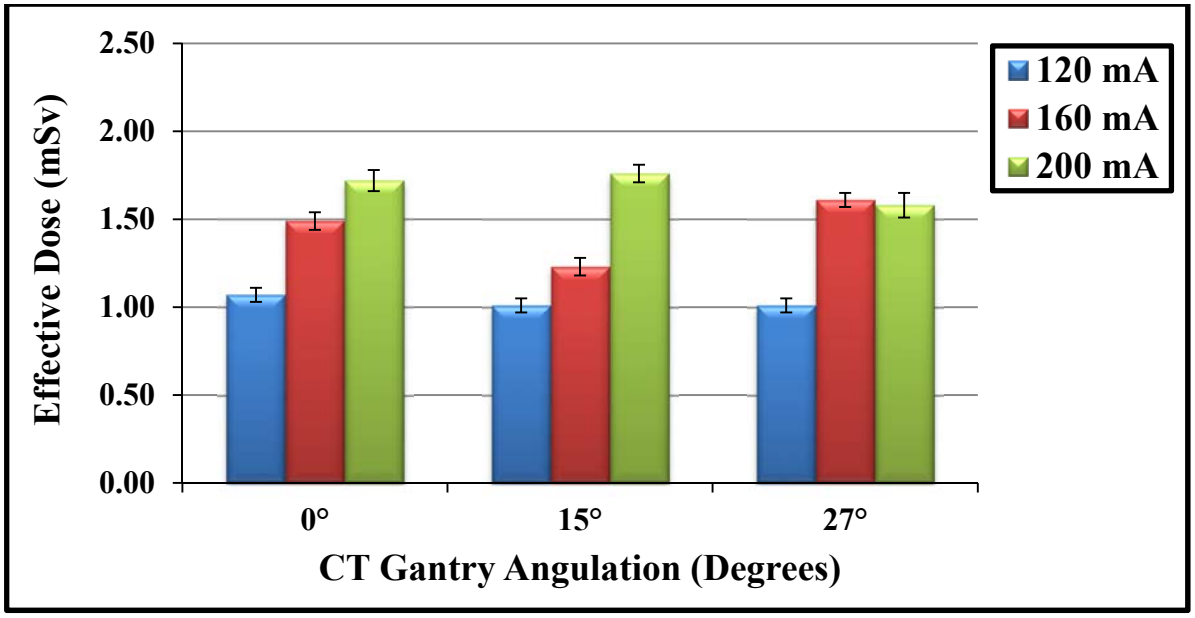

Figure 6-16: A bar chart illustrating a comparison of effective dose for different fixed tube currents at three different gantry angulations. Error bars denote the standard deviation of the data.

6.5 Eye Dose

The eye lens is an example of an organ with an attributed deterministic radiation effect: If the eye is exposed to a dose above a certain threshold, a cataract will develop. It is assumed that the minimum dose required to produce a detectable cataract is about 2 Gy for a single exposure and 5 Gy for fractionated or protracted exposure (ICRP, 2012). To avoid irradiation of the eyes, brain CT is normally planned to exclude the eyes from the imaged area. However as discussed in chapter three, in helical CT, over-ranging extends the irradiated area on both ends of the planned scanning range. Thus, the eyes receive a radiation dose, even though no images are reconstructed from data obtained in that area. The eye lens dose largely depends on the scanning parameters that control over-ranging (detector collimation and pitch), as well as on the actual distance from the eyes to the edge of the imaged volume (Schilham et al., 2010). The calculated eye dose for a typical helical CT examination of the head for an adult and paediatric when the eyes are outside of the imaged volume are illustrated below.

6.5.1 Adult Absorbed Eye Dose

Absorbed eye dose was measured for all 162 brain protocols and the data are presented in **(Table H - 1)** in **(Appendix (H)** on page **243**. An example of eye dose for the adult helical

protocol using the following settings: (rotation time 0.5 seconds, detector configuration of 0.5 x 16, pitch factors / Helical Pitch [Detail PF 0.688 / HP 11.0] and Sure Exp. 3D (ATC) [High Quality SD 1.80]) is shown in **(Table 6-21)** and **(Figure 6-17)**. The eye dose decreased slightly according to the change in gantry angulations from 0º to 15º whereas there is a statistical significant decrease in eye dose when changing CT gantry angulations from 0º to 27º. The percentage decrease in absorbed dose, according to gantry angulation settings is 5.5% change referring to the dose reduction between 0º and 15º and 51.3% to the reduction between 0º and 27º.

Table 6-21: Adult eye absorbed dose (mean/SD).			
Gantry Angulation	**0º**	**15º**	**27º**
Eye Dose (mGy)	32.1 ± 4	30.3 ± 3	15.6 ± 7

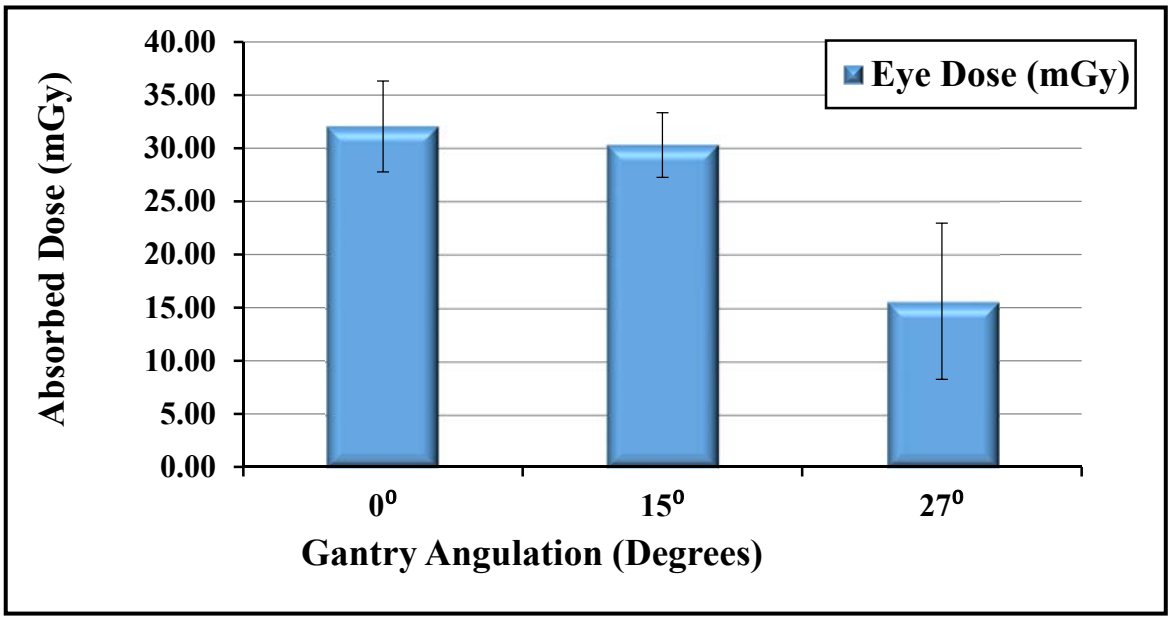

Figure 6-17: A bar chart illustrating a comparison of adult eye dose for three different gantry angulations for a representative protocol. Error bars denote the standard deviation of the data.

The Box & Whisker graph in **(Figure 6-18)** shows that the adult eye absorbed dose decreases as the CT gantry angulation increased across the range of protocols.

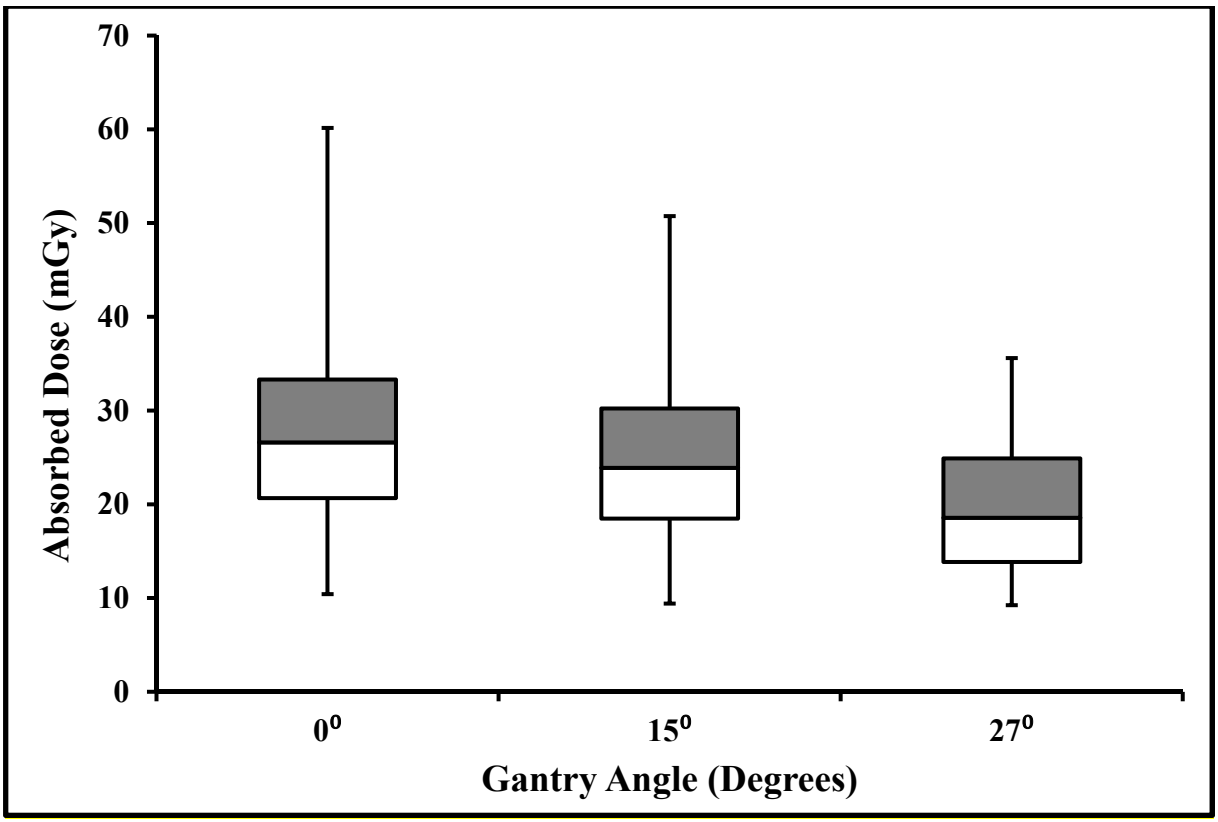

Figure 6-18: Box & Whisker graph showing the absorbed eye dose (mGy) for the adult helical protocols. Ends of the whiskers correspond to the maximum and minimum values, end of the boxes correspond to 1st and 3rd quartiles and the horizontal line refers to the median.

6.5.2 Paediatric Absorbed Eye Dose

Eye lenses absorbed dose was measured for 162 paediatric brain helical protocols and the results of the dose are illustrated in **(Table H - 2)** in **(Appendix H)** on page **244**. An example of eye absorbed dose for paediatric helical protocol using the following settings: (rotation time 0.5 seconds, detector configuration of 0.5 x 16, Pitch Factors / Helical Pitch [Detail PF 0.688 / HP 11.0] and Sure Exp. 3D (ATC) [High Quality SD 4.00]) is shown in **(Table 6-22)** and **(Figure 6-19)** the eye dose decreased slightly according to the change in gantry angulations. The percent of reduction in effective dose, according to gantry angulation settings was 9.53% change referring to the dose reduction between 0º and 15º degree and 24.36% to the reduction between 0º and 27º. Accordingly, as illustrated in the Box & Whisker graph in **(Figure 6-20)** paediatric eye absorbed doses decreased when CT gantry angulation increased.

Table 6-22: Paediatric eye absorbed dose (mean/SD).			
Gantry Angulation	**0°**	**15°**	**27°**
Eye Dose (mGy)	33.05 ± 3	29.90 ± 1	25.00 ± 3

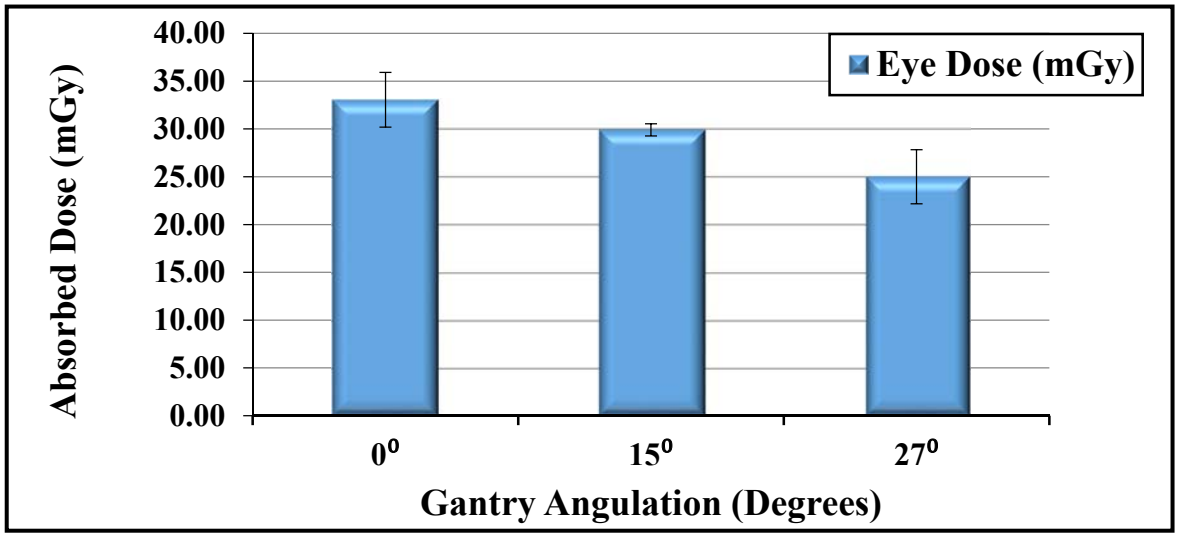

Figure 6-19: A bar chart illustrating a comparison of paediatric eye dose for three different gantry angulations for a representative protocol. Error bars denote the standard deviation of the data.

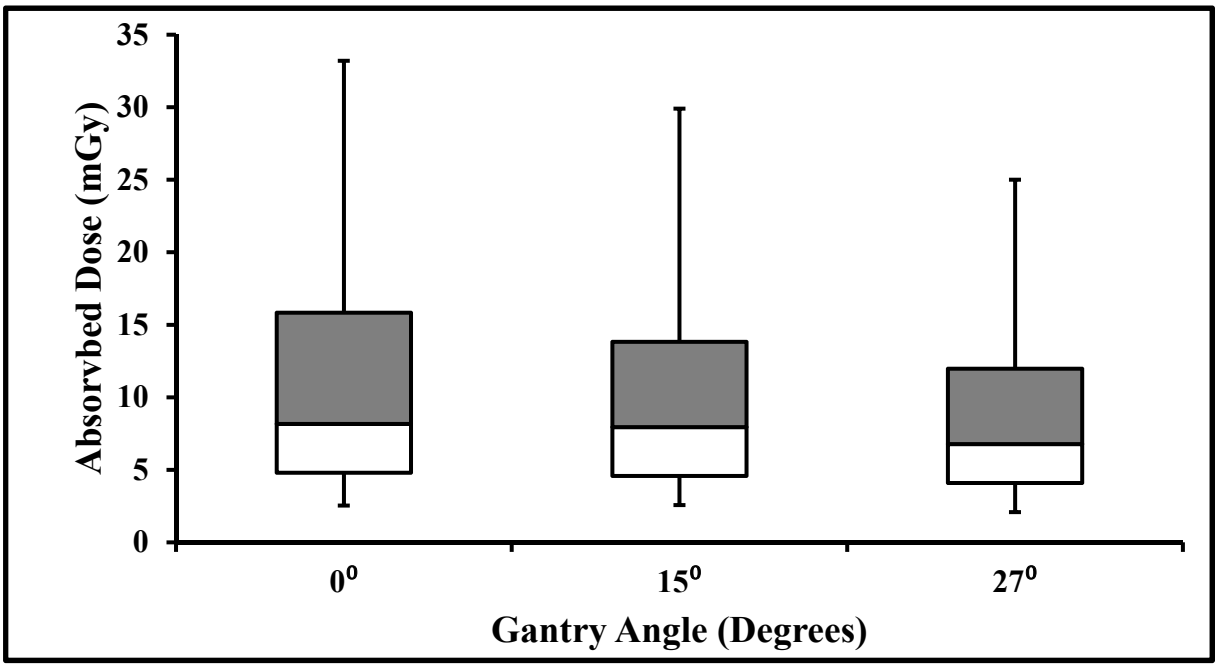

Figure 6-20: Box & Whisker graph showing absorbed eye dose (mGy) for the paediatric helical protocols. Ends of the whiskers correspond to the maximum and minimum values, end of the boxes correspond to 1st and 3rd quartiles and the horizontal line refers to the median.

6.6 Estimating Attributable Radiation Lifetime Cancer Risk

The attributable lifetime cancer risk estimation, based on BEIR VII modelling, was calculated for both male and female ages from 0 to 80 years old. Risk estimates were facilitated using the absorbed dose measurements (MOSFET) for the adult and paediatric ATOM phantoms. The attributable lifetime risk (number of cancer cases per million) was calculated for all 216 protocols for the adult phantom (including both sequential and helical protocols) and 162 protocols for the paediatric, and for both males and females. As an example, the lifetime attributable cancer risk for males and females for 9 protocols are illustrated in **(Table 6-23)** and **(Table 6-24)**, respectively. The box and whisker plots summarise the lifetime risk data for the male and female groups with age across all protocols. The lifetime risk for male and females of cancer increases as age decreases **(Figure 6-21)** and **(Figure 6-22)**. As can be seen from **(Figure 6-23)**, the gender differences are most apparent below the age of 30. Importantly, the selection of the brain CT protocol has the greatest impact on lifetime risk below the age of twenty as demonstrated by the length of the whiskers. The full range of lifetime cancer risk for both male and females are illustrated in **(Table I - 1)** and **(Table J - 1)** within **(Appendix's I & J)** on pages **245** to **248**. When referring to **(Table 6-23)** and **(Table 6-24)** full protocol acquisition parameters are presented in **(Appendix B)** within **(Table B - 1)** on pages **204** and in **(Appendix C)** within **(Table C - 1)** on page **213** for adult and paediatric respectively.

Table 6-23: Male lifetime attributable cancer risk case/10^6

	Age										
Protocol No.	**0**	**5**	**10**	**15**	**20**	**30**	**40**	**50**	**60**	**70**	**80**
1	46	29	14	11	8	5	5	4	3	2	1
2	24	15	13	11	8	5	5	4	3	2	1
3	16	10	12	9	8	5	4	3	3	2	1
4	39	24	11	9	7	4	4	3	2	1	1
5	23	14	10	8	6	4	4	3	2	1	1
6	15	11	10	8	6	4	3	3	2	1	1
7	33	21	8	7	5	3	3	2	2	1	<1
8	24	15	8	6	5	3	3	2	2	1	<1
9	17	10	7	6	5	3	3	2	2	1	<1

Table 6-24: Female lifetime attributable cancer risk case/10^6											
	Age										
Protocol No.	**0**	**5**	**10**	**15**	**20**	**30**	**40**	**50**	**60**	**70**	**80**
1	102	64	18	14	11	7	6	5	4	2	1
2	55	34	19	15	12	7	6	5	4	2	1
3	36	23	20	15	12	7	6	5	4	2	1
4	82	51	17	13	10	6	5	4	3	2	1
5	53	33	15	12	9	6	5	4	3	2	1
6	32	20	15	11	9	5	4	4	3	2	1
7	78	49	12	9	7	4	4	3	2	1	1
8	55	34	12	9	7	4	4	3	2	1	1
9	40	25	12	9	7	4	4	3	2	1	1

Figure 6-21: Box & Whisker graph showing male lifetime cancer risk cases/10^6. Ends of the whiskers correspond to the maximum and minimum values, end of the boxes correspond to 1st and 3rd quartiles and the horizontal line refers to the median.

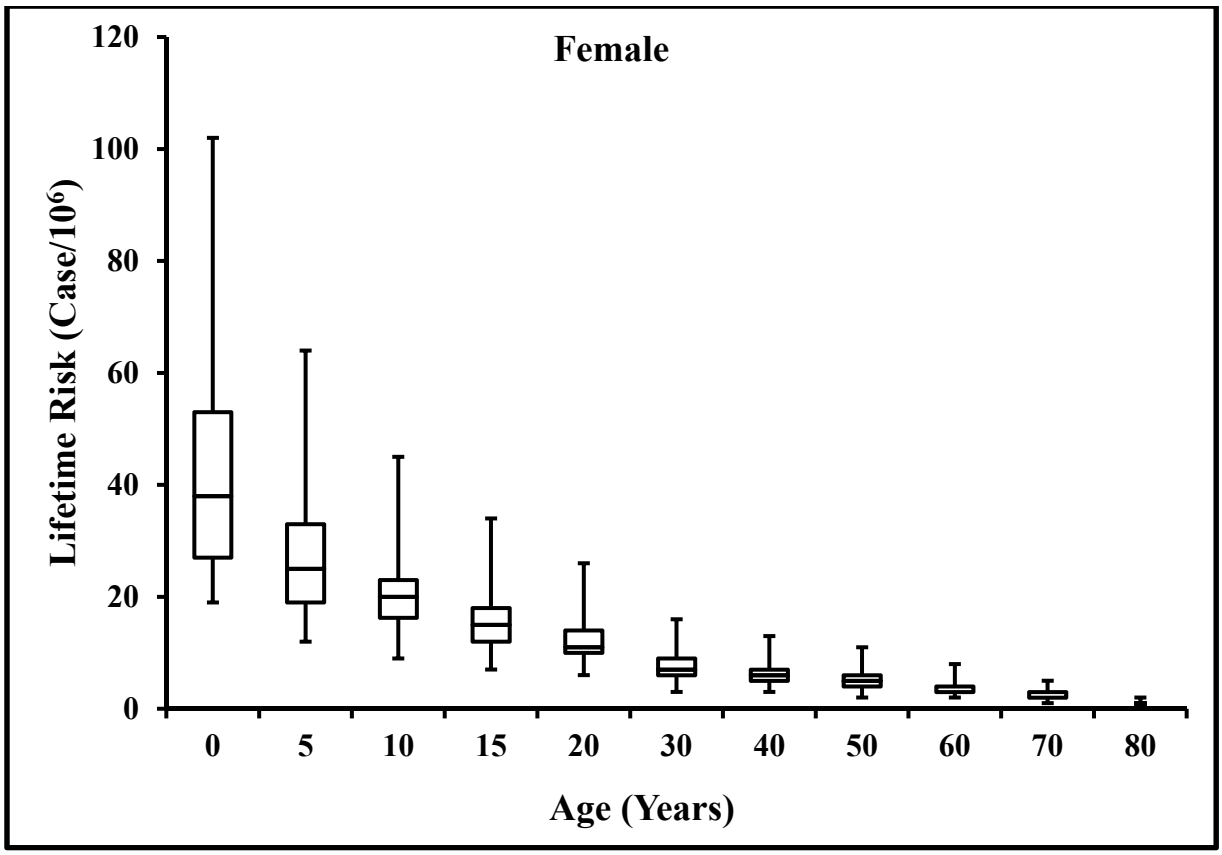

Figure 6-22: Box & Whisker graph showing female lifetime cancer risk cases/10^6 increases with as age decreases. Ends of the whiskers correspond to the maximum and minimum values, end of the boxes correspond to 1st and 3rd quartiles and the horizontal line refers to the median.

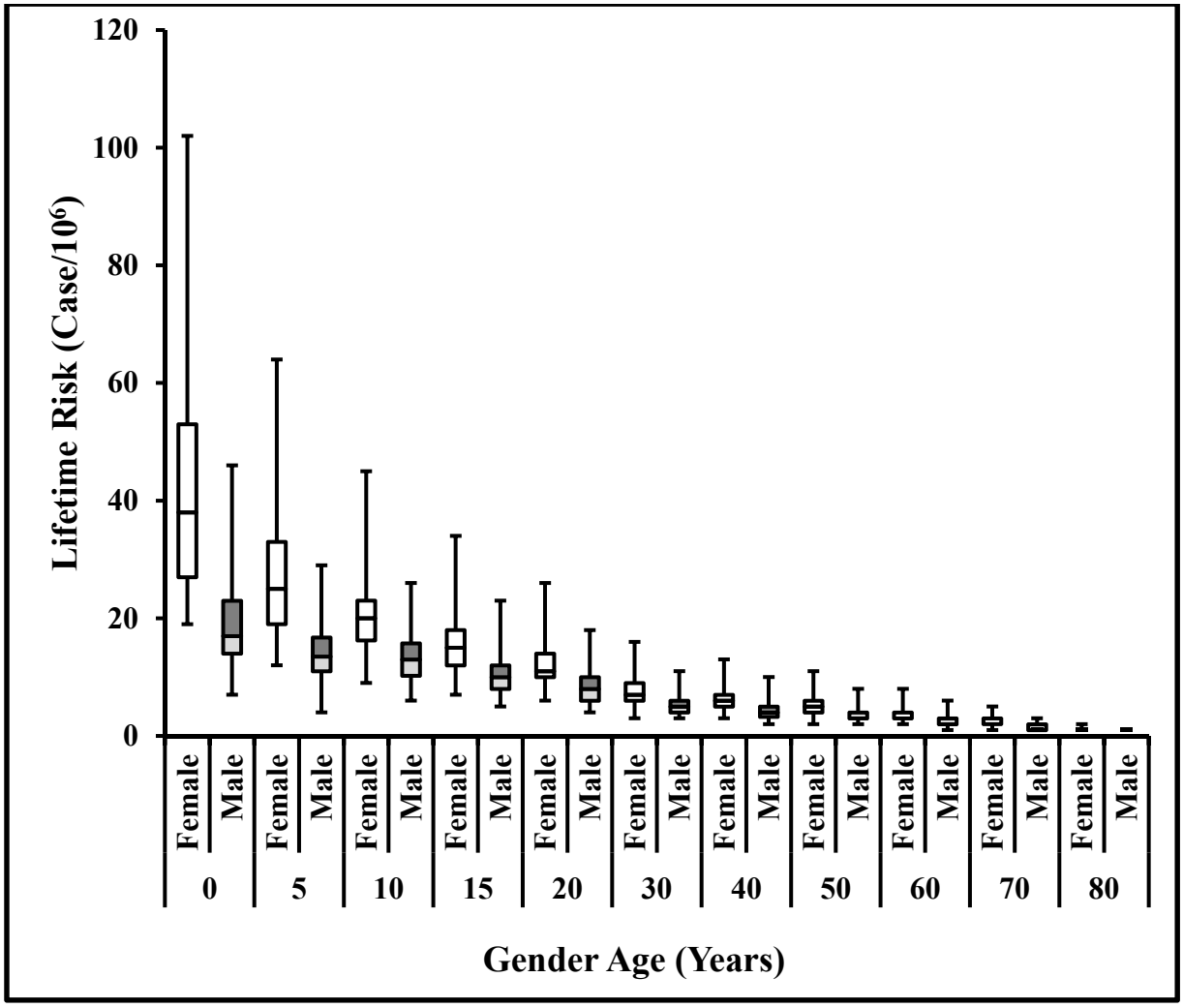

Figure 6-23: Box & Whisker male & female combined graph showing increase in lifetime cancer risk cases/10^6 for female and as the age of both male and female decreased.

6.7 A Tool to Estimate the Prospective Effective Risk for a Patient

The risk data presented above provides a useful summary of the relationships between risk, gender and age, however in order for the data to be informative for clinical practice a tool is necessary to understand the risk to a particular patient within a clinical scenario. To do this a Microsoft Excel Workbook has been developed that enables a practitioner to filter through the 216 protocols (adult) or 162 protocols (paediatric) based on the acquisition factors they are considering using. This enables them to easily compare the estimated attributable lifetime cancer risk associated with several protocols (or parameter changes) that they are considering. This demonstrates how the novel data generated from this thesis could be useful in informing radiographer decision-making prior to initiating a CT scan. Current clinical practices are for radiation dose assessment to be a retrospective process and commonly based on only $CTDI_{vol}$

and DLP dose estimates. $CTDI_{vol}$ and DLP have accepted limitations and the radiation estimate method proposed in thesis builds upon this. The worksheet also incorporates an option to select the accumulative risk for multiple brain CT scans. This may be useful in a situation where a patient has a long-term condition where multiple brain CT scans are expected to have to take place. Again, this approach to the prospective consideration of radiation risk for patients in a step change in radiographic practice. Although the data presented here are only applicable for the Toshiba 16 Aquilion CT scanner, from which dosimetry data were collected, similar data for CT scanners used in clinical practice could be collected and presented in a similar manner. The proposed risk estimation workbook has been published alongside a brief instruction manual within an online data repository known as Figshare, however, for the purpose of this thesis supplementary information on CD-ROM are included on the back of the thesis. A screen shot of the Microsoft Excel Workbook has been displayed in **(Figure 6-24)** and **(Figure 6-25)** illustrating the protocols and parameters available for selection and the subsequent predicted lifetime cancer risk for males and females.

	A	B	C	D	E	F	G
1							
2							
3	Detector Configuration (mm)	Pitch Factors / Helical Pitch	Sure Exp. 3D (ATC)	Tube Rotation Time (secs)	Tube Angulations (Degrees)	Protocol Number	Estimated Number of Exposures (1-5)
4	0.5x16	Detail PF 0.688 / HP 11.0	High Quality SD 1.80	0.5	0	1	1
5	0.5x16	Detail PF 0.688 / HP 11.0	Standard SD 2.00	0.5	0	2	1
6	0.5x16	Detail PF 0.688 / HP 11.0	Low Dose SD 2.20	0.5	0	3	1
7	0.5x16	Standard PF 0.938 / HP 15.0	High Quality SD 1.80	0.5	0	4	1
8	0.5x16	Standard PF 0.938 / HP 15.0	Standard SD 2.00	0.5	0	5	1
9	0.5x16	Standard PF 0.938 / HP 15.0	Low Dose SD 2.20	0.5	0	6	1
10	0.5x16	Fast PF 1.438 / HP 23.0	High Quality SD 1.80	0.5	0	7	1
11	0.5x16	Fast PF 1.438 / HP 23.0	Standard SD 2.00	0.5	0	8	1
12	0.5x16	Fast PF 1.438 / HP 23.0	Low Dose SD 2.20	0.5	0	9	1
13	0.5x16	Detail PF 0.688 / HP 11.0	High Quality SD 1.80	0.5	15	10	1
14	0.5x16	Detail PF 0.688 / HP 11.0	Standard SD 2.00	0.5	15	11	1
15	0.5x16	Detail PF 0.688 / HP 11.0	Low Dose SD 2.20	0.5	15	12	1
16	0.5x16	Standard PF 0.938 / HP 15.0	High Quality SD 1.80	0.5	15	13	1
17	0.5x16	Standard PF 0.938 / HP 15.0	Standard SD 2.00	0.5	15	14	1
18	0.5x16	Standard PF 0.938 / HP 15.0	Low Dose SD 2.20	0.5	15	15	1
19	0.5x16	Fast PF 1.438 / HP 23.0	High Quality SD 1.80	0.5	15	16	1
20	0.5x16	Fast PF 1.438 / HP 23.0	Standard SD 2.00	0.5	15	17	1
21	0.5x16	Fast PF 1.438 / HP 23.0	Low Dose SD 2.20	0.5	15	18	1
22	0.5x16	Detail PF 0.688 / HP 11.0	High Quality SD 1.80	0.5	27	19	1
23	0.5x16	Detail PF 0.688 / HP 11.0	Standard SD 2.00	0.5	27	20	1
24	0.5x16	Detail PF 0.688 / HP 11.0	Low Dose SD 2.20	0.5	27	21	1
25	0.5x16	Standard PF 0.938 / HP 15.0	High Quality SD 1.80	0.5	27	22	1
26	0.5x16	Standard PF 0.938 / HP 15.0	Standard SD 2.00	0.5	27	23	1
27	0.5x16	Standard PF 0.938 / HP 15.0	Low Dose SD 2.20	0.5	27	24	1
28	0.5x16	Fast PF 1.438 / HP 23.0	High Quality SD 1.80	0.5	27	25	1
29	0.5x16	Fast PF 1.438 / HP 23.0	Standard SD 2.00	0.5	27	26	1
30	0.5x16	Fast PF 1.438 / HP 23.0	Low Dose SD 2.20	0.5	27	27	1
31	1.0x16	Detail PF 0.688 / HP 11.0	High Quality SD 1.80	0.5	0	28	1
32	1.0x16	Detail PF 0.688 / HP 11.0	Standard SD 2.00	0.5	0	29	1
33	1.0x16	Detail PF 0.688 / HP 11.0	Low Dose SD 2.20	0.5	0	30	1
34	1.0x16	Standard PF 0.938 / HP 15.0	High Quality SD 1.80	0.5	0	31	1
35	1.0x16	Standard PF 0.938 / HP 15.0	Standard SD 2.00	0.5	0	32	1
36	1.0x16	Standard PF 0.938 / HP 15.0	Low Dose SD 2.20	0.5	0	33	1
37	1.0x16	Fast PF 1.438 / HP 23.0	High Quality SD 1.80	0.5	0	34	1
38	1.0x16	Fast PF 1.438 / HP 23.0	Standard SD 2.00	0.5	0	35	1
39	1.0x16	Fast PF 1.438 / HP 23.0	Low Dose SD 2.20	0.5	0	36	1
40	1.0x16	Detail PF 0.688 / HP 11.0	High Quality SD 1.80	0.5	15	37	1
41	1.0x16	Detail PF 0.688 / HP 11.0	Standard SD 2.00	0.5	15	38	1
42	1.0x16	Detail PF 0.688 / HP 11.0	Low Dose SD 2.20	0.5	15	39	1
43	1.0x16	Standard PF 0.938 / HP 15.0	High Quality SD 1.80	0.5	15	40	1
44	1.0x16	Standard PF 0.938 / HP 15.0	Standard SD 2.00	0.5	15	41	1
45	1.0x16	Standard PF 0.938 / HP 15.0	Low Dose SD 2.20	0.5	15	42	1
46	1.0x16	Fast PF 1.438 / HP 23.0	High Quality SD 1.80	0.5	15	43	1
47	1.0x16	Fast PF 1.438 / HP 23.0	Standard SD 2.00	0.5	15	44	1
48	1.0x16	Fast PF 1.438 / HP 23.0	Low Dose SD 2.20	0.5	15	45	1
49	1.0x16	Detail PF 0.688 / HP 11.0	High Quality SD 1.80	0.5	27	46	1
50	1.0x16	Detail PF 0.688 / HP 11.0	Standard SD 2.00	0.5	27	47	1
51	1.0x16	Detail PF 0.688 / HP 11.0	Low Dose SD 2.20	0.5	27	48	1
52	1.0x16	Standard PF 0.938 / HP 15.0	High Quality SD 1.80	0.5	27	49	1
53	1.0x16	Standard PF 0.938 / HP 15.0	Standard SD 2.00	0.5	27	50	1
54	1.0x16	Standard PF 0.938 / HP 15.0	Low Dose SD 2.20	0.5	27	51	1
55	1.0x16	Fast PF 1.438 / HP 23.0	High Quality SD 1.80	0.5	27	52	1
56	1.0x16	Fast PF 1.438 / HP 23.0	Standard SD 2.00	0.5	27	53	1
57	1.0x16	Fast PF 1.438 / HP 23.0	Low Dose SD 2.20	0.5	27	54	1
58	2.0x16	Detail PF 0.688 / HP 11.0	High Quality SD 1.80	0.5	0	55	1
59	2.0x16	Detail PF 0.688 / HP 11.0	Standard SD 2.00	0.5	0	56	1

Adult Eye Dose & Lifetime Risk

Figure 6-24: Effective risk prediction tool (Excel Workbook) showing the protocol parameters options.

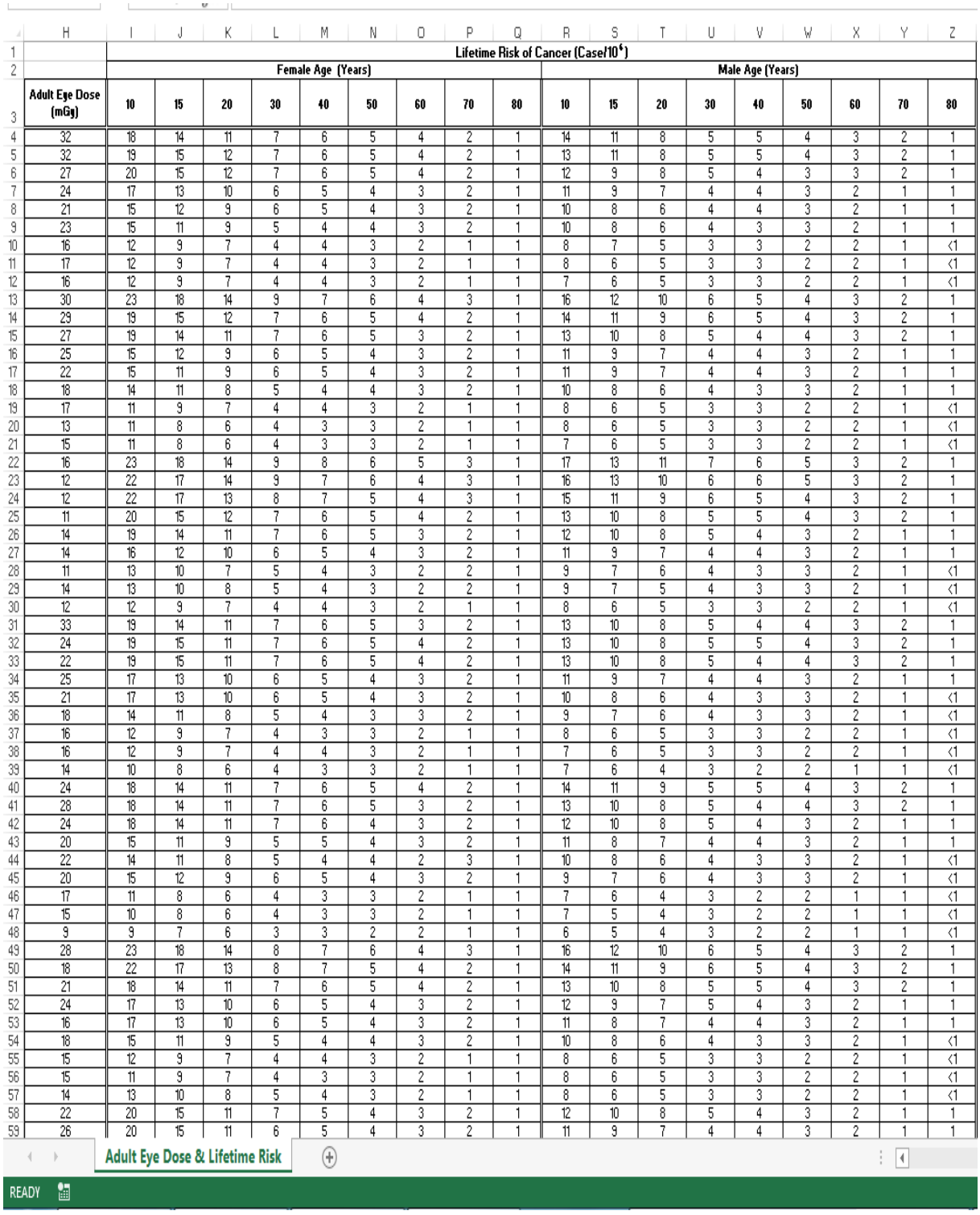

	H	I	J	K	L	M	N	O	P	Q	R	S	T	U	V	W	X	Y	Z
1		Lifetime Risk of Cancer (Case/10^4)																	
2		Female Age (Years)									Male Age (Years)								
3	Adult Eye Dose (mGy)	10	15	20	30	40	50	60	70	80	10	15	20	30	40	50	60	70	80
4	32	18	14	11	7	6	5	4	2	1	14	11	8	5	5	4	3	2	1
5	32	19	15	12	7	6	5	4	2	1	13	11	8	5	5	4	3	2	1
6	27	20	15	12	7	6	5	4	2	1	12	9	8	5	4	3	3	2	1
7	24	17	13	10	6	5	4	3	2	1	11	9	7	4	4	3	2	1	1
8	21	15	12	9	6	5	4	3	2	1	10	8	6	4	4	3	2	1	1
9	23	15	11	9	5	4	4	3	2	1	10	8	6	4	3	3	2	1	1
10	16	12	9	7	4	4	3	2	1	1	8	7	5	3	3	2	2	1	<1
11	17	12	9	7	4	4	3	2	1	1	8	6	5	3	3	2	2	1	<1
12	16	12	9	7	4	4	3	2	1	1	7	6	5	3	3	2	2	1	<1
13	30	23	18	14	9	7	6	4	3	1	16	12	10	6	5	4	3	2	1
14	29	19	15	12	7	6	5	4	2	1	14	11	9	6	5	4	3	2	1
15	27	19	14	11	7	6	5	3	2	1	13	10	8	5	4	4	3	2	1
16	25	15	12	9	6	5	4	3	2	1	11	9	7	4	4	3	2	1	1
17	22	15	11	9	6	5	4	3	2	1	11	9	7	4	4	3	2	1	1
18	18	14	11	8	5	4	4	3	2	1	10	8	6	4	3	3	2	1	1
19	17	11	9	7	4	4	3	2	1	1	8	6	5	3	3	2	2	1	<1
20	13	11	8	6	4	3	3	2	1	1	8	6	5	3	3	2	2	1	<1
21	15	11	8	6	4	3	3	2	1	1	7	6	5	3	3	2	2	1	<1
22	16	23	18	14	9	8	6	5	3	1	17	13	11	7	6	5	3	2	1
23	12	22	17	14	9	7	6	4	3	1	16	13	10	6	6	5	3	2	1
24	12	22	17	13	8	7	5	4	3	1	15	11	9	6	5	4	3	2	1
25	11	20	15	12	7	6	5	4	2	1	13	10	8	5	5	4	3	2	1
26	14	19	14	11	7	6	5	3	2	1	12	10	8	5	4	3	2	1	1
27	14	16	12	10	6	5	4	3	2	1	11	9	7	4	4	3	2	1	1
28	11	13	10	7	5	4	3	2	2	1	9	7	6	4	3	3	2	1	<1
29	14	13	10	8	5	4	3	2	2	1	9	7	5	4	3	3	2	1	<1
30	12	12	9	7	4	4	3	2	1	1	8	6	5	3	3	2	2	1	<1
31	33	19	14	11	7	6	5	3	2	1	13	10	8	5	4	4	3	2	1
32	24	19	15	11	7	6	5	4	2	1	13	10	8	5	5	4	3	2	1
33	22	19	15	11	7	6	5	4	2	1	13	10	8	5	4	4	3	2	1
34	25	17	13	10	6	5	4	3	2	1	11	9	7	4	4	3	2	1	1
35	21	17	13	10	6	5	4	3	2	1	10	8	6	4	3	3	2	1	<1
36	18	14	11	8	5	4	3	3	2	1	9	7	6	4	3	3	2	1	<1
37	16	12	9	7	4	3	3	2	1	1	8	6	5	3	3	2	2	1	<1
38	16	12	9	7	4	4	3	2	1	1	7	6	5	3	3	2	2	1	<1
39	14	10	8	6	4	3	3	2	1	1	7	6	4	3	2	2	1	1	<1
40	24	18	14	11	7	6	5	4	2	1	14	11	9	5	5	4	3	2	1
41	28	18	14	11	7	6	5	3	2	1	13	10	8	5	4	4	3	2	1
42	24	18	14	11	7	6	4	3	2	1	12	10	8	5	4	3	2	1	1
43	20	15	11	9	5	5	4	3	2	1	11	8	7	4	4	3	2	1	1
44	22	14	11	8	5	4	4	2	3	1	10	8	6	4	3	3	2	1	<1
45	20	15	12	9	6	5	4	3	2	1	9	7	6	4	3	3	2	1	<1
46	17	11	8	6	4	3	3	2	1	1	7	6	4	3	2	2	1	1	<1
47	15	10	8	6	4	3	3	2	1	1	7	5	4	3	2	2	1	1	<1
48	9	9	7	6	3	3	2	2	1	1	6	5	4	3	2	2	1	1	<1
49	28	23	18	14	8	7	6	4	3	1	16	12	10	6	5	4	3	2	1
50	18	22	17	13	8	7	5	4	2	1	14	11	9	6	5	4	3	2	1
51	21	18	14	11	7	6	5	4	2	1	13	10	8	5	5	4	3	2	1
52	24	17	13	10	6	5	4	3	2	1	12	9	7	5	4	3	2	1	1
53	16	17	13	10	6	5	4	3	2	1	11	8	7	4	4	3	2	1	1
54	18	15	11	9	5	4	4	3	2	1	10	8	6	4	3	3	2	1	<1
55	15	12	9	7	4	4	3	2	1	1	8	6	5	3	3	2	2	1	<1
56	15	11	9	7	4	3	3	2	1	1	8	6	5	3	3	2	2	1	<1
57	14	13	10	8	5	4	3	2	1	1	8	6	5	3	3	2	2	1	<1
58	22	20	15	11	7	5	4	3	2	1	12	10	8	5	4	3	2	1	1
59	26	20	15	11	6	5	4	3	2	1	11	9	7	4	4	3	2	1	1

Adult Eye Dose & Lifetime Risk

READY

Figure 6-25: Effective risk prediction tool showing lifetime risk for males and females (tool outcome).

Chapter 7 : Discussion

7.1 Chapter Overview

For CT examinations it can be beneficial to estimate both absorbed dose and effective dose in order to assess the risk and evaluate methods aimed at reducing dose. The primary aim of the dose measurements and calculations in this thesis were to estimate the attributable lifetime cancer risk. This specifically focused on assessing the risk of inducing cancer during the lifetime of an individual undergoing a CT brain scan. The secondary aim of this study was to understand the impact of different CT scan acquisition factors including gantry angle, both for paediatric and adults on the effective dose. To achieve these aims, a set of objectives were formulated, see chapter one, section **(1.3)** on page **5**. From these objectives, a research question was proposed; how do changes in CT protocols affect the effective risk from CT head scans in adults and children? The research question has been methodically tested and the results are presented in chapter **(6)** items **(6.1** to **6.7)** on pages **126** to **155**.

In this chapter, the results answering the research question will be discussed in two parts. The first part will examine the clinical implications of the absorbed and effective doses for helical and sequential protocols as well as the differences in radiation dose due to changes in CT scan parameters. Secondly, the results from the estimations of effective risk will be addressed. Fundamentally it was important to assess if patients having CT brain scans could be being exposed to high levels of radiation which could lead to the development of cancer during a patient's lifetime, especially in the young. This thesis will provide, for the first time, a prospective proactive method of estimating radiation risk (including age and gender) which is available prior to the start of the CT scan. Such a development is a major change from how CT scans are currently undertake and optimised.

7.2 Absorbed Dose (mGy)

In the literature, there are a limited number of studies providing information on organ and tissue absorbed doses for CT examinations on children (Brenner and Hall, 2007; Coursey et al., 2008; Fujii et al., 2007). This is largely due to the complexity of undertaking these types of measurements and the lack of resources and time for performing dosimetry experiments in the clinical environment. Furthermore, where studies exist, it is often difficult to make direct comparisons due to the many different variables that have considerable effect on the radiation

dose. These include the type of experimental or computational method for dosimetry, the representative age and type of anthropomorphic phantom used, the modelling of the CT scanner, if applicable, and/or the CT examination parameters (e.g. kVp, mAs, collimation, pitch and scan length).

Twenty-four organ and tissue doses, in both ATOM phantoms representing an adult and 1-year-old child, were obtained using MOSFET dosimeters for a range of head CT protocols (in total 432 protocols, 216 for each adult and paediatric phantoms, respectively). The results were used to calculate effective dose and for estimating induced cancer risk; see **(Table 6-1)** on page **127**, which shows an example of measured absorbed dose and calculated effective dose for a single protocol. The comparison of organ doses for helical adult brain protocols demonstrates that the highest dose was received by the brain tissue and eye lenses from 13.4 to 27.5 mGy and 16.2 to 32.1 mGy, respectively **(Table D - 1)** to **(Table D - 6)** in appendix **D** on pages **222 - 227**. However, changing the CT gantry angulation form 0^{o} to 27^{o} reduced the eye lens dose by 50% (from 32.05 to 15.60 mGy), see **(Table 6-21)** on page **149**. In terms of a head CT scan, there is a focus on bone marrow, thyroid gland and eye dose, due to the fact that these are the most radiosensitive. The lens of the eye does not need to be considered for stochastic effects such as cancer induction. However, it is useful to consider the deterministic effects, such as cataract formation, which have a threshold of about 0.5 Gy (ICRP, 2011). According to the ICRP 103 (2007) report, the tissue weighting factors for bone marrow and thyroid gland are 0.12 and 0.04, respectively. The major concern in a CT brain examination is the radiation administered to the eye lens, and that scans are potentially being overused (Owlia et al., 2014). This is because in routine clinical practice the CT gantry positioned will often be at 0°, making all or part of the patient's eye lens inevitably irradiated by the primary X-ray beam. As indicated in the ICRP 103 annual report, the lens of the eye is known to be radiosensitive, thus for CT brain examinations, as discussed later in the discussion **(section 7.5)**, it is important to reduce the absorbed dose to the lens of the eye by tilting the CT gantry to prevent them from an attributed deterministic radiation effect.

Organs on the periphery of the scan volume can have a significant variation in absorbed dose across the organ due to partial irradiation. The overall dose to the active bone marrow (ABM) was in the range 1.2 to 2.3 mGy and the dose to thyroid gland ranged from 0.6 to 1.0 mGy. The locations used to measure the absorbed dose to red bone marrow (RBM) are shown in appendix **A (Table A - 1)** and **(Table A - 2)** pages **197** to **199** for both adult and paediatric ATOM

phantoms, respectively. The absorbed doses for this tissue is not based on the simple average of multiple dosimeters in each organ (as detailed in the methods section **5.8.3** on page **118**) and has therefore been provided individually. The measured absorbed doses vary considerably for the locations selected for the RBM calculations. This is expected since these locations range from the skull to the pelvis and therefore may be directly irradiated, partially irradiated or completely outside of the scanned volume and reach of scattered radiation. This is evident in the variation (mean, SD) of measured absorbed doses for all protocols, although it can be most readily seen in the brain where the absorbed dose to the skull ranges from 2.2 ± 0.5 – 35.1 ± 2.3 mGy, while all other locations are less than 1 mGy. Similar values of ABM absorbed dose have been obtained on a study conducted by Lee et al. (2011); they indicate a received ABM absorbed dose of 1.8 mGy/100 mAs at 120 kVp in the head, whereas the thyroid dose was 0.3 mGy/100 mAs at 120 kVp in the head scan (Lee et al., 2011). According to Lee et al., (2007), the vertical placement of the thyroid can lead to significant differences in absorbed dose estimates as the thyroid will receive some shielding from the mandible bones. The calculated effective dose ranged from 0.34 – 1.55 mSv and from 0.27 – 1.13 mSv for helical and sequential CT brain protocols, respectively. The absorbed dose to thyroid gland for helical brain protocols received up to 1.5 times higher dose than for sequential CT protocols. The absorbed dose to ABM from the CT helical protocols were 2 to 4 times greater than for sequential protocols. The choice of using helical or sequential protocols are dependent on the reason the patient is having the CT scan. Helical mode is used for situations requiring faster scanning to reduce the potential for motion artefacts, whereas sequential scanning provides better image quality, especially for small structures with low tissue contrast (Pace & Zarb, 2015). Differences in the absorbed dose between the two protocols are likely to be the result of differences in the scan lengths (over-scanning) between the helical and sequential scanning modes. However, the scan range can be defined as actual imaging volume plus an additional half cycle at the beginning and the end of scanning volume to reconstruct the first and last slice in helical scanning mode. It must be a multiple of scan coverage less the overlapping zones in sequential scans. Also, the organs and tissues located inside the scan volume, or close to it, will receive a high dose compared to those located far from it. The percentage of ABM is age dependent, as recommended by ICRP report 70 (1995), and has a high tissue weighting factor of 0.12. For an adult aged 40 years old the ABM is distributed as 7.6% in the cranium, which is located within the brain scanning volume, 0.8% in mandible and 3.9% in C-spine which is located closely to the scanning volume. Whereas in a one-year old child the percentage of ABM is distributed as 25.1% in cranium, 2.4% in mandible and 2.8% in C-spine. As reported by Cohnen et al., (2000), the radiation

exposure to the bone marrow in the skull may be important because this is irradiated directly during a head CT scan and is radiosensitive. In particular, there are concerns regarding the risk of leukaemia induction as a result of exposure which is believed to represent 5% to 10% of the total marrow in adults. Thus, an approximate effective dose of 0.1 mSv may be applied during ‘‘standard’’ cranial CT. In children, CT of the brain results in a possible effective dose of up to 0.4 mSv to the calvarium, in which 25% to 30% of the bone marrow is localised. Since multiple scans may be performed in paediatric patients, (e.g., shunt and ventricle size control), emphasis should be placed on radiation protection and lowering exposure where possible. Also, the helical thyroid dose is high primarily because the thyroid is located in the thinnest region of the patient (the neck) and definitely outside on the periphery of the scan volume with scattered radiation exposure only (van der Molen and Geleijns, 2007).

Overall, it can be suggested that the decrease in organ dose observed with sequential scans may be due to one or a combination of differences in scan mechanics between the two modes, including (a) in helical scans, wherein the X-ray beam has to ramp up and ramp down the beam at the beginning and end of each scan, which are at different locations, or/and (b) a difference in physical beam collimation between axial and helical scan modes, or/and (c) inaccurate or imprecise table speed in helical mode (McDermott et al., 2009).

The comparison of organ and tissue absorbed doses measured in this thesis against those reported in the literature for paediatric CT relies on examining the work by Brenner et al. (2001; 2007). The absorbed doses measured in their first study (Brenner et al., 2001) are considerably higher than those measured in this thesis. One of the assumptions of their initial study was that adult CT parameters were being used on children (Paterson et al., 2001) and the corresponding organ absorbed dose estimates were made accordingly. For a paediatric patient, they calculated the brain dose to be 50 mGy from a single ‘typical’ CT scan of the head. This subsequently decreased to 35 mGy in their subsequent studies (Brenner et al., 2001; Brenner & Hall, 2007), which is still higher than the values measured in this thesis for a CT brain examinations (range from 2.1 to 27.5 mGy) depending on the protocol used. Similarly, the absorbed dose measured for the ABM was also higher than reported in this thesis which was 5 mGy in both of their studies (Brenner et al., 2001; 2007). In this thesis, these were approximately half (range 8.0 to 2.17 mGy).

7.3 Organ Positioning

As discussed in the methodology chapter (five), it is not feasible to conduct *in vivo* dosimetry in humans. However, an anthropomorphic ATOM phantom which simulates the human body can be used for this purpose. These type of phantoms provide the best representation of the human organs and tissues for dosimetry purposes and are more realistic than other phantoms available in terms of mimicking the real life situation (CIRS, 2006; Varchena, 2002). Differences between phantoms in terms of organ depth, the exterior shape of the trunk and diameter relative to the incoming radiation beam will affect the dose (Lee et al., 2007a; Zankl et al., 2005). Therefore, it is expected that there will be some variation in the calculated doses. Organs positioned inside the planned scan volume received higher absorbed doses compared to the other organs that were positioned at the border of the field of interest (e.g. eye lenses), or definitely outside with exposure to scattered radiation only (e.g. oral mucosa, salivary glands, thyroid gland and extrathoracic region). Oral mucosa received between 2.15 and 3.08 mGy, salivary glands between 2 to 3 mGy, thyroid gland between 0.36 and 0.76 mGy and extrathoracic region (ET) between 0.88 to 1.04 mGy for the helical adult brain protocol. However, comparing organ values to values calculated from sequential brain protocols, the absorbed dose for these organs almost all decreased by half. Whereas the radiation doses to the same organs for paediatric helical protocols were three times higher when compared to the dose obtained for helical adult brain protocol, that is due to the relative size and length of the adult phantom compared to the paediatric one as well as the size of the organs and the measuring points between phantoms in each organ.

Absorbed doses to the thyroid and ET region for CT brain examinations demonstrate a wide variation between the different scanning protocol parameters used for both paediatric and adult. Lee et al. (2011) have previously identified that the vertical placement of the thyroid can lead to significant differences in absorbed dose estimates. In both ATOM phantoms, the thyroid is located in the neck region, whereas for some other phantoms it is partially in the upper trunk region. In this more realistic anatomy, the thyroid will also receive some shielding from the facial bones (Lee et al., 2007a), but may also be directly irradiated in a head examination when changing CT gantry angulation, leading to variations in dose calculations. For this exposure situation, when these organs are located higher within the phantom, they are closer to the direct scan volume or are even positioned partially within it leading to the higher absorbed doses.

Anatomical variations in thyroid position between individuals should, therefore, be factored into any dosimetry comparisons.

Abdominal organs such as the adrenals, pancreas and kidneys are typically positioned lower in relation to the intended CT brain scanning volume (Lee et al., 2011). Therefore, for the CT brain examination the absorbed doses to these organs tend to be lower when compared to brain tissues. For this situation, when these organs are located lower within the phantom they are not closer to the direct scan volume, or are even positioned partially close to it leading to the lower absorbed doses.

The location of the testes can also lead to a difference in absorbed dose, which is evident in their location further away from the primary scan volume. The testes location can vary between phantoms (Lee et al., 2011). Therefore, if the angle of the CT gantry changes, the testes may be fully or partially subjected to scattered radiation depending on the phantom length. This location relative to the brain scanning volume is observed in the lower absorbed dose to the testes in the ATOM phantom representing an adult compared with the ATOM phantom representing one year old where the scan length and phantom length are different on both phantoms. Also, the absorbed doses to the testes predominantly vary according the changes in protocols parameters which are likely to result from differing levels of scattered radiation.

In addition to the overall size of a phantom, there are other internal disparities such as the location of organs that will also potentially affect dose estimates. In smaller phantoms, such as the one representing a one-year old child, the closer relative proximity of organs to the scanned volume will increase the dose. For an adult phantom, these organs will be further away from the directly irradiated area and as such the absorbed dose to these organs is decreased. This is an important point and will also vary in real life patients, it will, therefore need to be accepted that due to size variations dose estimates cannot be completely accurate for all (Lee et al., 2007; Zankl et al., 2005; Lee et al., 2011).

7.4 Absorbed Dose to Organ Substitution

The ATOM phantoms do not model all of the organs and tissues listed in ICRP 60 and ICRP 103 and often other organ absorbed doses are used as a substitute to approximate these doses. In this thesis, similar to Ludlow and colleagues (2008 & 2006); Roberts et al. (2009); Suomalainen et al. (2009); Tootell et al. (2014); Theodorakou et al. (2014) and ICRP 66 (1994), it was assumed that, for example, for measurements made in these physical phantoms, the

second measuring point of the cervical spine and oesophagus could be used to approximate the absorbed dose to the ET region. Also, the absorbed dose to the salivary glands and oral mucosa were approximated from by absorbed dose to the mandible from four measuring points (ICRP, 1994; Theodorakou et al., 2014).

In the ATOM phantoms the absorbed doses to the skin, muscles, lymph nodes and bone surface could not be measured nor included in the effective dose calculation as measuring points were not available for determining the absorbed dose to these organs. The effect of organ absorbed dose substitution can be seen in the high absorbed doses assigned to the salivary glands and oral mucosa in the both phantoms calculations, representing an adult and paediatric for the CT brain examinations. Also absorbed dose to these organs in paediatrics is higher compared to adult due to the phantom size variations as previously discussed. Results in this thesis, for all proposed protocols, demonstrates the absorbed dose to these tissues are in fact considerably less than the absorbed dose to the brain. This will also influence both the effective dose estimate and the effective risk calculation. As indicated in chapter **5 (section 5.5.3)** on page **107**, other studies have used a varying number of measurement locations, ranging from 20 to 66 for measuring absorbed dose. This thesis used 167 and 281 for the paediatric and adult ATOM phantoms, respectively.

The number of dosimeters per organ may cause additional uncertainty when deriving the mean absorbed dose to individual organs or tissues (Toivonen et al., 1996; Smith-Bindman et al., 2009). Aschan et al. (1999) and Brady et al. (2011) stated that the maximum error, caused by the use of one point instead of sampling the whole organ was found to be more than 11%. The organ used in their approximation was the kidney, the volume of which was estimated from the literature to be 150 cm^3. In their study, one or only a few reference points were used to represent the smallest organs, but dozens of reference points were needed for large organs.

Uncertainty can be caused by the use of multiple dose reference points, representing the entire volume of the organ and is estimated to be around 3%. The amount of inaccuracy from measuring one point within the organ versus the whole organ is dependent on the organ size, as indicated by Brady et al. (2011). Here it was found that the absorbed dose varied by up to 21% depending on the organ size. This variation in dose highlighted the necessity to use multiple measurement locations in organs and tissues, particularly those that are large, in order to accurately determine the mean organ or tissue absorbed dose. Also, an uncertainty of approximately 5% is generated in soft tissues close in contact with bone through interface

effects (Toivonen et al., 1996; Biswas et al., 2009). In this thesis, the method used is considered to be superior to several previously published studies in that multiple sampling points within different organs and tissues were used, and not just a single sampling point.

7.5 Eye Dose

CT scans of the brain, sinuses and petrous bones are commonly performed as the initial imaging test for a variety of indications, including trauma, suspected tumour, complicated infections and inflammatory conditions, as well as suspected congenital abnormalities and have the potential to expose the eye-lens to ionising radiation.

As reported by Schilham et al., (2010) the eye lens is an example of an organ with an attributed deterministic radiation effect, if the eye is exposed to a radiation dose above a certain threshold, a cataract will be formed. It is assumed that by ICRP 103 (2007) and ICRP 21 (1991) the minimum dose required to produce a detectable cataract is around 2 Gy for a single exposure and 5 Gy for fractionated or protracted exposure. In paediatrics, as indicated by ICRP 30 (2000) report, this threshold is even lower, with the development of cataracts having been documented at less than half this dose of radiation. Therefore, it is of paramount importance to shield the paediatric orbit from any unnecessary radiation during CT.

Typically, the dose to the eye is about 50 mGy, depending on the CT scanner characteristics and protocol that is used, see **(Appendix H)** within **(Table H - 1)** and **(Table H - 2)** on pages **243** and **244**, respectively. CT Brain scans are normally planned to exclude the eyes from the imaging volume and avoid irradiation. However, in helical CT, over-ranging extends the irradiated area on both ends of the planned scanning range. Thus, the eyes can receive a direct radiation dose, even though no images are reconstructed from data obtained from this area.

The eye lens dose largely depends on the scanning parameters that control over-ranging, which are detector collimation and pitch as well as the actual distance from the eyes to the edge of the imaged volume. In this thesis, due to the lack of movement of the head and neck in the ATOM phantom, there was some restriction in the position of the phantom. Clinically, avoidance of the primary beam irradiating through the eye lens region can be minimised by tilting the head (Schilham et al., 2010). Where this is not possible the CT gantry has to be tilted superiorly in order to avoid or minimise the extent of primary beam irradiation of the patient's orbit to keep the eyes outside the scan volume. A study by Wai-Keung LAI, (2015) found a drastic reduction

in the entrance surface dose (ESD) to the eye lens region by 92.5% when the CT gantry was tilted from 0° (overall ESD=30.7 mGy) to 30°crainially (overall ESD=2.4 mGy). This result agrees with the results of previous studies conducted by Heaney & Norvill, (2006); and Keil et al., (2008).

The calculated eye dose for the helical brain CT examination experiments undertaken within this thesis found a significant reduction to the eye lens dose when angling the gantry, and the percentages vary widely according to the helical protocol parameters used for both adult and paediatric phantoms. For adult results the reduction ranged from 12% to 41% when the CT gantry was tiled from 0^{o} (overall dose range 10.4 to 60.2 mGy) to 27^{o} (overall dose range from 9.2 to 35.6 mGy). Whereas the percentage reduction in eye lens doses for paediatrics ranged from 24% to 30% when changing CT gantry angulation from 0^{o} (overall dose range from 3.0 to 33.1 mGy) to 27^{o} (overall dose range from 2.1 to 25.0 mGy). The percentage dose reductions mentioned above were calculated when comparing the maximum and minimum absorbed dose for between the two CT gantry angulations 0^{o} and 27^{o}. Maximum (highest) doses were obtained when the eyes were in the scan volume (CT gantry not tilted).

Matsubara et al., (2011) demonstrated that the application of CT gantry tilting during CT brain examination (i.e., tilting the CT gantry towards the supra-orbital line of the patient in order to avoid or minimise the extent of primary X-ray beam irradiate the patient's orbit) could effectively reduce the overall dose delivered to the eye lens region by approximately 92%. Results of brain CT sequential protocol in this thesis found an excessive reduction in the absorbed dose to the eye lens region by 51.4% to 77% when the CT gantry was tilted from 0° (overall eye lens dose = 7 – 47.8 mGy) to 27°crainially (overall eye lens dose = 3.4 - 11 mGy).

Therefore, increasing gantry angle can be used as a way of reducing eye dose, examples of eye dose reductions for different protocols are illustrated by **(Table 6-21)**, **(Figure 6-17)** on page **149**, **(Figure 6-18)** on page **150** and **(Table 6-22**), **(Figure 6-19**), **(Figure 6-20)** on page **151** for adult and paediatric, respectively. Consequently, strategies to reduce eye lens dose during CT brain examinations still remain important to prevent deterministic effects. Comparing the absorbed dose to the eye for adult common clinical CT brain helical and sequential protocols, the percentage difference between the two protocols at 0^{o} angulation was 33% and the different between them at 27^{o} was 49%. In helical CT, over-ranging extends the irradiated area on both ends of the planned scanning range. Thus, the eyes receive a significant dose, even though no images are reconstructed from data obtained in that area. The eye lenses were positioned at the

border of the field of interest- a region is irradiated for which no images can be reconstructed. As stated by van der Molen and Geleijns (2007), an important factor that affects the absorbed dose to organs at the start and end of a scan volume is the additional length included for data interpolation for helical examinations. The exposed length is longer than the imaged length and depends on the pitch, beam collimation and reconstruction algorithm. These three different tilting options of the gantry angle can reduce the radiation dose to the eye lens effectively by avoiding direct exposure of this tissue. However, the dose drop-off is obvious once the eye lens is outside the primary beam. The absorbed dose drop-off suggests that the contribution from scattered radiation to the eye lens dose is small, probably because the eye lenses are located at the body surface where there is less scatter build-up than at locations at depth within the body.

7.6 CT Parameters

Tube potential, beam collimation, rotation time, tube current–time product or mA modulation indices are the starting points of the optimisation process to keep the dose 'as low as reasonably practicable' for diagnostic purposes (IR(ME)R, 2017). As in conventional radiography, a linear relationship exists between the tube current-time product and radiation dose; i.e. all dose quantities will change by the directly proportional amount as the applied mAs. When the tube potential is increased, both the tube output and the penetrating power of the beam are improved, while image contrast is adversely affected.

As reported in the literature, tube current is the most important parameter in CT that effects radiation dose followed by tube rotation time and tube kilovoltage. In CT, the tube current exposure time and tube potential can all be altered to give the appropriate exposure to the patient. However, users most commonly standardise the tube potential and gantry rotation time for a given clinical application. The fastest rotation time should typically be used to minimize motion blurring and artefacts, and the lowest kV consistent with the patient size should be selected to maximize image contrast. Hence tube current is the primary parameter that is adapted to patient size. Numerous investigators have shown that the manner in which mA should be adjusted as a function of patient size should be related to the overall attenuation, or thickness, of the anatomy of interest (McCollough et al., 2009). The exception is for imaging of the head, where attenuation is relatively well defined by age, since the primary attenuation comes from the skull and the process of bone formation in the skull is age dependent. For CT imaging of the head, the mAs reduction from an adult to a newborn of approximately a factor

of 2 to 2.5 is appropriate (Funama et al., 2005; McCollough et al., 2006 & 2009; Smith-Bindman et al., 2009).

In this thesis, it was found that, when using 100 kVp and 100 mA instead of 120 kVp, organ dose reductions of 19, 22 and 10% were found for the thyroid, eye lens and breast, respectively. However, the effective dose values were increased by 43% when increasing tube current from 120 to 200 mA and by 37% when changing the tube kilovoltage from 100 to 120 kV, see **(Table 6-19)**, **(Figure 6-15)** and **(Table 6-20)**, **(Figure 6-16)** on pages **147** and **148**, respectively. The trend in radiation dose change is expected but the amount of increase was much greater than would be expected in some cases; similar results have been reported by Funama et al. (2005) when changing the kV from 90 to 120 resulted in a dose increase of 30%. However, Raman et al. (2013), findings were consistent with Funama's, they stated that decreasing the tube potential from 120 to 100 kVp can result in a dose reduction of roughly 33%, and decreasing the tube potential further from 120 to 80 kVp can result in up to a 65% reduction in dose (Raman et al., 2013). Brody et al. (2007), indicated that the same CT examination parameters can be used for both for children and adults. Using the same CT parameters in children will have no effect on diagnostic accuracy of the CT scan but the radiation exposure may have been unnecessarily high. In fact, a change in these parameters with a resultant reduction in dose, ranging from approximately 50% to 90%, has been shown to be satisfactory for a paediatric CT examination (Brody et al., 2007).

A number of helical CT protocols, for both the adult and paediatric ATOM phantoms, made use of automatic tube current modulation, in which the tube current values varied during the examination to reduce dose to the patient whilst maintaining adequate image quality, this in turn had an effect on organ and effective doses. In this thesis, X-Y-Z tube current modulation was used, but the effects on organ absorbed and ED for adult phantom as the rotation time changed from 0.5 to 1.0 (S) almost doubled, see **(Table 6-5)** and **(Figure 6-2)** on page **133**. For example, scanning the adult phantom brain with '*high quality*' tube current modulation the effective dose was 0.71 and 1.17 mSv, respectively. The ED data does not, however, follow the same trend for the paediatric data, see **(Table 6-13)** and **(Figure 6-10)** on page **141**. By investigating the ATCM function for both adult and paediatric brain protocols, it appears that the tube current modulation was not functioning correctly for the majority of the adult brain protocols, see **(Figure 6-1)** on page **129**. The most recent report from the quality control tests performed on the Toshiba CT scanner used in this thesis indicated that the ATCM was working

within expected tolerances during the study period. Possible reasons behind the functionality issues for the ATCM are likely to be related to the construction of the phantom and the lack of anatomical noise (i.e. brain structures). ATCM, for a Toshiba scanner, is based on expected noise values (SD) and it is possible that the ATCM system was not able to distinguish between the regions of highest and lowest attenuations. Toshiba uses a combined system called Sure Exposure 3D. This ACTM system makes use of the frontal and lateral patient diameters and the detector intensities from the scout view to account for the oscillating tube current modulation during each gantry rotation. The system allows the operator to define the range within which the tube current can be modulated by selecting minimum and maximum mA limits. A clinical CT examination often covers different anatomic regions with variable attenuation values. Since the tube current is selected based on the region with the highest attenuation or the region that requires the highest image quality, the tube current is usually set to a high level when an ATCM system is not in use. Toshiba uses three different values of Sure Exposure 3D (ATCM), High Quality [SD 1.80], Standard [SD 2.00], Low Dose [SD 2.20] and also the same parameters with different values of SD, High Quality [SD 4.00], Standard SD [6.00] and Low Dose [SD 8.00] for adult and paediatric protocols, respectively. The effective dose calculations for the three parameters for the adult phantom were almost identical 0.71, 0.70 and 0.70 mSv, respectively with a <1% difference, see **(Table 6-8)** and **(Figure 6-5)** on page **135**. The percentage difference in effective dose values between detail and standard helical pitch factors were very small (approximately 11%), however, there was large percentage difference in effective dose between detail and fast helical pitch factors (around 35% reduction) as illustrated by **(Table 6-7)** and **(Figure 6-4)** on page **135**. The calculated ED reductions based on the paediatric phantom and the selected mA modulation values represent a larger difference in dose reduction, 47% and 66% between high quality and standard and high quality and low dose, respectively as shown in **(Table 6-16)** and **(Figure 6-13)** on page **144**. The helical pitch factors represent a small percentage difference in effective dose between detail and standard and detail and fast (15% and 21%, respectively) as shown in **(Table 6-15)** and **(Figure 6-12)** on page **143**. This reduction is related to the time that the X-ray beam is on, for a fast pitch the anatomy is covered quicker and the resultant dose to the patient is decreased. Papadakis et al. (2008) conducted study to assess the potential of a modern X, Y, Z ATCM system and fixed tube current (in a paediatric phantom, tube current (83 mAs) and effective tube current (mAseff) / quality 150 and in the adult phantom tube current (176 mAs) and effective tube current (mAseff) / quality 320) for CT head dose reduction in paediatric and adult MSCT. In AP ATCM scans, the dose reduction ranged between 15.4 and 30.9% for a 1 year old, and 15.5 and

57.4% for adult. In lateral ATCM scans, the corresponding dose reduction ranged between 27.2 and 35.7% and 15.0 and 61.7%, respectively. Similar results were achieved by Papadakis et al. in 2011, they again estimated the effective dose associated with fixed tube current and ATCM examinations and the relationship between the average reduction of tube current achieved by ATCM and the reductions in organ and effective dose. The percent organ dose reduction achieved when ATCM was activated in standard head and neck CT scans and ranged from 8.1% to 63.8% for a 1-year-old and 16.3% to 50.1% for an adult. Using the 1-year-old phantom, the ED values ranged from 1.71 to 2.82 mSv for fixed tube current and 0.99 to 2.38 mSv for ATCM scans. In the adult phantom, the ED ranged from 3.39 to 8.06 mSv for fixed tube current and 2.28 to 3.83 mSv for ATCM scans. Mean mAs reduction was linearly related to the ED reduction ($r^2 = 0.807$, $P < 0.0001$). The absolute percentage difference between % tube current and $\%ED_{MEAS}$ reduction was in most cases higher than 15%.

7.7 Helical and Sequential Protocols

The typical clinical adult protocols used for the dose calculations included helical and sequential CT brain examination. Helical and sequential CT scanning are both routine ways of imaging the brain. While helical scanning offers better multi-planar imaging operations, sequential scanning provides over-ranging free measurements and reduces z-axis blur. The examinations were performed with a tilted gantry to minimise dose to the lens of the eye as this is the standard clinical protocol. It is useful to examine the extent of the differences between the protocols when calculating adult CT doses. When evaluating differences between the maximum and minimum effective doses, the largest ratios were observed in helical CT protocol examinations, where the max/min ratios were 0.71 and 0.43 mSv, respectively, see helical protocols ED in **(Appendix D)** within **(Table D - 1)** to **(Table D - 6)** and **(Figure D - 1)** to **(Figure D - 5)** on pages **222** to **230** and the sequential protocols ED results in **(Appendix E)** within **(Table E - 1)** to **(Table E - 3)** and **(Figure E - 1)** to **(Figure E - 4)** on pages **231** to **233**. The spiral CT scanning resulted in large increases in ED due to large number of examinations performed and the average 'scanned patient volume' per examination, whereas the maximum and minimum ED calculated for sequential protocols were 0.31 and 0.51 mSv, respectively. In this study, helical scanning demonstrates wide variations in the radiation dose across the different protocols when compared to similar sequential CT brain examinations. As expected, the CT protocol used can dramatically affect the radiation dose received during a single CT examination, and this has a significant effect on annual population doses which may in turn lead to significant changes in the likelihood of adverse biologic changes due to exposure to medical radiation (Moorin et al., 2013). This is

particularly important when considering patients that may have multiple CT scans. Similar findings in a study conducted by Bischoff et al. (2010) state that although the sequential scanning mode significantly reduced radiation dose by 68% relative to the helical mode from 11.2 mSv to 3.6mSv ($p < 0.001$), the median diagnostic image quality scores were comparable in both groups (Bischoff et al., 2010).

As discussed in **(Section 7.3)** from this chapter, both the organ location in a phantom and the scan length difference between the child and adult will affect the absorbed dose to organs at the periphery of the imaging volume. Lechel et al. (2009) had similar findings with respect to organs on the border or partly inside the scan volume. In this work, they recommended that organ absorbed dose comparisons between different protocols could only be reliably made for those organs completely irradiated in both phantoms. Also, Li et al. (2011) and Turner et al. (2011) confirmed this finding for brain CT examinations. As stated by Van der Molen and Geleijns (2007), another important factor that affects the absorbed dose to organs at the start and end of a scan volume is the additional length included for data interpolation for helical examinations. The exposed length is longer than the imaged length and this depends on the pitch, beam collimation and reconstruction algorithm. For example, the over-ranging length for a pitch of 1-1.25 is approximately 5-6 cm (van der Molen and Geleijns, 2007), with half of this length added to each end of the scan.

The effects of over-ranging on absorbed dose due to the use of helical CT protocols assessed in this thesis and is clearly demonstrated on the dosimeter measurements that show the additional doses outside of the imaged scan volume are higher for helical examinations compared to sequential examinations. However, in helical CT examinations the scan volume was uniformly irradiated from all directions by a beam with constant output and a continuously moving table. The absorbed dose measured in this thesis to the organs outside the scan volume for common helical brain CT protocol were almost doubled when considered against those from sequential protocols (the absorbed dose to eyes, oral mucosa and salivary glands were 58.11, 5.30, 5.32 mGy and 39.15, 2.56, 2.57 mGy for helical and sequential protocols, respectively).

7.8 Effective Dose (mSv)

Although the overall effective dose (ED) reflects a patient's exposure to radiation, organ-specific doses may be more appropriate when estimating the lifetime cancer risk for non-uniform exposures such as CT. For example, if a patient undergoes an imaging study that

radiates only the brain, the patient's risk of cancer from that examination will primarily reflect the increased risk of brain cancer and that of the other organs as well.

The ED quantity was created in order to provide a metric that was related to the probability of health detriment due to stochastic effects from exposure to low doses of ionizing radiation. More reliance is often placed on ED values and risk estimates based on ED. Martin (2014) reviewed the uncertainties in the estimated values of ED and the associated risk coefficients for a reference patient in order to provide an indication of how much reliance can be placed on ED as an indicator of patient risk. There are uncertainties in the quantity ED that has been employed in many applications for which it was never intended and much greater accuracy has been attributed to it than is justified (Martin, 2014). ED is not intended to provide an individual (personalised) dose, but the dose to a reference (average) person. The relative uncertainty in estimated values of ED for medical exposures for a reference patient is seen to be about ±40%. It is therefore reasonable that ED should only be used to assess and compare the relative risks for a 'reference' patient, which are then described in general terms such as low, very low, minimal and negligible. The estimated risk of cancer may be a factor of three higher or lower when applied to a reference patient, and will be more variable when applied to an individual with height and weight variations (Martin, 2014).

Peer-reviewed scientific literature on radiation dosimetry, published between 1980 and 2007, providing values of ED relating to adults were reviewed by Mettler et al. (2008). They concluded that the representative values and ranges of EDs reported in the literature for various examinations and procedures wee 0.9 – 4.0 mSv and the average ED was 2 mSv, depending on the technical factors (voltage and/or tube current–time product and pitch factor). It was also reported that EDs to the neonate, for a head CT examination, were markedly higher than for adults, the EDs are usually within 50% of the adult dose. The ED calculated in this thesis were much lower than mentioned above and ranged from 0.54 – 1.8 mSv and 0.30 – 1.1 mSv for adult brain CT helical and sequential protocols, respectively, and according to the protocol parameters used. Whereas the calculated ED for helical paediatric protocols ranged from 0.40 to 2.1 mSv dependent in the protocol setting used. However, ED is a calculated as an all organs-averaged value that is used as a robust measure to compare detriment from cancer and hereditary effects due to various procedures involving ionizing radiation. Martin (2007), has pointed out a number of limitations in its use, including about 40% uncertainty for a reference 'average' patient.

In a study by Christner et al. (2010), two common methods used to estimate ED for adult CT examinations were compared: first, the gold standard method using MC simulations based on organ dose estimates that explicitly uses tissue-weighting coefficients as specified by ICRP; and, second, the computationally more simple method based on the DLP and a DLP to ED conversion coefficient, referred to as "k," which depends on only the an atomic region examined. Their compared results of ED for head CT calculations based in MC simulations and those calculated from DLP and k coefficients, results ranged from 0.4 - 0.9 mSv and from 0.5 – 1.3 mSv, respectively. These results are more or less very comparable to the results obtained in this thesis for adult helical brain CT protocols (0.43 – 1.5 mSv).

Using a standard head CT protocol, the ED for a 1-year old was calculated by Papadakis et al. (2011), using two different methods. The first was based on the DLP concept. The second method was based on the measurement of the absorbed dose in all radiosensitive organs of each phantom using TLDs. ED measured with TLDs was 1 mSv whereas that calculated from DLP was 3.4 mSv. The measured ED based on absorbed dose calculations fall within the range of ED doses measured within this thesis, however, the ED dose estimated using DLP was higher by 88.2% and 38.2% above the minimum and maximum rage measured in this thesis (0.4 – 2.1 mSv).

McCollough et al. (2012) reported on a CT community summit which brought together participants from academia, clinical practice, industry, and regulatory and funding agencies to identify the steps required to reduce the effective dose from routine CT examinations to less than 1 mSv, which is below annual background levels of ionizing radiation. They stated that scanner settings must be tailored to the size of the individual patient, ED is defined for scanner output values (volume CT dose index values) appropriate to an individual of similar size and shape as the ICRP's reference person (a 70–80-kg adult). This yields typical ED values of 1–2 mSv for routine head CT. The ED measured within this thesis was in the range supported by this report (0.43 – 1.5 mSv and 0.40 – 2.1 mSv for adult and paediatrics, respectively).

Also, the summit members stated that, current commercially available techniques such as ATCM, optimization of tube potential, beam-shaping filters, and dynamic z-axis collimators are important, and education to successfully implement these methods routinely is critically needed. Other methods that are just becoming widely available, such as iterative reconstruction, noise reduction, and post-processing algorithms, will also have an important role. Together,

these existing techniques can reduce dose by a factor of two to four and should be incorporated into routine clinical practice.

As mentioned previously the literature reported that tube current is the most important parameter in CT that effects radiation dose followed by tube rotation time and tube kilovoltage. This is consistent with the findings from this thesis, where the increase in tube current led to an increase in ED which was proportional to the mA used (ED increased from 1.8 to 3.1 mSv, as the mA changed from 120 to 200, when other parameters were kept consistent). Whereas changing the tube rotation time from 0.5 to 1 seconds, with 100kV and 100 mA, the ED value almost doubled (1.3 mSv and 2.4 mSv, respectively). However, the tube potential change from 100 kV to 120 kV, lead to increase in effective dose from 1.3 to 1.8 mSv, respectively. For the paediatric results reported in this thesis, manipulating the tube current values from 100, 120 to 200 mA resulted in an ED increase ranging from 38.5% to 61.5%. Whereas changing the rotation time from 0.5, 0.75 to 1 seconds, the ED dose increase ranged from 22.2% to 84.5% when other parameters were kept consistent. However, changing the tube potential from 100 kV to 120 kV was resulted in ED increase by 38.5%. Whereas in study by McCollough et al. (2012) switching tube potentials from 80 and 100 kV allowed for a dose reduction of up to 50% compared with a tube potential of 120 kV.

The ICRP defines ED as a parameter for expressing stochastic risk from radiation exposure and recommends its use only for radiation protection purposes (ICRP, 2007b). However, effective dose has found widespread application in evaluating doses from medical exposure due to its effectiveness in condensing a complex set of parameters for any exposure situation into a single quantity (McCollough et al., 2010). It is routinely used to compare doses resulting from variations in protocols or from different modalities. However, while taking into account the nature of the exposure, characteristics of specific individuals are not considered. Hence, effective dose provides a broad, generic estimate and is an indication only of the typical dose. Although it should not be applied to the individual, it is often used for dose assessments following radiation incident and other situations involving specific patients to express a relative risk.

ED, as reported by Wall et al. (2011), has several limitations when applied to medical populations. There are a number of important limitations in using ED for further details see **(Chapter 4 section 4.5)** on page **73**. ED (and ICRP's nominal probability coefficients for radiation-induced cancer and heritable effects) should not be used to assess risks to individual

patients of specific age, sex and nationality. These are applications for which it was not intended. It can, however, be a valuable tool for comparing the doses (and risks of aggregated detriment) to a reference person (of 'average' age, gender and nationality) from different medical diagnostic procedures and from other sources of radiation exposure (Martin, 2014).

Risk estimates based on ED are highly generic and include, for example, hereditary effects that are unlikely to be significant at doses relevant to diagnostic radiology. In addition, the weighting factors used in the calculation of ED do not take into account the strong variations of radiosensitivity with age and gender (Hall & Brenner, 2008) and as such newer methods are required. A number of national and international bodies have developed radiation risk models in recent years from which it is possible to calculate the lifetime risks of radiation-induced cancer as a function of the age and sex of the exposed person (BEIR VII, 2006; UNSCEAR, 2006; ICRP, 2007). All three models are primarily based on the same epidemiological data from the Japanese atomic bomb survivors' lifespan study (LSS) but with some significant differences in the risk projection and transfer models used by the three bodies (brief summaries of the main features of the risk models developed by ICRP, BEIR and UNSCEAR are given elsewhere by Wall et al. (2011)). The dependence of the radiation-induced cancer risk on sex and age at exposure varies with cancer sites in all three models. In this thesis, the BEIR risk models described in BEIR Publication VII (BEIR, 2006) were used to calculate the lifetime risks of radiation-induced cancer per unit dose as a function of organ, sex and age at exposure. The BEIR models were chosen because they are from a recognised international authority on radiation protection and provide a nominal probability coefficient for radiation-induced cancer for an age range from 0 to 80 years, for male and female persons.

Typical CT doses and associated radiation risks are not well understood. Primarily this is because the doses are not accurately known or easily calculated. Furthermore, there are large uncertainties, in addition to a lack of consensus, regarding the risk from radiation exposure at low doses. The BEIR VII Report supports the linear no threshold (LNT) model as the best descriptor of the relationship between solid cancer incidence and low dose radiation exposure (NRC, 2006). The LNT theory is widely accepted (Brenner et al., 2003) as the most plausible model for radiation induced cancers for low dose exposures and is also adopted by the International Commission on Radiological Protection (ICRP) as the basis of the international system of radiation protection (ICRP, 2007b).

Cancer risk estimation based on BEIR VII modelling is limited by the uncertainties that exist from using the Life Span Study (LSS) data to derive radiation induced cancer risk. The sources of uncertainty arise from transporting the cancer incidence and mortality from the Japanese atomic bomb survivors to a Western population. Furthermore, the biggest source of uncertainty involves the LSS data being extrapolated to low dose and different dose rate exposure situations. The risk modelling of BEIR VII is also affected by sampling variability in the model parameter estimates for the LSS data. Despite these inherent uncertainties, one of the most useful applications of the BEIR VII radiation risk models is for estimating the detriment from exposure situations where doses differ substantially across the body. The data is particularly useful in these situations i.e. CT brain examinations. The BEIR VII data develops risk estimates for cancer from exposure to low-level ionizing radiation using the most current data and epidemiological models available, incorporating data from atomic bomb survivor studies as well as medical and occupational radiation studies. Its review of available data supports the so-called linear no-threshold (LNT) risk model for low-dose exposures to low linear energy transfer radiation such as X-rays, whereby the risk of cancer proceeds in linear fashion with no lower threshold. Other studies have also applied the BEIR VII attributable cancer risks to CT exposures on the basis that it is the best method currently available (Little et al., 2009; Berrington et al., 2009; Brenner et al., 2001a; Brenner and Hall, 2007; Einstein et al., 2007a; Smith-Bindman et al., 2009).

There are conflicting opinions in the literature between those who believe that low radiation doses are more damaging than in a linear model; there are also those who believe that low radiation doses are less damaging than a linear model would predict or even that they are beneficial (Hall & Brenner, 2008). However, it is not necessary to take a position on this LNT controversy because the doses involved in CT scans, which account for the majority of the collective dose from diagnostic radiology, are just within the range where we have credible and direct epidemiological evidence for an increased cancer risk in human populations (ICRP, 1991 & 2005; ANS, 2001; BEIR, 2006; Andrew et al., 2007; Hall & Brenner, 2008).

This thesis is the first study to investigate the cancer risks associated with specific CT protocols, full details of these risk will be discussion in **(Section 7.9)**. Data was collected for brain CT examinations for adults and paediatrics. Cancer risk gives a much more individualised risk estimate and is a new approach which enables easily accessible information of the risk associated with a protocol to be ascertained by practitioners prospectively. Although this data

was limited to brain CT examinations, the methodological principle for the collection and presentation of data could be applied to other types of CT scan. In this thesis, the cancer risks associated with the radiation exposures from brain CT scans are calculated by measuring the organ doses involved as a function of age, gender and type of CT exam, and then applying estimates of age, gender, and organ specific risk-per-unit dose data that were ultimately derived from atom bomb survivors. Therefore, the risk estimates on an organ-by-organ basis, and finally, simply summed up the estimated risks for all the different organs, see **(Method section 5.9)** on page **119**. As discussed by Hall & Brenner, (2008) the organ doses for a typical CT study involving two or three scans are in the range where there is direct statistically significant evidence of increased cancer risk, and thus the corresponding CT-related risks can be directly assessed from epidemiological data, without the need to extrapolate measured risks to lower doses.

7.9 Effective Risk

CT accounts for only 5% of all X-ray examinations but represents between 40% and 67% of the total medical radiation dose received by the population (Bernier et al., 2012). Owing to the ease and speed of image acquisition linked to technological developments, proliferation of procedures has occurred and in turn has led to increased doses to patients. Ionising radiation from CT has become a public health concern, as there is a possible attributable future cancer risk (Bernier et al., 2012). Assessment of cancer risk after childhood radiation exposure remains a concern regardless of the radioprotection used for children. Children actually present an increased radiosensitivity of certain tissues compared with that of adults, which, combined with a longer life expectancy, could generate a greater cancer incidence (Bernier et al., 2012).

Hall and Brenner (2008) reported that ED is the only quantity available that provides a dose metric related to the risk of health detriment. It is argued that to define a new, simple, less confusing, easy-to-estimate quantity, based on defensible science, which more directly does the job of comparing the risks associated with different inhomogeneous doses, the new quantity should not only refer to cancer risks but should also be age dependent, or at least distinguish between paediatric and adult risks. These are the properties that one would ideally want of a quantity describing low-dose radiation risks from an inhomogeneous dose distribution, which would allow science-based comparisons between different exposure scenarios.

The risk to an individual from brain CT exposures is assessed from the mean absorbed dose to radiosensitive organs and tissues. Since the probability of cancer induction depends on the anatomy exposed, the level of exposure and the age and gender of the individual, these factors were also considered within this thesis (ICRP, 2007a). The absorbed dose homogeneity in an organ or tissue depends on the exposure situation and also the size or physical distribution of that organ or tissue in the phantom. For CT examinations, the exposure is a partial irradiation of the body which leads to heterogeneity of the absorbed dose distribution in some organs and tissues, particularly those that are not completely located within the scan volume. Furthermore, distributed tissues such as the skin and bone marrow will always exhibit a varying absorbed dose distribution for CT examinations due to the nature of the exposure. Consequently, these factors contribute to the difficulty and variability in CT organ dosimetry. Pearce et al. (2012), reported that the most recent risk projections suggest that, for children with normal life expectancy, the lifetime excess risk of any incidence of cancer for a head CT scan (with typical dose levels used in the USA) is about one cancer case per 1000 head CT scans for young children (<5 years), decreasing to about one cancer per 2000 scans for exposure at age 15 years. The estimated number of CT scans that will lead to the development of a cancer varied widely depending on the specific type of CT examination (protocol variations) and the patient's age and gender. An estimated 1 in 8100 women who had a routine head CT scan at age 40 years (1 in 11 080 men). For 20-year-old patients, the risks were approximately doubled, and for 60-year-old patients, they were approximately 50% lower (Smith-Bindman et al., 2010). The lifetime cancer risk of any incidence of cancer for brain CT estimated in this thesis, for 0 years old child was ranged from 21 – 102 and 7 – 46 cases per million for females and males, respectively.

The risk of exposure will also depend on the type of radiation, expressed by the equivalent dose that represent the absorbed dose multiplied by the radiation weighting factor (ICRP, 2007b), although for CT scan examinations this is numerically equal to the absorbed dose. The effective dose reflects the combined detriment from the risk of stochastic effects in different organs and tissues averaged over all ages and both genders. The ICRP makes recommendations regarding radiation and tissue weighting factors, which are revised to take account of new scientific information regarding the biological effectiveness of radiation and tissue and organ radiosensitivity. The recommendations in ICRP Publication 60 (ICRP, 1991) have been in use for many years and these have been revised in ICRP Publication 103 (ICRP, 2007b).

In the clinical environment of diagnostic radiology, it is beneficial to estimate both absorbed dose and ED from CT examinations for assessment of risk and to reduce the dose to the patient. Furthermore, the need for epidemiological research studies has been highlighted by the BEIR VII Report (NRC, 2006), especially to follow-up children receiving CT examinations. Several studies have investigated the effects of low dose radiation (Bernier et al., 2012; Hricak et al., 2011; Pearce et al., 2011) and these require consideration for paediatric CT doses. Therefore, CT dose calculation methods that are applicable to children are required in both the clinical and research contexts.

Direct methods of estimating CT dose have been investigated in this thesis. Actual clinical scenarios have been evaluated by using typical CT protocols that a one-year old child may undergo at a children's hospital as well as adult protocols (helical and sequential). According to this there are several important influencing factors on the directly measured and calculated absorbed doses that need to be considered. Consequently, these include the models that can be used to represent the organs and their position in the body, the type or model of CT scanner being used and/or modelled in the calculation and the scan parameters used in simulating the X-ray exposure. As reported in the literature the clinical conditions could not be matched exactly in the computational methods and therefore various assumptions and approximations had to be made. Consequently, the variables associated with each method could not be strictly controlled, but rather the conditions that have been used for each method provide the closest match to the clinical scenario (Lee et al., 2011). Effective risk is more defensible than the effective dose, which would be easier to interpret: it would be an effective lifetime radiation-attributable cancer risk (‘‘× per 1 000 000’’ individuals).

As illustrated in results chapter **6 (S**ection **6.6)** on page **152**, the effective risk was calculated using the BEIR VII (2006) risk estimates which provides a method to estimate a cancer based on the magnitude of a single radiation exposure and a patient’s age at the time of that exposure. This thesis estimated the number of patients undergoing CT that would lead to the development of radiation-induced cancer, by type of CT brain examination, age at the time of exposure, and gender. The derived number of cancer incidence cases using the BEIR VII report indicates a substantially higher lifetime attributable risk of cancer incidence in females compared with males, and also in younger patients as illustrated by **(Table 6-23)**, **(Table 6-24)** and **(Figure 6-21)** to **(Figure 6-23)** on pages **152** to **155**. For example, the number of lifetime risks calculated in this thesis at birth was 102 and 46 case/1 000 000 for females and males,

respectively and the lifetime risk at birth and 30-years for females were 102 and 7 cases/ 1000000, respectively. As indicated by Brody et al. (2007) there is a difference in cancer risk from radiation exposure to children when compared with adults. He suggested several reasons for this difference. First, for the most part, tissues and organs that are growing and developing are more sensitive to radiation effects than those that are fully mature. Second, the oncogenic effect of radiation may have a long (for example, decades) latent period. This latent period varies with the type of malignancy. Leukemia has a shorter period (approximately ≤10 years) than solid malignancies. An infant or child, therefore, has a longer life expectancy in which to manifest the potential oncogenic effects of radiation compared with older adults. For example, a solid radiation-induced malignancy with a 30-year latent period will more likely occur in a 10-year-old than in a 50-year-old, on the basis of life expectancy. Also, they summarized the radiation cancer risk at different ages and stated that those exposed at 50 years of age have approximately one third of the risk of a 30-year-old and that "projection of lifetime risks for those exposed at age 10 is more uncertain. Third, in the case of CT scanning, the radiation exposure from a fixed set of CT parameters results in a dose that is relatively higher for a child's smaller cross-sectional area compared with an adult. A cohort study by Krille et al. (2015) was taken to assess the risk of developing cancer, specifically leukaemia, tumours of the central nervous system and lymphoma, before the age of 15 years in children previously exposed to CT in Germany. Data for children with at least one CT between 1980 and 2010 were extracted from 20 hospitals. Cancer cases occurring between 1980 and 2010 were identified by stochastic linkage with the German Childhood Cancer Registry (GCCR). Cases were only included if diagnosis occurred at least 2 years after the first CT and no signs of cancer were recorded in the radiology reports. The cohort included information on 71,073 CT examinations in 44,584 children contributing 161,407 person-years at risk with 46 cases initially identified through linkage with the GCCR.

Radiation doses have varied significantly between the different types of CT studies. As reported in the literature the overall median effective doses ranged from 2 millisieverts (mSv) for a routine head CT scan to 31 mSv for a multiphase abdomen and pelvis CT scan (depending on the scan protocol) (Smith-Bindman et al., 2009). Within each type of CT study, effective doses varied significantly within and across institutions, with a mean 13-fold variation between the highest and lowest dose for each study type (McCollough et al., 2009; Smith-Bindman et al., 2009). The estimated number of CT scans that will lead to the development of a cancer varied widely depending on the specific type of CT examination and the patient's age and

gender. In this thesis, an estimated 6 in 10^6 women who underwent a single helical CT head scan at the age of 40 years would develop cancer as a result of having that CT scan (5 in 10^6 men), compared with an estimated 3 in 10^6 women who had a routine (sequential) head CT scan at the same age (2 in 10^6 men). For 20-year-old patients and less, the risks were approximately doubled, and for 60-year-old patients and more, they were approximately 93% lower. According to the example above, an important aspect of risk calculation is to push the concept that we should not only consider risk associated with one CT examination but also for serial CT imaging in patients i.e. those with hydrocephalus.

The calculated cancer incidence risk for CT brain examinations were also applied to the entire 0-80 years age group, see **appendix I**, **(Table I - 1)** on page **245** and **appendix J**, **(Table J - 1)** on pages **248**. As the data was obtained using an ATOM phantom representing a one-year old child they were utilised to calculate the risk for ages of 0 and 5 years and adult phantom data for ages from 10 to 80 years, the risks will be underestimated for infants, whilst being overestimated for adolescents and hence will provide an intermediate estimate of the level of risk for the entire protocols. In addition to reduced CT parameters for younger, smaller children and higher site-specific radiation risk coefficients for younger children, there can also be variations in different organs with age. For example, almost all bone marrow is active (red bone marrow) at birth and with age gradually becomes inactive, with only about a third remaining active in adulthood (ICRP, 2002). Therefore, the bone marrow absorbed dose which directly correlates with risk of cancer incidence will vary with age, particularly in childhood. The radiation risks calculated for a CT scan undertaken on a phantom representing a one-year old child provides a reasonable benchmark for the average risk across the 0-5-year age band. The radiation risks calculated for a CT scan using an adult phantom is more suitable for the average risk across the age band from 10-80 years.

As discussed in **chapter 4 (Section 4.6)** on page **78,** paediatric CT is different from adult CT and also from any other sort of radiological examinations. The organ doses are clearly higher for children than for adults. Also, paediatric CT is increasing in frequency quite rapidly and probably more so than adult CT, and children are much more sensitive to radiation-induced cancer than adults (McCollough et al., 2009; Muhogora et al., 2010). Brenner et al. (2007), estimated that more than 62 million CT scans per year are currently performed in the United States, including at least 4 million on children. The growth of CT in paediatrics has been driven primarily by the decrease in the time needed to perform a scan (now less than 1 second) and

has largely eliminating the need for anaesthesia to prevent the child from moving during image acquisition. According to McDermott et al. (2009), approximately 2.7 million CT examinations were performed on paediatric patients under the age of 15 years, and about one-third of children who undergo CT will have three or more examinations. Multiple CT examinations expose patients to increased radiation dose, which is a concern to the medical community (McDermott et al., 2009). As mentioned by Dougeni et al., (2012), monitoring trends in CT dose is currently particularly important, especially in paediatrics, as the technology is evolving rapidly. The organ doses delivered from a common CT scan result in an increased risk of radiation induced carcinogenesis, particularly for children (Dougeni et al., 2012). According to the BEIR VII report, developing and growing organs are more sensitive to radiation than those that are fully mature, which in addition to a longer life expectancy, and possible increased repeated examinations, produces a greater paediatric risk of potential radiation damage. Brenner et al. (2001), reported a paediatric fatal cancer risk of 0.11% and 0.055% (approximately 1 in 900 and 1 in 1800) for abdominal or head CT respectively, for a single slice CT scan of a 1-year old child. CT is of particular interest because of its relatively high radiation dose and wide use. Consensus statements on radiation risk suggest that it is reasonable to act on the assumption that low-level radiation may have a small risk of causing cancer. However, the medical community should seek ways to decrease radiation exposure by using radiation doses as low as reasonably achievable and by performing these studies only when necessary (Strauss & Kaste, 2006; Brody et al., 2007). There is wide agreement that the benefits of clinically justified CT scan far outweigh the risks. Paediatric health care professionals' roles in the use of CT on children include deciding when a CT scan is justified and discussing the risk with patients and families. Radiologists should be a source of consultation when forming imaging strategies and should create specific protocols, in conjunction with radiographers, regarding the scanning techniques optimised for paediatric patients. Families and patients should be encouraged to ask questions about the risks and benefits of CT scanning (Brody et al., 2007).

Organ doses are larger in a child when compared to an adult. For example, if an organ located on the proximal side of the body relative to the X-ray source it will receive roughly the same dose in both adult and child. However, as the X-ray source rotates, that same organ will be on the distal side of the body relative to the X-ray source; now that organ is partly shielded by the body tissue proximal to it, reducing the organ dose. But for this reduction in dose, partial shielding will be much less for a thin individual, such as a child, compared to a thicker adult.

Also, there is a need to think about the issue of multiple CT scans in patients. Data reported by Brenner, (2002) showed that, 30% of patients who undergo CT have at least 3 scans, 7% have at least 5, and 4% have at least 9. In study by Krille et al., (2015), data capture from more than 44,584 patients from 20 hospitals; generated 71,073 eligible examinations and 161,407 person-years of data with a mean follow-up of 4.1 years. About 71% of the cohort were only exposed to one CT and 7% had four or more CTs with a maximum of 49 CT examinations (a case of hydrocephalus). 37% of all CT scans were performed in children younger than 5 years, 29% in children aged 5–<10 years and 34% in children aged 10–<15 years. Among children who had only one CT, 68% had received head CTs and 10% chest CTs. Among those with more than one CT, about 76% had received at least one head CT. Based on the published doses by Miglioretti et al. (2013), average cumulative radiation doses of 11.7 mGy were estimated here for the bone marrow, 34.4 mGy for the brain and 5.8 mGy for the colon per person in the cohort. Thus, to better understand the cumulative dose and risk from multiple CT scans, the dose should be multiplied by the number of CT scans that any given individual will have. Accordingly, clinical scenarios can be simulated to predict the cumulative lifetime risk of cancer from commonly used Toshiba Aquilion paediatric CT brain protocols presented in **(Table 7-1)** below:

Table 7-1: Toshiba Aquillion protocols for paediatric CT head scans

Size of child	kV	mA	Rotation Time	Helical/axial Acquisition	Slice Thickness
3mths - 3years	100	180	0.5	Helical	0.5
3 - 5 years	100	200	0.75	Helical	0.5
6 – 12 years	120	200	0.75	Helical	0.5

First scenario (trauma), if a 7-year-old girl was riding a bike and suddenly fell and injured her head and was admitted to the Emergency Department at her local hospital. On admission, she was transferred to the X-ray department for a brain CT scan. In this case, for Toshiba CT scanner the protocol that would have to be used is a helical brain CT (6 – 12 years). In this thesis, the effective dose calculated for this protocol was 3.58 mSv and the estimated lifetime cancer risk is in the range from 107 to 77 per 10^6 for 5 and 10 years, respectively. If she deteriorated then she might undergo for a follow-up scan, still as an in-patient, to evaluate the situation further and then possibly a follow-up scan after 6 months. This means that both her cumulative effective dose (10.74 mSv) and lifetime cancer risk (321 to 231 per 10^6 for 5 and 10 years, respectively) would rise by factor of 3.

Second scenario, in the case of a suspected space occupying lesion, if a 5-year-old boy presented complaining of a headache and a recent seizure he is then likely to be referred for an

urgent brain CT scan. According to his age a brain CT protocol for 3 – 5 year old's would be used. The calculated effective dose for this protocol is 2.41 mSv and the estimated lifetime cancer risk is 35 per 10^6. If he was admitted to hospital for surgery, a pre-operative CT brain scan is likely to be required to guide the surgeon and after surgery a CT brain scan might be performed to look for complications. He could then have another CT scan after six months for follow up. All these scans will increase the cumulative effective dose (9.64 mSv) and lifetime cancer risk (140 per 10^6) by factor of 4.

The third scenario is the case of epilepsy, for example if newborn girl is diagnosed with epilepsy then a CT brain scan could be performed yearly to follow up her progress. In this case the three different CT protocols as described in the above table will be used. The 3 months to 3 years protocol for the first three years once/year and the 3 – 5 years protocol for 2 years and 6 – 12 years protocol for 5 years. This could mean that her cumulative effective dose and lifetime risk in the first three years is 4.77 mSv and 42 – 69 per 10^6, respectively and when aged from 3 to 5 years 4.82 mSv and 71 – 115 per 10^6, respectively. Whereas from 6 to 10 years the cumulative effective dose 17.9 mSv and the risk ranged from 77 – 107 per 10^6.

In contrast, if a 40-year-old man was working for a construction company and suddenly fell and injured his head and was admitted to the Emergency Department referred for a brain CT scan. In this case for the Toshiba CT scanner the protocol that would have to be used is an adult helical brain CT. In this thesis, for his age and the protocol used, the effective dose would be 1.3 mSv and the estimated lifetime cancer risk is 8 per 10^6. He could go for a follow-up scan after 6 months. This means the cumulative effective dose will be 2.6 mSv and the cumulative of lifetime cancer risk induction is 16 per 10^6 for 5 and 10 years, respectively.

The risk prediction model developed for estimating lifetime cancer risk in this thesis can be used pre-scanning to prospectively predict the probability of inducing cancer in future according to the selected CT scan protocol parameters. The data obtained and calculated for the two ATOM phantoms (adult and one-year old child) could be implemented to estimate the risk for ages from 0 to 80 years old patients, which might for children underestimate the risk to ages less than one year old and overestimate to ages more than one year. This model can be further developed by using additional phantoms to represent the different age groups to calculate the lifetime cancer risk induction, and be used by CT venders to develop CT scanners which incorporate software algorithms for cancer risk calculations and in turn display the probability on the operator console.

As stated by Brenner and Hall (2007), the risk to the individual from diagnostic radiation exposure is small and in most cases, for a properly justified procedure, the benefit to the individual will outweigh any risk. However, with increasing rates of CT usage the application of small levels of risk to a large population produces a health concern. Based on CT usage in 2007, it is estimated that 1.5% to 2.0% of all cancers in the US may be caused by CT imaging (Brenner and Hall, 2007). The total number of CT scans in the US has increased annually by 8% to 15%, which is a greater rate than population growth (Mettler et al., 2009, 2008; NCRP, 2009) and similar trends are seen in the UK (Hall and Brenner, 2008).

Potential increases in future cancer risk, attributable to the rapid expansion in CT use have been estimated with risk projection models, which are derived mainly from studies of survivors of the atomic bombs in Japan. These studies have been criticised because of concerns about how applicable the findings from this group are to the relatively low doses of radiation exposure from CT scans and to non-Japanese populations. Some investigators claim that there are no risks, or even beneficial effects, associated with low-dose radiation. Only a few direct studies of cancer risk in patients who have undergone CT scans have been undertaken to date. Pearce et al. (2012), conducted a study to directly assess the question of whether cancer risks are increased after CT scans in childhood and young adulthoods. They assess the risks of leukaemia and brain tumours because they are the endpoints of greatest concern as the RBM and brain are highly radiosensitive tissues, especially in childhood. Furthermore, these tissues are also some of the most highly exposed to ionising radiation from childhood CT scans, and leukaemias and brain tumours are the most common childhood cancers. Their results show significant associations between the estimated radiation doses from CT scans to the RBM and brain and subsequent incidence of leukaemia and brain tumours.

Assuming typical doses for scans in children aged younger than 15 years, cumulative ionising radiation doses from 2 to 3 head CTs (ie, ~60 mGy) could almost triple the risk of brain tumours and 5 to 10 head CTs (~50 mGy) could triple the risk of leukaemia. The absorbed dose to the brain for an ATOM phantom representing a one-year old child ranged from 2.2 to 28.1 mGy depending on the individual CT brain protocol used. This means that the cumulative absorbed dose for three brain CT scans would be in the region of 6.6 to 84.1 mGy and would imply a heightened risk of leukaemia or brain tumour induction.

As we know, CT is a valuable diagnostic modality technique in which new clinical applications continue to be identified and the benefits generally outweigh individual risks. However, as CT

images are easy, painless and quick to obtain, although the immediate benefit to the individual patient can be substantial, and since radiation doses are among the highest from all diagnostic procedures, the justification criteria should be reinforced and careful consideration of the use of CT is necessary, given the increasing frequency of such examinations, perhaps by carefully considering the protocol used (by simply applying the risk estimation tool created in this thesis).

Radiologists and CT operators must understand the radiation dose estimates associated with this modality and the need to optimize image quality and dose for the clinical objective of the examination. Careful selection of CT scan parameters is imperative to optimize the imaging protocol and to generate diagnostic quality CT images with the least radiation exposure. However, according to the scenarios mentioned above there is evidence which suggests that cumulative radiation exposure will increase future risk of malignancy and that it should be modelled and considered proactively when undertaking examinations. This is not a finding- we of course know that having more scans will increase risk. The point of this is that it enables practitioners to balance the protocol they use along with the projected number of CT scans that will be required for the patient, and therefore this enables them to clearly and simply understand the impact of their acquisition factors on the patients' risk of induced cancer.

Wiest et al. (2002) reported that in 2001, 30% of patients had more than three CT examinations in their medical histories, 7% had more than five examinations, and 4% had more than nine examinations. Specific patient populations with chronic conditions or recurrent symptoms have been found to have high rates of repeat imaging. Sodickson et al. (2009), found high rates of recurrent CT imaging, exceeding those of Wiest et al. (2002), with 33% of patients having undergone more than five CT examinations, and 5% of patients having undergone at least 22 CT examinations in their administrative database over the 22-year study period. 15% of the cohort had accrued cumulative CT effective doses in excess of 100 mSv, 4% receiving over 250 mSv, and 1% receiving over 399 mSv, these are in the dose realm in which there is convincing epidemiologic evidence of increased cancer risk. Their LAR calculations predict that CT imaging of this cohort would produce 98 additional radiation-induced cancers, including 62 fatal cancers.

A cohort study was undertaken in Australia by Mathews et al. (2013), to assess the cancer risk in children and adolescents following exposure to low dose ionising radiation from diagnostic CT scans. The study included 10.9 million people identified from Australian Medicare records, aged 0-19 years on 1 January 1985 or born between 1 January 1985 and 31 December 2005; all

exposures to CT scans were funded by Medicare during 1985-2005 and were identified for this cohort. The cohort study results showed, 60 674 cancers were recorded, including 3150 in 680 211 people exposed to a CT scan at least one year before any cancer diagnosis. The mean duration of follow-up after exposure was 9.5 years. Overall cancer incidence was 24% greater for exposed than for unexposed people, after accounting for age, sex, and year of birth (incidence rate ratio (IRR) 1.24 (95% confidence interval 1.20 to 1.29); P<0.001). They reported a dose-response relationship, and the IRR increased by 0.16 (0.13 to 0.19) for each additional CT scan. The IRR was greater after exposure at younger ages (P<0.001). At 1-4, 5-9, 10-14, and 15 or more years since first exposure, IRRs were 1.35 (1.25 to 1.45), 1.25 (1.17 to 1.34), 1.14 (1.06 to 1.22), and 1.24 (1.14 to 1.34), respectively. The absolute excess incidence rate for all cancers combined was 9.38 per 100 000-person years at risk. The average effective radiation dose per scan was estimated as 4.5 mSv.

Absolute excess risk estimates are necessary to put the risks into perspective with the benefits of the scans. It is essential that radiologists, radiographers and medical physicists are aware of the radiation doses and their lifetime cancer risks of using CT for young people, particularity children. It is necessary to find the acceptable threshold of image quality with the minimum possible radiation exposure to the patient, in agreement with the ALARA principle. It is worth reminding ourselves that in this thesis image quality has not been considered at any point; however, the lowest dose image cannot be accepted as image quality may not be sufficient for diagnostic purposes which could lead to repeat the CT scan that should be avoided at any point to reduce the patient cumulative dose and risk. Patients (and carers, in the case of paediatric patients) should be made aware of the calculated risks corresponding to their radiological examination. Thus, it is useful to have a software program that can calculate the probability of lifetime risk of cancer induction and display this information on CT console prior to making an exposure which takes into account the imaging parameters, age and gender of the patient.

7.10 Lifetime Risk Excel Spreadsheet Calculation Tool

In this thesis, calculated lifetime attributable risks were made for all the possible selections of CT brain protocols parameters by developing a Microsoft Excel workbook which included the functionality to enable the user to select acquisition parameters, gender, age and number of expected scans and see the estimated the risk of cancer induction (and absorbed eye dose) for the chosen CT protocol/s. As stated the spreadsheet enables estimation based not only on acquisition parameters but also gender and age. This spreadsheet is unique, in terms of the

philosophical concept and the data contained within it. Although this spreadsheet is only applicable for the CT scanner used in this thesis, the methodological approach applied in this thesis could be translated to any CT scanner for any manufacturer. Perhaps a way forwards would be to develop new Monte Carlo methodologies for each CT scanner, in order to provide anticipated estimates of effective risk specific to the actual patient (being based upon CT scanner characteristics, protocol specifics as well as age and gender). Further mathematical modeling could also be provided, whereby the probability of further imaging could be introduced, thereby taking into account a scenario like 'this patient may require 5 CT scans over the next year'. As represented in the results chapter **(Sections 6.6** and **6.7)** on pages **152** to **155**, the risk estimation workbook has been published alongside a brief instruction manual within an online data repository, this is not yet publically available (embargo period 12 months), but for the purpose of this thesis access has been granted to the examiners (enclosed on a CD in the back of this thesis, supplementary item 1). The limitation of this workbook is it is only applicable to estimate the lifetime cancer risk induction for a Toshiba 16 Aquilion CT scanners. This approach can be adopted by CT scanner vendors to be turned into software to calculate the number of estimated cancer risk cases per 10^6 for all available clinical protocol options in use prior to expose the patient to radiation. This will help the radiologist and radiographers to justify the examination and reduce the dose to the patient by adjusting the scan parameters.

7.11 Study Limitations

Although this thesis makes a significant contribution to estimating lifetime attributable cancer risks for male and females from 0 to 80 years, and how they might contribute to the induction of cancer among patients accessing brain CT procedures, it does have number of limitations: -

1. Only two ATOM phantoms representing a one-year old child and adult were used for the lifetime cancer risk estimates. This is a limitation as it may not be representative of the entire patient population. Usually, patients with a smaller size receive higher organ dose when the same scanning technique is used. However, there is only a small variation in terms of the head size for adult patients. Therefore, the dose variations among patients should be small. Paediatric patients will receive higher organ doses for the same scanning protocols. As previously stated the 1 year old and adult phantoms used only represent 'average' sizes and that there is no account within this work for variations within an age group.

2. The ATOM phantoms do not model all organs and tissues listed in ICRP 60 and ICRP 103 and often other organ absorbed doses are used as a substitute to approximate these doses. Also, to calculate the effective dose, the organ dose for bone surface, skin, lymphatic nodes and muscles were set to zero. The error introduced by this step was expected to be small, given that each of these organs had a weighting factor of 1%. Furthermore, lymphatic nodes and muscles were not irradiated directly and the skin and bone surface were only partially irradiated.

3. The adult phantom data represent some errors from the ATCM functionality, previously explained within the discussion that might be due to the lack of internal brain structures and noise detection ability of the CT ATCM software.

7.12 Recommendations for Future Work

1. This study should be replicated using a different range of ATOM phantoms representing age groups of (neonate, and 5-year-old; male and female) to estimate the effective risk for different size of phantoms.

2. A prospective study should be conducted to compare directly measured effective dose estimates with those determined from mathematical models including k factors and ImpACT software.

3. A similar study should be conducted using dose optimisation and image quality techniques, as there needs to be a study, with practitioners and patients, evaluating the risk cancer prediction tool and how it can be developed and implemented.

4. CT manufacturers should introduce effective risk estimates within their systems, prior to exposures being made. The effectiveness of such introductions would need appropriate evaluation using a careful designed research study.

7.13 Thesis Novelty

No other study has estimated the lifetime cancer risks for patients undergoing CT brain examinations for different ages, from 0 to 80 years for both male and female. In this thesis, the variations in absorbed dose to organs and tissues for brain CT protocols using helical and sequential for adult, and helical only for the one year old on two different ATOM phantoms, were measured and used to calculate the lifetime cancer induction as reported by BEIR VII

report (2006). Consequently, prior to this study, there was no up to date knowledge on the relationship between paediatric CT brain examinations and the possibility of developing cancer risk among patients accessing CT procedures.

This thesis adds new knowledge to academic/clinical literature because it shows that lifetime cancer risk from CT brain examinations can be calculated according to the patient's age and gender for all possible CT protocol options prior to exposing the patients to ionising radiation. Also, it provides healthcare professionals with the information needed in order to make decisions about the justification and the necessity of CT examinations. Furthermore, it helps the practitioner to choose the appropriate protocol for the patient age and size as well implementing the dose reduction techniques such as ATCM, or altering the protocol parameters to suite the patient being scanned. Manufacturers should develop ways of displaying the radiation risk at the CT console prior to performing the scan. Findings from this thesis creates the need for raising awareness of the stochastic radiation risks for patients undergoing CT examinations, especially for paediatrics and young patients and also those undergoing repeated CT examinations.

This thesis has proposed a simple yet scientifically reliable tool for prospectively calculating radiation cancer risk for ages from 0 to 80 including male and female for different CT brain protocols used on the Toshiba 16 Aquilion CT scanner, which allow the operator or the researcher an opportunity to estimate the risk prior to exposing the patient to ionising radiation. This is a new philosophical concept in radiation risk management and could lead to changes in practices and developments on scanner software.

7.14 Thesis Recommendations

1. There is the need to create awareness of the stochastic risks for CT scans, in particular when scanning children.

2. Risk of cancer increase as age decreases. The potential radiation dose for children is very high and needs to be controlled. CT dose optimisation in children has a big impact on effective dose and overall radiation risk.

3. Where applicable, ATCM should be used for brain scans to reduce the radiation absorbed dose and cancer risk.

4. CT vendors should consider providing, on their CT equipment, radiation risk assessment software that can prospectively display the risks of inducing cancer at the scanner console. This would help CT operators and radiographers to better understand protocol selection and the effect of acquisition parameter adjustments.

5. Referrals for patients, especially young people, should not be accepted for CT scans if there are other imaging modalities available such as MRI or US, or if CT is not capable of providing the necessary diagnostic information.

6. Adult protocols should not be used to scan children. If the adult protocol has been selected then the scan parameters should be manipulated to suit the patient size and weight.

7.15 Conclusion

The aim of this thesis was to assess the medical radiation exposure of adult and paediatric patients from brain CT examinations. Radiation risk coefficients that are specific to the site of cancer induction, the age at exposure and gender are made available in the BEIR VII Report (NRC, 2006). These risks are applied to organ absorbed doses in order to assess age and gender specific radiation detriment. However, determining organ absorbed doses for CT exposure is complex, which is evidenced by the large number of mostly indirect methods currently available. Furthermore, few publications addressed experimental organ dosimetry methods in paediatric CT or the magnitude of organ absorbed doses for clinically used protocols.

Within this work, absorbed doses to organ and tissues have been measured for CT brain examinations using MOSFETs loaded in ATOM phantoms representing of an adult and 1-year old child and for the Toshiba 16 Aquilion CT scanner. The results for this study demonstrate effective doses from the CT head examinations ranging from 0.34 – 1.55 mSv and 0.31 – 2.01 mSv for adults and paediatrics, respectively. Some values of effective dose were lower than has been previously reported in the literature (e.g. McCollough and Yu, 2009). Typical effective dose values of 1 to 14 mSv have been reported for head CT examinations.

The MOSFET measurements for estimating the average absorbed dose to an organ or tissue demonstrated that directly and fully irradiated organs and tissues lead to more consistent dose measurements throughout their volume. Organs and tissues in the periphery of the scan volume had a range of dose measurements and were also affected by over-ranging in helical scanning. Even organs distant from the scanned volume had a small amount of radiation exposure, likely

the result of exposure to scattered radiation. MOSFETs were also investigated and found to be have suitable agreement with TLDs, overall, they offered a higher dose on (average 10% higher), although being a more practical alternative for regular use in the clinical environment.

MOSFETs offer an alternative dosimetry method that is fast and easy to use. However, they do require initial calibration and conversion factors must be derived for all beam qualities and energies that are to be used. This is performed at acceptance and is labour intensive. Further studies are required to assess the necessary frequency of calibration, both over time and relative to the cumulative dose that each MOSFET receives. Furthermore, MOSFETs have a lifespan related to cumulative exposure and hence must be replaced on a semi-regular basis. Also, MOSFETs are small, fragile and require careful handling and provide a real-time result.

MOSFETs are finding increased application as a potential dosimetry tool for medical exposures. However, considering that effective dose is intended to be a broad estimate of typical dose, the real-time nature of MOSFETs may lead to the acceptance of some of these limitations.

Experiments within this thesis confirm that increasing pitch proportionately reduces patient radiation dose on a helical CT scanner when other parameters are held constant. Also, ATCM did not modulated correctly for some of the adult helical protocols; however, a reduction in effective dose, particularly when changing from high quality to low dose techniques, have been shown.

From the measured absorbed doses, effective doses were derived based on ICRP 103. Effective dose is not a physical quantity but an estimate of biological detriment reflecting the risk from radiation exposure. It is a useful generic quantity that can be used for optimisation in diagnostic radiology. However, differences between the ICRP 60 and ICRP 103 tissue weighting factors arise from the changes that reflect the lower weighting now applied to the brain for direct irradiation, the increased assessed radiosensitivity of the breast and the remainder organs collectively and the decrease in assessed radiosensitivity for the gonads.

CT is an extremely important imaging modality for infants and children. Despite this importance, and increasing use, the risks of radiation and a lack of attention to these risks are only recently being addressed. Paediatric health care providers are an essential element in the selection of CT evaluation of children. Because of this, it is necessary to understand the benefits and radiation risks of CT and work with radiologists to develop strategies that reduce exposure

from CT in infants and children. Also monitoring of trends in CT patient doses is currently particularly important, especially in paediatrics, as the technology is evolving rapidly. The organ doses delivered from a common CT scan result in an increased risk of radiation induced carcinogenesis, particularly for children. Our experiment results showed paediatric and young people are at higher risk of cancer incidence than adults, and also that the risk much higher in females than males.

Because the risks to individuals from diagnostic radiation exposures are generally small, it is often difficult to study them directly. However, because of the large number of people exposed annually, even small risks could translate into a considerable number of future cancers. Referring medical practitioners need guidance to determine whether an imaging study is needed and, if an imaging study is required, which type of imaging study will yield the necessary clinical information at the lowest achievable radiation dose, because reducing radiation exposure from diagnostic procedures is a shared responsibility of the referring medical practitioner and the radiological medical practitioner. Thus, in the future, better metrics, such as lifetime attributable cancer risk, will hopefully become the norm.

The best strategies for radiologists and technologists to reduce the radiation to patients who undergo CT examinations is by modifying basic scanning parameters such as peak kilovoltage, milliampere-second, and pitch; they can also alter their scanning protocols by reducing the number of images or data sets acquired during a CT study.

The best way to reduce the radiation dose to paediatric patients is to avoid unnecessary CT exams and to look for alternative diagnostic imaging modalities with less or no exposure to ionising radiation. Paediatric protocols with scanning parameters specifically designed for children must be used. These protocols usually include tube current modulation, a child-size bowtie filter and scanning field of view (FOV), or a weight or size-based technique chart that can determine the appropriate kV and/or mAs for each patient.

For children undergoing CT examinations, providing a better understanding of the lifetime attributable radiation risks will hopefully lead to better justification for scans in the future. Furthermore, it will be a driver for undertaking dose optimisation at institutions where the doses are much higher. Overall, the risk due to radiation exposure for an appropriately justified and well optimized CT scan for an ill hospitalized child will almost always be much lower than the risk associated with not performing the scan. The risk projections in this thesis must be

considered in the context of the substantial diagnostic and/or treatment benefit gained from a justified and optimised CT scan.

There is no question that the benefit of an appropriately indicated CT scan far exceeds the associated estimated risk or that CT providers need to prescribe the minimal amount of radiation required to obtain images adequate for evaluating the patient's condition. Additionally, the medical community needs to better educate the public to the risks and benefits associated with CT, such that they can make informed decisions regarding their healthcare.

This thesis proposes a novel method to estimate effective lifetime risk of radiation-induced cancer from CT brain examinations in order to compare different brain CT protocols (acquisition parameters). Absorbed dose measurements when considered in relation to the age and gender of the patient can help provide prospective estimations of effective risk, a potentially more useful indicator of the possible effects of radiation exposure from CT head examinations. This risk estimation method can be used to prospectively compare different CT brain protocol parameters immediately prior to imaging. Risk data, using this method, can be prospectively taken into account when planning a CT brain examination, especially for young ages and those undergoing serial imaging. Using the prospective proactive evaluation of radiation risk data (spreadsheet) provided in this thesis, or via the CT console can help to estimate the probability of cancer induction and cataract formation from specific CT brain protocols and can be used by practitioners and manufacturers when developing CT technology and protocols in the future.

Overall, there is a large variability in scanning protocols and a resultant large range of effective doses, reflecting the increasing complexity of CT scanning. High radiation doses were observed in some paediatric protocols undertaken with high quality imaging parameters. Feedback and education about these parameters is needed to avoid inappropriate high radiation doses. It is important that the CT technique is tailored to the child, is only used when there are good clinical indications and that the radiation risk is proactively considered prior to scanning. In brief, among this thesis the following can be concluded:

- Increasing kV from 100 to 120 kVp lead to up 33% increase in ED.
- Increasing mA from 120 to 200 mA resulted in 39% increase in ED.
- Slow (detail) to a fast helical pitch showed 36% reduction in ED.

- Detector configuration change (0.5 to 2.0 x 16 mm) illustrated 2 to 25% increase in ED, depending on pitch used.

- Changing in CT gantry angles have no change to ED but do affect eye lens dose.

- Risk of cancer induction increases as age decrease. The potential dose for children is very high and needs to be actively controlled. CT dose optimization in children has big impact on both ED and ER and accurate estimations of both parameters are needed prior to the scan.

Appendices

Appendix A: Location and number of dosimeters within the sections of the adult and paediatric ATOM phantoms

Table A - 1: Location and number of dosimeters within the slices of the adult ATOM phantom (Adult).

Organs	Phantom slice number	Number of Dosimeters	Total Organ Dosimeters	
Brain	2	1	11	
Brain	3	4		
Brain	4	4		
Brain	5	2		
Cranium Active Bone Marrow (ABM)	3	4	4	**85**
Mandible (ABM) Lt + Rt	7	2	6	
Mandible (ABM) Lt + Rt	8	2		
Mandible (ABM) Lt + Rt	9	2		
C-Spine (ABM)	8	1	2	
C-Spine (ABM)	10	1		
Clavicle (ABM) Lt + Rt	12	4	10	
Clavicle (ABM) Lt + Rt	13	6		
Sternum (ABM)	13	1	4	
Sternum (ABM)	14	1		
Sternum (ABM)	16	1		
Sternum (ABM)	18	1		
T/L Spine (ABM)	13	1	9	
T/L Spine (ABM)	16	1		
T/L Spine (ABM)	19	1		
T/L Spine (ABM)	22	1		
T/L Spine (ABM)	25	1		
T/L Spine (ABM)	27	1		
T/L Spine (ABM)	29	1		
T/L Spine (ABM)	31	1		
T/L Spine (ABM)	33	1		
Ribs (ABM) Lt + Rt	14	6	18	
Ribs (ABM) Lt + Rt	17	6		
Ribs (ABM) Lt + Rt	20	6		
Scapular (ABM) Lt + Rt	14	4	10	
Scapular (ABM) Lt + Rt	15	2		
Scapular (ABM) Lt + Rt	16	2		
Scapular (ABM) Lt + Rt	17	2		
Pelvis (ABM) Lt + Rt	30	4	16	
Pelvis (ABM) Lt + RT	31	4		
Pelvis (ABM) Lt + RT	32	2		
Pelvis (ABM) Lt + Rt	34	4		
Pelvis (ABM) Lt + Rt	36	2		
Pelvis (ABM) Lt + Rt	33	2	2	
Femora (ABM) Lt + Rt	35	2	4	
Femora (ABM) Lt + Rt	38	2		

Continued **(Table A - 1)**

Organs	Phantom slice number	Number of Dosimeters	Total Organ Dosimeters
Eyes Lt + Rt	5	2	2
Thyroid Lt + Rt	10	2	6
Thyroid Lt + Rt	11	2	
Thyroid Lt + Rt	12	2	
Oesophagus	12	1	3
Oesophagus	15	1	
Oesophagus	19	1	
Lungs Lt + Rt	12	2	36
Lungs Lt + Rt	14	6	
Lungs Lt + Rt	16	10	
Lungs Lt + Rt	18	11	
Lungs Lt + Rt	20	7	
Thymus Lt + Rt	13	2	4
Thymus Lt + Rt	14	2	
Breast Lt + Rt	17	2 male/8 Female	10
Heart	17	1	2
Heart	18	1	
Spleen	20	2	12
Spleen	21	3	
Spleen	22	4	
Spleen	23	3	
Adrenals Lt	20	1	2
Adrenals Rt	22	1	
Liver	20	13	29
Liver	22	7	
Liver	23	4	
Liver	24	3	
Liver	25	2	
Stomach	21	2	14
Stomach	22	4	
Stomach	24	4	
Stomach	26	4	
Kidneys	21	1	16
Kidneys Lt	22	2	
Kidneys Lt + Rt	23	3	
Kidneys Rt + Lt	24	4	
Kidneys Lt + Rt	25	3	
Kidneys Rt	26	2	
Kidneys Rt	27	1	

Continued **(Table A - 1)**

Organs	Phantom slice number	Number of Dosimeters	Total Organ Dosimeters
Pancreas	23	2	5
Pancreas	24	3	
Gall Bladder	24	2	5
Gall Bladder	25	3	
Intestine Lt + Rt	27	4	16
Intestine Lt + Rt	29	5	
Intestine	31	5	
Intestine	33	1	
Intestine	35	1	
Bladder	32	4	16
Bladder	33	4	
Bladder	34	4	
Bladder	35	4	
Prostate	35	3	3
Testes Lt + Rt	38	2	2
Total Dosimeters			**281**

Table A - 2: Location and number of dosimeters within the slices of the ATOM phantom (Paediatric).

No	Organ	Phantom Slice No	Depth	Number of Dosimeters	Total Organ Dosimeters
1	Brain 1	2	10	3	9
2	Brain 2	2	10		
3	Brain 3	2	10		
4	Brain 4	3	15	3	
5	Brain 5	3	15		
6	Brain 6	3	15		
7	Brain 7	4	20	3	
8	Brain 8	4	20		
9	Brain 9	4	20		
10	Eye 1	4	15	2	2
11	Eye 2	4	15		
12	Cranium ABM 1	4	3	4	4
13	Cranium ABM 2	4	3		
14	Cranium ABM 3	4	3		
15	Cranium ABM 4	4	3		
16	C-Spine (ABM) 1	6	5	1	1
17	Mandible (ABM) 1	6	3	3	3
18	Mandible (ABM) 2	6	3		
19	Mandible (ABM) 3	6	13		
20	C-Spine (ABM) 2	7	5	1	1
21	Thyroid 1	7	20	2	2
22	Thyroid 2	7	20		
23	Oesophagus 1	8	3	1	1

Continued **(Table A - 2)**

No	Organ	Phantom Slice No	Depth	Number of Dosimeters	Total Organ Dosimeters
24	Clavicle (ABM) 1	8	10	2	2
25	Clavicle (ABM) 2	8	10		
26	Lung 1	9	5	4	4
27	Lung 2	9	5		
28	Lung 3	9	5		
29	Lung 4	9	5		
30	Rib 1	9	3	4	4
31	Rib 2	9	3		
32	Rib 3	9	3		
33	Rib 4	9	3		
34	Scapulae (ABM) 1	9	3	4	4
35	scapulae (ABM) 2	9	3		
36	scapulae (ABM) 3	9	3		
37	scapulae (ABM) 4	9	3		
38	T/L Spine (ABM) 1	9	5	1	1
39	Thymus 1	9	3	1	1
40	Sternum (ABM) 1	9	3	1	1
41	Thymus 2	9	3	1	1
42	Sternum (ABM) 2	10	3	1	1
43	Lung 5	10	5	5	5
44	Lung 6	10	5		
45	Lung 7	10	5		
46	Lung 8	10	5		
47	Lung 9	10	5		
48	Breast 1	10	12	2	2
49	Breast 2	10	12		
50	Oesophagus 2	10	5	1	1
51	Heart 1	10		1	1
52	Rib 5	11	3	6	6
53	Rib 6	11	3		
54	Rib 7	11	3		
55	Rib 8	11	3		
56	Rib 9	11	3		
57	Rib 10	11	3		
58	Sternum (ABM) 3	11	3	1	1
59	T/L Spine (ABM) 2	11	5	1	1
60	Lung 10	11	5	7	7
61	Lung 11	11	5		
62	Lung 12	11	5		
63	Lung 13	11	5		
64	Lung 14	11	5		
65	Lung 15	11	5		
66	Lung 16	11	5		
67	Heart 2	11		1	1

Continued **(Table A - 2)**

No	Organ	Phantom Slice No	Depth	Number of Dosimeters	Total Organ Dosimeters
68	Rib 11	12	3	6	6
69	Rib 12	12	3		
70	Rib 13	12	3		
71	Rib 14	12	3		
72	Rib 15	12	3		
73	Rib 16	12	3		
74	Stomach 1	12	17	1	1
75	Oesophagus 3	12	5	1	1
76	Lung 17	12	5	9	9
77	Lung 18	12	5		
78	Lung 19	12	5		
79	Lung 20	12	5		
80	Lung 21	12	5		
81	Lung 22	12	5		
82	Lung 23	12	5		
83	Lung 24	12	5		
84	Lung 25	12	5		
85	T/L Spine (ABM) 3	13	5	1	1
86	Stomach 2	13	4	1	1
87	Stomach 3	13	4	1	1
88	Stomach 4	13	4	1	1
89	Stomach 5	13	20	1	1
90	Stomach 6	13	20	1	1
91	Pancreas 1	13	5	1	1
92	Pancreas 2	13	5	1	1
93	Pancreas 3	13	5	1	1
94	Spleen 1	13	20	1	1
95	Spleen 2	13	20	1	1
96	Spleen 3	13	3	1	1
97	Liver 1	13	5	1	1
98	Liver 2	13	5	1	1
99	Liver 3	13	5	1	1
100	Adrenal 1	13	11	1	1
101	Adrenal 2	13	19	1	1
102	Kidney 1	13	19	1	1
103	Kidney 2	14	20	1	1
104	Kidney 3	14	20	1	1
105	Kidney 4	14	4	1	1
106	Kidney 5	14	12	1	1
107	Kidney 6	14	12	1	1
108	Gallbladder 1	14	18	1	1
109	Spleen 4	14	13	1	1

Continued **(Table A - 2)**

No	Organ	Phantom Slice No	Depth	Number of Dosimeters	Total Organ Dosimeters
110	Liver 4	14	5	1	1
111	Liver 5	14	5	1	1
112	Liver 6	14	5	1	1
113	Liver 7	15	5	1	1
114	Liver 8	15	5	1	1
115	Kidney 7	15	3	1	1
116	Kidney 8	15	13	1	1
117	T/L Spine (ABM) 4	15	5	1	1
118	Gallbladder 2	15	3	1	1
119	Intestine 1	15	5	1	1
120	Intestine 2	15	5	1	1
121	Intestine 3	15	5	1	1
122	Intestine 4	16	5	1	1
123	Intestine 5	16	5	1	1
124	Intestine 6	16	5	1	1
125	Intestine 7	16	5	1	1
126	Pelvis 1	17	3	1	1
127	Pelvis 2	17	3	1	1
128	T/L Spine (ABM) 5	17	5	1	1
129	Ovaries 1	17	15	1	1
130	Ovaries 2	17	15	1	1
131	Uterus 1	17	21	1	1
132	Intestine 8	17	5	1	1
133	Intestine 9	17	5	1	1
134	Intestine 10	17	5	1	1
135	Intestine 11	17	5	1	1
136	Intestine 12	18	5	1	1
137	Pelvis 3	18	5	1	1
138	Pelvis 4	18	5	1	1
139	T/L Spine (ABM) 6	18	5	1	1
140	Bladder 1	18	3	1	1
141	Bladder 2	18	18	1	1
142	Bladder 3	18	18	1	1
143	Bladder 4	18	18	1	1
144	Bladder 5	18	18	1	1
145	Bladder 6	19	7	1	1

Continued **(Table A - 2)**

No	Organ	Phantom Slice No	Depth	Number of Dosimeters	Total Organ Dosimeters
146	Upper ½ Femora (ABM) 1	19	5	1	1
147	Upper ½ Femora (ABM) 2	19	5	1	1
148	Testes 1	20	22	1	1
149	Testes 2	20	22	1	1
150	Upper ½ Femora (ABM) 3	20	5	1	1
151	Upper ½ Femora (ABM) 4	20	5	1	1
152	Lowe ½ Femora (ABM) 1	22	5	1	1
153	Lowe ½ Femora (ABM) 2	22	5	1	1
154	Lowe ½ Femora (ABM) 3	23	5	1	1
155	Lowe ½ Femora (ABM) 4	23	5	1	1
156	Tibiae, Fibulae (ABM) 1	25	5	1	1
157	Tibiae, Fibulae (ABM) 2	25	5	1	1
158	Tibiae, Fibulae (ABM) 3	28	5	1	1
159	Tibiae, Fibulae (ABM) 4	28	5	1	1
160	Humeri (ABM) 1	Right Arm		1	1
161	Humeri (ABM) 2			1	1
162	Radii, Ulnae (ABM) 1	Right Arm		1	1
163	Radii, Ulnae (ABM) 2			1	1
164	Humeri (ABM) 3	Left Arm		1	1
165	Humeri (ABM) 4			1	1
166	Radii, Ulnae (ABM) 3	Left Arm		1	1
167	Radii, Ulnae (ABM) 4			1	1
Total Dosimeters			**167**		

Appendix B: Full Details of Adult Helical and Sequential CT protocols Parameters Examined Using MOSFET Dosimeters

Table B - 1: Details of adult brain helical protocol parameters used.

No	Tube Rotation Time (Secs)	Tube Angulations (Degrees)	Image Thicknesses (mm)	Detector Configuration (mm)	Pitch Factors / Helical Pitch	Sure Exp. 3D (ATC)
1	0.5	0	2	0.5x16	Detail PF 0.688 / HP 11.0	High Quality SD 1.80
2	0.5	0	2	0.5x16	Detail PF 0.688 / HP 11.0	Standard SD 2.00
3	0.5	0	2	0.5x16	Detail PF 0.688 / HP 11.0	Low Dose SD 2.20
4	0.5	0	2	0.5x16	Standard PF 0.938 / HP 15.0	High Quality SD 1.80
5	0.5	0	2	0.5x16	Standard PF 0.938 / HP 15.0	Standard SD 2.00
6	0.5	0	2	0.5x16	Standard PF 0.938 / HP 15.0	Low Dose SD 2.20
7	0.5	0	2	0.5x16	Fast PF 1.438 / HP 23.0	High Quality SD 1.80
8	0.5	0	2	0.5x16	Fast PF 1.438 / HP 23.0	Standard SD 2.00
9	0.5	0	2	0.5x16	Fast PF 1.438 / HP 23.0	Low Dose SD 2.20
10	0.5	15	2	0.5x16	Detail PF 0.688 / HP 11.0	High Quality SD 1.80
11	0.5	15	2	0.5x16	Detail PF 0.688 / HP 11.0	Standard SD 2.00
12	0.5	15	2	0.5x16	Detail PF 0.688 / HP 11.0	Low Dose SD 2.20
13	0.5	15	2	0.5x16	Standard PF 0.938 / HP 15.0	High Quality SD 1.80
14	0.5	15	2	0.5x16	Standard PF 0.938 / HP 15.0	Standard SD 2.00
15	0.5	15	2	0.5x16	Standard PF 0.938 / HP 15.0	Low Dose SD 2.20
16	0.5	15	2	0.5x16	Fast PF 1.438 / HP 23.0	High Quality SD 1.80
17	0.5	15	2	0.5x16	Fast PF 1.438 / HP 23.0	Standard SD 2.00
18	0.5	15	2	0.5x16	Fast PF 1.438 / HP 23.0	Low Dose SD 2.20
19	0.5	27	2	0.5x16	Detail PF 0.688 / HP 11.0	High Quality SD 1.80
20	0.5	27	2	0.5x16	Detail PF 0.688 / HP 11.0	Standard SD 2.00
21	0.5	27	2	0.5x16	Detail PF 0.688 / HP 11.0	Low Dose SD 2.20
22	0.5	27	2	0.5x16	Standard PF 0.938 / HP 15.0	High Quality SD 1.80
23	0.5	27	2	0.5x16	Standard PF 0.938 / HP 15.0	Standard SD 2.00

204

Continued **(Table B - 1)**

No	Tube Rotation Time (Secs)	Tube Angulations (Degrees)	Image Thicknesses (mm)	Detector Configuration (mm)	Pitch Factors / Helical Pitch	Sure Exp. 3D (ATC)
24	0.5	27	2	0.5x16	Standard PF 0.938 / HP 15.0	Low Dose SD 2.20
25	0.5	27	2	0.5x16	Fast PF 1.438 / HP 23.0	High Quality SD 1.80
26	0.5	27	2	0.5x16	Fast PF 1.438 / HP 23.0	Standard SD 2.00
27	0.5	27	2	0.5x16	Fast PF 1.438 / HP 23.0	Low Dose SD 2.20
28	0.5	0	4	1.0x16	Detail PF 0.688 / HP 11.0	High Quality SD 1.80
29	0.5	0	4	1.0x16	Detail PF 0.688 / HP 11.0	Standard SD 2.00
30	0.5	0	4	1.0x16	Detail PF 0.688 / HP 11.0	Low Dose SD 2.20
31	0.5	0	4	1.0x16	Standard PF 0.938 / HP 15.0	High Quality SD 1.80
32	0.5	0	4	1.0x16	Standard PF 0.938 / HP 15.0	Standard SD 2.00
33	0.5	0	4	1.0x16	Standard PF 0.938 / HP 15.0	Low Dose SD 2.20
34	0.5	0	4	1.0x16	Fast PF 1.438 / HP 23.0	High Quality SD 1.80
35	0.5	0	4	1.0x16	Fast PF 1.438 / HP 23.0	Standard SD 2.00
36	0.5	0	4	1.0x16	Fast PF 1.438 / HP 23.0	Low Dose SD 2.20
37	0.5	15	4	1.0x16	Detail PF 0.688 / HP 11.0	High Quality SD 1.80
38	0.5	15	4	1.0x16	Detail PF 0.688 / HP 11.0	Standard SD 2.00
39	0.5	15	4	1.0x16	Detail PF 0.688 / HP 11.0	Low Dose SD 2.20
40	0.5	15	4	1.0x16	Standard PF 0.938 / HP 15.0	High Quality SD 1.80
41	0.5	15	4	1.0x16	Standard PF 0.938 / HP 15.0	Standard SD 2.00
42	0.5	15	4	1.0x16	Standard PF 0.938 / HP 15.0	Low Dose SD 2.20
43	0.5	15	4	1.0x16	Fast PF 1.438 / HP 23.0	High Quality SD 1.80
44	0.5	15	4	1.0x16	Fast PF 1.438 / HP 23.0	Standard SD 2.00
45	0.5	15	4	1.0x16	Fast PF 1.438 / HP 23.0	Low Dose SD 2.20
46	0.5	27	4	1.0x16	Detail PF 0.688 / HP 11.0	High Quality SD 1.80
47	0.5	27	4	1.0x16	Detail PF 0.688 / HP 11.0	Standard SD 2.00
48	0.5	27	4	1.0x16	Detail PF 0.688 / HP 11.0	Low Dose SD 2.20
49	0.5	27	4	1.0x16	Standard PF 0.938 / HP 15.0	High Quality SD 1.80

205

Continued **(Table B - 1)**

No	Tube Rotation Time (Secs)	Tube Angulations (Degrees)	Image Thicknesses (mm)	Detector Configuration (mm)	Pitch Factors / Helical Pitch	Sure Exp. 3D (ATC)
50	0.5	27	4	1.0x16	Standard PF 0.938 / HP 15.0	Standard SD 2.00
51	0.5	27	4	1.0x16	Standard PF 0.938 / HP 15.0	Low Dose SD 2.20
52	0.5	27	4	1.0x16	Fast PF 1.438 / HP 23.0	High Quality SD 1.80
53	0.5	27	4	1.0x16	Fast PF 1.438 / HP 23.0	Standard SD 2.00
54	0.5	27	4	1.0x16	Fast PF 1.438 / HP 23.0	Low Dose SD 2.20
55	0.5	0	8	2.0x16	Detail PF 0.688 / HP 11.0	High Quality SD 1.80
56	0.5	0	8	2.0x16	Detail PF 0.688 / HP 11.0	Standard SD 2.00
57	0.5	0	8	2.0x16	Detail PF 0.688 / HP 11.0	Low Dose SD 2.20
58	0.5	0	8	2.0x16	Standard PF 0.938 / HP 15.0	High Quality SD 1.80
59	0.5	0	8	2.0x16	Standard PF 0.938 / HP 15.0	Standard SD 2.00
60	0.5	0	8	2.0x16	Standard PF 0.938 / HP 15.0	Low Dose SD 2.20
61	0.5	0	8	2.0x16	Fast PF 1.438 / HP 23.0	High Quality SD 1.80
62	0.5	0	8	2.0x16	Fast PF 1.438 / HP 23.0	Standard SD 2.00
63	0.5	0	8	2.0x16	Fast PF 1.438 / HP 23.0	Low Dose SD 2.20
64	0.5	15	8	2.0x16	Detail PF 0.688 / HP 11.0	High Quality SD 1.80
65	0.5	15	8	2.0x16	Detail PF 0.688 / HP 11.0	Standard SD 2.00
66	0.5	15	8	2.0x16	Detail PF 0.688 / HP 11.0	Low Dose SD 2.20
67	0.5	15	8	2.0x16	Standard PF 0.938 / HP 15.0	High Quality SD 1.80
68	0.5	15	8	2.0x16	Standard PF 0.938 / HP 15.0	Standard SD 2.00
69	0.5	15	8	2.0x16	Standard PF 0.938 / HP 15.0	Low Dose SD 2.20
70	0.5	15	8	2.0x16	Fast PF 1.438 / HP 23.0	High Quality SD 1.80
71	0.5	15	8	2.0x16	Fast PF 1.438 / HP 23.0	Standard SD 2.00
72	0.5	15	8	2.0x16	Fast PF 1.438 / HP 23.0	Low Dose SD 2.20

206

Continued **(Table B - 1)**

No	Tube Rotation Time (Secs)	Tube Angulations (Degrees)	Image Thicknesses (mm)	Detector Configuration (mm)	Pitch Factors / Helical Pitch	Sure Exp. 3D (ATC)
73	0.5	27	8	2.0x16	Detail PF 0.688 / HP 11.0	High Quality SD 1.80
74	0.5	27	8	2.0x16	Detail PF 0.688 / HP 11.0	Standard SD 2.00
75	0.5	27	8	2.0x16	Detail PF 0.688 / HP 11.0	Low Dose SD 2.20
76	0.5	27	8	2.0x16	Standard PF 0.938 / HP 15.0	High Quality SD 1.80
77	0.5	27	8	2.0x16	Standard PF 0.938 / HP 15.0	Standard SD 2.00
78	0.5	27	8	2.0x16	Standard PF 0.938 / HP 15.0	Low Dose SD 2.20
79	0.5	27	8	2.0x16	Fast PF 1.438 / HP 23.0	High Quality SD 1.80
80	0.5	27	8	2.0x16	Fast PF 1.438 / HP 23.0	Standard SD 2.00
81	0.5	27	8	2.0x16	Fast PF 1.438 / HP 23.0	Low Dose SD 2.20
82	1.0	0	2	0.5x16	Detail PF 0.688 / HP 11.0	High Quality SD 1.80
83	1.0	0	2	0.5x16	Detail PF 0.688 / HP 11.0	Standard SD 2.00
84	1.0	0	2	0.5x16	Detail PF 0.688 / HP 11.0	Low Dose SD 2.20
85	1.0	0	2	0.5x16	Standard PF 0.938 / HP 15.0	High Quality SD 1.80
86	1.0	0	2	0.5x16	Standard PF 0.938 / HP 15.0	Standard SD 2.00
87	1.0	0	2	0.5x16	Standard PF 0.938 / HP 15.0	Low Dose SD 2.20
88	1.0	0	2	0.5x16	Fast PF 1.438 / HP 23.0	High Quality SD 1.80
89	1.0	0	2	0.5x16	Fast PF 1.438 / HP 23.0	Standard SD 2.00
90	1.0	0	2	0.5x16	Fast PF 1.438 / HP 23.0	Low Dose SD 2.20
91	1.0	15	2	0.5x16	Detail PF 0.688 / HP 11.0	High Quality SD 1.80
92	1.0	15	2	0.5x16	Detail PF 0.688 / HP 11.0	Standard SD 2.00
93	1.0	15	2	0.5x16	Detail PF 0.688 / HP 11.0	Low Dose SD 2.20
94	1.0	15	2	0.5x16	Standard PF 0.938 / HP 15.0	High Quality SD 1.80
95	1.0	15	2	0.5x16	Standard PF 0.938 / HP 15.0	Standard SD 2.00
96	1.0	15	2	0.5x16	Standard PF 0.938 / HP 15.0	Low Dose SD 2.20
97	1.0	15	2	0.5x16	Fast PF 1.438 / HP 23.0	High Quality SD 1.80

207

Continued **(Table B - 1)**

No	Tube Rotation Time (Secs)	Tube Angulations (Degrees)	Image Thicknesses (mm)	Detector Configuration (mm)	Pitch Factors / Helical Pitch	Sure Exp. 3D (ATC)
98	1.0	15	2	0.5x16	Fast PF 1.438 / HP 23.0	Standard SD 2.00
99	1.0	15	2	0.5x16	Fast PF 1.438 / HP 23.0	Low Dose SD 2.20
100	1.0	27	2	0.5x16	Detail PF 0.688 / HP 11.0	High Quality SD 1.80
101	1.0	27	2	0.5x16	Detail PF 0.688 / HP 11.0	Standard SD 2.00
102	1.0	27	2	0.5x16	Detail PF 0.688 / HP 11.0	Low Dose SD 2.20
103	1.0	27	2	0.5x16	Standard PF 0.938 / HP 15.0	High Quality SD 1.80
104	1.0	27	2	0.5x16	Standard PF 0.938 / HP 15.0	Standard SD 2.00
105	1.0	27	2	0.5x16	Standard PF 0.938 / HP 15.0	Low Dose SD 2.20
106	1.0	27	2	0.5x16	Fast PF 1.438 / HP 23.0	High Quality SD 1.80
107	1.0	27	2	0.5x16	Fast PF 1.438 / HP 23.0	Standard SD 2.00
108	1.0	27	2	0.5x16	Fast PF 1.438 / HP 23.0	Low Dose SD 2.20
109	1.0	0	4	1.0x16	Detail PF 0.688 / HP 11.0	High Quality SD 1.80
110	1.0	0	4	1.0x16	Detail PF 0.688 / HP 11.0	Standard SD 2.00
111	1.0	0	4	1.0x16	Detail PF 0.688 / HP 11.0	Low Dose SD 2.20
112	1.0	0	4	1.0x16	Standard PF 0.938 / HP 15.0	High Quality SD 1.80
113	1.0	0	4	1.0x16	Standard PF 0.938 / HP 15.0	Standard SD 2.00
114	1.0	0	4	1.0x16	Standard PF 0.938 / HP 15.0	Low Dose SD 2.20
115	1.0	0	4	1.0x16	Fast PF 1.438 / HP 23.0	High Quality SD 1.80
116	1.0	0	4	1.0x16	Fast PF 1.438 / HP 23.0	Standard SD 2.00
117	1.0	0	4	1.0x16	Fast PF 1.438 / HP 23.0	Low Dose SD 2.20
118	1.0	15	4	1.0x16	Detail PF 0.688 / HP 11.0	High Quality SD 1.80
119	1.0	15	4	1.0x16	Detail PF 0.688 / HP 11.0	Standard SD 2.00
120	1.0	15	4	1.0x16	Detail PF 0.688 / HP 11.0	Low Dose SD 2.20
121	1.0	15	4	1.0x16	Standard PF 0.938 / HP 15.0	High Quality SD 1.80
122	1.0	15	4	1.0x16	Standard PF 0.938 / HP 15.0	Standard SD 2.00

208

Continued **(Table B - 1)**

No	Tube Rotation Time (Secs)	Tube Angulations (Degrees)	Image Thicknesses (mm)	Detector Configuration (mm)	Pitch Factors / Helical Pitch	Sure Exp. 3D (ATC)
123	1.0	15	4	1.0x16	Standard PF 0.938 / HP 15.0	Low Dose SD 2.20
124	1.0	15	4	1.0x16	Fast PF 1.438 / HP 23.0	High Quality SD 1.80
125	1.0	15	4	1.0x16	Fast PF 1.438 / HP 23.0	Standard SD 2.00
126	1.0	15	4	1.0x16	Fast PF 1.438 / HP 23.0	Low Dose SD 2.20
127	1.0	27	4	1.0x16	Detail PF 0.688 / HP 11.0	High Quality SD 1.80
128	1.0	27	4	1.0x16	Detail PF 0.688 / HP 11.0	Standard SD 2.00
129	1.0	27	4	1.0x16	Detail PF 0.688 / HP 11.0	Low Dose SD 2.20
130	1.0	27	4	1.0x16	Standard PF 0.938 / HP 15.0	High Quality SD 1.80
131	1.0	27	4	1.0x16	Standard PF 0.938 / HP 15.0	Standard SD 2.00
132	1.0	27	4	1.0x16	Standard PF 0.938 / HP 15.0	Low Dose SD 2.20
133	1.0	27	4	1.0x16	Fast PF 1.438 / HP 23.0	High Quality SD 1.80
134	1.0	27	4	1.0x16	Fast PF 1.438 / HP 23.0	Standard SD 2.00
135	1.0	27	4	1.0x16	Fast PF 1.438 / HP 23.0	Low Dose SD 2.20
136	1.0	0	8	2.0x16	Detail PF 0.688 / HP 11.0	High Quality SD 1.80
137	1.0	0	8	2.0x16	Detail PF 0.688 / HP 11.0	Standard SD 2.00
138	1.0	0	8	2.0x16	Detail PF 0.688 / HP 11.0	Low Dose SD 2.20
139	1.0	0	8	2.0x16	Standard PF 0.938 / HP 15.0	High Quality SD 1.80
140	1.0	0	8	2.0x16	Standard PF 0.938 / HP 15.0	Standard SD 2.00
141	1.0	0	8	2.0x16	Standard PF 0.938 / HP 15.0	Low Dose SD 2.20
142	1.0	0	8	2.0x16	Fast PF 1.438 / HP 23.0	High Quality SD 1.80
143	1.0	0	8	2.0x16	Fast PF 1.438 / HP 23.0	Standard SD 2.00
144	1.0	0	8	2.0x16	Fast PF 1.438 / HP 23.0	Low Dose SD 2.20
145	1.0	15	8	2.0x16	Detail PF 0.688 / HP 11.0	High Quality SD 1.80
146	1.0	15	8	2.0x16	Detail PF 0.688 / HP 11.0	Standard SD 2.00

209

Continued **(Table B - 1)**

No	Tube Rotation Time (Secs)	Tube Angulations (Degrees)	Image Thicknesses (mm)	Detector Configuration (mm)	Pitch Factors / Helical Pitch	Sure Exp. 3D (ATC)
147	1.0	15	8	2.0x16	Detail PF 0.688 / HP 11.0	Low Dose SD 2.20
148	1.0	15	8	2.0x16	Standard PF 0.938 / HP 15.0	High Quality SD 1.80
149	1.0	15	8	2.0x16	Standard PF 0.938 / HP 15.0	Standard SD 2.00
150	1.0	15	8	2.0x16	Standard PF 0.938 / HP 15.0	Low Dose SD 2.20
151	1.0	15	8	2.0x16	Fast PF 1.438 / HP 23.0	High Quality SD 1.80
152	1.0	15	8	2.0x16	Fast PF 1.438 / HP 23.0	Standard SD 2.00
153	1.0	15	8	2.0x16	Fast PF 1.438 / HP 23.0	Low Dose SD 2.20
154	1.0	27	8	2.0x16	Detail PF 0.688 / HP 11.0	High Quality SD 1.80
155	1.0	27	8	2.0x16	Detail PF 0.688 / HP 11.0	Standard SD 2.00
156	1.0	27	8	2.0x16	Detail PF 0.688 / HP 11.0	Low Dose SD 2.20
157	1.0	27	8	2.0x16	Standard PF 0.938 / HP 15.0	High Quality SD 1.80
158	1.0	27	8	2.0x16	Standard PF 0.938 / HP 15.0	Standard SD 2.00
159	1.0	27	8	2.0x16	Standard PF 0.938 / HP 15.0	Low Dose SD 2.20
160	1.0	27	8	2.0x16	Fast PF 1.438 / HP 23.0	High Quality SD 1.80
161	1.0	27	8	2.0x16	Fast PF 1.438 / HP 23.0	Standard SD 2.00
162	1.0	27	8	2.0x16	Fast PF 1.438 / HP 23.0	Low Dose SD 2.20

210

Table B - 2: Adult sequential brain protocol parameters used.					
No	**Tube Rotation Time (Secs)**	**Tube Angulations (Degrees)**	**Image Thicknesses (mm)**	**Detector Configuration (mm)**	**Sure Exp. 3D (ATC)**
163	0.5	0	2	0.5x4	High Quality SD 1.80
164	0.5	0	2	0.5x4	Standard SD 2.00
165	0.5	0	2	0.5x4	Low Dose SD 2.20
166	0.5	0	4	1.0x4	High Quality SD 1.80
167	0.5	0	4	1.0x4	Standard SD 2.00
168	0.5	0	4	1.0x4	Low Dose SD 2.20
169	0.5	0	8	2.0x4	High Quality SD 1.80
170	0.5	0	8	2.0x4	Standard SD 2.00
171	0.5	0	8	2.0x4	Low Dose SD 2.20
172	0.5	15	2	0.5x4	High Quality SD 1.80
173	0.5	15	2	0.5x4	Standard SD 2.00
174	0.5	15	2	0.5x4	Low Dose SD 2.20
175	0.5	15	4	1.0x4	High Quality SD 1.80
176	0.5	15	4	1.0x4	Standard SD 2.00
177	0.5	15	4	1.0x4	Low Dose SD 2.20
178	0.5	15	8	2.0x4	High Quality SD 1.80
179	0.5	15	8	2.0x4	Standard SD 2.00
180	0.5	15	8	2.0x4	Low Dose SD 2.20
181	0.5	27	2	0.5x4	High Quality SD 1.80
182	0.5	27	2	0.5x4	Standard SD 2.00
183	0.5	27	2	0.5x4	Low Dose SD 2.20
184	0.5	27	4	1.0x4	High Quality SD 1.80
185	0.5	27	4	1.0x4	Standard SD 2.00
186	0.5	27	4	1.0x4	Low Dose SD 2.20
187	0.5	27	8	2.0x4	High Quality SD 1.80
188	0.5	27	8	2.0x4	Standard SD 2.00
189	0.5	27	8	2.0x4	Low Dose SD 2.20

211

Continued **(Table B - 2)**

No	Tube Rotation Time (Secs)	Tube Angulations (Degrees)	Image Thicknesses (mm)	Detector Configuration (mm)	Sure Exp. 3D (ATC)
190	1.0	0	2	0.5x4	High Quality SD 1.80
191	1.0	0	2	0.5x4	Standard SD 2.00
192	1.0	0	2	0.5x4	Low Dose SD 2.20
193	1.0	0	4	1.0x4	High Quality SD 1.80
194	1.0	0	4	1.0x4	Standard SD 2.00
195	1.0	0	4	1.0x4	Low Dose SD 2.20
196	1.0	0	8	2.0x4	High Quality SD 1.80
197	1.0	0	8	2.0x4	Standard SD 2.00
198	1.0	0	8	2.0x4	Low Dose SD 2.20
199	1.0	15	2	0.5x4	High Quality SD 1.80
200	1.0	15	2	0.5x4	Standard SD 2.00
201	1.0	15	2	0.5x4	Low Dose SD 2.20
202	1.0	15	4	1.0x4	High Quality SD 1.80
203	1.0	15	4	1.0x4	Standard SD 2.00
204	1.0	15	4	1.0x4	Low Dose SD 2.20
205	1.0	15	8	2.0x4	High Quality SD 1.80
206	1.0	15	8	2.0x4	Standard SD 2.00
207	1.0	15	8	2.0x4	Low Dose SD 2.20
208	1.0	27	2	0.5x4	High Quality SD 1.80
209	1.0	27	2	0.5x4	Standard SD 2.00
210	1.0	27	2	0.5x4	Low Dose SD 2.20
211	1.0	27	4	1.0x4	High Quality SD 1.80
212	1.0	27	4	1.0x4	Standard SD 2.00
213	1.0	27	4	1.0x4	Low Dose SD 2.20
214	1.0	27	8	2.0x4	High Quality SD 1.80
215	1.0	27	8	2.0x4	Standard SD 2.00
216	1.0	27	8	2.0x4	Low Dose SD 2.20

212

Appendix C: Full Details of Paediatric Helical CT protocols Parameters used.

Table C - 1: Paediatric helical brain protocol parameters used.

No	Tube Rotation Time (Secs)	Tube Angulations (Degrees)	Image Thicknesses (mm)	Detector Configuration (mm)	Pitch Factors / Helical Pitch	Sure Exp. 3D (ATC)
1	0.5	0	2	0.5x16	Detail PF 0.688 / HP 11.0	High Quality SD 4.00
2	0.5	0	2	0.5x16	Detail PF 0.688 / HP 11.0	Standard SD 6.00
3	0.5	0	2	0.5x16	Detail PF 0.688 / HP 11.0	Low Dose SD 8.00
4	0.5	0	2	0.5x16	Standard PF 0.938 / HP 15.0	High Quality SD 4.00
5	0.5	0	2	0.5x16	Standard PF 0.938 / HP 15.0	Standard SD 6.00
6	0.5	0	2	0.5x16	Standard PF 0.938 / HP 15.0	Low Dose SD 8.00
7	0.5	0	2	0.5x16	Fast PF 1.438 / HP 23.0	High Quality SD 4.00
8	0.5	0	2	0.5x16	Fast PF 1.438 / HP 23.0	Standard SD 6.00
9	0.5	0	2	0.5x16	Fast PF 1.438 / HP 23.0	Low Dose SD 8.00
10	0.5	15	2	0.5x16	Detail PF 0.688 / HP 11.0	High Quality SD 4.00
11	0.5	15	2	0.5x16	Detail PF 0.688 / HP 11.0	Standard SD 6.00
12	0.5	15	2	0.5x16	Detail PF 0.688 / HP 11.0	Low Dose SD 8.00
13	0.5	15	2	0.5x16	Standard PF 0.938 / HP 15.0	High Quality SD 4.00
14	0.5	15	2	0.5x16	Standard PF 0.938 / HP 15.0	Standard SD 6.00
15	0.5	15	2	0.5x16	Standard PF 0.938 / HP 15.0	Low Dose SD 8.00
16	0.5	15	2	0.5x16	Fast PF 1.438 / HP 23.0	High Quality SD 4.00
17	0.5	15	2	0.5x16	Fast PF 1.438 / HP 23.0	Standard SD 6.00
18	0.5	15	2	0.5x16	Fast PF 1.438 / HP 23.0	Low Dose SD 8.00
19	0.5	27	2	0.5x16	Detail PF 0.688 / HP 11.0	High Quality SD 4.00
20	0.5	27	2	0.5x16	Detail PF 0.688 / HP 11.0	Standard SD 6.00
21	0.5	27	2	0.5x16	Detail PF 0.688 / HP 11.0	Low Dose SD 8.00
22	0.5	27	2	0.5x16	Standard PF 0.938 / HP 15.0	High Quality SD 4.00
23	0.5	27	2	0.5x16	Standard PF 0.938 / HP 15.0	Standard SD 6.00
24	0.5	27	2	0.5x16	Standard PF 0.938 / HP 15.0	Low Dose SD 8.00

213

Continued **(Table C - 1)**

No	Tube Rotation Time (Secs)	Tube Angulations (Degrees)	Image Thicknesses (mm)	Detector Configuration (mm)	Pitch Factors / Helical Pitch	Sure Exp. 3D (ATC)
25	0.5	27	2	0.5x16	Fast PF 1.438 / HP 23.0	High Quality SD 4.00
26	0.5	27	2	0.5x16	Fast PF 1.438 / HP 23.0	Standard SD 6.00
27	0.5	27	2	0.5x16	Fast PF 1.438 / HP 23.0	Low Dose SD 8.00
28	0.5	0	4	1.0x16	Detail PF 0.688 / HP 11.0	High Quality SD 4.00
29	0.5	0	4	1.0x16	Detail PF 0.688 / HP 11.0	Standard SD 6.00
30	0.5	0	4	1.0x16	Detail PF 0.688 / HP 11.0	Low Dose SD 8.00
31	0.5	0	4	1.0x16	Standard PF 0.938 / HP 15.0	High Quality SD 4.00
32	0.5	0	4	1.0x16	Standard PF 0.938 / HP 15.0	Standard SD 6.00
33	0.5	0	4	1.0x16	Standard PF 0.938 / HP 15.0	Low Dose SD 8.00
34	0.5	0	4	1.0x16	Fast PF 1.438 / HP 23.0	High Quality SD 4.00
35	0.5	0	4	1.0x16	Fast PF 1.438 / HP 23.0	Standard SD 6.00
36	0.5	0	4	1.0x16	Fast PF 1.438 / HP 23.0	Low Dose SD 8.00
37	0.5	15	4	1.0x16	Detail PF 0.688 / HP 11.0	High Quality SD 4.00
38	0.5	15	4	1.0x16	Detail PF 0.688 / HP 11.0	Standard SD 6.00
39	0.5	15	4	1.0x16	Detail PF 0.688 / HP 11.0	Low Dose SD 8.00
40	0.5	15	4	1.0x16	Standard PF 0.938 / HP 15.0	High Quality SD 4.00
41	0.5	15	4	1.0x16	Standard PF 0.938 / HP 15.0	Standard SD 6.00
42	0.5	15	4	1.0x16	Standard PF 0.938 / HP 15.0	Low Dose SD 8.00
43	0.5	15	4	1.0x16	Fast PF 1.438 / HP 23.0	High Quality SD 4.00
44	0.5	15	4	1.0x16	Fast PF 1.438 / HP 23.0	Standard SD 6.00
45	0.5	15	4	1.0x16	Fast PF 1.438 / HP 23.0	Low Dose SD 8.00
46	0.5	27	4	1.0x16	Detail PF 0.688 / HP 11.0	High Quality SD 4.00
47	0.5	27	4	1.0x16	Detail PF 0.688 / HP 11.0	Standard SD 6.00
48	0.5	27	4	1.0x16	Detail PF 0.688 / HP 11.0	Low Dose SD 8.00
49	0.5	27	4	1.0x16	Standard PF 0.938 / HP 15.0	High Quality SD 4.00
50	0.5	27	4	1.0x16	Standard PF 0.938 / HP 15.0	Standard SD 6.00

214

Continued **(Table C - 1)**

No	Tube Rotation Time (Secs)	Tube Angulations (Degrees)	Image Thicknesses (mm)	Detector Configuration (mm)	Pitch Factors / Helical Pitch	Sure Exp. 3D (ATC)
51	0.5	27	4	1.0x16	Standard PF 0.938 / HP 15.0	Low Dose SD 8.00
52	0.5	27	4	1.0x16	Fast PF 1.438 / HP 23.0	High Quality SD 4.00
53	0.5	27	4	1.0x16	Fast PF 1.438 / HP 23.0	Standard SD 6.00
54	0.5	27	4	1.0x16	Fast PF 1.438 / HP 23.0	Low Dose SD 8.00
55	0.5	0	8	2.0x16	Detail PF 0.688 / HP 11.0	High Quality SD 4.00
56	0.5	0	8	2.0x16	Detail PF 0.688 / HP 11.0	Standard SD 6.00
57	0.5	0	8	2.0x16	Detail PF 0.688 / HP 11.0	Low Dose SD 8.00
58	0.5	0	8	2.0x16	Standard PF 0.938 / HP 15.0	High Quality SD 4.00
59	0.5	0	8	2.0x16	Standard PF 0.938 / HP 15.0	Standard SD 6.00
60	0.5	0	8	2.0x16	Standard PF 0.938 / HP 15.0	Low Dose SD 8.00
61	0.5	0	8	2.0x16	Fast PF 1.438 / HP 23.0	High Quality SD 4.00
62	0.5	0	8	2.0x16	Fast PF 1.438 / HP 23.0	Standard SD 6.00
63	0.5	0	8	2.0x16	Fast PF 1.438 / HP 23.0	Low Dose SD 8.00
64	0.5	15	8	2.0x16	Detail PF 0.688 / HP 11.0	High Quality SD 4.00
65	0.5	15	8	2.0x16	Detail PF 0.688 / HP 11.0	Standard SD 6.00
66	0.5	15	8	2.0x16	Detail PF 0.688 / HP 11.0	Low Dose SD 8.00
67	0.5	15	8	2.0x16	Standard PF 0.938 / HP 15.0	High Quality SD 4.00
68	0.5	15	8	2.0x16	Standard PF 0.938 / HP 15.0	Standard SD 6.00
69	0.5	15	8	2.0x16	Standard PF 0.938 / HP 15.0	Low Dose SD 8.00
70	0.5	15	8	2.0x16	Fast PF 1.438 / HP 23.0	High Quality SD 4.00
71	0.5	15	8	2.0x16	Fast PF 1.438 / HP 23.0	Standard SD 6.00
72	0.5	15	8	2.0x16	Fast PF 1.438 / HP 23.0	Low Dose SD 8.00
73	0.5	27	8	2.0x16	Detail PF 0.688 / HP 11.0	High Quality SD 4.00
74	0.5	27	8	2.0x16	Detail PF 0.688 / HP 11.0	Standard SD 6.00
75	0.5	27	8	2.0x16	Detail PF 0.688 / HP 11.0	Low Dose SD 8.00
76	0.5	27	8	2.0x16	Standard PF 0.938 / HP 15.0	High Quality SD 4.00

215

Continued **(Table C - 1)**

No	Tube Rotation Time (Secs)	Tube Angulations (Degrees)	Image Thicknesses (mm)	Detector Configuration (mm)	Pitch Factors / Helical Pitch	Sure Exp. 3D (ATC)
77	0.5	27	8	2.0x16	Standard PF 0.938 / HP 15.0	Standard SD 6.00
78	0.5	27	8	2.0x16	Standard PF 0.938 / HP 15.0	Low Dose SD 8.00
79	0.5	27	8	2.0x16	Fast PF 1.438 / HP 23.0	High Quality SD 4.00
80	0.5	27	8	2.0x16	Fast PF 1.438 / HP 23.0	Standard SD 6.00
81	0.5	27	8	2.0x16	Fast PF 1.438 / HP 23.0	Low Dose SD 8.00
82	0.75	0	2	0.5x16	Detail PF 0.688 / HP 11.0	High Quality SD 4.00
83	0.75	0	2	0.5x16	Detail PF 0.688 / HP 11.0	Standard SD 6.00
84	0.75	0	2	0.5x16	Detail PF 0.688 / HP 11.0	Low Dose SD 8.00
85	0.75	0	2	0.5x16	Standard PF 0.938 / HP 15.0	High Quality SD 4.00
86	0.75	0	2	0.5x16	Standard PF 0.938 / HP 15.0	Standard SD 6.00
87	0.75	0	2	0.5x16	Standard PF 0.938 / HP 15.0	Low Dose SD 8.00
88	0.75	0	2	0.5x16	Fast PF 1.438 / HP 23.0	High Quality SD 4.00
89	0.75	0	2	0.5x16	Fast PF 1.438 / HP 23.0	Standard SD 6.00
90	0.75	0	2	0.5x16	Fast PF 1.438 / HP 23.0	Low Dose SD 8.00
91	0.75	15	2	0.5x16	Detail PF 0.688 / HP 11.0	High Quality SD 4.00
92	0.75	15	2	0.5x16	Detail PF 0.688 / HP 11.0	Standard SD 6.00
93	0.75	15	2	0.5x16	Detail PF 0.688 / HP 11.0	Low Dose SD 8.00
94	0.75	15	2	0.5x16	Standard PF 0.938 / HP 15.0	High Quality SD 4.00
95	0.75	15	2	0.5x16	Standard PF 0.938 / HP 15.0	Standard SD 6.00
96	0.75	15	2	0.5x16	Standard PF 0.938 / HP 15.0	Low Dose SD 8.00
97	0.75	15	2	0.5x16	Fast PF 1.438 / HP 23.0	High Quality SD 4.00
98	0.75	15	2	0.5x16	Fast PF 1.438 / HP 23.0	Standard SD 6.00
99	0.75	15	2	0.5x16	Fast PF 1.438 / HP 23.0	Low Dose SD 8.00

216

Continued **(Table C - 1)**

No	Tube Rotation Time (Secs)	Tube Angulations (Degrees)	Image Thicknesses (mm)	Detector Configuration (mm)	Pitch Factors / Helical Pitch	Sure Exp. 3D (ATC)
100	0.75	27	2	0.5x16	Detail PF 0.688 / HP 11.0	High Quality SD 4.00
101	0.75	27	2	0.5x16	Detail PF 0.688 / HP 11.0	Standard SD 6.00
102	0.75	27	2	0.5x16	Detail PF 0.688 / HP 11.0	Low Dose SD 8.00
103	0.75	27	2	0.5x16	Standard PF 0.938 / HP 15.0	High Quality SD 4.00
104	0.75	27	2	0.5x16	Standard PF 0.938 / HP 15.0	Standard SD 6.00
105	0.75	27	2	0.5x16	Standard PF 0.938 / HP 15.0	Low Dose SD 8.00
106	0.75	27	2	0.5x16	Fast PF 1.438 / HP 23.0	High Quality SD 4.00
107	0.75	27	2	0.5x16	Fast PF 1.438 / HP 23.0	Standard SD 6.00
108	0.75	27	2	0.5x16	Fast PF 1.438 / HP 23.0	Low Dose SD 8.00
109	0.75	0	4	1.0x16	Detail PF 0.688 / HP 11.0	High Quality SD 4.00
110	0.75	0	4	1.0x16	Detail PF 0.688 / HP 11.0	Standard SD 6.00
111	0.75	0	4	1.0x16	Detail PF 0.688 / HP 11.0	Low Dose SD 8.00
112	0.75	0	4	1.0x16	Standard PF 0.938 / HP 15.0	High Quality SD 4.00
113	0.75	0	4	1.0x16	Standard PF 0.938 / HP 15.0	Standard SD 6.00
114	0.75	0	4	1.0x16	Standard PF 0.938 / HP 15.0	Low Dose SD 8.00
115	0.75	0	4	1.0x16	Fast PF 1.438 / HP 23.0	High Quality SD 4.00
116	0.75	0	4	1.0x16	Fast PF 1.438 / HP 23.0	Standard SD 6.00
117	0.75	0	4	1.0x16	Fast PF 1.438 / HP 23.0	Low Dose SD 8.00
118	0.75	15	4	1.0x16	Detail PF 0.688 / HP 11.0	High Quality SD 4.00
119	0.75	15	4	1.0x16	Detail PF 0.688 / HP 11.0	Standard SD 6.00
120	0.75	15	4	1.0x16	Detail PF 0.688 / HP 11.0	Low Dose SD 8.00
121	0.75	15	4	1.0x16	Standard PF 0.938 / HP 15.0	High Quality SD 4.00
122	0.75	15	4	1.0x16	Standard PF 0.938 / HP 15.0	Standard SD 6.00
123	0.75	15	4	1.0x16	Standard PF 0.938 / HP 15.0	Low Dose SD 8.00
124	0.75	15	4	1.0x16	Fast PF 1.438 / HP 23.0	High Quality SD 4.00

217

Continued **(Table C - 1)**

No	Tube Rotation Time (Secs)	Tube Angulations (Degrees)	Image Thicknesses (mm)	Detector Configuration (mm)	Pitch Factors / Helical Pitch	Sure Exp. 3D (ATC)
125	0.75	15	4	1.0x16	Fast PF 1.438 / HP 23.0	Standard SD 6.00
126	0.75	15	4	1.0x16	Fast PF 1.438 / HP 23.0	Low Dose SD 8.00
127	0.75	27	4	1.0x16	Detail PF 0.688 / HP 11.0	High Quality SD 4.00
128	0.75	27	4	1.0x16	Detail PF 0.688 / HP 11.0	Standard SD 6.00
129	0.75	27	4	1.0x16	Detail PF 0.688 / HP 11.0	Low Dose SD 8.00
130	0.75	27	4	1.0x16	Standard PF 0.938 / HP 15.0	High Quality SD 4.00
131	0.75	27	4	1.0x16	Standard PF 0.938 / HP 15.0	Standard SD 6.00
132	0.75	27	4	1.0x16	Standard PF 0.938 / HP 15.0	Low Dose SD 8.00
133	0.75	27	4	1.0x16	Fast PF 1.438 / HP 23.0	High Quality SD 4.00
134	0.75	27	4	1.0x16	Fast PF 1.438 / HP 23.0	Standard SD 6.00
135	0.75	27	4	1.0x16	Fast PF 1.438 / HP 23.0	Low Dose SD 8.00
136	0.75	0	8	2.0x16	Detail PF 0.688 / HP 11.0	High Quality SD 4.00
137	0.75	0	8	2.0x16	Detail PF 0.688 / HP 11.0	Standard SD 6.00
138	0.75	0	8	2.0x16	Detail PF 0.688 / HP 11.0	Low Dose SD 8.00
139	0.75	0	8	2.0x16	Standard PF 0.938 / HP 15.0	High Quality SD 4.00
140	0.75	0	8	2.0x16	Standard PF 0.938 / HP 15.0	Standard SD 6.00
141	0.75	0	8	2.0x16	Standard PF 0.938 / HP 15.0	Low Dose SD 8.00
142	0.75	0	8	2.0x16	Fast PF 1.438 / HP 23.0	High Quality SD 4.00
143	0.75	0	8	2.0x16	Fast PF 1.438 / HP 23.0	Standard SD 6.00
144	0.75	0	8	2.0x16	Fast PF 1.438 / HP 23.0	Low Dose SD 8.00
145	0.75	15	8	2.0x16	Detail PF 0.688 / HP 11.0	High Quality SD 4.00
146	0.75	15	8	2.0x16	Detail PF 0.688 / HP 11.0	Standard SD 6.00
147	0.75	15	8	2.0x16	Detail PF 0.688 / HP 11.0	Low Dose SD 8.00
148	0.75	15	8	2.0x16	Standard PF 0.938 / HP 15.0	High Quality SD 4.00
149	0.75	15	8	2.0x16	Standard PF 0.938 / HP 15.0	Standard SD 6.00

218

Continued **(Table C - 1)**

No	Tube Rotation Time (Secs)	Tube Angulations (Degrees)	Image Thicknesses (mm)	Detector Configuration (mm)	Pitch Factors / Helical Pitch	Sure Exp. 3D (ATC)
150	0.75	15	8	2.0x16	Standard PF 0.938 / HP 15.0	Low Dose SD 8.00
151	0.75	15	8	2.0x16	Fast PF 1.438 / HP 23.0	High Quality SD 4.00
152	0.75	15	8	2.0x16	Fast PF 1.438 / HP 23.0	Standard SD 6.00
153	0.75	15	8	2.0x16	Fast PF 1.438 / HP 23.0	Low Dose SD 8.00
154	0.75	27	8	2.0x16	Detail PF 0.688 / HP 11.0	High Quality SD 4.00
155	0.75	27	8	2.0x16	Detail PF 0.688 / HP 11.0	Standard SD 6.00
156	0.75	27	8	2.0x16	Detail PF 0.688 / HP 11.0	Low Dose SD 8.00
157	0.75	27	8	2.0x16	Standard PF 0.938 / HP 15.0	High Quality SD 4.00
158	0.75	27	8	2.0x16	Standard PF 0.938 / HP 15.0	Standard SD 6.00
159	0.75	27	8	2.0x16	Standard PF 0.938 / HP 15.0	Low Dose SD 8.00
160	0.75	27	8	2.0x16	Fast PF 1.438 / HP 23.0	High Quality SD 4.00
161	0.75	27	8	2.0x16	Fast PF 1.438 / HP 23.0	Standard SD 6.00
162	0.75	27	8	2.0x16	Fast PF 1.438 / HP 23.0	Low Dose SD 8.00

219

Table C - 2: Paediatric helical CT brain protocol parameters changes.					
No	**Angle**	**Rot. Time (S)**	**Slice thickness (mm)**	**KV**	**mA (fixed)**
01	0	0.5	0.5x16	100	120
02	0	0.75	0.5x16	100	120
03	0	1	0.5x16	100	120
04	15	0.5	0.5x16	100	120
05	15	0.75	0.5x16	100	120
06	15	1	0.5x16	100	120
07	27	0.5	0.5x16	100	120
08	27	0.75	0.5x16	100	120
09	27	1	0.5x16	100	120
10	0	0.5	0.5x16	100	160
11	0	0.75	0.5x16	100	160
12	0	1	0.5x16	100	160
13	15	0.5	0.5x16	100	160
14	15	0.75	0.5x16	100	160
15	15	1	0.5x16	100	160
16	27	0.5	0.5x16	100	160
17	27	0.75	0.5x16	100	160
18	27	1	0.5x16	100	160
19	0	0.5	0.5x16	100	200
20	0	0.75	0.5x16	100	200
21	0	1	0.5x16	100	200
22	15	0.5	0.5x16	100	200
23	15	0.75	0.5x16	100	200
24	15	1	0.5x16	100	200
25	27	0.5	0.5x16	100	200
26	27	0.75	0.5x16	100	200
27	27	1	0.5x16	100	200
28	0	0.5	0.5x16	120	120
29	0	0.75	0.5x16	120	120
30	0	1	0.5x16	120	120
31	15	0.5	0.5x16	120	120
32	15	0.75	0.5x16	120	120
33	15	1	0.5x16	120	120
34	27	0.5	0.5x16	120	120
35	27	0.75	0.5x16	120	120
36	27	1	0.5x16	120	120
37	0	0.5	0.5x16	120	160
38	0	0.75	0.5x16	120	160
39	0	1	0.5x16	120	160
40	15	0.5	0.5x16	120	160
41	15	0.75	0.5x16	120	160
42	15	1	0.5x16	120	160

Continued **(Table C - 2)**

No	Angle	Rot. Time (Secs)	Slice thickness (mm)	KV	mA (fixed)
43	27	0.5	0.5x16	120	160
44	27	0.75	0.5x16	120	160
45	27	1	0.5x16	120	160
46	0	0.5	0.5x16	120	200
47	0	0.75	0.5x16	120	200
48	0	1	0.5x16	120	200
49	15	0.5	0.5x16	120	200
50	15	0.75	0.5x16	120	200
51	15	1	0.5x16	120	200
52	27	0.5	0.5x16	120	200
53	27	0.75	0.5x16	120	200
54	27	1	0.5x16	120	200

Appendix D: Tables and graphs of adult helical effective dose results obtained using MOSFET

Table D - 1: Adult helical effective dose calculated for 0.5 CT gantry rotation time and CT gantry angle of 0°.			
Detector Configuration (mm)	**Pitch Factors / Helical Pitch**	**Sure Exp. 3D (ATC)**	**ED (mSv)**
0.5x16	Detail PF 0.688 / HP 11.0	High Quality SD 1.80	**0.71**
0.5x16	Detail PF 0.688 / HP 11.0	Standard SD 2.00	**0.70**
0.5x16	Detail PF 0.688 / HP 11.0	Low Dose SD 2.20	**0.70**
0.5x16	Standard PF 0.938 / HP 15.0	High Quality SD 1.80	**0.63**
0.5x16	Standard PF 0.938 / HP 15.0	Standard SD 2.00	**0.56**
0.5x16	Standard PF 0.938 / HP 15.0	Low Dose SD 2.20	**0.55**
0.5x16	Fast PF 1.438 / HP 23.0	High Quality SD 1.80	**0.46**
0.5x16	Fast PF 1.438 / HP 23.0	Standard SD 2.00	**0.45**
0.5x16	Fast PF 1.438 / HP 23.0	Low Dose SD 2.20	**0.43**
1.0x16	Detail PF 0.688 / HP 11.0	High Quality SD 1.80	**0.76**
1.0x16	Detail PF 0.688 / HP 11.0	Standard SD 2.00	**0.74**
1.0x16	Detail PF 0.688 / HP 11.0	Low Dose SD 2.20	**0.75**
1.0x16	Standard PF 0.938 / HP 15.0	High Quality SD 1.80	**0.64**
1.0x16	Standard PF 0.938 / HP 15.0	Standard SD 2.00	**0.61**
1.0x16	Standard PF 0.938 / HP 15.0	Low Dose SD 2.20	**0.55**
1.0x16	Fast PF 1.438 / HP 23.0	High Quality SD 1.80	**0.48**
1.0x16	Fast PF 1.438 / HP 23.0	Standard SD 2.00	**0.46**
1.0x16	Fast PF 1.438 / HP 23.0	Low Dose SD 2.20	**0.43**
2.0x16	Detail PF 0.688 / HP 11.0	High Quality SD 1.80	**0.73**
2.0x16	Detail PF 0.688 / HP 11.0	Standard SD 2.00	**0.71**
2.0x16	Detail PF 0.688 / HP 11.0	Low Dose SD 2.20	**0.63**
2.0x16	Standard PF 0.938 / HP 15.0	High Quality SD 1.80	**0.67**
2.0x16	Standard PF 0.938 / HP 15.0	Standard SD 2.00	**0.69**
2.0x16	Standard PF 0.938 / HP 15.0	Low Dose SD 2.20	**0.63**
2.0x16	Fast PF 1.438 / HP 23.0	High Quality SD 1.80	**0.62**
2.0x16	Fast PF 1.438 / HP 23.0	Standard SD 2.00	**0.62**
2.0x16	Fast PF 1.438 / HP 23.0	Low Dose SD 2.20	**0.56**
PF = Pitch Factor HP = Helical Pitch			

Table D - 2: Adult helical effective dose calculated for 1.0 CT gantry rotation time and CT gantry angle of 0^{o}.			
Detector Configuration (mm)	**Pitch Factors / Helical Pitch**	**Sure Exp. 3D (ATC)**	**ED (mSv)**
0.5x16	Detail PF 0.688 / HP 11.0	High Quality SD 1.80	**1.17**
0.5x16	Detail PF 0.688 / HP 11.0	Standard SD 2.00	**1.03**
0.5x16	Detail PF 0.688 / HP 11.0	Low Dose SD 2.20	**0.98**
0.5x16	Standard PF 0.938 / HP 15.0	High Quality SD 1.80	**0.91**
0.5x16	Standard PF 0.938 / HP 15.0	Standard SD 2.00	**0.82**
0.5x16	Standard PF 0.938 / HP 15.0	Low Dose SD 2.20	**0.78**
0.5x16	Fast PF 1.438 / HP 23.0	High Quality SD 1.80	**0.83**
0.5x16	Fast PF 1.438 / HP 23.0	Standard SD 2.00	**0.74**
0.5x16	Fast PF 1.438 / HP 23.0	Low Dose SD 2.20	**0.64**
1.0x16	Detail PF 0.688 / HP 11.0	High Quality SD 1.80	**1.24**
1.0x16	Detail PF 0.688 / HP 11.0	Standard SD 2.00	**1.20**
1.0x16	Detail PF 0.688 / HP 11.0	Low Dose SD 2.20	**0.92**
1.0x16	Standard PF 0.938 / HP 15.0	High Quality SD 1.80	**1.08**
1.0x16	Standard PF 0.938 / HP 15.0	Standard SD 2.00	**0.93**
1.0x16	Standard PF 0.938 / HP 15.0	Low Dose SD 2.20	**0.95**
1.0x16	Fast PF 1.438 / HP 23.0	High Quality SD 1.80	**0.89**
1.0x16	Fast PF 1.438 / HP 23.0	Standard SD 2.00	**0.77**
1.0x16	Fast PF 1.438 / HP 23.0	Low Dose SD 2.20	**0.75**
2.0x16	Detail PF 0.688 / HP 11.0	High Quality SD 1.80	**1.11**
2.0x16	Detail PF 0.688 / HP 11.0	Standard SD 2.00	**1.08**
2.0x16	Detail PF 0.688 / HP 11.0	Low Dose SD 2.20	**0.86**
2.0x16	Standard PF 0.938 / HP 15.0	High Quality SD 1.80	**1.08**
2.0x16	Standard PF 0.938 / HP 15.0	Standard SD 2.00	**1.01**
2.0x16	Standard PF 0.938 / HP 15.0	Low Dose SD 2.20	**0.76**
2.0x16	Fast PF 1.438 / HP 23.0	High Quality SD 1.80	**1.11**
2.0x16	Fast PF 1.438 / HP 23.0	Standard SD 2.00	**1.12**
2.0x16	Fast PF 1.438 / HP 23.0	Low Dose SD 2.20	**0.84**
PF = Pitch Factor HP = Helical Pitch			

Table D - 3: Adult helical effective dose calculated for 0.5 CT gantry rotation time and CT gantry angle of 15°.			
Detector Configuration (mm)	**Pitch Factors / Helical Pitch**	**Sure Exp. 3D (ATC)**	**ED (mSv)**
0.5x16	Detail PF 0.688 / HP 11.0	High Quality SD 1.80	**0.81**
0.5x16	Detail PF 0.688 / HP 11.0	Standard SD 2.00	**0.72**
0.5x16	Detail PF 0.688 / HP 11.0	Low Dose SD 2.20	**0.68**
0.5x16	Standard PF 0.938 / HP 15.0	High Quality SD 1.80	**0.58**
0.5x16	Standard PF 0.938 / HP 15.0	Standard SD 2.00	**0.57**
0.5x16	Standard PF 0.938 / HP 15.0	Low Dose SD 2.20	**0.52**
0.5x16	Fast PF 1.438 / HP 23.0	High Quality SD 1.80	**0.43**
0.5x16	Fast PF 1.438 / HP 23.0	Standard SD 2.00	**0.41**
0.5x16	Fast PF 1.438 / HP 23.0	Low Dose SD 2.20	**0.39**
1.0x16	Detail PF 0.688 / HP 11.0	High Quality SD 1.80	**0.70**
1.0x16	Detail PF 0.688 / HP 11.0	Standard SD 2.00	**0.69**
1.0x16	Detail PF 0.688 / HP 11.0	Low Dose SD 2.20	**0.64**
1.0x16	Standard PF 0.938 / HP 15.0	High Quality SD 1.80	**0.55**
1.0x16	Standard PF 0.938 / HP 15.0	Standard SD 2.00	**0.52**
1.0x16	Standard PF 0.938 / HP 15.0	Low Dose SD 2.20	**0.53**
1.0x16	Fast PF 1.438 / HP 23.0	High Quality SD 1.80	**0.39**
1.0x16	Fast PF 1.438 / HP 23.0	Standard SD 2.00	**0.38**
1.0x16	Fast PF 1.438 / HP 23.0	Low Dose SD 2.20	**0.34**
2.0x16	Detail PF 0.688 / HP 11.0	High Quality SD 1.80	**0.79**
2.0x16	Detail PF 0.688 / HP 11.0	Standard SD 2.00	**0.67**
2.0x16	Detail PF 0.688 / HP 11.0	Low Dose SD 2.20	**0.60**
2.0x16	Standard PF 0.938 / HP 15.0	High Quality SD 1.80	**0.68**
2.0x16	Standard PF 0.938 / HP 15.0	Standard SD 2.00	**0.60**
2.0x16	Standard PF 0.938 / HP 15.0	Low Dose SD 2.20	**0.47**
2.0x16	Fast PF 1.438 / HP 23.0	High Quality SD 1.80	**0.51**
2.0x16	Fast PF 1.438 / HP 23.0	Standard SD 2.00	**0.51**
2.0x16	Fast PF 1.438 / HP 23.0	Low Dose SD 2.20	**0.43**
PF = Pitch Factor HP = Helical Pitch			

Table D - 4: Adult helical effective dose calculated for 1.0 CT gantry rotation time and CT gantry angle of 15°.			
Detector Configuration (mm)	**Pitch Factors / Helical Pitch**	**Sure Exp. 3D (ATC)**	**ED (mSv)**
0.5x16	Detail PF 0.688 / HP 11.0	High Quality SD 1.80	**1.25**
0.5x16	Detail PF 0.688 / HP 11.0	Standard SD 2.00	**0.99**
0.5x16	Detail PF 0.688 / HP 11.0	Low Dose SD 2.20	**0.78**
0.5x16	Standard PF 0.938 / HP 15.0	High Quality SD 1.80	**0.99**
0.5x16	Standard PF 0.938 / HP 15.0	Standard SD 2.00	**0.84**
0.5x16	Standard PF 0.938 / HP 15.0	Low Dose SD 2.20	**0.73**
0.5x16	Fast PF 1.438 / HP 23.0	High Quality SD 1.80	**0.84**
0.5x16	Fast PF 1.438 / HP 23.0	Standard SD 2.00	**0.74**
0.5x16	Fast PF 1.438 / HP 23.0	Low Dose SD 2.20	**0.69**
1.0x16	Detail PF 0.688 / HP 11.0	High Quality SD 1.80	**1.35**
1.0x16	Detail PF 0.688 / HP 11.0	Standard SD 2.00	**1.18**
1.0x16	Detail PF 0.688 / HP 11.0	Low Dose SD 2.20	**1.08**
1.0x16	Standard PF 0.938 / HP 15.0	High Quality SD 1.80	**1.08**
1.0x16	Standard PF 0.938 / HP 15.0	Standard SD 2.00	**0.90**
1.0x16	Standard PF 0.938 / HP 15.0	Low Dose SD 2.20	**0.64**
1.0x16	Fast PF 1.438 / HP 23.0	High Quality SD 1.80	**0.70**
1.0x16	Fast PF 1.438 / HP 23.0	Standard SD 2.00	**0.71**
1.0x16	Fast PF 1.438 / HP 23.0	Low Dose SD 2.20	**0.66**
2.0x16	Detail PF 0.688 / HP 11.0	High Quality SD 1.80	**0.87**
2.0x16	Detail PF 0.688 / HP 11.0	Standard SD 2.00	**0.74**
2.0x16	Detail PF 0.688 / HP 11.0	Low Dose SD 2.20	**0.62**
2.0x16	Standard PF 0.938 / HP 15.0	High Quality SD 1.80	**0.77**
2.0x16	Standard PF 0.938 / HP 15.0	Standard SD 2.00	**0.64**
2.0x16	Standard PF 0.938 / HP 15.0	Low Dose SD 2.20	**0.58**
2.0x16	Fast PF 1.438 / HP 23.0	High Quality SD 1.80	**0.92**
2.0x16	Fast PF 1.438 / HP 23.0	Standard SD 2.00	**0.80**
2.0x16	Fast PF 1.438 / HP 23.0	Low Dose SD 2.20	**0.74**
PF = Pitch Factor HP = Helical Pitch			

Table D - 5: Adult helical effective dose calculated for 0.5 CT gantry rotation time and CT gantry angle of 27°.			
Detector Configuration (mm)	**Pitch Factors / Helical Pitch**	**Sure Exp. 3D (ATC)**	**ED (mSv)**
0.5x16	Detail PF 0.688 / HP 11.0	High Quality SD 1.80	**0.88**
0.5x16	Detail PF 0.688 / HP 11.0	Standard SD 2.00	**0.83**
0.5x16	Detail PF 0.688 / HP 11.0	Low Dose SD 2.20	**0.78**
0.5x16	Standard PF 0.938 / HP 15.0	High Quality SD 1.80	**0.70**
0.5x16	Standard PF 0.938 / HP 15.0	Standard SD 2.00	**0.66**
0.5x16	Standard PF 0.938 / HP 15.0	Low Dose SD 2.20	**0.57**
0.5x16	Fast PF 1.438 / HP 23.0	High Quality SD 1.80	**0.47**
0.5x16	Fast PF 1.438 / HP 23.0	Standard SD 2.00	**0.47**
0.5x16	Fast PF 1.438 / HP 23.0	Low Dose SD 2.20	**0.44**
1.0x16	Detail PF 0.688 / HP 11.0	High Quality SD 1.80	**0.81**
1.0x16	Detail PF 0.688 / HP 11.0	Standard SD 2.00	**0.76**
1.0x16	Detail PF 0.688 / HP 11.0	Low Dose SD 2.20	**0.67**
1.0x16	Standard PF 0.938 / HP 15.0	High Quality SD 1.80	**0.61**
1.0x16	Standard PF 0.938 / HP 15.0	Standard SD 2.00	**0.61**
1.0x16	Standard PF 0.938 / HP 15.0	Low Dose SD 2.20	**0.52**
1.0x16	Fast PF 1.438 / HP 23.0	High Quality SD 1.80	**0.45**
1.0x16	Fast PF 1.438 / HP 23.0	Standard SD 2.00	**0.42**
1.0x16	Fast PF 1.438 / HP 23.0	Low Dose SD 2.20	**0.42**
2.0x16	Detail PF 0.688 / HP 11.0	High Quality SD 1.80	**0.82**
2.0x16	Detail PF 0.688 / HP 11.0	Standard SD 2.00	**0.74**
2.0x16	Detail PF 0.688 / HP 11.0	Low Dose SD 2.20	**0.60**
2.0x16	Standard PF 0.938 / HP 15.0	High Quality SD 1.80	**0.71**
2.0x16	Standard PF 0.938 / HP 15.0	Standard SD 2.00	**0.64**
2.0x16	Standard PF 0.938 / HP 15.0	Low Dose SD 2.20	**0.58**
2.0x16	Fast PF 1.438 / HP 23.0	High Quality SD 1.80	**0.56**
2.0x16	Fast PF 1.438 / HP 23.0	Standard SD 2.00	**0.58**
2.0x16	Fast PF 1.438 / HP 23.0	Low Dose SD 2.20	**0.51**
PF = Pitch Factor HP = Helical Pitch			

Table D - 6: Adult helical effective dose calculated for 1.0 CT gantry rotation time and CT gantry angle of 27°.			
Detector Configuration (mm)	**Pitch Factors / Helical Pitch**	**Sure Exp. 3D (ATC)**	**ED (mSv)**
0.5x16	Detail PF 0.688 / HP 11.0	High Quality SD 1.80	**1.13**
0.5x16	Detail PF 0.688 / HP 11.0	Standard SD 2.00	**1.00**
0.5x16	Detail PF 0.688 / HP 11.0	Low Dose SD 2.20	**0.87**
0.5x16	Standard PF 0.938 / HP 15.0	High Quality SD 1.80	**1.01**
0.5x16	Standard PF 0.938 / HP 15.0	Standard SD 2.00	**0.83**
0.5x16	Standard PF 0.938 / HP 15.0	Low Dose SD 2.20	**0.75**
0.5x16	Fast PF 1.438 / HP 23.0	High Quality SD 1.80	**0.88**
0.5x16	Fast PF 1.438 / HP 23.0	Standard SD 2.00	**0.88**
0.5x16	Fast PF 1.438 / HP 23.0	Low Dose SD 2.20	**0.83**
1.0x16	Detail PF 0.688 / HP 11.0	High Quality SD 1.80	**1.55**
1.0x16	Detail PF 0.688 / HP 11.0	Standard SD 2.00	**1.28**
1.0x16	Detail PF 0.688 / HP 11.0	Low Dose SD 2.20	**1.10**
1.0x16	Standard PF 0.938 / HP 15.0	High Quality SD 1.80	**1.24**
1.0x16	Standard PF 0.938 / HP 15.0	Standard SD 2.00	**1.19**
1.0x16	Standard PF 0.938 / HP 15.0	Low Dose SD 2.20	**0.97**
1.0x16	Fast PF 1.438 / HP 23.0	High Quality SD 1.80	**0.87**
1.0x16	Fast PF 1.438 / HP 23.0	Standard SD 2.00	**0.79**
1.0x16	Fast PF 1.438 / HP 23.0	Low Dose SD 2.20	**0.77**
2.0x16	Detail PF 0.688 / HP 11.0	High Quality SD 1.80	**0.92**
2.0x16	Detail PF 0.688 / HP 11.0	Standard SD 2.00	**0.75**
2.0x16	Detail PF 0.688 / HP 11.0	Low Dose SD 2.20	**0.66**
2.0x16	Standard PF 0.938 / HP 15.0	High Quality SD 1.80	**0.76**
2.0x16	Standard PF 0.938 / HP 15.0	Standard SD 2.00	**0.75**
2.0x16	Standard PF 0.938 / HP 15.0	Low Dose SD 2.20	**0.56**
2.0x16	Fast PF 1.438 / HP 23.0	High Quality SD 1.80	**0.98**
2.0x16	Fast PF 1.438 / HP 23.0	Standard SD 2.00	**0.90**
2.0x16	Fast PF 1.438 / HP 23.0	Low Dose SD 2.20	**0.78**
PF = Pitch Factor HP = Helical Pitch			

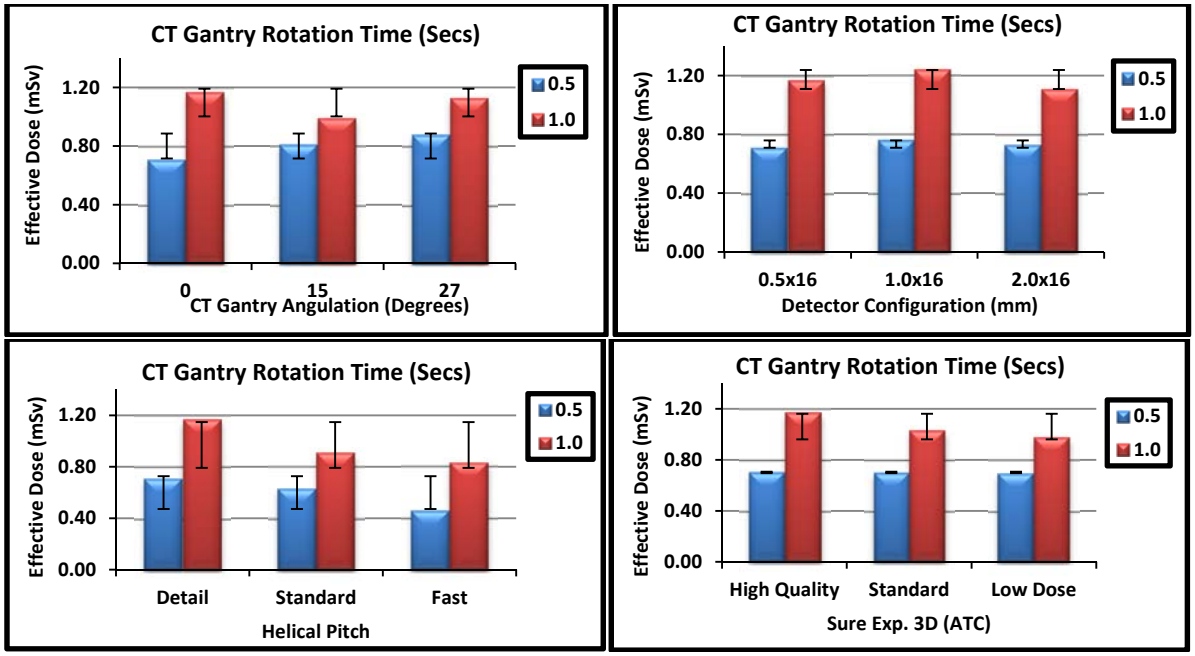

Figure D - 1: Graphs showing the relationship of CT gantry rotation time with detector configurations, CT gantry angulations, helical pitch and sure Exp. 3D (ATC).

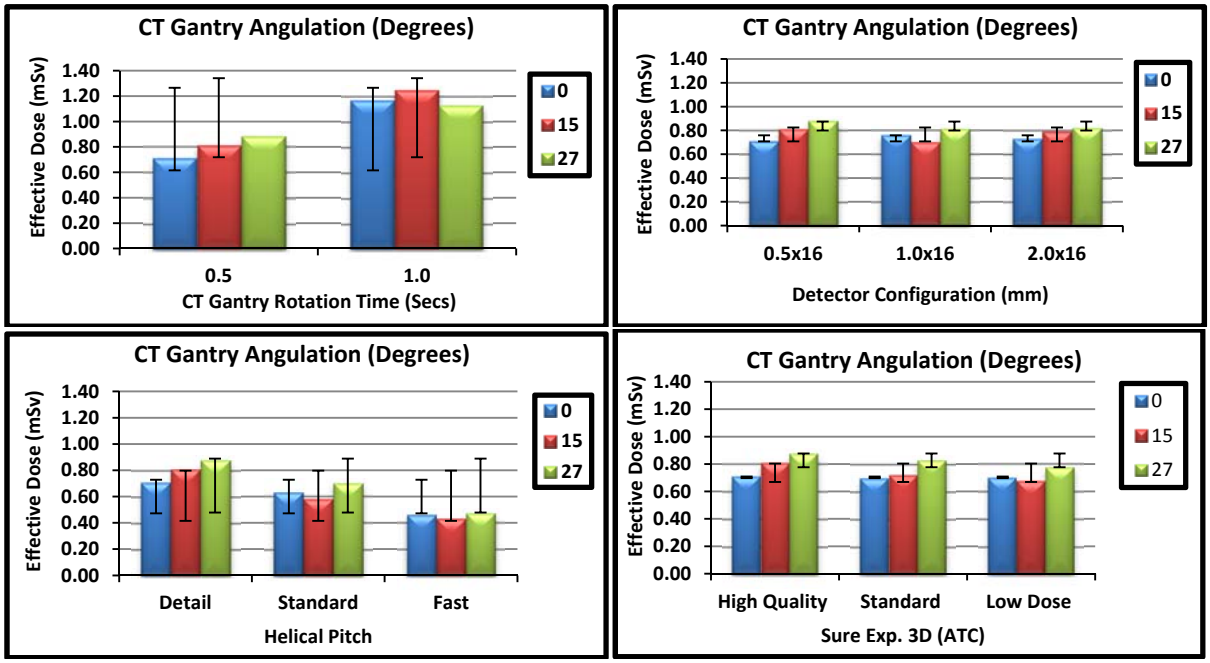

Figure D - 2: Graphs showing the relationship of CT gantry angulations with CT gantry rotation time, detector configurations, helical pitch and sure Exp. 3D (ATC).

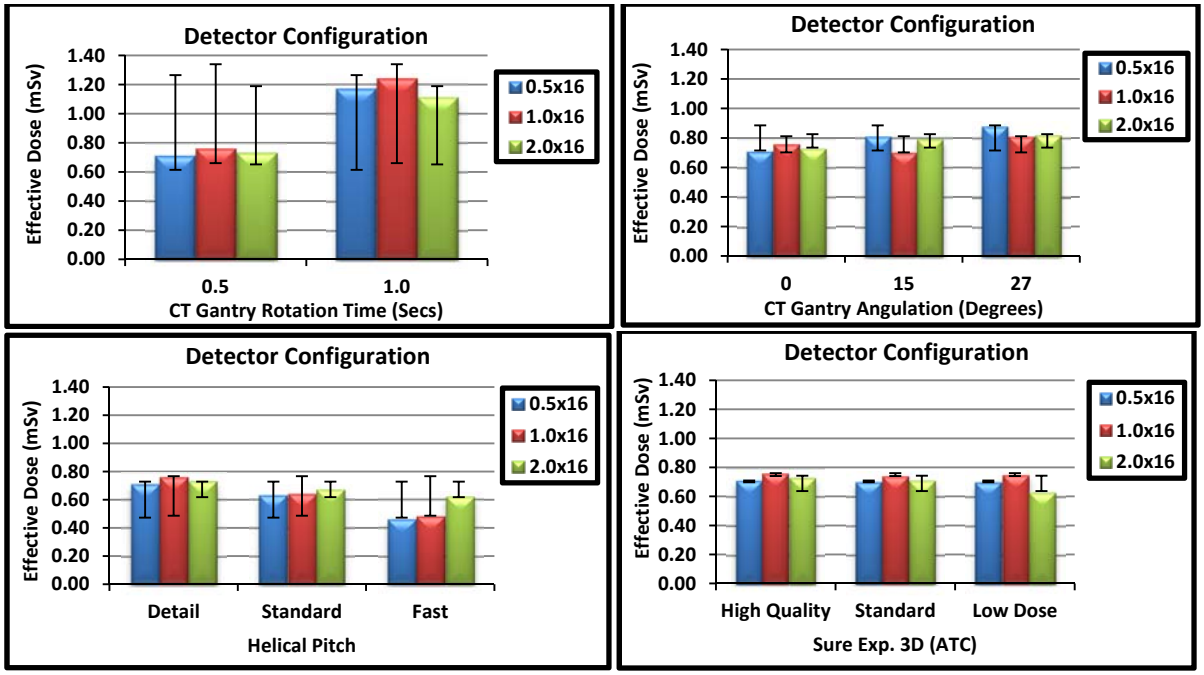

Figure D - 3: Graphs showing the relationship of detector configurations with CT gantry rotation time, CT gantry angulations, helical pitch and sure Exp. 3D (ATC).

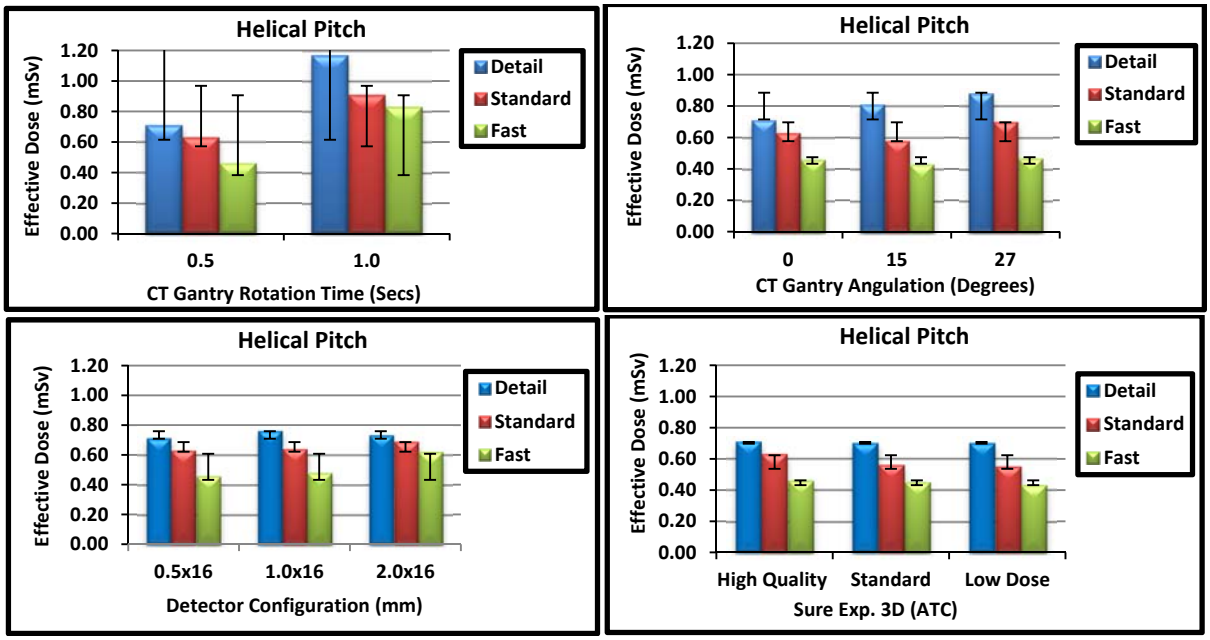

Figure D - 4: Graphs showing the relationship of helical pitch with CT gantry rotation time, CT gantry angulations, detector configurations and sure Exp. 3D (ATC).

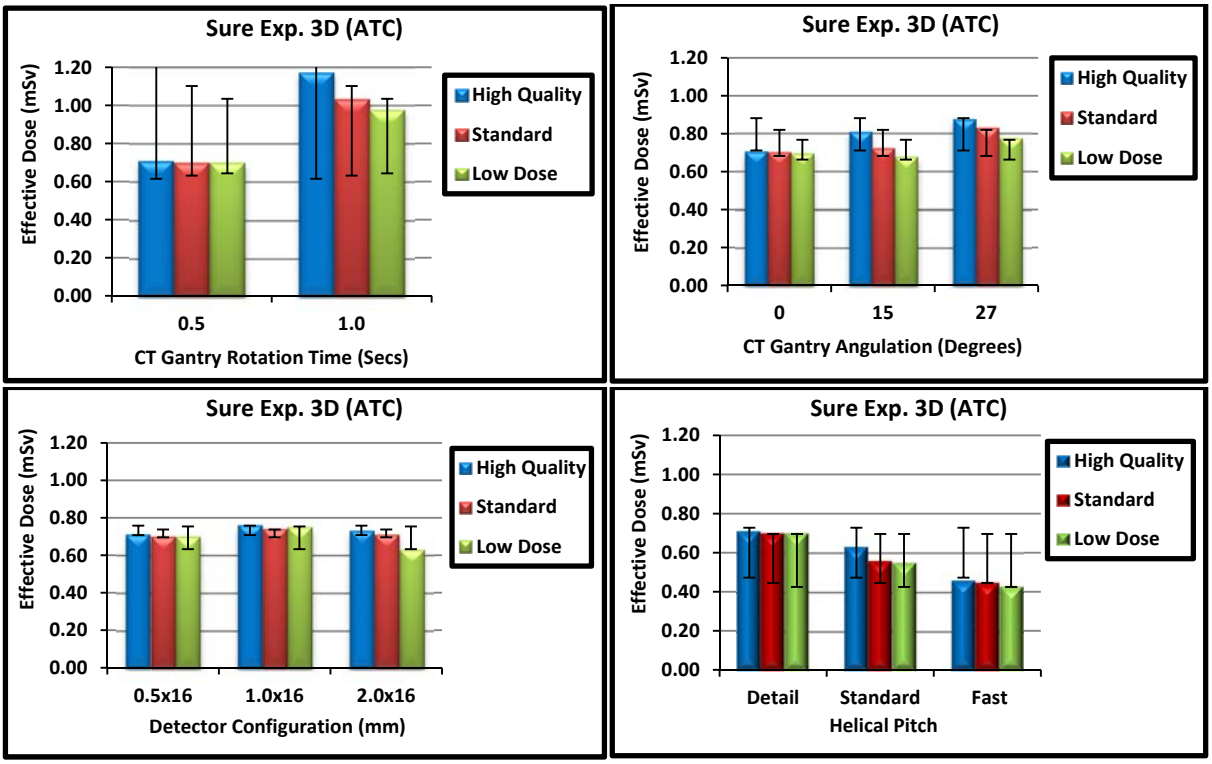

Figure D - 5: Graphs showing the relationship of helical pitch with CT gantry rotation time, CT gantry angulations, detector configurations and sure Exp. 3D (ATC).

Appendix E: Tables and graphs of adult sequential effective dose results obtained using MOSFET

Table E - 1: Sequential effective dose calculated for CT gantry angle of 0°.

Tube Rotation Time (S)	Detector Configuration (mm)	Sure Exp. 3D (ATC)	ED (mSv)
0.5	0.5x4	High Quality SD 1.80	**0.37**
0.5	0.5x4	Standard SD 2.00	**0.33**
0.5	0.5x4	Low Dose SD 2.20	**0.37**
0.5	1.0x4	High Quality SD 1.80	**0.43**
0.5	1.0x4	Standard SD 2.00	**0.36**
0.5	1.0x4	Low Dose SD 2.20	**0.40**
0.5	2.0x4	High Quality SD 1.80	**0.61**
0.5	2.0x4	Standard SD 2.00	**0.51**
0.5	2.0x4	Low Dose SD 2.20	**0.48**
1	0.5x4	High Quality SD 1.80	**0.55**
1	0.5x4	Standard SD 2.00	**0.54**
1	0.5x4	Low Dose SD 2.20	**0.52**
1	1.0x4	High Quality SD 1.80	**0.72**
1	1.0x4	Standard SD 2.00	**0.69**
1	1.0x4	Low Dose SD 2.20	**0.65**
1	2.0x4	High Quality SD 1.80	**0.98**
1	2.0x4	Standard SD 2.00	**0.85**
1	2.0x4	Low Dose SD 2.20	**0.77**

Table E - 2: Sequential effective dose calculated for CT gantry angle of 15°.

Tube Rotation Time (S)	Detector Configuration (mm)	Sure Exp. 3D (ATC)	ED (mSv)
0.5	0.5x4	High Quality SD 1.80	**0.30**
0.5	0.5x4	Standard SD 2.00	**0.32**
0.5	0.5x4	Low Dose SD 2.20	**0.27**
0.5	1.0x4	High Quality SD 1.80	**0.39**
0.5	1.0x4	Standard SD 2.00	**0.36**
0.5	1.0x4	Low Dose SD 2.20	**0.35**
0.5	2.0x4	High Quality SD 1.80	**0.51**
0.5	2.0x4	Standard SD 2.00	**0.49**
0.5	2.0x4	Low Dose SD 2.20	**0.47**
1	0.5x4	High Quality SD 1.80	**0.64**
1	0.5x4	Standard SD 2.00	**0.58**
1	0.5x4	Low Dose SD 2.20	**0.52**
1	1.0x4	High Quality SD 1.80	**0.71**
1	1.0x4	Standard SD 2.00	**0.65**
1	1.0x4	Low Dose SD 2.20	**0.66**
1	2.0x4	High Quality SD 1.80	**0.98**
1	2.0x4	Standard SD 2.00	**0.91**
1	2.0x4	Low Dose SD 2.20	**0.75**

Table E - 3: Sequential effective dose calculated for CT gantry angle of 27°.

Tube Rotation Time (S)	Detector Configuration (mm)	Sure Exp. 3D (ATC)	ED (mSv)
0.5	0.5x4	High Quality SD 1.80	**0.38**
0.5	0.5x4	Standard SD 2.00	**0.39**
0.5	0.5x4	Low Dose SD 2.20	**0.34**
0.5	1.0x4	High Quality SD 1.80	**0.44**
0.5	1.0x4	Standard SD 2.00	**0.43**
0.5	1.0x4	Low Dose SD 2.20	**0.39**
0.5	2.0x4	High Quality SD 1.80	**0.63**
0.5	2.0x4	Standard SD 2.00	**0.58**
0.5	2.0x4	Low Dose SD 2.20	**0.56**
1	0.5x4	High Quality SD 1.80	**0.75**
1	0.5x4	Standard SD 2.00	**0.66**
1	0.5x4	Low Dose SD 2.20	**0.63**
1	1.0x4	High Quality SD 1.80	**0.87**
1	1.0x4	Standard SD 2.00	**0.73**
1	1.0x4	Low Dose SD 2.20	**0.73**
1	2.0x4	High Quality SD 1.80	**1.13**
1	2.0x4	Standard SD 2.00	**0.96**
1	2.0x4	Low Dose SD 2.20	**0.78**

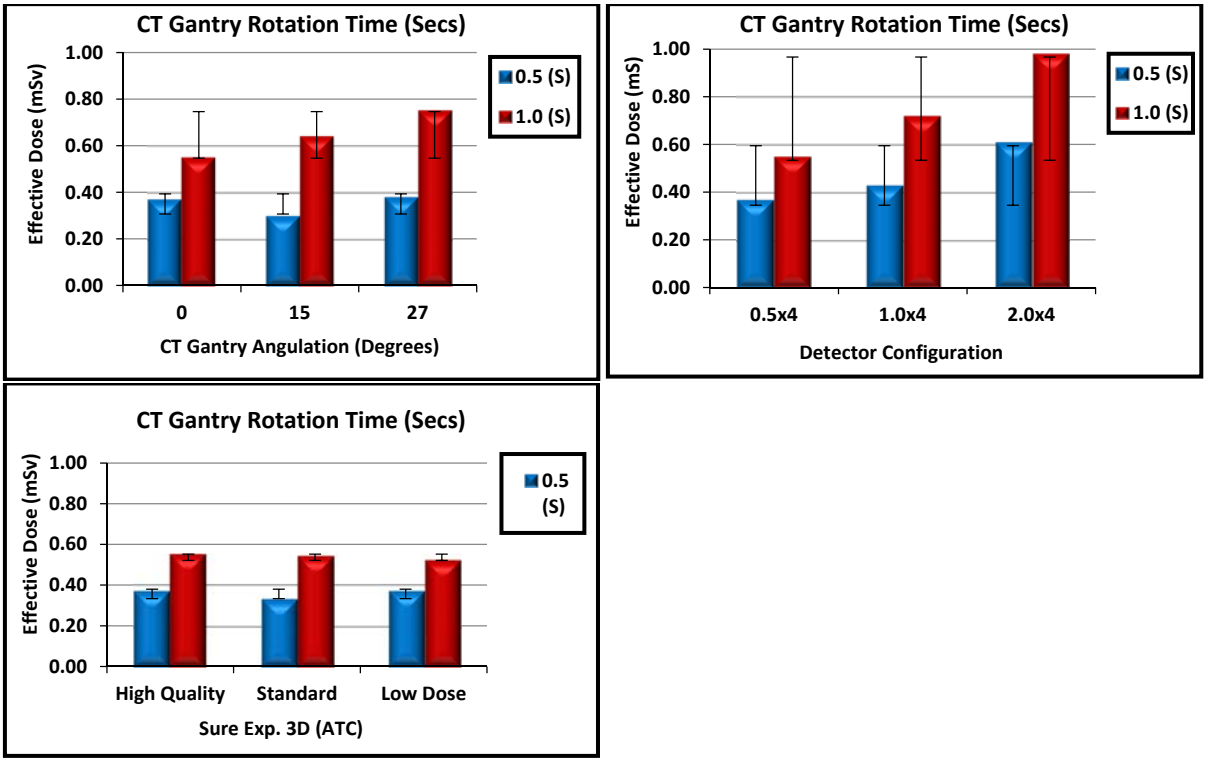

Figure E - 1: Graphs showing the relationship of CT gantry rotation time with CT gantry angulations, detector configurations and Sure Exp. 3D (ATC).

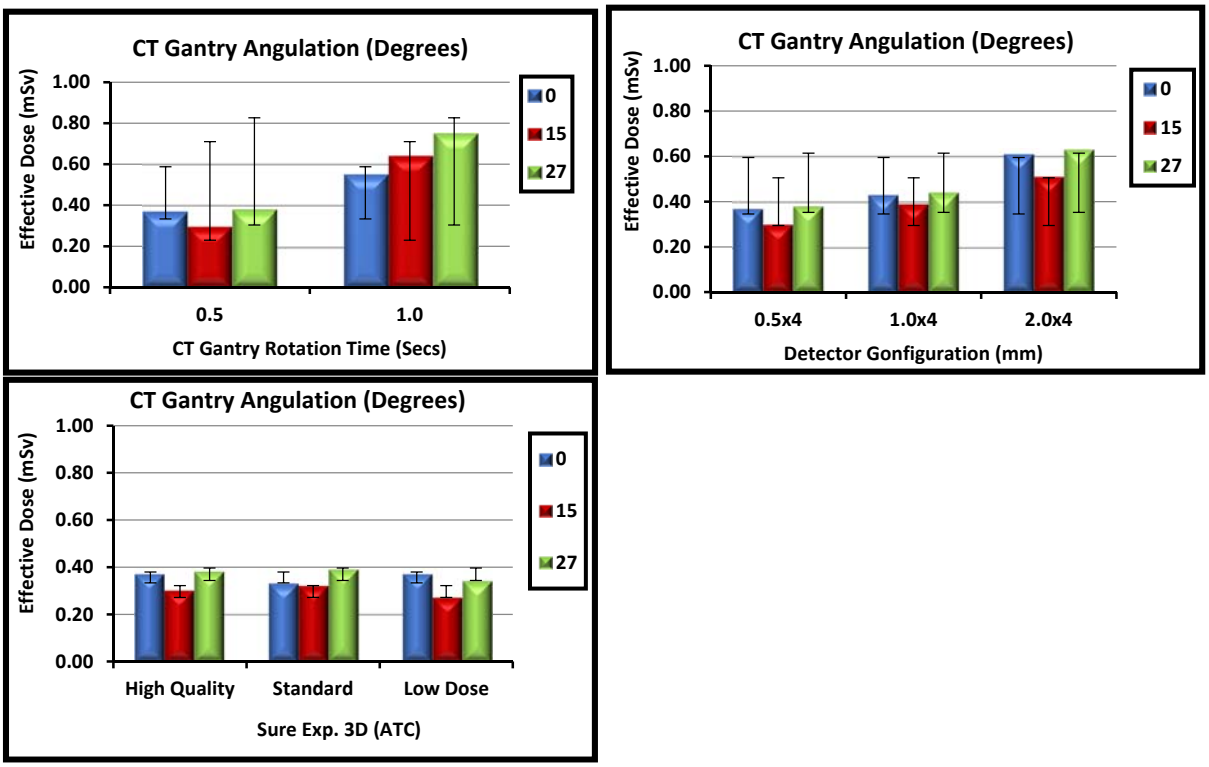

Figure E - 2: Graphs showing the relationship of CT gantry angulations with CT gantry rotation time, detector configurations and Sure Exp. 3D (ATC).

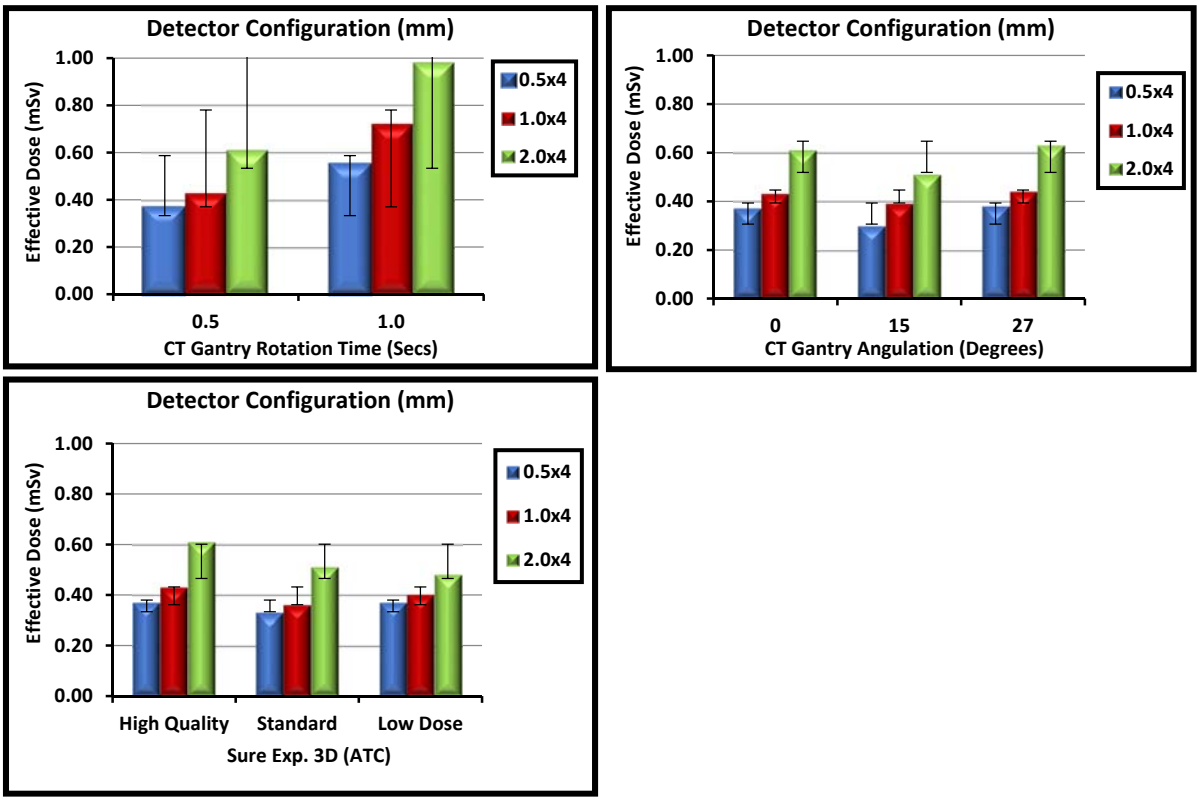

Figure E - 3: Graphs showing the relationship of detector configurations with CT gantry rotation time, CT gantry angulations, and Sure Exp. 3D (ATC).

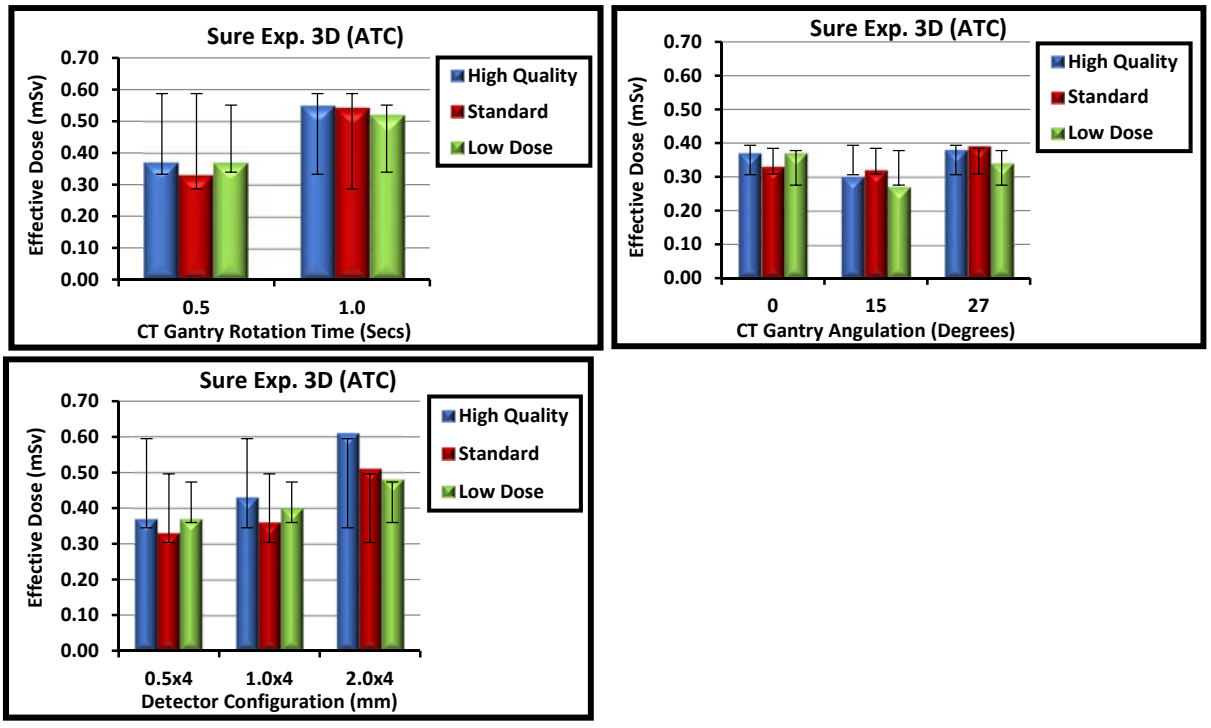

Figure E - 4: Graphs showing the relationship of sure Exp. 3D (ATC) with CT gantry rotation time, CT gantry angulations and detector configurations.

Appendix F: Tables and graphs of Paediatric helical effective dose results obtained using MOSFET

Table F - 1: Paediatric helical protocols effective dose calculated for 0.5 CT gantry rotation time and CT gantry angle of 0°.

Detector Configuration (mm)	Pitch Factors / Helical Pitch	Sure Exp. 3D (ATC)	ED (mSv)
0.5x16	Detail PF 0.688 / HP 11.0	High Quality SD 4.00	**2.01**
0.5x16	Detail PF 0.688 / HP 11.0	Standard SD 6.00	**1.08**
0.5x16	Detail PF 0.688 / HP 11.0	Low Dose SD 8.00	**0.68**
0.5x16	Standard PF 0.938 / HP 15.0	High Quality SD 4.00	**1.71**
0.5x16	Standard PF 0.938 / HP 15.0	Standard SD 6.00	**1.02**
0.5x16	Standard PF 0.938 / HP 15.0	Low Dose SD 8.00	**0.62**
0.5x16	Fast PF 1.438 / HP 23.0	High Quality SD 4.00	**1.58**
0.5x16	Fast PF 1.438 / HP 23.0	Standard SD 6.00	**1.15**
0.5x16	Fast PF 1.438 / HP 23.0	Low Dose SD 8.00	**0.77**
1.0x16	Detail PF 0.688 / HP 11.0	High Quality SD 4.00	**1.02**
1.0x16	Detail PF 0.688 / HP 11.0	Standard SD 6.00	**0.59**
1.0x16	Detail PF 0.688 / HP 11.0	Low Dose SD 8.00	**0.41**
1.0x16	Standard PF 0.938 / HP 15.0	High Quality SD 4.00	**1.00**
1.0x16	Standard PF 0.938 / HP 15.0	Standard SD 6.00	**0.53**
1.0x16	Standard PF 0.938 / HP 15.0	Low Dose SD 8.00	**0.40**
1.0x16	Fast PF 1.438 / HP 23.0	High Quality SD 4.00	**1.22**
1.0x16	Fast PF 1.438 / HP 23.0	Standard SD 6.00	**0.69**
1.0x16	Fast PF 1.438 / HP 23.0	Low Dose SD 8.00	**0.43**
2.0x16	Detail PF 0.688 / HP 11.0	High Quality SD 4.00	**0.71**
2.0x16	Detail PF 0.688 / HP 11.0	Standard SD 6.00	**0.42**
2.0x16	Detail PF 0.688 / HP 11.0	Low Dose SD 8.00	**0.33**
2.0x16	Standard PF 0.938 / HP 15.0	High Quality SD 4.00	**0.65**
2.0x16	Standard PF 0.938 / HP 15.0	Standard SD 6.00	**0.39**
2.0x16	Standard PF 0.938 / HP 15.0	Low Dose SD 8.00	**0.31**
2.0x16	Fast PF 1.438 / HP 23.0	High Quality SD 4.00	**0.75**
2.0x16	Fast PF 1.438 / HP 23.0	Standard SD 6.00	**0.46**
2.0x16	Fast PF 1.438 / HP 23.0	Low Dose SD 8.00	**0.33**

PF = Pitch Factor
HP = Helical Pitch

Table F - 2: Paediatric helical protocols effective dose calculated for 0.75 CT gantry rotation time and CT gantry angle of 0°.

Detector Configuration (mm)	Pitch Factors / Helical Pitch	Sure Exp. 3D (ATC)	ED (mSv)
0.5x16	Detail PF 0.688 / HP 11.0	High Quality SD 4.00	**1.95**
0.5x16	Detail PF 0.688 / HP 11.0	Standard SD 6.00	**1.06**
0.5x16	Detail PF 0.688 / HP 11.0	Low Dose SD 8.00	**0.71**
0.5x16	Standard PF 0.938 / HP 15.0	High Quality SD 4.00	**1.74**
0.5x16	Standard PF 0.938 / HP 15.0	Standard SD 6.00	**0.93**
0.5x16	Standard PF 0.938 / HP 15.0	Low Dose SD 8.00	**0.61**
0.5x16	Fast PF 1.438 / HP 23.0	High Quality SD 4.00	**2.06**
0.5x16	Fast PF 1.438 / HP 23.0	Standard SD 6.00	**1.14**
0.5x16	Fast PF 1.438 / HP 23.0	Low Dose SD 8.00	**0.75**
1.0x16	Detail PF 0.688 / HP 11.0	High Quality SD 4.00	**1.05**
1.0x16	Detail PF 0.688 / HP 11.0	Standard SD 6.00	**0.62**
1.0x16	Detail PF 0.688 / HP 11.0	Low Dose SD 8.00	**0.45**
1.0x16	Standard PF 0.938 / HP 15.0	High Quality SD 4.00	**1.02**
1.0x16	Standard PF 0.938 / HP 15.0	Standard SD 6.00	**0.58**
1.0x16	Standard PF 0.938 / HP 15.0	Low Dose SD 8.00	**0.40**
1.0x16	Fast PF 1.438 / HP 23.0	High Quality SD 4.00	**1.25**
1.0x16	Fast PF 1.438 / HP 23.0	Standard SD 6.00	**0.64**
1.0x16	Fast PF 1.438 / HP 23.0	Low Dose SD 8.00	**0.46**
2.0x16	Detail PF 0.688 / HP 11.0	High Quality SD 4.00	**0.72**
2.0x16	Detail PF 0.688 / HP 11.0	Standard SD 6.00	**0.44**
2.0x16	Detail PF 0.688 / HP 11.0	Low Dose SD 8.00	**0.37**
2.0x16	Standard PF 0.938 / HP 15.0	High Quality SD 4.00	**0.62**
2.0x16	Standard PF 0.938 / HP 15.0	Standard SD 6.00	**0.40**
2.0x16	Standard PF 0.938 / HP 15.0	Low Dose SD 8.00	**0.35**
2.0x16	Fast PF 1.438 / HP 23.0	High Quality SD 4.00	**0.85**
2.0x16	Fast PF 1.438 / HP 23.0	Standard SD 6.00	**0.51**
2.0x16	Fast PF 1.438 / HP 23.0	Low Dose SD 8.00	**0.35**

PF = Pitch Factor
HP = Helical Pitch

Table F - 3: Paediatric helical protocols effective dose calculated for 0.5 CT gantry rotation time and CT gantry angle of 15º.

Detector Configuration (mm)	Pitch Factors / Helical Pitch	Sure Exp. 3D (ATC)	ED (mSv)
0.5x16	Detail PF 0.688 / HP 11.0	High Quality SD 4.00	**1.82**
0.5x16	Detail PF 0.688 / HP 11.0	Standard SD 6.00	**0.99**
0.5x16	Detail PF 0.688 / HP 11.0	Low Dose SD 8.00	**0.61**
0.5x16	Standard PF 0.938 / HP 15.0	High Quality SD 4.00	**1.58**
0.5x16	Standard PF 0.938 / HP 15.0	Standard SD 6.00	**0.91**
0.5x16	Standard PF 0.938 / HP 15.0	Low Dose SD 8.00	**0.57**
0.5x16	Fast PF 1.438 / HP 23.0	High Quality SD 4.00	**1.52**
0.5x16	Fast PF 1.438 / HP 23.0	Standard SD 6.00	**0.95**
0.5x16	Fast PF 1.438 / HP 23.0	Low Dose SD 8.00	**0.68**
1.0x16	Detail PF 0.688 / HP 11.0	High Quality SD 4.00	**0.98**
1.0x16	Detail PF 0.688 / HP 11.0	Standard SD 6.00	**0.51**
1.0x16	Detail PF 0.688 / HP 11.0	Low Dose SD 8.00	**0.39**
1.0x16	Standard PF 0.938 / HP 15.0	High Quality SD 4.00	**0.86**
1.0x16	Standard PF 0.938 / HP 15.0	Standard SD 6.00	**0.53**
1.0x16	Standard PF 0.938 / HP 15.0	Low Dose SD 8.00	**0.38**
1.0x16	Fast PF 1.438 / HP 23.0	High Quality SD 4.00	**1.15**
1.0x16	Fast PF 1.438 / HP 23.0	Standard SD 6.00	**0.62**
1.0x16	Fast PF 1.438 / HP 23.0	Low Dose SD 8.00	**0.47**
2.0x16	Detail PF 0.688 / HP 11.0	High Quality SD 4.00	**0.63**
2.0x16	Detail PF 0.688 / HP 11.0	Standard SD 6.00	**0.40**
2.0x16	Detail PF 0.688 / HP 11.0	Low Dose SD 8.00	**0.32**
2.0x16	Standard PF 0.938 / HP 15.0	High Quality SD 4.00	**0.62**
2.0x16	Standard PF 0.938 / HP 15.0	Standard SD 6.00	**0.40**
2.0x16	Standard PF 0.938 / HP 15.0	Low Dose SD 8.00	**0.30**
2.0x16	Fast PF 1.438 / HP 23.0	High Quality SD 4.00	**0.81**
2.0x16	Fast PF 1.438 / HP 23.0	Standard SD 6.00	**0.44**
2.0x16	Fast PF 1.438 / HP 23.0	Low Dose SD 8.00	**0.36**

PF = Pitch Factor
HP = Helical Pitch

Table F - 4: Paediatric helical protocols effective dose calculated for 0.75 CT gantry rotation time and CT gantry angle of 15º.

Detector Configuration (mm)	Pitch Factors / Helical Pitch	Sure Exp. 3D (ATC)	ED (mSv)
0.5x16	Detail PF 0.688 / HP 11.0	High Quality SD 4.00	**1.76**
0.5x16	Detail PF 0.688 / HP 11.0	Standard SD 6.00	**1.01**
0.5x16	Detail PF 0.688 / HP 11.0	Low Dose SD 8.00	**0.64**
0.5x16	Standard PF 0.938 / HP 15.0	High Quality SD 4.00	**1.59**
0.5x16	Standard PF 0.938 / HP 15.0	Standard SD 6.00	**0.83**
0.5x16	Standard PF 0.938 / HP 15.0	Low Dose SD 8.00	**0.57**
0.5x16	Fast PF 1.438 / HP 23.0	High Quality SD 4.00	**1.78**
0.5x16	Fast PF 1.438 / HP 23.0	Standard SD 6.00	**0.98**
0.5x16	Fast PF 1.438 / HP 23.0	Low Dose SD 8.00	**0.66**
1.0x16	Detail PF 0.688 / HP 11.0	High Quality SD 4.00	**0.93**
1.0x16	Detail PF 0.688 / HP 11.0	Standard SD 6.00	**0.53**
1.0x16	Detail PF 0.688 / HP 11.0	Low Dose SD 8.00	**0.42**
1.0x16	Standard PF 0.938 / HP 15.0	High Quality SD 4.00	**0.91**
1.0x16	Standard PF 0.938 / HP 15.0	Standard SD 6.00	**0.52**
1.0x16	Standard PF 0.938 / HP 15.0	Low Dose SD 8.00	**0.36**
1.0x16	Fast PF 1.438 / HP 23.0	High Quality SD 4.00	**1.21**
1.0x16	Fast PF 1.438 / HP 23.0	Standard SD 6.00	**0.62**
1.0x16	Fast PF 1.438 / HP 23.0	Low Dose SD 8.00	**0.46**
2.0x16	Detail PF 0.688 / HP 11.0	High Quality SD 4.00	**0.69**
2.0x16	Detail PF 0.688 / HP 11.0	Standard SD 6.00	**0.41**
2.0x16	Detail PF 0.688 / HP 11.0	Low Dose SD 8.00	**0.31**
2.0x16	Standard PF 0.938 / HP 15.0	High Quality SD 4.00	**0.65**
2.0x16	Standard PF 0.938 / HP 15.0	Standard SD 6.00	**0.39**
2.0x16	Standard PF 0.938 / HP 15.0	Low Dose SD 8.00	**0.33**
2.0x16	Fast PF 1.438 / HP 23.0	High Quality SD 4.00	**0.82**
2.0x16	Fast PF 1.438 / HP 23.0	Standard SD 6.00	**0.49**
2.0x16	Fast PF 1.438 / HP 23.0	Low Dose SD 8.00	**0.36**

PF = Pitch Factor
HP = Helical Pitch

Table F - 5: Paediatric helical protocols effective dose calculated for 0.5 CT gantry rotation time and CT gantry angle of 27º.			
Detector Configuration (mm)	**Pitch Factors / Helical Pitch**	**Sure Exp. 3D (ATC)**	**ED (mSv)**
0.5x16	Detail PF 0.688 / HP 11.0	High Quality SD 4.00	**1.73**
0.5x16	Detail PF 0.688 / HP 11.0	Standard SD 6.00	**0.90**
0.5x16	Detail PF 0.688 / HP 11.0	Low Dose SD 8.00	**0.60**
0.5x16	Standard PF 0.938 / HP 15.0	High Quality SD 4.00	**1.50**
0.5x16	Standard PF 0.938 / HP 15.0	Standard SD 6.00	**0.82**
0.5x16	Standard PF 0.938 / HP 15.0	Low Dose SD 8.00	**0.56**
0.5x16	Fast PF 1.438 / HP 23.0	High Quality SD 4.00	**1.49**
0.5x16	Fast PF 1.438 / HP 23.0	Standard SD 6.00	**0.99**
0.5x16	Fast PF 1.438 / HP 23.0	Low Dose SD 8.00	**0.62**
1.0x16	Detail PF 0.688 / HP 11.0	High Quality SD 4.00	**0.93**
1.0x16	Detail PF 0.688 / HP 11.0	Standard SD 6.00	**0.54**
1.0x16	Detail PF 0.688 / HP 11.0	Low Dose SD 8.00	**0.34**
1.0x16	Standard PF 0.938 / HP 15.0	High Quality SD 4.00	**0.85**
1.0x16	Standard PF 0.938 / HP 15.0	Standard SD 6.00	**0.46**
1.0x16	Standard PF 0.938 / HP 15.0	Low Dose SD 8.00	**0.31**
1.0x16	Fast PF 1.438 / HP 23.0	High Quality SD 4.00	**1.06**
1.0x16	Fast PF 1.438 / HP 23.0	Standard SD 6.00	**0.59**
1.0x16	Fast PF 1.438 / HP 23.0	Low Dose SD 8.00	**0.39**
2.0x16	Detail PF 0.688 / HP 11.0	High Quality SD 4.00	**0.66**
2.0x16	Detail PF 0.688 / HP 11.0	Standard SD 6.00	**0.37**
2.0x16	Detail PF 0.688 / HP 11.0	Low Dose SD 8.00	**0.30**
2.0x16	Standard PF 0.938 / HP 15.0	High Quality SD 4.00	**0.66**
2.0x16	Standard PF 0.938 / HP 15.0	Standard SD 6.00	**0.35**
2.0x16	Standard PF 0.938 / HP 15.0	Low Dose SD 8.00	**0.28**
2.0x16	Fast PF 1.438 / HP 23.0	High Quality SD 4.00	**0.85**
2.0x16	Fast PF 1.438 / HP 23.0	Standard SD 6.00	**0.53**
2.0x16	Fast PF 1.438 / HP 23.0	Low Dose SD 8.00	**0.37**
PF = Pitch Factor HP = Helical Pitch			

Table F - 6: Paediatric helical protocols effective dose calculated for 0.75 CT gantry rotation time and CT gantry angle of 27º**.**			
Detector Configuration (mm)	**Pitch Factors / Helical Pitch**	**Sure Exp. 3D (ATC)**	**ED (mSv)**
0.5x16	Detail PF 0.688 / HP 11.0	High Quality SD 4.00	**1.73**
0.5x16	Detail PF 0.688 / HP 11.0	Standard SD 6.00	**0.89**
0.5x16	Detail PF 0.688 / HP 11.0	Low Dose SD 8.00	**0.62**
0.5x16	Standard PF 0.938 / HP 15.0	High Quality SD 4.00	**1.51**
0.5x16	Standard PF 0.938 / HP 15.0	Standard SD 6.00	**0.82**
0.5x16	Standard PF 0.938 / HP 15.0	Low Dose SD 8.00	**0.56**
0.5x16	Fast PF 1.438 / HP 23.0	High Quality SD 4.00	**1.77**
0.5x16	Fast PF 1.438 / HP 23.0	Standard SD 6.00	**0.96**
0.5x16	Fast PF 1.438 / HP 23.0	Low Dose SD 8.00	**0.60**
1.0x16	Detail PF 0.688 / HP 11.0	High Quality SD 4.00	**0.89**
1.0x16	Detail PF 0.688 / HP 11.0	Standard SD 6.00	**0.52**
1.0x16	Detail PF 0.688 / HP 11.0	Low Dose SD 8.00	**0.39**
1.0x16	Standard PF 0.938 / HP 15.0	High Quality SD 4.00	**0.86**
1.0x16	Standard PF 0.938 / HP 15.0	Standard SD 6.00	**0.53**
1.0x16	Standard PF 0.938 / HP 15.0	Low Dose SD 8.00	**0.33**
1.0x16	Fast PF 1.438 / HP 23.0	High Quality SD 4.00	**1.04**
1.0x16	Fast PF 1.438 / HP 23.0	Standard SD 6.00	**0.59**
1.0x16	Fast PF 1.438 / HP 23.0	Low Dose SD 8.00	**0.41**
2.0x16	Detail PF 0.688 / HP 11.0	High Quality SD 4.00	**0.63**
2.0x16	Detail PF 0.688 / HP 11.0	Standard SD 6.00	**0.37**
2.0x16	Detail PF 0.688 / HP 11.0	Low Dose SD 8.00	**0.31**
2.0x16	Standard PF 0.938 / HP 15.0	High Quality SD 4.00	**0.58**
2.0x16	Standard PF 0.938 / HP 15.0	Standard SD 6.00	**0.35**
2.0x16	Standard PF 0.938 / HP 15.0	Low Dose SD 8.00	**0.28**
2.0x16	Fast PF 1.438 / HP 23.0	High Quality SD 4.00	**0.83**
2.0x16	Fast PF 1.438 / HP 23.0	Standard SD 6.00	**0.56**
2.0x16	Fast PF 1.438 / HP 23.0	Low Dose SD 8.00	**0.33**
PF = Pitch Factor HP = Helical Pitch			

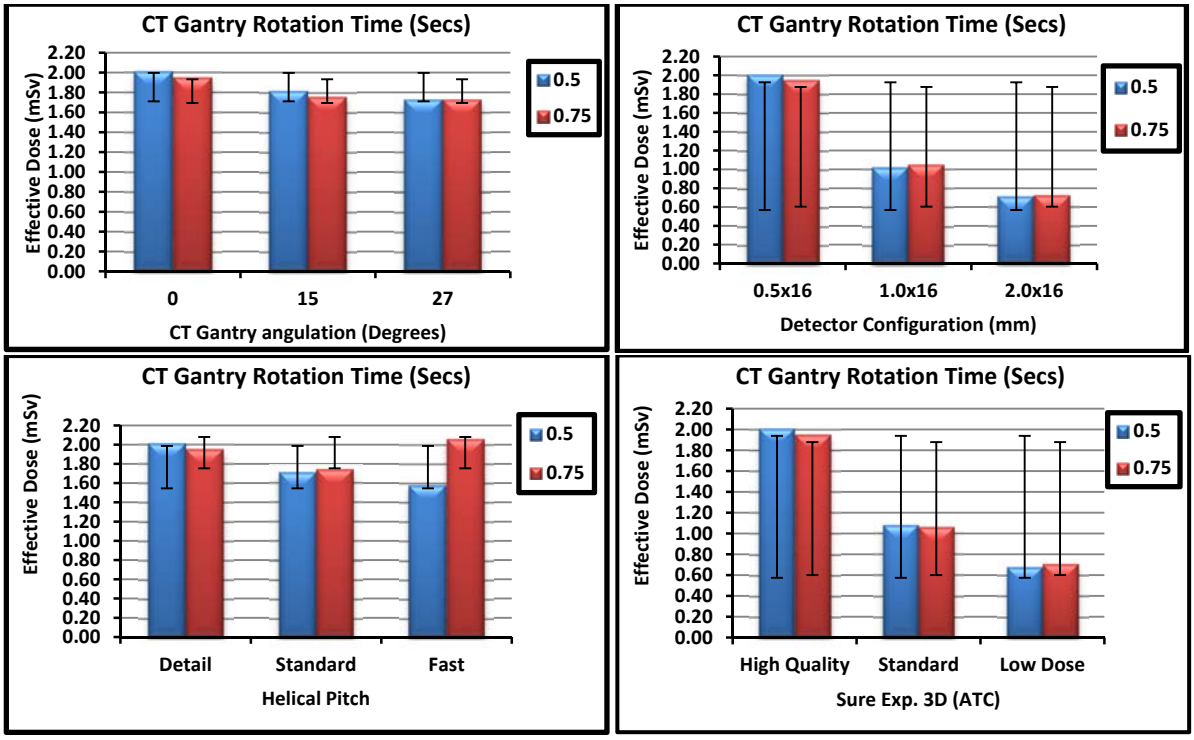

Figure F - 1: Graphs showing the relationship of CT gantry rotation times with CT gantry angulations, detector configurations, helical pitch and sure Exp. 3D (ATC).

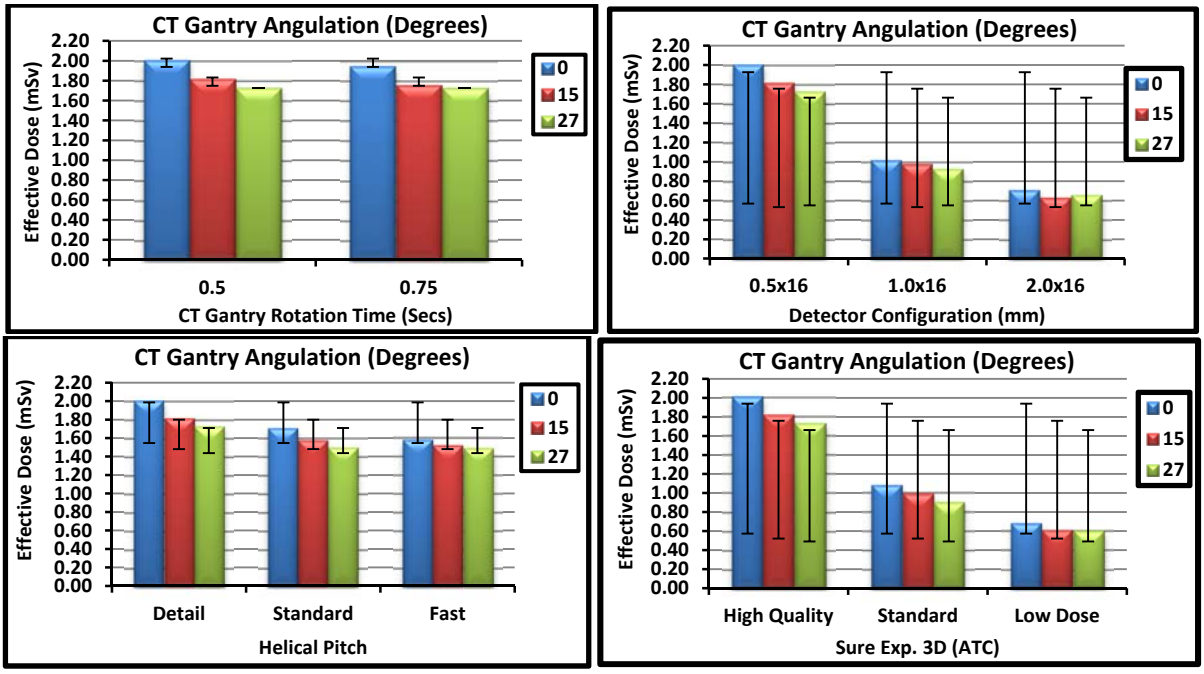

Figure F - 2: Graphs showing the relationship of CT gantry angulations with CT gantry rotation times, detector configurations, helical pitch and sure Exp. 3D (ATC).

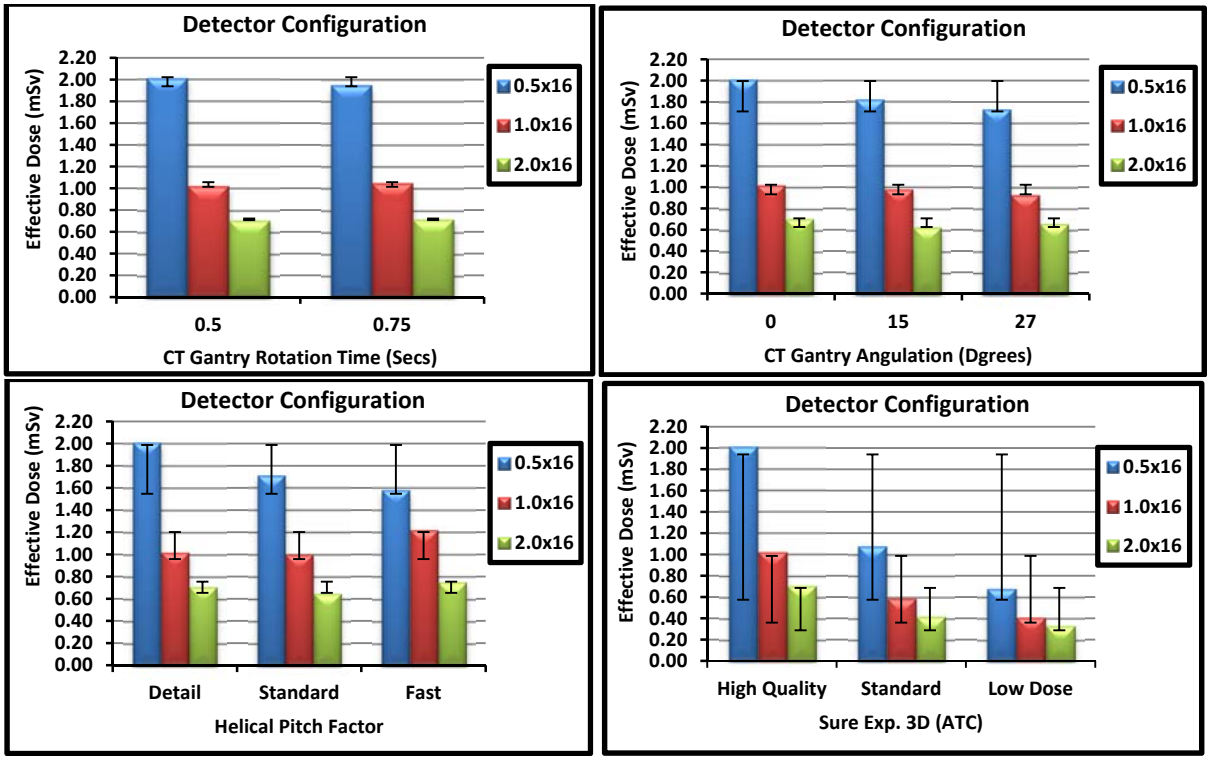

Figure F - 3: Graphs showing the relationship of detector configurations with CT gantry rotation times, CT gantry angulations, helical pitch and sure Exp. 3D (ATC).

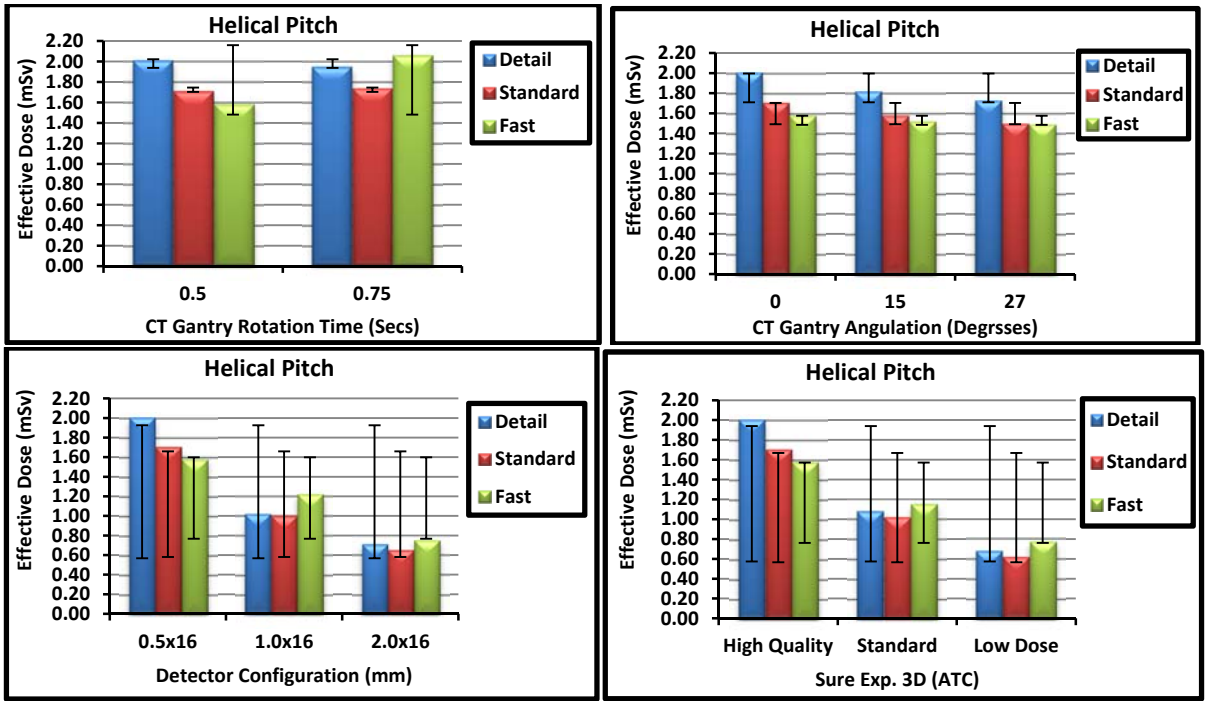

Figure F - 4: Graphs showing the relationship of helical pitch with CT gantry rotation times, CT gantry angulations, detector configurations and sure Exp. 3D (ATC).

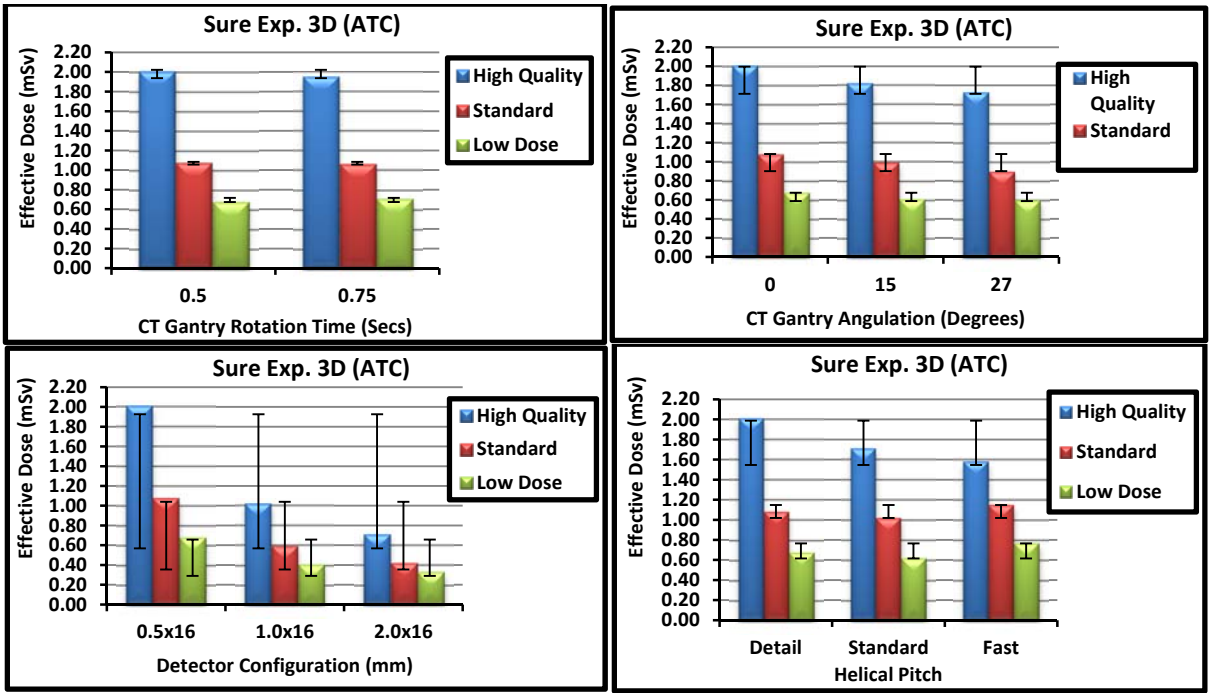

Figure F - 5: Graphs showing the relationship of sure Exp. 3D (ATC) with CT gantry rotation times, CT gantry angulations, detector configurations and helical pitch.

Appendix G: Tables and graphs of varying parameters of Paediatric helical protocols, effective dose results obtained using MOSFET

Table G - 1: Paediatric protocol parameters changes effective dose at 0° angle.

Rotation Time (Secs)	Detector Configuration (mm)	KVp	mA (fixed)	Effective Dose (mSv)
0.5	0.5x16	100	120	1.07
0.75	0.5x16	100	120	1.49
1	0.5x16	100	120	1.99
0.5	0.5x16	100	160	1.49
0.75	0.5x16	100	160	1.86
1	0.5x16	100	160	2.63
0.5	0.5x16	100	200	1.72
0.75	0.5x16	100	200	2.49
1	0.5x16	100	200	3.30
0.5	0.5x16	120	120	1.49
0.75	0.5x16	120	120	2.19
1	0.5x16	120	120	3.08
0.5	0.5x16	120	160	2.11
0.75	0.5x16	120	160	2.95
1	0.5x16	120	160	3.84
0.5	0.5x16	120	200	2.57
0.75	0.5x16	120	200	3.72
1	0.5x16	120	200	4.72

Table G - 2: Paediatric protocol parameters changes effective dose at 15° angle.

Rotation Time (Secs)	Detector Configuration (mm)	KVp	mA (fixed)	Effective Dose (mSv)
0.5	0.5x16	100	120	1.01
0.75	0.5x16	100	120	1.50
1	0.5x16	100	120	1.88
0.5	0.5x16	100	160	1.23
0.75	0.5x16	100	160	1.82
1	0.5x16	100	160	2.49
0.5	0.5x16	100	200	1.76
0.75	0.5x16	100	200	2.35
1	0.5x16	100	200	2.94
0.5	0.5x16	120	120	1.41
0.75	0.5x16	120	120	2.06
1	0.5x16	120	120	2.90
0.5	0.5x16	120	160	1.82
0.75	0.5x16	120	160	2.93
1	0.5x16	120	160	3.95
0.5	0.5x16	120	200	2.48
0.75	0.5x16	120	200	3.66
1	0.5x16	120	200	4.89

Table G - 3: Paediatric protocol parameters changes effective dose 27° angle.

Rotation Time (Secs)	Detector Configuration (mm)	KVp	mA (fixed)	Effective Dose (mSv)
0.5	0.5x16	100	120	1.01
0.75	0.5x16	100	120	1.53
1	0.5x16	100	120	2.02
0.5	0.5x16	100	160	1.61
0.75	0.5x16	100	160	1.94
1	0.5x16	100	160	2.65
0.5	0.5x16	100	200	1.58
0.75	0.5x16	100	200	2.16
1	0.5x16	100	200	3.33
0.5	0.5x16	120	120	1.60
0.75	0.5x16	120	120	2.38
1	0.5x16	120	120	2.97
0.5	0.5x16	120	160	1.96
0.75	0.5x16	120	160	2.97
1	0.5x16	120	160	3.86
0.5	0.5x16	120	200	2.41
0.75	0.5x16	120	200	3.57
1	0.5x16	120	200	4.81

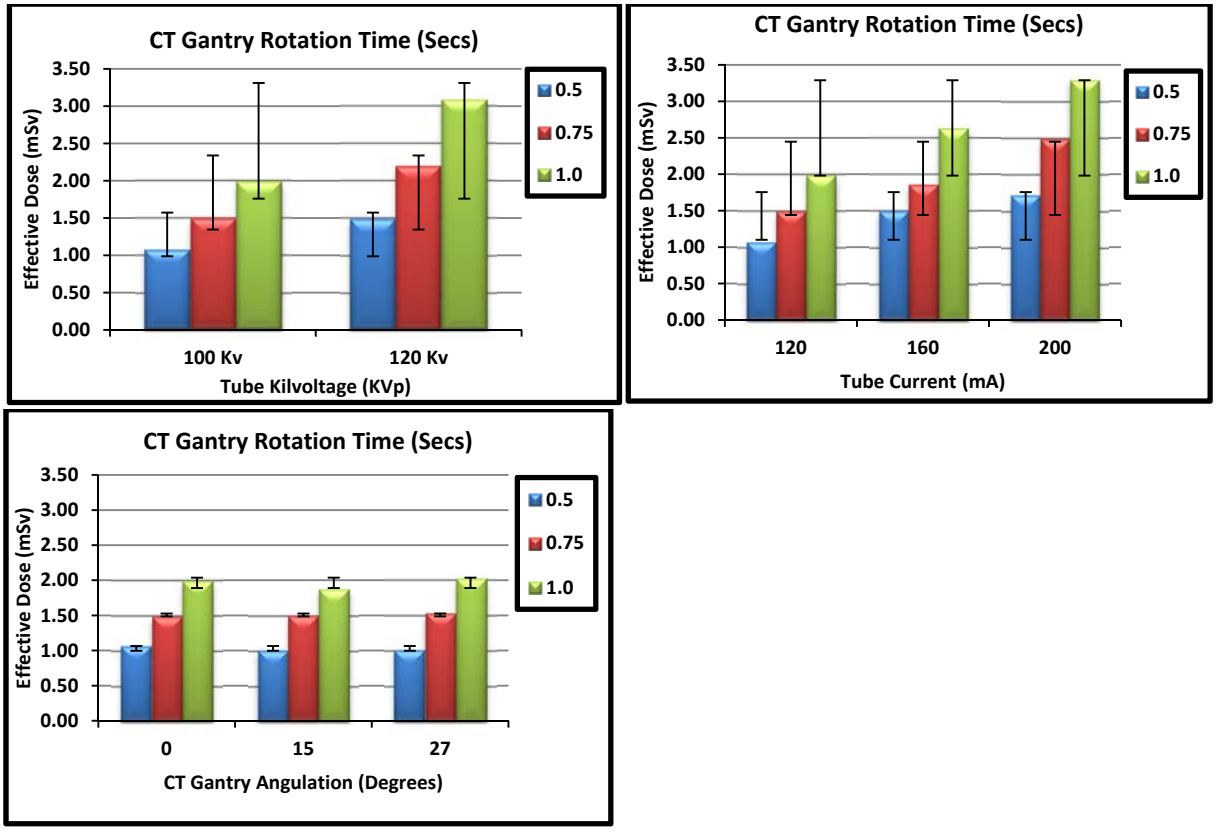

Figure G - 1: Graphs showing the relationship of CT gantry rotation time with tube kilovoltage (KVp), tube current (mA) and CT gantry angulations.

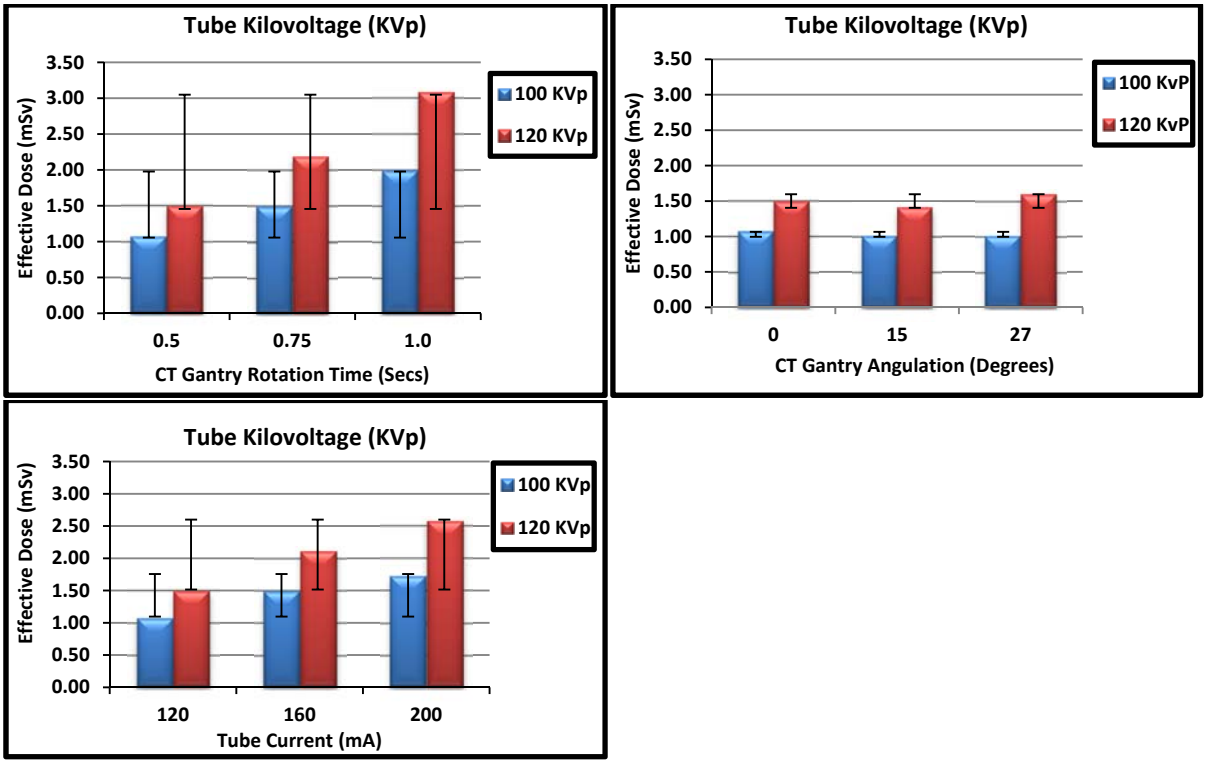

Figure G - 2: Graphs showing the relationship of tube kilovoltage (KVp) with CT gantry rotation time, CT gantry angulations and tube current (mA).

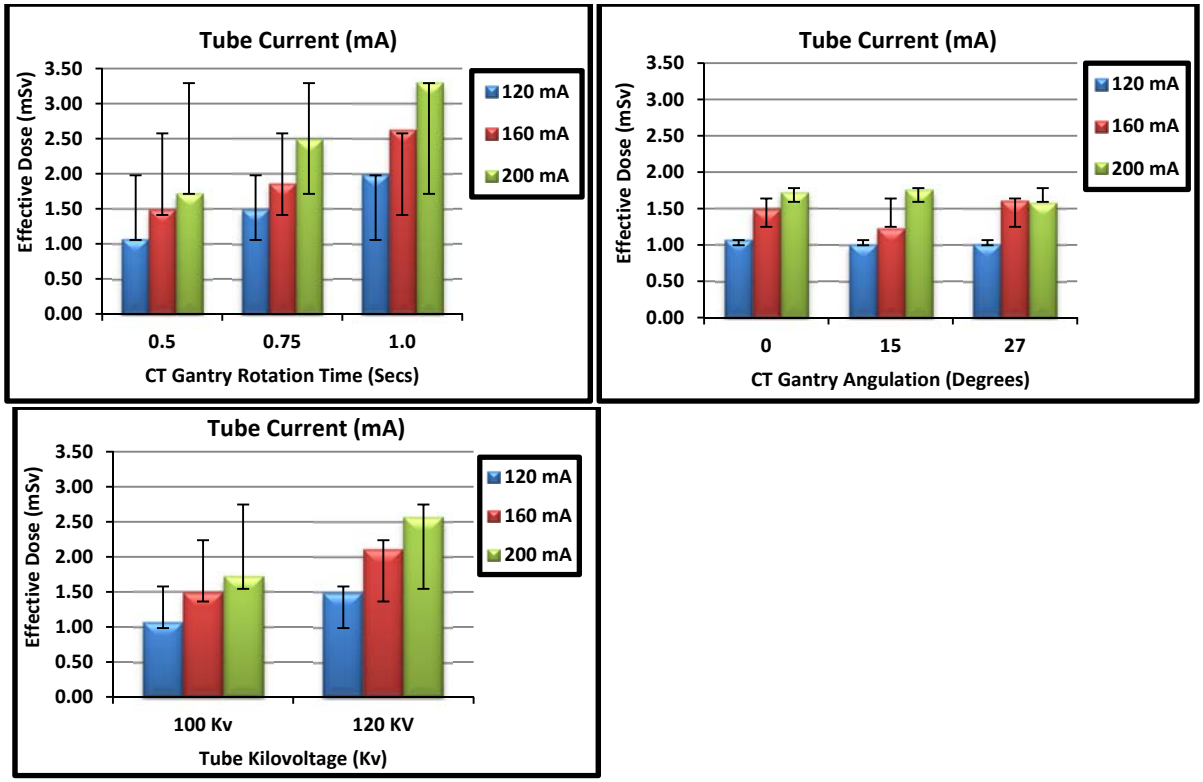

Figure G - 3: Graphs showing the relationship of tube current (mA) with CT gantry rotation time, CT gantry angulations and tube kilovoltage (KVp).

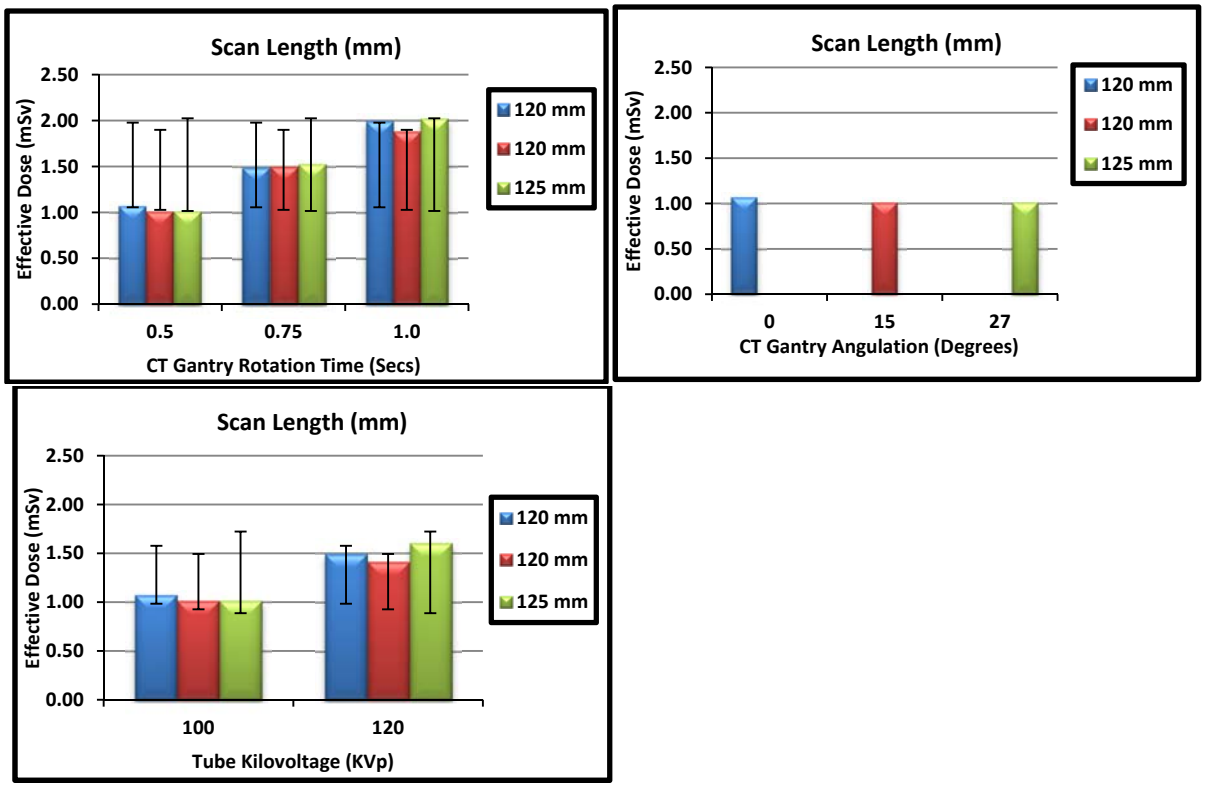

Figure G - 4: Graphs showing the relationship of scan lengths with CT gantry rotation time, CT gantry angulations, tube kilovoltage (KVp) and tube current (mA).

Appendix H: Tables of Adult and Paediatric Helical Protocols on Eye Absorbed dose, results obtained using MOSFET

Table H - 1: Adult brain protocols, eye absorbed dose (mGy).

Tube Rotation Time (S)	Detector Configuration (mm)	Pitch Factors / Helical Pitch	Sure Exp. 3D (ATC)	Eye Dose (mGy) / Gantry Angulations		
				0°	15°	27°
0.5	0.5x16	Detail PF 0.688 / HP 11.0	High Quality SD 1.80	**32.05**	**30.30**	**15.60**
0.5	0.5x16	Detail PF 0.688 / HP 11.0	Standard SD 2.00	**32.00**	**28.95**	**11.75**
0.5	0.5x16	Detail PF 0.688 / HP 11.0	Low Dose SD 2.20	**26.60**	**26.80**	**12.05**
0.5	0.5x16	Standard PF 0.938 / HP 15.0	High Quality SD 1.80	**24.05**	**25.00**	**10.92**
0.5	0.5x16	Standard PF 0.938 / HP 15.0	Standard SD 2.00	**20.75**	**22.35**	**14.30**
0.5	0.5x16	Standard PF 0.938 / HP 15.0	Low Dose SD 2.20	**23.25**	**18.15**	**13.75**
0.5	0.5x16	Fast PF 1.438 / HP 23.0	High Quality SD 1.80	**15.85**	**16.90**	**10.52**
0.5	0.5x16	Fast PF 1.438 / HP 23.0	Standard SD 2.00	**16.95**	**13.40**	**14.35**
0.5	0.5x16	Fast PF 1.438 / HP 23.0	Low Dose SD 2.20	**16.2**	**14.55**	**12.20**
0.5	1.0x16	Detail PF 0.688 / HP 11.0	High Quality SD 1.80	**32.80**	**23.85**	**28.15**
0.5	1.0x16	Detail PF 0.688 / HP 11.0	Standard SD 2.00	**24.15**	**28.05**	**18.35**
0.5	1.0x16	Detail PF 0.688 / HP 11.0	Low Dose SD 2.20	**22.35**	**23.95**	**20.65**
0.5	1.0x16	Standard PF 0.938 / HP 15.0	High Quality SD 1.80	**24.95**	**20.00**	**23.95**
0.5	1.0x16	Standard PF 0.938 / HP 15.0	Standard SD 2.00	**21.40**	**22.15**	**16.20**
0.5	1.0x16	Standard PF 0.938 / HP 15.0	Low Dose SD 2.20	**17.70**	**20.45**	**17.70**
0.5	1.0x16	Fast PF 1.438 / HP 23.0	High Quality SD 1.80	**16.40**	**16.70**	**15.30**
0.5	1.0x16	Fast PF 1.438 / HP 23.0	Standard SD 2.00	**15.85**	**14.50**	**14.85**
0.5	1.0x16	Fast PF 1.438 / HP 23.0	Low Dose SD 2.20	**13.95**	**9.40**	**14.20**
0.5	2.0x16	Detail PF 0.688 / HP 11.0	High Quality SD 1.80	**22.20**	**30.00**	**23.75**
0.5	2.0x16	Detail PF 0.688 / HP 11.0	Standard SD 2.00	**25.95**	**21.80**	**23.60**
0.5	2.0x16	Detail PF 0.688 / HP 11.0	Low Dose SD 2.20	**19.90**	**21.80**	**15.90**
0.5	2.0x16	Standard PF 0.938 / HP 15.0	High Quality SD 1.80	**20.65**	**18.75**	**18.80**
0.5	2.0x16	Standard PF 0.938 / HP 15.0	Standard SD 2.00	**16.85**	**17.75**	**19.90**
0.5	2.0x16	Standard PF 0.938 / HP 15.0	Low Dose SD 2.20	**17.20**	**19.00**	**14.85**
0.5	2.0x16	Fast PF 1.438 / HP 23.0	High Quality SD 1.80	**12.46**	**10.64**	**16.05**
0.5	2.0x16	Fast PF 1.438 / HP 23.0	Standard SD 2.00	**16.25**	**10.96**	**9.24**
0.5	2.0x16	Fast PF 1.438 / HP 23.0	Low Dose SD 2.20	**10.41**	**12.00**	**13.70**
1	0.5x16	Detail PF 0.688 / HP 11.0	High Quality SD 1.80	**58.40**	**42.75**	**12.90**
1	0.5x16	Detail PF 0.688 / HP 11.0	Standard SD 2.00	**51.75**	**37.35**	**12.75**
1	0.5x16	Detail PF 0.688 / HP 11.0	Low Dose SD 2.20	**47.25**	**31.60**	**9.54**
1	0.5x16	Standard PF 0.938 / HP 15.0	High Quality SD 1.80	**43.85**	**44.30**	**13.60**
1	0.5x16	Standard PF 0.938 / HP 15.0	Standard SD 2.00	**32.90**	**34.70**	**12.05**
1	0.5x16	Standard PF 0.938 / HP 15.0	Low Dose SD 2.20	**38.35**	**25.85**	**13.70**
1	0.5x16	Fast PF 1.438 / HP 23.0	High Quality SD 1.80	**30.55**	**31.55**	**19.45**
1	0.5x16	Fast PF 1.438 / HP 23.0	Standard SD 2.00	**30.40**	**28.30**	**27.80**
1	0.5x16	Fast PF 1.438 / HP 23.0	Low Dose SD 2.20	**26.60**	**27.05**	**24.75**
1	1.0x16	Detail PF 0.688 / HP 11.0	High Quality SD 1.80	**60.15**	**47.10**	**35.55**
1	1.0x16	Detail PF 0.688 / HP 11.0	Standard SD 2.00	**52.40**	**50.75**	**32.25**
1	1.0x16	Detail PF 0.688 / HP 11.0	Low Dose SD 2.20	**45.15**	**44.65**	**35.60**
1	1.0x16	Standard PF 0.938 / HP 15.0	High Quality SD 1.80	**40.55**	**37.45**	**33.65**
1	1.0x16	Standard PF 0.938 / HP 15.0	Standard SD 2.00	**39.45**	**42.30**	**31.70**
1	1.0x16	Standard PF 0.938 / HP 15.0	Low Dose SD 2.20	**33.95**	**19.55**	**27.30**
1	1.0x16	Fast PF 1.438 / HP 23.0	High Quality SD 1.80	**29.60**	**31.90**	**28.25**
1	1.0x16	Fast PF 1.438 / HP 23.0	Standard SD 2.00	**27.90**	**29.30**	**26.75**
1	1.0x16	Fast PF 1.438 / HP 23.0	Low Dose SD 2.20	**26.05**	**27.45**	**24.95**
1	2.0x16	Detail PF 0.688 / HP 11.0	High Quality SD 1.80	**46.60**	**28.30**	**31.10**
1	2.0x16	Detail PF 0.688 / HP 11.0	Standard SD 2.00	**34.70**	**21.65**	**25.45**
1	2.0x16	Detail PF 0.688 / HP 11.0	Low Dose SD 2.20	**32.80**	**19.70**	**20.80**
1	2.0x16	Standard PF 0.938 / HP 15.0	High Quality SD 1.80	**33.45**	**24.15**	**23.05**
1	2.0x16	Standard PF 0.938 / HP 15.0	Standard SD 2.00	**31.05**	**19.10**	**21.35**
1	2.0x16	Standard PF 0.938 / HP 15.0	Low Dose SD 2.20	**27.95**	**18.30**	**16.65**
1	2.0x16	Fast PF 1.438 / HP 23.0	High Quality SD 1.80	**28.20**	**30.70**	**27.70**
1	2.0x16	Fast PF 1.438 / HP 23.0	Standard SD 2.00	**21.45**	**18.40**	**21.75**
1	2.0x16	Fast PF 1.438 / HP 23.0	Low Dose SD 2.20	**25.35**	**14.10**	**20.55**

Table H - 2: Paediatric brain protocols, eye absorbed dose (mGy).						
Tube Rotation Time (S)	**Detector Configurations (mm)**	**Pitch Factors / Helical Pitch**	**Sure Exp. 3D (ATC)**	**Eye Dose (mGy)/ Gantry Angulations**		
				0°	**15°**	**27°**
0.5	0.5x16	Detail PF 0.688 / HP 11.0	High Quality SD 4.00	**33.05**	**29.90**	**25.00**
0.5	0.5x16	Detail PF 0.688 / HP 11.0	Standard SD 6.00	**17.90**	**15.55**	**13.05**
0.5	0.5x16	Detail PF 0.688 / HP 11.0	Low Dose SD 8.00	**11.75**	**9.80**	**8.86**
0.5	0.5x16	Standard PF 0.938 / HP 15.0	High Quality SD 4.00	**26.20**	**28.05**	**21.85**
0.5	0.5x16	Standard PF 0.938 / HP 15.0	Standard SD 6.00	**16.90**	**13.95**	**12.35**
0.5	0.5x16	Standard PF 0.938 / HP 15.0	Low Dose SD 8.00	**9.62**	**7.86**	**7.03**
0.5	0.5x16	Fast PF 1.438 / HP 23.0	High Quality SD 4.00	**22.50**	**21.40**	**21.35**
0.5	0.5x16	Fast PF 1.438 / HP 23.0	Standard SD 6.00	**16.15**	**13.45**	**11.90**
0.5	0.5x16	Fast PF 1.438 / HP 23.0	Low Dose SD 8.00	**10.35**	**8.93**	**7.06**
0.5	1.0x16	Detail PF 0.688 / HP 11.0	High Quality SD 4.00	**15.65**	**15.40**	**12.30**
0.5	1.0x16	Detail PF 0.688 / HP 11.0	Standard SD 6.00	**7.80**	**8.24**	**6.37**
0.5	1.0x16	Detail PF 0.688 / HP 11.0	Low Dose SD 8.00	**5.62**	**4.35**	**4.27**
0.5	1.0x16	Standard PF 0.938 / HP 15.0	High Quality SD 4.00	**14.20**	**12.35**	**10.35**
0.5	1.0x16	Standard PF 0.938 / HP 15.0	Standard SD 6.00	**6.04**	**7.49**	**5.18**
0.5	1.0x16	Standard PF 0.938 / HP 15.0	Low Dose SD 8.00	**4.90**	**4.60**	**3.67**
0.5	1.0x16	Fast PF 1.438 / HP 23.0	High Quality SD 4.00	**15.15**	**16.05**	**13.10**
0.5	1.0x16	Fast PF 1.438 / HP 23.0	Standard SD 6.00	**7.61**	**6.83**	**7.57**
0.5	1.0x16	Fast PF 1.438 / HP 23.0	Low Dose SD 8.00	**4.78**	**4.63**	**3.49**
0.5	2.0x16	Detail PF 0.688 / HP 11.0	High Quality SD 4.00	**9.12**	**7.95**	**6.78**
0.5	2.0x16	Detail PF 0.688 / HP 11.0	Standard SD 6.00	**4.51**	**3.45**	**3.95**
0.5	2.0x16	Detail PF 0.688 / HP 11.0	Low Dose SD 8.00	**2.94**	**2.70**	**3.17**
0.5	2.0x16	Standard PF 0.938 / HP 15.0	High Quality SD 4.00	**8.32**	**6.46**	**6.60**
0.5	2.0x16	Standard PF 0.938 / HP 15.0	Standard SD 6.00	**3.98**	**3.27**	**3.37**
0.5	2.0x16	Standard PF 0.938 / HP 15.0	Low Dose SD 8.00	**2.54**	**2.57**	**2.89**
0.5	2.0x16	Fast PF 1.438 / HP 23.0	High Quality SD 4.00	**6.79**	**5.86**	**6.72**
0.5	2.0x16	Fast PF 1.438 / HP 23.0	Standard SD 6.00	**3.91**	**4.48**	**4.04**
0.5	2.0x16	Fast PF 1.438 / HP 23.0	Low Dose SD 8.00	**3.17**	**2.95**	**3.27**
0.75	0.5x16	Detail PF 0.688 / HP 11.0	High Quality SD 4.00	**33.20**	**29.90**	**24.85**
0.75	0.5x16	Detail PF 0.688 / HP 11.0	Standard SD 6.00	**16.75**	**15.00**	**11.90**
0.75	0.5x16	Detail PF 0.688 / HP 11.0	Low Dose SD 8.00	**10.35**	**9.75**	**8.96**
0.75	0.5x16	Standard PF 0.938 / HP 15.0	High Quality SD 4.00	**26.55**	**26.25**	**22.80**
0.75	0.5x16	Standard PF 0.938 / HP 15.0	Standard SD 6.00	**13.95**	**12.05**	**12.80**
0.75	0.5x16	Standard PF 0.938 / HP 15.0	Low Dose SD 8.00	**9.34**	**7.95**	**7.06**
0.75	0.5x16	Fast PF 1.438 / HP 23.0	High Quality SD 4.00	**30.80**	**29.20**	**24.55**
0.75	0.5x16	Fast PF 1.438 / HP 23.0	Standard SD 6.00	**17.15**	**14.80**	**12.15**
0.75	0.5x16	Fast PF 1.438 / HP 23.0	Low Dose SD 8.00	**9.18**	**9.32**	**7.97**
0.75	1.0x16	Detail PF 0.688 / HP 11.0	High Quality SD 4.00	**17.55**	**14.25**	**13.20**
0.75	1.0x16	Detail PF 0.688 / HP 11.0	Standard SD 6.00	**7.98**	**8.16**	**6.03**
0.75	1.0x16	Detail PF 0.688 / HP 11.0	Low Dose SD 8.00	**5.53**	**4.53**	**4.46**
0.75	1.0x16	Standard PF 0.938 / HP 15.0	High Quality SD 4.00	**15.90**	**12.75**	**10.43**
0.75	1.0x16	Standard PF 0.938 / HP 15.0	Standard SD 6.00	**8.69**	**7.08**	**6.33**
0.75	1.0x16	Standard PF 0.938 / HP 15.0	Low Dose SD 8.00	**4.67**	**4.05**	**3.94**
0.75	1.0x16	Fast PF 1.438 / HP 23.0	High Quality SD 4.00	**18.30**	**16.05**	**12.00**
0.75	1.0x16	Fast PF 1.438 / HP 23.0	Standard SD 6.00	**6.67**	**8.18**	**6.19**
0.75	1.0x16	Fast PF 1.438 / HP 23.0	Low Dose SD 8.00	**5.23**	**4.96**	**4.71**
0.75	2.0x16	Detail PF 0.688 / HP 11.0	High Quality SD 4.00	**7.08**	**7.96**	**7.74**
0.75	2.0x16	Detail PF 0.688 / HP 11.0	Standard SD 6.00	**4.46**	**4.83**	**4.74**
0.75	2.0x16	Detail PF 0.688 / HP 11.0	Low Dose SD 8.00	**3.01**	**3.09**	**3.12**
0.75	2.0x16	Standard PF 0.938 / HP 15.0	High Quality SD 4.00	**6.67**	**6.47**	**6.49**
0.75	2.0x16	Standard PF 0.938 / HP 15.0	Standard SD 6.00	**4.04**	**4.18**	**3.25**
0.75	2.0x16	Standard PF 0.938 / HP 15.0	Low Dose SD 8.00	**3.16**	**2.67**	**2.40**
0.75	2.0x16	Fast PF 1.438 / HP 23.0	High Quality SD 4.00	**8.02**	**6.60**	**6.77**
0.75	2.0x16	Fast PF 1.438 / HP 23.0	Standard SD 6.00	**4.62**	**4.58**	**3.76**
0.75	2.0x16	Fast PF 1.438 / HP 23.0	Low Dose SD 8.00	**3.64**	**2.90**	**2.09**

Appendix I: Tables of Estimated Cases of Lifetime Cancer Risk for both adult and paediatric male and females ages from 10 to 80 years for 162 helical brain CT scan protocols (case/10^6)

Table I - 1: Adult and Paediatric helical brain protocols; Lifetime cancer risk for male and female case/10^6.

protocol	Female age (case/10^6)											Male age (case/10^6)										
	0	5	10	15	20	30	40	50	60	70	80	0	5	10	15	20	30	40	50	60	70	80
1	102	64	18	14	11	7	6	5	4	2	1	46	29	14	11	8	5	5	4	3	2	1
2	55	34	19	15	12	7	6	5	4	2	1	24	15	13	11	8	5	5	4	3	2	1
3	36	23	20	15	12	7	6	5	4	2	1	16	10	12	9	8	5	4	3	3	2	1
4	82	51	17	13	10	6	5	4	3	2	1	39	24	11	9	7	4	4	3	2	1	1
5	53	33	15	12	9	6	5	4	3	2	1	23	14	10	8	6	4	4	3	2	1	1
6	32	20	15	11	9	5	4	4	3	2	1	15	11	10	8	6	4	3	3	2	1	1
7	78	49	12	9	7	4	4	3	2	1	1	33	21	8	7	5	3	3	2	2	1	<1
8	55	34	12	9	7	4	4	3	2	1	1	24	15	8	6	5	3	3	2	2	1	<1
9	40	25	12	9	7	4	4	3	2	1	1	17	10	7	6	5	3	3	2	2	1	<1
10	95	58	23	18	14	9	7	6	4	3	1	46	28	16	12	10	6	5	4	3	2	1
11	52	32	19	15	12	7	6	5	4	2	1	23	14	14	11	9	6	5	4	3	2	1
12	31	19	19	14	11	7	6	5	3	2	1	15	13	13	10	8	5	4	4	3	2	1
13	84	52	15	12	9	6	5	4	3	2	1	39	25	11	9	7	4	4	3	2	1	1
14	50	31	15	11	9	6	5	4	3	2	1	22	14	11	9	7	4	4	3	2	1	1
15	32	20	14	11	8	5	4	4	3	2	1	14	10	10	8	6	4	3	3	2	1	1
16	88	56	11	9	7	4	4	3	2	1	1	36	23	8	6	5	3	3	2	2	1	<1
17	53	33	11	8	6	4	3	3	2	1	1	24	15	8	6	5	3	3	2	2	1	<1
18	40	25	11	8	6	4	3	3	2	1	1	16	10	7	6	5	3	3	2	2	1	<1
19	96	60	23	18	14	9	8	6	5	3	1	44	27	17	13	11	7	6	5	3	2	1
20	51	32	22	17	14	9	7	6	4	3	1	23	14	16	13	10	6	6	5	3	2	1
21	35	22	22	17	13	8	7	5	4	3	1	17	15	15	11	9	6	5	4	3	2	1
22	80	49	20	15	12	7	6	5	4	2	1	38	24	13	10	8	5	5	4	3	2	1
23	46	29	19	14	11	7	6	5	3	2	1	20	13	12	10	8	5	4	3	2	1	1
24	34	21	16	12	10	6	5	4	3	2	1	14	11	11	9	7	4	4	3	2	1	1
25	89	56	13	10	7	5	4	3	2	2	1	38	24	9	7	6	4	3	3	2	1	<1
26	57	36	13	10	8	5	4	3	2	2	1	25	15	9	7	5	4	3	3	2	1	<1
27	35	22	12	9	7	4	4	3	2	1	1	15	10	8	6	5	3	3	2	2	1	<1
28	52	32	19	14	11	7	6	5	3	2	1	23	14	13	10	8	5	4	4	3	2	1
29	32	20	19	15	11	7	6	5	4	2	1	15	13	13	10	8	5	5	4	3	2	1
30	25	19	19	15	11	7	6	5	4	2	1	14	13	13	10	8	5	4	4	3	2	1
31	51	32	17	13	10	6	5	4	3	2	1	22	13	11	9	7	4	4	3	2	1	1
32	29	18	17	13	10	6	5	4	3	2	1	12	10	10	8	6	4	3	3	2	1	<1
33	23	15	14	11	8	5	4	3	3	2	1	10	9	9	7	6	4	3	3	2	1	<1
34	66	42	12	9	7	4	3	3	2	1	1	26	16	8	6	5	3	3	2	2	1	<1
35	42	26	12	9	7	4	4	3	2	1	1	16	10	7	6	5	3	3	2	2	1	<1
36	23	14	10	8	6	4	3	3	2	1	1	10	6	7	6	4	3	2	2	1	1	<1
37	54	33	18	14	11	7	6	5	4	2	1	24	15	14	11	9	5	5	4	3	2	1
38	28	17	18	14	11	7	6	5	3	2	1	15	13	13	10	8	5	4	4	3	2	1
39	24	15	18	14	11	7	6	4	3	2	1	14	12	12	10	8	5	4	3	2	1	1
40	47	30	15	11	9	5	5	4	3	2	1	20	13	11	8	7	4	4	3	2	1	1
41	29	19	14	11	8	5	4	4	2	3	1	12	10	10	8	6	4	3	3	2	1	<1
42	24	15	15	12	9	6	5	4	3	2	1	11	9	9	7	6	4	3	3	2	1	<1
43	66	41	11	8	6	4	3	3	2	1	1	26	16	7	6	4	3	2	2	1	1	<1
44	41	26	10	8	6	4	3	3	2	1	1	16	10	7	5	4	3	2	2	1	1	<1
45	29	19	9	7	6	3	3	2	2	1	1	11	7	6	5	4	3	2	2	1	1	<1
46	56	35	23	18	14	8	7	6	4	3	1	23	15	16	12	10	6	5	4	3	2	1
47	32	20	22	17	13	8	7	5	4	2	1	15	14	14	11	9	6	5	4	3	2	1
48	19	12	18	14	11	7	6	5	4	2	1	14	13	13	10	8	5	5	4	3	2	1
49	52	33	17	13	10	6	5	4	3	2	1	21	13	12	9	7	5	4	3	2	1	1
50	29	18	17	13	10	6	5	4	3	2	1	12	11	11	8	7	4	4	3	2	1	1
51	19	15	15	11	9	5	4	4	3	2	1	12	10	10	8	6	4	3	3	2	1	<1
52	65	41	12	9	7	4	4	3	2	1	1	26	17	8	6	5	3	3	2	2	1	<1
53	35	22	11	9	7	4	3	3	2	1	1	15	9	8	6	5	3	3	2	2	1	<1
54	25	16	13	10	8	5	4	3	2	1	1	10	8	8	6	5	3	3	2	2	1	<1
55	45	29	20	15	11	7	5	4	3	2	1	17	10	12	10	8	5	4	3	2	1	1
56	27	17	20	15	11	6	5	4	3	2	1	13	11	11	9	7	4	4	3	2	1	1
57	21	14	18	13	10	6	5	4	3	2	1	12	11	11	8	6	4	3	3	2	1	1
58	41	26	17	13	10	6	5	4	3	2	1	15	9	11	8	7	4	4	3	2	1	1

Continued **(Table I - 1)**

protocol	Female age (case/10^6)											Male age (case/10^6)										
	0	**5**	**10**	**15**	**20**	**30**	**40**	**50**	**60**	**70**	**80**	**0**	**5**	**10**	**15**	**20**	**30**	**40**	**50**	**60**	**70**	**80**
59	25	16	20	15	11	6	5	4	3	2	1	12	11	11	8	7	4	4	3	2	1	1
60	22	18	18	13	10	5	4	3	2	2	1	12	10	10	7	6	4	3	2	2	1	<1
61	53	34	19	14	10	6	4	3	2	1	1	18	11	9	7	6	3	3	2	2	1	<1
62	34	22	18	13	9	5	4	3	2	1	1	11	7	9	7	5	3	3	2	2	1	<1
63	24	16	17	12	9	5	4	3	2	1	1	10	8	8	6	5	3	2	2	1	1	<1
64	40	25	22	17	13	8	6	5	4	2	1	16	14	14	11	9	5	5	4	3	2	1
65	25	16	18	14	11	7	5	4	3	2	1	14	12	12	9	7	5	4	3	2	1	1
66	23	15	16	12	10	6	5	4	3	2	1	13	11	11	8	7	4	4	3	2	1	1
67	42	27	18	14	11	6	5	4	3	2	1	15	11	11	9	7	4	4	3	2	1	1
68	24	16	15	11	9	5	4	4	3	2	1	12	10	10	8	6	4	3	3	2	1	<1
69	21	14	12	9	7	4	4	3	2	1	1	7	4	8	7	5	3	3	2	2	1	<1
70	58	37	13	10	7	4	4	3	2	1	1	20	12	8	7	5	3	3	2	2	1	<1
71	29	18	14	10	8	4	4	3	2	1	1	11	8	8	6	5	3	3	2	2	1	<1
72	26	17	12	9	7	4	3	3	2	1	1	9	7	7	6	4	3	2	2	1	1	<1
73	43	28	22	17	13	8	7	5	4	2	1	17	15	15	12	9	6	5	4	3	2	1
74	25	16	20	15	12	7	6	5	4	2	1	15	14	14	11	8	5	5	4	3	2	1
75	21	14	16	12	10	6	5	4	3	2	1	13	12	12	9	7	4	4	3	2	1	1
76	44	28	19	14	11	7	8	5	3	2	1	16	12	12	10	8	5	4	3	2	1	1
77	24	15	16	12	9	6	5	4	3	2	1	13	11	11	8	7	4	4	3	2	1	1
78	20	13	17	13	10	6	5	4	3	2	1	12	10	10	8	6	4	3	3	2	1	<1
79	61	40	15	11	8	5	4	3	2	2	1	20	13	9	7	6	4	3	3	2	1	<1
80	38	25	18	13	10	6	4	3	2	1	1	12	9	9	7	6	3	3	2	2	1	<1
81	26	17	15	11	8	5	4	3	2	1	1	11	9	9	7	5	3	3	2	2	1	<1
82	97	60	32	25	19	12	10	8	6	4	2	46	28	21	17	13	8	7	6	4	3	1
83	58	36	28	21	17	10	9	7	5	3	1	25	19	19	15	12	8	7	5	4	2	1
84	39	25	26	20	15	10	8	7	5	3	1	20	18	18	14	11	7	6	5	4	2	1
85	90	56	24	18	14	9	8	6	5	3	1	40	25	17	13	10	7	6	5	3	2	1
86	47	29	23	17	13	8	7	5	4	3	1	21	15	15	12	9	6	5	4	3	2	1
87	33	21	20	15	12	7	6	5	4	2	1	16	14	14	11	8	5	5	4	3	2	1
88	101	63	23	18	14	8	7	6	4	3	1	45	28	15	12	9	6	5	4	3	2	1
89	59	37	22	17	13	8	6	5	4	2	1	25	15	13	10	8	5	5	4	3	2	1
90	40	25	18	13	10	6	5	4	3	2	1	16	12	12	9	7	5	4	3	2	1	1
91	91	57	36	28	22	14	11	9	6	4	2	42	26	23	18	14	9	8	7	5	3	1
92	57	36	28	21	17	10	9	7	5	3	1	24	15	16	15	12	7	6	5	4	2	1
93	36	23	21	16	13	8	7	6	4	3	1	18	16	16	12	10	6	5	4	3	2	1
94	85	52	27	21	16	10	8	7	5	3	1	40	25	19	15	12	8	7	5	4	2	1
95	46	29	24	18	14	9	8	6	5	3	1	20	17	17	13	10	7	6	5	3	2	1
96	34	21	21	16	12	8	6	5	4	2	1	16	14	14	11	8	5	5	4	3	2	1
97	97	60	22	17	13	8	7	6	4	3	1	43	27	16	13	10	6	5	5	3	2	1
98	53	33	21	16	12	8	6	5	4	2	1	24	15	14	11	9	6	5	4	3	2	1
99	36	23	19	14	11	7	6	5	3	2	1	15	13	13	10	8	5	4	4	3	2	1
100	94	59	32	24	19	12	10	8	6	4	2	42	26	22	18	14	9	8	6	4	3	1
101	51	32	28	21	16	10	9	7	5	3	2	22	20	20	15	12	8	7	5	4	2	1
102	36	23	25	19	14	9	7	6	5	3	1	18	17	17	13	10	7	6	5	3	2	1
103	85	53	28	21	17	10	9	7	5	3	2	38	24	20	15	12	8	7	6	4	2	1
104	46	29	23	18	14	9	7	6	5	3	1	20	17	17	13	10	7	6	5	3	2	1
105	32	20	20	16	12	7	6	5	4	2	1	17	14	14	11	9	5	5	4	3	2	1
106	97	60	24	18	14	9	7	6	5	3	1	44	27	17	13	10	7	6	5	3	2	1
107	56	35	25	19	15	9	8	6	5	3	1	24	17	15	13	10	7	6	5	3	2	1
108	35	22	23	17	13	8	7	6	4	3	1	17	16	16	12	10	6	5	4	3	2	1
109	49	31	33	25	20	12	10	8	6	4	2	25	20	20	17	13	8	7	6	4	3	1
110	33	21	33	25	20	12	10	8	6	4	2	21	19	19	16	13	8	7	6	4	2	1
111	26	25	25	19	14	8	7	6	4	3	1	17	14	14	13	10	6	5	4	3	2	1
112	50	32	27	20	16	10	8	7	5	3	1	21	13	18	14	11	7	6	5	4	2	1
113	31	26	20	19	15	9	7	6	4	3	1	19	17	17	13	10	6	6	5	3	2	1
114	27	25	25	20	15	9	8	6	4	3	1	17	15	15	12	9	6	5	4	3	2	1
115	70	44	23	17	13	8	6	5	4	2	1	27	17	14	11	9	5	5	4	3	2	1
116	38	24	22	17	13	8	6	5	4	2	1	15	13	13	10	8	5	4	4	3	2	1
117	28	18	19	14	11	7	6	4	3	2	1	13	12	12	9	7	5	4	3	2	1	1
118	50	30	38	29	23	14	12	10	7	5	2	23	15	26	20	16	10	9	7	5	3	1
119	28	17	32	25	19	12	10	8	6	4	2	24	23	23	18	14	9	8	6	5	3	1
120	27	21	21	23	18	11	9	8	6	4	2	22	20	18	16	13	8	7	6	4	2	1
121	53	34	28	22	17	10	9	7	5	3	2	21	19	18	16	13	8	7	6	4	2	1
122	32	25	25	19	15	9	8	6	5	3	1	20	18	18	14	11	7	6	5	4	2	1
123	23	14	18	14	11	6	5	4	3	2	1	13	12	12	9	7	5	4	3	2	1	1

Continued **(Table I - 1)**

protocol	Female age (case/10^6)											Male age (case/106)										
	0	**5**	**10**	**15**	**20**	**30**	**40**	**50**	**60**	**70**	**80**	**0**	**5**	**10**	**15**	**20**	**30**	**40**	**50**	**60**	**70**	**80**
124	73	47	20	15	12	7	6	5	4	2	1	27	17	14	11	8	5	5	4	3	2	1
125	37	23	20	15	12	7	6	5	3	2	1	15	13	13	10	8	5	4	3	2	1	1
126	27	18	17	13	10	6	5	4	3	2	1	13	12	12	9	7	5	4	3	2	1	1
127	52	32	45	34	26	16	13	11	8	5	2	29	25	25	23	18	11	10	8	6	3	1
128	32	20	35	27	21	13	11	9	7	4	2	27	25	25	20	16	10	9	7	5	3	1
129	31	29	28	23	18	11	10	8	6	4	2	23	22	21	17	13	8	7	6	4	3	1
130	52	33	35	27	21	13	11	8	6	4	2	21	13	22	17	14	9	8	6	4	3	1
131	33	30	30	25	19	12	10	8	6	4	2	23	21	20	17	13	9	7	6	4	3	1
132	20	13	27	20	16	10	8	7	5	3	1	8	5	18	14	11	7	6	5	4	2	1
133	62	39	25	19	14	9	7	6	4	3	1	26	16	16	12	10	6	5	4	3	2	1
134	38	24	21	16	12	8	6	5	4	3	1	17	15	15	11	9	6	5	4	3	2	1
135	24	15	22	17	13	8	7	5	4	3	1	15	13	13	11	9	5	5	4	3	2	1
136	44	28	28	21	16	10	8	7	5	3	1	19	17	17	14	11	7	6	5	4	2	1
137	30	27	25	23	17	10	8	6	5	3	1	17	15	15	13	10	6	6	5	3	2	1
138	26	23	21	18	13	8	7	5	4	2	1	15	13	13	11	9	6	5	4	3	2	1
139	38	29	27	23	17	9	7	6	4	3	1	18	16	16	13	10	6	5	4	3	2	1
140	27	23	23	20	15	9	7	5	4	3	1	16	14	14	12	9	6	5	4	3	2	1
141	23	15	20	15	11	7	6	4	3	2	1	14	11	11	10	8	5	4	3	2	1	1
142	57	37	34	25	18	10	7	6	4	3	1	19	17	16	13	10	6	5	4	3	2	1
143	35	23	40	28	20	10	7	5	4	2	1	18	16	16	12	9	6	5	4	3	2	1
144	26	24	24	18	13	7	5	4	3	2	1	15	13	13	10	8	5	4	3	2	1	1
145	42	27	23	18	14	9	7	6	4	3	1	16	10	15	12	10	6	5	4	3	2	1
146	27	19	17	14	11	7	6	5	4	2	1	14	12	12	10	8	5	5	4	3	2	1
147	21	19	17	13	10	6	5	4	3	2	1	12	11	11	8	7	4	4	3	2	1	1
148	43	28	19	14	11	7	6	5	4	2	1	15	13	13	11	8	5	5	4	3	2	1
149	27	17	17	13	10	6	5	4	3	2	1	13	11	11	9	7	4	4	3	2	1	1
150	24	15	16	12	9	6	5	4	3	2	1	12	10	10	8	6	4	3	3	2	1	1
151	57	37	23	17	13	8	6	5	4	2	1	20	15	15	11	9	6	5	4	3	2	1
152	36	23	21	16	12	7	6	5	4	2	1	12	8	13	10	8	5	4	4	3	2	1
153	25	16	20	15	11	7	6	4	3	2	1	13	11	11	9	7	5	4	3	2	1	1
154	40	26	25	19	15	9	7	6	4	3	1	17	16	15	13	10	7	6	5	3	2	1
155	23	15	20	15	12	7	6	5	4	2	1	16	12	13	11	9	5	5	4	3	2	1
156	22	14	17	13	10	6	5	4	3	2	1	12	11	11	9	7	5	4	3	2	1	1
157	39	25	19	15	12	7	6	5	4	2	1	15	13	13	11	8	5	5	4	3	2	1
158	24	16	20	15	11	7	6	5	3	2	1	13	11	11	10	8	5	4	3	2	1	1
159	20	13	14	11	8	5	4	4	3	2	1	11	10	10	8	6	4	3	3	2	1	<1
160	58	38	28	21	16	9	8	6	4	3	1	20	15	14	13	10	6	5	4	3	2	1
161	44	29	24	18	14	8	7	5	4	3	1	16	14	14	12	9	6	5	4	3	2	1
162	23	21	21	16	12	7	6	5	4	2	1	14	12	12	10	8	5	4	4	3	2	1

Appendix J: Adult Cancer Risk Estimated Cases for 54 Sequential Protocols for Male and Female aged from 10 to 80 years (case/10^6)

Table J - 1: Adult brain sequential protocols; Lifetime cancer risk for male and female case/10^6.

protocol	Female age (case/10^6)									Male age (case/10^6)								
	10	**15**	**20**	**30**	**40**	**50**	**60**	**70**	**80**	**10**	**15**	**20**	**30**	**40**	**50**	**60**	**70**	**80**
163	10	7	6	4	3	3	2	1	1	6	5	4	3	2	2	1	1	<1
164	9	7	5	3	3	2	2	1	<1	6	5	4	2	2	2	1	1	<1
165	9	7	6	3	3	2	2	1	<1	5	4	3	2	2	2	1	1	<1
166	11	8	6	4	3	3	2	1	1	7	6	5	3	3	2	2	1	<1
167	10	8	6	4	3	2	2	1	1	7	5	4	3	2	2	1	1	<1
168	9	7	6	4	3	2	2	1	1	7	5	4	3	2	2	1	1	<1
169	16	13	10	6	5	4	3	2	1	10	8	6	4	4	3	2	1	1
170	13	10	8	5	4	3	3	2	1	9	7	6	4	3	3	2	1	<1
171	13	10	8	5	4	3	3	2	1	9	7	5	3	3	3	2	1	<1
172	8	6	5	3	3	2	2	1	<1	6	5	4	2	2	2	1	1	<1
173	9	7	5	3	3	2	2	1	<1	6	5	4	2	2	2	1	1	<1
174	7	5	4	3	2	2	1	1	<1	5	4	3	2	2	1	1	1	<1
175	10	8	6	4	3	3	2	1	1	7	6	5	3	3	2	1	1	<1
176	10	8	6	4	3	3	2	1	1	7	5	4	3	2	2	1	1	<1
177	10	8	6	4	3	3	2	1	1	7	5	4	3	2	2	1	1	<1
178	14	11	8	5	4	4	3	2	1	10	8	6	4	4	3	2	1	1
179	12	10	7	5	4	3	3	2	1	9	7	6	4	3	3	2	1	<1
180	12	10	7	5	4	3	2	2	1	9	7	6	4	3	3	2	1	<1
181	10	8	6	4	3	3	2	1	1	7	6	4	3	2	2	1	1	<1
182	11	8	6	4	3	3	2	1	1	7	6	4	3	2	2	1	1	<1
183	9	7	6	3	3	2	2	1	1	7	5	4	3	2	2	1	1	<1
184	11	9	7	4	4	3	2	1	1	8	7	5	3	3	2	2	1	<1
185	12	10	7	5	4	3	2	1	1	8	6	5	3	3	2	2	1	<1
186	10	8	6	4	3	3	2	1	1	7	6	5	3	3	2	2	1	<1
187	17	13	10	6	5	4	3	2	1	11	9	7	5	4	3	2	1	1
188	15	12	9	6	5	4	3	2	1	11	8	7	4	4	3	2	1	1
189	14	11	9	5	5	4	3	2	1	10	8	6	4	3	3	2	1	1
190	15	11	9	5	5	4	3	2	1	10	8	6	4	3	3	2	1	1
191	15	11	9	6	5	4	3	2	1	10	8	6	4	4	3	2	1	1
192	14	11	8	5	4	4	3	2	1	10	8	6	4	3	3	2	1	<1
193	19	15	11	7	6	5	4	2	1	14	11	9	5	5	4	3	2	1
194	20	15	12	7	6	5	4	2	1	13	10	8	5	4	4	3	2	1
195	18	14	11	7	5	4	3	2	1	12	9	7	5	4	3	2	1	1
196	25	19	15	9	8	6	5	3	1	18	14	11	7	6	5	3	2	1
197	22	17	13	8	7	6	4	3	1	16	13	10	6	5	5	3	2	1
198	19	15	12	7	6	5	4	2	1	14	11	9	6	5	4	3	2	1
199	17	13	10	6	5	4	3	2	1	12	9	7	5	4	3	2	1	1
200	16	13	10	6	5	4	3	2	1	11	8	7	4	4	3	2	1	1
201	15	11	9	5	5	4	3	2	1	10	8	6	4	4	3	2	1	1
202	20	15	12	7	6	5	4	2	1	14	11	9	6	5	4	3	2	1
203	18	14	11	7	6	5	3	2	1	13	10	8	5	4	4	3	2	1
204	18	14	11	7	5	4	3	2	1	12	9	7	5	4	3	2	1	1
205	27	21	16	10	8	7	5	3	1	18	14	11	7	6	5	4	2	1
206	24	18	14	9	8	6	5	3	1	18	14	11	7	6	5	3	2	1
207	20	15	12	8	7	5	4	3	1	15	12	9	6	5	4	3	2	1
208	20	15	12	7	6	5	4	2	1	14	11	9	5	5	4	3	2	1
209	19	14	11	7	6	5	4	2	1	13	10	8	5	4	4	3	2	1
210	17	13	10	6	5	4	3	2	1	12	10	8	5	4	3	2	1	1
211	25	19	15	9	8	6	5	3	1	17	13	10	7	6	5	3	2	1
212	20	15	12	7	6	5	4	2	1	15	11	9	6	5	4	3	2	1
213	20	16	12	8	6	5	4	2	1	14	11	9	6	5	4	3	2	1
214	31	24	18	11	10	8	6	4	2	21	17	13	8	7	6	4	2	1
215	26	20	15	10	8	7	5	3	1	19	15	11	7	6	5	4	2	1
216	21	16	13	8	7	5	4	3	1	15	12	9	6	5	4	3	2	1

Appendix K: ED for Toshiba Aquilion 16 standard CT head scans protocols (adult and paediatric)

Table K - 1: Toshiba Aquilion helical protocol for adult CT head scans							
Angle (Degrees)	Rotation Time (S)	Image Thickness (mm)	Detector Configuration (mm)	Pitch factor / Helical Pitch	Sure Exp. 3D (ATC)	kV	Effective Dose (mSv)
0	1.0	5.0	0.5x16	Detail PF 0.688 / HP 11.0	High Quality 1.80	120	**1.3**
15							**1.5**
27							**1.5**

Table K - 2: Toshiba Aquilion sequential protocol for adult CT head scans						
Angle (Degrees)	Rotation Time (S)	Image Thickness (mm)	Detector Configuration (mm)	Sure Exp. 3D (ATC)	kV	Effective Dose (mSv)
0	1.0	4.0	2.0x4.0	off	120	**0.81**
15						**0.78**
27						**0.83**

Table K - 3: Toshiba Aquilion 3 months -3years protocol for paediatric CT head scans						
Angle (Degrees)	Rotation Time (S)	Image Thickness (mm)	Detector Configuration (mm)	kV	mA (fixed)	Effective Dose (mSv)
0	0.5	0.5	0.5x16	100	180	**1.5**
15						**1.6**
27						**1.7**

Table K - 4: Toshiba Aquilion 3 – 5 years protocol for paediatric CT head scans						
Angle (Degrees)	Rotation Time (S)	Image Thickness (mm)	Detector Configuration (mm)	kV	mA (fixed)	Effective Dose (mSv)
0	0.75	0.75	0.5x16	100	200	**2.4**
15						**2.7**
27						**2.5**

Table K - 5: Toshiba Aquilion 6 – 12 years protocol for paediatric CT head scans						
Angle (Degrees)	Rotation Time (S)	Image Thickness (mm)	Detector Configuration (mm)	kV	mA (fixed)	Effective Dose (mSv)
0	0.75	0.75	0.5x16	120	200	**3.6**
15						**3.5**
27						**3.6**

Appendix L: Toshiba Aquilion 16 standard CT head scans protocols ER Estimated Cases for adult and paediatric protocols for male and female aged from 0 – 5 and 10 - 80 years (case/10^6), respectively

Table L - 1: Toshiba Aquilion 16 adult brain standard helical protocol Lifetime cancer risk for male and female case/10^6.

gantry angle	Female age (case/10^6)									Male age (case/10^6)								
	10	**15**	**20**	**30**	**40**	**50**	**60**	**70**	**80**	**10**	**15**	**20**	**30**	**40**	**50**	**60**	**70**	**80**
0º	34	26	20	12	10	8	6	4	2	23	18	14	9	8	6	4	3	1
15º	41	32	25	15	13	11	8	5	2	28	22	18	11	10	8	6	3	1
27º	43	32	25	15	13	11	8	5	2	29	23	18	11	10	8	6	3	1

Table L - 2: Toshiba Aquilion 16 adult brain standard sequential protocol Lifetime cancer risk for male and female case/10^6.

gantry angle	Female age (case/10^6)									Male age (case/10^6)								
	10	**15**	**20**	**30**	**40**	**50**	**60**	**70**	**80**	**10**	**15**	**20**	**30**	**40**	**50**	**60**	**70**	**80**
0º	22	17	13	8	7	5	4	3	1	15	12	9	6	5	4	3	2	1
15º	22	17	13	8	7	6	4	3	1	15	12	10	6	5	4	3	2	1
27º	23	18	14	8	7	6	4	3	1	16	12	10	6	5	4	3	2	1

Table L - 3: Toshiba Aquilion 16 paediatric brain standard 3months -3years protocol Lifetime cancer risk for male and female case/10^6.

gantry angle	Female age (case/10^6)		Male age (case/10^6)	
	0	**5**	**0**	**5**
0º	69	42	36	22
15º	89	55	39	24
27º	97	60	44	28

Table L - 4: Toshiba Aquilion 16 paediatric brain standard 3 – 5 years protocol Lifetime cancer risk for male and female case/10^6.

gantry angle	Female age (case/10^6)		Male age (case/10^6)	
	0	**5**	**0**	**5**
0º	115	71	57	35
15º	148	89	78	48
27º	144	88	68	42

Table L - 5: Toshiba Aquilion 16 paediatric brain standard 6 – 12 years protocol Lifetime cancer risk for male and female case/10^6.

gantry angle	Female age (case/10^6)		Male age (case/10^6)	
	0	**5**	**0**	**5**
0º	174	107	84	52
15º	179	111	84	52
27º	179	111	86	54

Appendix M: Paediatric Effective Dose Data Normality and Correlation Statistical Tests

Table M - 1: Paediatric effective dose (mSv) summary statistics including an indication of the normality of the data.

Protocol Parameters		Mean, SD	Minimum	Maximum	P -Value Shapiro-Wilk
Tube rotation time (seconds)	0.5	0.74 ± 0.05	0.28	2.01	0.20
	0.75	0.76 ± 0.05	0.28	2.06	0.21
Gantry angulation (degree)	0º	0.80 ± 0.06	0.31	2.06	0.20
	15º	0.74 ± 0.06	0.30	1.82	0.20
	27º	0.71 ± 0.05	0.28	1.72	0.20
Detector configuration (mm)	0.5x16	1.10 ± 0.06	0.56	2.06	0.20
	1.0x16	0.66 ± 0.04	0.31	1.25	0.18
	2.0x16	0.49 ± 0.1	0.28	0.85	0.21
Helical Pitch (mm/rotation)	11	0.75 ± 0.06	0.30	2.01	0.20
	15	0.69 ± 0.05	0.28	1.74	0.20
	23	0.81 ± 0.06	0.33	2.06	0.21
Sure Exp. 3D (SD)	4.00	1.14 ± 0.06	0.58	2.06	0.20
	6.00	0.65 ± 0.03	0.35	1.15	0.20
	8.00	0.45 ± 0.02	0.28	0.77	0.21

Appendix N: List of Trainings Undertaken During the Course of the PhD

(All certified by the University of Salford, Manchester, UK)

Session No.	Title of training session	Date
Session 1	Seminar on doing Research – the scientific way • Ethics	10th February, 2014
Session 2	Introduction to Endnote X7 Reference Manager-beginners • Creating an EndNote Library • Importing references from databases • Creating references from PDF files	18th February, 2014
Session 3	Doing a literature review • How to use keywords and MeSH headings to search for published literature	19th February, 2014
Session 4	Electronic resources for researchers	12th March, 2014
Session 5	Seminar on Myers Briggs Type Indicator personality tool • To improve effectiveness of communication, team working, decision making and problem solving • To help researchers understand themselves, the impact they have on others, and how different personality styles and preferences can work together in complementary ways in a research environment	12th March, 2014
Session 6	Endnote training (advanced)	19th March, 2014
Session 7	TLDs training session - 1	1st April, 2014
Session 8	TLDs training session - 2	2nd April, 2014
Session 9	Completing a learning agreement and the PhD progression points	10th April, 2014
Session 10	Introduction to SPSS statistics package – beginners • Input primary data and excel data into SPSS • Upload previously coded data • Label and manipulate dataset to generate results and summary	17th April, 2014
Session 11	SPSS with Statistics – advanced • How to run parametric and non-parametric statistics • Edit graphical output from SPSS • How to report results from SPSS	18th April, 2014
Session 12	Referencing your work APA (Harvard) style	12th April, 2014
Session 13	Supporting and Motivating your Research	22nd April, 2014
Session 14	Critical Thinking at Postgraduate Level	25th April, 2014
Session 15	Structuring your research	30th April, 2014
Session 16	Writing research method section of a thesis	6th May,2014

Session 17	Statistics with SPSS – Questions and answers session webinar • The facilitator answered questions from the previous two SPSS sessions	23rd May, 2014
Session 18	Word Scopus workshop (Scopus Writing)	10 Sessions-1.5 hour each
Session 19	Research ideas, Questions and Theoretical Frameworks	5th November, 2014
Session 20	Literature Searching and a Literary Review Skills	5th November, 2014
Session 21	Training on Endnote X7 Reference Manager-advanced • Creating groups in Endnote library • Creating in-text citations • Formatting bibliographies in Microsoft Word	18th November, 2014
Session 22	Intellectual property rights for research students	2nd December, 2014
Session 23	Structuring your Research Findings	31st January, 2015
Session 24	How to get published with the IEEE	17th February, 2015
Session 25	MOSFETs training course – Day 1	22nd May, 2015
Session 26	MOSFETs training course – Day 2	23rd May, 2015
Session 27	Thinking and Writing Critically	24th May, 2015
Session 28	Finding Journal Articles: Health and Social Care • Searching the SOLAR library catalogue • Finding journal articles for health and social care subjects • How to save favourites and search results	25th February, 2016
Session 29	Critical Thinking and Critical Writing at Doctoral Level • Analyse and chart professional progression using a critical reflective process and learning style analysis • Develop skills to evaluate research critically and include an evidence-based research to promote optimal findings • Examine critically reflective practice, problem solving and creative ethical decision making	18th May, 2016

Appendix O: List of Developed Skills

No	Type of skill
1	How to search for published literature using scientific databases
2	How to critically analyse published literature
3	How to use published literature for writing
4	How to use Microsoft word, excel and PowerPoint at the advanced level
5	How to conduct scientific research at the PhD level
6	How to use Endnote reference manager for in-text citation
7	How to operate and use the Computer Tomography (CT) machine
8	How to use TLD system for the direct measurement of dose
9	How to use MOSFET system for the direct measurement of dose
10	How to write journal papers and design posters for conference presentation
11	How to work effectively with people of different personality traits
12	How to use the Unfors dosimeter for dose measurements and QA protocols
13	How to use the SPSS statistical software to analyse data
14	How to present at a conference
15	A variety of reading skills
16	How to think and write critically at the PhD level
17	How to use the DR and CR X-ray machine
18	How to use RadiAnt DICOM Viewer (64-bit) software for image manipulation
19	How to use the ImageJ software for Hounsfield unit calculation
20	How to use parametric and non-parametric statistical tests
21	How to develop a questionnaire

Reference List

AAPM. (2012). The American Association of Physicists in Medicine (AAPM). Adult Routine Head (Brain) CT Protocols Version 1.1. Retrieved from: https://www.aapm.org/pubs/CTProtocols/documents/AdultRoutineHeadCT.

AAPM. (2016). The American Association of Physicists in medicine (AAPM). Adult Routine Head (Brain) CT Protocols Version 2.0. Retrieved from: https://www.aapm.org/pubs/CTProtocols/documents/AdultRoutineHeadCT.

ACR. (2010). American College of Radiology. CT Accreditation Program Requirements. 13 September 2010. Journal of the American College of Radiology, 8(11), pp.795-803.

Akhlaghi, P., Hakimabad, H. M., & Motavalli, L. R. (2014). An overview of exposure parameters, dose measurements and strategies for dose reduction in pediatric CT examinations. Radioprotection, 49(1), 9-15.

Alessio, A. M., & Phillips, G. S. (2010). A paediatric CT dose and risk estimator. Pediatr Radiol, 40 (11), 1816-1821.

Allisy-Roberts, P., & Williams, J. R. (2007). Farr's physics for medical imaging: Elsevier Health Sciences.

Arch, M. E., & Frush, D. P. (2008). Paediatric body MDCT: a 5-year follow-up survey of scanning parameters used by paediatric radiologists. American Journal of Roentgenology, 191 (2), 611-617.

Archambault, L., Briere, T. M., Pönisch, F., Beaulieu, L., Kuban, D. A., Lee, A., & Beddar, S. (2010). Toward a Real-Time In Vivo Dosimetry System Using Plastic Scintillation Detectors. International Journal of Radiation Oncology*Biology*Physics, 78(1), 280-287.

Asbury, C., (2011). Brain imaging technologies and their applications in neuroscience. The Dana Foundation, pp.1-45.

ASN. (2001). ANS, American Nuclear Society. Health Effects of Low-Level Radiation - Position Statement 41. June 2001. Journal of nuclear cardiology: official publication of the American Society of Nuclear Cardiology, 8 (1), G5.

Atherton, J. V., & Huda, W. (1996). Energy imparted and effective doses in computed tomography. Medical Physics, 23 (5), 735-741.

Attix, F. (2004). Introduction to Radiological Physics and Radiation Protection: Wiley& Sons.

Attix, F. H. (2008). Introduction to radiological physics and radiation dosimetry. New York John Wiley & Sons.

Attix, F. H., & Tochilin, E. (2016). Sources, Fields, Measurements, and Applications: Radiation Dosimetry (Vol. 3): Academic Press.

Aurengo, A., Averbeck, D., Bonnin, A., Le Guen, B., Masse, R., Monier, R., de Vathaire, F. (2005). French Academy of Sciences-French National Academy of Medicine Dose-effect relationships and estimation of the carcinogenic effects of low doses of ionizing radiation.

Axelsson, B., Persliden, J., & Schuwert, P. (1996). Dosimetry for computed tomography examination of children. Radiation Protection Dosimetry, 64 (3), 221-226.

Bagg, S. A., Steenburg, S. D., & Ravenel, J. G. (2008). Handling of outside trauma studies: a survey of program directors. Journal of the American College of Radiology, 5 (5), 657-663.

Baliga, B. J. (2008). Power mosfets Fundamentals of Power Semiconductor Devices (pp. 276-503): Springer.

Balonov, M., & Shrimpton, P. (2012). Effective dose and risks from medical x-ray procedures. Annals of the ICRP, 41(3), 129-141.

Bauhs, J. A., Vrieze, T. J., Primak, A. N., Bruesewitz, M. R., & McCollough, C. H. (2008). CT dosimetry: comparison of measurement techniques and devices 1. RadioGraphics, 28 (1), 245-253.

BEIR VII. (2006). Committee to Assess Health Risks from Exposure to Low Levels of Ionizing Radiation. Health Risks from Exposure to Low Levels of Ionizing Radiation. BEIR VII. Phase 2, Washington, DC: National Research Council. Paper presented at the National Academy of Science.

Bernier, M., Rehel, J., Brisse, H., Wu-Zhou, X., Caer-Lorho, S., Jacob, S., Laurier, D. (2012). Radiation exposure from CT in early childhood: a French large-scale multicentre study. The British Journal of Radiology.

Bibb, R., Eggbeer, D., & Paterson, A. (2015). 2 - Medical Imaging Medical Modelling (Second Edition) (pp. 7-34). Oxford: Woodhead Publishing.

Bicron, H. (2001). Model 4500 manual TLD reader with winrems: operator's manual. Solon, Bicron.

Bischoff, B., Hein, F., Meyer, T., Krebs, M., Hadamitzky, M., Martinoff, S., Hausleiter, J. r. (2010). Comparison of sequential and helical scanning for radiation dose and image quality: results of the Prospective Multicenter Study on Radiation Dose Estimates of Cardiac CT Angiography (PROTECTION) I Study. American Journal of Roentgenology, 194 (6), 1495-1499.

Biswas, D., Bible, J. E., Bohan, M., Simpson, A. K., Whang, P. G., & Grauer, J. N. (2009). Radiation exposure from musculoskeletal computerized tomographic scans. JBJS, 91(8), 1882-1889.

Blackwell, C. D., Gorelick, M., Holmes, J. F., Bandyopadhyay, S., & Kuppermann, N. (2007). Pediatric head trauma: changes in use of computed tomography in emergency departments in the United States over time. Annals of emergency medicine, 49 (3), 320-324.

Blecher, C. M. (2010). Alarm about computed tomography scans is unjustified. The Medical journal of Australia, 192 (12), 723.

Bongartz, G., Golding, S., Jurik, A., Leonardi, M., Van Persijn Van Meerten, E., Rodríguez, R., Jessen, K. (2004). European guidelines for multislice computed tomography. European Commission.

Boone, J. M. (2012). Reply to "Comment on the 'Report of AAPM TG 204: Size-specific dose estimates (SSDE) in paediatric and adult body CT examinations" [AAPM Report 204, 2011]. Medical Physics, 39 (7), 4615-4616.

Boone, J. M., Geraghty, E. M., Seibert, J. A., & Wootton-Gorges, S. L. (2003). Dose reduction in paediatric CT: A rational approach 1. Radiology, 228 (2), 352-360.

Borrás, C., Huda, W., & Orton, C. G. (2010). The use of effective dose for medical procedures is inappropriate. Medical Physics, 37 (7), 3497-3500.

Bos, A. (2001). High sensitivity thermoluminescence dosimetry. Nuclear Instruments and Methods in Physics Research Section B: Beam Interactions with Materials and Atoms, 184 (1), 3-28.

Bos, A. (2007). Theory of thermoluminescence. Radiation Measurements, 41, S45-S56.

Brady, Z., Cain, T. M., & Johnston, P. N. (2011). Paediatric CT imaging trends in Australia. Journal of medical imaging and radiation oncology, 55 (2), 132-142.

Brady, Z., Cain, T., & Johnston, P. (2012). Comparison of organ dosimetry methods and effective dose calculation methods for paediatric CT. Australasian physical & engineering sciences in medicine, 35 (2), 117-134.

Brady, Z., Ramanauskas, F., Cain, T., & Johnston, P. (2014). Assessment of paediatric CT dose indicators for the purpose of optimisation. The British Journal of Radiology.

Brain basic. (2015). Brain Basics: Know Your Brain. National Institute of Neurological Disorders and Stroke. Retrieved from: http://www.ninds.nih.gov/disorders/brain_basics/brain_basics_know_your_brain.pdf

Brenner, D. (2008). Effective dose: a flawed concept that could and should be replaced. The British Journal of Radiology.

Brenner, D. J. (2002). Estimating cancer risks from pediatric CT: going from the qualitative to the quantitative. Pediatr Radiol, 32 (4), 228-231.

Brenner, D. J. (2010). Slowing the increase in the population dose resulting from CT scans. Radiation research, 174(6b), 809-815.

Brenner, D. J. (2014). What we know and what we don't know about cancer risks associated with radiation doses from radiological imaging. The British Journal of Radiology, 87(1035), 20130629. doi:10.1259/bjr.20130629

Brenner, D. J., & Hall, E. J. (2007). Computed tomography—an increasing source of radiation exposure. New England Journal of Medicine, 357 (22), 2277-2284.

Brenner, D. J., & Hall, E. J. (2012). Cancer risks from CT scans: now we have data, what next? : Radiological Society of North America, Inc.

Brenner, D. J., & Hricak, H. (2010). Radiation exposure from medical imaging: time to regulate? Jama, 304 (2), 208-209.

Brenner, D. J., Doll, R., Goodhead, D. T., Hall, E. J., Land, C. E., Little, J. B., Puskin, J. S. (2003). Cancer risks attributable to low doses of ionizing radiation: assessing what we really know. Proceedings of the National Academy of Sciences, 100 (24), 13761-13766.

Brenner, D. J., Elliston, C. D., Hall, E. J., & Berdon, W. E. (2001a). Estimated risks of radiation-induced fatal cancer from paediatric CT. American Journal of Roentgenology, 176 (2), 289-296.

Brenner, D. J., Elliston, C. D., Hall, E. J., & Berdon, W. E. (2001b). Estimates of the cancer risks from paediatric CT radiation are not merely theoretical: Comment on "Point/Counterpoint: In x-ray computed tomography, technique factors should be selected appropriate to patient size. Against the Proposition" [Med. Phys. 28, 1543–1545 (2001)]. Medical Physics, 28 (11), 2387-2388.

Brenner, D. J., Elliston, C. D., Hall, E. J., & Berdon, W. E. (2001c). Response to the statement by The Society for Paediatric Radiology on radiation risks from paediatric CT scans. Pediatr Radiol, 31(6), 389-391.

Brink, J. A., & Amis Jr, E. S. (2010). Image wisely: a campaign to increase awareness about adult radiation protection 1: Radiological Society of North America, Inc.

Brink, J. A., Goske, M. J., & Patti, J. A. (2011). Informed consent for radiologic procedures. Jama, 305 (9), 888-890.

Brisse, H. J., Robilliard, M., Savignoni, A., Pierrat, N., Gaboriaud, G., De Rycke, Y., Rosenwald, J.-C. (2009). Assessment of organ absorbed doses and estimation of effective doses from pediatric anthropomorphic phantom measurements for multi-detector row CT with and without automatic exposure control. Health physics, 97 (4), 303-314.

Brix, G., Lechel, U., Veit, R., Truckenbrodt, R., Stamm, G., Coppenrath, E., Nagel, H.-D. (2004). Assessment of a theoretical formalism for dose estimation in CT: an anthropomorphic phantom study. Eur Radiol, 14 (7), 1275-1284.

Brix, G., Nagel, H., Stamm, G., Veit, R., Lechel, U., Griebel, J., & Galanski, M. (2003). Radiation exposure in multi-slice versus single-slice spiral CT: results of a nationwide survey. Eur Radiol, 13 (8), 1979-1991.

Broder, J. S. (2008). CT utilization: the emergency department perspective. Pediatr Radiol, 38(4), 664.

Broder, J., & Preston, R. (2011). Chapter 1 - Imaging the Head and Brain Diagnostic Imaging for the Emergency Physician (pp. 1-45). Saint Louis: W.B. Saunders.

Brody, A. S., Frush, D. P., Huda, W., & Brent, R. L. (2007). Radiation risk to children from computed tomography. Paediatrics, 120 (3), 677-682.

Budoff, M. J. (2009). Maximizing dose reductions with cardiac CT. The international journal of cardiovascular imaging, 25 (2), 279-287.

Bushberg, J. T., & Boone, J. M. (2011). The essential physics of medical imaging: Lippincott Williams & Wilkins.

Bushberg, J. T., Seibert, J., Leidholdt, E., & Boone, J. (2002). Computed tomography. The essentials of medical imaging. Philadelphia: Lippincott Williams & Wilkins, 355-356.

Bushong, S. C. (2000). Computed Tomography: Essential of Medical Imaging Series. The MacGraw-Hill Companies, New York.

Bushong, S. C. (2013). Radiologic Science for Technologists-E-Book: Physics, Biology, and Protection (10th ed): Elsevier Health Sciences.

Butler, P., & Mitchell, A. W. (2012). Applied radiological anatomy (2nd ed.): Cambridge University Press.

Byng, J., Mainprize, J., & Yaffe, M. (1998). X-ray characterization of breast phantom materials. Phys Med Biol, 43(5), 1367.

Calabrese, E. J., & O'Connor, M. K. (2014). Estimating risk of low radiation doses–a critical review of the BEIR VII Report and its use of the linear no-threshold (LNT) hypothesis. Radiation research, 182 (5), 463-474.

Camargo-Mendoza, R. E., Poletti, M. E., Costa, A. M., & Caldas, L. V. (2011). Measurement of some dosimetric parameters for two mammography systems using thermoluminescent dosimetry. Radiation Measurements, 46 (12), 2086-2089.

Campbell, J., Kalra, M. K., Rizzo, S., Maher, M. M., & Shepard, J.-A. (2005). Scanning beyond anatomic limits of the thorax in chest CT: findings, radiation dose, and automatic tube current modulation. American Journal of Roentgenology, 185 (6), 1525-1530.

Caon, M., Bibbo, G., & Pattison, J. (1999). An EGS4-ready tomographic computational model of a 14-year-old female torso for calculating organ doses from CT examinations. Phys Med Biol, 44 (9), 2213.

Cardis, E., Vrijheid, M., Blettner, M., Gilbert, E., Hakama, M., Hill, C., Schubauer-Berigan, M. (2007). The 15-Country Collaborative Study of Cancer Risk among Radiation Workers in the Nuclear Industry: estimates of radiation-related cancer risks. Radiation research, 167 (4), 396-416.

Carolan, M. G. (2003). Semiconductor dosimetry of epithermal neutron beams for Boron neutron capture therapy.

Carvajal, M. A., Vilches, M., Guirado, D., Lallena, A. M., Banqueri, J., & Palma, A. J. (2010). Readout techniques for linearity and resolution improvements in MOSFET dosimeters. Sensors and Actuators A: Physical, 157(2), 178-184.

Chapple, C., Willis, S., & Frame, J. (2002). Effective dose in paediatric computed tomography. Phys Med Biol, 47 (1), 107.

Cheung, T., Butson, M. J., & Yu, P. (2009). Energy dependence corrections to MOSFET dosimetric sensitivity. Australasian Physics & Engineering Sciences in Medicine, 32 (1), 16-20.

Chodick, G., Kim, K., Shwarz, M., Horev, G., Shalev, V., & Ron, E. (2009). Radiation risks from pediatric computed tomography scanning. Pediatric endocrinology reviews: PER, 7 (2), 29-36.

Chodick, G., Ronckers, C., Ron, E., & Shalev, V. (2006). The utilization of paediatric computed tomography in a large Israeli Health Maintenance Organization. Pediatr Radiol, 36 (6), 485-490.

Christner, J. A., Kofler, J. M., & McCollough, C. H. (2010). Estimating effective dose for CT using dose–length product compared with using organ doses: consequences of adopting International Commission on Radiological Protection Publication 103 or dual-energy scanning. American Journal of Roentgenology, 194 (4), 881-889.

Chuang, C. F., Verhey, L. J., & Xia, P. (2002). Investigation of the use of MOSFET for clinical IMRT dosimetric verification. Medical Physics, 29 (6), 1109-1115.

Chwals, W. J., Robinson, A. V., Sivit, C. J., Alaedeen, D., Fitzenrider, E., & Cizmar, L. (2008). Computed tomography before transfer to a level I pediatric trauma center risks duplication with associated increased radiation exposure. J Pediatr Surg, 43 (12), 2268-2272.

CIRS. (2013). CIRS tissue simulation and phantom technology. ATOM Dosimetry verification phantoms model 701 - 706 data sheet; 2013. 2428 Almeda Avenue Suite 316, Norfolk, Virginia 23513 USA. Retrieved from: http://www.cirsinc.com/file/Products/701_706/701_706_DS.pdf

Cody, D. D., & Mahesh, M. (200). Technologic Advances in Multidetector CT with a Focus on Cardiac Imaging 1. RadioGraphics, 27 (6), 1829-1837.

Cohen, A., Hughes, K., Fahey, N., Caldwell, B., Wang, C. H., & Park, S. (2016). Wide Variation in Radiation Exposure During Computerized Tomography. Urology, 95, 47-53.

Cohen, M. D. (2009). Pediatric CT radiation dose: how low can you go? American Journal of Roentgenology, 192 (5), 1292-1303.

Cohnen, M., Fischer, H., Hamacher, J., Lins, E., Kötter, R., & Mödder, U. (2000). CT of the head by use of reduced current and kilovoltage: relationship between image quality and dose reduction. American Journal of Neuroradiology, 21 (9), 1654-1660.

Cohnen, M., Wittsack, H.-J., Assadi, S., Muskalla, K., Ringelstein, A., Poll, LMödder, U. (2006). Radiation exposure of patients in comprehensive computed tomography of the head in acute stroke. American Journal of Neuroradiology, 27 (8), 1741-1745.

Colagrande, S., Origgi, D., Zatelli, G., Giovagnoni, A., & Salerno, S. (2014). CT exposure in adult and paediatric patients: a review of the mechanisms of damage, relative dose and consequent possible risks. La radiologia medica, 119 (10), 803-810.

Commission, C. o. t. E. (1997). Council directive 97/43/EURATOM of 30 June 1997 on health protection of individuals against the dangers of ionizing radiation in relation to medical exposure. Official Journal of the European Communities, 180, 22-27.

Commission, E. P., Medicines, E. D. f. t. Q. o., & Healthcare. (2010). European pharmacopoeia (Vol. 1): Council of Europe.

Commission, I. E. (2010). Medical electrical equipment—Part 2-44: particular requirements for the basic safety and essential performance of X-ray equipment for computed tomography. International Standard IEC, 60601-60602.

Cook, S. H., Fielding, J. R., & Phillips, J. D. (2010). Repeat abdominal computed tomography scans after pediatric blunt abdominal trauma: missed injuries, extra costs, and unnecessary radiation exposure. J Pediatr Surg, 45 (10), 2019-2024.

Coursey, C. A., & Frush, D. P. (2008). CT and radiation: What radiologists should know? Applied radiology, 37 (3), 22.

Coursey, C., Frush, D. P., Yoshizumi, T., Toncheva, G., Nguyen, G., & Greenberg, S. B. (2008). Pediatric chest MDCT using tube current modulation: effect on radiation dose with breast shielding. American Journal of Roentgenology, 190(1), W54-W61.

Coutts, S. B., Lev, M. H., Eliasziw, M., Roccatagliata, L., Hill, M. D., Schwamm, L. H., Buchan, A. M. (2004). ASPECTS on CTA Source Images Versus Unenhanced CT. Stroke, 35(11), 2472-2476.

Cretti, F., & Perugini, G. (2016). Patient dose evaluation for the whole-body low-dose multidetector CT (WBLDMDCT) skeleton study in multiple myeloma (MM). La radiologia medica, 121 (2), 93-105.

Cristy, M. (1981). Active bone marrow distribution as a function of age in humans. Phys Med Biol, 26 (3), 389.

Crossman, A. R., & Neary, D. (2014). Neuroanatomy: an illustrated colour text: Elsevier Health Sciences.

Davis, T., & Ings, A. (2014). Head injury: triage, assessment, investigation and early management of head injury in children, young people and adults (NICE guideline CG 176). Archives of Disease in Childhood-Education and Practice, edpract-2014-306797.

Dawson, P. (2004). Patient dose in multislice CT: why is it increasing and does it matter? The British Journal of Radiology, 77(suppl_1), S10-S13.

de Campo, J. F., & de Campo, M. P. (2010). Is informed consent necessary for computed tomography in children and young adults? The Medical journal of Australia, 192 (7), 423.

de Gonzalez, A. B., & Darby, S. (2004). Risk of cancer from diagnostic X-rays: estimates for the UK and 14 other countries. The lancet, 363 (9406), 345-351.

de González, A. B., Mahesh, M., Kim, K.-P., Bhargavan, M., Lewis, R., Mettler, F., & Land, C. (2009). Projected cancer risks from computed tomographic scans performed in the United States in 2007. Archives of internal medicine, 169 (22), 2071-2077.

de Mendivil, A. O., Alcalá-Galiano, A., Ochoa, M., Salvador, E., & Millán, J. M. (2013). Brainstem Stroke: Anatomy, Clinical and Radiological Findings. Seminars in Ultrasound, CT and MRI, 34 (2), 131-141.

Deak, P. D., Smal, Y., & Kalender, W. A. (2010). Multisection CT protocols: Sex-and age-specific conversion factors used to determine effective dose from dose-length product 1. Radiology, 257 (1), 158-166.

Dekaban, A. S., & Sadowsky, D. (1978). Changes in brain weights during the span of human life: relation of brain weights to body heights and body weights. Annals of neurology, 4 (4), 345-356.

DeMarco, J., Cagnon, C., Cody, D., Stevens, D., McCollough, C. H., Zankl, M., McNitt-Gray, M. (2007). Estimating radiation doses from multidetector CT using Monte Carlo simulations: effects of different size voxelized patient models on magnitudes of organ and effective dose. Phys Med Biol, 52 (9), 2583.

Den Harder, A.M., Willemink, M.J., Bleys, R.L., de Jong, P.A., Budde, R.P., Schilham, A.M. and Leiner, T., (2014). Dose reduction for coronary calcium scoring with hybrid and model-based iterative reconstruction: an ex vivo study. The international journal of cardiovascular imaging, 30 (6), pp.1125-1133.

DeWerd, L. A., & Wagner, L. K. (1999). Characteristics of radiation detectors for diagnostic radiology. Applied radiation and isotopes, 50 (1), 125-136.

Dobrzyński, L., Fornalski, K. W., & Feinendegen, L. E. (2015). Cancer Mortality Among People Living in Areas with Various Levels of Natural Background Radiation. Dose-Response, 13(3), 1559325815592391. Doi: 10.1177/1559325815592391

Donnelly, L. F. (2005). Reducing radiation dose associated with pediatric CT by decreasing unnecessary examinations. American Journal of Roentgenology, 184 (2), 655-657.

Donnelly, L. F., & Frush, D. P. (2001). Fallout from recent articles on radiation dose and pediatric CT. Pediatr Radiol, 31 (6), 388-388.

Donnelly, L. F., Emery, K. H., Brody, A. S., Laor, T., Gylys-Morin, V. M., Anton, C. G., Frush, D. P. (2001). Minimizing radiation dose for pediatric body applications of single-detector helical CT: strategies at a large children's hospital. American Journal of Roentgenology, 176 (2), 303-306.

Donnelly, L.F., (2002). Lessons from history. Pediatric radiology, 32 (4), pp.287-292.

Dorfman, A. L., Fazel, R., Einstein, A. J., Applegate, K. E., Krumholz, H. M., Wang, Y., Nallamothu, B. K. (2011). Use of medical imaging procedures with ionizing radiation in children: a population-based study. Archives of pediatrics & adolescent medicine, 165 (5), 458-464.

Dougeni, E., Faulkner, K., & Panayiotakis, G. (2012). A review of patient dose and optimisation methods in adult and paediatric CT scanning. European Journal of Radiology, 81 (4), e665-e683.

Dowsett, D., Kenny, P. A., & Johnston, R. E. (2006). The Physics of Diagnostic Imaging Second Edition: CRC Press.

Dubbins, P., Price, J., Johnson, K., Maguire, S. A., Wall, M., Jaspan, T., Kemp, A. M. (2008). Standards for radiological investigations of suspected non-accidental injury.

Duggan, L., Warren-Forward, H., Smith, T., & Kron, T. (2014). Investigation of dose reduction in neonatal radiography using specially designed phantoms and LiF: Mg, Cu, P TLDs. The British Journal of Radiology.

Duzenli, C., Hilts, M., & Jirasek, A. (2005). Technical considerations for implementation of x-ray CT polymer gel dosimetry. Physics in Medicine & Biology: An official journal of the Institute of Physical Sciences in Medicine (8), 1727-1746.

Einstein, A. J., Henzlova, M. J., & Rajagopalan, S. (2007). Estimating risk of cancer associated with radiation exposure from 64-slice computed tomography coronary angiography. Jama, 298 (3), 317-323.

Einstein, A. J., Moser, K. W., Thompson, R. C., Cerqueira, M. D., & Henzlova, M. J. (2007). Radiation dose to patients from cardiac diagnostic imaging. Circulation, 116 (11), 1290-1305.

Elbakri, I. A., & Kirkpatrick, I. D. (2013). Dose-length product to effective dose conversion factors for common computed tomography examinations based on Canadian clinical experience. Canadian Association of Radiologists Journal, 64 (1), 15-17.

Elliott, A. (2009). Issues in medical exposures. Journal of radiological Protection, 29 (2A), A107.

European Commission. (1996). European protocol on dosimetry in mammography. European Commission Report EUR 16263 EN (Luxembourg: European Commission). Retrieved from: http:// www.europa.eu.int

Farrell-Carnahan, L., Franke, L., Graham, C., & McNamee, S. (2013). Subjective sleep disturbance in veterans receiving care in the Veterans Affairs Polytrauma System following blast-related mild traumatic brain injury. Military medicine, 178 (9), 951-956.

Fazel, R., Krumholz, H. M., Wang, Y., Ross, J. S., Chen, J., Ting, H. H., Nallamothu, B. K. (2009). Exposure to low-dose ionizing radiation from medical imaging procedures. New England Journal of Medicine, 361 (9), 849-857.

FDA. (2009). US Food Drug Administration. Safety investigation of CT brain perfusion scans: initial notification. FDA website. www. fda. gov/MedicalDevices/Safety/AlertsandNotices/ucm193293. htm. Published October, 8.

FDA. (2010). US Food and Drug Administration. FDA Safety Investigation of CT Brain Perfusion Scans: Update 9 November. American Journal of Neuroradiology, 31 (1), 2-3.

Fenton, S. J., Hansen, K. W., Meyers, R. L., Vargo, D. J., White, K. S., Firth, S. D., & Scaife, E. R. (2004). CT scan and the pediatric trauma patient—are we overdoing it? J Pediatr Surg, 39 (12), 1877-1881.

Fernández-Gil, M. Á., Palacios-Bote, R., Leo-Barahona, M., & Mora-Encinas, J. (2010). Anatomy of the brainstem: a gaze into the stem of life. Paper presented at the Seminars in Ultrasound, CT and MRI.

Field, A. (2015). Discovering statistics using IBM SPSS statistics (4th ed.): Sage.

Flohr, T. G., Schaller, S., Stierstorfer, K., Bruder, H., Ohnesorge, B. M., & Schoepf, U. J. (2005). Multi–detector row CT systems and image-reconstruction techniques. Radiology, 235(3), 756-773.

Fricke, B. L., Donnelly, L. F., Frush, D. P., Yoshizumi, T., Varchena, V., Poe, S. A., & Lucaya, J. (2003). In-plane bismuth breast shields for pediatric CT: effects on radiation dose and image quality using experimental and clinical data. American Journal of Roentgenology, 180 (2), 407-411.

Frush, D. P. (2008). Pediatric dose reduction in computed tomography. Health physics, 95 (5), 518-527.

Frush, D. P. (2009). Radiation safety. Pediatr Radiol, 39 (3), pp.385-390.

Frush, D. P., & Yoshizumi, T. (2006). Conventional and CT angiography in children: dosimetry and dose comparisons. Pediatr Radiol, 36 (2), 154.

Frush, D. P., Donnelly, L. F., & Rosen, N. S. (2003). Computed tomography and radiation risks: what pediatric health care providers should know. Pediatrics, 112 (4), 951-957.

Frush, D. P., Donnelly, L. F., & Rosen, N. S. (2003). Computed tomography and radiation risks: what pediatric health care providers should know. Pediatrics, 112 (4), 951-957.

Fuchs, T., Kachelrieß, M., & Kalender, W. A. (2000). Technical advances in multi–slice spiral CT. European Journal of Radiology, 36 (2), 69-73.

Fujii, K., Aoyama, T., Koyama, S. and Kawaura, C., 2007. Comparative evaluation of organ and effective doses for paediatric patients with those for adults in chest and abdominal CT examinations. The British journal of radiology, 80 (956), pp.657-667.

Fujii, K., Aoyama, T., Yamauchi-Kawaura, C., Koyama, S., Yamauchi, M., Ko, S., Nishizawa, K. (2009). Radiation dose evaluation in 64-slice CT examinations with adult and paediatric anthropomorphic phantoms. The British Journal of Radiology.

Funama, Y., Awai, K., Nakayama, Y., Kakei, K., Nagasue, N., Shimamura, M., Yamashita, Y. (2005). Radiation dose reduction without degradation of low-contrast detectability at abdominal multisection CT with a low–tube voltage technique: phantom study 1. Radiology, 237 (3), 905-910.

Fung, K. K. (2004). Investigation of dosimetric characteristics of the high sensitivity LiF: Mg, Cu, P thermoluminescent dosemeter and its applications in diagnostic radiology—a review. Radiography, 10 (2), 145-150.

Galanski, M., Nagel, H., & Stamm, G. (2005). Paediatric CT exposure practice in the Federal Republic of Germany. Results of a nation-wide survey in, 6, 2006.

Galanski, M., Nagel, H., & Stamm, G. (2007). Paediatric CT exposure practice in the federal republic of Germany: results of a nationwide survey in 2005–2006. Medizinische Hochschule, Hannover.

Galup-Montoro, C., & Schneider, M. C. (2007). MOSFET modeling for circuit analysis and design: World scientific.

Galup-Montoro, C., Schneider, M.C., Cunha, A.I.A., de Sousa, F.R., Klimach, H. and Siebel, O.F., (2007), September. The advanced compact MOSFET (ACM) model for circuit analysis and design. In Custom Integrated Circuits Conference, 2007. CICC'07. IEEE (pp. 519-526). IEEE.

GE Medical System. (2001). Dose in Computed Tomography Basics, Challenges, and Solutions. Technical Report, 71113-BE France.

Geleijns, J., Wang, J., & McCollough, C. (2010). The use of breast shielding for dose reduction in pediatric CT: arguments against the proposition. Pediatr Radiol, 40 (11), 1744-1747.

Gerber, T. C., Kuzo, R. S., & Morin, R. L. (2005). Techniques and parameters for estimating radiation exposure and dose in cardiac computed tomography. The international journal of cardiovascular imaging, 21 (1), 165-176.

Ghotbi, N., Ohtsuru, A., Ogawa, Y., Morishita, M., Norimatsu, N., Namba, H., Yamashita, S. (2006). Pediatric CT scan usage in Japan: results of a hospital survey. Radiation medicine, 24 (8), 560-567.

Giacco, G., Cannata, V., Furetta, C., Santopietro, F., & Fariello, G. (2001). On the use of pediatric phantoms in the dose evaluation during computed tomography (CT) thorax examinations. Medical Physics, 28 (2), 199-204.

Giedd, J. N. (2008). The Teen Brain: Insights from Neuroimaging. Journal of Adolescent Health, 42(4), 335-343.

Golding, S., & Shrimpton, P. (2002). Radiation dose in CT: are we meeting the challenge? The British Journal of Radiology, 75 (889), 1-4.

Goldman, L. W. (2007). Principles of CT: radiation dose and image quality. J Nucl Med Technol, 35 (4), 213-225.

Goldman, L. W. (2008). Principles of CT: multislice CT. J Nucl Med Technol, 36 (2), 57-68.

Goo, H. W. (2012). CT radiation dose optimization and estimation: an update for radiologists. Korean journal of radiology, 13 (1), 1-11.

Gordon, W. A., Zafonte, R., Cicerone, K., Cantor, J., Brown, M., Lombard, L., Chandna, T. (2006). Traumatic brain injury rehabilitation: state of the science. American Journal of Physical Medicine & Rehabilitation, 85 (4), 343-382.

Goske, M. J., & Bulas, D. (2009). Improving health literacy: informed decision-making rather than informed consent for CT scans in children. Pediatr Radiol, 39 (9), 901-903.

Goske, M. J., Applegate, K. E., Boylan, J., Butler, P. F., Callahan, M. J., Coley, B. D., Jaramillo, D. (2008a). The Image Gently campaign: working together to change practice. American Journal of Roentgenology, 190 (2), 273-274.

Goske, M. J., Applegate, K. E., Boylan, J., Butler, P. F., Callahan, M. J., Coley, B. D., Jaramillo, D. (2008b). The 'Image Gently'campaign: increasing CT radiation dose awareness through a national education and awareness program. Pediatr Radiol, 38 (3), 265-269.

Gower-Thomas, K., Lewis, M., Shiralkar, S., Snow, M., Galland, R., & Rennie, A. (2002). Doctors' knowledge of radiation exposures is deficient. BMJ: British Medical Journal, 324 (7342), 919.

Graham, D. T., & Cloke, P. J. (2003). Principles of radiological physics (4th ed.): Elsevier Health Sciences.

Graser, A., Wintersperger, B., Suess, C., Reiser, M., & Becker, C. (2006). Dose reduction and image quality in MDCT colonography using tube current modulation. American Journal of Roentgenology, 187 (3), 695-701.

Gray, H. (2014). Anatomy of the human body (20th ed.): Lea & Febiger.

Gray, H., Standring, S., Anand, N., Birch, R., Collins, P., Crossman, A.R., Gleeson, M., Jawaheer, G., Smith, A.L., Spratt, J.D. and Stringer, M.D., (2016). Gray's anatomy: the anatomical basis of clinical practice. Elsevier.

Griffey, R. T., & Sodickson, A. (2009). Cumulative radiation exposure and cancer risk estimates in emergency department patients undergoing repeat or multiple CT. American Journal of Roentgenology, 192(4), 887-892.

Groves, A., Owen, K., Courtney, H., Yates, S., Goldstone, K., Blake, G., & Dixon, A. (2014). 16-detector multislice CT: dosimetry estimation by TLD measurement compared with Monte Carlo simulation. The British Journal of Radiology.

Guimaraes, C. C., Moralles, M., & Okuno, E. (2008). Performance of GEANT4 in dosimetry applications: Calculation of X-ray spectra and kerma-to-dose equivalent conversion coefficients. Radiation Measurements, 43(9), 1525-1531.

Gupta, A. K., Nelson, R. C., Johnson, G. A., Paulson, E. K., Delong, D. M., & Yoshizumi, T. T. (2003). Optimization of Eight-Element Multi–Detector Row Helical CT Technology for Evaluation of the Abdomen 1. Radiology, 227 (3), 739-745.

Haaga, J. R. (2001). Radiation dose management: weighing risk versus benefit. American Journal of Roentgenology, 177(2), 289-291.

Hadley, J. L., Agola, J., & Wong, P. (2006). Potential impact of the American College of Radiology appropriateness criteria on CT for trauma. American Journal of Roentgenology, 186 (4), 937-942.

Haines, D. E. (2004). Neuroanatomy: An atlas of structures, sections, and systems (Vol. 153): Lippincott Williams & Wilkins.

Hall, E. J., & Giaccia, A. J. (2006). Radiobiology for the Radiologist: Lippincott Williams & Wilkins.

Hall, E.J. and Brenner, D.J., (2008). Cancer risks from diagnostic radiology.The British journal of radiology, 81 (965), pp.362-378.

Halliburton, S. S., Sola, S., Kuzmiak, S. A., Obuchowski, N. A., Desai, M., Flamm, S. D., & Schoenhagen, P. (2008). Effect of dual-source cardiac computed tomography on patient

radiation dose in a clinical setting: comparison to single-source imaging. J Cardiovasc Comput Tomogr, 2 (6), 392-400.

Hamberg, L. M., Rhea, J. T., Hunter, G. J., & Thrall, J. H. (2003). Multi–Detector Row CT: Radiation Dose Characteristics 1. Radiology, 226 (3), 762-772.

Hammer, G. P., Seidenbusch, M. C., Regulla, D. F., Spix, C., Zeeb, H., Schneider, K., & Blettner, M. (2011). Childhood cancer risk from conventional radiographic examinations for selected referral criteria: results from a large cohort study. American Journal of Roentgenology, 197 (1), 217-223.

Hara, A. K., Paden, R. G., Silva, A. C., Kujak, J. L., Lawder, H. J., & Pavlicek, W. (2009). Iterative reconstruction technique for reducing body radiation dose at CT: feasibility study. American Journal of Roentgenology, 193 (3), 764-771.

Hara, N., Onoguchi, M., Takenaka, K., Matsubara, K., Ujita, H., & Kenko, Y. (2010). Assessment of patient exposure to X-radiation from SPECT/CT scanners. J Nucl Med Technol, 38 (3), 138-148.

Hart, D., & Wall, B. (2004). UK population dose from medical X-ray examinations. European Journal of Radiology, 50 (3), 285-291.

Hart, D., Wall, B., Hillier, M., & Shrimpton, P. (2010). Frequency and collective dose for medical and dental X-ray examinations in the UK, 2008. Health Protection Agency.

Hashemi-Malayeri, B., & Williams, J. (2003). A practical approach for the assessment of patient doses from CT examinations. Radiography, 64, 35.

Heaney, D., & Norvill, C. (2006). A comparison of reduction in CT dose through the use of gantry angulations or bismuth shields. Australasian Physics & Engineering Sciences in Medicine, 29 (2), 172-178.

Heggie, J., Kay, J., & Lee, W. (2006). Importance in optimization of multi-slice computed tomography scan protocols. Australasian radiology, 50 (3), 278-285.

Hendee, W. R., & O'Connor, M. K. (2012). Radiation risks of medical imaging: separating fact from fantasy. Radiology, 264 (2), 312-321.

Hendee, W. R., & Ritenour, E. (2002). Medical Imaging Physics. Wiley-Liss. Inc., New York.

Hendee, W. R., Becker, G. J., Borgstede, J. P., Bosma, J., Casarella, W. J., Erickson, B. A., Wallner, P. E. (2010). Addressing overutilization in medical imaging 1. Radiology, 257 (1), 240-245.

Hine, G. J., & Brownell, G. L. (2013). Radiation dosimetry: Elsevier.

Hobbie, R. K., & Roth, B. J. (2007). Intermediate physics for medicine and biology: Springer Science & Business Media.

Hoehn, K., & Marieb, E. N. (2010). Human anatomy and physiology (9th ed.): San Francisco: Benjamin Cummings. ISBN 0-321-60261-7.

Hofer, M. (2010). CT teaching manual. A systematic approach to CT reading. (4th ed.).

Hohl, C., Mühlenbruch, G., Wildberger, J., Leidecker, C., Süss, C., Schmidt, T., Mahnken, A. (2006). Estimation of radiation exposure in low-dose multislice computed tomography of the heart and comparison with a calculation program. Eur Radiol, 16 (8), 1841-1846.

Hollingsworth, C. L., Yoshizumi, T. T., Frush, D. P., Chan, F. P., Toncheva, G., Nguyen, G., . Hurwitz, L. M. (2007). Pediatric cardiac-gated CT angiography: assessment of radiation dose. American Journal of Roentgenology, 189 (1), 12-18.

Holmes-Siedle, A. (1974). The space-charge dosimeter: General principles of a new method of radiation detection. Nuclear Instruments and Methods, 121 (1), 169-179.

Hopper, K. D. (2002). Orbital, thyroid, and breast superficial radiation shielding for patients undergoing diagnostic CT. Seminars in Ultrasound, CT and MRI, 23 (5), 423-427.

Hourdakis, J., & Nowotny, R. (2014). Instrumentation for Dosimetry. Chapter 21 Diagnostic radiology physics: A handbook for teachers and students. Endorsed by: American Association of Physicists in Medicine, Asia-Oceania Federation of Organizations for Medical Physics, European Federation of Organisations for Medical Physics.

Hricak, H., Brenner, D. J., Adelstein, S. J., Frush, D. P., Hall, E. J., Howell, R. W., Suleiman, O. H. (2011). Managing radiation use in medical imaging: a multifaceted challenge. Radiology, 258 (3), 889-905.

Hsieh, J. (2009). Computed tomography: principles, design, artifacts, and recent advances (2nd ed.): SPIE Bellingham, WA.

Hsieh, J., Nett, B., Yu, Z., Sauer, K., Thibault, J.-B., & Bouman, C. A. (2013). Recent advances in CT image reconstruction. Current Radiology Reports, 1 (1), 39-51.

Hua, F., Ma, J., Ha, T., Kelley, J. L., Kao, R. L., Schweitzer, J. B., Li, C. (2009). Differential roles of TLR2 and TLR4 in acute focal cerebral ischemia/reperfusion injury in mice. Brain Research, 1262(Supplement C), 100-108.

Huda, W. (2002). Effective doses to adult and pediatric patients. Pediatr Radiol, 32 (4), 272-279.

Huda, W., & Mettler, F. A. (2011). Volume CT Dose Index and Dose-Length Product Displayed during CT: What Good Are They? 1. Radiology, 258 (1), 236-242.

Huda, W., & Ogden, K. M. (2008). Comparison of head and body organ doses in CT. Phys Med Biol, 53(2), N9.

Huda, W., & Slone, R. M. (2003). Review of radiologic physics: Lippincott Williams & Wilkins.

Huda, W., & Vance, A. (2007). Patient radiation doses from adult and pediatric CT. American Journal of Roentgenology, 188 (2), 540-546.

Huda, W., Magill, D., & He, W. (2011). CT effective dose per dose length product using ICRP 103 weighting factors. Medical Physics, 38 (3), 1261-1265.

Huda, W., Ogden, K. M., Lavallee, R. L., Roskopf, M. L., & Scalzetti, E. M. (2012). KERMA ratios in pediatric CT dosimetry. Pediatr Radiol, 42 (5), 527-535.

Huda, W., Scalzetti, E. M., & Levin, G. (2000). Technique factors and image quality as functions of patient weight at abdominal CT 1. Radiology, 217 (2), 430-435.

Hunold, P., Vogt, F. M., Schmermund, A., Debatin, J. r. F., Kerkhoff, G., Budde, T., Barkhausen, J. r. (2003). Radiation Exposure during Cardiac CT: Effective Doses at Multi–Detector Row CT and Electron-Beam CT 1. Radiology, 226 (1), 145-152.

Hurwitz, L. M., Reiman, R. E., Yoshizumi, T. T., Goodman, P. C., Toncheva, G., Nguyen, G., & Lowry, C. (2007). Radiation Dose from Contemporary Cardiothoracic Multidetector CT Protocols with an Anthropomorphic Female Phantom: Implications for Cancer Induction 1. Radiology, 245 (3), 742-750.

Hurwitz, L. M., Yoshizumi, T. T., Goodman, P. C., Frush, D. P., Nguyen, G., Toncheva, G., & Lowry, C. (2007). Effective dose determination using an anthropomorphic phantom and metal oxide semiconductor field effect transistor technology for clinical adult body multidetector array computed tomography protocols. Journal of Computer Assisted Tomography, 31 (4), 544-549.

Hurwitz, L. M., Yoshizumi, T. T., Goodman, P. C., Nelson, R. C., Toncheva, G., Nguyen, G. B., Anderson-Evans, C. (2009). Radiation dose savings for adult pulmonary embolus 64-MDCT using bismuth breast shields, lower peak kilovoltage, and automatic tube current modulation. American Journal of Roentgenology, 192 (1), 244-253.

IAEA. (1996). No, IAEA Safety Series. 115, International Basic Safety Standards for Protection against Ionizing Radiation and for the Safety of Radiation Sources. International Atomic Energy Agency, Vienna.

ICRP Publication 102. (2007). International Commission on Radiological Protection. Managing patient dose in multi-detector computed tomography (MDCT). Annals of the ICRP Publication 102. (0702030473). Retrieved from Oxford: ICRP: http://sascrad.de/attachments/File/ICRP-Report_102_ (Auszug).pdf

ICRP. (1977). Recommendations of the ICRP. ICRP Publication 26 Ann ICRP; 1977: 3. Retrieved from http://www.icrp.org/publications.asp.

ICRP. (1991). International Commission on Radiological Protection. The 1990 Recommendations of the International Commission on Radiological Protection. ICRP Publication 60. Annals of the ICRP, (1991); 21 (1-3): 1-201. Retrieved from http://www.icrp.org/publication.aspid=ICRP Publication 60

ICRP. (1994). International Commission on Radiological Protection. Human respiratory tract model for radiological protection. ICRP Publication 66. Ann ICRP. Oxford, UK: Pergamon Press., 1994, 53 (1-4), 107-114.

ICRP. (1995). ICRP, International Commission on Radiological Protection. Age-dependent doses to members of the public from intake of radionuclides: Part 3 ingestion dose coeffcients. ICRP Publication 69. Annals of the ICRP, 1995, 25 (1): 1-74.

ICRP. (2002). Basic anatomical and physiological data for use in radiological protection: reference values: ICRP Publication 89. Annals of the ICRP, 32 (3), 1-277.

ICRP. (2005). Annals of the International Commission on Radiological Protection. Low-dose extrapolation of radiation-related cancer risk. Annals of the ICRP Publication 99, 35 (4), 1-140.

ICRP. (2007a). International Commission on Radiological Protection. The (2007) Recommendations of the International Commission on Radiological Protection. ICRP Publication 103. Annals of the ICRP, 2007b, 37 (2-4):1-332.

ICRP. (2007b). International Commission on Radiological Protection. Radiological protection in medicine. ICRP Publication 105. Ann ICRP, 37 (6), 1-63.

ICRP. (2007c). International Commission on Radiological Protection. Managing patient dose in multi-detector computed tomography (MDCT). ICRP Publication 102. Annals of the ICRP, 2007a, 37 (1):1-79.: Elsevier.

Igbaseimokumo, U. (2009). Brain CT Scans in Clinical Practice: Springer Verlag Science & Business Media.

ImPACT. (2006). Imaging performance assessment of CT scanners: a medical devices agency evaluation group. CT scanner matching data, tables of CTDI values in air, $CTDI_w$, and phantom factor values. Retrieved from http://www.impactscan.org

ImPACT. (2011). ImPACT CT Dosimetry Calculator St. George's Hospital London, UK. Retrieved from http://www.impactscan.org/ctdosimetry.htm

Izak-Biran, T., Malch, S., Shamai, Y., & Alfassi, Z. (1996). Low pre-and post-irradiation fading of LiF: Mg, Ti (TLD-100, TLD-600, TLD-700) using a preheat technique. Radiat Prot Dosimetry, 64 (4), 269-274.

Jablonski, A. (1935). Nature131, 839 (1933). Jablonski, A.: Z. Physik, 94, 38.

Jacob, K., Vivian, G., & Steel, J. (2004). X-ray dose training: are we exposed to enough? Clinical radiology, 59 (10), 928-934.

Jaffe, T. A., Nelson, R. C., Johnson, G. A., Lee, E. R., Yoshizumi, T. T., Lowry, C. R., Paulson, E. K. (2006). Optimization of Multiplanar Reformations from Isotropic Data Sets Acquired with 16–Detector Row Helical CT Scanner 1. Radiology, 238 (1), 292-299.

Jaffe, T. A., Yoshizumi, T. T., Toncheva, G., Anderson-Evans, C., Lowry, C., Miller, C. M., Ravin, C. E. (2009). Radiation dose for body CT protocols: variability of scanners at one institution. American Journal of Roentgenology, 193 (4), 1141-1147.

Jansen, J. T., & Shrimpton, P. C. (2011). Calculation of normalised organ and effective doses to adult reference computational phantoms from contemporary computed tomography scanners. Prog Nuc Sci Technol, 2, 165-171.

Jarry, G., DeMarco, J., Beifuss, U., Cagnon, C., & McNitt-Gray, M. (2003). A Monte Carlo-based method to estimate radiation dose from spiral CT: from phantom testing to patient-specific models. Phys Med Biol, 48 (16), 2645.

Jiménez, S., Jiménez, J. R., Crespo, M., Santamarta, E., Bousoño, C., & Rodríguez, J. (2006). Computed tomography in children with cystic fibrosis: a new way to reduce radiation dose. Archives of disease in childhood, 91 (5), 388-390.

Johns, P. a. (2014). Clinical neuroscience: an illustrated colour text (First edition. ed.): Edinburgh New York: Churchill Livingstone/Elsevier.

Jones, A., Pazik, F., Hintenlang, D., & Bolch, W. (2005). MOSFET dosimeter depth-dose measurements in heterogeneous tissue-equivalent phantoms at diagnostic x-ray energies. Medical Physics, 32 (10), 3209-3213.

Jones, D., & Shrimpton, P. (1991). Normalised Organ Doses Calculated Using Monte Carlo Techniques: National Radiological Protection Board.

Jones, D., Shrimpton, P. C., & Britain, G. (1991). Survey of CT practice in the UK. Part 3: Normalised organ doses calculated using Monte Carlo techniques: National Radiological Protection Board Chilton, UK.

Jones, D.G. and Wall, B.F., (1985). Organ doses from medical x-ray examinations calculated using Monte Carlo techniques (No. NRPB-R--186). National Radiological Protection Board.

Jones, D.G. and Wall, B.F., (1985). Organ doses from medical x-ray examinations calculated using Monte Carlo techniques (No. NRPB-R-186). National Radiological Protection Board.

Jones, D.G., Shrimpton, P.C. and Britain, G., (1991). Survey of CT practice in the UK. Part 3: Normalised organ doses calculated using Monte Carlo techniques. Chilton, UK: National Radiological Protection Board.

Kadane, J. B., & Lazar, N. A. (2004). Methods and criteria for model selection. Journal of the American statistical Association, 99 (465), 279-290.

Kaelin, M. A., & Bayona, M. (2004). Attributable risk applications in epidemiology. College Entrance Examination Board, 6-7.

Kalender, W. A. (2006). X-ray computed tomography. Phys Med Biol, 51 (13), R29.

Kalender, W. A. (2011). Computed tomography: fundamentals, system technology, image quality, applications: John Wiley & Sons.

Kalender, W. A. (2014). Dose in x-ray computed tomography. Phys Med Biol, 59 (3), R129.

Kalender, W.A., (2006). X-ray computed tomography. Physics in medicine and biology, 51(13), p. R29.

Kalender, W.A., (2014). Dose in x-ray computed tomography. Physics in medicine and biology, 59 (3), p. R129.

Kalra, M. K., Maher, M. M., Rizzo, S., & Saini, S. (2004). Radiation exposure and projected risks with multidetector-row computed tomography scanning: clinical strategies and technologic developments for dose reduction. Journal of Computer Assisted Tomography, 28, S46-S49.

Kalra, M. K., Maher, M. M., Toth, T. L., Hamberg, L. M., Blake, M. A., Shepard, J.-A., & Saini, S. (2004). Strategies for CT radiation dose optimization 1. Radiology, 230 (3), 619-628.

Kalra, M. K., Maher, M. M., Toth, T. L., Schmidt, B., Westerman, B. L., Morgan, H. T., & Saini, S. (2004). Techniques and applications of automatic tube current modulation for CT 1. Radiology, 233 (3), 649-657.

Kalra, M. K., Rizzo, S. M., & Novelline, R. A. (2005). Reducing radiation dose in emergency computed tomography with automatic exposure control techniques. Emergency radiology, 11 (5), 267-274.

Kandel, M., & Tollet, M. (2016). Anatomy of the Nervous System Brain–Computer Interfaces 1 (pp. 1-24): John Wiley & Sons, Inc.

Karsli, T., Kalra, M. K., Self, J. L., Rosenfeld, J. A., Butler, S., & Simoneaux, S. (2009). What physicians think about the need for informed consent for communicating the risk of cancer from low-dose radiation? Pediatr Radiol, 39 (9), 917-925.

Kathren, R. L. (1964). William H. Rollins (1852-1929): x-ray protection pioneer. Journal of the history of medicine and allied sciences, 287-294.

Kawaura, C., Aoyama, T., Koyama, S., Achiwa, M., & Mori, M. (2006). Organ and effective dose evaluation in diagnostic radiology based on in-phantom dose measurements with novel photodiode-dosemeters. Radiat Prot Dosimetry, 118 (4), 421-430.

Keat, N., (2005). CT scanner automatic exposure control systems, Medicines and Healthcare Products Regulatory Agency (MHRA) evaluation report 05016. London: MHRA, pp.1-57.

Keijzers, G. B., & Britton, C. J. (2010). Doctors' knowledge of patient radiation exposure from diagnostic imaging requested in the emergency department. Medical journal of Australia, 193 (8), 450.

Khan, F. M., & Gibbons, J. P. (2014). Khan's the physics of radiation therapy: Lippincott Williams & Wilkins.

Khursheed, A., Hillier, M., Shrimpton, P., & Wall, B. (2002). Influence of patient age on normalized effective doses calculated for CT examinations. The British Journal of Radiology, 75 (898), 819-830.

Kim, J.-E., & Newman, B. (2010). Evaluation of a radiation dose reduction strategy for pediatric chest CT. American Journal of Roentgenology, 194 (5), 1188-1193.

Kitis, G., Furetta, C., Prokic, M., & Prokic, V. (2000). Kinetic parameters of some tissue equivalent thermoluminescence materials. Journal of Physics D: Applied Physics, 33(11), 1252.

Kleinerman, R. A. (2006). Cancer risks following diagnostic and therapeutic radiation exposure in children. Pediatr Radiol, 36(2), 121-125. Doi: 10.1007/s00247-006-0191-5.

Kleinman, P. L., Strauss, K. J., Zurakowski, D., Buckley, K. S., & Taylor, G. A. (2010). Patient size measured on CT images as a function of age at a tertiary care children's hospital. American Journal of Roentgenology, 194 (6), 1611-1619.

Klig, J. E. (2006). Issues of computerized tomography scans in children and implications for emergency care. Current opinion in pediatrics, 18 (3), 231-233.

Klingenbeck-Regn, K., Schaller, S., Flohr, T., Ohnesorge, B., Kopp, A. F., & Baum, U. (1999). Subsecond multi-slice computed tomography: basics and applications. European Journal of Radiology, 31 (2), 110-124.

Klotz, E., & König, M. (1999). Perfusion measurements of the brain: using dynamic CT for the quantitative assessment of cerebral ischemia in acute stroke. European Journal of Radiology, 30 (3), 170-184.

Knoll, G. (2000). Radiation Detection and Measurement 3rd edition John Wiley and Sons. New York.

Knoll, G. F. (2010). Radiation detection and measurement (fourth edition ed.). New York, N.Y.; Chichester John Wiley & Sons.

Kobayashi, M., Asada, Y., Matsubara, K., Haba, T., Matsunaga, Y., Kawaguchi, A., Kato, R. (2015). Evaluation of effective dose using the k-factor of optimal scan range for CT examination. Open J. Radiol, 5, 142-148.

Koivisto, J. H., Wolff, J. E., Kiljunen, T., Schulze, D., & Kortesniemi, M. (2015). Characterization of MOSFET dosimeters for low-dose measurements in maxillofacial anthropomorphic phantoms. Journal of Applied Clinical Medical Physics, 16(4).

Koller, C., Eatough, J., & Bettridge, A. (2014). Variations in radiation dose between the same model of multislice CT scanner at different hospitals. The British Journal of Radiology.

Korir, G., Wambani, J., & Korir, I. (2012). Patient doses using multidetector computed tomography scanners in Kenya. Radiat Prot Dosimetry, 151 (2), 267-271.

Korn, A., Fenchel, M., Bender, B., Danz, S., Hauser, T., Ketelsen, D., Ernemann, U. (2012). Iterative reconstruction in head CT: image quality of routine and low-dose protocols in comparison with standard filtered back-projection. American Journal of Neuroradiology, 33 (2), 218-224.

Kortov, V. (2007). Materials for thermoluminescent dosimetry: Current status and future trends. Radiation Measurements, 42 (4), 576-581.

Krille, L., Dreger, S., Schindel, R., Albrecht, T., Asmussen, M., Barkhausen, J., Forsting, M. (2015). Risk of cancer incidence before the age of 15 years after exposure to ionising radiation from computed tomography: results from a German cohort study. Radiation and environmental biophysics, 54(1), 1-12.

Kubo, T., Lin, P.-J. P., Stiller, W., Takahashi, M., Kauczor, H.-U., Ohno, Y., & Hatabu, H. (2008). Radiation dose reduction in chest CT: a review. American Journal of Roentgenology, 190 (2), 335-343.

Kuppermann, N. (2008). Pediatric head trauma: the evidence regarding indications for emergent neuroimaging. Pediatr Radiol, 38 (4), 670.

Kwoh, Y. S., Hou, J., Jonckheere, E. A., & Hayati, S. (1988). A robot with improved absolute positioning accuracy for CT guided stereotactic brain surgery. IEEE Transactions on Biomedical Engineering, 35 (2), 153-160.

Lacroix, F., Archambault, L., Gingras, L., Guillot, M., Beddar, A. S., & Beaulieu, L. (2008). Clinical prototype of a plastic water-equivalent scintillating fiber dosimeter array for QA applicationsa). Medical Physics, 35 (8), 3682-3690.

Larson, D. B., Johnson, L. W., Schnell, B. M., Goske, M. J., Salisbury, S. R., & Forman, H. P. (2011). Rising use of CT in child visits to the emergency department in the United States, 1995–2008. Radiology, 259 (3), 793-801.

Lavallee, M., Beaulieu, L., & Gingras, L. (2006). Sci-Sat AM (1) General-09: Dose dependence of MOSFET sensitivity for clinical photon energy spectra between 30kV and 60Co. Medical Physics, 33 (7), 2674-2674.

Lavallee, M.-C., Gingras, L., & Beaulieu, L. (2006). Energy and integrated dose dependence of MOSFET dosimeter sensitivity for irradiation energies between 30kV and Co60. Medical Physics, 33 (10), 3683-3689.

Lechel, U., Becker, C., Langenfeld-Jäger, G., & Brix, G. (2009). Dose reduction by automatic exposure control in multidetector computed tomography: comparison between measurement and calculation. Eur Radiol, 19 (4), 1027-1034.

Lee, C. I., Haims, A. H., Monico, E. P., Brink, J. A., & Forman, H. P. (2004). Diagnostic CT Scans: Assessment of Patient, Physician, and Radiologist Awareness of Radiation Dose and Possible Risks 1. Radiology, 231 (2), 393-398.

Lee, C., Kim, K. P., Long, D., Fisher, R., Tien, C., Simon, S. L., Bolch, W. E. (2011). Organ doses for reference adult male and female undergoing computed tomography estimated by Monte Carlo simulations. Medical Physics, 38 (3), 1196-1206.

Lee, C., Lee, C., Staton, R. J., Hintenlang, D. E., Arreola, M. M., Williams, J. L., & Bolch, W. E. (2007). Organ and effective doses in pediatric patients undergoing helical multislice computed tomography examination. Medical Physics, 34 (5), 1858-1873.

Lee, C.-W., Ferain, I., Afzalian, A., Yan, R., Akhavan, N. D., Razavi, P., & Colinge, J.-P. (2010). Performance estimation of junctionless multigate transistors. Solid-State Electronics, 54(2), 97-103.

LeHeron, J. (1993). CTDOSE-a computer program to enable the calculation of organ doses and dose indices for CT examinations. Christchurch, New Zealand: Ministry of Health, National Radiation Laboratory.

Lehnert, B. E., & Bree, R. L. (2010). Analysis of appropriateness of outpatient CT and MRI referred from primary care clinics at an academic medical center: how critical is the need for improved decision support? Journal of the American College of Radiology, 7 (3), 192-197.

Lemoigne, Y., & Caner, A. (2011). Radiation protection in medical physics: Springer Science & Business Media.

Lewis M. (2005). Radiation dose issues in multi-slice CT scanning. ImPACT technology update, no. 3 (1). MHRA–ImPACT.

Lewis, M., Keat, N. and Edyvean, S., (2006). 32 to 64 Slice CT Scanner Comparison Report: Version 14. Centre for Evidence-based Purchasing.

Lewis, M., Keat, N. and Edyvean, S., (2006). Sixteen slice CT scanner comparison report-version 14. Im-PACT Report, 6012.

Lewis, M.A. and Edyvean, S., (2014). Patient dose reduction in CT. The British journal of radiology, 78 (934), pp.880-883.

Lin, E. C. (2010). Radiation Risk from Medical Imaging. Mayo Clinic Proceedings, 85(12), 1142-1146. Doi: https://doi.org/10.4065/mcp.2010.0260

Linet, M. S., Kim, K. P., Miller, D. L., Kleinerman, R. A., Simon, S. L., & de Gonzalez, A. B. (2010). Historical review of occupational exposures and cancer risks in medical radiation workers. Radiation research, 174 (6b), 793-808.

Linet, M. S., Kim, K., & Rajaraman, P. (2009). Children's Exposure to Diagnostic Medical Radiation and Cancer Risk: Epidemiologic and Dosimetric Considerations. Pediatr Radiol, 39(Suppl 1), S4. Doi:10.1007/s00247-008-1026-3

Linet, M. S., Slovis, T. L., Miller, D. L., Kleinerman, R., Lee, C., Rajaraman, P., & Berrington de Gonzalez, A. (2012). Cancer risks associated with external radiation from diagnostic imaging procedures. CA: a cancer journal for clinicians, 62 (2), 75-100.

Linton, O. W., & Mettler Jr, F. A. (2003). National conference on dose reduction in CT, with an emphasis on pediatric patients. American Journal of Roentgenology, 181 (2), 321-329.

Liou, J. J., & Schwierz, F. (2003). RF MOSFET: recent advances, current status and future trends. Solid-State Electronics, 47 (11), 1881-1895.

Little, M. P., Wakeford, R., Tawn, E. J., Bouffler, S. D., & Berrington de Gonzalez, A. (2009). Risks Associated with Low Doses and Low Dose Rates of Ionizing Radiation: Why Linearity May Be (Almost) the Best We Can Do. Radiology, 251(1), 6-12.

Livingstone, R., Eapen, A., Dip, N., & Hubert, N. (2006). Achieving reduced radiation doses for CT examination of the brain using optimal exposure parameters. Indian Journal of Radiology and Imaging, 16 (2), 247.

Lockwood, D., Einstein, D., & Davros, W. (2007). Diagnostic imaging: Radiation dose and patients' concerns. Journal of Radiology Nursing, 26 (4), 121-124.

Lucaya, J., Piqueras, J., García-Peña, P., Enríquez, G., García-Macías, M., & Sotil, J. (2000). Low-dose high-resolution CT of the chest in children and young adults: dose, cooperation, artifact incidence, and image quality. American Journal of Roentgenology, 175 (4), 985-992.

Lumbreras, B., Vilar, J., González-Álvarez, I., Guilabert, M., Parker, L., Pastor-Valero, M., Hernández-Aguado, I. (2016). Evaluation of clinicians' knowledge and practices regarding medical radiological exposure: findings from a mixed-methods investigation (survey and qualitative study). BMJ open, 6 (10), e012361.

Luo, L. Z. (2008). Extensive fade study of Harshaw LiF TLD materials. Radiation Measurements, 43 (2), 365-370.

Ma, H., Elbakri, I.A. and Reed, M., (2013). Estimation of organ and effective doses from newborn radiography of the chest and abdomen. Radiation protection dosimetry, 156 (2), pp.160-167.

Marco, A. (2013). AAPM Computed Tomography Radiation Dose Education Slides - Tsrm. Retrieved from: http://www.aapm.org/pubs/CTProtocols/documents/CTTerminologyLexicon.pdf

Margo, J. (2009). CT scans pose risk of cancer. Australian Financial Review 12 March 2009.

Martin, C.J., (2014). Effective dose: how should it be applied to medical exposures? The British journal of radiology, 80 (956), pp.639-647.

Martini, F. H., Timmons, M. J., & Tallitsch, R. B. (2005). Human Anatomy, The nervous system: The brain and cranial nerves (5th ed.): Benjamin Cummings.

Mary, G.-C. (2016). CT Brain Anatomy. Retrieved from: http://www.radiologymasterclass.co.uk/tutorials/ct/ct_brain_anatomy/ct_brain_anatomy_start

Mathews, J. D., Forsythe, A. V., Brady, Z., Butler, M. W., Goergen, S. K., Byrnes, G. B., Guiver, T. A. (2013). Cancer risk in 680 000 people exposed to computed tomography scans in childhood or adolescence: data linkage study of 11 million Australians. BMJ, 346, f2360.

Matsumoto, K., Jinzaki, M., Tanami, Y., Ueno, A., Yamada, M., & Kuribayashi, S. (2011). Virtual monochromatic spectral imaging with fast kilovoltage switching: Improved image quality as compared with that obtained with conventional 120-kVp CT. Radiology, 259(1), 257-62.

Mayo, J. R., Aldrich, J., & Muller, N. L. (2003). Radiation exposure at chest CT: a statement of the Fleischner Society 1. Radiology, 228 (1), 15-21.

McCann, C., & Alasti, H. (2004). Comparative evaluation of image quality from three CT simulation scanners. J Appl Clin Med Phys, 5 (4), 55-70.

McCollough, C. H. (2005). Automatic exposure control in CT: are we done yet? Radiology, 237 (3), 755-756.

McCollough, C. H. (2008). CT dose: how to measure, how to reduce. Health physics, 95 (5), 508-517.

McCollough, C. H. (2010). Diagnostic reference levels. Image Wisely [Internet], 1-6.

McCollough, C. H., & Schueler, B. A. (2000). Calculation of effective dose. Medical Physics, 27 (5), 828-837.

McCollough, C. H., Bruesewitz, M. R., & Kofler Jr, J. M. (2006). CT dose reduction and dose management tools: overview of available options 1. RadioGraphics, 26 (2), 503-512.

McCollough, C. H., Bushberg, J. T., Fletcher, J. G., & Eckel, L. J. (2015). Answers to Common Questions About the Use and Safety of CT Scans. Mayo Clinic Proceedings, 90(10), 1380-1392. Doi: 10.1016/j.mayocp.2015.07.011.

McCollough, C. H., Christner, J. A., & Kofler, J. M. (2010). How effective is effective dose as a predictor of radiation risk? American Journal of Roentgenology, 194 (4), 890-896.

McCollough, C. H., Leng, S., Yu, L., Cody, D. D., Boone, J. M., & McNitt-Gray, M. F. (2011). CT dose index and patient dose: they are not the same thing. Radiology, 259 (2), 311-316.

McCollough, C. H., Primak, A. N., Braun, N., Kofler, J., Yu, L., & Christner, J. (2009). Strategies for reducing radiation dose in CT. Radiol Clin North Am, 47 (1), 27-40.

McCollough, C., Cody, D., Edyvean, S., & Medicine, A. A. o. P. i. (2008). The measurement, reporting, and management of radiation dose in CT: report of AAPM task group 23 of the Diagnostic Imaging Council CT Committee. 2008. No. 96. American Association of Physicists in Medicine (AAPM), 96.

McCollough, C., Cody, D., Edyvean, S., Geise, R., Gould, B., Keat, N., McNitt-Gray, M. (2008). The measurement, reporting, and management of radiation dose in CT. Report of AAPM Task Group, 23 (23), 1-28.

McCollough, C., Cody, D., Edyvean, S., Rich, G., Gould, B., Keat, N., McNitt-Gray, M. (2008). AAPM Task Group 23; CT dosimetry. Diagnostic Imaging Council CT Committee. The measurement, reporting, and management of radiation dose in CT: report (96).

McDermott, A., White, R. A., Mc-Nitt-Gray, M., Angel, E., & Cody, D. (2009). Pediatric organ dose measurements in axial and helical multislice CT. Medical Physics, 36 (5), 1494-1499.

McNitt-Gray, M. F. (2002). AAPM/RSNA physics tutorial for residents: topics in CT: radiation dose in CT 1. RadioGraphics, 22 (6), 1541-1553.

Mehta, S. (2007). Neuroimaging for paediatric minor closed head injuries. Paediatrics & child health, 12 (6), 482.

Mendelson, R. M., Fox, R. A., & de Klerk, N. H. (2010). Alarm about computed tomography scans is unjustified. The Medical journal of Australia, 193 (4), 246-246.

Metter, R. B., Rittenberger, J. C., Guyette, F. X., & Callaway, C. W. (2011). Association between a quantitative CT scan measure of brain edema and outcome after cardiac arrest. Resuscitation, 82 (9), 1180-1185.

Mettler Jr, F. A., Bhargavan, M., Faulkner, K., Gilley, D. B., Gray, J. E., Ibbott, G. S., Stabin, M. G. (2009). Radiologic and Nuclear Medicine Studies in the United States and Worldwide: Frequency, Radiation Dose, and Comparison with Other Radiation Sources—1950–2007 1. Radiology, 253 (2), 520-531.

Mettler Jr, F. A., Thomadsen, B. R., Bhargavan, M., Gilley, D. B., Gray, J. E., Lipoti, J. A., Mahesh, M. (2008). Medical radiation exposure in the US in 2006: preliminary results. Health physics, 95 (5), 502-507.

Mettler Jr, F. A., Wiest, P. W., Locken, J. A., & Kelsey, C. A. (2000). CT scanning: patterns of use and dose. Journal of radiological Protection, 20 (4), 353.

Miglioretti, D. L., Johnson, E., Williams, A., Greenlee, R. T., Weinmann, S., Solberg, L. I., Vanneman, N. (2013). The use of computed tomography in pediatrics and the associated radiation exposure and estimated cancer risk. JAMA pediatrics, 167 (8), 700-707.

Mijnheer, B., Beddar, S., Izewska, J. and Reft, C., (2013). In vivo dosimetry in external beam radiotherapy. Medical physics, 40 (7).

Miksys, N., Gordon, C. L., Thomas, K., & Connolly, B. L. (2010). Estimating effective dose to pediatric patients undergoing interventional radiology procedures using anthropomorphic phantoms and MOSFET dosimeters. American Journal of Roentgenology, 194 (5), 1315-1322.

Millar, N. (2001). Biology statistics made simple using Excel. School science review, 83, 23-34.

Mobile MOSFET. (2007). Best medical Canada operator's manual for the mobile MOSFET wireless dosimetry system for use with mobileMOSFT software viresion 2.2 and above. Best Medical Canada Ltd. 25B Northside Road Ottawa, ON K2H 8S1 Canada.

Mohan, R., Singh, A., & Gundappa, M. (2011). Three-dimensional imaging in periodontal diagnosis-Utilization of cone beam computed tomography. Journal of Indian Society of Periodontology, 15 (1), 11.

Moore, K. L., Dalley, A. F., & Agur, A. M. (2013). Clinically oriented anatomy: Lippincott Williams & Wilkins.

Moorin, R. E., Forsyth, R., Gibson, D. J., & Fox, R. (2013). Radiation dosimetry assessment of routine CT scanning protocols used in Western Australia. Journal of radiological Protection, 33 (2), 295.

Morgan, W. F., & Bair, W. J. (2013). Issues in low dose radiation biology: the controversy continues. A perspective. Radiation research, 179(5), 501-510.

Morin, R. L., Gerber, T. C., & McCollough, C. H. (2003). Radiation dose in computed tomography of the heart. Circulation, 107 (6), 917-922.

Moscovitch, M., & Horowitz, Y. (2006). Thermoluminescent materials for medical applications: LiF: Mg, Ti and LiF: Mg, Cu, P. Radiation Measurements, 41, S71-S77.

Moser, J. B., Sheard, S. L., Edyvean, S., & Vlahos, I. (2017). Radiation dose-reduction strategies in thoracic CT. Clinical radiology, 72(5), 407-420.

Moss, M., & McLean, D. (2006). Paediatric and adult computed tomography practice and patient dose in Australia. Australasian radiology, 50 (1), 33-40.

MR/CT Committee of the Society of Pediatric Radiology, (2001). Risks and benefits in pediatric CT. Pediatric Radiology, 31 (6), pp.387-387.

MR/CT Committee of the Society of Pediatric Radiology, 2001. Risks and benefits in pediatric CT. Pediatric Radiology, 31 (6), pp.387-387.

Muhogora, W., Ahmed, N., Alsuwaidi, J., Beganovic, A., Ciraj-Bjelac, O., Gershan, V., Manatrakul, N. (2010). Paediatric CT examinations in 19 developing countries: frequency and radiation dose. Radiat Prot Dosimetry, 140 (1), 49-58.

Muhogora, W., Ahmed, N., Beganovic, A., Benider, A., Ciraj-Bjelac, O., Gershan, V., Manatrakul, N. (2009). Patient doses in CT examinations in 18 countries: initial results from International Atomic Energy Agency projects. Radiat Prot Dosimetry, 136 (2), 118-126.

Mukundan Jr, S., Wang, P. I., Frush, D. P., Yoshizumi, T., Marcus, J., Kloeblen, E., & Moore, M. (2007). MOSFET dosimetry for radiation dose assessment of bismuth shielding of the eye in children. American Journal of Roentgenology, 188 (6), 1648-1650.

Mulkens, T. H., Bellinck, P., Baeyaert, M., Ghysen, D., Van Dijck, X., Mussen, E., Termote, J.-L. (2005). Use of an Automatic Exposure Control Mechanism for Dose Optimization in Multi–Detector Row CT Examinations: Clinical Evaluation 1. Radiology, 237 (1), 213-223.

Mulkens, T., Salgado, R., & Bellinck, P. (2007). Dose optimization and reduction in CT of the head and neck, including brain. Radiation Dose from Adult and Pediatric Multidetector Computed Tomography, 135-151.

Mullins, M. E., Lev, M. H., Bove, P., O'Reilly, C. E., Saini, S., Rhea, J. T., Gonzalez, R. G. (2004). Comparison of image quality between conventional and low-dose nonenhanced head CT. American Journal of Neuroradiology, 25(4), 533-538.

Nagel, H. (2005). Significance of overbeaming and overranging effects of single-and multi-slice CT scanners. Biomed Tech (Berl), 50 (suppl 1), 395-396.

Nagel, H. D. (2007). CT parameters that influence the radiation dose Radiation dose from adult and pediatric multidetector computed tomography (pp. 51-79): Springer.

Nagel, S., Sinha, D., Day, D., Reith, W., Chapot, R., Papanagiotou, P., Fassbender, K. (2017). e-ASPECTS software is non-inferior to neuroradiologists in applying the ASPECT score to computed tomography scans of acute ischemic stroke patients. International Journal of Stroke, 12(6), 615-622.

Nawfel, R. D., Judy, P. F., Silverman, S. G., Hooton, S., Tuncali, K., & Adams, D. F. (2000). Patient and Personnel Exposure during CT Fluoroscopy-guided Interventional Procedures 1. Radiology, 216 (1), 180-184.

NCRP. (1988). Exposure of the US population from diagnostic medical radiation: NCRP Report No. 100.

NCRP. (2001). Evaluation of the Linear-Nonthreshold Dose-Response Model for Ionizing Radiation. Bethesda, MD: National Council on Radiation Protection and Measurements; 2001: NCRP Report No. 136.

NCRP. (2009). NCRP report N. 160, ionizing radiation exposure of the population of the United States, medical exposure—are we doing less with more, and is there a role for health physicists? Health physics, 97 (1), 1-5.

Ngaile, J. E., & Msaki, P. (2006). Estimation of patient organ doses from computed tomography examinations in Tanzania. Journal of Applied Clinical Medical Physics, 7 (3), pp.80-94.

Nicholson, R., & Fetherston, S. (2002). Primary radiation outside the imaged volume of a multislice helical CT scan. The British Journal of Radiology, 75(894), 518-522.

Nickoloff, E. L., & Alderson, P. O. (2001). Radiation exposures to patients from CT: reality, public perception, and policy. American Journal of Roentgenology, 177 (2), 285-287.

Nickoloff, E. L., Dutta, A. K., & Lu, Z. F. (2003). Influence of phantom diameter, kVp and scan mode upon computed tomography dose index. Medical Physics, 30 (3), 395-402.

Nievelstein, R. A., van Dam, I. M., & van der Molen, A. J. (2010). Multidetector CT in children: current concepts and dose reduction strategies. Pediatr Radiol, 40 (8), 1324-1344.

Nishizawa, K., Mori, S.-I., Ohno, M., Yanagawa, N., Yoshida, T., Akahane, K., Wada, S.-I. (2008). Patient dose estimation for multi-detector-row CT examinations. Radiat Prot Dosimetry, 128 (1), 98-105.

Nolte, J. (2002). The human brain: an introduction to its functional anatomy (5th ed.): Mosby Year book/George Stamathis.

Nowinski, W.L., (2011). Introduction to brain anatomy. In Biomechanics of the Brain (pp. 5-40). Springer New York.

NRC. (2006). National Research Council of the National Academies. Board on Radiation Effects Research. Health risks from exposure to low levels of ionizing radiation: BEIR VII phase 2 (Vol. 7). Washington, DC, US: National Academies Press.

Oberhofer, M., & Scharmann, A. (1981). Applied thermoluminescence dosimetry: Adam Hilger Ltd.

O'Daniel, J. C., Stevens, D. M., & Cody, D. D. (2005). Reducing radiation exposure from survey CT scans. American Journal of Roentgenology, 185 (2), 509-515.

Oktyabrsky, S. and Peide, D.Y. eds., (2010). Fundamentals of III-V semiconductor MOSFETs (pp. 163-165). New York: Springer.

Olarinoye, I., & Sharifat, I. (2010). A protocol for setting dose reference level for medical radiography in nigeria: a review. Bayero journal of pure and applied sciences, 3(1).

Origgi, D., Vigorito, S., Villa, G., Bellomi, M., & Tosi, G. (2006). Survey of computed tomography techniques and absorbed dose in Italian hospitals: a comparison between two methods to estimate the dose–length product and the effective dose and to verify fulfilment of the diagnostic reference levels. Eur Radiol, 16 (1), 227-237.

Orrison, W. W., Snyder, K. V., Hopkins, L. N., Roach, C. J., Ringdahl, E. N., Nazir, R., & Hanson, E. H. (2011). Whole-brain dynamic CT angiography and perfusion imaging. Clinical radiology, 66(6), 566-574.

Osmond, M. H., Klassen, T. P., Wells, G. A., Correll, R., Jarvis, A., Joubert, G., McConnell, D. (2010). CATCH: a clinical decision rule for the use of computed tomography in children with minor head injury. Canadian Medical Association Journal, 182 (4), 341-348.

Pace, I., & Zarb, F. (2015). A comparison of sequential and spiral scanning techniques in brain CT. Radiologic technology, 86 (4), 373-378.

Palmer, J., (2008). Lead Apron Shielding for Fetal Dose Reduction during CT Pulmonary Angiography. Diss Dept of Physics Univ of Surrey.

Parker, M., Kelleher, N., Hoots, J., Chung, J., Fatouros, P., & Benedict, S. H. (2008). Absorbed radiation dose of the female breast during diagnostic multidetector chest CT and dose reduction with a tungsten–antimony composite breast shield: preliminary results. Clinical radiology, 63 (3), 278-288.

Paterson, A., & Frush, D. (2007). Dose reduction in paediatric MDCT: general principles. Clinical radiology, 62 (6), 507-517.

Paterson, A., Frush, D. P., & Donnelly, L. F. (2001). Helical CT of the body: are settings adjusted for paediatric patients? American Journal of Roentgenology, 176 (2), 297-301.

Pearce, M. S., Salotti, J. A., Little, M. P., McHugh, K., Lee, C., Kim, K. P., Craft, A. W. (2012). Radiation exposure from CT scans in childhood and subsequent risk of leukaemia and brain tumours: a retrospective cohort study. The lancet, 380 (9840), 499-505.

Pearce, M. S., Salotti, J. A., McHugh, K., Metcalf, W., Kim, K. P., Craft, A. W., Ron, E. (2011). CT scans in young people in Northern England: trends and patterns 1993–2002. Pediatr Radiol, 41 (7), 832-838.

Perisinakis, K., Damilakis, J., Voloudaki, A., Papadakis, A., & Gourtsoyiannis, N. (2001). Patient dose reduction in CT examinations by optimising scanogram acquisition. Radiat Prot Dosimetry, 93 (2), 173-178.

Picano, E. (2004a). Informed consent and communication of risk from radiological and nuclear medicine examinations: how to escape from a communication inferno. BMJ: British Medical Journal, 329 (7470), 849.

Picano, E. (2004b). Sustainability of medical imaging. BMJ: British Medical Journal, 328 (7439), 578.

Pointer, D. (2008). Computed tomography (CT) scan image reconstruction on the SRC-7. Proceedings of the Fourth Annual Reconfigurable Systems Summer Institute (RSSF08).

Prasad, K. N., Cole, W. C., & Hasse, G. M. (2004). Health risks of low dose ionizing radiation in humans: a review. Experimental Biology and Medicine, 229(5), 378-382.

Preston, R. J. (2008). Update on linear non-threshold dose-response model and implications for diagnostic radiology procedures. Health physics, 95 (5), 541-546.

Prince, J.L. and Links, J.M., (2006). Medical imaging signals and systems. Upper Saddle River, New Jersey: Pearson Prentice Hall.

Prins, R. D., Thornton, R. H., Schmidtlein, C. R., Quinn, B., Ching, H., & Dauer, L. T. (2011). Estimating radiation effective doses from whole body computed tomography scans based on US soldier patient height and weight. BMC Med Imaging, 11 (1), 20.

Prokop, M., (2003). General principles of MDCT. European journal of radiology, 45, pp. S4-S10.

PSR. (2010). Professional Services Review. Report to the Professions 2008-09. Canberra, Australian Capital Territory, Australia, 2010.

Qronfla, M.M., Kinsara, A.A., Maimani, A.A., Abulfaraj, W.H., Bhuiyan, S.I. and Elmohor, E., 2005. Application of European commission reference dose levels in some common CT examinations in King AbdulAziz University Hospital. Transactions of the American Nuclear Society, 93, pp.814-815.

Radiation, U. N. S. C. o. t. E. o. A. (2013). UNSCEAR 2013 Report Volume I. Report to the general assembly scientific annex A: Levels and effects of radiation exposure due to the nuclear accident after the 2011 great east-Japan earthquake and tsunami. United Nations.

Raman, S. P., Johnson, P. T., Deshmukh, S., Mahesh, M., Grant, K. L., & Fishman, E. K. (2013). CT dose reduction applications: available tools on the latest generation of CT scanners. Journal of the American College of Radiology, 10 (1), 37-41.

Rapalino, O., Kamalian, S., Kamalian, S., Payabvash, S., Souza, L., Zhang, D., Pomerantz, S. (2012). Cranial CT with adaptive statistical iterative reconstruction: improved image quality with concomitant radiation dose reduction. American Journal of Neuroradiology, 33 (4), 609-615.

Rehani, M. M. (2010). Radiation protection in newer imaging technologies. Radiat Prot Dosimetry, 139(1-3), 357-362.

Rehani, M. M., Bongartz, G., Kalender, W., Golding, S., Gordon, L., Murakami, T., & Shrimpton, P. (2000). Managing patient dose in computed tomography. Ann ICRP, 30 (4), 7-45.

Rehani, M., Kalra, M., McCollough, C., Nagel, H., Collins, L. and Kalender, W., (2006). Managing Patient Dose in Multi-Detector Computed Tomography (MDCT). IC o. R. Protection, Education., ed.

Rehani, M., Kalra, M., McCollough, C., Nagel, H., Collins, L. and Kalender, W., (2006). Managing Patient Dose in Multi-Detector Computed Tomography (MDCT). IC o. R. Protection, Ed., ed.

Renowden, S. (2012). Normal anatomy of the brain on CT and MRI with a few normal variants. Pract Neurol, 12(4), 225-233.

Rice, H. E., Frush, D. P., Harker, M. J., Farmer, D., Waldhausen, J. H., & Committee, A. E. (2007). Peer assessment of pediatric surgeons for potential risks of radiation exposure from computed tomography scans. J Pediatr Surg, 42 (7), 1157-1164.

Rivera, T. (2012). Thermoluminescence in medical dosimetry. Applied radiation and isotopes, 71, pp.30-34.

Roberts, J.A., Drage, N.A., Davies, J. and Thomas, D.W., (2014). Effective dose from cone beam CT examinations in dentistry. The British journal of radiology, 82 (973), pp.35-40.

Robinson, A., Hill, E., & Harpen, M. (1986). Radiation dose reduction in pediatric CT. Pediatr Radiol, 16 (1), 53-54.

Rogers, L. F. (2001). Taking care of children: check out the parameters used for helical CT. American Journal of Roentgenology, 176 (2), 287-287.

Rohen, J. W., Yokochi, C., & Lütjen-Drecoll, E. (2006). Color atlas of anatomy: a photographic study of the human body: Schattauer Verlag.

Rohen, J. W., Yokochi, C., & Lütjen-Drecoll, E. (2016). Anatomy a photographic Atlas (8th ed.): Schattauer Verlag, Stuttgart, Germany.

Romans, L. E. (2011). Computed tomography for technologists: A Comprehensive Text: Lippincott Williams & Wilkins.

Rosner, B. (2015). Fundamentals of biostatistics: Nelson Education.

Rossaint, R., Bouillon, B., Cerny, V., Coats, T. J., Duranteau, J., Fernández-Mondéjar, E., Nardi, G. (2016). The European guideline on management of major bleeding and coagulopathy following trauma. Critical care, 20(1), 100.

Rothenberg, L., & Pentlow, K. (1992). Radiation dose in CT. RadioGraphics, 12 (6), 1225-1243.

Royal, H.D., (2008), September. Effects of low level radiation—what's new? Paper presented at the Seminars in nuclear medicine (Vol. 38, No. 5, pp. 392-402). WB Saunders.

Rubin, G. D. (2000). Data explosion: the challenge of multidetector-row CT. European Journal of Radiology, 36 (2), 74-80.

Rubin, G. D. (2003). 3-D imaging with MDCT. European Journal of Radiology, 45, S37-S41.

Russell, M., Fink, J. R., Rebeles, F., Kanal, K., Ramos, M., & Anzai, Y. (2008). Balancing radiation dose and image quality: clinical applications of neck volume CT. American Journal of Neuroradiology, 29 (4), 727-731.

Rustemeyer, P., Streubühr, U., & Suttmoeller, J. (2004). Low-dose dental computed tomography: significant dose reduction without loss of image quality. Acta radiologica, 45 (8), 847-853.

Sabarudin, A., & Sun, Z. (2013). Radiation dose measurements in coronary CT angiography. World J Cardiol, 5 (12), 459-464.

Scalzetti, E. M., Huda, W., Bhatt, S., & Ogden, K. M. (2008). A method to obtain mean organ doses in a Rando phantom. Health physics, 95 (2), 241-244.

Schardt, P., Deuringer, J., Freudenberger, J., Hell, E., Knüpfer, W., Mattern, D., & Schild, M. (2004). New x-ray tube performance in computed tomography by introducing the rotating envelope tube technology. Medical Physics, 31 (9), 2699-2706.

Schauer, D. A., & Linton, O. W. (2009). National council on radiation protection and measurements report shows substantial medical exposure increase: Radiological Society of North America, Inc. pp.293-296.

Schauer, D. A., & Linton, O. W. (2009). NCRP report No. 160, ionizing radiation exposure of the population of the United States, medical exposure—are we doing less with more, and is there a role for health physicists? Health physics, 97 (1), 1-5.

Scheck, R., Coppenrath, E., Kellner, M., Lehmann, K., Rock, C., Rieger, J., Hahn, K. (1998). Radiation dose and image quality in spiral computed tomography: multicentre evaluation at six institutions. The British Journal of Radiology, 71 (847), 734-744.

Schilham, A., van der Molen, A. J., Prokop, M., & de Jong, H. W. (2010). Overranging at Multisection CT: An Underestimated Source of Excess Radiation Exposure 1. RadioGraphics, 30 (4), 1057-1067.

Schmidt, R., & Kalender, W. (2002). A fast voxel-based Monte Carlo method for scanner-and patient-specific dose calculations in computed tomography. Physica Medica, 18 (2), 43-54.

Schueller-Weidekamm, C., Schaefer-Prokop, C. M., Weber, M., Herold, C. J., & Prokop, M. (2006). CT angiography of pulmonary arteries to detect pulmonary embolism:

improvement of vascular enhancement with low kilovoltage settings 1. Radiology, 241 (3), 899-907.

Scoccianti, S., Detti, B., Gadda, D., Greto, D., Furfaro, I., Meacci, F., Giacomelli, I. (2015). Organs at risk in the brain and their dose-constraints in adults and in children: a radiation oncologist's guide for delineation in everyday practice. Radiotherapy and Oncology, 114 (2), 230-238.

Seeram, E., (2015). Computed Tomography-E-Book: Physical Principles, Clinical Applications, and Quality Control. Elsevier Health Sciences.

Sessions, J., Roshau, J., Tressler, M., Hintenlang, D., Arreola, M., Williams, J., Bolch, W. (2002). Comparisons of point and average organ dose within an anthropomorphic physical phantom and a computational model of the newborn patient. Medical Physics, 29 (6), 1080-1089.

Shah, R., Gupta, A., Rehani, M., Pandey, A., & Mukhopadhyay, S. (2005). Effect of reduction in tube current on reader confidence in paediatric computed tomography. Clinical radiology, 60 (2), 224-231.

Sheet, T. F. (2011). National Institute of Neurological Disorders and Stroke, National Institutes of Health. Updated Feb, 18.

Sherer, M., Visconti, P., Ritenour, E., & Haynes, K. (2011). Radiation Protection in Medical Radiography (6th ed). Publishing Services Manager: Catherine Jackson.

Shrimpton, P., Hillier, M., Lewis, M., & Dunn, M. (2005). Doses from computed tomography (CT) examinations in the UK-2003 review (Vol. 67): NRPB.

Shrimpton, P., Hillier, M., Meeson, S., & Golding, S. (2014). Doses from computed tomography (CT) examinations in the UK-2011 review (Vol. 67): NRPB.

Shrimpton, P.C., Hillier, M.C., Lewis, M.A. and Dunn, M., (2006). National survey of doses from CT in the UK: 2003. The British journal of radiology, 79 (948), pp.968-980.

Shuryak, I., Sachs, R. K., & Brenner, D. J. (2010). Cancer risks after radiation exposure in middle age. J Natl Cancer Inst, 102 (21), 1628-1636.

Siebel, O. F., Pereira, J. G., Souza, R. S., Ramirez-Fernandez, F. J., Schneider, M. C., & Galup-Montoro, C. (2015). A very-low-cost dosimeter based on the off-the-shelf CD4007 MOSFET array for in vivo radiotherapy applications. Radiation Measurements, 75(Supplement C), 53-63.

Siegel, M. J., Schmidt, B., Bradley, D., Suess, C., & Hildebolt, C. (2004). Radiation dose and image quality in pediatric CT: effect of technical factors and phantom size and shape 1. Radiology, 233 (2), 515-522.

Silva, A. C., Lawder, H. J., Hara, A., Kujak, J., & Pavlicek, W. (2010). Innovations in CT dose reduction strategy: application of the adaptive statistical iterative reconstruction algorithm. American Journal of Roentgenology, 194 (1), 191-199.

Silverman, P. M., Kalender, W. A., & Hazle, J. D. (2001). Common terminology for single and multislice helical CT. American Journal of Roentgenology, 176 (5), 1135-1136.

Simantirakis, G., Hourdakis, C., Economides, S., Kaisas, I., Kalathaki, M., Koukorava, C., Vogiatzi, S. (2014). Diagnostic reference levels and patient doses in computed tomography examinations in Greece. Radiat Prot Dosimetry, 163(3), 319-324.

Simon, S. L., Weinstock, R. M., Doody, M. M., Neton, J., Wenzl, T., Stewart, P., Freedman, D. M. (2006). Estimating historical radiation doses to a cohort of US radiologic technologists. Radiation research, 166 (1), 174-192.

Singh, S., Kalra, M. K., Gilman, M. D., Hsieh, J., Pien, H. H., Digumarthy, S. R., & Shepard, J.-A. O. (2011). Adaptive statistical iterative reconstruction technique for radiation dose reduction in chest CT: a pilot study. Radiology, 259 (2), 565-573.

Singh, S., Kalra, M. K., Moore, M. A., Shailam, R., Liu, B., Toth, T. L., Westra, S. J. (2009). Dose Reduction and Compliance with Pediatric CT Protocols Adapted to Patient Size, Clinical Indication, and Number of Prior Studies 1. Radiology, 252 (1), 200-208.

Singh, S., Kalra, M. K., Shenoy-Bhangle, A. S., Saini, A., Gervais, D. A., Westra, S. J., & Thrall, J. H. (2012). Radiation dose reduction with hybrid iterative reconstruction for pediatric CT. Radiology, 263 (2), 537-546.

Smith, A., Dillon, W., Gould, R., & Wintermark, M. (2007). Radiation dose-reduction strategies for neuroradiology CT protocols. American Journal of Neuroradiology, 28 (9), 1628-1632.

Smith, M. M., & Smith, T. L. (2001). Pocket Atlas of Normal CT Anatomy of the Head and Brain (2nd ed. Vol. 11): Lippincott Williams & Wilkins.

Smith-Bindman, R. (2010). Is computed tomography safe? The New England journal of medicine, 363 (1), p.1.

Smith-Bindman, R., Lipson, J., Marcus, R., Kim, K.-P., Mahesh, M., Gould, R., Miglioretti, D. L. (2009). Radiation dose associated with common computed tomography examinations and the associated lifetime attributable risk of cancer. Archives of internal medicine, 169 (22), 2078-2086.

Sodickson, A., Baeyens, P. F., Andriole, K. P., Prevedello, L. M., Nawfel, R. D., Hanson, R., & Khorasani, R. (2009). Recurrent CT, cumulative radiation exposure, and associated radiation-induced cancer risks from CT of adults 1. Radiology, 251 (1), 175-184.

Sodickson, A., Baeyens, P. F., Andriole, K. P., Prevedello, L. M., Nawfel, R. D., Hanson, R., & Khorasani, R. (2009). Recurrent CT, cumulative radiation exposure, and associated radiation-induced cancer risks from CT of adults. Radiology, 251(1), 175-184.

Sorantin, E., Riccabona, M., Stücklschweiger, G., Guss, H., & Fotter, R. (2013). Experience with volumetric (320 rows) pediatric CT. European Journal of Radiology, 82 (7), 1091-1097.

Soye, J.A. and Paterson, A., (2008). A survey of awareness of radiation dose among health professionals in Northern Ireland. The British journal of radiology, 81 (969), pp.725-729.

Standring, S. (2008). Gray's anatomy: the anatomical basis of clinical practice (14th ed.): Elsevier Health Sciences.

Statkiewicz-Sherer, M. A., Visconti, P. J., Ritenour, E. R. (2010). Radiation Protection in Medical Radiography (6th ed.). London: Mosby.

Stewart, F., Akleyev, A., Hauer-Jensen, M., Hendry, J., Kleiman, N., Macvittie, T., Muirhead, C. (2012). ICRP publication 118: ICRP statement on tissue reactions and early and late effects of radiation in normal tissues and organs–threshold doses for tissue reactions in a radiation protection context. Annals of the ICRP, 41 (1), 1-322.

Strauss, K. J., & Goske, M. J. (2011). Estimated pediatric radiation dose during CT. Pediatr Radiol, 41 (2), 472.

Strauss, K. J., Goske, M. J., Frush, D. P., Butler, P. F., & Morrison, G. (2009). Image Gently Vendor Summit: working together for better estimates of pediatric radiation dose from CT. American Journal of Roentgenology, 192 (5), 1169-1175.

Strauss, K. J., Goske, M. J., Kaste, S. C., Bulas, D., Frush, D. P., Butler, P., Applegate, K. E. (2010). Image gently: ten steps you can take to optimize image quality and lower CT dose for pediatric patients. American Journal of Roentgenology, 194 (4), 868-873.

Street, M., Brady, Z., Every, B. V., & Thomson, K. R. (2009). Radiation exposure and the justification of computed tomography scanning in an Australian hospital emergency department. Internal Medicine Journal, 39 (11), 713-719.

Studdert, D. M., Mello, M. M., Sage, W. M., DesRoches, C. M., Peugh, J., Zapert, K., & Brennan, T. A. (2005). Defensive medicine among high-risk specialist physicians in a volatile malpractice environment. Jama, 293 (21), 2609-2617.

Suess, C., & Chen, X. (2002). Dose optimization in pediatric CT: current technology and future innovations. Pediatr Radiol, 32 (10), 729-734.

Suzuki, K., & Yamashita, S. (2012). Low-dose Radiation Exposure and Carcinogenesis. Japanese Journal of Clinical Oncology, 42(7), 563-568. doi:10.1093/jjco/hys078.

Szczykutowicz, T.P., Bour, R.K., Pozniak, M. and Ranallo, F.N., (2015). Compliance with AAPM Practice Guideline 1. a: CT Protocol Management and Review—from the perspective of a university hospital. Journal of applied clinical medical physics, 16 (2), pp.443-457.

Tack, D., & Gevenois, P.-A. (2004). Radiation dose in computed tomography of the chest. Jbr-Btr, 87 (6), pp.281-288.

Tapiovaara, M., Lakkisto, M., & Servomaa, A. (1997). A PC-based Monte Carlo program for calculating patient doses in medical x-ray examinations: Finnish Centre for Radiation and Nuclear Safety.

Theodorakou, C., Walker, A., Horner, K., Pauwels, R., Bogaerts, R., Jacobs Dds, R. and SEDENTEXCT Project Consortium, (2014). Estimation of paediatric organ and effective doses from dental cone beam CT using anthropomorphic phantoms. The British Journal of Radiology, 85 (1010), pp.153-160.

Thermo. (2007). TLD-100H, Thermo Scientific, Franklin, Massachusetts, US. Thermo scientific materials and assemblies for thermoluminescent dosimetry: Product overview.

ThermoScientific. (2015). High Sensitivity LIF: Mg, Cu, P Thermoluminescent Dosimetry Materials, Chips 2015 [cited 2017]. Retrieved from: https://www.thermofisher.com/order/catalog/product/SCP18815#%2Flegacy=thermoscientific.com.

Thomas, K. E., Parnell-Parmley, J. E., Haidar, S., Moineddin, R., Charkot, E., BenDavid, G., & Krajewski, C. (2006). Assessment of radiation dose awareness among pediatricians. Pediatr Radiol, 36 (8), 823-832.

Thomson, J., & Wise, K. (2004). Changes in CT radiation doses in Australia from 1994 to 2002. Radiographer: The Official Journal of the Australian Institute of Radiography, The, 51 (2), p.81.

Tian, X., Li, X., Segars, W. P., Frush, D. P., & Samei, E. (2015). Prospective estimation of organ dose in CT under tube current modulation. Medical Physics, 42(4), 1575-1585.

Tijssen, M., Hofman, P., Stadler, A., van Zwam, W., de Graaf, R., van Oostenbrugge, R. J., Postma, A. (2014). The role of dual energy CT in differentiating between brain haemorrhage and contrast medium after mechanical revascularisation in acute ischaemic stroke. Eur Radiol, 24 (4), 834-840.

Toivonen, M., Aschan, C., Rannikko, S., Karila, K., & Savolainen, S. (1996). Organ dose determinations of X-ray examinations using TL detectors for verification of computed doses. Radiat Prot Dosimetry, 66 (1-4), 289-294.

Tootell, A. K., Szczepura, K. R., & Hogg, P. (2013). Optimising the number of thermoluminescent dosimeters required for the measurement of effective dose for

computed tomography attenuation correction data in SPECT/CT myocardial perfusion imaging. Radiography, 19 (1), 42-47.

Tootell, A., Szczepura, K., & Hogg, P. (2014). An overview of measuring and modelling dose and risk from ionising radiation for medical exposures. Radiography, 20 (4), 323-332.

Tootell, A., Szczepura, K., & Hogg, P. (2014). Comparison of effective dose and lifetime risk of cancer incidence of CT attenuation correction acquisitions and radiopharmaceutical administration for myocardial perfusion imaging. The British Journal of Radiology, 87 (1041), 20140110.

TOSHIBA, M. S. C. (2004). Operation manual for whole-body X-ray CT scanner, Toshiba Medical systems corporationToshiba Aquilion 16. (2B201-313E*B).

Townsend, B. A., Callahan, M. J., Zurakowski, D., & Taylor, G. A. (2010). Has pediatric CT at children's hospitals reached its peak? American Journal of Roentgenology, 194 (5), 1194-1196.

Tricarico, F., Hlavacek, A. M., Schoepf, U. J., Ebersberger, U., Nance, J. W., Vliegenthart, R., Savino, G. (2013). Cardiovascular CT angiography in neonates and children: image quality and potential for radiation dose reduction with iterative image reconstruction techniques. Eur Radiol, 23 (5), 1306-1315.

Triolo, A., Brai, M., Bartolotta, A., & Marrale, M. (2006). Glow curve analysis of TLD-100H irradiated with radiation of different LET: Comparison between two theoretical methods. Nuclear Instruments and Methods in Physics Research Section A: Accelerators, Spectrometers, Detectors and Associated Equipment, 560 (2), 413-417.

Tsapaki, V., Aldrich, J. E., Sharma, R., Staniszewska, M. A., Krisanachinda, A., Rehani, M., Papailiou, J. (2006). Dose Reduction in CT while Maintaining Diagnostic Confidence: Diagnostic Reference Levels at Routine Head, Chest, and Abdominal CT—IAEA-coordinated Research Project 1. Radiology, 240 (3), 828-834.

Tsapaki, V., Kottou, S., & Papadimitriou, D. (2001). Application of European Commission reference dose levels in CT examinations in Crete, Greece. The British Journal of Radiology, 74 (885), 836-840.

Tzedakis, A., Damilakis, J., Perisinakis, K., Stratakis, J., & Gourtsoyiannis, N. (2005). The effect of z overscanning on patient effective dose from multidetector helical computed tomography examinations. Medical Physics, 32 (6), 1621-1629.

Uffmann, M., & Schaefer-Prokop, C. (2009). Digital radiography: The balance between image quality and required radiation dose. European Journal of Radiology, 72(2), 202-208. doi: https://doi.org/10.1016/j.ejrad.2009.05.060.

Ulzheimer, S. and Flohr, T., (2009). Multislice CT: current technology and future developments. In Multislice CT (pp. 3-23). Springer Berlin Heidelberg.

UNSCEAR, U. N. S. C. o. t. E. o. A. R. (2008). Effects of Ionizing Radiation: Report to the General Assembly, with scientific annexes (Vol. 1): United Nations Publications.

UNSCEAR, United Nations. Scientific Committee on the Effects of Atomic Radiation, (2008). Report of the United Nations Scientific Committee on the Effects of Atomic Radiation: Fifty-Sixth Session (10-18 July 2008) (No. 46). United Nations Publications.

UNSCEAR. (2000). United Nations. Scientific Committee on the Effects of Atomic Radiation. Sources and effects of ionizing radiation: sources (Vol. 1). New York, NY: USA: United Nations Publications.

UNSCEAR. (2000a). Sources and effects of ionizing radiation: Sources and effects of ionizing radiation. Report to the general assembly with scientific annexes, vol. II. Effects. (Vol. II). New York: United Nations Publications.

UNSCEAR. (2006). United Nations Scientific Committee on the Effects of Atomic Radiation. Effects of ionizing radiation: United Nations Scientific Committee on the Effects of Atomic Radiation—UNSCEAR 2006 report, volume II—report to the general assembly, with scientific annexes C, D, and E. UN; 2009. United Nations Office at Vienna: United Nations.

UNSCEAR. (2010). United Nations Scientific Committee on the Effects of Atomic Radiation. Sources and Effects of Ionizing Radiation. Volume I. New York, US. 1.

Valentin, J. (2003). Biological effects after prenatal irradiation (embryo and fetus): ICRP Publication 90 Approved by the Commission in October 2002. Annals of the ICRP, 33 (1), 1-206.

Valentin, J., (2007). Managing patient dose in multi-detector computed tomography (MDCT) (pp. 1-79). Elsevier.

Valentin, J., (2007). The 2007 recommendations of the international commission on radiological protection (pp. 1-333). Elsevier Oxford, UK.

Van De Graaff, K. M., Morton, D. A., & Crawley, J. L. (2012). A photographic atlas for the anatomy and physiology laboratory: Morton Publishing Company.

Van der Molen, A. J., & Geleijns, J. (2007). Overranging in Multisection CT: Quantification and Relative Contribution to Dose—Comparison of Four 16-Section CT Scanners 1. Radiology, 242 (1), 208-216.

Van der Molen, A. J., Schilham, A., Stoop, P., Prokop, M., & Geleijns, J. (2013). A national survey on radiation dose in CT in The Netherlands. Insights Imaging, 4 (3), 383-390.

Van Straten, M., Venema, H., Majoie, C., Freling, N., Grimbergen, C., & den Heeten, G. (2007). Image quality of multisection CT of the brain: thickly collimated sequential scanning versus thinly collimated spiral scanning with image combining. American Journal of Neuroradiology, 28 (3), 421-427.

VanDam, J., & Marinello, G. (2006). Methods for in vivo dosimetry in external radiotherapy (Second edition). Brussels (Belgium): ESTRO.

Varchena, V. (2002). Paediatric phantoms. Pediatr Radiol, 32 (4), pp. 280-284.

Vassileva, J., Rehani, M. M., Applegate, K., Ahmed, N. A., Al-Dhuhli, H., & Al-Naemi, H. M. (2013). IAEA survey of paediatric computed tomography practice in 40 countries in Asia, Europe, Latin America and Africa: procedures and protocols. Eur Radiol, 23 (3), 623-631.

Venselaar, J., Meigooni, A. S., Baltas, D., & Hoskin, P. J. (2012). Comprehensive brachytherapy: physical and clinical aspects: Taylor & Francis.

Verdun, F. R., Gutierrez, D., Vader, J. P., Aroua, A., Alamo-Maestre, L. T., Bochud, F., & Gudinchet, F. (2008). CT radiation dose in children: a survey to establish age-based diagnostic reference levels in Switzerland. Eur Radiol, 18 (9), 1980-1986.

Verdun, F. R., Lepori, D., Monnin, P., Valley, J.-F., Schnyder, P., & Gudinchet, F. (2004). Management of patient dose and image noise in routine pediatric CT abdominal examinations. Eur Radiol, 14 (5), 835-841.

Verdun, F.R., Gutierrez, D., Vader, J.P., Aroua, A., Alamo-Maestre, L.T., Bochud, F. and Gudinchet, F., (2008). CT radiation dose in children: a survey to establish age-based diagnostic reference levels in Switzerland. European radiology, 18 (9), pp.1980-1986.

Vilar-Palop, J., Vilar, J., Hernández-Aguado, I., González-Álvarez, I., & Lumbreras, B. (2016). Updated effective doses in radiology. Journal of radiological Protection, 36 (4), 975.

Vock, P. (2005). CT dose reduction in children. Eur Radiol, 15 (11), 2330-2340.

Von der Haar, T., Klingenbeck-Regn, K., & Hupke, R. (1998). Improvement of CT performance by UFC detector technology Advances in CT IV (pp. 9-15): Springer.

Vorona, G. A., Ceschin, R. C., Clayton, B. L., Sutcavage, T., Tadros, S. S., & Panigrahy, A. (2011). Reducing abdominal CT radiation dose with the adaptive statistical iterative reconstruction technique in children: a feasibility study. Pediatr Radiol, 41 (9), 1174-1182.

Wall, B., Haylock, R., Jansen, J., Hillier, M., Hart, D., & Shrimpton, P. (2011). Radiation risks from medical X-ray examinations as a function of the age and sex of the patient. Health Protection Agency Centre for Radiation, Chemical and Environmental Hazards. HPA-CRCE-028.

Wall, B.F., Kendall, G.M., Edwards, A.A., Bouffler, S., Muirhead, C.R. and Meara, J.R., (2014). What are the risks from medical X-rays and other low dose radiation? The British Journal of Radiology, 79 (940), pp.285-294.

Wallace, A. B., Goergen, S. K., Schick, D., Soblusky, T., & Jolley, D. (2010). Multidetector CT dose: clinical practice improvement strategies from a successful optimization program. Journal of the American College of Radiology, 7 (8), 614-624.

Walsh, L., Shore, R., Auvinen, A., Jung, T., & Wakeford, R. (2014). Risks from CT scans—what do recent studies tell us? Journal of radiological Protection, 34 (1), E1.

Wang, B., Xu, X. G., & Kim, C.-H. (2005). Monte Carlo study of MOSFET dosemeter characteristics: dose dependence on photon energy, direction and dosemeter composition. Radiat Prot Dosimetry, 113 (1), 40-46.

WHO, W. H. O. (2016). Communicating radiation risks in paediatric imaging: information to support health care discussions about benefit and risk. Geneva: World Health Organization.

Wiest, P. W., Locken, J. A., Heintz, P. H., & Mettler, F. A. (2002). CT scanning: a major source of radiation exposure. Paper presented at the Seminars in Ultrasound, CT and MRI.

Winslow, J. F., Hyer, D. E., Fisher, R. F., Tien, C. J., & Hintenlang, D. E. (2009). Construction of anthropomorphic phantoms for use in dosimetry studies. Journal of Applied Clinical Medical Physics, 10(3), 195-204.

Wood, G. C., & Boucher, B. (2012). Management of acute traumatic brain injury. PSAP-VIII: Neurology and Psychiatry, pp.139-156.

Wrixon, A. (2008). New recommendations from the International Commission on Radiological Protection—a review. Phys Med Biol, 53 (8), R41.

Xu, X.G. and Eckerman, K.F., (2010). Computational phantoms for radiation dosimetry: a 40-year history of evolution. Handbook of anatomical models for radiation dosimetry: CRC Press, 1, pp.3-41.

Yates, S.J., Pike, L.C. and Goldstone, K.E., (2014). Effect of multislice scanners on patient dose from routine CT examinations in East Anglia. The British journal of radiology, 77 (918), pp.472-478.

Yoshizumi, Sarder, M., Goodman, P. C., Frush, D. P., Barnes, L., & Nguyen, G. (2003). Application of MOSFET Technology in CT Organ Dose Assessment. Medical Physics, 30 (1422).

Yoshizumi, T. T., Goodman, P. C., Frush, D. P., Nguyen, G., Toncheva, G., Sarder, M., & Barnes, L. (2007). Validation of metal oxide semiconductor field effect transistor technology for organ dose assessment during CT: comparison with thermoluminescent dosimetry. American Journal of Roentgenology, 188 (5), 1332-1336.

Younis, R. T., Anand, V. K., & Davidson, B. (2002). The role of computed tomography and magnetic resonance imaging in patients with sinusitis with complications. The Laryngoscope, 112 (2), 224-229.

Yu, L., & Leng, S. (2016). Image reconstruction techniques. American College of Radiology. 1-6.

Yu, L., Leng, S. and McCollough, C.H., 2012. Dual-energy CT–based monochromatic imaging. American journal of Roentgenology, 199 (5_supplement), pp. S9-S15.

Zankl, M., Panzer, W., Petoussi-Henss, H., & Drexler, G. (1995). Organ doses for children from computed tomographic examinations. Radiat Prot Dosimetry, 57 (1-4), 393-396.

Zarb, F., McEntee, M., & Rainford, L. (2012). Maltese CT doses for commonly performed examinations demonstrate alignment with published DRLs across Europe. Radiat Prot Dosimetry, 150 (2), 198-206.

Zenone, F., Aimonetto, S., Catuzzo, P., Peruzzo Cornetto, A., Marchisio, P., Natrella, M., Tofani, S. (2012). Effective dose delivered by conventional radiology to Aosta Valley population between 2002 and 2009. The British Journal of Radiology, 85(1015), e330-e338. doi:10.1259/bjr/19099861.

Zhou, G., Wong, D., Nguyen, L., & Mendelson, R. (2010). Student and intern awareness of ionising radiation exposure from common diagnostic imaging procedures. Journal of medical imaging and radiation oncology, 54 (1), 17-23.

Ziqiang, P., & Binglin, X. (2000). United Nations Scientific Committee on the effects of atomic radiation (UNSCEAR) and its forty-ninth session. Radiation Protection (Taiyuan), 20 (5), 312-317.